

ISSN: 2249-6645

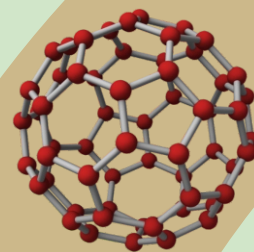


International Journal of Modern Engineering Research (IJMER)

Volume 4

Issue 2

February 2014



International Journal of Modern Engineering Research (IJMER)

Editorial Board

Executive Managing Editor

Prof. Shiv Kumar Sharma
India

Editorial Board Member

Dr. Jerry Van
Department of Mechanical, USA

Dr. George Dyrud
Research centre dy. Director of Civil Engineering, New Zealand

Dr. Masoud Esfal
R& D of Chemical Engineering, Australia

Dr. Nouby Mahdy Ghazaly
Minia University, Egypt

Dr. Stanley John
Department of Textile Engineering, United Kingdom

Dr. Valfitaf Rasoul
Professor and HOD of Electromechanical, Russian

Dr. Mohammed Ali Hussain
HOD, Sri Sai Madhavi Institute of Science & Technology, India

Dr. Manko dora
Associate professor of Computer Engineering, Poland

Dr. Ahmed Nabih Zaki Rashed
Menoufia University, Egypt

Ms. Amani Tahat
Ph.D physics Technical University of Catalonia-Spain

Associate Editor Member

Dr. Mohd Nazri Ismail
University of Kuala Lumpur (UniKL), Malaysia

Dr. Kamaljit I. Lakhtaria
Sir Padmapat Singhaniya University, Udaipur

Dr. Rajesh Shrivastava
Prof. & Head Mathematics & computer Deptt. Govt. Science & commerce College Benazir. M.P

Dr. Asoke Nath
Executive Director, St. Xavier's College, West Bengal, India

Prof. T. Venkat Narayana Rao
Head, CSE, HITAM Hyderabad

Dr. N. Balasubramanian
Ph. D (Chemical Engg), IIT Madras

Jasvinder Singh Sadana
M. TECH, USIT/GGSIPU, India

Dr. Bharat Raj Singh

Associate Director, SMS Institute of Technology, Lucknow

DR. RAVINDER RATHEE

C. R. P, Rohtak, Haryana

Dr. S. Rajendran

Research Supervisor, Corrosion Research Centre Department of Chemistry, GTN Arts College, Dindigul

Mohd Abdul Ahad

Department of Computer Science, Faculty of Management and Information Technology, Jamia Hamdad, New Delhi

Kunjai Mankad

Institute of Science & Technology for Advanced Studies & Research (ISTAR)

NILANJAN DEY

JIS College of Engineering, Kalyani, West Bengal

Dr. Hawz Nwayu

Victoria Global University, UK

Prof. Plewin Amin

Crewe and Alsager College of Higher Education, UK

Dr. (Mrs.) Annifer Zalic

London Guildhall University, London

Dr. (Mrs.) Malin Askiy

Victoria University of Manchester

Dr. ABSALOM

Sixth form College, England

Dr. Nimrod Nivek

London Guildhall University, London

Finite Element Analysis of Convective Micro Polar Fluid Flow through a Porous Medium in Cylindrical Annulus

¹Dr. B. Tulasi Lakshmi Devi, ²Dr. B. Srinivasa Reddy, ³G. V. P. N. Srikanth,
⁴Dr. G. Srinivas

^{1,3,4}Department of Mathematics, Guru Nanak Institute of Technology, Hyderabad, India

²Department of Applied Mathematics, Yogi Vemana University, Kaddapah, A.P., India

ABSTRACT: We analyze a finite element solution for the mixed convection micro polar flow through a porous medium in a cylindrical annulus. The governing partial differential equations are solved numerically by using finite element technique. The effect of Darcy parameter and Heat source parameter and surface condition on velocity, micro rotation and temperature functions has been studied.

Keywords: Porous medium, Micro polar Fluids, Convection, Cylindrical annulus.

I. INTRODUCTION

In recent years there have been considerable advancement in the study of free convection in a porous annulus because of its natural occurrence and of its importance in many branches of science and engineering. This is of fundamental importance to a number of technological applications, such as underground disposal of radioactive waste materials, cooling of nuclear fuel in shipping flasks and water filled storage bays, regenerative heat exchangers containing porous materials and petroleum reservoirs, burying of drums containing heat generating chemicals in the earth, storage of agricultural products, ground water flow modeling, nuclear reactor assembly, thermal energy storage tanks, insulation of gas cooled reactor vessels, high performance insulation for building, and cold storage, free convective heat transfer inside a vertical annulus filled with isotropic porous medium has been studied by many researchers, notable among them are Havstad et. al., [7], Reda [15], Prasad et. al., [12,13], Prasad et. al., [14], Hickon et. al., [8], and Shiva kumara et. al., [16], they concluded that radius ratio and Rayleigh number influence the heat and fluid flow significantly.

Eringen [5] presented the theory of micro polar fluid which explains adequately the internal characteristics of the substructure particles subject to rotations and deformations, Ariman [1] Sylvester et. al., [17] and Ariman et. al., [2] confirmed that the micropolar fluid serves a better model for animal blood. The liquid crystals, suspension solutions and certain polymeric fluids consisting of randomly oriented barlike elements of dumbbell molecules, behave as micro polar fluid. Kazakai and Ariman [10] introduced the heat conducting micropolar fluid and investigated the flow between two parallel plates. Eringen [6] extended the theory further to include heat conduction and viscous dissipation. The application of this theory may be searched in biomechanics.

Berman [4] has studied the flow of a viscous liquid under a constant pressure gradient between two concentric cylinders at rest. Inger [9] solved the problem when the walls are permeable and the outer cylinder is sliding with a constant axial velocity relative to the stationary inner one. Mishra and Acharya [11] examined the elastico viscous effects in the flow considered by Inger [9]. Sastri and Maiti solved the problem of combined convective flow of micro polar fluid in an annulus.

The problem of massive blowing into aerodynamic body flow fields is a complex 1 for a realistic flow configuration. However the study the simplified flow models exhibits some of the essential physical features involving the interaction of blowing with a shear flow. The classical Couette – Poiseuille shear flow is an idealized model for this purpose to investigate to micro polar structures at least theoretically on such a flow Agarwal and Dhanpal [3] have analyzed the connective micro polar fluid flow and heat transfer between two concentric porous circular cylinders when the outer cylinder moves parallel to itself with a constant velocity. A problem solved by Inger [9] in viscous fluids.

In this paper we make an investigation of connective heat transfer flow micro polar fluid in a cylindrical annulus between the porous concentric cylinders $r = a$ and $r = b$. By employing Galerkin finite element analysis with line elements with three nodes the transport equations of linear momentum, angular momentum and energy are solved to obtain velocity, micro concentration and temperature distributions.

II. FORMULATION OF THE PROBLEM

Consider the steady motion of an incompressible micro polar fluid through an annulus of two infinitely long porous circular cylinders of radii a and b ($a - b = h > 0$) respectively. The fluid is injected through the inner cylinder with arbitrary radial velocity u_b and in view of continuity, also flows outward through the moving cylinder with a radial velocity u_a . The cylindrical polar co-ordinate system (r, θ, z) with z co-ordinate along the axis of the cylinders is chosen to specify the problem.

The velocity and micro rotation are taken in the form

$$\begin{aligned} v_r &= u(r), \quad v_\theta = v = 0, \quad v_z = w(r) \\ v_r &= 0, \quad v_\theta = v = (r), \quad v_z = 0 \end{aligned} \quad 2.1$$

the basic equations are:

$$\text{Continuity:} \quad \frac{\partial u}{\partial r} + \frac{u}{r} = 0 \quad 2.2$$

$$\text{Momentum:} \quad \rho u \frac{\partial u}{\partial r} = - \frac{\partial p}{\partial r} + (\mu + k) \left(\frac{\partial^2 u}{\partial r^2} + \frac{1}{r} \frac{\partial u}{\partial r} - \frac{u}{r^2} \right) \quad 2.3$$

$$\rho u \frac{\partial w}{\partial r} = - \frac{\partial p}{\partial z} + (\mu + k) \left(\frac{\partial^2 w}{\partial r^2} + \frac{1}{r} \frac{\partial w}{\partial r} \right) + \frac{k}{r} \frac{\partial}{\partial r} (rN) \quad 2.4$$

First stress Momentum:

$$\rho j u \frac{\partial N}{\partial r} = r \left(\frac{\partial^2 N}{\partial r^2} + \frac{1}{r} \frac{\partial N}{\partial r} - \frac{N}{r^2} \right) - k \frac{\partial w}{\partial r} - 2kN \quad 2.5$$

$$\text{Energy:} \quad \rho C_p w \frac{\partial T}{\partial z} = k_f \left(\frac{\partial^2 T}{\partial r^2} + \frac{1}{r} \frac{\partial T}{\partial r} \right) \quad 2.6$$

Where T is the temperature, N is the micro rotation ρ the density, p the pressure, j the micro inertia, C_p the specific heat, k_f the thermal conductivity, μ the fluid viscosity, k is the material constants.

At $r = b$, $u = u_b$, $w = 0$, $v = 0$, $T = T_0 + A_0 z$

At $r = a$, $u = u_a$, $w = 0$, $v = 0$, $T = T_1 + A_0 z$ 2.7

Where the fluid is assumed to adhere to the solid boundaries. A_0 is the constant of proportionality and T_0, T_1 are the constant wall temperatures of inner and outer cylinders temperatures of inner and outer cylinders respectively at $z = 0$.

The integration of (2.2) yields

$$ur = C, \text{ a constant} \quad 2.8$$

$$\Rightarrow ru = au_a = bu_b \Rightarrow u = \frac{au_a}{r}$$

Also in view of the boundary condition on temperature, we may write

$$T = T_0 + A_0(z) + \theta(r) \quad 2.9$$

Introducing the non-dimensional variables r', w', p', θ and N as

$$\begin{aligned} r' &= \frac{r}{a}, \quad w' = \frac{w}{a}, \quad p' = \frac{p}{\rho u^2 / a^2} \\ \theta &= \frac{T - T_0}{T_i - T_0}, \quad N' = \frac{(u+k)w}{\rho \mu^2 a^2} \end{aligned} \quad 2.10$$

The governing equations in the non-dimensional form are

$$\frac{d^2 w'}{d r'^2} + \left(1 - \frac{\lambda}{1+\Delta} \right) \frac{1}{r'} \frac{d w'}{d r'} = -\pi_1 + D_1^{-1} - G\theta - \frac{\Delta}{r'} \frac{d}{d r'} (r' N') \quad 2.11$$

$$\frac{d^2 N'}{d r'^2} + (1 - \lambda A) \frac{1}{r'} \frac{d N'}{d r'} - \left(\frac{1}{r'^2} - \frac{2\Delta}{A} \right) N' = \frac{\Delta}{A} \frac{1}{r'} \frac{d w'}{d r'} \quad 2.12$$

$$P_r N_T w' = \frac{d^2 \theta}{d r'^2} + \frac{1}{r'} \frac{d \theta}{d r'} \quad 2.13$$

where

$$\Delta = \frac{k}{\mu} \quad (\text{Micropolar parameter}) \quad A = \frac{r}{\mu J} \quad (\text{Micropolar parameter})$$

$$A_1 = \frac{\beta}{\mu a^2} \quad \lambda = \frac{a u_a}{\nu} \quad (\text{Suction parameter})$$

$$D^{-1} = \frac{L^2}{k} \quad (\text{Darcy parameter}) \quad G = \frac{\beta g \Delta T L^3}{\nu^2} \quad (\text{Grashof number})$$

$$G_1 = \frac{G}{1+\Delta} \quad \Delta_1 = \frac{\Delta}{1+\Delta}$$

$$P_r = \frac{\mu C_p}{k_f} \quad (\text{Prandtl number})$$

The boundary conditions are

$$w = 0, \quad \theta = 1, \quad N = 0 \quad \text{on} \quad r = 1$$

$$w = 0, \quad \theta = 0, \quad N = 0 \quad \text{on} \quad r = s$$

In order to predict the heat and mass transfer behavior in the porous medium equations (2.11) – (2.13) are solved by using finite element method. A simple 3-noded triangular element is considered. ψ , θ and ϕ vary inside the element and can be expressed as

$$\psi = N_1 \psi_1 + N_2 \psi_2 + N_3 \psi_3$$

$$\theta = N_1 \theta_1 + N_2 \theta_2 + N_3 \theta_3$$

$$\phi = N_1 \phi_1 + N_2 \phi_2 + N_3 \phi_3$$

Gela kin's method is used to convert the partial differential equation (2.11) – (2.13) into matrix form of equations. Details of FEM formulations and good understanding of the subject is given in the books [3, 4]. The matrix equations are, assembled to get global matrix equations for the whole domain, which is then solved iteratively, to obtain θ , ψ and ϕ in porous medium. In order to get accurate results, tolerance level of solution for θ , ψ and ϕ are set at 10^{-5} and 10^{-9} respectively. Element size in domain varies. Large number of elements are located near the walls where large variations in θ , ψ and ϕ are expected. The mesh is symmetrical about central horizontal and vertical lines of the cavity. Sufficiently dense mesh is chosen to make the solution mesh invariant. The mesh size of 3200 elements has good accuracy in predicting the heat transfer behavior of the porous medium. The computations are carried out on high-end computer.

III. RESULTS AND DISCUSSION

On solving the equations, given by the finite element technique the velocity, micro rotation and temperature distributions are obtained. The Prandtl number p_r , material constants A & A are taken to be constant, at 0.733, 1 and 1 respectively whereas the effect of other important parameters, namely micro polar parameter Δ , the section Reynolds number λ , Grashof number G and Darcy parameter D^{-1} has been studied for these functions and the corresponding profiles are shown in figs. 1.

Fig. 1 depicts the variation of velocity function W with Grashof number G . The actual axial velocity W is in the vertically downwards direction and $w < 0$ represents the actual flow. Therefore $w > 0$ represents the reversal flow. We notice from fig. 1 that $w > 0$ for $G > 0$ and $w < 0$ for $G < 0$ except in the vicinity of outer cylinder $r = 2$. the reversal flow exists everywhere in the region ($1.1 \leq r \leq 1.8$) for $G > 0$ and in the neighborhood of $r = 2$ for $G < 0$. The region of reversed flow enlarges with $G \leq 2 \times 10^3$ and shrinks with higher $G \geq 3 \times 10^3$. Also it grows in size with $|G| (< 0)$. $|w|$ enhances with $G \leq 2 \times 10^3$ and reduces with higher $G \geq 3 \times 10^3$. $|w|$ experiences a depreciation in the case of cooling of the boundaries with maximum at $r = 1.5$. The variation of w with Darcy parameter D^{-1} . It is found that lesser the permeability of the porous medium larger $|w|$ in the flow region (fig. 2). The influence of micro rotation parameter Δ on w is shown in fig. 3. As the micro polar parameter $\Delta \leq 3$ increases, the velocity continuously increases and decreases with higher $\Delta \geq 5$, with maximum attained in the vicinity of $r = 1$. Fig. 4 represents w with suction parameter λ . IT is found that the axial velocity experiences an enhancement with increase in $\lambda \leq 0.03$ and depreciates with higher $\lambda \geq 0.05$. Fig. 5 depicts w with the width of the annular region. We notice that the axial velocity continuously decreases with increase in the width S of the annular region. Thus the velocity enhances in the narrow gap region and depreciates in the wide gap case. The effect of radiation parameter N_1 on w is exhibited in Fig. 6. IT is observed that the velocity w enhances with increase in $N_1 \leq 1.0$ except in a narrow region adjacent to $r = 2$ and for higher $N_1 \geq 1.5$, it experiences an enhancement in the entire flow region.

The micro rotation (N) is shown in figs 7-12 for different values of G , Δ , λ , S and N_1 . It is found that the values of micro rotation for $G > 0$ are negative and positive for $G < 0$. An increase in $|G| \leq 2 \times 10^3$ editor an enhancement in N and for higher $|G| \geq 3 \times 10^3$, it reduces in the region adjacent to $r = 1$ and enhances in the reform adjacent to $r = 2$ with maximum at $r = 1.5$ (fig. 7). From fig. 8 we find that lesser the permeability of the porous medium larger the micro oration everywhere in the flow region. The effect of N on micro polar parameter Δ in shown in Fig. 9. We notice that an increase in $\Delta \leq 3$ leads to an enhancement in $|N|$ and for higher $\Delta \geq 5$, it enhances the first half ($1.1 \leq r \leq 1.5$) and reduces in the second half ($1.6 \leq r \leq 1.9$). Fig. 10 illustrates that the micro oration enhances in the first half and reduces in the second half with increase in $\lambda \leq 0.02$ and for higher values of $\lambda \geq 0.03$ we notice an increment in $|N|$ everywhere in the flow region. Form fig. 11 we find that the micro rotation depreciates in the narrow gap case and enhances in the wide gap case. Fig. 12 illustrates that the micro rotation $|N|$ enhances with increase in the radiation parameter $N_1 \leq 1.5$ and for higher $N_1 \geq 2.5$, the micro rotation enhances in the let half and depreciates in the second half of the flow region.

The non-dimensional temperature (θ) is shown in figs. 13 – 17 for different values of G , λ , Δ , S and N_1 . Fig. 13 illustrates that non-dimensional temperature is positive for all variations. The actual temperature enhances with increase in $G \leq 2 \times 10^3$ and depreciates with higher $G \geq 3 \times 10^3$. Also it enhances with $G < 0$. The variation of θ with D^{-1} shows that lesser the permeability of the porous medium larger the actual temperature in the flow region (Fig. 14), Fig. 15 illustrates that an increase in the micro rotation parameter Δ increases the actual temperature continuously with maximum attained at $r=1.5$. The variation of θ with suction parameter λ shows that the temperature enhances with increase in $\lambda \geq 0.03$. For further increase in $\lambda \geq 0.05$, the temperature depreciates in the first half and enhances in the second half. The influence of the suction of the boundary on θ is shown in fig. 16. IT is found that increase in $S \leq 0.6$ reduces θ in the left half and enhances it in the right half and for $S = 0.7$, θ reduces in the flow region except in a region adjacent to $r=1$. For further increase in S we notice an enhancement in the central flow region and depreciation in θ in the regions abutting the cylinders $r = 1$ & 2. Fig. 17 represents the temperature with radiation parameter N_1 . It is found that an increase in N_1 enhances θ in the left half and depreciates in the right half and for higher values $N_1 \geq 1.5$ we observe depreciation in the first half and enhancement in the second half.

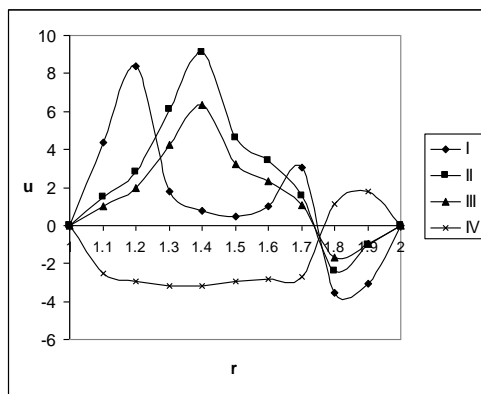


Fig. 1 : Variation of velocity (u) with G
 I II III IV
 G 10^3 3×10^3 5×10^3 -10^3

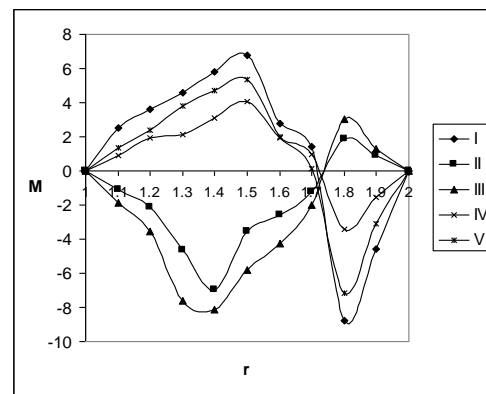


Fig. 2 : Variation of velocity (u) with G
 I II III IV V
 G -3×10^3 -5×10^3 10^3 2×10^3 3×10^3

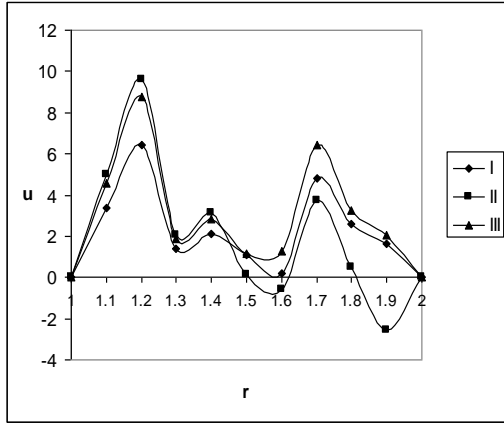


Fig. 3 : Variation of velocity (u) with Δ
 I II III
 Δ 1 3 5

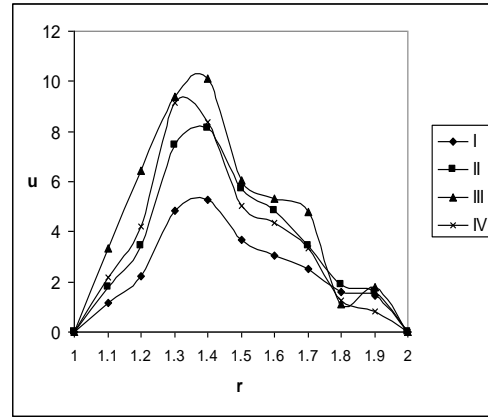


Fig. 4 : Variation of velocity (u) with λ
 I II III IV
 λ 0.01 0.02 0.03 0.05

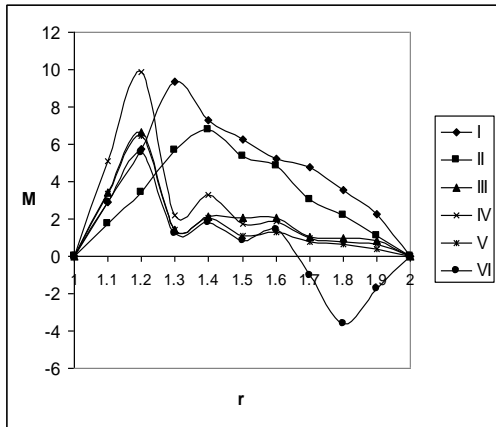


Fig. 5 : Variation of velocity (u) with S
 I II III IV V VI
 S 0.4 0.5 0.6 0.7 0.8 0.9

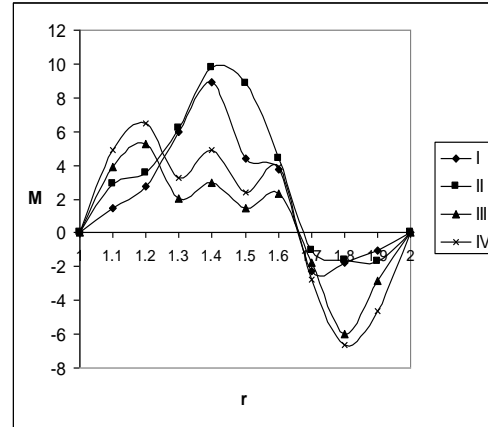


Fig. 6 : Variation of velocity (u) with N_t
 I II III IV
 N_t 0.5 1.0 1.5 2.5

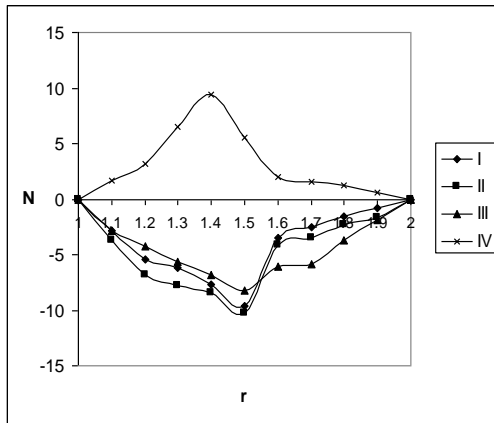


Fig. 7 : Variation of micro rotation (N) with G
 I II III IV
 G 10^3 3×10^3 5×10^3 -10^3

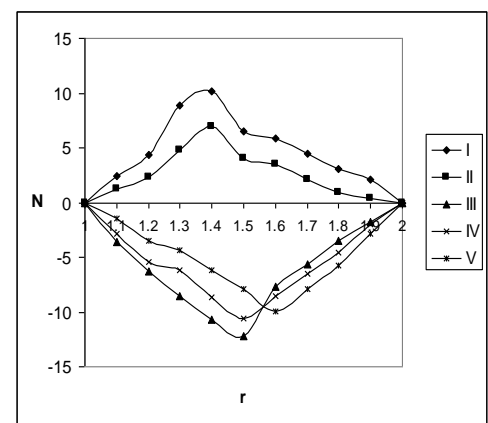


Fig. 8 : Variation of micro rotation (N) with G
 I II III IV V
 G -3×10^3 -5×10^3 10 20 30

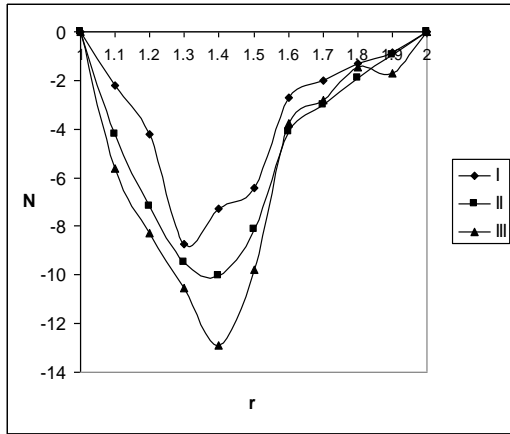


Fig. 9 : Variation of micro rotation (N) with Δ
 I II III
 Δ 1 3 5

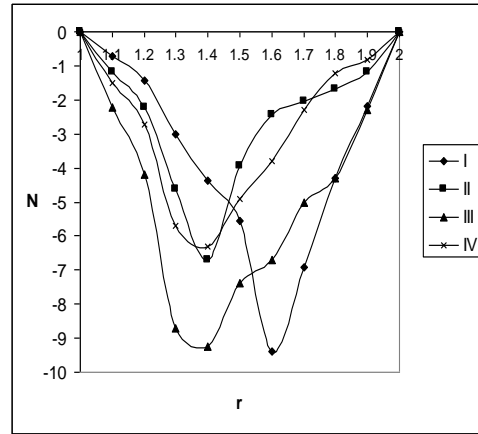


Fig. 10 : Variation of micro rotation (N) with λ
 I II III IV
 λ 0.01 0.02 0.03 0.05

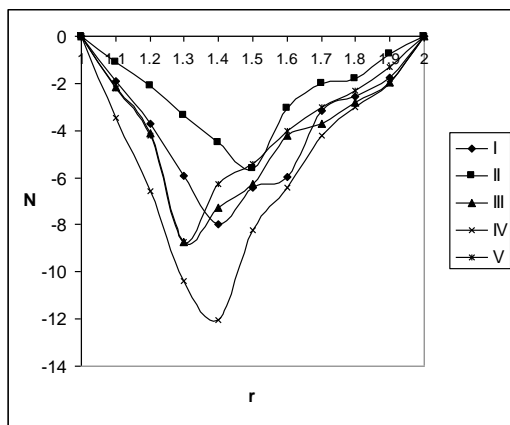


Fig. 11 : Variation of micro rotation (N) with S
 I II III IV V VI
 S 0.4 0.5 0.6 0.7 0.8 0.9

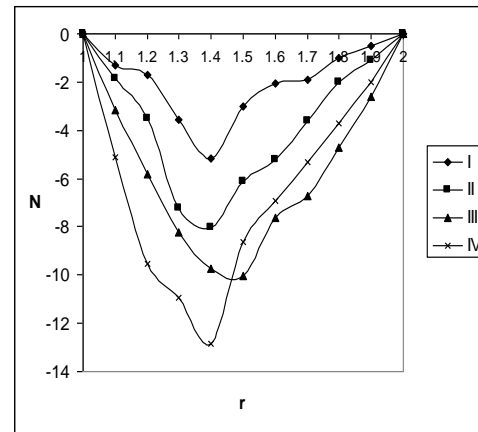


Fig. 12 : Variation of micro rotation (N) with N_t
 I II III IV
 N_t 0.5 1.0 1.5 2.5

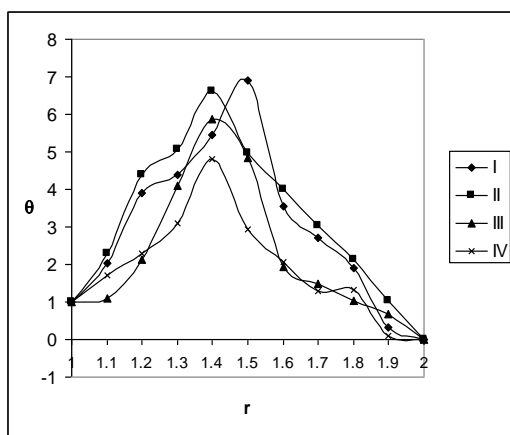


Fig. 13 : Variation of temperature (θ) with G
 I II III IV
 G 10^3 3×10^3 5×10^3 -10^3

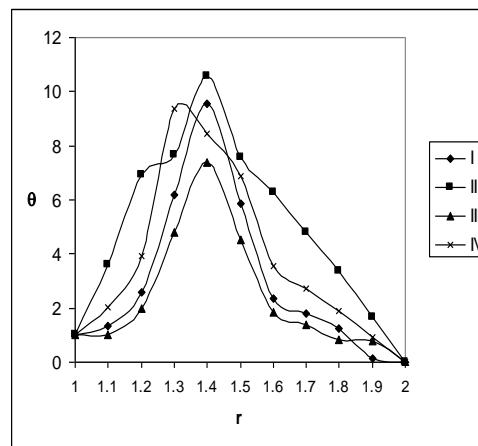


Fig. 14 : Variation of temperature (θ) with G
 I II III IV V
 G -3×10^3 -5×10^3 10 20 30

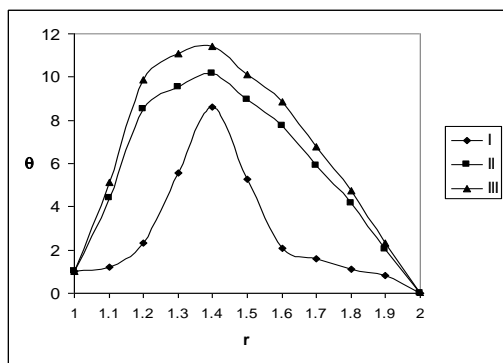


Fig. 15: Variation of temperature (θ) with Δ

	I	II	III
Δ	1	3	5

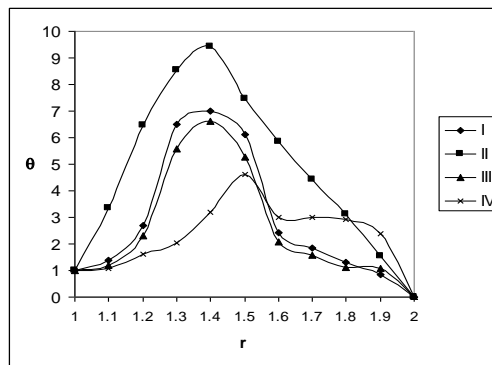


Fig. 16: Variation of temperature (θ) with λ

	I	II	III	IV
λ	0.01	0.02	0.03	0.05

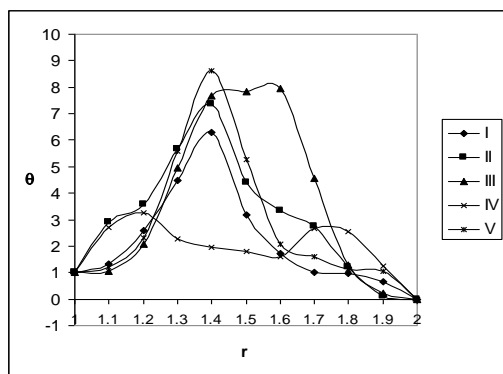


Fig. 17: Variation of temperature (θ) with S

	I	II	III	IV	V	VI
S	0.4	0.5	0.6	0.7	0.8	0.9

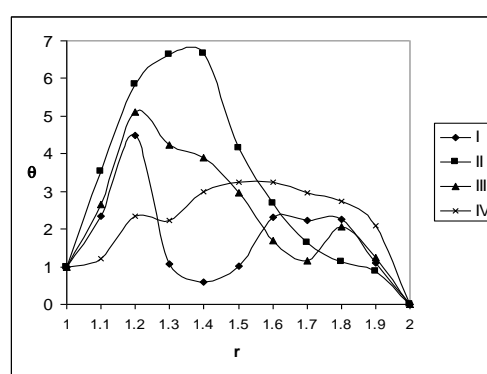


Fig. 18: Variation of temperature (θ) with N_t

	I	II	III	IV
N_t	0.5	1.0	1.5	2.5

REFERENCES

- [1] T. ARIMAN, *J. Biomech.* 4, 185 (1971).
- [2] T. ARIMAN, M.A.TURK and N.D.SYLVESTER, *Int. J. Engng. sci.* 11, 905 (1973).
- [3] R.S. AGARWAL¹ and C. DHANAPAL² Numerical solution of micro polar fluid flow and heat transfer between two co-axial porous circular cylinders *Int. J. Engng. Sci.* vol. 26. No.11, pp. 1133-1142, 1988.
- [4] A.S. BERMAN, *J. appl. Phys.* 29, 71 (1958).
- [5] A.C. ERINGEN, *J. Math. Mech.* 16, 1 (1966).
- [6] A.C. ERINGEN, *J. Math. Analysis Applic.* 38 480 (1972).
- [7] HAVSTAD, M.A, BURNS, P.J. convective heat transfer in vertical cylindrical Annuli filled with porous medium, *Int. J. Heat Mass Transfer.* 25 (1982), 11, pp. 1755-1766.
- [8] HICKON, C.E, GARTLING, D.K. A Numerical study of natural convection in a vertical Annulus porous layer, *Int. J. Heat Mass Transfer*, 28 (1985) 3, pp. 720-723.
- [9] G.R.INGER, *phys. Fluids* 12, 1741 (1969).
- [10] Y. KAIZAKI and T. ARIMAN, *Rheol. Acta* 10 319 (1971).
- [11] S.P.MISHRA and B.P. ACHARYA. *Ind. J. phys.* 46, 469 (1972).
- [12] PRASAD, V., KULACKI, F.A. Natural convection in a vertical porous Annulus, *Int. J. Heat Mass Transfer* 27 (1984), 2 pp. 207-219.
- [13] PRASAD, V. KULACKI, F.A. Natural convection in porous media bounded by short concentric cylinders, *ASME J. Heat Transfer*, 107 (1985), 1, pp. 147-154
- [14] PRASAD, V., KULACKI, F.A, KEYHANI, M. Natural convection in porous media, *J. Fluid Mechanics*, 150 (1985), 3, pp. 89-119.
- [15] REDA, D.C. Natural convection experiments in a liquid saturated porous medium bounded by vertical coaxial cylinders, *ASME J. Heat Transfer*, 105 (1983), 4, pp. 795-802.
- [16] SHIVAKUMARA, I.S, PRASANNA, B.M.R, RUDRAISH, N. VENKATACHALAPPA, M. Numerical study of natural convection in a vertical cylindrical Annulus using Non-Darcy equation. *J. Porous Media*, 5 (2003), 2, pp. 87-102.
- [17] N.D. SYLVESTER, M.A, TURK and T. ARIMAN *Trans. Soc. Rheol.* 17, 1 (1973).

Biogas as a Alternate Source Of Energy And Creating Awareness Among Rural People

Neeraj Kumar¹, Sachin Gupta², Bharat atary³

Assistant Professor, Department of ME¹

Assistant Professor, Department of CSE²

Assistant Professor, Department of ME³

Maharishi Markandeshwar Group of Institutions (Ramba) Karnal, India

ABSTRACT: This paper deals with the use of biogas as a alternate source of energy and creating awareness among rural people. Biogas refer to a gas made from anaerobic digestion of agricultural and animal waste. The gas is useful as a fuel substitute for firewood, dung, agricultural residues, petrol and electricity. Biogas, a clean and renewable form of energy could very well substitute (especially in the rural sector) for conventional sources of energy (fossil fuels, oil, etc.) which are causing ecological–environmental problems biogas digester involves anaerobic fermentation process in which different groups of bacteria act upon complex organic materials in the absence of air to produce biogas.

Keywords: Alternate Source, Biogas, Methane, Waste, Biogas plant.

I. INTRODUCTION

Biogas is a gas whose primary elements are methane (CH₄) and carbon dioxide (CO₂) and may have small amount of hydrogen sulphide (H₂S), Moisture and siloxanes. It is a mixture of methane (CH₄), 50 to 70% carbon dioxide (CO₂), 30 to 40% hydrogen (H₂), 5 to 10% nitrogen (N₂) and 1 to 2% hydrogen sulphide (H₂S). Water vapour (0.3%). biogas is about 20% lighter than air and has an ignition temperature in the range of 650 to 750°C. It is a colourless and odourless gas that burns with 60% efficiency in a conventional biogas stove. It is a product of the natural decomposition of any organic substance of animal or plant. It refers to a gas produced by the biological breakdown of organic matter in the absence of oxygen organic waste such as dead plant and animal material, animal dung and kitchen waste can be converted into a gaseous fuel called biogas. The main source for production of biogas are cattle dung, night soil, poultry or piggery dropping, agricultural residues animals manure, wood waste from forestry and industry, residues from food and paper industries, municipal green wastes, sewage sludge dedicated energy crops such as short rotation (3 to 15 years) grasses, sugar crops (sugarcane, beet), starch crops (corn, wheat) and oil crops (soy, sunflower, palm oil), kitchen waste, household waste, green waste, human waste. The components of biogas – methane and carbon dioxide- act as greenhouse gases that harm the environment if released unburned into the atmosphere. The production of biogas in biogas plants prevents uncontrolled emission of methane into the atmosphere and, by generating renewable energy in the form of biogas, reduces the use of fossil fuel.

II. BIOMASS CONVERSION PROCESS

Biomass conversion process is divided into three categories, such as:

- (i) Direct combustion
- (ii) Thermo chemical conversion
- (iii) Biochemical conversion

2.1 Direct combustion

Process of burning in presence of oxygen to produce heat and by products is called combustion complete combustion to ashes is called is incineration. The process of combustion is applicable to solid, liquid and gaseous fuel. Such as wood dung, vegetable waste can be dried and burnt to provide heat or converted into low calorific value gas by “pyrolysis”.

2.1.1 Pyrolysis process

In this process organic material to gases solid and liquids by heating to 500 °C to 900 °C in the absence of oxygen product of wood pyrolysis are methanol, charcoal and acidic acid all forms of organic materials

including such as rubber and plastic can be converted to a fuel gas which contains CO, CH₄, other hydrocarbons (C_nH_m) CO₂ and N₂.

2.2 Thermo chemical conversion

Thermo chemical conversion process converts the biomass and its residues to fuel, chemical and power using gasification and pyrolysis technologies.

2.3 Biochemical conversion

Biochemical conversion by micro-organisms converting biomass to biofuels are slow processes taking place at low temp. The principal conversion process is fermentation. fermentation is a process of decomposition of organic matter by micro-organism. e.g- decomposition of suger to form ehanol and carbondioxide by yeast and ethanol forming acetic acid in making vinegar.

2.3.1 Gassification

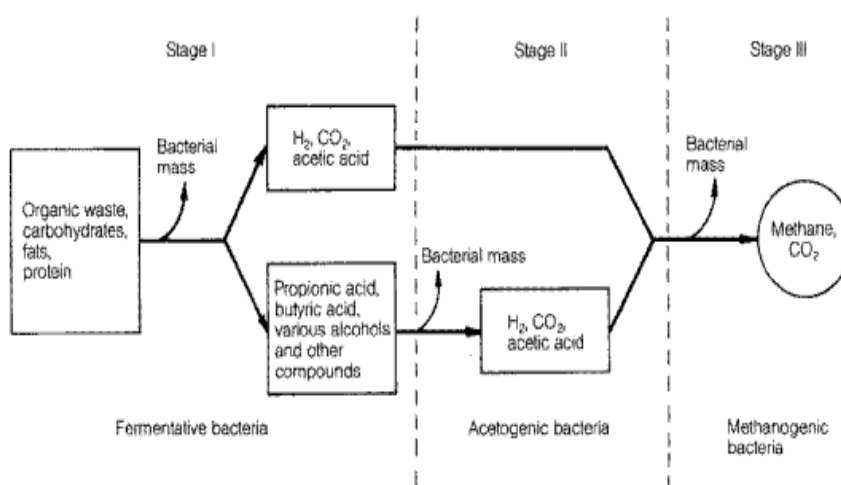
Heating biomass with about one-third of the oxygen necessary for complete combustion produces a mixture of carbon dioxide and hydrogen known as syngas. Paralysis heating biomass in the absence of oxygen produce a liquid pyrolysis oil both syngas and pyrolysis oil can be used as fuels both can also be chemically converted to other valuable fuels and chemicals. „ Gobar Gas” mainly because cow dung has been the material for its production. It is not only the excreta of the cattle, but also the piggery waste as well as poultry droppings are very effectively used for biogas generation. A few other material through which biogas can be generated are algae, crop residues. Biogas is produced by digestion, pyrolysis or hydro gasification. Digestion is a biological process that occurs in the absence of oxygen and in the presence of anaerobic organisms at ambient pressures and temperatures of 35-70 C. The container in which this digestion takes place is known as the digester.

2.4 Anaerobic digestion

Biogas technology is concerned to micro organisms. These are living creatures which are microscopic in size and are invisible to unaided eyes. There are different types of micro organisms. They are called bacteria, fungi, virus etc. Bacteria again can be classified into two types' beneficial bacteria and harmful bacteria. Bacteria can be divided into two major groups based on their oxygen requirement. Those which grow in presence of oxygen are called aerobic while the others grow in absence of gaseous oxygen are called anaerobic. When organic matter undergoes fermentation (process of chemical change in organic matter brought about by living organisms) through anaerobic digestion, gas is generated. This gas is known as bio-gas. Biogas is generated through fermentation or bio-digestion of various wastes by a variety of anaerobic and facultative-organisms. Facultative bacteria are capable of growing both in presence and absence of air or oxygen.

III. STEPS IN BIOGAS PRODUCTION

Biogas microbes consist of a large group of complex and differently acting microbe species, notable the methane-producing bacteria. The whole biogas-process can be divided into three steps: hydrolysis, acidification, and methane formation. Three types of bacteria are involved



3.1 Hydrolysis

In the first step (hydrolysis), the organic matter is enzymolyzed externally by extracellular enzymes (cellulose, amylase, protease and lipase) of microorganisms. Bacteria decompose the long chains of the complex carbohydrates, proteins and lipids into shorter parts. For example, polysaccharides are converted into monosaccharide. Proteins are split into peptides and amino acids.

3.2 Acidification

Acid-producing bacteria, involved in the second step, convert the intermediates of fermenting bacteria into acetic acid (CH_3COOH), hydrogen (H_2) and carbon dioxide (CO_2). These bacteria are facultatively anaerobic and can grow under acid conditions. To produce acetic acid, they need oxygen and carbon. For this, they use the oxygen solved in the solution or bounded-oxygen. Hereby, the acid-producing bacteria create an anaerobic condition which is essential for the methane producing microorganisms. Moreover, they reduce the compounds with a low molecular weight into alcohols, organic acids, amino acids, carbon dioxide, hydrogen sulphide and traces of methane. From a chemical standpoint, this process is partially endergonic (i.e. only possible with energy input), since bacteria alone are not capable of sustaining that type of reaction. Acid-producing bacteria, involved in the second step, convert the intermediates of fermenting bacteria into acetic acid (CH_3COOH), hydrogen (H_2) and carbon dioxide (CO_2). These bacteria are facultative anaerobic and can grow under acid conditions. To produce acetic acid, they need oxygen and carbon. For this, they use the oxygen solved in the solution or bound oxygen. Hereby, the acid producing bacteria create an anaerobic condition which is essential for the methane producing microorganisms. Moreover, they reduce the compounds with a low molecular weight into alcohols, organic acids, amino acids, carbon dioxide, hydrogen sulphide and traces of methane.

3.3 Methane formation

Methane-producing bacteria, involved in the third step, decompose compounds with a low molecular weight. For example, they utilize hydrogen, carbon dioxide and acetic acid to form methane and carbon dioxide. Under natural conditions, methane producing microorganisms occur to the extent that anaerobic conditions are provided, e.g. under water (for example in marine sediments), in ruminant stomach and in marshes. They are obligatory anaerobic and very sensitive to environmental changes. In contrast to the acidogenic and acetogenic bacteria, the methanogenic bacteria belong to the archaeobacter genus, i.e. to a group of bacteria with a very heterogeneous morphology and a number of common biochemical and molecular-biological properties that distinguish them from all other bacterial general. The main difference lies in the makeup of the bacteria's cell walls.

3.3.1 Symbiosis of bacteria

Methane and acid-producing bacteria act in a symbiotically manner. On the one hand, acid producing bacteria create an atmosphere with ideal parameters for methane-producing bacteria (anaerobic conditions, compounds with a low molecular weight). On the other hand, methane-producing microorganisms use the intermediates of the acid producing bacteria.[2] Without consuming them, toxic conditions for the acid-producing microorganisms would develop. In practical fermentation processes the metabolic actions of various bacteria all act in concert. No single bacteria are able to produce fermentation products alone.

IV. PARAMETERS AND PROCESS OPTIMIZATION

The metabolic activity involved in microbiological methanation is dependent on the following factors:

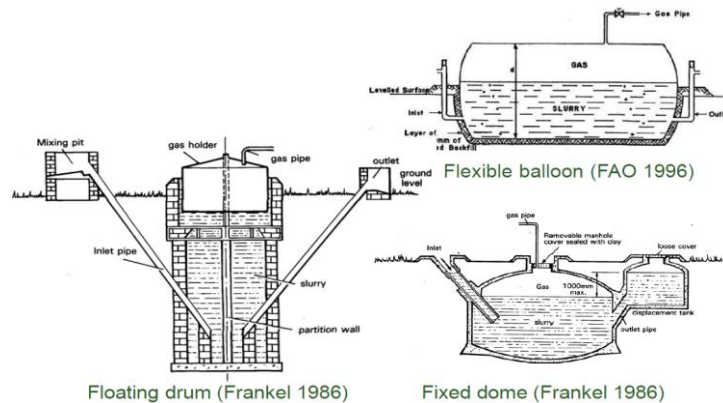
- (i). Substrate temperature
- (ii). Available nutrients
- (iii). Retention time (flow-through time)
- (iv). pH level
- (v). Nitrogen inhibition and C/N ratio
- (vi). Substrat solid content and agitation

Each of the various types of bacteria responsible for the three stages of the methanogenesis affected differently by the above parameters. Since interactive effects between the various determining factors exist, no precise quantitative data on gas production as a function of the above factors are available. Thus, discussion of the various factors is limited to their qualitative effects on the process of fermentation.

V. CASE STUDY: FLOATING-DRUM & FIXED-DOME TYPE PLANT

5.1 Floating-drum plants

Floating-drum plants consist of an underground digester and a moving gas-holder. The gas-holder floats either directly on the fermentation slurry or in a water jacket of its own. The gas is collected in the gas drum, which rises or moves down, according to the amount of gas stored. The gas drum is prevented from tilting by a guiding frame. If the drum floats in a water jacket, it cannot get stuck, even in substrate with high solid content.



5.2 The Drum

In the past, floating-drum plants were mainly built in India. A floating-drum plant consists of a cylindrical or dome-shaped digester and a moving, floating gas-holder, or drum. The gas-holder floats either directly in the fermenting slurry or in a separate water jacket. The drum in which the biogas collects has an internal and/or external guide frame that provides stability and keeps the drum upright. If biogas is produced, the drum moves up, if gas is consumed, the gas-holder sinks back.

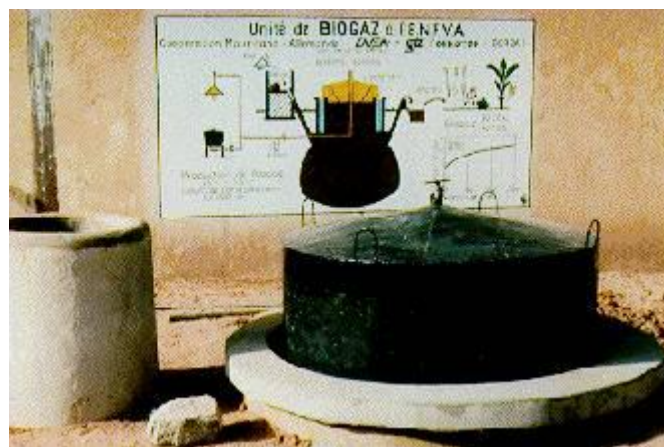


Figure 2: Basic Structure of the Drum

Floating-drum plants are used chiefly for digesting animal and human feces on a continuous-feed mode of operation, i.e. with daily input. They are used most frequently by small- to middle-sized farms (digester size: 5-15m³) or in institutions and larger agro-industrial estates (digester size: 20-100m³).

5.3 Fixed-dome Plants

A fixed-dome plant consists of a digester with a fixed, non-movable gas holder, which sits on top of the digester. When gas production starts, the slurry is displaced into the compensation tank. Gas pressure increases with the volume of gas stored and the height difference between the slurry level in the digester and the slurry level in the compensation tank. The costs of a fixed-dome biogas plant are relatively low. It is simple as no moving parts exist. There are also no rusting steel parts and hence a long life of the plant (20 years or more) can be expected. The plant is constructed underground, protecting it from physical damage and saving space. While the underground digester is protected from low temperatures at night and during cold seasons, sunshine and warm seasons take longer to heat up the digester. No day/night fluctuations of temperature in the digester

positively influence the bacteriological processes. The construction of fixed dome plants is labor-intensive, thus creating local employment. Fixed-dome plants are not easy to build. They should only be built where construction can be supervised by experienced biogas technicians. Otherwise plants may not be gas-tight (porosity and cracks). The basic elements of a fixed dome plant (here the Nicarao Design) are shown in the figure below.

VI. CONCLUSION

Biogas as a alternate source of energy because it is a very cheap gas .it is a renewable source of energy. Waste includes all items that people no longer have any use for, which they either intend to get rid of or have already discarded. Additionally, wastes are such items which people are require to discard, for example by lay because of their hazardous properties. Many items can be considered as waste e.g., household rubbish, sewage sludge, wastes from manufacturing activities, packaging items, discarded cars, old televisions, garden waste, old paint containers etc. Thus all our daily activities can give rise to a large variety of different wastes arising from different sources. Biowaste refers to livestock manures, the biodegradable part of municipal wastes including food and garden wastes, treated sewage sludge, organic industrial wastes such as paper and textiles and compost. They are a major contributor to greenhouse gas emissions and pollution of waters courses if not managed properly. Biowaste can be degraded anaerobically in a biogas digester to produce biogas and other gases. One excellent source of energy is Biogas. This is produced when bacteria decompose organic material such as garbage and sewage, especially in the absence of oxygen. Biogas is a mixture of about 60 percent methane and 40 percent Carbon dioxide. Methane is the main component of natural gas. It is relatively clean burning, colorless, and odorless. This gas can be captured and burned for cooking and heating. This is already being done on a large scale in some countries of the world. Farms that produce a lot of manure, such as hog and dairy farms, can use biogas generators to produce methane.

REFERENCES

- [1] Eze J. I. ^{1,2*} and Ojike O. ^{1,2} , Anaerobic production of biogas from maize wastes International Journal of the Physical Sciences Vol. 7(6), pp. 982 - 987, 2 February, 2012.
- [2] Kumar et al. Ministry of Non- Conventional Energy Sources)(Source; 2009-10 MNRE Annual Report , Kumar et al, IJES, 2010)
- [3] Ev Mamdouh A. El-Messery*, Gaber AZ. Ismail*,Anwaar K. Arafa**,J evaluation of Municipal Solid Waste Management in Egyptian Rural Areas,Egypt Public Health Assoc Vol. 84 No. 1 & 2, 2009.
- [4] Usman M. A., Olanipekun O. O., Kareem O. M,Biogas Generation from Domestic Solid Wastes in Mesophilic Anaerobic Digestion,International Journal of Research in Chemistry and Environment ,Vol. 2 Issue 1 January 2012(200-205) ,ISSN 2248-9649
- [5] Eze J. I. ^{1,2} and Ojike O. ^{1,2,1}, “Anaerobic production of biogas from maize wastes”, National Center for Energy Research and Development, University of Nigeria, Nsukka, Enugu State, Nigeria.Department of Food Science and Technology, University of Nigeria, Nsukka, Enugu State, Nigeria.Accepted 20 January, 2012
- [6] Richard Arthura, Martina Francisca Baidooa , Edward Antwi, ”Biogas as a potential renewable energy source: A Ghanaian case study”, Accepted 8 November 2010
- [7] Cooper, E.L. 1997. Agriscience: Fundamentals & Applications. Delmar Publishers, Albany,New York),-scienceResources
- [8] Teodorita Al Seadi, DominikRutz, Heinz Prassl, Michael Köttner, Tobias Finsterwalder,Silke Volk, Rainer Janssen, ISBN 978-87-992962-0-0,Published by University of Southern Denmark Esbjerg, NielsBohrsVej 9-10,(project Information and Advisory Service on Appropriate Technology (ISAT)
- [9] Amaratunga, M.: Structural Behaviour and Stress Conditions of Fixed Dome Type of Biogas Units. Elhalwagi, M.M. (Ed.): Biogas Technology, Transfer and Diffusion, London & New York, pp. 295-301. 1986. 0001182; ISBN: 1-85166-000-3
- [10] Van Buren, A.; Crook, M.: A Chinese Biogas Manual - Popularising Technology in the Countryside. Intermediate Technology Publications Ltd. London (UK), 1979, sixth impression 1985, 135 P. ISBN: 0903031655
- [11] Fulford, D.: Fixed Concrete Dome Design. Biogas - Challenges and Experience from Nepal. Vol I. United Mission to Nepal, 1985, pp. 3.1-3.10.

On Contra – RW Continuous Functions in Topological Spaces

M. Karpagadevi¹, A. Pushpalatha²

¹Assistant Professor, S.V.S. College of Engineering, Coimbatore, India

²Assistant Professor, Government Arts College, Udumalpet, India

ABSTRACT: In this paper we introduce and investigate some classes of functions called contra-rw continuous functions. We get several characterizations and some of their properties. Also we investigate its relationship with other types of functions.

Mathematics Subject Classification: 54C08, 54C10

Keywords: Contra rw-continuous, Almost Contra rw-continuous, Contra rw-irresolute

I. Introduction

In 1996, Dontchev[1] presented a new notion of continuous function called contra-continuity. This notion is a stronger form of LC-Continuity. In 2007, Benchalli.S.S. and Wali.R.S.[2] introduced RW-closed set in topological spaces. In 2012, Karpagadevi.M. and Pushpalatha.A.[3] introduced RW-continuous maps and RW-irresolute maps in topological spaces. The purpose this paper is to define a new class of continuous functions called Contra-rw continuous functions and almost Contra rw-Continuous function and investigate their relationships to other functions.

II. Preliminaries

Throughout this paper X and Y denote the topological spaces (X, τ) and (Y, σ) respectively and on which no separation axioms are assumed unless otherwise explicitly stated. For any subset A of a space (X, τ) , the closure of A , the interior of A and the complement of A are denoted by $cl(A)$, $int(A)$ and A^c respectively. (X, τ) will be replaced by X if there is no chance of confusion. Let us recall the following definitions as per requesters.

Definition 2.1: A Subset A of (X, τ) is called

- (i) generalized closed set (briefly g-closed) [5] if $cl(A) \subseteq U$ whenever $A \subseteq U$ and U is open in X .
- (ii) regular generalized closed set (briefly rg-closed)[6] if $cl(A) \subseteq U$ whenever $A \subseteq U$ and U is regular open in X .

The Complement of the above mentioned closed sets are their respective open sets.

Definition 2.2: A Subset A of a Space X is called rw-closed [2] if $cl(A) \subseteq U$ whenever $A \subseteq U$ and U is regular semiopen in X .

Definiton 2.3: A Map $f: (X, \tau) \rightarrow (Y, \sigma)$ is said to be

- (i) rw-continuous[3] if $f^{-1}(V)$ is rw-closed in (X, τ) for every closed set V in (Y, σ)
- (ii) rw-irresolute[3] if $f^{-1}(V)$ is rw-closed in (X, τ) for every rw-closed set V of (Y, σ)
- (iii) rw-closed[2] if $f(F)$ is rw-closed in (Y, σ) for every rw-closed set F of (X, τ)
- (iv) rw-open[2] if $f(F)$ is rw-open in (Y, σ) for every rw-open set F of (X, τ)

Definiton 2.4: A Map $f: (X, \tau) \rightarrow (Y, \sigma)$ is said to be contra-continuous [1] if $f^{-1}(V)$ is closed in (X, τ) for every open set V in (Y, σ) .

III. Contra RW-Continuous Function

In this section we introduce the notions of contra rw-continuous, contra rw-irresolute and almost contra rw-continuous functions in topological spaces and study some of their properties.

Definition 3.1: A function $f: (X, \tau) \rightarrow (Y, \sigma)$ is called contra rw-continuous if $f^{-1}(V)$ is rw-closed set in X for each open set V in Y .

Example 3.2: Let $X=Y=\{a,b,c\}$ with topologies $\tau = \{X, \phi, \{a\}, \{b\}, \{a,b\}\}$ and $\sigma = \{Y, \phi, \{a,b\}\}$. Let $f: X \rightarrow Y$ be a map defined by $f(a) = a, f(b) = b$ and $f(c) = c$. Clearly f is contra rw-continuous.

Theorem 3.3: Every contra-continuous function is contra rw-continuous.

Proof: The proof follows from the fact that every closed set is rw-closed set.

Remark 3.4: The converse of the above theorem need not be true as seen from the following example.

Example 3.5: Let $X=Y=\{a,b,c\}$ with topologies $\tau = \{X, \phi, \{a\}, \{b\}, \{a,b\}\}$ and $\sigma = \{Y, \phi, \{a,b\}\}$. Let $f: X \rightarrow Y$ be a map defined by $f(a) = a, f(b) = b$ and $f(c) = c$. Clearly f is contra rw-continuous but not contra-continuous since $f^{-1}(\{a,b\}) = \{a,b\}$ which is not closed in X .

Theorem 3.6: If a function $f: X \rightarrow Y$ is contra rw-continuous, then f is contra-continuous.

Proof: Let V be an open set in Y . Since f is contra rw-continuous, $f^{-1}(V)$ is closed in X . Hence f is contra-continuous.

Remark 3.7: The concept of rw-continuity and contra rw-continuity is independent as shown in the following examples.

Example 3.8 : Let $X=Y=\{a,b,c\}$ with topologies $\tau = \{X, \phi, \{a\}, \{b\}, \{a,b\}\}$ and $\sigma = \{Y, \phi, \{b,c\}\}$. Let $f: X \rightarrow Y$ be a map defined by $f(a) = a, f(b) = b$ and $f(c) = c$. Clearly f is contra rw-continuous but not rw-continuous since $f^{-1}(\{a\}) = \{a\}$ is not rw-closed in X where $\{a\}$ is closed in Y .

Example 3.9 : Let $X=Y=\{a,b,c\}$ with topologies $\tau = \{X, \phi, \{a\}, \{b\}, \{a,b\}\}$ and $\sigma = \{Y, \phi, \{b\}\}$. Define $f: X \rightarrow Y$ identity mapping. Then clearly f is rw-continuous but not contra rw-continuous since $f^{-1}(\{b\}) = \{b\}$ is not rw-closed in X where $\{b\}$ is closed in Y .

Theorem 3.10: Every contra rw-continuous function is contra rg-continuous.

Proof: Since every rw-closed set is rg-closed, the proof is obvious.

Remark 3.11: The converse of the above theorem need not be true as seen from the following example.

Example 3.12: Let $X=Y=\{a,b,c,d\}$ with topologies $\tau = \{X, \phi, \{a\}, \{b\}, \{a,b\}, \{a,b,c\}\}$ and $\sigma = \{Y, \phi, \{a\}, \{b\}, \{a,b,c\}\}$. Let $f: X \rightarrow Y$ be a map defined by $f(a) = c, f(b) = d, f(c) = a$ and $f(d) = b$. Clearly f is contra rg-continuous but not contra rw-continuous since $f^{-1}(\{a\}) = \{c\}$ is not rw-closed in X where $\{a\}$ is open in Y .

Remark 3.13: The composition of two contra rw-continuous functions need not be contra rw-continuous as seen from the following example.

Example 3.14: Let $X=Y=Z=\{a,b,c\}$ with topologies $\tau = \{X, \phi, \{a\}, \{b\}, \{a,b\}\}$ and $\sigma = \{Y, \phi, \{a,b\}\}$ and $\eta = \{Z, \phi, \{a\}\}$. Let $f: X \rightarrow Y$ be a map defined by $f(a) = c, f(b) = b$ and $f(c) = a$ and $g: Y \rightarrow Z$ is defined by $g(a) = b, g(b) = c$ and $g(c) = a$. Then clearly f and g are contra rw-continuous. But $g \circ f: X \rightarrow Z$ is not contra rw-continuous since $(g \circ f)^{-1}\{a\} = f^{-1}(g^{-1}\{a\}) = f^{-1}(\{c\}) = \{a\}$ is not rw-closed in X .

Theorem 3.15: If $f: (X, \tau) \rightarrow (Y, \sigma)$ is contra rw-continuous and $g: Y \rightarrow Z$ is a continuous function, then $g \circ f: X \rightarrow Z$ is contra rw-continuous.

Proof: Let V be open in Z . Since g is continuous, $g^{-1}(V)$ is open in Y . Then $f^{-1}(g^{-1}(V))$ is rw-closed in X since f is contra rw-continuous. Thus $(g \circ f)^{-1}(V)$ is rw-closed in X . Hence $g \circ f$ is contra rw-continuous.

Theorem 3.16: If $f: X \rightarrow Y$ is rw-irresolute and $g: Y \rightarrow Z$ is contra continuous function then $g \circ f: X \rightarrow Z$ is contra rw-continuous.

Proof: Since every contra continuous is contra rw-continuous, the proof is obvious.

Theorem 3.17: If $f: X \rightarrow Y$ is contra rw-continuous then for every $x \in X$, each $F \in C(Y, f(x))$, there exists $U \in RWO(X, x)$ such that $f(U) \subset F$ (ie) For each $x \in X$, each closed subset F of Y with $f(x) \in F$, there exists a rw-open set U of Y such that $x \in U$ and $f(U) \in F$.

Proof: Let $f: X \rightarrow Y$ be contra rw-continuous. Let F be any closed set of Y and $f(x) \in F$ where $x \in X$. Then $f^{-1}(F)$ is rw-open in X . Also $x \in f^{-1}(F)$. Take $U = f^{-1}(F)$. Then U is a rw-open set containing x and $f(U) \subseteq F$.

Theorem 3.18: Let (X, τ) be a rw-connected space (Y, σ) be any topological space. If $X \rightarrow Y$ is surjective and contra rw-continuous then Y is not a discrete space.

Proof: Suppose Y is discrete space. Let A be any proper non-empty subset of Y . Then A is both open and closed in Y . Since f is contra rw-continuous, $f^{-1}(A)$ is both rw-open and rw-closed in X . Since X is rw-connected, the only subset of Y which are both rw-open and rw-closed are X and \emptyset . Hence $f^{-1}(A) = X$. Then it contradicts to the fact that $f: X \rightarrow Y$ surjective. Hence Y is not a discrete space.

Definition 3.19: A function $f: X \rightarrow Y$ is called almost contra rw-continuous if $f^{-1}(V)$ is rw-closed set in X for every regular open set V in Y .

Example 3.20: Let $X=Y=Z=\{a,b,c\}$ with topologies $\tau = \{X, \emptyset, \{a\}, \{b\}, \{a,b\}\}$ and $\sigma = \{Y, \emptyset, \{a\}, \{c\}, \{a,c\}\}$. Define $f: X \rightarrow Y$ by $f(a) = a$, $f(b) = b$ and $f(c) = c$. Here f is almost contra rw-continuous since $f^{-1}(\{a\}) = \{a\}$ is rw-closed in X for every regular open set $\{a\}$ in Y .

Theorem 3.21: Every contra rw-continuous function is almost contra rw-continuous.

Proof: The proof follows from the definition and fact that every regular open set is open.

Definition 3.22: A function $f: X \rightarrow Y$ is called contra rw-irresolute if $f^{-1}(V)$ is rw-closed in X for each rw-open set V in Y .

Definition 3.23: A function $f: X \rightarrow Y$ is called perfectly contra rw-irresolute if $f^{-1}(V)$ is rw-closed and rw-open in X for each rw-open set V in Y .

Theorem 3.24: A function $f: X \rightarrow Y$ is perfectly contra rw-irresolute if and only if f is contra rw-irresolute and rw-irresolute.

Proof: The proof directly follows from the definitions.

Remark 3.25: The following examples shows that the concepts of rw-irresolute and contra rw-irresolute are independent of each other.

Example 3.26: Let $X=Y=Z=\{a,b,c\}$ with topologies $\tau = \{X, \emptyset, \{a\}, \{b\}, \{a,b\}\}$ and $\sigma = \{Y, \emptyset, \{a\}, \{c\}, \{a,c\}\}$. Define $f: X \rightarrow Y$ by $f(a) = a$, $f(b) = b$ and $f(c) = c$. Here f is contra rw-irresolute but not rw-irresolute since $f^{-1}(\{a,b\}) = \{a,b\}$ is not rw-open in X .

Example 3.27: Let $X=Y=Z=\{a,b,c\}$ with topologies $\tau = \{X, \emptyset, \{a\}, \{b\}, \{a,b\}\}$ and $\sigma = \{Y, \emptyset, \{a\}, \{c\}, \{a,c\}\}$. Define $f: X \rightarrow Y$ by $f(a) = a$, $f(b) = b$ and $f(c) = c$. Here f is rw-irresolute but not contra rw-irresolute since $f^{-1}(\{b\}) = \{b\}$ is not rw-closed in X .

Theorem 3.28: Let $f: X \rightarrow Y$ and $g: Y \rightarrow Z$ be a function then

(i) If g is rw-irresolute and f is contra rw-irresolute then $g \circ f$ is contra rw-irresolute

(ii) If g is contra rw-irresolute and f is rw-irresolute then $g \circ f$ is contra rw-irresolute

Proof: (i) Let U be a rw-open in Z . Since g is rw-irresolute, $g^{-1}(U)$ is rw-open in Y . Thus $f^{-1}(g^{-1}(U))$ is rw-closed in X . Since f is contra rw-irresolute (ie) $(g \circ f)^{-1}(U)$ is rw-closed in X . This implies that $g \circ f$ is contra rw-irresolute.

(ii) Let U be a rw-open in Z . Since g is contra rw-irresolute, $g^{-1}(U)$ is rw-closed in Y . Thus $f^{-1}(g^{-1}(U))$ is rw-closed in X since f is rw-irresolute (ie) $(g \circ f)^{-1}(U)$ is rw-closed in X . This implies that $g \circ f$ is contra rw-irresolute.

Theorem 3.29: Every perfectly contra rw-irresolute function is contra rw-irresolute and rw-irresolute.

Proof: The proof directly follows from the definitions.

Remark 3.30: The following two examples shows that a contra rw-irresolute function may not be perfectly contra rw-irresolute and rw-irresolute function may not be perfectly contra rw-irresolute.

Example 3.31: In example 3.29, f is rw-irresolute but not perfectly contra rw-irresolute and in example 3.28, f is contra rw-irresolute but not perfectly contra rw-irresolute.

Theorem 3.32: A function is perfectly contra rw-irresolute iff f is contra rw-irresolute and rw-irresolute.

Proof: The proof directly follows from the definitions.

REFERENCES

- [1]. Dontchev.J.”Contra-continuous functions and strongly s closed spaces”, International J.Math&Math.Sci.19 (1996).303-310.
- [2]. Benchalli.S.S. and Wali.R.S, “On RW-closed sets in topological spaces”, Bull. Malays. Math. Sci. Soc (2) 30(2) (2007), 99-110.
- [3]. Karpagadevi.M. and Pushpaltha. A., “RW-Continuous maps and RW-irresolute maps in topological spaces”, International Journal of Mathematics Trends and Technology, Vol.4, Issue 2-2013, 21-25.
- [4]. Karpagadevi.M. and Pushpaltha. A., “RW-Closed maps and RW- Open maps in topological spaces”, International Journal of Computer Applications Technology and Research, Vol.2, Issue 2-2013, 91-93.
- [5]. Levine.N. ”Generalized closed sets in topology”, Rend.Circ.Mat.Palermo 19.1970,89-96.
- [6]. Palaniappan.N and Rao.K.C. “Regular generalized closed sets”, Kyungpook Math J 33, 1993, 211-219.
- [7]. Syed Ali Fathima.S. and Mariasingam.M. “On contra #rg-Continuous functions”, International Journal of Modern Engineering Research, Vol.3.Issue.2, March-April.2013 pp.939-943

Heart Disease Prediction Using Associative Relational Classification Technique (Acar) With Som Neural Network

Amit Sahu¹, Mayank saxena²

Department of Computer Science & Engineering PCST, Bhopal, India

ABSTRACT: Mining of medical diagnoses of data is very difficult task in current data mining approach. The heart disease data is collective information of blood pressure, Cholesterol problem, diabetes and another complex disease. The relational of one disease to another is rare so classification task is very difficult. So prediction of heart disease is very critical. in the process of data mining rule based classification technique used for prediction. The rule based classification technique based on association rule mining. The better rule mining technique the better classification and predication of heart disease. in this paper proposed a association based ensemble classification method for heart disease prediction. the association ensemble classifier based on association rule mining and self –organized map network model. For the association rule used Apriori-like algorithm. This algorithm generates numbers of rules for all combination of factor of heart disease and divided into different level such as high level , middle level and low level, the all level ensemble through SOM network and generate optimized set of heart disease prediction.

Keywords: Heart Disease, Associative Classification, Ensemble and SOM Network

I. INTRODUCTION

The diversity of lifestyle invites much disease in our body. In all disease heart disease which is also called cardiovascular disease is considered as one of the leading cause of death in the world with high prevalence in the Asia subcontinent [1, 2]. There are several risk factors which account for the heart disease such as age, sex, smoking etc. Patients with Hereditary risk factors (such as: high blood pressure, diabetes) have more chances of heart disease. Some risk factors are controllable. While having so many risk factors, it is a complicated task to analyze heart disease on the basis of patient's report [4]. Particularly, doctors take decision on their intuition and experience rather than on the knowledge-rich data hidden in the database. In healthcare transactions, data is too complex and huge to be processed and analyzed by traditional methods. It requires high skills and experiences for correct decisions. Classification based on association rules, also called associative classification, is a technique that uses association rules to build classifier. Generally it contains two steps: first it finds all the class association rules (CARs) whose right-hand side is a class label, and then selects strong rules from the CARs to build a classifier [5]. In this way, associative classification can generate rules with higher confidence and better understandability comparing with traditional approaches. Thus associative classification has been studied widely in both academic world and industrial world, and several effective algorithms [6] have been proposed successively. However, all the above algorithms only focus on processing data organized in a single relational table. In practical application, data is often stored dispersedly in multiple tables in a relational database. Simply converting multi-relational data into a single flat table may lead to the high time and space cost, moreover, some essential semantic information carried by the multi-relational data may be lost. Thus the existing associative classification algorithms cannot be applied in a relational database directly [7]. We propose a novel algorithm, ACAR, for associative classification which can be applied in multi-relational data environment. The main idea of ACAR is to mine relevant features of each class label in each table respectively, and generate strong classification rules[8]. The ensemble of different rules in different level used SOM based ensemble classifier. The SOM based ensemble classifier classified the data very accurately. The self-organizing map (SOM) is one of the most popular algorithms in the classification of data with a good performance regarding rate of classification[9]. The SOM is a widely used unsupervised neural network for clustering high dimensional input data and mapping these data into a two-dimensional representation space. Self-organizing map is one of the most fascinating topics in the neural network field. The SOM introduced by Kohonen (1982), is a neural network that maps signals from a high-dimensional space to a one- or two-dimensional discrete lattice of neuron units. Each neuron stores a weight. The SOM organizes unknown data into groups of similar patterns, according to a similarity criterion. Such networks can learn to detect regularities and correlations in

their input and adapt their future responses to that input accordingly. An important feature of this neural network is its ability to process noisy data[13]. The map preserves topological relationships between inputs in a way that neighboring inputs in the input space are mapped to neighboring neurons in the map space. The rest of paper is organized as follows. In Section II discuss related work of associative classification. The Section III proposed method for classification. The section IV discusses experimental result and finally followed section V conclusion and future scope

II. RELATED WORK

In this section discuss the related work in the field of medical data classification using associative classification using neural network and other optimization technique. The neural network is important area of research in the field of data mining classification. The neural network optimized the level of classification and improved the ratio of classification.

[1] In this paper author proposed an ensemble method and classification for heart diseases and to improve the decision of the classifiers for heart disease diagnosis. Homogeneous ensemble is applied for heart disease classification and finally results are optimized by using Genetic algorithm. Data is evaluated by using IO-fold cross validation and performance of the system is evaluated by classifiers accuracy, sensitivity and specificity to check the feasibility of our system. Comparison of our methodology with existing ensemble technique has shown considerable improvements in terms of classification accuracy. The focused on the optimized heart disease classification problem. Genetic Algorithm has been found a very good technique for optimization and searching for quality solution. The proposed framework of SVM classifier ensemble and optimization of results using Genetic Algorithm technique improved the classification accuracy as compared to existing work.

[2] In this paper author proposed a genetic algorithm based feature selection for the heart diseases and the details are, we presented a genetic algorithm (GA) based feature-selection method to find informative features that play a significant role in discrimination of samples. Selected subsets from multiple GA runs were used to build a classifier. The proposed approach can be combined with various classifiers to improve classification performance and selection of the most discriminative features. Starting with a set of pre-selected features by using a filter (1000 features), we used a GA combined with Fisher's linear discriminate analysis (LDA) to explore the space of feature subsets. In fact, our proposed approach employs GA and uses the LDA classifier to evaluate the fitness of a given candidate feature subset. An external test set was chosen by using Kohonen self-organizing maps (SOMs) to evaluate the performance of feature selection at the final stage. The proposed method can be used to diagnose CHD in patients without using any angiographic techniques, which may have a high risk of death for the individuals.

[3] In this paper author discussed on data mining method for heart disease, the details are data classification is based on supervised machine learning algorithms which result in accuracy, time taken to build the algorithm. Tanagra tool is used to classify the data and the data is evaluated using 10-fold cross validation and the results are compared. The selection of algorithms is based on their performance, but not around the test dataset itself, and also comprising the predictions of the classification models on the test instance. Training data are produced by recording the predictions of each algorithm, using the full training data both for training and for testing. Performance is determined by running 10-fold cross-validations and averaging the evaluations for each training dataset. Several approaches have been proposed for the characterization of learning domain. the performance of each algorithm on the data attribute is recorded. The algorithms are ranked according to their performance of the error rate. Author also deals with the results in the field of data classification obtained with Naive Bayes algorithm, Decision list algorithm and k-nn algorithm, and on the whole performance made known Naive Bayes Algorithm when tested on heart disease datasets. Naive Bayes algorithm is the best compact time for processing dataset and shows better performance in accuracy prediction.

[4] In this paper author described a heart beat classification system using optimization techniques such as particle swarm optimization, to proposes a novel system to classify three types of electrocardiogram beats, namely normal beats and two manifestations of heart arrhythmia. This system includes three main modules: a feature extraction module, a classifier module, and an optimization module. In the feature extraction module, a proper set combining the shape features and timing features is proposed as the efficient characteristic of the patterns. In the classifier module, a multi-class support vector machine (SVM)-based classifier is proposed. For the optimization module, a particle swarm optimization algorithm is proposed to search for the best value of the SVM parameters and upstream by looking for the best subset of features that feed the classifier. Simulation results show that the proposed algorithm has very high recognition accuracy. This high efficiency is achieved with only little features, which have been selected using particle swarm optimizer.

[5] In this paper author presented a Back propagation neural network and genetic algorithm for medical diseases diagnosis classification, by using the Three-Term Back propagation (TBP) network based on the Elitist

Multiobjective Genetic Algorithm (MOGA). One of the recent MOGAs is a Non-dominated Sorting Genetic Algorithm II (NSGA-II), which is used to reduce or optimize the error rate and network structure of TBP simultaneously to achieve more accurate classification results. In addition accuracy, sensitivity, specificity and 10-fold cross validation are used as performance evaluation indicators to evaluate the outcome of the proposed method.

[6] In This paper author analyses the performance of various classification function techniques in data mining for prediction heart disease from the heart disease data set. The classification algorithms used and tested in work are Logistics, Multi-layer Perception and Sequential Minimal Optimization algorithms. The performance factor used for analyzing the efficiency of algorithm are clustering accuracy and error rate. The result show logistics classification function efficiency is better than multi-layer perception and sequential minimal optimization. Three classification algorithms techniques in data mining are intelligent for predicting heart disease. They are function based Logistic, Multilayer perception and Sequential Minimal Optimization algorithm. By analyzing the experimental results, it is observed that the logistic classification algorithms technique turned out to be best classifier for heart disease prediction because it contains more accuracy and least error rate. In future we tend to improve performance efficiency by applying other data mining techniques and optimization techniques. It is also enhanced by reducing the attributes for the heart disease dataset.

[7] In This paper author describes about a prototype using data mining techniques, namely Naïve Bayes and WAC (weighted associative classifier). It enables significant knowledge, e.g. patterns, relationships between medical factors related to heart disease, to be established. It can serve a training tool to train nurses and medical students to diagnose patients with heart disease. It is a web based user friendly system and can be used in hospitals if they have a data ware house for their hospital. Presently we are analyzing the performances of the two classification data mining techniques by using various performance measures.

[8] In this paper author discussed on a diseases Using Genetic Algorithm and Ensemble Support Vector Machine, Support vector machine (SVM) is believed to be more efficient than neural network and traditional statistical-based classifiers. an ensemble of SVM classifiers use multiple models to obtain better predictive accuracy and are more stable than models consist of a single model. Genetic algorithm (GA), on the other hand, is able to find optimal solution within an acceptable time, and is faster than dynamic programming with exhaustive searching strategy. By taking the advantage of GA in quickly selecting the salient features and adjusting SVM parameters, it was combined with ensemble SVM to design a clinical decision support system (CDSS) for the diagnosis of patients with severe OSA, and then followed by PSG to further discriminate normal, mild and moderate patients. The results show that ensemble SVM classifiers demonstrate better diagnosing performance than models consisting of a single SVM model and logistic regression analysis.

[9] In this paper The aim of author for this work is to design a GUI based Interface to enter the patient record and predict whether the patient is having Heart disease or not using Weighted Association rule based Classifier. The prediction is performed from mining the patient's historical data or data repository. In Weighted Associative Classifier (WAC), different weights are assigned to different attributes according to their predicting capability. It has already been proved that the Associative Classifiers are performing well than traditional classifiers approaches such as decision tree and rule induction.

[10] In this paper author Enhanced the Prediction of Heart Disease with Feature Subset Selection based on a Genetic Algorithm, Genetic algorithm is used to determine the attributes which contribute more towards the diagnosis of heart ailments which indirectly reduces the number of tests which are needed to be taken by a patient. Thirteen attributes are reduced to 6 attributes using genetic search. Subsequently, three classifiers like Naive Bays, Classification by clustering and Decision Tree are used to predict the diagnosis of patients with the same accuracy as obtained before the reduction of number of attributes. Also, the observations exhibit that the Decision Tree data mining technique outperforms other two data mining techniques after incorporating feature subset selection with relatively high model construction time.

III. PROPOSED METHODOLOGY

In this section discuss the proposed methodology of ensemble associative classification based on SOM network and also discuss the associative classification. the ensemble classification technique improved the classification and prediction of heart disease.

III.A Associative classification (ACAR)

Let D is the dataset. Let I be the set of all items in D and C be the set of class labels. We say that a data case $d_i \in D$ contains $X \subseteq I$, a subset of items, if $X \subseteq d_i$. A class association rule (CAR) is an implication of the form $X \rightarrow c$, where $X \subseteq I$, and $c \in C$. Bing Liu et al. [22] first proposed the AC approach, named classification based on association algorithm (CBA), for building a classifier based on the set of discovered class association rules. The difference between rule discovery in AC and conventional frequent item set mining is that the former

task may carry out multiple frequent item set mining processed for mining rules of different classes simultaneously. Data mining in associative classification (AC) framework usually consists of two steps [10] Generating all the class association rules (CARs) which has the form of $I_{set} = > c$, where I_{set} is an item set and c is a class.

Building a classifier based on the generated CARs. Generally, a subset of the association rules was selected to form a classifier and AC approaches are based on the confidence measure to select rules [12].

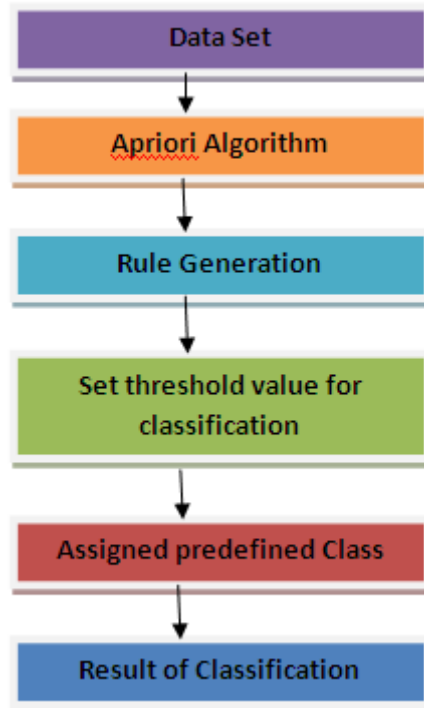


Figure .1 Association Classifications

III.B PROPOSED METHOD

Proposed models are creating for data training for minority and majority class data sample for processing of associative classification level of rules. The associative classification process a data input for training phase for SMOTE and CMTNN sampling technique for classifier. While single-layer SOM networks can potentially learn virtually any input output relationship, SOM networks with single layers might learn complex relationships more quickly[12]. The function SOM creates wiener and successor matrix. For example, a ensemble layer network has connections from layer 1 to layer 2, layer 2 to layer 3, and layer 1 to layer 3. The ensemble -layer network also has connections from the input to all cascaded layers. The additional connections might improve the speed at which the network learns the desired relationship. SOM artificial intelligence model is similar to feed-forward back-propagation neural network in using the back-propagation algorithm for weights updating, but the main symptom of this network is that each layer of neurons related to all previous layer of neurons. Tan-sigmoid transfer function, log - sigmoid transfer function and pure linear threshold functions were used to reach the optimized status.

1. Data are passes through ACR
2. ACR makes a multi-level rule set using rule mining algorithm
3. level of rules going to SOM ensemble process
4. The training phase data are passes through SMOTE AND CMTNN sampler
5. The sampling of data passes through SOM AND balanced the data for minority and majority ratio of class
6. The sampled data assigned to k-type binary class
7. Binary class data are coded in bit form
8. if code bit value is single assigned the class value
9. Else data goes to training phase
10. . Balanced part of training is updated
11. Find accuracy and relative mean Error
12. Exit

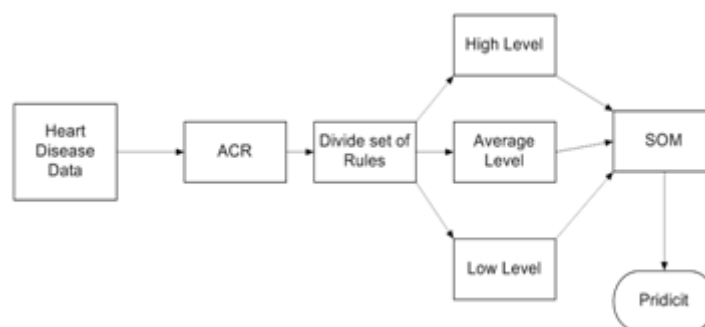


Figure 2 proposed model for ensemble based associative classification with SOM network

IV. EXPERIMENTAL RESULT ANALYSIS

It is simulating on mat lab 7.8.0 and for this work we use Intel 1.4 GHz Machine. MATLAB is a high-level technical computing language and interactive environment for algorithm development, data visualization, data analysis, and numeric computation Matlab is a software program that allows you to do data manipulation and visualization, calculations, math and programming. It can be used to do very simple as well as very sophisticated tasks. Three datasets (Cleveland, SPECT and Statlog) are obtained from UCI machine learning repository and other is indian dataset [10]. IO-folds cross validation is applied in all experiments. Training and testing sets are generated randomly form the dataset. In table I is the comparison of performance between ACAR and the proposed scheme. The figure clearly shows that classifiers perform best on Cleveland dataset. Considerable performance has also been achieved on other datasets by using ensemble based optimizing technique.

	Method	Support	Confidence	Accuracy (%)	Runtime (sec)
Cleveland	ACAR	0.3	0.5	84.57	7.4375
	AC-EN	0.3	0.5	90.1	6.879
SPECT	ACAR	0.3	0.5	89.36	8.451
	AC-EN	0.3	0.5	92.34	9.678
	ACAR	0.3	0.5	90.31	5.7812
Statlog	AC-EN	0.3	0.5	91.54	4.561
Indian dataset	ACAR	0.3	0.5	81.23	7.891
	AC-EN	0.3	0.5	86.23	5.671

Table I. Maximum accuracy of the ACAR and ensemble ACAR

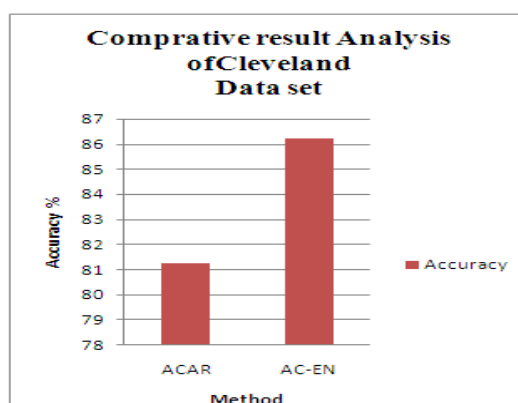


Figure 3 shows that comparative result of Cleveland data set this data set is collection of heart disease. the proposed algorithm shows that better prediction of ACAR algorithm.

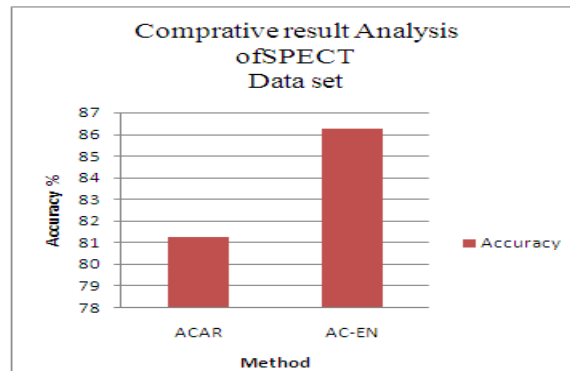


Figure 4 shows that comparative result of SPECT data set this data set is collection of heart disease. The proposed algorithm shows that better prediction of ACAR algorithm.

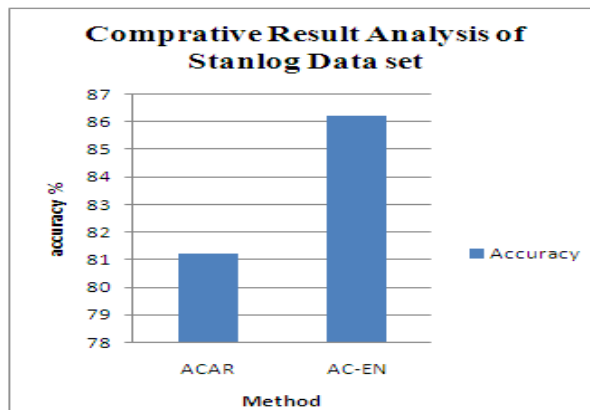


Figure 5 shows that comparative result of STANLOG data set this data set is collection of heart disease. The proposed algorithm shows that better prediction of ACAR algorithm.

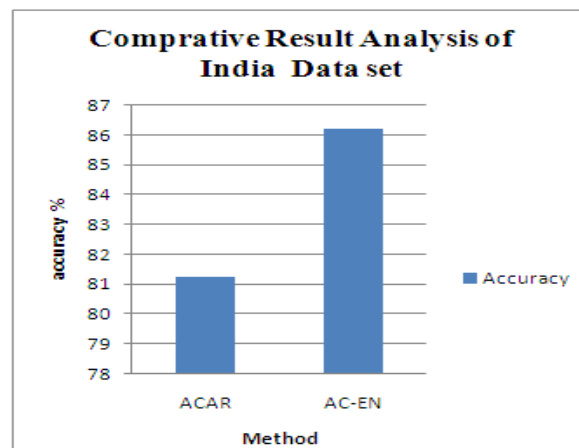


Figure 6 shows that comparative result of Indian data set this data set is collection of heart disease. The proposed algorithm shows that better prediction of ACAR algorithm.

V. CONCLUSION AND FUTURE WORK

Currently, ACAR uses a support-confidence framework to discover frequent item sets and generate classification rules. It may discover more relevant features of each class label by using related measures extending current framework. Also the current algorithm could be improved in terms of efficiency by using the optimization technique. Multiple relational classification algorithm modified by SOM so improved rate of classification in comparison of ACAR. In the process of SOM the calculation complexity are increases, the complexity of time are also increases. Our proposed algorithm test heart disease data set. In this data set the rate of classification is 92%. We also use another data set Indian heart disease and estimate some little bit difference of rate of classification is 91%. The rate of classification increases in previous method on the consideration of

time complexity. In future we minimize the complexity of time and also increase the rate of classification using Meta heuristic function such as ant colony optimization, power of swarm (pos) and dendrites cell algorithm

REFERENCES

- [1]. [1] Benish Fida, Muhammad Nazir, Nawazish Naveed, Sheeraz Akram "Heart Disease Classification Ensemble Optimization Using Genetic Algorithm" Ieee 2011. Pp 19-25.
- [2]. [2] Mahdi Vasighi, Ali Zahraei, Saeed Bagheri, Jamshid Vafaeimanesh "Diagnosis Of Coronary Heart Disease Based On Hnmr Spectra Of Human Blood Plasma Using Genetic Algorithm-Based Feature Selection" Wiley Online Library 2013. 318-322.
- [3]. [3] Asha Rajkumar, G.Sophia Reena" Diagnosis Of Heart Disease Using Data Mining Algorithm" Global Journal Of Computer Science And Technology ,Vol-10 2010. Pp 38-44.
- [4]. [4] Ali Khazae " Heart Beat Classification Using Particle Swarm Optimization" Intelligent Systems And Applications, 2013. Pp 25-33.
- [5]. [5] Ashraf Osman Ibrahim, Siti Mariyam Shamsuddin, Nor Bahiah Ahmad, Sultan Noman Qasem "Three-Term Backpropagation Network Based On Elitist Multiobjective Genetic Algorithm For Medical Diseases Diagnosis Classification" Life Science Journal 2013. Pp 1815-1823.
- [6]. [6] Pramod Kumar Yadav K.L.Jaiswal, Shamsheer Bahadur Patel, D. P.Shukla "Intelligent Heart Disease Prediction Model Using Classification Algorithms" International Journal Of Computer Science And Mobile Computing Vol-2, 2013. Pp 102-107.
- [7]. [7] N. Aditya Sundar, P. Pushpa Latha, M. Rama Chandra "Performance Analysis Of Classification Data Mining Techniques Over Heart Disease Data Base" International Journal Of Engineering Science & Advanced Technology Vol-2, 2012. Pp 470-478.
- [8]. [8] Liang-Wen Hang, Hsuan-Hung Lin, Yi-Wu Chiang Hsiang-Ling Wang, Yung-Fu Chen " Diagnosis Of Severe Obstructive Sleep Apnea With Model Designed Using Genetic Algorithm And Ensemble Support Vector Machine" Applied Mathematics & Information Sciences, 2013. Pp 227-237.
- [9]. [9] Jyoti Soni, Uzma Ansari, Dipesh Sharma, Sunita Soni "Intelligent And Effective Heart Disease Prediction System Using Weighted Associative Classifiers" International Journal On Computer Science And Engineering Vol-3, 2011. Pp 285-2397.
- [10]. [10] M. Anbarasi, E. Anupriya, N.Ch.S.N.Iyengar "Enhanced Prediction Of Heart Disease With Feature Subset Selection Using Genetic Algorithm" International Journal Of Engineering Science And Technology Vol-2. 2010, Pp 5370-5376.
- [11]. [11] J. H. Eom, S. C. Kim and B.T. Zhang, "AptaCDSS-E: A classifier ensemble-based clinical decision support system for cardiovascular disease level prediction", Expert Systems with Applications 34, 2008, Pp 2465-2479.
- [12]. [12] R. Das, I. Turkoglu, A. Sengur "Effective diagnosis of heart disease through neural networks ensembles"Expert Systems with Applications, 2009, Volume 36, Issue 4, Pp 7675-7680.
- [13]. [13] A. Ebrahimzadeh, A. Khazae"Detection of premature ventricular contractions using MLP neural networks: A comparative study Measurement" 2010. Pp 103-112.
- [14]. [14] S. Osowski, T. Markiewicz, L. T. Hoai "Recognition and classification system of arrhythmia using ensemble of neural networks Measurement" vol. 41, 2008, Pp 610-617

Design of Elliptical Patch Antenna with Single & Double U-Slot for Wireless Applications: A Comparative Approach

P.Surya Anuja¹, V.Uday Kiran², Ch.Kalavathi³, G.N.Murthy⁴, G.Santhi Kumari⁵
^{1,2,3,4,5}Dept. of Electronics, Lendi Institute of Engineering & Technology.

ABSTRACT: A novel approach in the field of wireless communication industry continues to drive the requirements for small, compatible, and affordable multiband antennas. To overcome the challenges of multi-frequency operation a new scheme of multiband is proposed. So, in this we are taking elliptical probe-fed antenna with double U-shaped slot in order to increase the bandwidth to an extent. The presented antennas are suitable for multiband wireless communication systems.

Keywords: Microstrip patch antenna, multiband, U-shaped slot, elliptical patch antenna.

I. INTRODUCTION

Now a day's wireless communication devices needed more and more frequency bands because of increasing wireless service requirements. Due to this specification the demand for multiband antenna design is increasing continuously. Multiband antennas have derived rapidly increasing attention in modern wireless communication systems in which the downward compatibility and the roaming capability among multi-standards are demanded. For example, The global system for mobile communication (GSM), The wireless local area networks (WLAN), The general packet radio services (GPRS), The universal mobile telecommunication systems (UMTS) are generally a dual band or multiband wireless standards communication devices. Microstrip patch antennas consist basically of three layers, a metallic layer with the antenna element pattern, a dielectric substrate and another metallic layer as the ground plane. These antennas are relatively easy to manufacture because of their simple planar configuration and the compact structure. They are light in weight and have the capability to be integrated with other microwave circuits. It has a radiating patch on one side of a dielectric substrate which has a ground plane on the other side. The patch is generally made of conducting material such as copper or gold and can take any possible shape.

Microstrip patch antennas are increasing in popularity for use in wireless applications due to their low-profile structure. They have a very high antenna quality factor (Q). To design the multiband antenna we have different feeding techniques in which we are using coaxial cable or probe feed technique. The coaxial feed or probe feed is a very common technique used for feeding microstrip patch antennas. The inner conductor of the coaxial connector extends through the dielectric and is soldered to the radiating patch, while the outer conductor is connected to the ground plane. The main advantage of this type of feeding scheme is that the feed can be placed at any desired location inside the patch in order to match with its input impedance. It is easy to fabricate. However, its main disadvantage is that it provides narrow bandwidth and is difficult to model since a hole has to be drilled in the substrate and the connector protrudes outside the ground plane, thus not making it completely planar for thick substrates.

Since the dimension of the patch is treated a circular loop, the actual radius of the patch is given by (Balanis, 1982)

$$a = \frac{F}{\left\{1 + \frac{2h}{\pi \epsilon_r F} \left[\ln \left(\frac{\pi F}{2h} \right) + 1.7726 \right] \right\}^{1/2}}$$

Where,

$$F = \frac{8.791 \times 10^9}{f_r \sqrt{\epsilon_r}}$$

Above does not take into consideration the fringing effect. Since fringing makes the patch electrically larger, the effective radius of patch is used and is given by (Balanis, 1982).

$$a_e = a \left\{ 1 + \frac{2h}{\pi \epsilon_r a} \left[\ln \left(\frac{\pi a}{2h} \right) + 1.7726 \right] \right\}^{1/2}$$

Hence, the resonant frequency for the dominant TM_{110} should be modified by using above equation and expressed as

$$f_{rc} = \frac{1.8412v_0}{2\pi a\sqrt{\epsilon_r}}$$

where v_0 is the free space speed of light.

II. ANTENNA DESIGN & ANALYSES

Here, antenna is designed using a HFSS (High Frequency Structural Simulator), it is one of several commercial tools used for antenna design. The multi-band elliptical patch antenna is designed to operate at particular frequency bands. The antenna consists of elliptical patch with U-shaped slot by coaxial or probe fed. U-shaped slot is used to increase the Bandwidth. The antenna is printed on the FR4 epoxy substrate with dielectric constant (ϵ_r) =4.4, thickness of 0.8mm.

The designing of antenna is done by following steps.

Design Requirements:

Input Impedance =100 Ω

Resonant Frequency of the Antenna=10GHz

Relative permittivity of the substrate = 4.4

Dielectric loss tangent =0.02

Procedure:

1) Designing the Microstrip patch

a) Draw the substrate dimensions 3cm x 3cm x 1.9mm.

b) Draw the elliptical patch and trace on the top face of the substrate. The elliptical patch has Dimensions Radius-0.525cm

Along x axis: 1.93cm

Along y axis: 1.93cm

Material used: FR-4 Epoxy

c) Draw an Air box on starting from the bottom of the substrate with the same length and width .The height of the air box can be any value. Here the dimensions are taken to be 3cm x 3cm x 1.9cm.

d) Draw an Air box below the substrate of dimensions 3cm x 3cm x 1.9cm.

e) We need to define a wave port .To do so draw a circle on the XY plane of dimensions such that it covers the trace. Make sure you select the XY Plane from the menu before drawing

2) Assigning Materials

a) Select the substrate to assign material

b) Assign a User defined material with a relative permittivity of 4.4 and dielectric loss tangent of 0.02 to the substrate.

3) Assigning Boundaries and Excitations

a) Select the bottom face of the substrate and Assign the Perfect E boundary to it.

b) Assign the Radiation boundary to the top and bottom air boxes.

4) Making "U" slit around probe

a) 1st u slit of length 0.4cm and breadth 0.6cm

b) 2nd u slit of length 0.25cm and breadth 0.25cm

Here as we are observing the comparison between the elliptical patch with single U-slot and double U-slot. So we are comparing return loss, 3D gain plot, 2D gain plot and Radiation pattern. Designs of both single and double U-slot are shown below.

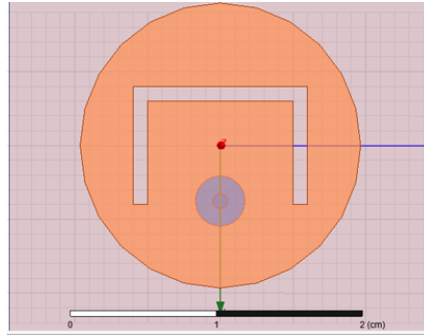


Fig. 1. Design of elliptical patch antenna with single U-slot

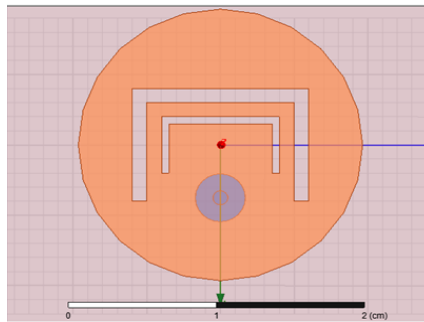


Fig. 2. Shows the design of elliptical patch antenna with double U-slot

The model of the HFSS will be in this form with the x,y and z co-ordinates, the rectangular shape is the substrate in which the antenna is designed, and the elliptical antenna is fed with coaxial cable on that double U-slot is placed and the optimization is done. This is the closer view of the design process given in following figure (2).

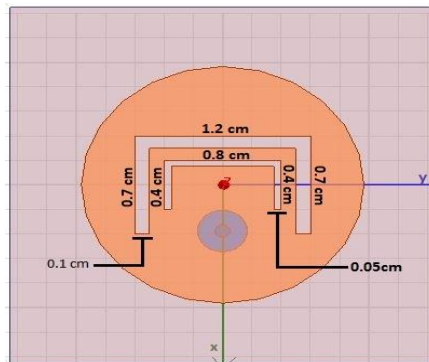


Fig. 3. Represents the closer view

III. RESULTS & DISCUSSION

In the design process after the simulation, we will get Return loss, Input impedance (S11 parameters), 3D total gain, 2D gain total. So we are showing a comparison between the single U-slot and double U-shaped slot.

Parameters	Single U-Slot	Double U-Slot
Operating Frequency	10GHz	10GHz
Return loss	6.30GHz at -11 dB	4.6 to 6.25 GHz.
Substrate material	FR4 Epoxy	FR4 Epoxy
Feed material	Teflon(tm)	Teflon(tm)

Table 1. Comparison between single U-slot and double U-slot

Below figures are the results of elliptical patch antenna with single U-slot.

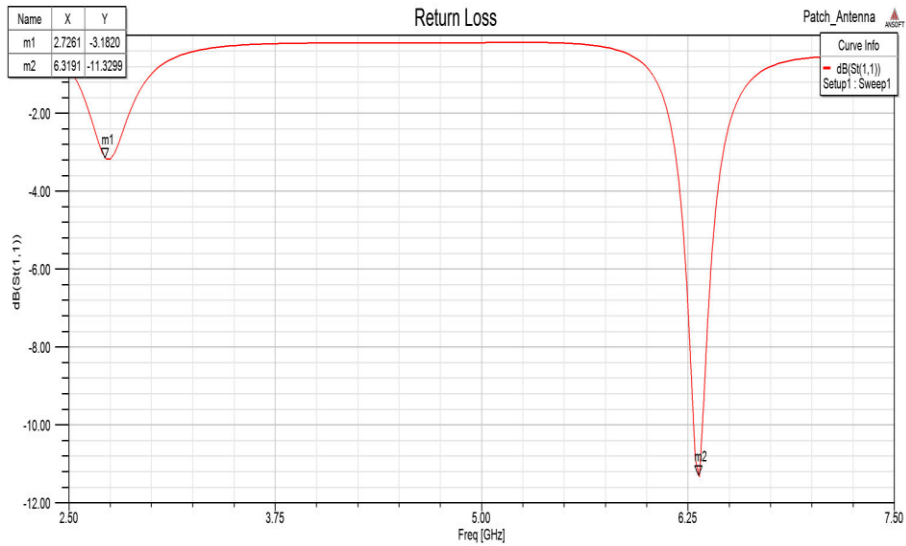


Fig.4. Represents Return loss

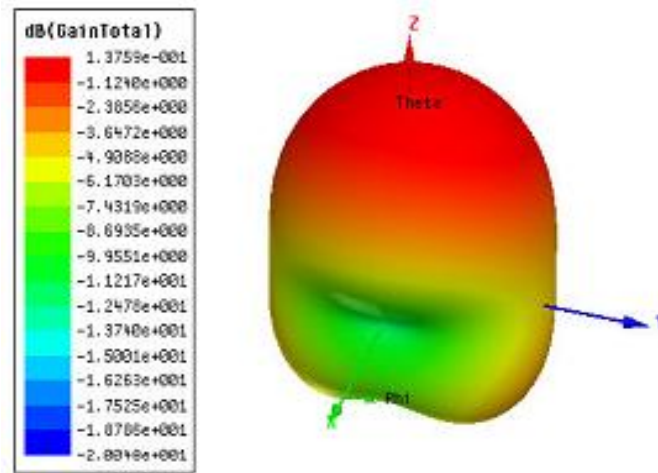


Fig. 5. Represents 3D gain total

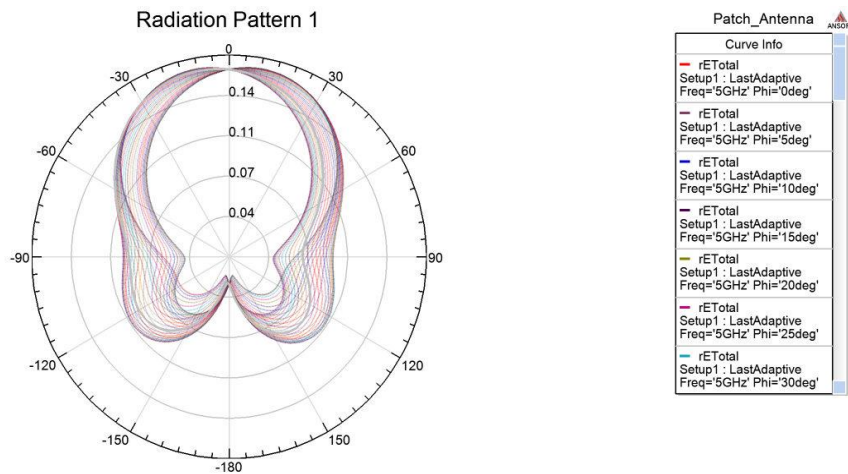


Fig. 6. Represents 2D gain total

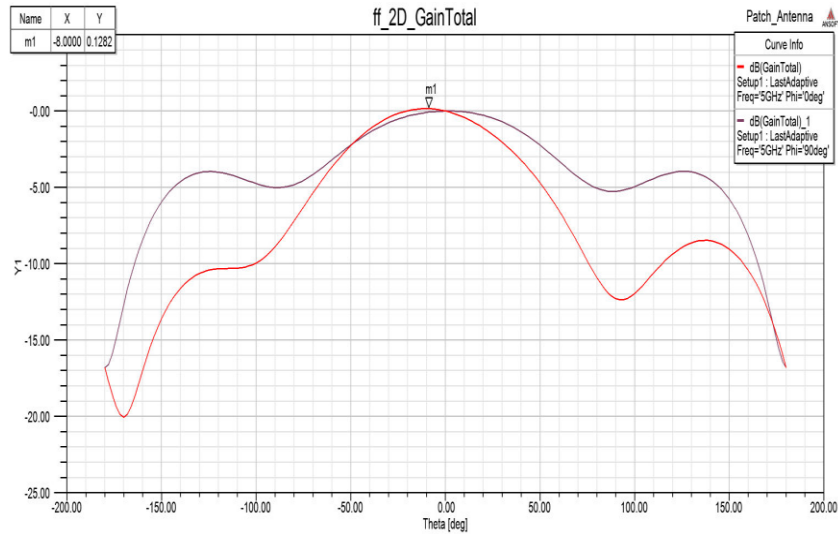


Fig. 7. Represents 2D gain total

And the results of elliptical patch antenna with double U-shaped slot are below.

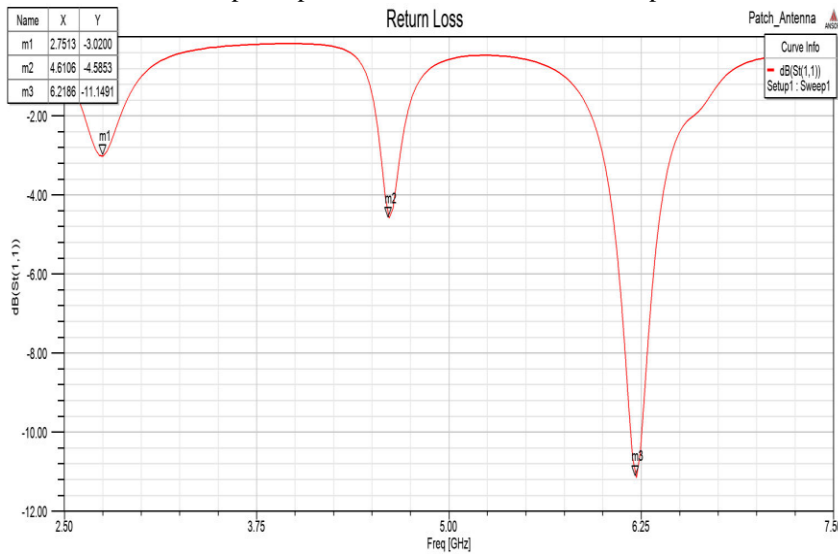


Fig. 8. Represents Return losses

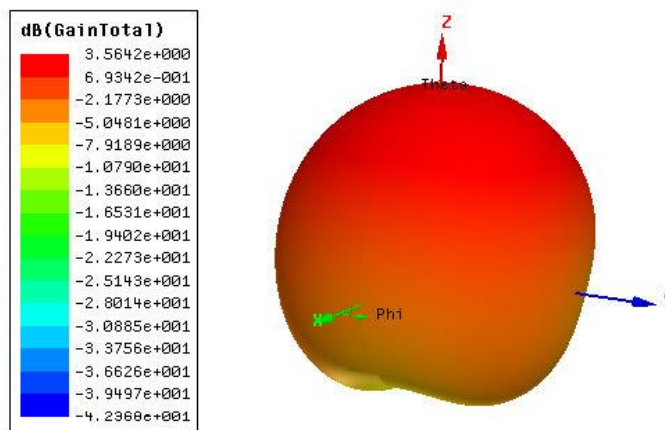


Fig. 9. Represents the 3D gain total

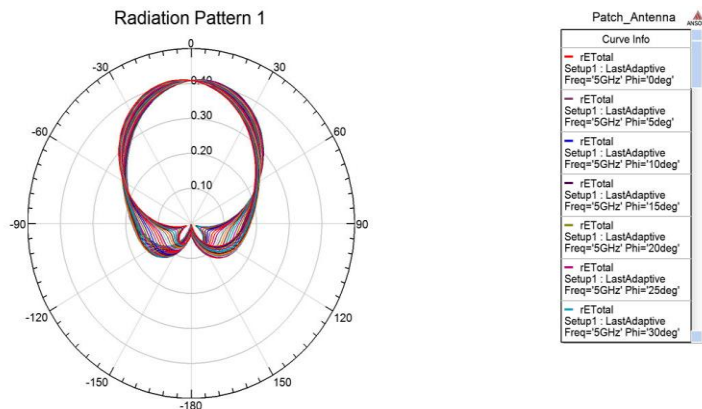


Fig. 10. Represents the Radiation pattern



Fig. 11. Represents the 2D gain total

The antenna gain is the key performance figure which combines the antenna’s directivity and electrical efficiency. A plot of the gain as a function of direction is called the radiation pattern. The term antenna gain also describes how much power is transmitted in the direction of peak radiation of that of an isotropic source. The gain of a real antenna can be as high as 40-50 dB for very large dish antennas. Directivity can be as low as 1.76 dB for a real antenna.

ACKNOWLEDGEMENTS

This is solely informing that “Design of elliptical patch antenna with single & double U-slot for wireless applications: a comparative approach” paper was completed by the support of our college.

We would like to thank Management of Lendi Institute of Engineering & Technology, Dr.V.V.Rama Reddy (Principal) Dr. M.Rajan Babu (Head of the Department), Mr.B.Sridhar, Professor, and Mr. D.Naresh Kumar, Associate Professor, (Project coordinators).

IV. CONCLUSION

In this paper, antenna is designed with a novel shape derived from the U-shaped slot with an elliptical patch antenna structure. The antenna operated with a multiband frequency making it most suitable for the wireless applications. The antenna achieves good impedance matching and gain in the entire band of operation. The antenna does serve well in radiating in all frequencies of operation with good radiation efficiency.

REFERENCES

- [1] Antenna theory analysis and design by CONSTANTINE A. BALANIS
- [2] Ratnesh kumari and Mithilesh kumar (member IEEE), Design of Multiband antennas for wireless communication, 2013 International conference on Communication Systems and Network Technologies.
- [3] J.Chen, S.T.Fan, W.Hu, and C.H.Liang, Design of Tri-band printed monopole antenna for WLAN and WIMAX applications, progress in Electromagnetics Research C, Vol. 23, 265-275, 2011.

- [4] Joseph Costantine, Karim Y.Kabalan, Ali El-Hajj, and Mohammad Rammal, New Multi-Band Microstrip Antenna Design for Wireless Communications, IEEE Antennas and Propagation Magazine, Vol. 49, No. 6, December 2007..
- [5] A.Beno and D.S.Emmanuel, High gain inverted U-shaped miniaturized patch antenna for multiband wireless applications, May 2012.
- [6] Hussain Falih Mahdi, Simulation of Rectangular Microstrip Antenna by Integrating Matlab in Visual Basic, Diyala Journal of Engineering Sciences, Vol.03, No. 01, pp. 16-24, June 2010.
- [7] ANTENNA THEORY AND WAVE PROPAGATION by K.D.Prasad.
- [8] A new dual-band microstrip antenna with U-shaped slot, J.Ghalibafan and A.R.Attari.

Security in Wireless Sensor Networks Using Broadcasting

Sneh Lata¹, Sandeep Gupta²
^{1,2}Hindu College of Engineering

ABSTRACT: *Wireless sensor networks as one of the growing technology in the coming decades has posed various unique challenges to researchers. A WSN typically consists of several base stations and thousands of sensor nodes, which are resource limited devices with low processing, energy, and storage capabilities. While the set of challenges in sensor networks are diverse, we focus on security of Wireless Sensor Network in this paper. As today's world is growing more towards the Wireless technology, our aim must be towards providing the best security features to Wireless Sensor Network (WSN). We propose some of the security requirements for Wireless Sensor Network. Further, security being vital to the acceptance and use of sensor networks for many applications. We propose an efficient broadcast authentication scheme for wireless sensor networks in this paper.*

Keywords: *Broadcast, security, sensors, Wireless sensor network(WSN).*

I. INTRODUCTION

A sensor is a device that translates parameters or events in the physical world into signals that can be measured and analyzed. Sensor networks refer to a heterogeneous system combining tiny sensors and actuators with general purpose computing elements. Wireless Sensor Networks are diverse due to the availability of micro-sensors and low-power wireless communications. Unlike the traditional sensors, in the remote sensor network, a vast numbers of sensors are densely deployed. These sensor nodes will perform significant signal processing, computation and network self-configuration to achieve scalable, robust and long-lived networks. Broadcast is an important communication primitive in wireless sensor networks. It is highly desirable to broadcast commands and data to the sensor nodes due to the large number of sensor nodes and the broadcast nature of wireless communication. Due to the limited signal range, it is usually necessary to have some receivers of a broadcast packet forward it in order to propagate the packet throughout the network (e.g., through flooding, or probabilistic broadcasting). Broadcast authentication is a basic and important security mechanism in a WSN because broadcast is a natural communication method in a wireless environment. When base stations want to send commands to thousands of sensor nodes, broadcasting is a much more efficient method than unicasting to each node individually. A wireless sensor network (WSN) can cheaply monitor an environment for diverse industries, such as healthcare, military, or home. A WSN typically consists of several base stations and thousands of sensor nodes, which are resource limited devices with low processing, energy, and storage capabilities. In WSN security, various types of attacks like Denial of service attack, sybil attack, wormhole attack, blackhole attack create problem. Distributing data through wireless communication is also bandwidth limited. A message authentication code (MAC) is an authentication tag derived by applying an authentication scheme and a secret key to a message. MAC is an efficient symmetric cryptographic primitive for two-party authentication; however, MAC is not suitable for broadcast communication without additional modification. Because the sender and its receivers share the same secret key, any one of the receivers can impersonate the sender and forge messages to other receivers. That is, both sender and receivers can sign messages. This problem stems from the symmetric property of MAC. Therefore, to achieve authenticated broadcasts, it is necessary to establish an asymmetric mechanism in which only the sender can sign messages, and the receivers can only verify messages.

II. WSN ARCHITECTURE

WSN architecture[1] is shown in following fig: –
Internet

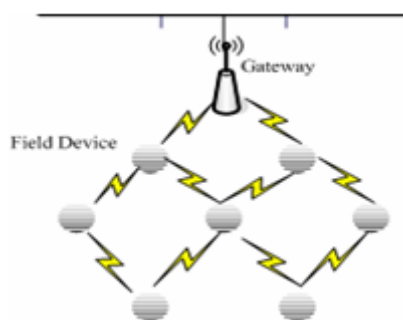


Fig 1 :- An example of WSN

Components:-

- **Sensor nodes (Field devices)** – Field devices are mounted in the process, they characterize or control the process or process equipment. A router is a special type of field device that does not have process sensor or control equipment and as such does not interface with the process itself.
- **Gateway or Access points** – A Gateway enables communication between Host application and field devices.
- **Network manager** – A Network Manager is responsible for configuration of the network, scheduling communication between devices, management of the routing tables and monitoring and reporting the health of the network.
- **Security manager** – The Security Manager is responsible for the generation, storage, and management of keys.

III. SECURITY REQUIREMENTS

Sensor networks are used in a number of domains that handle sensitive information. Due to this, there are many considerations that should be investigated and are related with protecting sensitive information traveling between nodes[2].

A. Data Confidentiality

Data confidentiality is the most important issue in network security. Confidentiality requirement is needed to ensure that sensitive information is well protected and not revealed to unauthorized third parties. A sensor network should not leak sensor readings to its neighbors.

B. Authentication

In the case of sensor networks, it is essential for each sensor node and base station to have the ability to verify that the data received was really send by a trusted sender and not by an adversary that tricked legitimate nodes into accepting false data. If such a case happens and false data are supplied into the network, then the behavior of the network could not be predicted and most of times will not outcome as expected.

C. Data Integrity

An adversary may be unable to steal information. However, this doesn't mean the data is safe. Lack of integrity could result in many problems since the consequences of using inaccurate information could be disastrous. Thus, data integrity ensures that any received data has not been altered in transit.

D. Availability

The wireless sensor network will introduce some extra costs to adjust the traditional encryption algorithms. Availability ensures that services and information can be accessed at the time that they are required. Lack of availability may affect the operation of many critical real time applications. Therefore, it is critical to ensure resilience to attacks targeting the availability of the system and find ways to fill in the gap created by the capturing or disablement of a specific node by assigning its duties to some other nodes in the network.

IV. PROTOCOLS

A Hop-by-Hop Broadcast Source Authentication Protocol[5] for WSN to mitigate DoS Attacks. Denial of Service (DoS) is produced by the unintentional failure of nodes or malicious action. The simplest DoS attack tries to exhaust the resources available to the victim node, by sending extra unnecessary packets and thus prevents legitimate network users from accessing services or resources to which they are entitled. Broadcast communication is a dominant communication pattern in WSN. As a major security concern, the broadcast source authentication is needed to mitigate impersonation of a broadcast source, modifications of its broadcasted data. Broadcast Source Authentication Protocols (BSAPs); one class of them is time asymmetry-based BSAPs like TESLA protocol. These BSAPs operate delayed key-disclosure to secure broadcast communications, but they suffer from a kind of DoS attack, called resource-draining attack, in which an attacker floods the network with fake messages that all sensors of the network buffer and forward, then later verify, thus causing buffer overflow and batteries depletion. We propose the H2BSAP protocol, to overcome this kind of DoS attacks, by

achieving a hop-by-hop authentication of broadcasted messages, thus limiting the damage of an attacker to its one-hop neighbors only, instead of the entire network. In addition, like TESLA[6], H²BSAP suffers from scalability issue, because it does not efficiently support multiple broadcast sources in the network. An asymmetric mechanism such as public key cryptography is generally required for broadcast authentication. Otherwise, a malicious receiver can easily forge any packet from the sender. uTESLA introduces asymmetry by delaying the disclosure of symmetric keys. A sender broadcasts a message with a Message Authentication Code (MAC) generated with a secret key K , which is disclosed after a certain period of time. When a receiver gets this message, if it can ensure that the packet was sent before the key was disclosed, the receiver buffers this packet and authenticates the packet when it later receives the disclosed key. To continuously authenticate broadcast packets, uTESLA divides the time period for broadcast into multiple intervals, assigning different keys to different time intervals. All packets broadcast in a particular time interval are authenticated with the same key assigned to that time interval. Multi-level uTESLA technique to extend the capabilities of uTESLA. The basic idea is to construct a multi-level uTESLA structure, where any higher-level uTESLA instance is only used to authenticate the commitments of its immediate lower-level ones and the lowest level uTESLA instances are actually used to authenticate the data packets. This extension enables the original uTESLA to cover a long time period and support a large number of receivers. Assume a sensor network application requires m uTESLA instances, which may be used by different senders during different periods of time. For convenience, assume $m = 2k$, where k is an integer. Before deployment, the central server pre-computes m uTESLA instances, each of which is assigned a unique, integer-valued ID between 1 and m . Merkle Hash Tree technique is used to authenticate and distribute mTESLA parameters. This method removes the authentication delay as well as the vulnerability to DOS attacks during the distribution of mTESLA parameters, and at the same time allows a large number of senders.

V. COMPARISON BETWEEN MERKLE TREE AND MULTI MTESLA PROTOCOL

Compared with the multi-level mTESLA schemes[7][8], the most significant gain of the proposed approach is the removal of the authentication delay in distributing the mTESLA parameters. The multi-level mTESLA schemes are subject to DOS attacks against the distribution of mTESLA parameters because of the authentication delay. Specifically, receivers cannot authenticate parameter distribution messages immediately after receiving them, and thus have to buffer such messages. An attacker may send a large amount of messages to consume receivers' buffers and thus prevent the receiver from saving the authentic messages. With the proposed approach, senders may still duplicate parameter distribution messages to deal with communication failures. However, unlike multi-level mTESLA schemes, a sender does not have to compete with malicious attackers, since it can immediately authenticate the parameter distribution message instead of keeping it in the buffer for future authentication. In other words, with the proposed approach, it is sufficient for a receiver to receive one copy of each parameter distribution message. In general, our approach allows late binding of mTESLA instances with senders. For example, the central server may reserve some mTESLA instances during deployment time and distribute them to mobile sinks as needed during the operation of the sensor networks. This allows us to add new senders dynamically by simply generating enough number of instances at the central server for later joined senders.

VI. THE EFFICIENT SCHEME

We propose using a cryptographic hash function Hash for example SHA-1[3][10] to construct H as follows

- A. split the output of the hash function into k substrings of length $\log t$ each;[4]
- B. interpret each $(\log t)$ -bit substring as integer written in binary;
- C. combine these integers to form the subset of T of size at most k .

We believe that such H satisfies our definition it certainly does if the cryptographic hash function is modeled as a random oracle.

Such construction of H results in the scheme we call HORS (for "Hash to Obtain Random subset")

This scheme involves three phases and termed as HORS (Hash to Obtain Random Subset). The phases are[12]

1. Key Generation
2. Signing
3. Verifying

Key generation

Input : p, d, l

Output: Key Pair

Private Key $K_{pri} = (k, s_1, s_2, \dots, s_p)$

Public Key $K_{pub} = (k, v_1, v_2, \dots, v_{ln d})$

1. Randomly generate p l -bit Random numbers as private key.

2. Generate public key

Use p balls as pre-image of leaves to build c Merkle trees with height $\ln p$. Take $\ln d$ tree root as public key with each public key as sequence period.

3. Distribute Public key.

Signing(Base Station or Sender)

Input: message m , K_{pri} , one-time session key(k_1)

Output: Digital Envelope

1. Encrypt m with k_1 .

2. Compute Hash(H_1) of m .

3. k_1 encrypted with K_{pri} .

Verification(Sensor nodes or receiver)

Input: Digital Envelope

Output: accept or reject

1. Decrypt k_1 with its own K_{pub}

2. Extract original message m with k_1

3. Compute Hash(H_2) of decrypted message m .

4. Compare H_1 with H_2

If $(H_1) = (H_2)$

then output accept;

else output reject:

VII. CONCLUSION

The scheme which we have discussed is also efficient in many ways. As it provides security from adversary that, in any case if it could extract public key that is in transit and get the confidential message out of it. Then the adversary could not encrypt it in the same way as did by the sender. As a result the receiver come to know that there is problem somewhere in transit. Our scheme exhibits many nice properties including individual authentication, robustness to packet loss, and low overhead in computation, communication and storage. This scheme improves upon Hash to Obtain Random Subset (HORS) in terms of reducing the large key storage requirement. This scheme devised a simple and efficient Broadcast Authentication for Wireless Sensor Network.

REFERENCES

- [1]. Y. W. Law and P. Havinga. How to secure a wireless sensor network. pages 89–95, Dec. 2005.
- [2]. Mayank Saraogi. Security in Wireless Sensor Networks. In ACM SenSys, 2004.
- [3]. Huei-Ru Tseng, Rong-Hong Jan and Wu Yang, "An Improved Dynamic User Authentication Scheme for Wireless Sensor Networks", IEEE Global Communications Conference (GLOBECOM 2007, Washington, DC, USA), pages 986-990, Nov. 2007.
- [4]. Shang-Ming Chang, Shihpyng Shieh, Warren W. Lin, Chih-Ming Hsieh, "An Efficient Broadcast Authentication Scheme in Wireless Sensor Networks"
- [5]. D. Liu, P. Ning, S. Zhu, and S. Jajodia, "Practical broadcast authentication in sensor networks," in Proc. 2nd Annual International Conf. Mobile Ubiquitous Syst.: Networking Services (MobiQuitous 2005), July 2005, pp. 118-132.
- [6]. Chakib Bekara and Maryline Laurent-Maknavicius and Kheira Bekara Institut Telecom, Telecom and Management Sud-Paris CNRS Samovar UMR 5157, 9 rue Charles Fourier, 91000 Evry, France, 'H²BSAP: A Hop-by-Hop Broadcast Source Authentication Protocol for WSN to mitigate DoS attack'.
- [7]. Tsern-Huei Lee, "Simple Dynamic User Authentication Protocols for Wireless Sensor Networks", Second International Conference on Sensor Technologies and Applications (SENSORCOMM'08), pages 657-660, France, 2008.
- [8]. D. Liu and P. Ning, "Multi-level mTESLA: Broadcast authentication for distributed sensor networks," ACM Trans. Embedded Computing Systems (TECS), vol. 3, no. 4, pp. 800-836, 2004.
- [9]. I. Akyildiz and I. Kasimoglu, "Wireless sensor and actor networks: research challenges," Ad Hoc Networks 2(4), pages 351-367, 2004.
- [10]. W. Du, R. Wang, and P. Ning "An efficient scheme for authenticating public keys in sensor networks," in Proc. 6th ACM International Symposium Mobile Ad Hoc Networking Computing (MobiHoc), 2005, pp. 58-67.
- [11]. S. Datema. A Case Study of Wireless Sensor Network Attacks. Master's thesis, Delft University of Technology, September 2005.
- [12]. J. Drissi and Q. Gu, "Localized broadcast authentication in large sensor networks," in ICNS '06: Proceedings of the International conference on Networking and Services, 2006, p. 25.

“To Improve Thermal Efficiency of 27mw Coal Fired Power Plant”

Amit Kumar Vishwakarma¹, Gopal Kumar Choudhary², Rajendra Prasad Sahu³
^{1,2,3}Assistant Professor, Department of Mechanical Engineering, Technocrats Institute of Technology, Bhopal, M.P 462021

ABSTRACT: Booming demand for electricity, especially in the developing countries, has raised power generation technologies in the headlines. At the same time the discussion about causes of global warming has focused on emissions originating from power generation and on CO₂ reduction technologies such as:

- (1) Alternative primary energy sources,
- (2) Capture and storage of CO₂,
- (3) Increasing the efficiency of converting primary energy content into electricity.

In the dissertation, the thermal efficiency of the power plant is improved when Control of furnace draft (nearer to balanced draft). Oxygen level decreases percentage of flue gases. Above this level heat losses are increases & below this carbon mono-oxide is formed. Steam power plant is using fuel to generate electrical power. The used of the fuel must be efficient so the boiler can generate for the maximum electrical power. By the time the steam cycle in the boiler, it also had heat losses through some parts and it effect on the efficiency of the boiler. This project will analyze about the parts of losses and boiler efficiency. to find excess air which effect heat losses in boiler. By using the 27 MW coal fired thermal power plant of **Birla Corporation Limited, Satna (M.P.)** the data is collect by using types of Combustion & heat flow in boiler. Result of the analysis show that the efficiency of boiler depends on mass of coal burnt & type of combustion .This study is fulfilling the objective of analysis to find the boiler efficiency and heat losses in boiler for 27 MW thermal power plant of Birla Corporation Limited, Satna (M.P.)

Keywords: Rankine Cycle, AFBC Boiler, Ash Handling System, Coal Fired Thermal Power Plant

I. INTRODUCTION

Thermal power plants convert heat (via mechanical energy) into electrical energy. The most important types are coal, gas and nuclear power stations. Thermal power plants are the backbone of our electricity system. Their efficiency is typically between 30 and 50%. Based on this, it is often concluded that thermal power stations are inadequate, waste energy, and need to be replaced by 'better' facilities. To evaluate this conclusion, one needs to look at the physical properties of heat energy, as well as at the fine-print in efficiency calculations, defined by man.

Rapid growth of electrical energy demand, not only in developing countries, discussions on fossil fuel reserves and the impact of thermal power generation on global warming, have increased the focus on alternative primary energy sources and the efficiency improvement techniques for the conversion of the fossil fuels into electricity. Development efforts are ongoing to reduce, capture and/or store CO₂ emitted from burning fossil fuels. The following is a quote from the McKinsey report of May 2007 “Curbing the energy demand growth”.

QUOTE Reducing current losses from electricity generation and distribution is another substantial opportunity. Power generation used 155 QBTUs (Quad =10¹⁵) – representing a hefty 37% of global energy use – to generate 57 QBTUs of deliverable electricity in 2003. In short, close to two-thirds of the energy put to the process is lost before it reaches the final end user.

UNQUOTE In this essay, we will look at some of the auxiliary load in fossil-fueled power stations and see what can be done to reduce this part of the losses. Thermal power stations use 3% to 10 % of their gross generation capacity for auxiliary processes. A conventional coal-fired thermal power plant uses slightly more (5 – 10%) of the electricity it produces for the auxiliary load. For a combined-cycle power plant, the auxiliary consumption can be less than 3.5 %. Auxiliary processes are required to keep the generator running; they are,

for instance, conveying fuel coal to coal mills and maintaining the cooling water flowing through the condenser. Most of the auxiliary power demand, up to 80%, is used by large electric motors that are typically connected to the medium voltage switchboard, supplied through auxiliary transformers. The increasing demand for “clean coal” and CO₂ emission capture and storage technologies will increase the auxiliary electricity consumption of electric power generation. Power stations, especially base-load ones, are running at full load all the time. It is easy to imagine that not much change or control is needed for the auxiliary processes in such cases. The fact is however, that very few power stations run at their maximum capacity throughout the year; instead the capacity is being adjusted all the time to match demand and various operation conditions and parameters. See Figure 1 illustrating a one year capacity utilization curve and Figure 2 for the corresponding operating hours of a 27 MW steam generator

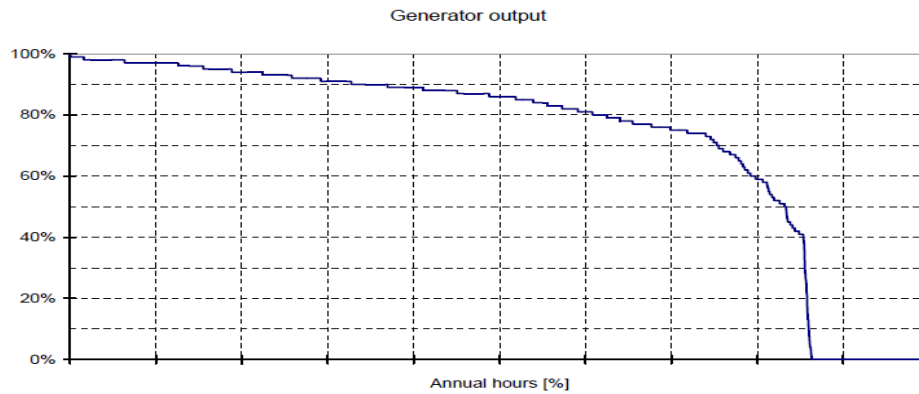


Fig 1: CAPACITY UTILIZATION CURVE OF A 27 MW STEAM GENERATOR.

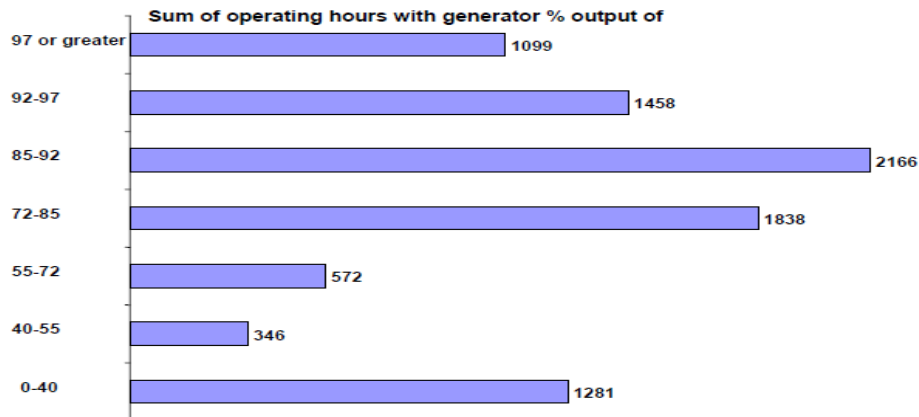


Fig 2: OPERATING HOURS AT VARIOUS LOAD RANGES OF A 27 MW STEAM GENERATOR.

1.1 EFFICIENCY:

The efficiency of a power station is indicated with the Greek character η , and is defined as follows:

$$\eta = \frac{\text{output of station}}{\text{input of station}} \times 100$$

This definition applies to any power plant. It seems to be straight forward, but in practice, a few problems arise with it. First, power plants themselves use electricity for their operation (lighting, pumps, etc.). Using the total amount of electricity generated yields the ‘gross Efficiency’, while subtracting the power plants own use gives ‘net efficiency’. Comparisons are only meaningful based on net efficiency.

The energy efficiency of a conventional thermal power station, considered as salable energy as a percent of the heating value of the fuel consumed, is typically 33% to 48%. This efficiency is limited as all heat engines are governed by the laws of thermodynamics. The rest of the energy must leave the plant in the form of heat. This waste heat can go through a condenser and be disposed of with cooling water or incooling towers. If the waste heat is instead utilized for district heating, it is called co-generation. An important class of thermal power station are associated with desalination facilities; these are typically found in desert countries with large supplies of natural gas and in these plants, freshwater production and electricity are equally important co-

products. The outstanding efficiency of variable speed fans has been discussed in this paper. The fan input power varies as the cube of the speed and while satisfying the system requirements at maximum continuous rating or at lower loads, power savings are maximized as compared to any other method of flow control. Sometimes it is difficult to match all three parameters (flow, pressure and speed) at the maximum efficiency point. To select a fan at maximum efficiency, sometimes the fan needs to be selected at a speed other than synchronous speed, which becomes possible with a variable speed drive. Also, a fan has higher efficiency when inlet vanes or inlet dampers are totally eliminated. Through the energy efficiency of variable speed fan, investment in electric variable speed drives can typically prove to be the most economical choice in all cases with longer than few years operating period. This is especially the situation in cases where investment must be split over several years and the alternative is to install and operate a heavily throttled fixed speed fan dimensioned to future demand.

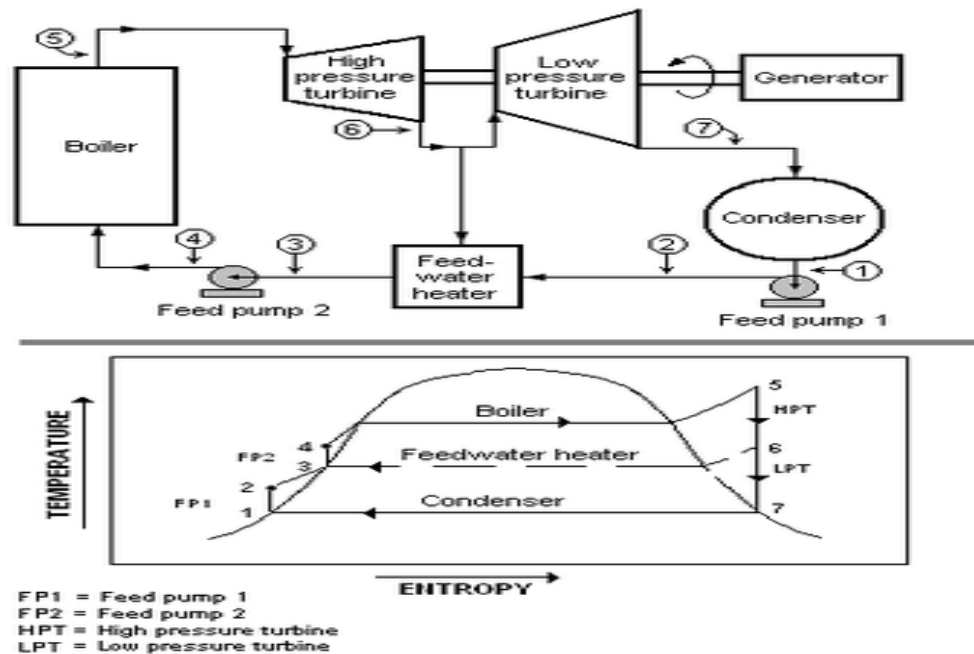


Fig 3 : A Rankine Cycle With A Two-Stage Steam Turbine And A Single Feed Water Heater.

Above the critical point for water of 374 °C and 22.06 MPa there is no phase transition from water to steam, but only a gradual decrease in density. Boiling does not occur and it is not possible to remove impurities via steam separation. In this case a super critical steam plant is required to utilize the increased thermodynamic efficiency by operating at higher temperatures. These plants, also called *once-through* plants because boiler water does not circulate multiple times, require additional water purification steps to ensure that any impurities picked up during the cycle will be removed. This purification takes the form of high pressure ion exchange units called condensate polishers between the steam condenser and the feed water heaters. Sub-critical fossil fuel power plants can achieve 36–40% efficiency. Super critical designs have efficiencies in the low to mid 40% range, with new "ultra critical" designs using pressures of 30.3 MPa and dual stage reheat reaching about 48% efficiency.

Current nuclear power plants operate below the temperatures and pressures that coal-fired plants do. This limits their thermodynamic efficiency to 30–32%. Some advanced reactor designs being studied, such as the Very high temperature reactor, Advanced gas-cooled reactor and Super critical water reactor, would operate at temperatures and pressures similar to current coal plants, producing comparable thermodynamic efficiency.

1.2 ELECTRICITY COST:

The direct cost of electric energy produced by a thermal power station is the result of

- (1) Cost of fuel,
- (2) Capital cost for the plant,
- (3) Operator labour,
- (4) Maintenance,
- (5) Ash handling and disposal.

Indirect, social or environmental costs such as the economic value of environmental impacts, or environmental and health effects of the complete fuel cycle and plant decommissioning, are not usually assigned

to generation costs for thermal stations in utility practice, but may form part of an environmental impact assessment.

1.3 WHY POWER PLANT EFFICIENCY IS IMPORTANT:

Increased efficiency implies :

- Same MW / Electricity from less quantity of coal
- 1% efficiency improvement implies:
- ~3% reduction in coal consumption and
- ~3% reduction CO₂/GHG & particulate emission

Generation efficiency : percentage energy content of the fuel being converted into electrical energy. Focus needed on technology options to improve generation efficiency of existing & new power stations.

- Efficiency of modern coal power plant = 34-36%
- Efficiency of old power plant = 20-30%

II. LITERATURE REVIEW

2.1 INTRODUCTION:

In this chapter, all the important information related of this project is stated. Besides that, the literature review can give a brief explanation about the steam power plant and its operation also the effect of the excess air & unburnt carbon loss. Some of the points in this chapter can give extra information which is useful while doing this project.

2.2 THE USE OF THE STEAM:

Steam is a critical recourse in today's industrial world. It is essential for cooling and heating of large buildings, driving equipment such as pump and compressors and for powering ships. However, its most importance priority remains as source of power for the production of electricity. Steam is extremely valuable because it can be produced anywhere in this world by using the heat that comes from the fuels that are available in this area. Steam also has unique properties that are very important in producing energy. Steam is basically recycled, from a steam to water and then back to steam again, all in manner that is nontoxic in nature. The steam plant of today are a combination of complex engineered system that work to produce steam in the most efficient manner that is economically feasible. Whether the end product of this steam is electricity, heat or a steam process required to develop a needed product such as paper, the goal is to have that product produced at the lowest cost possible. The heat required to produce the steam is a significant operating cost that affects the ultimate cost of the end product. (Everett, 2005)

2.3 STEAM IS EFFICIENT AND ECONOMIC TO GENERATE:

Water is plentiful and inexpensive. It is non-hazardous to health and environmentally, sound. In its gaseous form, it is a safe and efficient energy carrier. Steam can hold five or six times as much potential energy as an equivalent mass of water. When water is heated in a boiler, it begins to absorb energy. Depending on the pressure in the boiler, the water will evaporate at a certain temperature to form steam. The steam contains a large quantity of stored energy which will eventually be transferred to the process or the space to be heated. It can be generated at high pressures to give high steam temperatures. The higher the pressure, the higher the temperature. More heat energy is contained within high temperature steam so its potential to do work is greater.

- Modern shell boilers are compact and efficient in their design, using multiple passes and efficient burner technology to transfer a very high proportion of the energy contained in the fuel to the water, with minimum emissions.
- The boiler fuel may be chosen from a variety of options, including combustible waste, which makes the steam boiler an environmentally sound option amongst the choices available for providing heat. Centralized boiler plant can take advantage of low interruptible gas tariffs, because any suitable standby fuel can be stored for use when the gas supply is interrupted.
- Highly effective heat recovery systems can virtually eliminate blow down costs, return valuable condensate to the boiler house and add to the overall efficiency of the steam and condensate loop.

The increasing popularity of Combined Heat and Power (CHIP) systems demonstrates the high regard for steam systems in today's environment and energy conscious industries. (Everett, 2005)

2.4 ENERGY IS EASILY TRANSFERRED TO THE PROCESS:

Steam provides excellent heat transfer. When the steam reaches the plant, the condensation process efficiently transfers the heat to the product being heated. Steam can surround or be injected into the product being heated. It can fill any space at a uniform temperature and will supply heat by condensing at a constant temperature; this eliminates temperature gradients which may be found along any heat transfer surface - a problem which is so often a feature of high temperature oils or hot water heating, and may result in quality

problems, such as distortion of materials being dried. Because the heat transfer properties of steam are so high, the required heat transfer area is relatively small. This enables the use of more compact plant, which is easier to install and takes up less space in the plant. A modern packaged unit for steam heated hot water rated to 1200 kW and incorporating a steam plate heat exchanger and all the controls, requires only 0.7 m² floor spaces. In comparison, a packaged unit incorporating a shell and tube heat exchanger would typically cover an area of two to three times that size.

2.5 THE STEAM PLANT CYCLE:

The simplest steam cycle of practical value is called the Rankine cycle, which originated around the performance of the steam engine. The steam cycle is important because it connects processes that allow heat to be converted to work on a Continuous basis. This simple cycle was based on dry saturated steam being supplied by a boiler to a power unit such as a turbine that drives an electric generator. Dry saturated steam is at the temperature that corresponds to the boiler pressure, is not superheated, and does not contain moisture. The steam from the turbine exhausts to a condenser, from which the condensed steam is pumped back into the boiler. It is also called a condensing cycle, and a simple schematic of the system is shown in Fig. 4.

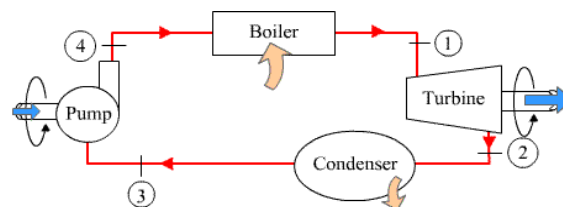
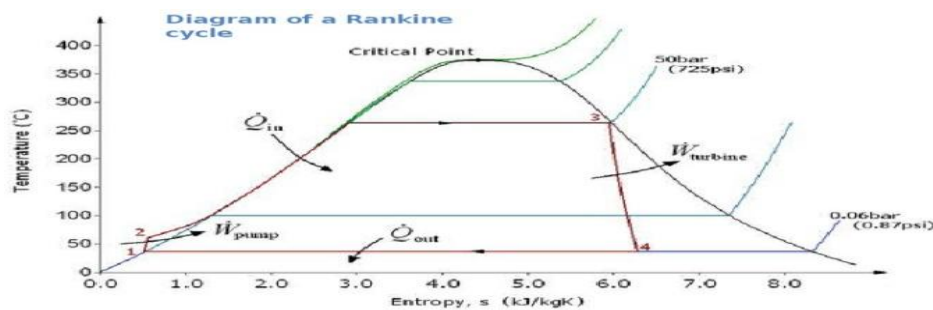


Fig 4 : Steam Plant Cycle



$$\text{Rankine thermal efficiency} = \frac{h_3 - h_4}{h_3 - h_1}$$

Fig 5: Rankine Thermal Cycle

This schematic also shows heat (Q_{in}) being supplied to the boiler and a generator connected to the turbine for the production of electricity. Heat (Q_{out}) is removed by the condenser, and the pump supplies energy (W_p) to the feed water in the form of a pressure increase to allow it to flow through the boiler. A higher plant efficiency is obtained if the steam is initially superheated, and this means that less steam and less fuel are required for a specific output. (Superheated steam has a temperature that is above that of dry saturated steam at the same pressure and thus contains more heat content, called enthalpy, Btu/lb.) If the steam is reheated and passed through a second turbine, cycle efficiency also improves, and moisture in the steam is reduced as it passes through the turbine. This moisture reduction minimizes erosion on the turbine blades. When saturated steam is used in a turbine, the work required rotating the turbine results in the steam losing energy, and a portion of the steam condenses as the steam pressure drops. The amount of work that can be done by the turbine is limited by the amount of moisture that it can accept without excessive turbine blade erosion. This steam moisture content generally is between 10 and 15 percent. Therefore, the moisture content of the steam is a limiting factor in turbine design. With the addition of superheat, the turbine transforms this additional energy into work without forming moisture, and this energy is basically all recoverable in the turbine. A reheater often is used in a large utility. (Kenneth, 2005).

2.6 FEEDWATER:

The feed water system requires accessories to supply the correct amount of water in the proper condition to the boiler. A feed water accessory is equipment that is not directly attached to the boiler that controls the quantity, pressure, and/or temperature of water supplied to the boiler. Maintaining the correct level of water in the boiler is critical for safety and efficiency. If the water level in the boiler is too high, water can be carried over into steam lines, which can lead to water hammer and line rupture. If the water level in the boiler is too low, heat from the furnace cannot be properly transferred to the water. This can cause overheating and damage

to boiler tubes and heating surfaces. Significant damage from over heating can lead to a boiler explosion. Feedwater is treated and regulated automatically to meet the demand for steam. Valves are installed in feedwater lines to permit access for maintenance and repair. The feedwater system must be capable of supplying water to the boiler in all circumstances and includes feedwater accessories required for the specific boiler application, In a steam heating system.) Heat necessary for providing comfort in the building starts at the boiler. Water in the boiler is heated and turns to steam. Steam leaves the boiler through the main steam line (boiler outlet) where it enters the main steam header-. From the main steam header, main branch lines direct the steam up a riser to the heating unit (heat exchanger). Heat is released to the building space as steam travels through the heating unit, Steam in the heating unit cools and turns into condensate. The condensate is separated from the steam by a steam trap that allows condensate, but not steam to pass. The condensate is directed through the condenser return line to the condensate return tank. The feed water pump pumps the condensate and/or water back to the boiler through check valves and stop valves on the feed water line. Feed water enters the boiler and is turned to steam to repeat the process. (Kenneth, 2005)

2.7 BOILER EFFICIENCY:

Boiler Efficiency may be indicated by

1. Combustion Efficiency indicates the burners ability to burn fuel measured by unburned fuel and excess air in the exhaust
2. Thermal Efficiency - indicates the heat exchangers effectiveness to transfer heat from the combustion process to the water or steam in the boiler, exclusive radiation and convection losses
3. Fuel to Fluid Efficiency - indicates the overall efficiency of the boiler inclusive thermal efficiency of the heat exchanger, radiation and convection losses - output divided by input. Boiler Efficiency is in general indicated by either Thermal Efficiency or Fuel to Fluid Efficiency depending the context. (Chattopadhyay, 2005)

2.8 BOILER LOSSES:

1. Dry flue gas loss.
2. Moisture in combustion air loss
3. Unburnt carbon loss – carbon in ash loss.
4. Unburnt gas loss, due to incomplete combustion of carbon,
5. Wet flue gas loss loss due to moisture in fuel & due to moisture formed by combustion of H₂ in fuel
6. Radiation & Unaccounted losses. (Dr. V.K. Sethi,2011)

III. MAJOR ENERGY SAVING POTENTIAL AREAS IN THERMAL POWER PLANT

Thermal power plant is designated sector as per EC act 2001. Most thermal power plant uses 30-40% of energy value of primary fuels. The remaining 60-70% is lost during generation, transmission and distribution of which major loss is in the form of heat. Thermal power consist of various sub cycles / systems like air & flue gas cycle, main steam, feed water & condensate cycle , fuel & ash cycle, Equipment cooling water (ECW), auxiliary cooling water (ACW) system, Compressed air system, Electrical auxiliary power & lighting system, HVAC system etc.. There is tremendous scope of energy saving potential in each system/cycle which is given below.

3.1 AIR & FLUE GAS CYCLE:

- (i) Optimizing excess air ratio: - It reduces FD fan & ID fan loading.
- (ii) Replacement of oversize FD and PA fan: - Many thermal power plants have oversize fan causing huge difference between design & operating point leads to lower efficiency. Hence fan efficiency can be improved by replacing correct size of fan. If replacement is not possible, Use of HT VFD for PA & ID fan can be the solution.
- (iii) Attending the air & flue gas leakages: - Leakages in air & flue gas path increases fan loading. Use of Thermo vision monitoring can be adopted to identify leakages in flue gas path.
- (iv) Air preheater performance is one crucial factor in leakage contribution. If APH leakage exceeds design value then it requires corrective action.

3.2 STEAM FEEDWATER & CONDENSATE CYCLE:

- (i) BFP scoop operation in three element mode instead of DP mode: - In three element mode throttling losses across FRS valve reduces leads to reduction in BFP power.
- (ii) Optimization of level set point in LP & HP heater: - Heater drip level affects TTD & DCA of heater which finally affect feed water O/L temp. Hence it requires setting of drip level set point correctly.
- (iii) Charging of APRDS from CRH line instead of MS line: - APRDS charging from cold reheat (CRH) is always more beneficial than from MS line charging.
- (iv) Isolation of steam line which is not in use: - It is not advisable to keep steam line unnecessary charge if steam is not utilized since there energy loss occurred due to radiation. For example deareator extraction

can be charged from turbine Extraction/CRH or from APRDS. In normal running APRDS Extraction is not used so same can be kept isolated.

- (v) Replacement of BFP cartridge: - BFP draws more current If Cartridge is wore out, causing short circuit of feed water Flow inside the pump. It affects pump performance. Hence cartridge replacement is necessary.
- (vi) Attending passing recirculation valve of BFP: - BFP Power consumption Increases due to passing of R/C valve. It requires corrective action.
- (vii) Installation of HT VFD for CEP: - CEP capacity is underutilized and also there is pressure loss occurs across Deareator level control valve. There is large scope of energy saving which can be accomplished by use of HT VFD for CEP or impeller trimming.

3.3 FUEL & ASH CYCLE:

- (i) Optimized ball loading in Ball tube mill :- Excessive ball loading increases mill power. Hence ball loading is to be Optimized depending upon coal fineness report.
- (ii) Use of Wash Coal or Blending with A- grade coal : - F-grade coal has high ash content. Overall performance can be improved by using Wash coal or blending of F-grade coal with A- grade coal instead of only using F- grade coal.
- (iii) Avoiding idle running of conveyors & crusher in CHP
- (iv) Use of Dry ash Evacuation instead of WET deashing System: - Dry deashing system consumes less power & also minimizes waste reduction.
- (v) Optimize mill maintenance:- Mill corrective/preventive maintenance is to be optimized depending parameter like- running hrs, mill fineness, bottom ash unburnt particle, degree of reject pipe chocking etc.

3.4 ELECTRICAL & LIGHTING SYSTEM:

- (i) Optimizing Voltage level of distribution transformer: - It is found that Operating voltage level is on higher side than required causing more losses. It is required to reduce the voltage level by tap changing.
- (ii) Use of Auto star/delta/star converter for under loaded motor Lighting: - Use of electronic chock instead of conventional use copper Chock, Use of CFL, Replacement of mercury vapor lamp by metal Halide lamp. Use of timer for area lighting is the methods can be used. Lighting has tremendous potential of saving.

3.5 ECW & ACW SYSTEM:

- (i) **Isolating ECW supply of standby auxiliaries:** - Many times standby coolers are kept charged from ECW side. Also Standby equipment's auxiliaries like Lube oil system kept running for reliability. We can isolate Standby cooler from ECW system & switching of standby auxiliaries, doing trade off between return & reliability.
- (ii) **Improving condenser performance by condenser tube cleaning & use of highly efficient debris filter:** Tube cleaning by bullet shot method increases condenser performance, condenser tube cleaning is necessary which is to be carried out in overhaul. Also highly advanced debris filter contribute condenser performance.
- (iii) **Application of special coating on CW pump impeller:** - It improves pump impeller profile condition, increasing pump performance.

3.6 COMPRESSED AIR SYSTEM:-

- (i) **Optimizing discharge air pressure by tuning loading/unloading cycle:** - It helpful to reduce sp. Power consumption.
- (ii) **Use of heat of compression air dryer instead of electrically heated air dryer:** - Heat of compression air dryer use heat generated in compression cycle, thus reduces sp. Power consumption.
- (iii) **Use of screw compressor instead reciprocating compressor:** - Sp. Power consumption of screw compressor is less than reciprocating air compressor leads to reduce aux. power consumption.

3.7 HVAC SYSTEM:

- (i) Cooling tower performance improvement
- (ii) Installing absorption refrigeration system instead of vapor compression system Use of wind turbo ventilators instead of conventional motor driven exhauster

IV. OBJECTIVES OF THE STUDY

- To increase the thermal efficiency of 27 MW coal fired power plant.
- To identify and bring forth the operation and working of a typical thermal power plant with special reference to Birla **Corporation Limited, Satna (M.P.)**.
- To explore the various avenues and areas, where the waste related to energy consumption can be minimized.
- To identify and study the key factors for improving the energy efficiency of a thermal power.

- To study the various environmental issues in relation to the working efficiency of the thermal power plants.

V. DESCRIPTION OF COAL FIRED POWER PLANT

- (1) Pulverized coal
- (2) Fluidized Bed Combustion
- (3) Atmospheric Fluidized Bed Combustion Boiler
- (4) Ash Handling System
- (5) Super heater
- (6) Economizer

5.1 PULVERIZED COAL:

A pulverized coal-fired boiler is an industrial or utility boiler that generates thermal energy by burning pulverized coal (also known as powdered coal or coal dust since it is as fine as face powder in cosmetic makeup) that is blown into the firebox.

The basic idea of a firing system using pulverized fuel is to use the whole volume of the furnace for the combustion of solid fuels. Coal is ground to the size of a fine grain, mixed with air and burned in the flue gas flow. Biomass and other materials can also be added to the mixture. Coal contains mineral matter which is converted to ash during combustion. The ash is removed as bottom ash and fly ash. The bottom ash is removed at the furnace bottom. This type of boiler dominates the electric power industry, providing steam to drive large turbines. Pulverized coal provides the thermal energy which produces about 50% of the world's electric supply. Pulverized coal power plants account for about 97% of the world's coal-fired capacity. The conventional types of this technology have an efficiency of around 35%. For a higher efficiency of the technology supercritical and ultra-supercritical coal-fired technologies have been developed. These technologies can combust pulverized coal and produce steam at higher temperatures and under a higher pressure, so that an efficiency level of 45% can be reached (ultra-supercritical plants). Supercritical power plants have become the system of choice in most industrialized countries, while ultra-supercritical plant technology is still in the process of demonstration. Supercritical and ultra-supercritical plants are more expensive (because of the higher requirements to the steel needed to stand the higher pressure and temperature) but the higher efficiency results in cost savings during the technical lifetime of the plants.

In a pulverized coal-fired boiler of a large power plant, an oxygen analyzer is essential for combustion control. A pulverized coal-fired boiler is an industrial or utility boiler that generates thermal energy by burning pulverized coal (also known as powdered coal or coal dust). This type of boiler dominates the electric power industry, providing steam to drive large turbines. Pulverized coal provides the thermal energy which reduces about 50% of the world's electric supply. Exhaust gases from the pulverized coal boiler contain a large quantity of dust and flow very fast. Oxygen analyzers that employ a sampling method may be subject to wear or clogging, resulting in increased maintenance workload and cost. A solution to this problem is the ZR22/ZR402 Direct In-Situ Zirconia Oxygen Analyzer that has no sampling system and utilizes a long-life sensor. A probe protector is attached to protection it against wear.

5.1.1: PROCESS: Coal is inexpensive and readily available. coal produces a large quantity of ashes when it is burned; necessitating pulverized coal-fired boilers to be equipped with an ash removal system such as a cyclone. Exhaust gases from these boilers contain a large quantity of dust (10 to 30 g/Nm³) and flow very fast as the result of the large volume of air being blown into the boiler. For oxygen measurement in large ducts, a probe with a long insertion length is used.

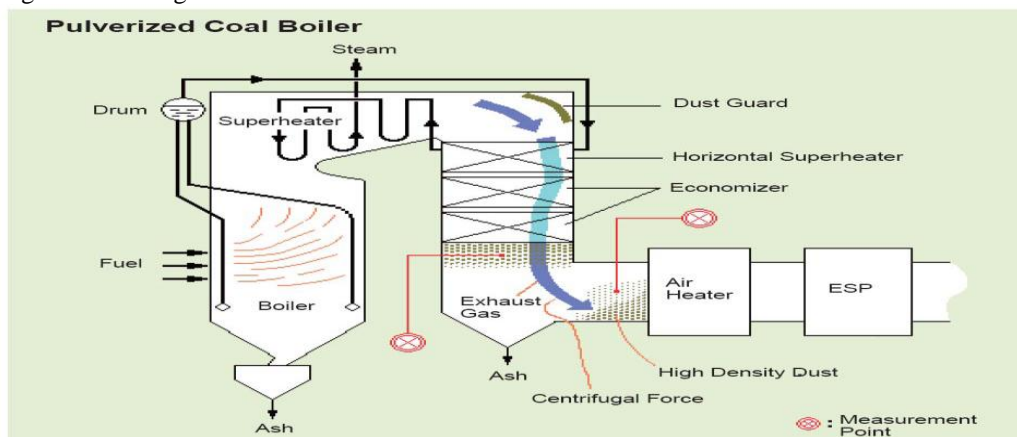


Fig 7: Pulverized Coal Boiler

5.1.2: COMBUSTION EFFICIENCY

Operating your boiler with an optimum amount of excess air will minimize heat loss up the stack and improve combustion efficiency. Combustion efficiency is a measure of how effectively the heat content of a fuel is transferred into usable heat. The stack temperature and flue gas oxygen (or carbon dioxide) concentrations are primary indicators of combustion efficiency.

Given complete mixing, a precise or stoichiometric amount of air is required to completely react with a given quantity of fuel. In practice, combustion conditions are never ideal, and additional or “excess” air must be supplied to completely burn the fuel.

The correct amount of excess air is determined from analyzing flue gas oxygen or carbon dioxide concentrations. Inadequate excess air results in unburned combustibles (fuel, soot, smoke, and carbon monoxide), while too much results in heat lost due to the increased flue gas flow—thus lowering the overall boiler fuel-to-steam efficiency. The table relates stack readings to boiler performance

5.1.3: FLUE GAS ANALYZER:

The percentage of oxygen in the flue gas can be measured by inexpensive gas-absorbing test kits. More expensive (ranging in cost from \$500 to \$1,000) hand-held, computer-based analyzers display percent oxygen, stack gas temperature, and boiler efficiency. They are a recommended investment for any boiler system with annual fuel costs exceeding \$50,000.

5.1.4: OXYGEN TRIM SYSTEM:

When fuel composition is highly variable (such as refinery gas, hog fuel, or multi-fuel boilers), or where steam flows are highly variable, an online oxygen analyzer should be considered. The oxygen “trim” system provides feedback to the burner controls to automatically minimize excess combustion air and optimize the air-to-fuel ratio.

To ensure complete combustion of the fuel used, combustion chambers are supplied with excess air. Excess air increase the amount of oxygen and the probability of combustion of all fuel.

- when fuel and oxygen in the air are in perfectly balance - the combustion is said to be **stoichiometric**
- The combustion efficiency will increase with increased excess air, until the heat loss in the excess air is larger than the heat provided by more efficient combustion.

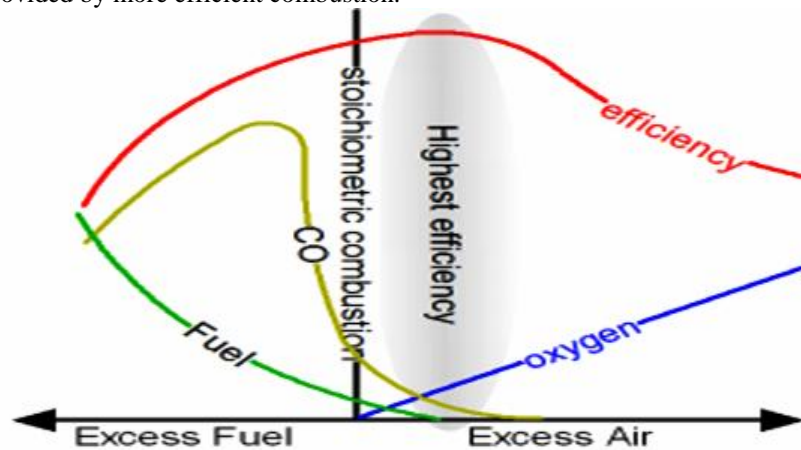


Fig 8 : COBUSTION EFFICIENCY

Typical excess air to achieve highest efficiency for different fuels are 15 - 60% for coal

Carbon dioxide - CO₂ - is a product of the combustion and the content in the flue gas is an important indication of the combustion efficiency.

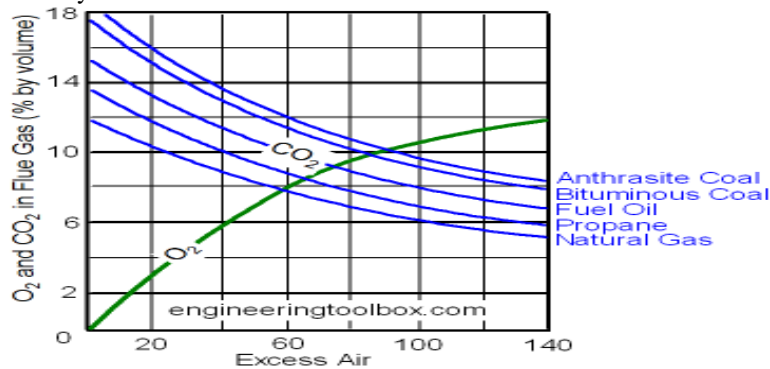


Fig 9: EXCESS AIR VS O2&CO2 IN FLUE GAS (% BY VOLUME)

An optimal content of carbon dioxide - CO_2 - after combustion is approximately 10% for natural gas and approximately 13% for lighter oils.

5.2 FLUIDIZED BED COMBUSTION:

The major portion of the coal available in India is of low quality, high ash content and low calorific value. The traditional grate fuel firing systems have got limitations and are techno-economically unviable to meet the challenges of future. Fluidized bed combustion has emerged as a viable alternative and has significant advantages over conventional firing system and offers multiple benefits – compact boiler design, fuel flexibility, higher combustion efficiency and reduced emission of noxious pollutants such as SO_x and NO_x . The fuels burnt in these boilers include coal, washery rejects, rice husk, bagasse & other agricultural wastes. The fluidized bed boilers have a wide capacity range- 0.5 T/hr to over 100 T/hr.

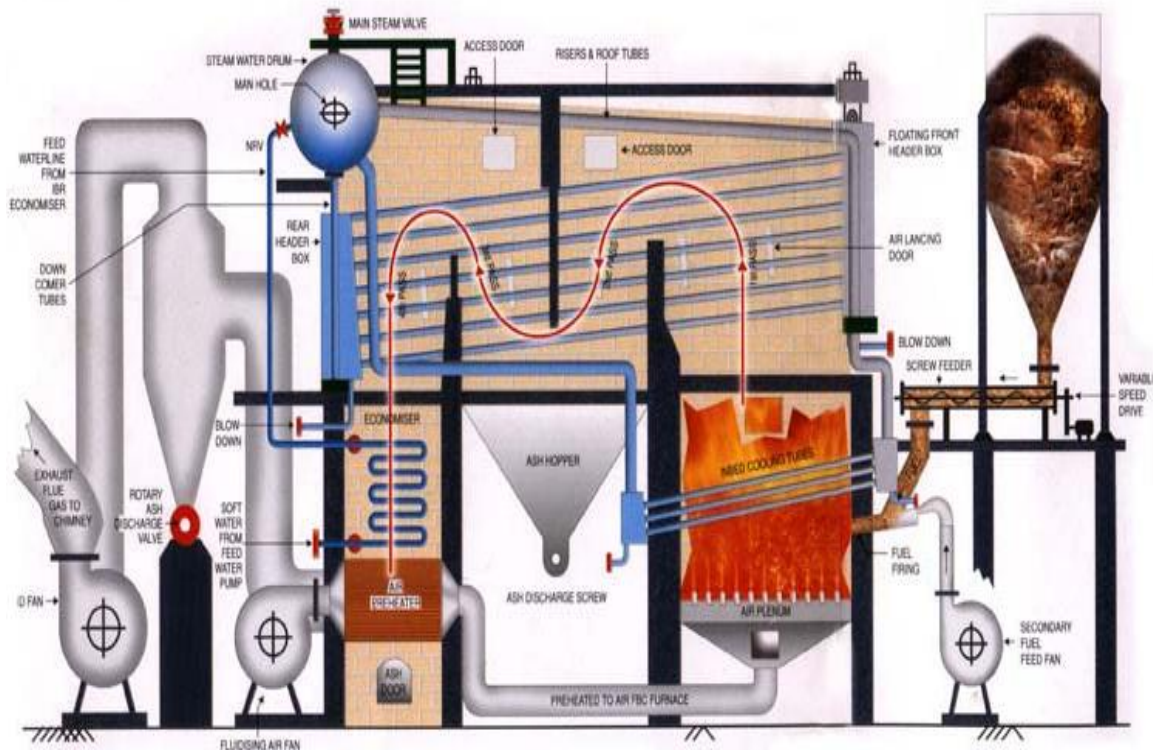


FIG 10 : MECHANISM OF FLUIDISED BED COMBUSTION

When an evenly distributed air or gas is passed upward through a finely divided bed of solid particles such as sand supported on a fine mesh, the particles are undisturbed at low velocity. As air velocity is gradually increased, a stage is reached when the individual particles are suspended in the air stream – the bed is called “fluidized”. With further increase in air velocity, there is bubble formation, vigorous turbulence, rapid mixing and formation of dense defined bed surface. The bed of solid particles exhibits the properties of a boiling liquid and assumes the appearance of a fluid – “bubbling fluidized bed”.

At higher velocities, bubbles disappear, and particles are blown out of the bed. Therefore, some amounts of particles have to be recirculated to maintain a stable system – “circulating fluidized bed”. This principle of fluidization is illustrated in Figure1.

Fluidization depends largely on the particle size and the air velocity. The mean solids velocity increases at a slower rate than does the gas velocity, as illustrated in Figure 6.2. The difference between the mean solid velocity and mean gas velocity is called as slip velocity. Maximum slip velocity between the solids and the gas is desirable for good heat transfer and intimate contact. If sand particles in a fluidized state is heated to the ignition temperatures of coal, and coal is injected continuously into the bed, the coal will burn rapidly and bed attains a uniform temperature. The fluidized bed combustion (FBC) takes place at about $840^{\circ}C$ to $950^{\circ}C$. Since this temperature is much below the ash fusion temperature, melting of ash and associated problems are avoided. The lower combustion temperature is achieved because of high coefficient of heat transfer due to rapid mixing in the fluidized bed and effective extraction of heat from the bed through in-bed heat transfer tubes and walls of the bed. The gas velocity is maintained between minimum fluidization velocity and particle entrainment velocity. This ensures stable operation of the bed and avoids particle entrainment in the gas stream.

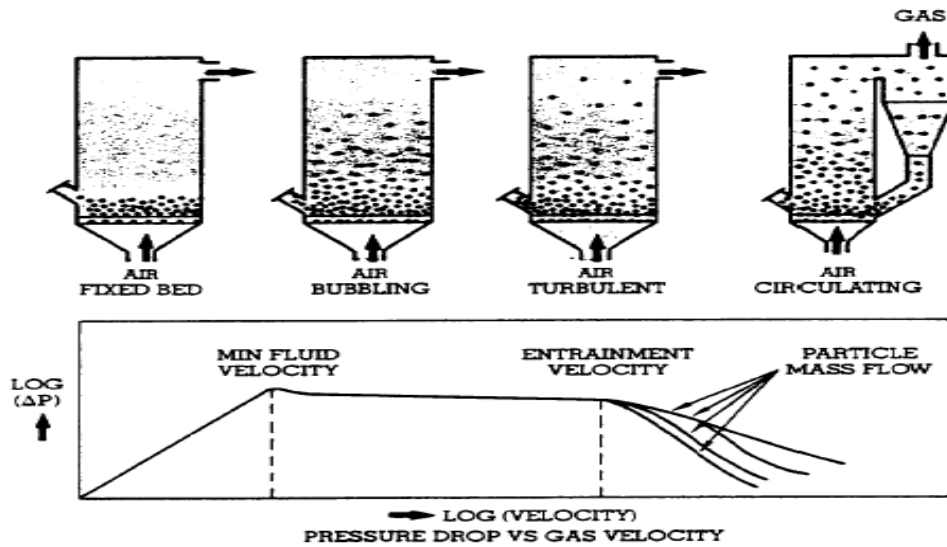


Fig 11: Relation Between Gas Velocity And Solid Velocity

Combustion process requires the three “T”s that is Time, Temperature and Turbulence. In FBC, turbulence is promoted by fluidisation. Improved mixing generates evenly distributed heat at lower temperature. Residence time is many times greater than conventional grate firing. Thus an FBC system releases heat more efficiently at lower temperatures.

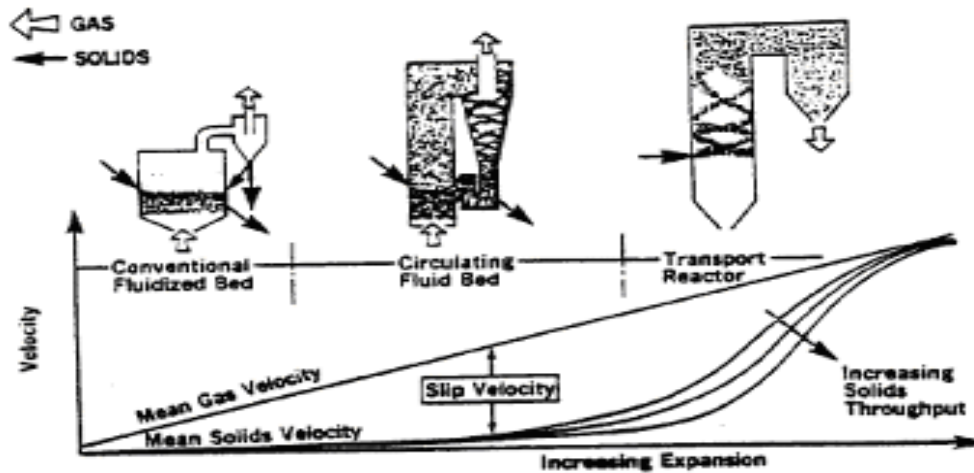


Fig 12: Velocity Vs Increasing Expansion

Firing. Thus an FBC system releases heat more efficiently at lower temperatures. Since limestone is used as particle bed, control of sulfur dioxide and nitrogen oxide emissions in the combustion chamber is achieved without any additional control equipment. This is one of the major advantages over conventional boilers.

5.3 ATMOSPHERIC FLUIDIZED BED COMBUSTION:

In AFBC, coal is crushed to a size of 1 – 10 mm depending on the rank of coal, type of fuel feed and fed into the combustion chamber. The atmospheric air, which acts as both the fluidization air and combustion air, is delivered at a pressure and flows through the bed after being preheated by the exhaust flue gases. The velocity of fluidising air is in the range of 1.2 to 3.7 m /sec. The rate at which air is blown through the bed determines the amount of fuel that can be reacted. Almost all AFBC/ bubbling bed boilers use in-bed evaporator tubes in the bed of limestone, sand and fuel for extracting the heat from the bed to maintain the bed temperature. The bed depth is usually 0.9 m to 1.5 m deep and the pressure drop averages about 1 inch of water per inch of bed depth. Very little material leaves the bubbling bed – only about 2 to 4 kg of solids are recycled per ton of fuel burned. Typical fluidized bed combustors of this type are shown in Figures 9.1 and 9.2

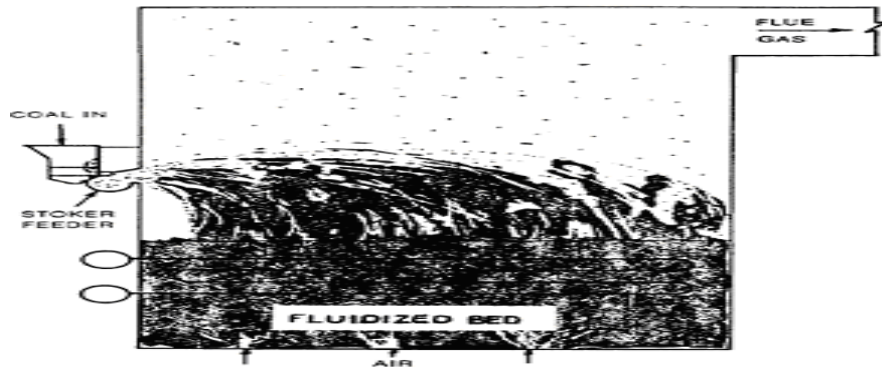


Fig 13: Bubbling Bed Boiler

The combustion gases pass over the super heater sections of the boiler, flow past the economizer, the dust collectors and the air preheaters before being exhausted to atmosphere.

The main special feature of atmospheric fluidized bed combustion is the constraint imposed by the relatively narrow temperature range within which the bed must be operated. With coal, there is risk of clinker formation in the bed if the temperature exceeds 950°C and loss of combustion efficiency if the temperature falls below 800°C . For efficient sulphur retention, the temperature should be in the range of 800°C to 850°C .

5.3.1 GENERAL ARRANGEMENTS OF AFBC BOILER

AFBC boilers comprise of following systems:

- i) Fuel feeding system
- ii) Air Distributor
- iii) Bed & In-bed heat transfer surface
- iv) Ash handling system

5.3.2 MANY OF THESE ARE COMMON TO ALL TYPES OF FBC BOILERS :

1. FUEL FEEDING SYSTEM

For feeding fuel, sorbents like limestone or dolomite, usually two methods are followed: under bed pneumatic feeding over-bed feeding.

5.2.4.1 UNDER BED PNEUMATIC FEEDING :

If the fuel is coal, it is crushed to 1-6 mm size and pneumatically transported from feed hopper to the combustor through a feed pipe piercing the distributor. Based on the capacity of the boiler, the number of feed points is increased, as it is necessary to distribute the fuel into the bed uniformly.

5.4.4.2 OVER-BED FEEDING :

The crushed coal, 6-10 mm size is conveyed from coal bunker to a spreader by a screw conveyor. The spreader distributes the coal over the surface of the bed uniformly. This type of fuel feeding system accepts over size fuel also and eliminates transport lines, when compared to under-bed feeding system.

5.4.3 AIR DISTRIBUTOR :

The purpose of the distributor is to introduce the fluidizing air evenly through the bed cross section thereby keeping the solid particles in constant motion, and preventing the formation of defluidization zones within the bed. The distributor, which forms the furnace floor, is normally constructed from metal plate with a number of perforations in a definite geometric pattern. The perforations may be located in simple nozzles or nozzles with bubble caps, which serve to prevent solid particles from flowing back into the space below the distributor.

The distributor plate is protected from high temperature of the furnace by:

- i) Refractory Lining
- ii) A Static Layer of the Bed Material or
- iii) Water Cooled Tubes.

5.3.3 BED & IN-BED HEAT TRANSFER SURFACE:

5.3.3.1 BED

The bed material can be sand, ash, crushed refractory or limestone, with an average size of about 1 mm. Depending on the bed height these are of two types: shallow bed and deep bed.

At the same fluidizing velocity, the two ends fluidise differently, thus affecting the heat transfer to an immersed heat transfer surfaces. A shallow bed offers a lower bed resistance and hence a lower pressure drop and lower fan power consumption. In the case of deep bed, the pressure drop is more and this increases the effective gas velocity and also the fan power.

5.3.3.2 IN-BED HEAT TRANSFER SURFACE :

In a fluidized in-bed heat transfer process, it is necessary to transfer heat between the bed material and an immersed surface, which could be that of a tube bundle, or a coil. The heat exchanger orientation can be horizontal, vertical or inclined. From a pressure drop point of view, a horizontal bundle in a shallow bed is more attractive than a vertical bundle in a deep bed. Also, the heat transfer in the bed depends on number of parameters like (i) bed pressure (ii) bed temperature (iii) superficial gas velocity (iv) particle size (v) Heat exchanger design and (vi) gas distributor plate design.

5.3.4 ADVANTAGES OF FLUIDIZED BED COMBUSTION BOILERS

1. HIGH EFFICIENCY

FBC boilers can burn fuel with a combustion efficiency of over 95% irrespective of ash content. FBC boilers can operate with overall efficiency of 84% (plus or minus 2%).

2. REDUCTION IN BOILER SIZE

High heat transfer rate over a small heat transfer area immersed in the bed result in overall size reduction of the boiler.

3. FUEL FLEXIBILITY

FBC boilers can be operated efficiently with a variety of fuels. Even fuels like flotation slimes, washer rejects, agro waste can be burnt efficiently. These can be fed either independently or in combination with coal into the same furnace.

4. ABILITY TO BURN LOW GRADE FUEL

FBC boilers would give the rated output even with inferior quality fuel. The boilers can fire coals with ash content as high as 62% and having calorific value as low as 2,500 kcal/kg. Even carbon content of only 1% by weight can sustain the fluidised bed combustion.

5. ABILITY TO BURN FINES

Coal containing fines below 6 mm can be burnt efficiently in FBC boiler, which is very difficult to achieve in conventional firing system.

6. POLLUTION CONTROL

SO₂ formation can be greatly minimised by addition of limestone or dolomite for high sulphur coals. 3% limestone is required for every 1% sulphur in the coal feed. Low combustion temperature eliminates NO_x formation.

7. LOW CORROSION AND EROSION

The corrosion and erosion effects are less due to lower combustion temperature, softness of ash and low particle velocity (of the order of 1 m/sec).

8. EASIER ASH REMOVAL – NO CLINKER FORMATION

Since the temperature of the furnace is in the range of 750 – 900 °C in FBC boilers, even coal of low ash fusion temperature can be burnt without clinker formation. Ash removal is easier as the ash flows like liquid from the combustion chamber. Hence less manpower is required for ash handling.

9. LESS EXCESS AIR – HIGHER CO₂ IN FLUE GAS

The CO₂ in the flue gases will be of the order of 14 – 15% at full load. Hence, the FBC boiler can operate at low excess air - only 20 – 25%.

10. SIMPLE OPERATION, QUICK START-UP

High turbulence of the bed facilitates quick start up and shut down. Full automation of start up and operation using reliable equipment is possible.

11. FAST RESPONSE TO LOAD FLUCTUATIONS

Inherent high thermal storage characteristics can easily absorb fluctuation in fuel feed rates. Response to changing load is comparable to that of oil fired boilers.

12. NO SLAGGING IN THE FURNACE-NO SOOT BLOWING

In FBC boilers, volatilisation of alkali components in ash does not take place and the ash is non sticky. This means that there is no slagging or soot blowing.

13 PROVISIONS OF AUTOMATIC COAL AND ASH HANDLING SYSTEM

Automatic systems for coal and ash handling can be incorporated, making the plant easy to operate comparable to oil or gas fired installation.

14 PROVISION OF AUTOMATIC IGNITION SYSTEM

Control systems using micro-processors and automatic ignition equipment give excellent control with minimum manual supervision.

15 HIGH RELIABILITY

The absence of moving parts in the combustion zone results in a high degree of reliability and low maintenance costs.

16 REDUCED MAINTENANCE

Routine overhauls are infrequent and high efficiency is maintained for long periods.

17 QUICK RESPONSES TO CHANGING DEMAND

A fluidized bed combustor can respond to changing heat demands more easily than stoker fired systems. This makes it very suitable for applications such as thermal fluid heaters, which require rapid responses.

18 HIGH EFFICIENCY OF POWER GENERATION

By operating the fluidized bed at elevated pressure, it can be used to generate hot pressurized gases to power a gas turbine. This can be combined with a conventional steam turbine to improve the efficiency of electricity generation and give a potential fuel savings of at least 4%.

5.4. ASH HANDLING SYSTEM:

5.4.1: BOTTOM ASH REMOVAL:

In the FBC boilers, the bottom ash constitutes roughly 30 - 40 % of the total ash, the rest being the fly ash. The bed ash is removed by continuous over flow to maintain bed height and also by intermittent flow from the bottom to remove over size particles, avoid accumulation and consequent defluidization. While firing high ash coal such as washery rejects, the bed ash overflow drain quantity is considerable so special care has to be taken.

5.4.2 FLY ASH REMOVAL:

The amount of fly ash to be handled in FBC boiler is relatively very high, when compared to conventional boilers. This is due to elutriation of particles at high velocities. Fly ash carried away by the flue gas is removed in number of stages; firstly in convection section, then from the bottom of air preheater/economizer and finally a major portion is removed in dust collectors. The types of dust collectors used are cyclone, bagfilters, electrostatic precipitators (ESP's) or some combination of all of these. To increase the combustion efficiency, recycling of fly ash is practiced in some of the units.

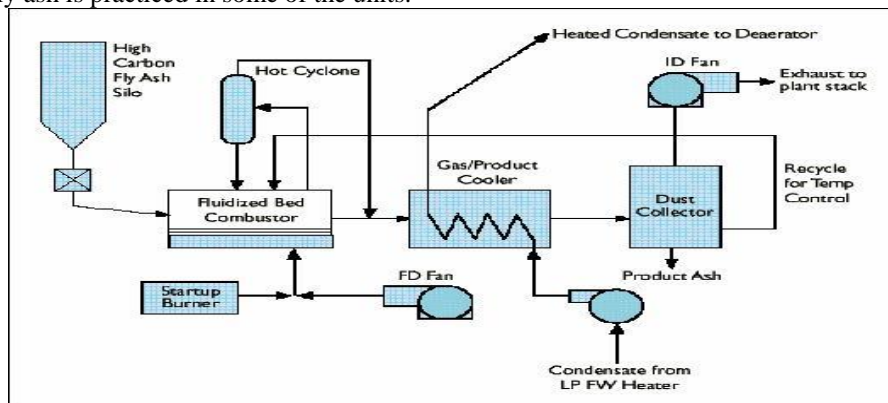


Fig 15: Fly Ash Removal

5.5 SUPERHEATER:

Steam superheaters are widely used in steam generators and heat-recovery steam generators (HRSGs). Their purpose is to raise steam temperature from saturation conditions to the desired final temperature, which can be as high as 550°C in some cases. When used in steam turbines, superheated steam decreases steam heat rate of the turbine and thus improves the turbine and overall plant power output and efficiency. Also, steam conditions at the steam turbine exit will have little or no moisture, depending on the pressure ratio; moisture in the last few stages of a steam turbine can damage the turbine blades. This article outlines some of the design considerations and performance aspects of super heater. A superheater is a device used to convert saturated steam or wet steam into dry steam used for power generation or processes. There are three types of superheaters namely: radiant, convection, and separately fired. A superheater can vary in size from a few tens of feet to several hundred feet.

- A radiant superheater is placed directly in the combustion chamber.
- A convection superheater is located in the path of the hot gases.
- A separately fired superheater, as its name implies, is totally separated from the boiler.

A superheater is a device in a steam engine, when considering locomotives, that heats the steam generated by the boiler again, increasing its thermal energy and decreasing the likelihood that it will condense inside the engine. Superheaters increase the efficiency of the steam engine, and were widely adopted. Steam which has been superheated is logically known as superheated steam; non-superheated steam is called saturated steam or wet steam. Superheaters were applied to steam locomotives in quantity from the early 20th century, to

most steam vehicles, and to stationary steam engines. This equipment is still an integral part of power generating stations throughout the world.

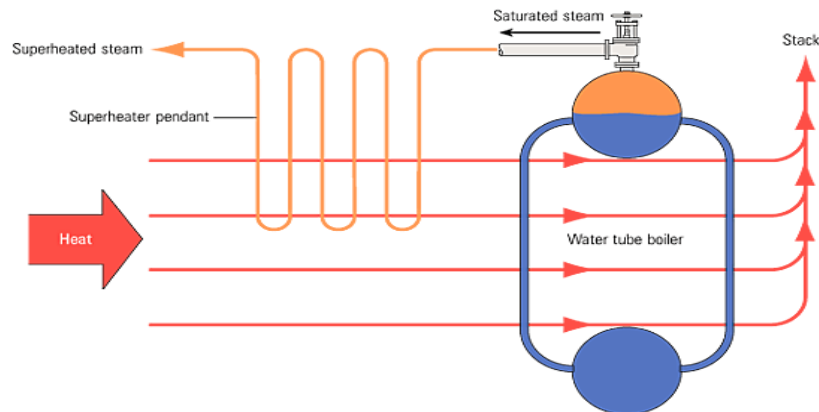


Fig 16: A Water Tube Boiler With A Superheater

5.5.1 ADVANTAGE & DISADVANTAGES:

The main advantages of using a superheater are reduced fuel and water consumption but there is a price to pay in increased maintenance costs. In most cases the benefits outweighed the costs and superheaters were widely used. An exception was shunting locomotives (switchers). British shunting locomotives were rarely fitted with superheaters. In locomotives used for mineral traffic the advantages seem to have been marginal. For example, the North Eastern Railway fitted superheaters to some of its NER Class P mineral locomotives but later began to remove them.

Without careful maintenance superheaters are prone to a particular type of hazardous failure in the tube bursting at the U-shaped turns in the superheater tube. This is difficult to both manufacture, and test when installed, and a rupture will cause the superheated high-pressure steam to escape immediately into the large flues, then back to the fire and into the cab, to the extreme danger of the locomotive crew.

5.6 ECONOMIZER:

In boilers, economizers are heat exchange devices that heat fluids, usually water, up to but not normally beyond the boiling point of that fluid. Economizers are so named because they can make use of the enthalpy in fluid streams that are hot, but not hot enough to be used in a boiler, thereby recovering more useful enthalpy and improving the boiler's efficiency. They are a device fitted to a boiler which saves energy by using the exhaust gases from the boiler to preheat the cold water used to fill it.

A feedwater economizer reduces steam boiler fuel requirements by transferring heat from the flue gas to incoming feedwater. Boiler flue gases are often rejected to the stack at temperatures more than 100°F to 150°F higher than the temperature of the generated steam. Generally, boiler efficiency can be increased by 1% for every 40°F reduction in flue gas temperature. By recovering waste heat, an economizer can often reduce fuel requirements by 5% to 10% and pay for itself in less than 2 years. The table provides examples of the potential for heat recovery. Economizers or economisers are mechanical devices intended to reduce energy consumption, or to perform another useful function like preheating a fluid. The term economizer is used for other purposes as well. Boiler, powerplant, and heating, ventilating, and air-conditioning (HVAC). In boilers, economizers are heat exchange devices that heat fluids, usually water, up to but not normally beyond the boiling point of that fluid. Economizers are so named because they can make use of the enthalpy in fluid streams that are hot, but not hot enough to be used in a boiler, thereby recovering more useful enthalpy and improving the boiler's efficiency. They are a device fitted to a boiler which saves energy by using the exhaust gases from the boiler to preheat the cold water used to fill it (the feed water).

METHODOLOGY:

- (1) I adopted for the conduct of my Project study was basically Survey and Observation.
- (2) it was relatively easy for me to understand the working and operations of the plant, but still there were many areas
- (3) I was quite unacquainted with and hence had to take help and assistance from text books, journals, magazines and reference material provided by Birla Corporation Limited, Birla vikas cement.27MW thermal power plant.
- (4) I studied the operations of the power plant 1x27, and was able to explore and identify the various avenues and areas related to energy conservation and waste reduction.

- (5) My focus of study was to enhance the Thermal efficiency of Boiler at different stages of working cycle by unburnt carbon .
- (6) I went on to studying the various aspects of the working of a Thermal Power Plant. Keeping in mind the need of today that is the methods and measures adopted by Organizations and Government initiatives.
- (7) I thought why not study the factors responsible for achieving and improving thermal efficiency in 27MW coal fired power plants.

A NOTE ON THERMAL ENERGY CONSUMPTION

• **SATNA CEMENT WORKS :**

Specific fuel consumption depend on various factors like Coal quality with respect to

- (1) Calorific value,
- (2) Ash content and
- (3) Moisture content.

Specific Fuel consumption in terms of Kcal/kg Clinker was more during the year 2008-2009, while percentage consumption of coal was lowest. This is due to more UHV and low coal ash content in coal during this year, as compared to other two years. In 2009-2010, fuel consumption was more than 2008-2009, due to low UHV of coal than previous and manufacturing Low Alkali sulphate resistant Cement for Export. To Produce Low Alkali Clinker, Fuel consumption increases due to running of Alkali By-pass System to extract Alkali dust from Kiln inlet at 1000 °C. A Comparative table below confirms above statement.

	Unit	2009-2010	2010-2011	2011-2012
Specific Heat Consumption	Kcal/kg Clkr	754	760	746
Coal Consumption	Kg/hr	20209	20152	20082
Specific Heat of Coal (UHV)	Kcal/kg coal	4089	4223	4145
Ash Content	%	31.97	30.97	31.22
Moisture Content	%	2.89	2.92	3.24
Coal Consumption	Tons/day	14459245	14459152	14459040

CASE STUDY:

• **ECONOMIZER:**

Specification Box Econ. Rev.1, 04.04.2012

Boiler Economizer Specification – Rectangular Design

This specification defines the minimum requirements that must be met for the design and fabrication of vertical gas flow, horizontal tube economizers. No deviation from this specification is permissible without documented approval.

I. Description of Operation

The purpose of the equipment is to recover waste heat using the established principle of a gas to liquid heat exchanger. The economizer should be a bare, welded, or extruded finned tube coil assembly installed either inside or parallel to the boiler exhaust stack or duct. Feedwater under pressure will circulate in the tubes of the coil and heat will be transferred from the flue gases to the water.

II. The Heat Exchanger

- Furnish economizer, as described below, to recover waste heat from the boiler exhaust stack.
- The economizer shall be a rectangular box type, completely packaged unit, utilizing bare tube or extended surface.
- The economizer shall be counterblow type arranged to allow the boiler exhaust gas to travel vertically upward, while the feed water travels vertically downward (or vice versa).
- Structural steel, inlet and outlet transitions, when required, shall be provided with the economizer. The structural steel shall be designed to support the economizer, inlet and outlet transition, and stack.

III. Construction Features

- All pressure parts shall conform to the applicable provisions of the current ASME Power Boiler Code. The economizer shall be properly name plated and code stamped. The design pressure shall meet or exceed the design pressure of the boiler.
- Tubes shall of the welded type, 2” O.D. with a minimum wall thickness of .120”.

- Return bends shall be cold bent or manufactured by a forging process. Cold bends shall be assumed to have a 30% thin out or less for code calculation purposes; hot forged bends shall have no thin out of wall thickness. Headers shall be SA 106 B material, Sch. 80 minimum. Vent, drain, and safety relief valve connections shall be a minimum of ¾” npt and shall include a plug.
- The method of tube-to-header attachment shall be welded. Compression fittings, as they are not an accepted Section I joint, shall not be used.
- All coils shall be completely drainable by gravity.
- Method of tube supports shall allow for free flow of hot gases around the welds, return bends and manifolds. The outlet feedwater temperatures shall be at least 30°F below the saturation temperature. The tubes shall be arranged for tube internal acid cleaning, and tube external soot blowing (for fuels other than natural gas).
- For fuels other than natural gas, the economizer shall be provided with a soot blower lane, soot blower wall box (es), and distal bearings. Soot blowers shall be installed transverse to the tubes.
- A gas tight inner seal welded 10 Ga. steel shall be insulated and covered with 30 Ga. thick corrugated, galvanized, carbon steel metal lagging.
- **Finned tubes:**
 1. The tube pitch shall be square to ensure ease in cleaning for fuels other than natural gas or the equivalent in which case triangular (staggered) tube pitch is allowable.
 2. Fin pitch shall be: 6 fins/inch for natural gas, 4 fins/inch for #2 fuel oil, and 3 fins/inch for #6 fuel oil. For solid fuels such as coal or wood, a maximum of 2 fins/inch shall be used.
 3. The fin attachment shall be by high frequency weld process. Tension wrapped, embedded, or brazed finned tubes are not acceptable.
 4. The fin material shall be carbon steel.
 - All exterior surfaces not galvanized shall be painted with high temperature black paint.
 - Economizer shall be protected to prevent damage during shipping.
 - Maximum allowable pressure drops will be 15 PSIG for the feedwater and 1.5” W. C. for the flue gas.
 - Insulation shall be 8 lb density mineral wool and of sufficient thickness to yield a skin temperature no greater than 140°F.
 - As a minimum, 10% of the tube to tube welds will be radiographed.
 - The economizer’s performance, while in a commercially clean condition, shall be guaranteed by the manufacturer.
 - Three sets of operating and instruction manuals shall be furnished at time of shipment to include: ASME Code Report; material test reports; nameplate facsimile; economizer assembly drawings; other as required by customer or engineering specifications.
 - Economizer shall be designed to operate at 100 percent load without bypassing any flue gas or feedwater.

TECHNICAL DATA

OBSERVATION

27MW Coal Fired Thermal Power Plant

- (1) Capacity of boiler = 65 TPH X 2 = 130 TPH
- (2) Type of Boiler = Coal Fired, Semi door, Natural draught, Balanced draft, Single drum, Water Tube
- (3) Type of Combustion = Atmospheric Fluidized Bed Combustion
- (4) Pressure of superheated steam = 86.4 Bar
- (5) Temperature of superheated steam = 505⁰ C
- (6) Temperature of feed water = 188⁰ C
- (7) G.C.V. of Coal = 16568.64 KJ /Kg (3960Kcal/kg)
- (8) N.C.V. of Coal = 15878.28 KJ/Kg
- (9) Gas plenum Pressure At furnace = - 1.8 mm WC
- (10) Oxygen level = 4.8%
- (11) Ash content in coal = 45-52%
- (12) Temperature of Flue Gases leaving in chimney = 138⁰ C
- (13) Temperature of Boiler house = 32⁰ C
- (14) Total steam generated (m_s)=103416 Kg/Hr
- (15) Total coal consumption (m_f)= 20082 Kg/Hr
- (16) Output of station = 24.33 MW

(17) FOR ECONOMIZER

- a. Inlet temperature of feed water = 188⁰C
- b. Outlet temperature of feed water = 293⁰C
- c. Inlet temperature of Flue gases = 550⁰C
- d. Outlet temperature of Flue gases = 243⁰C
- e. Inlet draught = -4 mmWC
- f. Outlet draft = - 34.8 mmWC

(18) FOR SUPERHEATER

- a. Inlet temperature of flue gases = 575⁰C
- b. outlet temperature of flue gases = 550⁰C
- c. primary heat transfer = pendent convective type
- d. secondary heat transfer = radiant type

(19) FOR REHEATER

- a. inlet temperature of steam = 423⁰C
- b. outlet temperature of superheated steam = 502⁰C
- c. pressure of superheated steam = 84.4 kg/cm²

(20) FOR STEAM CONDENSER

- a. inlet pressure of steam = -0.88 mmWC
- b. outlet pressure of steam = -0.88 mmWC
- c. inlet temperature of steam = 48.26 kg/cm²
- d. outlet temperature of steam = 49⁰C

(21) FOR STEAM TURBINE

- a. inlet pressure of superheated steam = 82.88 kg/cm²
 - b. exit pressure of steam = 0.43 kg/cm²
 - c. inlet temperature of superheated steam = 500⁰C
 - d. inlet temperature of superheated steam = 48⁰C
 - e. steam turbine heat rate = 2631 kcal/kwh
 - f. speed of steam turbine = 7059 rpm (rated)
- (22) speed of generator = 1500 rpm (rated)

(23) FOR BOILER NO. 1

- a) Mass of steam (m_s)= 1343 T/day=55958 Kg/Hr
- b) Mass of Coal consumption (m_f)= 260.8 T/day= 10866 Kg/Hr
- c) Mass of Gases formed = 76392 Kg/Hr
- d) Mass of Unburnt Coal = 472 Kg/ Hr
- e) Excess air for combustion = 61 T/hr to 56 T/Hr

(24) FOR BOILER NO 2

- a) Mass of steam (m_s)= 1139 T/day=47458 Kg/Hr
- b) Mass of Coal consumption (m_f)= 221.2 t/day= 9216Kg/Hr
- c) Mass of Gases formed = 70534 Kg/Hr
- d) Mass of Unburnt Coal = 390 Kg/ Hr
- e) Excess air for combustion = 60 T/hr to 55 T/Hr

CALCULATION:

• **FOR BOILER NO 1**

We know that

- 1. Pressure of superheated steam (P) = 86.4 kg/cm²
- 2. Temperature of superheated steam (T) = 505⁰C
- 3. Mass of steam (m_s) = 55958 Kg/Hr
- 4. Mass of coal (m_f) = 10866 Kg/hr
- 5. C.V. of Coal = 16568.64 KJ/Kg

To calculate

- 1. Equivalent evaporation (E)= ?
- 2. Boiler Efficiency = ?
- 3. Heat Balance Sheet=?

We know that:

Equivalent evaporation (E)= $\frac{me (h_{sup} - h_{f1})}{2257}$ kg /kg of coal

$$\text{Boiler efficiency } (\eta_{\text{boiler}}) = \frac{m_s (h_{\text{sup}} - h_{f1})}{m_f \times \text{CV of coal}} \times 100$$

From steam table

For superheated steam at P= 86.4 bar , Temperature =505^oC

Enthalpy of steam (h_{sup}) = 3390.5 KJ/Kg

Enthalpy of feed water at 188^oC

$$h_{f1} = 1 \times 4.184 (188-0)$$

$$h_{f1} = 786.59 \text{ KJ/Kg}$$

Equivalent mass (m_e)

$$m_e = \frac{\text{mass of steam}}{\text{mass of coal}} \text{ kg/kg of coal}$$

$$m_e = \frac{55958}{10866}$$

$$m_e = 5.149 \text{ kg/kg of coal}$$

(1) EQUIVALENT EVAPORATION (E)

$$\text{Equivalent evaporation (E)} = \frac{m_e (h_{\text{sup}} - h_{f1})}{2257} \text{ kg /kg of coal}$$

$$E = \frac{5.149 (3390.5 - 786.59)}{2257}$$

$$E = \frac{5.149 \times 2603.91}{2257}$$

$$E = 5.94 \text{ Kg/Kg of coal}$$

BOILER (1)EFFICIENCY (η_{boiler})

$$\text{Boiler efficiency } (\eta_{\text{boiler}}) = \frac{m_s (h_{\text{sup}} - h_{f1})}{m_f \times \text{CV of coal}} \times 100$$

$$\eta_{\text{boiler}} = \frac{55958 (3390.5 - 786.59)}{10866 \times 16568.64} \times 100$$

$$\eta_{\text{boiler}} = \frac{55958 \times 2603.91}{180034842.24} \times 100$$

$$\eta_{\text{boiler}} = \frac{145709595.78}{180034842.24} \times 100$$

$$\eta_{\text{boiler}} = 80.93 \%$$

(2) HEAT BALANCE SHEET :

HEAT SUPPLIED	KJ	HEAT UTILISATION	KJ	% UTILISATION
Heat supplied by coal (Kg / hr)	Q _s = m _f X CV of coal Q _s = 180034842.24	(1)heat utilized to generate superheated steam	Q ₁ = m _s (h _{sup} - h _{f1}) = 145709595.78	80.93%
		(2)heat carried by dry flue gases	Q ₂ = 8907074	4.94%
		(3)heat lost due to unburnt coal	Q ₃ = 7820398	4.34%
		(4)heat lost due to convection & radiation	Q ₄ = 17597774.14	9.77%

(1) Heat supplied :

$$Q_s = m_f \times \text{CV of coal}$$

$$Q_s = 10866 \times 16568.64$$

$$Q_s = 180034842.24 \text{ KJ}$$

(2) Heat utilized to generate superheated steam

$$Q_1 = m_s (h_{\text{sup}} - h_{f1})$$

$$Q_1 = 55958 (3390.5 - 786.59)$$

$$Q_1 = 145709595.78 \text{ KJ}$$

(3) Heat carried by dry flue gases

$$Q_2 = m_g \times C_{pg} (T_g - T_a)$$

$$= 76390 \times 1.1 (138-32)$$

$$Q_2 = 8907074 \text{ KJ}$$

(4) Heat lost due to unburnt coal

$$Q_3 = m_{uf} \times \text{CV of coal}$$

$$= 472 \times 16568.64$$

$$Q_3 = 7820398 \text{ KJ}$$

(5) Heat lost due to convection & radiation

$$Q_4 = Q_s - (Q_1 + Q_2 + Q_3)$$

$$Q_4 = 17597774.14 \text{ KJ}$$

FOR BOILER NO 2

We know that:

- | | | |
|----|--|----------------------|
| 1. | Pressure of superheated steam (P) | = 86.4 bar |
| 2. | Temperature of superheated steam (T) | = 505 ⁰ C |
| 3. | Mass of superheated steam (m _s) | = 47458 Kg/hr |
| 4. | Mass of coal consumption (m _f) | = 9216 Kg/hr |
| 5. | Temperature of feed water (t ⁰ C) | = 188 ⁰ C |
| 6. | C.V. of coal | = 16568.64 KJ/Kg |

CALCULATION:

- (1) Equivalent evaporation (E)=?
- (2) Boiler efficiency (η_{boiler})=?
- (3) Heat balance sheet = ?

From steam table for superheated steam

At P=86.4 bar , T=505⁰C

Enthalpy of superheated steam (h_{sup}) = 3390.5 kJ/Kg

At feed water temperature =188⁰ C

Enthalpy of feed water (h_{f1}) = 1 x 4.184 (188-0)

$$h_{f1} = 786.59 \text{ KJ/Kg}$$

$$m_e = \frac{m_s}{m_f} = \frac{\text{mass of steam}}{\text{mass of coal}}$$

$$m_e = \frac{47458}{9216}$$

$m_e = 5.149 \text{ Kg/kg of coal}$
$h_{sup} = 3390.5 \text{ kJ/Kg}$
$h_{f1} = 786.59 \text{ KJ/Kg}$

(1) EQUIVALENT EVAPORATION (E)

$$E = \frac{m_e (h_{sup} - h_{f1})}{2257}$$

$$E = \frac{5.149(3390.5 - 786.59)}{2257}$$

$$E = 5.94 \text{ kg/kg of coal}$$

(2) BOILER(2) EFFICIENCY (η_{boiler})

$$\eta_{boiler} = \frac{m_s (h_{sup} - h_{f1})}{m_f \times \text{CV of coal}} \times 100$$

$$\eta_{boiler} = \frac{47458 (3390.5 - 786.59)}{9216 \times 16568.64} \times 100$$

$$\eta_{boiler} = \frac{47458 \times 2603.91}{152696586.24} \times 100$$

$$\eta_{boiler} = \frac{123576360.78}{152696586.24} \times 100$$

$$\eta_{boiler} = 80.93\%$$

(3) **HEAT BALANCE SHEET :**

Heat Supplied	KJ	Heat utilized	KJ	% Utilised
Heat supplied by coal (Kg per hour)	$Q_s = m_f \times CV$ of coal =152696586.24	1.Heat utilized to generate superheated steam	=123576360.78	80.93%
		2.Heat carried by dry flue gases	$Q_2 = m_g \times C_{pg}(T_g - T_a)$ =8224264.4	5.38%
		3.Heat lost due to unburnt coal	$Q_3 = m_{uf} \times CV$ of coal =6461769.60	4.235%
		4.Heat lost due to convection & radiation	$Q_4 = Q_s - (Q_1 + Q_2 + Q_3)$ =14434191.46	9.46%

Heat supplied by coal

$Q_s = m_f \times CV$ of coal

$Q_s = 9216 \times 16568.64$

$Q_s = 152696586.24$ KJ

(1) Heat utilized to generate superheated steam

$Q_1 = m_s (h_{sup} - h_{f1})$

$Q_1 = 47458 \times (3390.5 - 786.59)$

$Q_1 = 47458 \times 2603.61$

$Q_1 = 123576360.78$ KJ

(2) Heat carried by dry flue gases

$Q_2 = m_g \times C_{pg}(T_g - T_a)$

$Q_2 = 70534 \times 1.1 (138 - 32)$

$Q_2 = 8224264.4$ KJ

(3) Heat lost due to unburnt coal

$Q_3 = m_{uf} \times CV$ of coal

$Q_3 = 390 \times 16568.64$

$Q_3 = 6461769.60$ KJ

(4) Heat lost due to convection & radiation

$Q_4 = Q_s - (Q_1 + Q_2 + Q_3)$

$Q_4 = 152696586.24 + 123576360.78 + 8224264.4 + 6461769.60$

$Q_4 = 14434191.46$ KJ

**• COAL SAMPLE GAVES BY WEIGHT PER KG OF COAL (PER KG OF COAL/HR) :
PERCENTAGE VOLUMETRIC ANALYSIS OF SAMPLE OF FLUE GASES OF 27 MW COAL
FIRED POWER PLANT OF BCL,SATNA**

CO₂ = 12%

CO = 0.7%

O₂ = 7.8%

N₂ = 79.5% (by difference)

& GRAVIMETRIC % ANALYSIS OF COAL PER HR

C = 55%

H₂ = 3.5%

O₂ = 4.7%

Incombustible = 36.8% (by difference)

CALCULATION :

(1) Weight of dry flue gases per kg of coal per hr

(2) Weight of excess air per kg of coal per hr

• WEIGHT OF EXCESS AIR PER KG OF COAL PER HR

ELEMENT ,WT (kg)	O2 used	DRY PRODUCT
C= 0.55	$0.55 \times 8/3 = 1.47$	$0.55 \times 11/3 = 2.017(\text{CO}_2)$
H ₂ = 0.035	$0.035 \times 8 = 0.28$	
O ₂ = 0.047	-----	

Total O₂ = 1.75 kg

(i) **Minimum weight of air needed for combustion =**
 = $1.75 \times 100/23$
 Min. air = 7.61 Kg
 Excess air supplied is about 10%
 = 7.61×0.10
 = 0.761 kg

Total air supplied for combustion = Min. air + Excess air
 = $7.61 + 0.761$
 = 8.371 Kg

Weight of N₂ in flue gases
 = $8.371 \times 77/100$
 = 6.44 kg

Minimum weight of air needed = $(1.75 - 0.047) \times 100/23$
 = 7.404 Kg

• **WEIGHT OF DRY FLUE GASES PER KG OF COAL PER HR:**

Name of gas	Volume per m ³ of DFG (x)	Molecular wt (y)	Relative volume Z= xy	Wt. per kg of DFG Z=Z/ ΣZ
CO ₂	0.12	44	5.28	0.1746
CO	0.007	28	0.196	0.00648
N ₂	0.795	28	22.26	0.7364
O ₂	0.078	32	2.496	0.08257

$\Sigma Z = 30.23$

Amount of carbon present per kg of gases=

Amount of carbon in 0.1746 kg of CO₂ + Amount of carbon in 0.00648 kg of CO
 = $3/11 \times 0.1746 + 3/7 \times 0.00648$
 = $0.04762 + 0.00278$
 = 0.0504 kg

Also,

Carbon in coal = 0.55 kg

Weight of DFG per kg of coal/hr
 = [wt of C in 1 kg of coal] / [wt of C in 1 kg of flue gas]
 = $0.55 / 0.0504$
 = 10.91 kg

Weight of excess oxygen per kg of DFG
 = $0.09524 - 4/7 \times 0.00648$
 = $0.09524 - 0.0037$
 = 0.9154 kg [allowing for unburnt carbon monoxide]

Weight of excess oxygen = 10.91×0.09154
 = 0.9987 ≈ 1 kg

Weight of excess air = $1 \times 100/23$

Weight of excess air= 4.35 kg

• **OVERALL PLANT EFFICIENCY :**

At full load on turbine =24330 kW ,& total coal burnt = 20082 kg/hr

Total mass of coal = $47458 + 9216 = 20082$ Kg/hr

$$\eta_{\text{overall}} = \frac{\text{output of station} \times 860}{\text{coal burnt} \times \text{cv of coal}} \times 100$$

$$\eta_{\text{overall}} = \frac{24330 \times 860}{20082 \times 3960} \times 100$$

$$\eta_{\text{overall}} = 26.31 \%$$

Where 860 is the conversion factor which makes both numerator & denominator in same unit

But in the Birla Corporation Limited 27MW Thermal power Plant

Power generation is 24330 KW

Total coal burnt = 20082 – (472+390)

= 20082 - 862

$$m_f = 19220 \text{ kg/hr}$$

$$\eta_{\text{overall}} = \frac{\text{output of station} \times 860}{\text{coal burnt} \times \text{cv of coal}} \times 100$$

$$\eta_{\text{overall}} = \frac{24330 \times 860}{20082 \times 3960} \times 100$$

$$\eta_{\text{overall}} = \frac{20923800}{79409880} \times 100$$

$$\eta_{\text{overall}} = 26.34 \%$$

MODIFICATION:

For Boiler No. 1

Total combustion of coal = 10866 - (unburnt coal X 0.01)

$$m_f = 10866 - (472 \times 0.01)$$

$$m_f = 10866 - 47.2$$

$$m_f = 10861.287 \text{ kg/hr}$$

Increases in boiler efficiency

$$\eta_{\text{boiler}} = \frac{ms (hsup - hf1)}{mf \times CV \text{ of coal}} \times 100$$

$$\eta_{\text{boiler}} = \frac{55958 (3390.5 - 786.59)}{10861.287 \times 16568.64} \times 100$$

$$\eta_{\text{boiler}} = \frac{145709595.78}{179956638.3} \times 100$$

$$\eta_{\text{boiler}} = 80.96 \%$$

• **Increase s in boiler (1) efficiency**

Increase s in boiler efficiency= 80.96 - 80.93

$$\text{Increases in boiler (1) efficiency} = 0.03\% \text{ to } 0.06\%$$

Increase in efficiency upto 0.03 % to 0.06%

• **In Boiler No. 2**

Total combustion of coal = 9216 - (unburnt coal X 0.01)

$$m_f = 9216 - (390 \times 0.01)$$

$$m_f = 9216 - 3.9$$

$$m_f = 9212.1 \text{ kg/hr}$$

Increases in boiler efficiency

$$\eta_{\text{boiler}} = \frac{ms (hsup - hf1)}{mf \times CV \text{ of coal}} \times 100$$

$$\eta_{\text{boiler}} = \frac{47458 (3390.5 - 786.59)}{9212.1 \times 16568.64} \times 100$$

$$\eta_{\text{boiler}} = \frac{123576360.8}{152631968.5} \times 100$$

$$\eta_{\text{boiler}} = 80.96 \%$$

• **Increase s in boiler (2) efficiency:**

Increase s in boiler efficiency= 80.96 - 80.93

$$\text{Increases in boiler (2) efficiency} = 0.03\% \text{ to } 0.06\%$$

• **INCREASES IN OVERALL PLANT EFFICINCY**

$$\eta_{\text{overall}} = \frac{\text{output of station (KW)} \times 860}{\text{coal burnt} \times \text{CV of coal}} \times 100$$
$$\eta_{\text{overall}} = \frac{24330 \times 860}{20073.38 \times 3960} \times 100$$
$$\eta_{\text{overall}} = \frac{20923800}{79490584.8} \times 100$$

$$\eta_{\text{overall}} = 26.32\%$$

Increase in Overall plant Efficiency in %

increase in overall efficiency = 26.32 – 26.31

$$\text{increase in overall plant efficiency} = 0.01\% \text{ to } 0.02\%$$

RESULT & DISCUSSION

• RESULT:

- (1) Efficiency of boiler (1) = 80.93%
- (2) Efficiency of boiler (2) = 80.93 %
- (3) Overall plant efficiency = 26.31 %

After modification

- (1) Efficiency of boiler (1) = 80.93% to 80.99%
- (2) Efficiency of boiler (2) = 80.93 % to 80.99%
- (3) Overall plant efficiency = 26.31 % to 26.32%

Increase in boiler efficiency is from 0.03 to 0.06%

➤ Increases in overall plant efficiency is 0.01 % to 0.02%

• DISCUSSION :

If the excesses air supplied is very large amount then the ignition temperature required for combustion of coal is decrease which effect the combustion efficiency of coal is reduced and due to this losses in boiler is maximized & formation of carbon monoxide is increase. So quantity of excess air is to maintained. And furnace draft pressure is also effect the combustion of coal. The furnace draft pressure is maintained about the balanced draft.

REFERENCES

- [1]. Thermal Power Technology By Dr. V.K. Sethi , First Edition, Chapter3 page no. 23,chapter no. 4,page no.53,
- [2]. Energy Conversion System –I, By Bhupendra Gupta, Second Edition Chapter No. 1, page no. 5, page no. 17
- [3]. Thermal Engg. By R.K. Rajput, chapter no. 10,page no.496,chapter no.11 page no.555, page no. 558,chapter no. 12,page no. 580, page no. 583
- [4]. Power plant Technology by G.D. Rai, edition third(2003), chapter no. 7 page no.241,page no.246 ,chapter no. 3, page no. 193,page no. 207
- [5]. www.birlacorporationlimited.com/27mwtpusatna, paragraph 3
- [6]. Data from 27MW thermal power plant of BCL, satna
- [7]. Bullock, A., 2010, Ash Handling: Why Dry Bottoms are better than Wet Bottoms, Power-Gen Worldwide, May 1.
- [8]. NETL, 2009c, Opportunities to Improve the Efficiency of Existing Coal-Fired Power Plants, Workshop Report, July 15–16.
- [9]. Congressional Research Service, Increasing Efficiency of Coal-Fired Power Plants, Richard J. Campbell, December 20, 2013
Topper, J. (2011), Status of Coal Fired Power Plants ,World-Wide, Joint IEA-CEA Workshop on High Efficiency, Low Emission (HELE) Roadmap, New Delhi, India, 29 November, www.iea.org/media/workshops/2011/cea/Topper.pdf
- [10]. Energy Analysis and Efficiency Improvement of a Coal Fired Thermal Power Plant By R. Mahamud, M.M.K. Khan, M.G. Rasul and M.G. Leinster.

FPGA Based Power Efficient Channelizer For Software Defined Radio

Ms. Anuradha S.Deshmukh¹, Ms. Kalpana U. Pandey², Mr. Roshan P. Ghodkhande³

^{1, 2,3}Data Meghe Institute Of Engineering & Tech.Sawangi (Meghe)

ABSTRACT: Multiple communication channel support in RF transmission, such as that in a Software Defined Radio (SDR) warrants the use of channelizers to extract required channels from the received RF frequency band and to perform follow-on baseband processing. This paper describes the process of channelization as it applies to low power and high-efficiency applications in wireless and Satellite Communications (SATCOM) domains. Smaller bandwidths and changing requirements of bandwidth calls for a programmable channel selection mechanism whereby channels and the resulting bandwidth can be selected based on target application, which is the primary principle in the Software Defined Radio based systems.

Keywords: Software defined radio, Channelization, Digital filter banks, Reconfigurability . Low complexity

I. INTRODUCTION

A software-defined radio (SDR) system is a radio communication system which can tune to any frequency band and receive any modulation across a large frequency spectrum by means of a programmable hardware which is controlled by software. A Software radio is an enabling technology for future radio transceivers, allowing the realisation of multi-mode, multi-band, and reconfigurable base stations and terminals. However, considerable research efforts and breakthroughs in technology are required before the ideal software radio can be realised. The basic idea of SDR is to replace the conventional analog signal processing in radio transceivers by digital signal processing by placing the analog to digital converter (ADC) in receivers as close to the antenna as possible. Thus SDR should be able to support multiple communication standards by dynamically reconfiguring the same hardware platform. Also, SDR should be able to use the same architecture for any number of channels by simply reconfiguring the digital front-end as compared to a conventional radio transceiver whose complexity grows linearly with the number of received channels.

In this paper, we review some of the existing digital filter banks and investigate the potential of these filter banks for channelization in multi-standard SDR receivers. We also present two of our low complexity, reconfigurable filter bank architectures for SDR channelizers.

II. OBJECTIVES OF THE PROPOSED TOPIC

The overall objective of this work has been to develop a low-power Channelizer design that can be implemented on FPGA device. The design consists of schematic entry and RTL descriptions in Verilog. Specific tasks include:

1. Improvements of Polyphase Channelizer.
2. Efficient M-Path Polyphase channelization architecture is designed for highly efficient and low-cost (power and area) designs.
3. For providing a complete solution to the problem on hand, we need to address two aspects: 1) Programmability and 2) Low-Power and efficient design techniques. In a channelizer design, we need to perform basic channelization and secondary signal processing operations.

2.1. FILTER BANKS FOR SDR CHANNELIZERS

In this section, we review existing digital filter banks and discuss their suitability for channelization in SDR receivers.

1. Per-Channel (PC) Approach

The PC approach is based on a parallel arrangement of many one-channel channelizers. Each one-channel channelizer performs the channelization process. The PC approach is a straight forward approach and hence relatively simple. But the main drawback is that, the number of branches of filtering-DDC-SRC is directly proportional to the number of received channels. Hence the PC approach is not efficient when the number of received channels is large. Furthermore, if the channels are of uniform bandwidth, a filter bank approach would be a cost-effective solution than the PC approach. Its hardware cost is very high, which has led to the development of DFT filter banks.

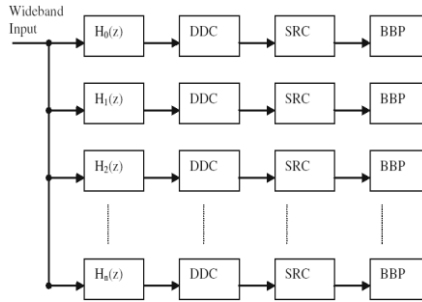


Figure 3 Per-Channel approach based channelization.

2. DFT Filter Banks

DFT filter bank is a uniformly modulated filter bank, which has been developed as an efficient substitute for PC approach when the number of channels need to be extracted is more, and the channels are of uniform bandwidth (for example many single-standard communication channels need to be extracted). The main advantage of DFT filter bank is that, it can efficiently utilize the polyphase decomposition of filters.

However, DFTFBs have following limitations for multi-standard receiver applications:

2.1. DFTFBs cannot extract channels with different bandwidths. This is because DFTFBs are modulated filter banks with equal bandwidth of all bandpass filters.

Therefore, for multi-standard receivers, distinct DFTFBs are required for each standard. Hence the complexity of a DFTFB increases linearly with the number of received standards.

2.2. Due to fixed channel stacking, the channels must be properly located for selecting them with the DFTFB. The channel stacking of a particular standard depends on the sample rate and the DFT size. To use the same DFTFB for another standard, the sample rate at the input of the DFTFB must be adapted accordingly. This requires additional sample rate converters (SRCs), which would increase the complexity and cost of DFTFBs.

2.3. If the channel bandwidth is very small compared to wideband input signal the prototype filter must be highly selective resulting in very high-order filter. As the order of the filter increases, the complexity increases linearly. Ideally, the reconfigurability of the filter bank must be accomplished by reconfiguring the same prototype filter in the filter bank to process the signals of the new communication standard with the least possible overhead, instead of employing separate filter banks for each standard. However reconfiguration of DFTFB suffers from following overheads:

1. The prototype filter needs to be reconfigured. Generally DFTFB employs the polyphase decomposition. Hence reconfiguration can involve changing the number of polyphase branches which is a tedious and expensive task.
2. Downsampling factor needs to be changed. If down sampling is to be done after filtering, then we need separate digital down converters. This will add more cost.
3. The DFT needs to be reformulated accordingly which is also expensive.

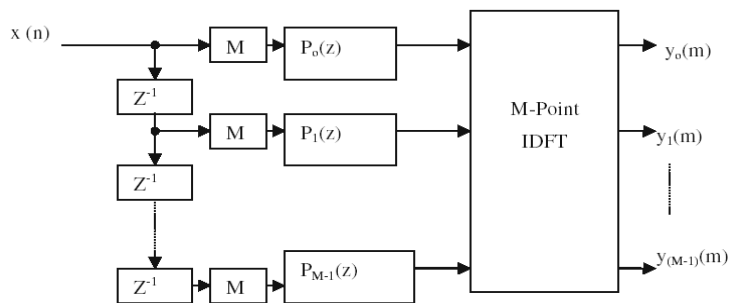


Figure 7 DFT filter bank.

In the case of multiple channel extraction of single standard signal i. e., extraction of many channels of identical bandwidth, the complexity of PC approach is given by $N.L.f_s$, where N is the number of channels extracted, L is the total length of filters employed in all

the branches for PC approach and f_s is the sampling frequency. The complexity of DFTFB is only $L.f_s$ which is N times lower than PC approach. But in the case of SDR, multiple channels of multiple standards need to be extracted.

In that case, the complexity of PC approach and DFTFB are $N.C.s$ and $N.S.s$ respectively, where NC and NS are the number of channels and number of standards respectively. Thus the complexity of these channelizers can be reduced further if (1) the length of filter, L, can be reduced and (2) the same filter bank can be reconfigured to the new standard. Thus there is a need for developing new filter bank architectures for SDR receivers

3. ALTERNATIVE FILTER BANKS

A Goertzel filter bank (GFB) based on modified Goertzel algorithm was proposed in as a substitute to DFTFB. In GFB, the DFT is replaced by a modified Goertzel algorithm which performs the modulation of the prototype low-pass frequency response to any centre frequency which is not possible using DFT. This will eliminate the limitation of fixed channel stacking associated with DFTFBs.

This paper is an attempt towards design of FBs with reduced area complexity and improved reconfigurability when compared with conventional resampling-based FBs. The frequency response masking (FRM) technique was originally proposed for designing low complexity sharp transition-band finite impulse response (FIR) filters. A reconfigurable low complexity channel filter for SDR receivers based on the FRM technique. The objective of the work in was to realize a channel filter to extract a single channel (frequency band) from the wideband input signal.

New low complexity reconfigurable architecture for the modal filter which can simultaneously extract multiple channels is also presented in this paper. The proposed modal filter architecture can generate simultaneous frequency responses employing different delay line adders. Coefficient multiplication, which is the most power consuming operation, is done only once for obtaining different frequency responses simultaneously in the proposed modal filter architecture. Consequently the proposed FB offers low multiplier complexity when compared with other FBs in the literature. The proposed FB has been compared with the conventional PC approach, DFTFB, GFB.

III. FREQUENCY RESPONSE MASKING BASED FILTER BANKS

Ideally, the reconfigurability of the receiver must be accomplished in such a way that the filter bank architecture serving the current communications standard must be reconfigured with least possible overhead to support a new communication standard while maintaining the parallel operation (simultaneous reception/transmission of multistandard channels). To realize a filter bank which can be reconfigured to accommodate multiple standards with reduced hardware overhead, we have proposed a frequency response masking (FRM) based reconfigurable filter bank (FRMFB). The FRM technique was originally proposed for designing application-specific low complexity sharp transition-band finite impulse response (FIR) filters.

Table 1 Comparison of channelization approaches,

Table 1 Comparison of channelization approaches.

Parameter		PC Approach	DFTFB	PFT
Computational complexity	For multiple uniform bandwidth channels	Poor	Excellent	Good
	For multiple non-uniform bandwidth channels	Poor	Poor	Poor
Silicon cost		Poor	Excellent	Good
Initial design flexibility	Independent channels	Yes	No	No
	Number of channels	Selectable	2^N	2^N
Reconfigurability		Poor	Very poor	Poor

IV. REVIEW OF FREQUENCY RESPONSE MASKING APPROACH

In this section, a brief review of the FRM approach is presented. An SDR channelizer consists of a bank of filters known as channel filters for extracting individual channels from the digitized wideband input signal. FIR filters are employed as channel filters because of their linear phase property and guaranteed stability. Sharp transition-band FIR filters are required in the channelizer to meet the stringent wireless communication specifications. In conventional FIR filter designs, higher order filters are required to obtain sharp transition-band.

The complexity of FIR filters increases with the filter order. Several approaches have been proposed for reducing the complexity of FIR filters. In an FRM technique was employed for the synthesis of sharp transition-band FIR filters with low complexity. The advantage of the FRM technique is that the bandwidths of the filters are not altered and the resulting filter will have many sparse coefficients (because the subfilters have wide transition-band) resulting in less complexity.

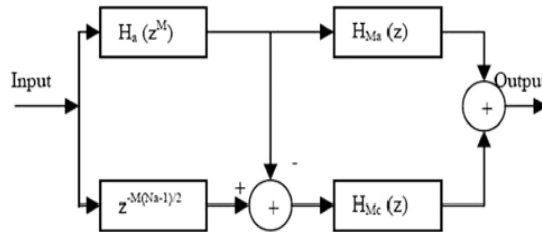


Fig. 1. FIR filter architecture based on FRM technique.

Fig. 1. FIR filter architecture based on FRM technique filters. The basic idea behind the FRM technique is to compose the overall sharp transition-band filter using several wide transition-band subfilters. In this paper, the sharp transition-band filter designed using FRM with necessary modifications has been employed as channel filter in an SDR channelizer.

The FRM approach can be more clearly explained with the help of Fig. 2. Fig. 2(a) represents the frequency response of an LPF $H_a(z)$. The passband and stopband edges of the modal filter are f_{ap} and f_{as} , respectively. The complementary filter of the modal filter $H_c(z)$ is shown in Fig. 2(b). Replacing each delay of $H_a(z)$ and $H_c(z)$ by M delays, two filters $H_a(z^M)$ and $H_c(z^M)$ are obtained, and their frequency responses are shown in Fig. 2(c). Two masking filters $H_{MA}(z)$ and $H_{MC}(z)$ as shown in Fig. 2(d), are used to mask $H_a(z^M)$ and $H_c(z^M)$, respectively. If the outputs of $H_{MA}(z)$ and $H_{MC}(z)$, are added, as shown in Fig. 1, the frequency response of the resulting filter $H(z)$ is shown in Fig. 2(e). Thus a sharp transition-band FIR filter is obtained using four subfilters. Since these subfilters are having wide transition-band specifications, the overall complexity will be much less than direct or conventional design of sharp transition-band FIR filters.

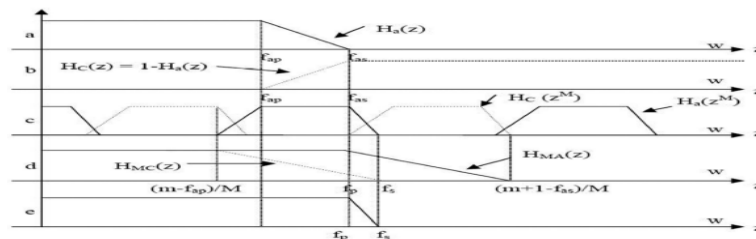


Fig. 2. Frequency response illustration of FRM approach.

In an SDR receiver, the specifications of the channelizer changes as the mode of communication changes. In conventional multi-mode channelizers a separate channelizer is needed for each mode, and reconfigurability is achieved by switching among distinct channelizers. This is not an efficient approach due to its increased hardware complexity and poor resource utilization. In this section, a reconfigurable filter bank is presented for SDR channelizers, which uses two blocks: a common hardware block at the front-end (modal filter) for multiple communication standards and a reconfigurable masking filter at the back-end. The complexity of the FB is dominated by the block at the front-end (as the order of the modal filter is substantially higher than that of the masking filter). Since the front-end hardware in the proposed scheme is the same (common) for all the communication standards, its complexity can be significantly reduced by using fixed-coefficient optimization techniques as in [12], which will ensure low complexity of the overall FB. However, in this paper, the idea discussed in has been extended by including the complete design details, generalized expressions for the modal and masking filters, practical design example, and actual implementation results on FPGA. The conventional FRM technique employs the direct form filter structure and therefore the critical path delay is proportional to filter length. But if transposed direct is employed, the critical path delay can be made independent of the filter length. Hence the transposed direct form is employed in the proposed FB. The proposed channelizer offers reconfigurability at two levels, named

- 1) architectural level, and 2) filter level.

A. Architectural Reconfigurability

The architectural reconfigurability of the FRM-based FB can be illustrated using the expressions (3). Though the proposed architecture is capable of handling multiple modes of communication, for ease of explanation, a dual-mode channelizer is used to illustrate reconfigurability. Let f_{p1} and f_{p2} be the passband frequencies and f_s

and f_{s2} be the stopband frequencies of the channels corresponding to two modes (communication standards) of operation, m_1 and m_2 respectively. Reconfigurability can be achieved by using the same subfilters in Fig. 1 for both the modes. The parameters f_{ap} and f_{as} remain unchanged for both the modes and therefore, the same modal filter is employed for both modes. The masking filters can be reconfigured by modifying the look up table (LUT) values which are explained in detail later. Thus,

$$f_{p1M1} ; b_{fp1M1c} = f_{p2M2} ; b_{fp2M2c} \quad (4)$$

$$f_{s1M1} ; b_{fs1M1c} = f_{s2M2} ; b_{fs2M2c} \quad (5)$$

where M_1 and M_2 denote the upsampling factors for the two modes m_1 and m_2 respectively, which can be obtained by solving (4) and (5). Thus by changing the number of delay elements, the same modal filter can be employed to work for both the modes. It is assumed that the two channels are at baseband or need to be down converted to baseband before filtering. However, the expressions (4) and (5) can be extended to bandpass channels also. The dual-mode channelizer can be extended to incorporate additional communication modes by choosing an appropriate n_{in} in addition to the architectural reconfigurability explained above, each of the subfilters of the proposed FB has been implemented such that they can be reconfigured. This enables the same FB architecture to operate for an entirely new communication standard.

The filter level reconfigurability is explained in the next section.

B. Filter Level Reconfigurability

Filter reconfigurability means changing the coefficients of each filter in Fig. 1 according to the specifications of the new standard. It is well known that one of the efficient ways to reduce the complexity of multiplication operation is to realize

it using shift and add operations. In contrast to conventional shift and add units used in previously proposed reconfigurable filter architectures, a binary common subexpressions (BCSs) based shift and add unit has been employed in the filter architectures.

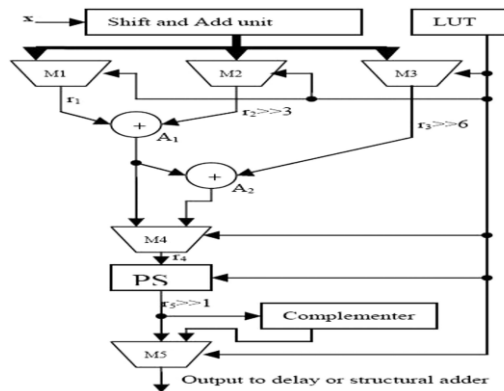


Fig. 3. Proposed reconfigurable filter architecture.

In two new reconfigurable FIR filter architectures based on a binary subexpression elimination (BSE) algorithm has been proposed. The architecture in consisted of a shift and add unit which will generate all the 3-bit BCSs using 3 adders. In this paper, the architecture in is modified for reducing its complexity. In the filter coefficients are stored in a LUT without any coding. As a result of this, if the first few bits are zeros, the adders employed in the architecture are unnecessarily used. The proposed architecture of the filter for an 8-bit coefficient is shown in Fig. 3. M_1 and M_2 are 8 : 1 multiplexers; M_3 is a 4 : 1 multiplexer and M_4 and M_5 are 2 : 1 multiplexers. The input is given to the shift and add unit whose output is shared among the multiplexers.

V. COMPLEXITY COMPARISON

In this section, we present a quantitative comparison of different filter banks reviewed in this paper. Table 2 shows the comparison of the multiplication rate of the PC approach, DFTFB, GFB [5], MPRB our FRMFB and CDFB. Multiplication complexity of a channelizer is defined as the total number of multiplications for extracting N_I number of channels (of same communication standard) simultaneously. The multiplications involved in a channelizer can be grouped into three categories: Multiplications associated with (1) Channel filtering; (2) Digital down conversion and (3) Modulation of filters (this is not applicable for PC approach, FRMFB and CDFB). In Table 1, L represents the number of non-zero coefficients of the prototype filter for the PC approach, DFTFB and GFB, l represents the additional number of non-zero coefficients of the modal filter (because of over design) and masking filters in the proposed CDFB, l_m represents the total number of non-zero coefficients for the modal filter and masking filters in the FRMFB (We have considered only non-zero coefficients as they will only result in multiplication complexity), and F_s represents the sampling frequency.

The multiplication complexities for PC approach, DFTFB and GFB are taken directly from. From Table 2, it is clear that the complexity of PC approach is directly proportional to the number of channels, N_I .

Thus higher the number of channels, the PC approach is not hardware efficient. It can be seen that, the complexity of filtering (multiplication) operation is same for the proposed DFTFB and GFB and slightly higher for CDFB (because of overdesigning and masking filters). The MPRB consists of an analysis DFTFB and a synthesis DFTFB and hence the complexity is exactly twice that of DFTFB. As the FRMFB and CDFB do not require any DFT, there are no modulation complexity associated with FRMFB and CDFB. However separate (N_f-1) digital down converters are required in the FRMFB and CDFB for converting all the channels except the low-pass channel to baseband. We have not considered FFT for the implementation of IDFT in DFTFB and MPRB, as FFT is appropriate only if the number of channels to be extracted is a power-of-two. From

Table 2, it can be seen that the over-all complexity of the proposed CDFB is lower than that of the PC approach, MPRB and GFB. Also, the proposed CDFB is less complex compared to DFTFB, when the number of channels, N_f , increases. The FRMFB has the least filter length because of the wide transition-band subfilters compared to other filterbanks and hence has the least over-all complexity

Table 2 Multiplication rate of channelizers.

	PC Approach	DFTFB	GFB [5]	MPRB [10]	FRMFB [16]	CDFB [19]
Filter	$N_f \cdot L$	L	L	$2L$	lm	$L+1$
DDC	N_f-1	-	-	-	N_f-1	N_f-1
Modulation of filters	-	N_f^2	$N_f \cdot L$	$2N_f^2$	-	-
Sum	$N_f \cdot (L+1)-1$	$L+N_f^2$	$L \cdot (1+N_f)$	$2(L+N_f^2)$	$lm+N_f-1$	$L+1+N_f-1$

However, the design of FRMFB is a tedious task as it follows separate design procedure for each bandpass channel. For the extraction of channels of different standards (non-uniform bandwidth channels), only PC approach and FRMFB can be employed efficiently. Hence for non-uniform bandwidth channel extraction, FRMFB is a very good substitute for PC approach because of former's inherent low complexity and easy reconfigurability. Similarly for the extraction of channels of uniform bandwidth, CDFB is an excellent substitute for DFTFB, GFB and MPRB.

VI. CONCLUSIONS

In this paper, Low complexity and reconfigurability are the two key requirements of filter banks in SDR receivers.

The proposed architecture is inherently less complex and offers two level of reconfigurability: 1) at architectural level and 2) at filter level. The FRM technique is modified to improve the speed and reduce the complexity.

The filter bank based on frequency response masking can be used as an efficient substitute for the per-channel approach and the filter bank .

In future, to increase the flexibility of the proposed reconfigurable FB multistage FRM techniques will be investigated .

REFERENCES

- [1]. Hentschel, T. and Fettweis, G. "Software Radio Receivers," CDMA Techniques for Third Generation Mobile Systems. Norwell, MA: Kluwer Academic Publishers, 1999.
- [2]. Mitola, J. Software Radio Architecture. Hoboken, NJ: Wiley, 2000.
- [3]. Hentschel, T. Channelization for software defined base-stations. Annales des Telecommunications, 5—6 (May—June 2002).
- [4]. Pucker, L. Channelization techniques for software defined radio. Spectrum Signal Processing Inc., Burnaby, B.C., Canada, Nov. 17—19, 2003.
- [5]. Kim, C., Shin, Y., Im, S., and Lee, W. SDR-based digital channelizer/de-channelizer for multiple CDMA signals. In Proceedings of IEEE Vehicular Technology Conference, vol. 6, Sept. 2000, 2862—2869.
- [6]. Fung, C. Y. and Chan, S. C. A multistage filter bank-based channelizer and its multiplier less realization. In Proceedings of IEEE International Symposium on Circuits and Systems, vol. 3, Phoenix, AZ, May 2002,
- [7]. Abu-Al-Saud, W. A. and Stuber, G. L. Efficient wideband channelizer for software radio systems using modulated PR filter banks. IEEE Transactions on Signal Processing, **52**, 10 (Oct. 2004), 2807—2820.
- [8]. Lim, Y. C. Frequency-response masking approach for the synthesis of sharp linear phase digital filters. IEEE Transactions on Circuits and Systems, **33** (Apr. 1986), 357—364.
- [9]. Hartley, R. I. Subexpression sharing in filters using canonic signed digit multipliers. IEEE Transactions on Circuits and Systems-II, **43** (Oct. 1996), 677—688.
- [10]. Peiro, M. M., Boemo, E. I., and Wanhammar, L. Design of high-speed multiplierless filters using a nonrecursive signed common subexpression algorithm. IEEE Transactions on Computer Aided Design of
- [11]. Integrated Circuits and Systems, **49**, 3 (Mar. 2002), [11] Xu, F., Chang, C. H., and Jong, C. C. Contention resolution algorithm for common sub
- [12]. expression elimination in digital filter design. IEEE Transactions on Circuits and Systems-II, (Oct. 2005)

Configurable Monitoring For Multi-Domain Networks

Aymen Belghith¹, Bernard Cousin², Samer Lahoud²

¹University of Sfax, Road of Aeroport Km 0.5, 3029 Sfax, Tunisia

²University of Rennes 1- IRISA, Campus de Beaulieu, 35042 Rennes Cedex, France

ABSTRACT: In this paper, we review the state-of-the-art monitoring architectures proposed for multi-domain networks. We establish the five requirements a multi-domain monitoring architecture must fulfilled. We note that these architectures do not support measurement configuration that enables the providers to perform flexible multi-domain measurements. Therefore, we propose a configurable multi-domain network monitoring architecture in order to give more flexibility in monitoring and solve the heterogeneity and interoperability problems. We also propose two collaboration schemes that can be applied in our configurable monitoring architecture. These collaboration schemes are based on the proactive selection and the reactive selection. We show through extensive simulations that the proactive collaboration scheme provides a more flexible multi-domain monitoring and reduces the delay and the overload of the monitoring establishment.

Keywords: About five key words in alphabetical order, separated by comma

I. INTRODUCTION

Network monitoring is necessary to guarantee precise and efficient management of a network communication system. It is required to control the Quality of Service (QoS) provided by the network. The performance requirements of the services are typically specified through a contract called Service Level Agreement (SLA). In order to guarantee the performance of the services, the network performance has to be verified by performing measurements on well chosen metrics. Once the metrics to be measured are determined, it is required to define the monitoring architecture to be used. A monitoring architecture can be based on standard protocols, proposed for intra-domain networks, or proposed for multi-domain networks.

Many monitoring architectures were standardized such as Real-time Traffic Flow Measurement (RTFM), IP Flow Information eXport (IPFIX), and Packet Sampling (PSAMP). The architecture of RTFM [1] contains four components: a manager that configures the measurement points (meters), a meter that performs the measurements, a meter reader that exports the results, and an analysis application that analyzes the results. The architectures of IPFIX [2] and PSAMP [3] contain three processes: a metering process which performs the measurements, an exporting process which exports the results, and a collecting process which analyzes the results. The major difference between these architectures is that PSAMP exports information about individual packets while IPFIX exports information about flows.

Some monitoring architectures were proposed for intra-domain networks. For example, the monitoring architecture of AQUILA [4] contains three tools: a tool that produces traffic that emulates the traffic generated by the Internet applications, a tool that injects probes into the network to evaluate the performance of a defined path, and a tool that monitors the QoS parameters. The intra-domain monitoring architecture proposed in [5] contains two services: a measurement service that measures a set of metrics and stores the results in a database and an evaluation and violation detection service that retrieves the results from the database, analyzes them, and sends notifications when detecting violations.

All the above architectures do not take into account the multi-domain heterogeneous structure of the network. They suppose that the same set of monitoring services can be provided by any equipment of the network homogeneously and independently of the domain owner of the equipment. This assumption is in general erroneous. Particularly, every domain wants to apply its own policy and its own monitoring process. This requirement is called the autonomously managed domain requirement. Moreover, each domain wants to keep some monitoring processes or measurement results private. This requirement is called the confidential domain requirement.

A domain can be either collaborative or non-collaborative. A domain is collaborative only and only if it is ready to share measurement results as well as information about its measurement points with distant domains. Obviously, when the domains do not collaborate, the networks monitoring becomes more complicated. However, it is very interesting to monitor the services even if the domains are non-collaborative because the assumption that all the domains are collaborative is in general erroneous. This requirement is called the non-collaborative monitoring requirement.

Monitoring is used to extract measurement results for performance analysis and, in multi-domain networks, these measurement results may have to be exchanged between different domains or sent to a third party for aggregation and multi-domain analysis. In order to have efficient and meaningful measurement results, we want to assess in this paper that the export parameters such as the export methods and the export protocols have to be configurable. This requirement is called the adaptive export process requirement. When the export parameters of the different domains are configurable, we can request a domain to modify, for example, its export method in order to have more frequent measurement results for better fault detection.

Due to the heterogeneity of the measurement parameters which can be used by different domains, we want to assess in this paper that the measurement parameters such as the metrics to be measured and the measurement protocols to be used have to be configurable. This requirement is called the adaptive measurement process requirement. This requirement is mandatory especially when active measurements are performed between two domains because these domains have to agree on the measurement process. Moreover, when the measurement parameters of the different domains are configurable, we can modify, for example, the measurement protocol used by two domains without applying any modification on other domains along the path of the monitored service. This modification allows the providers, for example, to use a more efficient measurement protocol without requiring implementing the same measurement protocol in all domains. This configuration capability also offers more flexibility since multi-domain measurements can be provided even if a non-collaborative domain exists in the path of the monitored service. Indeed, multi-domain measurements can be performed measurements between two adjacent domains and these multi-domain measurements require the configuration of these adjacent domains.

In this paper, we propose a configurable multi-domain network monitoring architecture that resolves the heterogeneity problems by providing the adaptive measurement process and the adaptive export process requirements. In this architecture, both the measurement parameters and the export parameters can be configured. For a more efficient monitoring adaptation, we propose that the analysis functional block reacts to anomaly detections and this also could require some adaptations of the monitoring process such as the reconfiguration of the monitoring. Therefore, the measurement parameters and the export parameters have to be reconfigured.

Our monitoring architecture also resolves the confidentiality problems and allows the different domains to use own monitoring processes by providing the confidential domain and the autonomously managed domain requirements, respectively. In order to provide the confidentiality of the domain topology, we propose to perform multi-domain monitoring only between measurement points located at the border of the domains. Furthermore, our monitoring architecture can perform measurements even if all domains are not collaborative by providing the non-collaborative monitoring requirement.

Our work studies functionalities required for multi-domain network monitoring, thus this paper will propose a functional architecture and the relevancy of a proposal has to be evaluated against the five requirements listed previously. Moreover, we propose, in this paper, two collaboration schemes. These collaboration schemes are used by our proposed configurable monitoring architecture in order to select the measurement points participating in the multi-domain monitoring and to configure the different parameters of the selected measurement points. These collaboration schemes are based on the proactive selection and the reactive selection, respectively.

This paper is organized as follows. In section II, we discuss the main architectures already proposed for multi-domain networks. We present our proposals for a configurable multi-domain network monitoring architecture in section III. In section IV, we perform a functional evaluation of our configurable multi-domain monitoring architecture. Section V presents the simulation model and performance evaluations and comparisons of our proposed collaboration schemes. Conclusions are provided in section VI.

II. STATE-OF-THE-ART MONITORING ARCHITECTURES FOR MULTI-DOMAIN NETWORKS

We identify four functional blocks that are used by the current monitoring architectures: a configuration block, a measurement block, an export block, and an analysis block. The configuration functional block configures the monitoring. The measurement functional block performs measurements. The export functional block exports measurement results for further analysis. The analysis functional block analyzes the measurement results. In this section, we discuss the main monitoring architectures proposed for multi-domain networks. We also verify whether these architectures allow the providers to perform multi-domain measurements and whether the monitoring is configurable.

II.1. INTERMON architecture

The objective of the INTERMON project is to improve the QoS in inter-domain networks and to analyze the traffic in large scale [6]. The INTERMON architecture consists of four layers: a tool layer, a tool adaptation layer, a central control and storage layer, and a user interface layer [7]. In each domain, a central server called Global Controller (GC) coordinates the interaction between the different components of the architecture. We can identify the following functional blocks:

- The measurement functional block, which is located in the tool layer, consists of active and passive measurement points.
- The configuration functional block, which is located in the tool adaptation layer, is responsible for configuration of the measurement points.
- The export functional block, which is located in the central control and storage layer, is responsible for the export of the results using IPFIX and the results are then stored in the global database.
- The analysis functional block that is located in the central control and storage layer is responsible for the data post processing.

The INTERMON architecture is applied in each domain and the communication between the different domains is performed using Authorization, Authentication, and Accounting (AAA) local servers. Each provider can request a distant provider to get intra-domain measurement results on one or some metrics. When receiving this request, the distant provider checks if the sender has the right to obtain such information, using the AAA server, and answers the request.

II.2. ENTHRONE architecture

The objective of the monitoring system of the ENTHRONE project is to verify whether the QoS performance are respected using active and passive measurements. The management monitoring architecture of ENTHRONE consists of three levels: Node level Monitoring (NodeMon), Network level Monitoring (NetMon), and Service level Monitor (ServMon) [8].

- The NodeMon performs intra-domain active and passive application-level measurements at the edge nodes. These per-flow measurements are used to detect SLA violations such as QoS degradations, and then launch failure localization procedures.
- The NetMon processes and aggregates the measurements collected by the different NodeMons belonging to its domain. Then, it exports only the relevant measurement results to the ServMon. Therefore, the ServMon minimizes the quantity of the exported information since it exports only the relevant measurement results. The exported measurement results depend on the analysis process.
- The ServMon is responsible for reporting the QoS measurements between the different domains using XML-based measurement statistic.

Two monitoring signaling protocols are added to the monitoring architecture: an inter-domain monitoring signaling protocol (EQoS-RM) and an intra-domain active measurement signaling protocol (EMon). A disadvantage of the ENTHRONE architecture is that the measurements are mostly done at an application-level. The EQoS-RM and the EMon are used for monitoring exchanges between the ServMons of the different domains and between the NodeMons of the same domain, respectively. The EMon also configures the characteristics of the active measurements sessions (such as the one-way delay and the flow identification) between the effective NodeMons.

II.3. EuQoS architecture

The Monitoring and Measurement System (MMS) of the EuQoS project provides traffic measurements in real-time [9]. The EuQoS architecture consists of:

- Measurement Points (MP) that perform QoS measurements.
- Measurement Controller (MC) that launches and terminates the intra-domain measurements and collects the results from the different MPs.
- Monitoring, Measurement and Fault Management (MMFM) module that stores the measurement results obtained from the MC in the Resource Management Database (RM DB). Each domain contains a single RM DB and this database is accessible for the MMFM modules of all the domains.

For QoS performance evaluation, Net Meter [10] is selected as the intra-domain measurement tool. This active tool provides measurements on QoS metrics such as the delay, the delay variation, and the packet loss ratio. Moreover, the Monitoring and Measurement System (MMS) of EuQoS provides real-time measurements using an on-line monitoring passive tool called Oreneta. The MMS is limited to monitor a single class of service in a single domain. An active measurement tool, called Link Load Measurement Tool (LLMT), was developed

by EuQoS to perform inter-domain measurements (on inter-domain links). The measurement results obtained by LLMT are then stored in the RM DB.

II.3. Synthesis of the state-of-the-art monitoring architectures for multi-domain networks

We note that the measurement, export, analysis and configuration functional blocks exist in the INTERMON and ENTHRONE monitoring architectures. Besides, the export block of the INTERMON architecture uses a standardized export process (IPFIX). Moreover, the INTERMON architecture provides the confidential domain requirement using the AAA servers. However, the INTERMON and ENTHRONE architectures do not allow the providers to perform full multi-domain measurements and they are limited to the exchange of the intra-domain measurement results between the providers. These architectures provide partial multi-domain measurements because inter-domain measurements are not performed. Moreover, these architectures require that all the domains are collaborative and each of them performs intra-domain measurements and exchanges its measurement results with other domains. Therefore, the non-collaborative monitoring requirement is not provided. Furthermore, the configuration block of the INTERMON and ENTHRONE architectures are limited to the configuration of the measurement points and the configuration of the active measurement sessions, respectively. However, these configurable parameters are not sufficient in a heterogeneous environment (see subsection III.1). Then, the adaptive measurement process requirement is not totally provided while the adaptive export process requirement is not provided.

The main advantage of the EuQoS monitoring architecture is that it performs full multi-domain measurements by providing intra-domain and inter-domain measurements. However, this architecture uses its own inter-domain measurement tool. Therefore, all the domains must use the same measurement tool and this does not respect the autonomously managed domain requirement. Moreover, there is no configuration functional block in the EuQoS architecture. Therefore, this monitoring architecture does not provide the adaptive measurement process and the adaptive export process requirements.

Therefore, we propose in the following a configurable multi-domain networks monitoring architecture that provides these five requirements: the autonomously managed domain, the confidential domain, the non-collaborative monitoring, the adaptive measurement process, and the adaptive export process requirements. Table I presents whether these five requirements are provided by the different monitoring architectures. In the following section, we present our proposals for a configurable multi-domain monitoring in section III.

III. PROPOSALS FOR A CONFIGURABLE MULTI-DOMAIN MONITORING

Our monitoring proposals should adapt to any compatible multi-domain network architecture like the architecture model defined by the IPSphere forum [11]. This model allows providers to overcome scalability and interoperability issues. The IPSphere forum has defined the role of each system entity: Administrative Owner (AO), Element Owner (EO), and customer. AO is the entity that is responsible for providing and guaranteeing end-to-end services over a multi-domain network. These services are requested by customers. EO is the entity that manages the resources of a network domain. Each service provided by the AO uses the resources of one or several EOs.

Table I. Multi-domain monitoring architectures vs monitoring requirements

Architectures	Autonomously managed domain	Confidential domain	Non-collaborative monitoring	Adaptive measurement process	Adaptive export process
INTERMON	Yes	Yes	No	Partially	No
ENTHRONE	Yes	No	No	Partially	No
EuQoS	No	No	No	No	No
Our configurable monitoring	Yes	Yes	Yes	Yes	Yes

The principal elements of our monitoring architecture are represented in Fig. I. Each domain contains measurement, export, analysis, and configuration blocks. We propose that the configuration block has the capacity to configure the measurement and the export blocks to overcome the heterogeneity issues. The configuration block can be initialized using a configuration file. To have more flexibility in monitoring, it is required to have a dynamic configuration. For example, when the analysis block detects a network failure, it can modify the measurement and/or the export parameters through the configuration block in order for instance to locate the source of the failure. The details of our monitoring architecture and our proposals for a configurable multi-domain network monitoring are giving in the following.

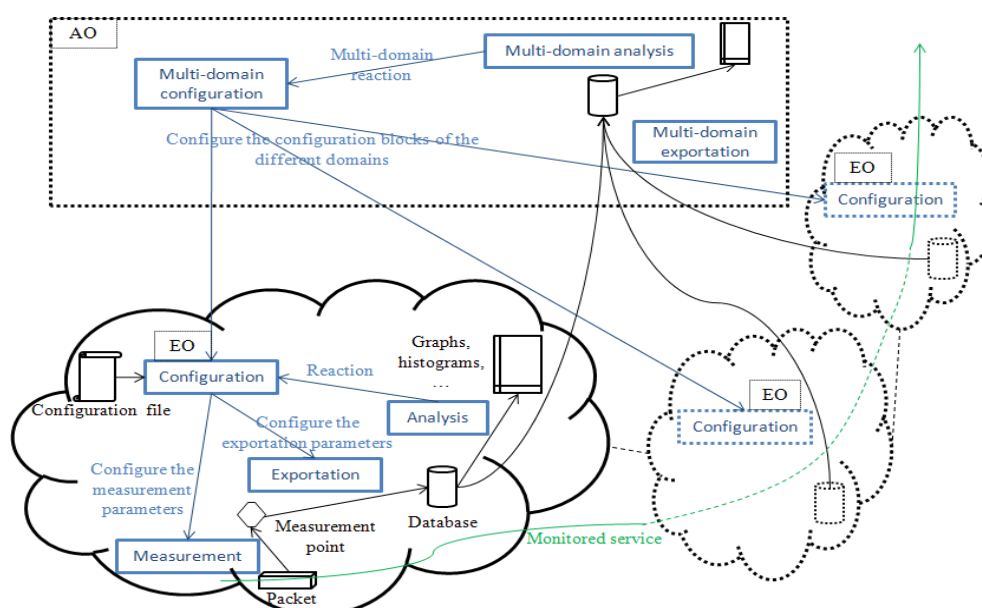


Figure I. Principal elements of a configurable multi-domain monitoring

III.1. Configurable parameters of network monitoring

In this section, we present the main parameters of the measurement and the export functional blocks that have to be configured. The parameters of the measurement functional block that should be adequately chosen in order to have an effective network monitoring in a heterogeneous environment are the following:

- **Metrics:** depend on the constraints defined in the contract that is already established between the user and the provider and recursively between providers on the service path. In this paper, we consider the metrics that have been standardized by the Internet Engineering Task Force (IETF) such as the network capacity [12], One Way Delay (OWD) [13], IP Packet Delay Variation (IPDV) [14], One Way Packet Loss (OWPL) [15], and connectivity [16]. We note that the International Telecommunication Union (ITU) defines additional metrics in [17] such as IP Packet Transfer Delay (IPTD), and IP Packet Loss Ratio (IPLR). However, these metrics can be easily mapped with the metrics defined by the IETF. For example, IPLR can be mapped with OWPL.
- **Monitoring type:** depends on the metrics to be measured as well as the capabilities of the measurement point. The monitoring can be passive or active. A measurement point can support passive monitoring and/or active monitoring. A well chosen monitoring type can ease the measurement process of the metrics. For example, the number of transmitted packets is adequately computed using passive monitoring, while delay is easily measured using active monitoring. Nevertheless, the same metric can be measured by both monitoring types.
- **Measurement protocols:** define the procedures used to perform the measurements of metrics into a network. A measurement protocol can be passive and/or active. For example, Bidirectional Forwarding Detection (BFD) [18], which is an active protocol, is used to determine the connectivity. In [19], it is recommended to use standardized measurement protocols in order to ensure the interoperability between heterogeneous measurement points. For example, it is recommended to use One Way Active Measurement Protocol (OWAMP) [20] to provide one-way measurements such as OWD. Two-way measurements can be provided using Two-Way Active Measurement Protocol (TWAMP) [21]. Once the measurement protocol is selected, its parameters have to be chosen. For example, when the measurement protocol is active, the characteristics of the additional traffic such as the packet size, the probe rate and the probe duration have to be chosen. The choice of the additional traffic characteristics depends on the model used to infer the network traffic.
- **Sampling methods:** determine when the packets are captured. These methods can reduce the network resource utilization of the path between the physical channel and the measurement point. This path is called the supervision path (see Fig. II). The sampling methods depend on the metrics to be measured. For example, the periodic and the random sampling can provide acceptable performance when measuring the delay and the packet loss [22]. When measuring the delay variation, the batch sampling provides the best performance. In practice, the periodic sampling is almost always used because this sampling method is easier to implement [23].

- Packet filtering methods: determine the packets that will not be taken into account in the measurements. These methods can reduce the network resource utilization (computations at the measurement point level). For example, a packet filtering method can specify to do not measure packets having a source IP address equal to 205.10.0.0/24. A packet filtering method can be applied on packet field(s), flow field(s), and/or service class field(s).

The parameters of the export functional block that should be configured are:

- Statistic computation methods: determine how the measurement results are computed. For example, when the OWD is measured, the export functional block can export the minimum OWD or the average OWD. Generally, the statistic computation method depends on the analysis process.
- item Export methods: determine when are the results exported. The export method has a direct influence on the reaction time of the analysis process and the utilization of the path between the measurement point and the database (where the measurement results are stored). We note that the results can be immediately exported when they are obtained using the real-time method. This export method has the advantage of speeding up the results analysis time and then reduce the violation detection delay. However, the quantity of exchanged data can be quite large. To reduce the network resource utilization, the results can be exported periodically. This method can also provide acceptable results analysis time when the export period is finely tuned. The results can also be exported in a random method. This export method has the advantage of following the random aspect of the failure generation instants. Another solution to reduce the network resource utilization while rapidly reacting against failures is to export results using a trigger mechanism. For example, the results are compared against thresholds. However, this method has the disadvantage that it requires additional processing in the measurement functional block. The results can also be exported when they are requested by the analysis block (on-demand, e.g. Simple Network Management Protocol (SNMP) [24] request) or once at the end of the measurement campaign. In both methods, long delays can affect the results analysis time.
- Export protocols: define the procedures used to send the measurement results from the measurement point to the analysis point. These measurement points can be stored in a database. For interoperability issues, standardized export protocols are more interesting. For example, export protocol IPFIX is used by two standardized monitoring architectures: IPFIX and PSAMP. The IPFIX protocol is described in [25].
- Collecting methods: gather several measurement results in the same packet. The collecting method (applied on the same metric, for example, the minimum delay) can be temporary or spatial. The temporary collecting method consists of gathering several measurement results obtained in different sampling periods. The spatial collecting method consists of gathering several measurement results obtained from different measurement points. The collecting methods can reduce the network resource utilization of the path between the measurement point and the database (export path, see Fig. II), and then minimize the amount of data stored in the database.
- Result filtering methods can minimize the amount of the measurement results to be exported while getting enough measurement results for efficient analysis. For example, a result filtering method can specify to do not export measurement results that have already been provided from packets having an source IP address equal to 205.10.0.0/24. A result filtering method can be applied on packet field(s), flow field(s), and/or service class field(s). The result filtering methods (like the collecting methods) can reduce the network resource utilization of export path, and then minimize the amount of data stored in the database.

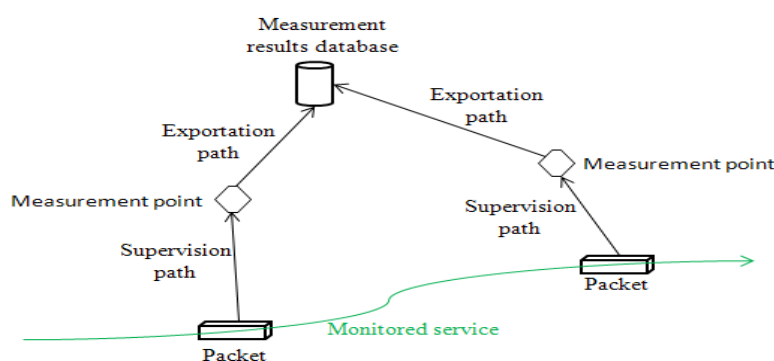


Figure II. Example of supervision paths and export paths

The main configurable parameters of the measurement and export functional blocks are presented in Table II.

III.2. Proposals for the measurement functional block

In intra-domain, each provider configures its domain with its own method without taking into account the monitoring characteristics of the other domains. However, in multi-domain, the providers have to share and exchange configuration information to perform multi-domain measurements. For example, the operators have to select the measurement protocol to be used. Indeed, each provider can have one or many measurement protocols. We note that it is possible to perform the monitoring between two points (without performing intermediate measurement, for example between measurement point *a2* and measurement point *b3* without performing measurements between measurement point *a2* and measurement point *b1*, see Fig. III) only if these measurement points support the same measurement protocol to be used.

Table III. Configurable parameters of the measurement and export functional blocks

Configurable parameters	Mandatory conditions	Examples of possible values
Metrics	Always mandatory	Delay, packet loss, etc.
Monitoring types	Always mandatory	Active, passive
Measurement protocols	Mandatory if the monitoring type is active (in this case, the additional traffic characteristics such as the probe size, and the probe rate have to be defined)	BFD, OWAMP, TWAMP, etc.
Sampling methods	Mandatory if the sampling is used (in this case, the sampling duration and the sampling frequency have to be defined)	Periodic, random, batch, etc.
Packet filtering methods	Mandatory if the filtering is used (in this case, the filtering rules have to be defined)	Filtering according to packet or flow field(s), etc.
Statistic computation methods	Always mandatory (this parameter depends on the metric measured)	Minimum delay, average delay, etc.
Export protocols	Always mandatory	IPFIX, etc.
Export methods	Always mandatory	Periodic, random, triggered, etc.
Collecting methods	Mandatory if the measurement results collecting is used	Temporary, spatial, etc.
Result filtering methods	Mandatory if the filtering of the measurement results is used (in this case, the filtering rules have to be defined)	Filtering according to packet or flow field(s), etc.

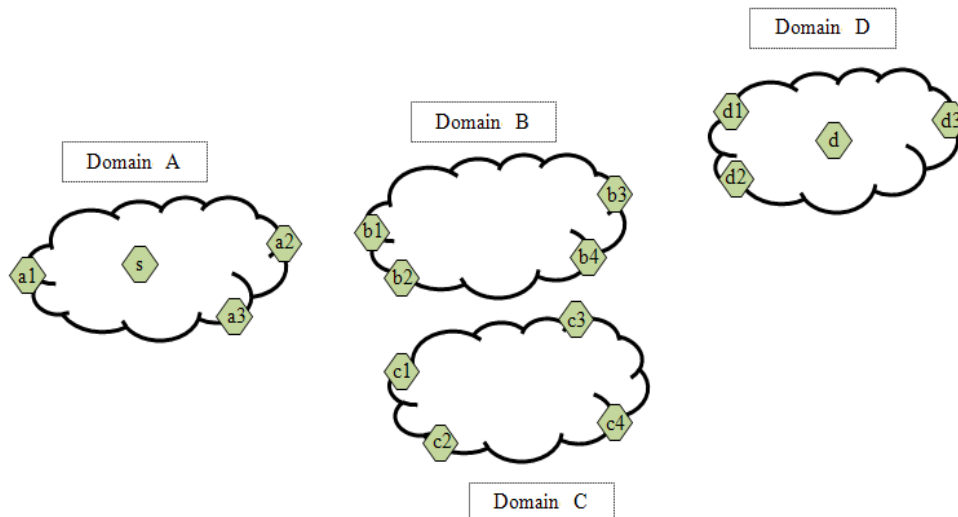


Fig. III. Multi-domain network monitoring scenario

In a close monitoring of a multi-domain flow or path, the providers have to perform multiple measurements (segment by segment) and the measurement results have to be correlated. The multiple domain measurements can be performed in two ways:

- All the providers use the same measurement protocol and measurement parameters and this makes easier the correlation of the measurement results. However, this assumption of homogeneity cannot always fulfill. For instance, let suppose a set of domains which share the same measurement protocol and have preselected a fixed measurement parameter set. Let suppose now that a new type of service requires a new monitoring method. When the homogeneity is a requirement, to monitor a new service, either all domains supported the new monitoring method or none. In the latter case, the new service cannot be properly monitored. In the first case, the new service will be monitored when and only when all domains support the new monitoring method. This could be unnecessary because the path to be monitored could use only a subset of the domains.
- The providers use different measurement protocols but two contiguous providers should mandatory run the same measurement protocol. Therefore, there is more flexibility in the choice of the measurement protocol to be used. However, the result correlation can become complex and each pair of providers have to select the measurement protocol to be used. This requires an additional negotiation phase for each choice of measurement protocol pair.

In both above ways, we make the assumption that the providers collaborate in the use of the measurement protocols. However, a provider may be non-collaborative; for instance, he does not want to publish measurement results on its traffic. A provider may do not support monitoring or the chosen measurement parameters are not available or its measurement capacity is already allocated to other services. In these cases, we can perform active measurements between his adjacent domains in order to monitor the traffic that traverses this domain. However, it can be difficult to perform a passive monitoring between the adjacent domains because it could be difficult to identify the traffic to be measured. Indeed, the outgoing border router of the non-collaborative domain (and thus the incoming border router of the following domain) cannot be assessed with sufficient precision. When monitoring a Label Switched Path (LSP) in Multi Protocol Label Switching (MPLS) networks, it is possible to perform active and passive monitoring on the adjacent domains as the path of an LSP is well-known.

In addition to the measurement protocol that is used in the remote measurement point, the local provider has to know at least the localization of the remote measurement point. However, confidentiality problems can take place since the router localization and then the network topology can be unveiled. One usual policy is to propose that only the localization of the border measurement points is unveiled to distant domains.

III.3. Proposals for the export functional block

For scalability and interoperability purposes, we recommend that the intra-domain export block exports the results to the AO for multi-domain analysis. The multi-domain analysis functional block verifies whether the measured network performance complies with the performance specified in the contract. When this functional block detects anomalies, some interventions of the multi-domain monitoring configuration are required (see Fig. 1).

For correlation purposes, it is required that statistic computation methods, the result filtering methods, and the collecting methods used are the same for all the measurement points located on the monitored path.

Finally, we propose that the export and the collecting methods are compatible in order to have meaningful results. For example, when the AO receives results from a domain that uses the periodic export method and from another domain that exports results using a trigger mechanism, the AO can analyze the measurement results if it can identify the trigger generation instants.

III.4. Proposals for the configuration functional block

We propose to locate the multi-domain configuration block at the AO since the global network resources are managed by this entity. Likewise, we propose that the intra-domain configuration block is coupled with the EO as this entity manages the resources of its network domain (see Fig. 1). The multi-domain configuration block is responsible for the configuration of all the domains that participate in the multi-domain monitoring by acting on their intra-domain configuration blocks.

We suppose that the client launches a multi-domain monitoring of a service by sending a multi-domain network monitoring request. When receiving this request, the AO configures the domains concerned by the multi-domain network monitoring of the service. These domains belong to the path of the monitored service. The measurement points that participate in this monitoring are selected by the AO. However, an EO can participate in the selection by preselecting a list of useful measurement points. The selection of the measurement points can be with or after the service establishment. The selection can be proactive or reactive. For both selection methods, the configuration blocks of the concerned domains have to transmit the information about the useful measurement points (or the information about all the available measurement points in its domain). The information about a measurement point consists in its localization (e.g. the Internet Protocol address of the

measurement point), its configurable parameters (see subsection III.1), and its monitoring capacity (that represents the maximum number of services that can be monitored simultaneously).

In proactive selection, each domain publishes the information about all its measurement points. When all the information is available, the AO can efficiently select the measurement points to be used. However, the transmitted information can be quite large. The proactive selection has two major drawbacks. First, the providers cannot preselect the measurement points to be used. Second, the providers have to transmit update messages when they need to update the list of the measurement points as well as their parameters or their monitoring capacities.

In reactive selection, the AO requests each concerned domain to transmit the information about the useful measurement points. Each provider preselects the measurement points and answers the request. The reactive selection allows the providers to avoid measurement points update procedure and decreases the amount of exchanged data for the publication (only preselected measurement points are sent). However, the selection has to be performed with each incoming multi-domain monitoring request. Furthermore, the AO can select the measurement points only when it receives all the responses from the domains concerned by the multi-domain monitoring. Therefore, the measurement points selection can receive extra delay.

In both above selection methods, we propose that the AO requests the configuration blocks of the domain on the monitored path to activate the selected measurement points.

In practice, the proactive selection mode is required when the monitoring establishment is performed simultaneously with the service establishment. The major advantage of this selection mode is that the LSP routing can take into account the characteristics of the measurement points. For example, the routing algorithm selects compatible measurement points which can still monitor further services, i.e. having monitoring capacity greater than zero. When the monitoring is established after the service establishment, the proactive selection mode becomes useless as there is no need to send all the measurement points characteristics to the AO. In this case, the reactive selection mode becomes more interesting

Finally, we propose that each intra-domain configuration block configures its measurement and export parameters (see Table II). This configuration can be determined locally when performing intra-domain network monitoring. However, this configuration has to be determined by the AO when performing multi-domain network monitoring for two reasons: the heterogeneity and the confidentiality. For example, when we perform active measurements between measurement point $a1$ belonging to domain A and measurement point $d2$ belonging to domain D (see Fig. 3), we have to configure these two measurement points in a coordinated way. For example, in a heterogeneous environment, in order to measure the delay, we have to select the same metric (for example OWD), the same statistic computation method (average OWD), the same measurement protocol (for example OWAMP), and the same export method (periodic, each 5 s). These monitoring parameters are selected among the set of the metrics, the statistic computation methods, the measurement protocols, and the export methods available at these two measurement points.

Even in a homogeneous environment (all the measurement points use the same parameters), the multi-domain monitoring configuration is still necessary for confidentiality reasons. Indeed, when we need, for example, to perform active measurements between measurement point s and measurement point $d2$ (see Fig. 3) without unveiling the localization of the measurement points located inside a local domain to any distant domain, we can perform multiple segmented measurements. For example, we can perform active measurements between measurement point s and $a1$ and between measurement point $a1$ and $d2$. Therefore, the localization of measurement point s is known by measurement point $a2$ that belongs to the same domain. Moreover, measurement point $d2$ uses only the localization of measurement point $a2$ that is located at the border of the distant domain.

IV. FUNCTIONAL EVALUATION OF OUR PROPOSED MONITORING ARCHITECTURE

Now, we evaluate our configurable multi-domain monitoring architecture functionally. Recall that we do not evaluate our propositions through prototype measurements or performance modeling since we study a functional architecture. We consider the scenario presented in Fig. III. It is required to perform measurements between measurement point s and measurement point $d3$ and these measurements are used to verify whether the delay constraint is respected (the end-to-end delay of the service has to be lower than 150 ms). The domains concerned by the monitoring are A , B , and D . The supported measurement protocols by the different measurement points that can participate in these measurements are presented in Table III. We assume that the service has been already established. The measurement protocols that can be used are $p1$, $p2$, and $p3$ and all these protocols can provide measurements on OWD using active monitoring. The statistic computation method of all the measurement points provides average delay. All the measurement points can export the measurement results periodically or using a trigger mechanism. From the list of the configurable parameters (see Table II), we

consider only the metric, the monitoring type, the measurement protocol, the statistic computation method, and the export method but we do not lose any generality if any additional configurable parameter is selected.

Table III. Supported measurement protocols by measurement points

Measurement points	Supported measurement protocols
s	p1
a2	p1 and p2
b1	p1 and p3
b3	p3
d2	p2 and p3
d3	p2

IV.1. Autonomously managed domain requirement

We note that we cannot perform measurements directly between measurement point *s* and measurement point *d3* because they do not support the same measurement protocol (these measurement points support *p1* and *p2*, respectively). Moreover, we also note that the inter-domain measurements are performed using two different measurement protocols: *p1* (performed between domain *A* and domain *B*, in particular between measurement point *a2* and measurement point *b1*) and *p3* (performed between domain *B* and domain *D*, in particular between measurement point *b3* and measurement point *d2*). So, even advanced inter-domain monitoring architecture (like the EuQoS architecture) cannot provide inter-domain measurement results in our scenario since the same measurement protocol has to be used in all multi-domain measurements.

Our proposed architecture allows the AO to configure and perform multi-domain monitoring between measurement point *s* and measurement point *d3* in spite of the heterogeneity of the measurement protocols of these measurement points. In fact, the AO can select measurement protocol *p1* between *s* and *a2* and between *a2* and *b1*, measurement protocol *p3* between *b1* and *b3* and between *b3* and *d2*, and measurement protocol *p2* between *d2* and *d3*. We note that the autonomously managed domain requirement is provided since the domains do not have to use the same monitoring process (in our scenario they can use different measurement protocols).

IV.2. Confidential domain requirement

Using our monitoring architecture, the characteristics of the measurement points located inside the domains and especially their localizations are not unveiled to the distant domains. For example, the measurement point *s* characteristics are known only by domain *A*. Only the characteristics of the border measurement points are unveiled to the distant domains (for example the characteristics of measurement point *a2* are unveiled to domain *B*). Therefore, the topology confidentiality of the different domains is assured using our configurable monitoring architecture. We also notice that the border measurement points do not have a global view of the possible values of the configuration parameters. For example, domain *A* does not know that measurement point *b1* supports measurement protocol *p3* and this specificity can be useful for confidentiality purposes. We note that the confidential domain requirement is provided.

IV.3. Non-collaborative monitoring requirement

Now, we assume that the AO thinks that domain *B* exports spurious measurement results. As consequence, the AO can decide to perform measurements between the adjacent domains of domain *B* along the path of the monitored service. Measurements can be performed between *a2* and *d2* and then these measurement points have to be reconfigured. For example, the AO specifies to domain *A* that measurement point *a2* will communicate with measurement point *d2* (instead of measurement point *b1*) using measurement protocol *p2* (instead of measurement protocol *p1*). This reaction can also be performed when domain *B* is or becomes non-collaborative. We note that the non-collaborative monitoring requirement is provided. We also note that the existing monitoring architectures cannot react in this situation. Indeed, the INTERMON and ENTHRONE architectures require that all domains used by the monitored service exchange their measurement results. The EuQoS architecture has no configuration block and therefore the measurement protocol used by measurement point *a1*, for example, cannot be replaced. In our case, measurement protocol *p1* is replaced by measurement protocol *p2* that represents the only common measurement protocol with the distant measurement point (*d2*).

IV.4. Adaptive export process requirement

We suppose that the AO selects the measurement result export method using a trigger mechanism in order to minimize the volume of data exported to the database. We assume that the measurement results are exported only if the delay exceeds 55 ms for measurements performed between measurement points belonging to the same domain (for example between measurement point s and measurement point $a2$) or if the delay exceeds 5 ms for measurements performed between measurement points belonging to two different domains (for example between measurement point $a2$ and measurement point $b1$). These thresholds are determined by the AO.

Now, we assume that the mean delay between measurement point $b1$ and measurement point $b3$ is equal to 60 ms. Then, since this intra-domain measurement value exceeds the corresponding threshold (55 ms), domain B exports measurement results to the AO. We propose that domain B , in a first stage, locally reacts to minimize the delay before the client detects service degradation. In order to verify whether the multi-domain delay constraint is respected (whether the end-to-end delay is lower than 150 ms), the AO can reconfigure the different domains by requesting them to replace their current export methods by the periodic export method. We note that the adaptive export process requirement is provided. After reconfiguring the export methods, the different domains periodically export their measurement results. We assume that the total average delay is equal to 130 ms. As the multi-domain constraint is respected, it is no necessary to perform further reactions. However, if the end-to-end delay exceeds 150 ms and domain B is the domain which does not respect its delay constraint, the AO may, for example, give penalty to the faulty domain, renegotiate the contracts between the different domains, and eliminate the faulty domain from the negotiation. The impact of configuration on monitoring reactions will be studied in future work. Anyhow, we think that it will introduce a great enhancement.

In general, the monitoring reactions are performed once the multi-domain analysis functional block detects anomalies, it has to react. We indicate that we do not consider anomaly diagnosis and fault detection. Many works have already been done on these important fields such as [26], [27], and [28], and our solutions should be compatible with any of them. The anomalies can be detected, for example, when the client announces service degradation or using the measurement results exported by the different domains. Detection fault mechanisms will be proposed and evaluated in future work.

IV.5. Adaptive measurement process requirement

We suppose that measurement protocol $p3$ is the least efficient. Now, we assume that measurement point $b3$ supports measurement protocol $p1$ (in addition of measurement protocol $p3$). As measurement point $b1$ also supports measurement protocol $p1$, we can reconfigure measurement point $b3$ and measurement point $b1$ without reconfiguring the other measurement points. This reconfiguration allows domain B to use a more efficient measurement protocol without disturbing domain A and domain D . This reconfiguration can also ease the measurement results collecting in the AO because measurement points s , $a2$, $b1$, and $b3$ use the same measurement protocol. We note that the adaptive measurement process requirement is provided.

V. PERFORMANCE EVALUATION OF THE PROPOSED COLLABORATION SCHEMES

V.1. Simulation model

In this section, we consider a topology formed by four domains and fourteen measurement points (see Fig. III). We consider only measurement points that are located at the border of the domains for confidentiality reasons. Domain A, Domain B, domain C, and domain D contains three measurement points ($a1$, $a2$, and $a3$), four measurement points ($b1$, $b2$, $b3$, and $b4$), four measurement points ($c1$, $c2$, $c3$, and $c4$), and three measurement points ($d1$, $d2$, and $d3$), respectively. The main simulation parameters are presented in Table IV}. The measurement point capacity represents the maximum number of services that this measurement point can monitor simultaneously. The incompatibility ratio represents the ratio of the measurement points that are not compatible with any other one. Two measurement points are compatible if and only if they can perform active measurement between them. For example, if the incompatibility ratio is equal to 0.1 and if there are 10 measurement points, then we have, in average, one measurement point that is not compatible with all the other ones.

Table IV. Simulation parameters

Simulation parameters	Values
Number of domains	4
Number of measurement points	14
Simulation time	1500 s

Monitoring requests arrival	is chosen according exponential distribution on the interval [1, 200]
Measurement point capacity	is chosen according uniform distribution on the interval [100, 120]
Incompatibility ratio	0 (all the MPS are compatibles), 0.1, 0.3, and 0.5 (the half of the measurement points are incompatible)

V.2. Simulation results for compatible measurement points

First, we interest in the case when all the measurement points are compatible (incompatibility ratio is equal to zero). We evaluate the blocking percentage due to the measurement points surcharge (the blocking percentage due to the measurement points incompatibility is equal to zero), the monitoring throughput (that represents the throughput of messages used to publish the measurement points characteristics and to configure the measurement points), and finally the delay of the monitoring establishment.

V.2.1. Blocking percentage evaluation

Fig. IV represents the blocking percentage as a function of the total number of the generated services during simulation. We note that, using the simulations parameters listed in Table IV, the blocking percentage is equal to zero for both collaboration schemes when the total number of services is lower than 200. Indeed, the measurement points do not reach their maximum monitoring capacity yet. From a total number of services approximately equal to 200, the blocking percentage of the reactive mode starts increasing while the blocking percentage of the proactive mode remains equal to zero until a total number of services equals to 300.

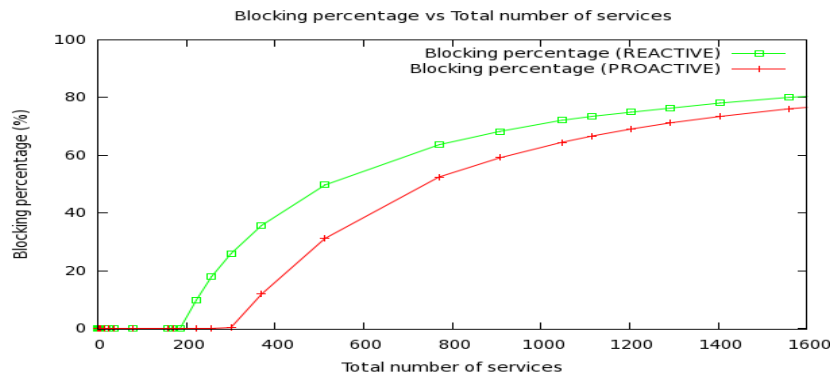


Fig. IV. Blocking percentage vs total number of the generated services during simulation

We notice that the proactive mode outperforms the reactive mode because when the first mode is applied, the AO has a global view on the capacity of all the measurement points. Therefore, the AO can select the measurement points that have the capacity to monitor further services. However, when the reactive mode is applied, the LSP for a given service is already established and so it can cross a measurement point that has already reached its maximum monitoring capacity.

When the number of services becomes very important, the curves of the proactive mode and of the reactive mode become close as most of the measurement points cannot monitor further services.

V.2.2. Throughput evaluation

Fig. V represents the monitoring throughput, the publication throughput, and the publication throughput as a function of the total number of services. The configuration throughput presented by the proactive mode is more important than that presented by the reactive mode. This is explained by the fact that the proactive mode allows our monitoring architecture to monitor more services than the reactive mode (the proactive mode is flexible and thus it generates lower monitoring requests blockage, see Fig. IV).

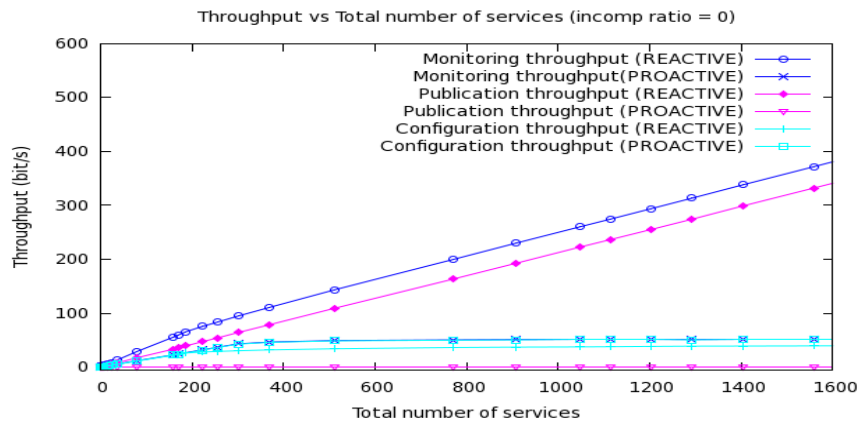


Fig. V. Throughput vs total number of services

Now, we consider the publication throughput. We note that the reactive mode generates higher publication throughput than the proactive mode. Indeed, we assumed that the refreshment period of the measurement points characteristics update is longer than the simulation time and therefore, when the proactive mode is used, each EO publishes the characteristics of its measurement points once during the simulation. However, when the reactive mode is used, the EO sends the list of the preselected measurement points at each monitoring request.

Recall that the monitoring throughput is equal to the configuration throughput added with the publication throughput. As the publication throughput is more important than the configuration throughput and therefore it has more effect on the monitoring throughput, we observe that the monitoring throughput of the reactive mode is higher than that of the proactive mode. Evidently, the monitoring throughput depends on the configuration and publication messages length as well as the number of accepted (non blocked) monitoring requests. The number of accepted monitoring requests depends on the monitoring capacity of the different measurement points as well as on the total number monitoring requests.

V.2.3. Delay evaluation

The mean delay of the monitoring establishment is presented in Table V. We note that the mean delay of the monitoring establishment when the reactive mode is used is greater than that when the proactive mode is used. This is because that, when the proactive mode is used, the AO has the characteristics of all the measurement points. Therefore, in opposition to the reactive mode, the AO can locally select the useful measurement points without needing to send messages (for requesting the list of the preselected measurement points) to the EOs concerned by the multi-domain monitoring and so waiting their responses.

Table V. Mean delay of the monitoring establishment

Collaboration mode	Proactive	Reactive
Mean delay	0.1 s	0.18 s

V.3. Simulation results for measurement points having different incompatibility ratios

Now, we study the blocking percentage for measurement points having incompatibility ratio equal to 0, 0.1, 0.3, and 0.5. Fig. VI represents the blocking percentage due to the MPs incompatibility as a function of the total number of services. Evidently, when all the MPS are compatible (incompatibility ratio is equal to zero), the blocking percentage due to the MPS incompatibility is equal to zero for the proactive and reactive modes (the curves of this incompatibility ratio are not presented in Fig. VI).

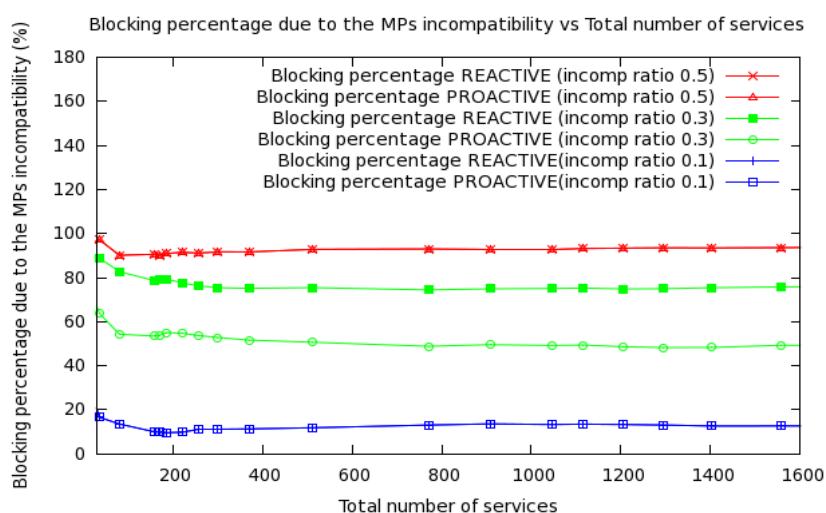


Fig. VI. Blocking percentage due to the MPs incompatibility vs total number of services (for different incompatibility ratios)

When the incompatibility ratio is equal to 0.1, the blocking percentage due to the MPs incompatibility is the same independently of the collaboration mode. This is due to the small solicitation of the incompatible measurement points for the multi-domain monitoring when the incompatibility ratio is too lower.

When the incompatibility ratio is equal to 0.3, the proactive mode outperforms the reactive mode. In fact, when the proactive mode is used, the AO endeavors to select compatible measurement points while the LSP paths are already established and then the measurement points that can participate in the multi-domain monitoring are limited when the reactive mode is used.

For an incompatibility ratio equal to 0.5, both collaboration mode presents the same blocking percentage due to the MPs incompatibility. Indeed, when the incompatibility ratio is important, even the proactive mode cannot find a path (especially if the path has to cross many domains and then many measurement points) that contains only compatible measurement points. However, we predict that the proactive mode becomes more and more efficient than the reactive mode, even if the incompatibility ratio is important, when the number of measurement points per domain increases (in our scenario, we have at most two measurement points that can link two domains). We will study the influence of the increasing of the number of measurement points as well as the increasing of the number of the domains in future work.

VI. CONCLUSION

In this paper, we have studied the state-of-the-art monitoring architectures proposed for multi-domain networks. We have concluded that these architectures assume that the set of monitoring methods is identical over all the domains. This assumption achieves the potential interoperability of the methods. However, in the case of autonomous domains (which is very common in practice), even with this homogeneous assumption, one important point is missed: the need of a coordinated and wise selection of the monitoring parameters to achieve an efficient monitoring of the multi-domain networks. Let us suppose that, for instance, one domain manages the sampling method (which is a configurable parameter of the measurement functional block) of a certain flow on a periodic basis which can be chosen between 100 ms and 200 ms, whereas another domain uses a period sampling between 100 ms and 500 ms. It could be wise to offer the capability to select, on a flow basis, either the lower period to have a precise monitoring or the larger period to have a lighter resource consumption. So, the adaptive measurement process requirement (as well as the adaptive export process requirement) must be provided.

We have supposed that in a multi-domain network, some domains can collaborate to monitor some segments of the monitored services whereas some domains do not want or cannot collaborate. In this context, it is required that the collaborative domains adjacent to the non-collaborative domains monitor a longer segment which spans the non-collaborative domain. Thus even non-adjacent domains (for instance the above domains which are adjacent to the non-collaborative domains) should have the mean to determine the most appropriated monitoring methods and parameters to use. We have shown that the non-collaborative monitoring requirement has to be provided.

Furthermore, we have shown that the autonomously managed-domain and the confidential domain requirements have an impact on every monitoring process: the measurement process, the export process, and the

reaction process. This requires and induces a flexible configuration of all (monitoring) processes, thus we have made proposals for these monitoring processes.

In conclusion, configurable monitoring is required by in any current architecture (for instance IPSphere) which manages multi-domain services. Our proposals fit with them and complement them with a flexible monitoring function.

ACKNOWLEDGEMENTS

This work has been performed within collaboration with Alcatel-Lucent Bell Labs France.

REFERENCES

- [1] Brownlee, N., Mills, C., Ruth, G.: Traffic Flow Measurement: Architecture. RFC 2722, October 1999.
- [2] Sadasivan, G., Brownlee, N., Claise, B., Quittek, J.: Architecture for IP Flow Information Export. RFC 5470, May 2009.
- [3] Claise, B., Johnson, Ed. A., Quittek, J.: Packet Sampling (PSAMP) Protocol Specifications. RFC 5476, March 2009.
- [4] Strohmeier, F., Dörken, H., Hechenleitner, B.: AQUILA distributed QoS measurement. In: International Conference on Advances in Communications and Control, Crete, Greece, 2001.
- [5] Molina-Jimenez, C., Shrivastava, S., Crowcroft, J., Gevos, P.: On the monitoring of Contractual Service Level Agreements. In: the first IEEE International Workshop on Electronic Contracting, WEC, San Diego, CA, USA, 2004.
- [6] Schmoll, C., Boschi, E.: Final Architecture Specification. Deliverable 15, INTERMON, 2004.
- [7] Boschi, E., D'Antonio, S., Malone, P., Schmoll, C.: INTERMON: An architecture for inter-domain monitoring, modelling and simulation. In: NETWORKING 2005, Pages 1397 - 1400, Springer Berlin / Heidelberg, 2005.
- [8] A. Mehaoua et al.: Service-driven inter-domain QoS monitoring system for large-scale IP and DVB networks. In: Computer Communications, Volume 29, 2006.
- [9] Dabrowski, M., Owezarski, P., Burakowski, W., Beben, A.: Overview of monitoring and measurement system in EuQoS multi-domain network. In: International Conference on Telecommunications and Multimedia (TEMU'06), Greece, 2006.
- [10] Net Meter. <http://www.hootech.com/NetMeter/> [6 October 2008].
- [11] Uzé, J.-M.: IPSphere Forum: status on technical specifications. In: TERENA Networking Conference 2007, Copenhagen, Denmark, 2007.
- [12] Chimento, P., Ishac, J.: Defining Network Capacity. RFC 5136, February 2008.
- [13] Almes, G., Kalidindi, S., Zekauskas M.: A One-way Delay Metric for IPPM. RFC 2679, September 1999.
- [14] Demichelis, C., Chimento, P.: IP Packet Delay Variation Metric for IP Performance Metrics (IPPM). RFC 3393, November 2002.
- [15] Almes, G., Kalidindi, S., Zekauskas, M.: A One-way Packet Loss Metric for IPPM. RFC 2680, September 1999.
- [16] Mahdavi, J., Paxson, V.: IPPM Metrics for Measuring Connectivity. RFC 2678, September 1999.
- [17] Telecommunication Standardization Sector of ITU: Internet protocol data communication service - IP packet transfer and availability performance parameters. Y.1540, March 2000.
- [18] Katz, D., Ward, D.: Bidirectional Forwarding Detection. draft-ietf-bfd-base-11.txt, January 2010.
- [19] Amante, S. et al.: Inter-provider Quality of Service. White paper draft 1.1, 2006.
- [20] Shalunov, S., Teitelbaum, B., Karp, A., Boote, J., Zekauskas, M.: A One Way Active Measurement Protocol (OWAMP). RFC 4656, September 2006.
- [21] Hedayat, K., Krzanowski, R., Morton, A., Yum, K., Babiarz, J.: A Two-Way Active Measurement Protocol (TWAMP). RFC 5357, October 2008.
- [22] Hill, J.: Assessing the accuracy of active probes for determining network delay, jitter and loss". MSc Thesis in High Performance Computing, 2002.
- [23] Evans, J. W., Filselfs, C.: Deploying IP and MPLS QoS for Multiservice Networks: Theory & Practice. Morgan Kaufmann, 2007.
- [24] Case, J., Fedor, M., Schoffstall, M., Davin, J.: A Simple Network Management Protocol (SNMP). RFC 1157, May 1990.
- [25] Claise, B.: Specification of the IP Flow Information Export (IPFIX) protocol for the exchange of IP traffic flow information. RFC 5101, January 2008.
- [26] Naidu, K.V.M., Panigrahi, D., Rastogi, R.: Detecting anomalies using end-to-end path measurements. In: the 27th Conference on Computer Communications, INFOCOM 2008, Phoenix, AZ, USA, 2008.
- [27] Barford, P., Duffield, N., Ron, A., Sommers, J.: Network performance anomaly detection and localization. In: the 28th Conference on Computer Communications, INFOCOM 2009, Rio de Janeiro, Brazil, 2009.
- [28] Chu, L.W., Zou, S.H., Cheng, S.D., Wang, W.D., Tian, C.Q.: A distributed multi-domain oriented fault diagnosis algorithm. In: the 2nd IEEE International Conference on Computer Science and Information Technology, Beijing, China, 2009.

Radiation and Mass Transfer Effects on MHD Natural Convection Flow over an Inclined Plate

R.L.V.Renuka Devi¹, T.Poornima², N. Bhaskar Reddy³, S.Venkataramana⁴
^{1,2,3,4}Department of Mathematics, Sri Venkateswara University, Tirupati, India

ABSTRACT: A numerical solution for the unsteady, natural convective flow of heat and mass transfer along an inclined plate is presented. The dimensionless unsteady, coupled, and non-linear partial differential conservation equations for the boundary layer regime are solved by an efficient, accurate and unconditionally stable finite difference scheme of the Crank-Nicolson type. The velocity, temperature, and concentration fields have been studied for the effect of Magnetic parameter, buoyancy ratio parameter, Prandtl number, radiation parameter and Schmidt number. The local skin-friction, Nusselt number and Sherwood number are also presented and analyzed graphically.

Keywords: Unsteady flow, Inclined plate, Finite difference method, Radiation, Mass transfer.

I. INTRODUCTION

The buoyancy force induced by density differences in a fluid cause's natural convection. Natural convection flows are frequently encountered in physics and engineering problems such as chemical catalytic reactors, nuclear waste material etc. Transient free convection is important in many practical applications such as thermal regulation process, security of energy systems etc. In literature, extensive research work has been performed to examine the effect of natural convection on flow past a plate. The first attempt in this direction was made by Callahan and Marner [1] who solved the non-linear system of equations by explicit finite difference scheme, which is not always convergent. Soundalgekar and Ganesan [2] studied the same problem by implicit finite difference scheme which is always stable and convergent. Recently, finite difference solution of natural convection flow over a heated plate with different inclination was studied by Begum et al. [3].

Two dimensional natural convection heat and mass transfer flow past a semi-infinite flat plate has been receiving the attention of many researchers because of its wide applications in industry and technological fields. Natural convection along an inclined plate has received less attention than the case of vertical and horizontal plates. Finite-difference technique has been used in natural convective flow analysis by many researchers. Callahan and Marner [4] have presented a paper on transient free convection with mass transfer effects and to solve the problem by explicit finite difference technique. Soundalgekar and Ganesan [5] solved the same problem using implicit finite difference technique and compared the result with those of Marner and Callahan [6] and both the results agree well. Chamkha et al. [7] presented similarity solutions for hydromagnetic simultaneous heat and mass transfer by natural convection from inclined plate with thermal heat generation or absorption employing implicit finite difference technique. Ganesan and Palani [8] studied free convection effects on the flow of water at 4°C past a semi-infinite inclined flat plate and solved the problem using implicit finite difference technique.

Magnetohydrodynamic flows have applications in meteorology, solar physics, cosmic fluid dynamics, astrophysics, geophysics and in the motion of earth's core. In addition from the technological point of view, MHD free convection flows have significant applications in the field of stellar and planetary magnetospheres, aeronautical plasma flows, chemical engineering and electronics. An excellent summary of applications is to be found in Hughes and Young [9]. Raptis [10] studied mathematically the case of time varying two dimensional natural convective flow of an incompressible, electrically conducting fluid along an infinite vertical porous plate embedded in a porous medium. Helmy [11] studied MHD unsteady free convection flow past a vertical porous plate embedded in a porous medium. Elbashbeshy [12] studied heat and mass transfer along a vertical plate in the presence of magnetic field.

In the context of space technology and in the processes involving high temperatures, the effects of radiation are of vital importance. Recent developments in hypersonic flights, missile re-entry, rocket combustion chambers, power plants for inter planetary flight and gas cooled nuclear reactors, have focused attention on thermal radiation as a mode of energy transfer, and emphasized the need for improved understanding of radiative transfer in these processes. Cess [13] presented radiation effects on the boundary layer flow of an absorbing fluid past a vertical plate, by using the Rosseland diffusion model. Several authors have also studied thermal radiating MHD boundary layer flows with applications in astrophysical fluid dynamics. Mosa [14] discussed one of the first models for combined radiative hydromagnetic heat transfer,

considering the case of free convective channel flows with an axial temperature gradient. Nath et al. [15] obtained a set of similarity solutions for radiative-MHD stellar point explosion dynamics using shooting method. Takhar et al. [16] studied radiation effects on MHD free convection flow past a semi infinite vertical plate where the viscosity and thermal conductivity were assumed constant. Azzam [17] studied radiation effects on the MHD mixed convective flow past a semi infinite moving vertical plate for the case of high temperature differences.

However, the interaction of natural convection flow of an electrically conducting fluid past an inclined plate in the presence of radiation and mass transfer has received little attention. Hence, in the present chapter an attempt is made to analyze the mass transfer effects on MHD natural convection flow along a heated inclined semi-infinite plate in the presence of radiation. The equations of continuity, linear momentum, energy and diffusion, which govern the flow field, are solved by an implicit finite difference method of Crank-Nicolson type. The behavior of the velocity, temperature, concentration, skin-friction, Nusselt number and Sherwood number has been discussed for variations in the physical parameters.

II. MATHEMATICAL ANALYSIS

An unsteady two-dimensional natural convection flow of a viscous, incompressible, electrically conducting, radiating fluid past a heated inclined semi infinite plate is considered. The fluid is assumed to be gray, absorbing-emitting but non-scattering. The x-axis is taken along the plate and the y-axis normal to it. Initially, it is assumed that the plate and the fluid are at the same temperature T'_∞ and concentration level C'_∞ everywhere in the fluid. At time $t > 0$, the temperature of the plate and the concentration level near the plate are raised to T'_w and C'_w respectively and are maintained constantly thereafter. A uniform magnetic field is applied in the direction perpendicular to the plate and that the induced magnetic field is neglected. The transverse applied magnetic field and magnetic Reynolds number are assumed to be very small, so that the induced magnetic field is negligible. It is assumed that the concentration C' of the diffusing species in the binary mixture is very less in comparison to the other chemical species, which are present, and hence the Soret and Dufour effects are negligible. It is also assumed that there is no chemical reaction between the diffusing species and the fluid. Then, under the above assumptions, in the absence of an input electric field, the governing boundary layer equations with Boussinesq's approximation are

$$\frac{\partial u}{\partial x} + \frac{\partial v}{\partial y} = 0 \tag{1}$$

$$\frac{\partial u}{\partial t'} + u \frac{\partial u}{\partial x} + v \frac{\partial u}{\partial y} = g\beta(T - T'_\infty)\sin\alpha + g\beta^*(C - C'_\infty)\sin\alpha + \nu \frac{\partial^2 u}{\partial y^2} - \frac{\sigma B_0^2}{\rho} u \tag{2}$$

$$\frac{\partial T'}{\partial t'} + u \frac{\partial T'}{\partial x} + v \frac{\partial T'}{\partial y} = \alpha \frac{\partial^2 T'}{\partial y^2} - \frac{1}{\rho c_p} \frac{\partial q_r}{\partial y} \tag{3}$$

$$\frac{\partial C'}{\partial t'} + u \frac{\partial C'}{\partial x} + v \frac{\partial C'}{\partial y} = D \frac{\partial^2 C'}{\partial y^2} \tag{4}$$

The initial and boundary conditions are

$$\begin{aligned} t' \leq 0 : u = 0, v = 0, T' = T'_\infty, C' = C'_\infty \\ t' > 0 : u = 0, v = 0, T' = T'_w, C' = C'_w \text{ at } y = 0 \\ u = 0, T' = T'_\infty, C' = C'_\infty \text{ at } x = 0 \\ u \rightarrow 0, T' \rightarrow T'_\infty, C' \rightarrow C'_\infty \text{ as } y \rightarrow \infty \end{aligned} \tag{5}$$

Where u, v are the velocity components in x, y directions respectively, t' - the time, g - the acceleration due to gravity, β - the volumetric coefficient of thermal expansion, β^* - the volumetric coefficient of expansion with concentration, T - the temperature of the fluid in the boundary layer, C - the species concentration in the boundary layer, ν - the kinematic viscosity, T'_w - the wall temperature, T'_∞ - the free stream temperature far away from the plate, C'_w - the concentration at the plate, C'_∞ - the free stream concentration far away from the plate, σ - the electrical conductivity, B_0 - the magnetic induction, ρ - the density of the fluid, α - the thermal diffusivity, c_p - the specific heat at constant pressure, q_r - the radiation heat flux and D - the species diffusion coefficient.

The second term on the right hand side of equation (2.3) represents the radiative heat flux; Thermal radiation is assumed to be present in the form of a unidirectional flux in the y-direction i.e., q_r (transverse to the surface).

By using the Rosseland approximation (Brewster [18]), the radiative heat flux q_r is given by

$$q_r = -\frac{4\sigma_s}{3k_e} \frac{\partial T'^4}{\partial y} \tag{6}$$

Where σ_s is the Stefan-Boltzmann constant and k_e - the mean absorption coefficient. It should be noted that by using the Rosseland approximation, the present analysis is limited to optically thick fluids. If the temperature differences within the flow are sufficiently small, then Equation (2.6) can be linearized by expanding T'^4 into the Taylor series about T'_∞ , which after neglecting higher order terms takes the form

$$T'^4 \cong 4T'_\infty{}^3 T' - 3T'_\infty{}^4 \tag{7}$$

In view of equations (2.6) and (2.7), equation (2.3) reduces to

$$\frac{\partial T'}{\partial t} + u \frac{\partial T'}{\partial x} + v \frac{\partial T'}{\partial y} = \alpha \frac{\partial^2 T'}{\partial y^2} + \frac{16\sigma_s T'_\infty{}^3}{3k_e \rho c_p} \frac{\partial^2 T'}{\partial y^2} \tag{8}$$

From the technological point of view, for the type of problem under conditions, the coefficient of skin-friction, heat and mass transfer are important.

Local and average skin-frictions are given respectively by

$$\tau'_x = -\mu \left(\frac{\partial u}{\partial y} \right)_{y=0} \tag{9}$$

$$\bar{\tau}_L = \frac{-1}{L} \int_0^L \mu \left(\frac{\partial u}{\partial y} \right)_{y=0} dx \tag{10}$$

Local and average Nusselt numbers are given respectively by

$$Nu_x = \frac{-x \left(\frac{\partial T'}{\partial y} \right)_{y=0}}{T'_w - T'_\infty} \tag{11}$$

$$\bar{Nu}_L = -\int_0^L \left[\left(\frac{\partial T'}{\partial y} \right)_{y=0} / (T'_w - T'_\infty) \right] dx \tag{12}$$

Local and average Sherwood numbers are given respectively by

$$Sh_x = \frac{-x \left(\frac{\partial C'}{\partial y} \right)_{y=0}}{C'_w - C'_\infty} \tag{13}$$

$$\bar{Sh}_L = -\int_0^L \left[\left(\frac{\partial C'}{\partial y} \right)_{y=0} / (C'_w - C'_\infty) \right] dx \tag{14}$$

In order to write the governing equations and the boundary conditions in dimensionless form, the following non-dimensional quantities are introduced.

$$X = \frac{x}{L}, \quad Y = \frac{yGr^{1/4}}{L}, \quad t' = \frac{L^2}{\nu} Gr^{-1/2}, \quad U = \frac{uLGr^{-1/2}}{\nu}, \quad V = \frac{vLGr^{-1/4}}{\nu}, \quad Gr = \frac{g\beta L^3(T'_w - T'_\infty)}{\nu^2}, \quad Gc = \frac{g\beta^* L^3(C'_w - C'_\infty)}{\nu^2} \tag{15}$$

$$T = \frac{T' - T'_\infty}{T'_w - T'_\infty}, \quad C = \frac{C' - C'_\infty}{C'_w - C'_\infty}, \quad M = \frac{\sigma B_0^2 \nu}{L^2}, \quad Pr = \frac{\nu}{\alpha}, \quad Sc = \frac{\nu}{D}, \quad N = \frac{\beta^*(C'_w - C'_\infty)}{\beta(T'_w - T'_\infty)}, \quad F = \frac{k_e k}{4\sigma_s T_\infty^3}$$

where L is the characteristic length of the plate and k-the thermal conductivity.

In view of (2.15), the equations (1), (2), (8) and (4) are reduced to the following non-dimensional form

$$\frac{\partial U}{\partial X} + \frac{\partial V}{\partial Y} = 0 \tag{16}$$

$$\frac{\partial U}{\partial t} + U \frac{\partial U}{\partial X} + V \frac{\partial U}{\partial Y} = \frac{\partial^2 U}{\partial Y^2} + (T + NC) \sin \alpha - MU \tag{17}$$

$$\frac{\partial T}{\partial t} + U \frac{\partial T}{\partial X} + V \frac{\partial T}{\partial Y} = \frac{1}{Pr} \left(1 + \frac{4}{3F} \right) \frac{\partial^2 T}{\partial Y^2} \quad (18)$$

$$\frac{\partial C}{\partial t} + U \frac{\partial C}{\partial X} + V \frac{\partial C}{\partial Y} = \frac{1}{Sc} \frac{\partial^2 C}{\partial Y^2} \quad (19)$$

where, Gr , M , F , Pr , N and Sc are thermal Grashof number, radiation parameter, Prandtl number, buoyancy ratio parameter and Schmidt number respectively.

The corresponding initial and boundary conditions are

$$\begin{aligned} t \leq 0 : U = 0, V = 0, T = 0, C = 0 \\ t > 0 : U = 0, V = 0, T = 1, C = 1 \quad \text{at } Y = 0 \\ U = 0, V = 0, T = 0, C = 0 \quad \text{at } X = 0 \\ U \rightarrow 0, T \rightarrow 0, C \rightarrow 0 \quad \text{as } Y \rightarrow \infty \end{aligned} \quad (20)$$

Local and average skin-frictions in non-dimensional form are

$$\tau'_x = Gr^{3/4} \left(\frac{\partial u}{\partial y} \right)_{y=0} \quad (21)$$

$$\bar{\tau} = Gr^{3/4} \int_0^1 \left(\frac{\partial u}{\partial y} \right)_{y=0} dX \quad (22)$$

Local and average Nusselt numbers in non-dimensional form are

$$Nu_x = -XGr^{1/4} \left(\frac{\partial T}{\partial Y} \right)_{y=0} \quad (23)$$

$$\bar{Nu} = -Gr^{1/4} \int_0^1 \left(\frac{\partial T}{\partial Y} \right)_{y=0} dX \quad (24)$$

Local and average Sherwood numbers in non-dimensional form are

$$Sh_x = -XGr^{1/4} \left(\frac{\partial C}{\partial Y} \right)_{y=0} \quad (25)$$

$$\bar{Sh} = -Gr^{1/4} \int_0^1 \left(\frac{\partial C}{\partial Y} \right)_{y=0} dX \quad (26)$$

III. METHOD OF SOLUTION

In order to solve the unsteady, non-linear, coupled equations (16) - (19), under the boundary conditions (20), an implicit finite difference scheme of Crank-Nicholson type has been employed. The region of integration is considered as a rectangle with sides $X_{\max} (=1)$ and $Y_{\max} (=14)$, where Y_{\max} corresponds to $Y = \infty$, which lies very well outside the momentum, energy and concentration boundary layers. The maximum value of Y was chosen as 14 after some preliminary investigations so that the last two of the boundary conditions of equation (20) are satisfied with in the tolerance limit 10^{-5} . The grid system is shown in the following figure A.

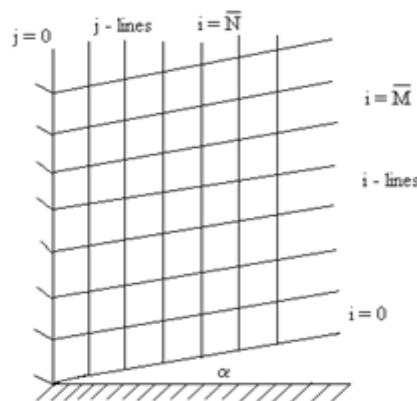


Figure A. Grid system

The finite difference equations corresponding to equations (16) - (19) are as follows

$$\frac{[U_{i,j}^{n+1} - U_{i-1,j}^{n+1} + U_{i,j}^n - U_{i-1,j}^n + U_{i,j-1}^{n+1} - U_{i-1,j-1}^{n+1} + U_{i,j-1}^n - U_{i-1,j-1}^n]}{4\Delta X} + \frac{[V_{i,j}^{n+1} - V_{i,j-1}^{n+1} + V_{i,j}^n - V_{i,j-1}^n]}{2\Delta Y} = 0 \quad (27)$$

$$\frac{[U_{i,j}^{n+1} - U_{i,j}^n]}{\Delta t} + U_{i,j}^n \frac{[U_{i,j}^{n+1} - U_{i-1,j}^{n+1} + U_{i,j}^n - U_{i-1,j}^n]}{2\Delta X} + V_{i,j}^n \frac{[U_{i,j+1}^{n+1} - U_{i,j-1}^{n+1} + U_{i,j+1}^n - U_{i,j-1}^n]}{4\Delta Y} =$$

$$\left(\frac{[T_{i,j}^{n+1} + T_{i,j}^n]}{2} + N \frac{[C_{i,j}^{n+1} + C_{i,j}^n]}{2} \right) \sin \alpha + \frac{[U_{i,j-1}^{n+1} - 2U_{i,j}^{n+1} + U_{i,j+1}^{n+1} + U_{i,j-1}^n - 2U_{i,j}^n + U_{i,j+1}^n]}{2(\Delta Y)^2} - M \frac{[U_{i,j}^{n+1} + U_{i,j}^n]}{2} \quad (28)$$

$$\frac{[T_{i,j}^{n+1} - T_{i,j}^n]}{\Delta t} + U_{i,j}^n \frac{[T_{i,j}^{n+1} - T_{i-1,j}^{n+1} + T_{i,j}^n - T_{i-1,j}^n]}{2\Delta X} + V_{i,j}^n \frac{[T_{i,j+1}^{n+1} - T_{i,j-1}^{n+1} + T_{i,j+1}^n - T_{i,j-1}^n]}{4\Delta Y} =$$

$$\frac{1}{Pr} \left(1 + \frac{4}{3F} \right) \frac{[T_{i,j-1}^{n+1} - 2T_{i,j}^{n+1} + T_{i,j+1}^{n+1} + T_{i,j-1}^n - 2T_{i,j}^n + T_{i,j+1}^n]}{2(\Delta Y)^2} \quad (29)$$

$$\frac{[C_{i,j}^{n+1} - C_{i,j}^n]}{\Delta t} + U_{i,j}^n \frac{[C_{i,j}^{n+1} - C_{i-1,j}^{n+1} + C_{i,j}^n - C_{i-1,j}^n]}{2\Delta X} + V_{i,j}^n \frac{[C_{i,j+1}^{n+1} - C_{i,j-1}^{n+1} + C_{i,j+1}^n - C_{i,j-1}^n]}{4\Delta Y} =$$

$$\frac{1}{Sc} \frac{[C_{i,j-1}^{n+1} - 2C_{i,j}^{n+1} + C_{i,j+1}^{n+1} + C_{i,j-1}^n - 2C_{i,j}^n + C_{i,j+1}^n]}{2(\Delta Y)^2} \quad (30)$$

Here, the subscript i -designates the grid point along the X-direction, j -along the Y-direction and the superscript n along the t -direction. An appropriate mesh size considered for the calculation is $\Delta X = 0.018$, $\Delta Y = 0.25$, and the time step $\Delta t = 0.01$. During any one time step, the coefficients $U_{i,j}^n$ and $V_{i,j}^n$ appearing in the difference equations are treated as constants. The values of C , T , U and V at time level $(n+1)$ using the known values at previous time level (n) are calculated as follows.

The finite difference equation (30) at every internal nodal point on a particular i -level constitute a tridiagonal system of equations. Such a system of equations is solved by using Thomas algorithm as discussed in Carnahan et al. [33]. Thus, the values of C are known at every internal nodal point on a particular i at $(n+1)^{\text{th}}$ time level. Similarly, the values of T are calculated from the equation (29). Using the values of C and T at $(n+1)^{\text{th}}$ time level in the equation (28), the values of U at $(n+1)^{\text{th}}$ time level are found in similar manner. Thus the values of C , T and U are known on a particular i -level. Then the values of V are calculated explicitly using the equation (27) at every nodal point at particular i -level at $(n+1)^{\text{th}}$ time level. This process is repeated for various i -levels. Thus the values of C, T, U and V are known, at all grid points in the rectangular region at $(n+1)^{\text{th}}$ time level.

Computations are carried out until the steady state is reached. The steady-state solution is assumed to have been reached, when the absolute difference between the values of U as well as temperature T and concentration C at two consecutive time steps are less than 10^{-5} at all grid points. The derivatives involved in the equations (21) - (26) are evaluated using five-point approximation formula and then the integrals are evaluated using Newton-Cotes closed integration formula.

IV. STABILITY OF THE SCHEME

In this section, the stability of the finite difference equations has been discussed using the well-known Von-Neumann technique. This method introduces an initial error represented by a finite Fourier series and examines how this error propagates during the solution. The general terms of the Fourier expansion for U , T and C at a time arbitrarily called $t = 0$ are assumed to be of the form $e^{i\phi x} e^{i\phi y}$ (here $i = \sqrt{-1}$). At a later time t , these terms will become

$$\begin{aligned} U &= F(t) e^{i\phi x} e^{i\phi y} \\ T &= G(t) e^{i\phi x} e^{i\phi y} \\ C &= H(t) e^{i\phi x} e^{i\phi y} \end{aligned} \quad (4.1)$$

Substituting (4.1) in the equations (27) – (30) under the assumption that the coefficients U and V are constants over any one time step and denoting the values after on time step by F', G' and H' , one may get after simplification.

$$\frac{(F' - F)}{\Delta t} + U \frac{(F' + F) (1 - e^{-i\phi\Delta X})}{2\Delta X} + V \frac{(F' + F) i \sin(\phi\Delta Y)}{2\Delta Y} = \left[\frac{(G' + G)}{2} + N \frac{(H' + H)}{2} \right] \sin \alpha + \frac{(F' + F) (\cos \phi\Delta Y - 1)}{(\Delta Y)^2} \quad (4.2)$$

$$\frac{(G' - G)}{\Delta t} + U \frac{(G' + G) (1 - e^{-i\phi\Delta X})}{2\Delta X} + V \frac{(G' + G) i \sin(\phi\Delta Y)}{2\Delta Y} = \left(1 + \frac{4}{3F} \right) \frac{(G' + G) (\cos \phi\Delta Y - 1)}{\text{Pr}(\Delta Y)^2} \quad (4.3)$$

$$\frac{(H' - H)}{\Delta t} + U \frac{(H' + H) (1 - e^{-i\phi\Delta X})}{2\Delta X} + V \frac{(H' + H) i \sin(\phi\Delta Y)}{2\Delta Y} = \frac{(H' + H) (\cos \phi\Delta Y - 1)}{\text{Sc}(\Delta Y)^2} \quad (4.4)$$

Equations (4.2) – (4.4) can be written as

$$(1+A)F' = (1-A)F + \frac{\Delta t}{2} [(G' + G) + N(H' + H)] \sin \alpha \quad (4.5)$$

$$(1+B) G' = (1-B)G \quad (4.6)$$

$$(1+E) H' = (1-E)H \quad (4.7)$$

where

$$A = \frac{U}{2} \frac{\Delta t}{\Delta X} (1 - e^{-i\phi\Delta X}) + \frac{V}{2} \frac{\Delta t}{\Delta Y} i \sin(\phi\Delta Y) \quad B = \frac{U}{2} \frac{\Delta t}{\Delta X} (1 - e^{-i\phi\Delta X}) + \frac{V}{2} \frac{\Delta t}{\Delta Y} i \sin(\phi\Delta Y) - (\cos \phi\Delta Y - 1) \frac{\Delta t}{(\Delta Y)^2} \quad E = \frac{U}{2} \frac{\Delta t}{\Delta X} (1 - e^{-i\phi\Delta X}) + \frac{V}{2} \frac{\Delta t}{\Delta Y} i \sin(\phi\Delta Y) - (\cos \phi\Delta Y - 1) \frac{\Delta t}{\text{Sc}(\Delta Y)^2}$$

After eliminating G' and H' in the equation (4.5) using the equations (4.6) and (4.7), the resultant equation and equations (4.6) and (4.7) can be written in matrix form as follows.

$$\begin{bmatrix} F' \\ G' \\ H' \end{bmatrix} = \begin{bmatrix} \frac{1-A}{1+A} & D_1 & D_2 \\ 0 & \frac{1-B}{1+B} & 0 \\ 0 & 0 & \frac{1-E}{1+E} \end{bmatrix} \begin{bmatrix} F \\ G \\ H \end{bmatrix} \quad (4.8)$$

where $D_1 = \frac{\Delta t \sin \alpha}{(1+A)(1+B)}$ and $D_2 = \frac{\Delta t \sin \alpha}{(1+A)(1+E)}$

Now, for the stability of the finite difference scheme, the modulus of each eigen value of the amplification matrix must not exceed unity. Since this matrix in the equation (4.8) is triangular, the eigen values are diagonal elements. Hence, the eigen values of the amplification matrix are $(1-A)/(1+A)$, $(1-B)/(1+B)$ and $(1-E)/(1+E)$. Assuming that U is everywhere non-negative and V is everywhere non-positive we get

$$\begin{aligned}
 A &= 2a \sin^2\left(\frac{\phi\Delta X}{2}\right) + 2c \sin^2\left(\frac{\phi\Delta Y}{2}\right) \\
 &+ i(a \sin \phi\Delta X + b \sin \phi\Delta Y) \\
 B &= 2a \sin^2\left(\frac{\phi\Delta X}{2}\right) + 2\left(1 + \frac{4}{3F}\right) \frac{c}{Pr} \sin^2\left(\frac{\phi\Delta Y}{2}\right) \\
 &+ i(a \sin \phi\Delta X + b \sin \phi\Delta Y) \\
 A &= 2a \sin^2\left(\frac{\phi\Delta X}{2}\right) + \frac{2}{Sc} c \sin^2\left(\frac{\phi\Delta Y}{2}\right) \\
 &+ i(a \sin \phi\Delta X + b \sin \phi\Delta Y)
 \end{aligned}$$

where

$$a = \frac{U\Delta t}{2\Delta X}, \quad b = \frac{|V|\Delta t}{2\Delta Y} \quad \text{and} \quad c = \frac{\Delta t}{(\Delta Y)^2}$$

Since the real part of A is greater than or equal to zero, $|(1-A)/(1+A)| \leq 1$ always. Similarly, $|(1-B)/(1+B)| \leq 1$ and $|(1-E)/(1+E)| \leq 1$.

Hence, the scheme is unconditionally stable. The local truncation error is $O(\Delta t^2 + \Delta Y^2 + \Delta X)$ and it tends to zero as Δt , ΔY and ΔX tend to zero. Therefore the scheme is compatible. The stability and compatibility ensures convergence.

V. RESULTS AND DISCUSSION

The aim of present study is to investigate the effect of radiation and mass transfer on an unsteady free convection flow of a viscous incompressible electrically conducting fluid over an inclined heated plate. A representative set of numerical results is shown graphically in Figs.1-20, to illustrate the influence of physical parameters viz., radiation parameter F , buoyancy ratio parameter N , Prandtl number Pr , Schmidt number Sc , and magnetic parameter M on the velocity, temperature, concentration, skin-friction, Nusselt number and Sherwood number. Here the value of Pr is chosen as 0.72, which corresponds to air. The values of Sc are chosen such that they represent Helium (0.24), Ammonia (0.78). The other parameters are arbitrarily chosen.

In order to ascertain the accuracy of the numerical results, the present study is compared with the previous study. The velocity profiles of the present problem for $Sc = 0.0$, $Pr = 0.72$, $N = 0.0$, $M=0.0$, $F=0.0$, $t=0.40$, $\alpha=60^\circ$, $X = 1.0$ are compared with the available solution of Begum et al [3] in Fig.1. It is observed that the present results are in good agreement with that of Begum et al. [3].

The effects of inclined angle α , on the transient velocity are displayed in Fig.2. It is noticed that the velocity increases with increasing values of the inclined angle. The effects of the magnetic parameter M on the transient velocity are illustrated in Fig.3. It is seen that, as expected, the velocity decreases with an increase in the magnetic parameter. The magnetic parameter is found to retard the velocity at all points of the flow field. It is because that the application of transverse magnetic field will result in a resistive type force (Lorentz force) similar to drag force which tends to resist the fluid flow and thus reducing its velocity. Also, the boundary layer thickness decreases with an increase in the magnetic parameter. The effect of N , on the transient velocity is displayed in Fig.4. It is noticed that the velocity increases with increasing values of the buoyancy ratio parameter. The effect of F , on the transient velocity is displayed in Fig.5. It can be seen that an increase in the thermal radiation parameter produces significant decreases in the velocity boundary layer.

The steady state temperature for different values of M is displayed in Fig.6. It can be seen that an increase in the magnetic parameter produces significant increases in the temperature boundary layer. Fig.7 shows the distribution of steady state temperature against Y for various N values. The profiles in Fig.7 attest that with an increase in N the thermal boundary layer will be decreased in thickness and there will be a corresponding uniformity of temperature distributions across the boundary layer. The effect of radiation parameter on the transient temperature can be observed from Fig.8. It can be seen that an increase in the radiation parameter leads to a decrease in the temperature.

Fig.9 shows the distribution of T against Y for various Pr values. The profiles in Fig.9 attest that with an increase in Pr the thermal boundary layer will be decreased in thickness and there will be a corresponding uniformity of temperature distributions across the boundary layer. It is observed that the maximum temperature

correspond to lower Pr values. The profiles also steepen and intersect the abscissa faster for higher Pr fluids i.e. temperatures across the boundary layer (normal to wall) reach zero faster.

The steady state concentration for the different values M is displayed in Fig.10. It can be seen that an increase in the magnetic parameter produces significant increase in the concentration boundary layer. The effect of N , on the steady state concentration is displayed in Fig.11. It is noticed that the concentration decreases with increasing values of the buoyancy ratio parameter. The effect of F , on the steady state concentration is represented in Fig.12. It is noticed that the concentration decreases with increasing values of the radiation parameter. Fig.13 shows the distribution of transient concentration against Y for various Sc values. The profiles in Fig.13 attest that with an increase in Sc the concentration boundary layer will be decreased in thickness and there will be a corresponding uniformity of concentration distributions across the boundary layer.

Fig.14 illustrates the effects of M , N and F on the local skin-friction. The local skin-friction is found to decrease due to an increase in the magnetic field strength. An increase in N or F produces an increase in the local skin-friction. The effects M , N and F on the average skin-friction are shown in Fig.15. It is observed that the average skin-friction increases as N or F increases, and it decreases as M increases. Figs.16 and 17 show the effect of Pr and F on the local and average Nusselt numbers respectively. It is observed that the local and average Nusselt numbers increase as Pr increases, and decrease as F increases. Figs.18, 19 and 20 display the effect of Sc and F on the local and average Sherwood numbers respectively. It can be observed that as Sc or F increases the local and average Sherwood numbers increase.

VI. CONCLUSIONS

An Unsteady two dimensional natural convection boundary layer flow of heat and mass transfer over heated plate with different inclinations in the presence of radiation has been studied. Implicit finite difference scheme of Crank-Nicolson type was employed to obtain the solution of the governing equations. The present solutions were validated by comparing with solutions existing in the literature. Our results show a good agreement with the existing work in the literature. The results are summarized as follows:

1. Magnetic field elevates the temperature and concentration, and reduces the velocity.
2. The angle of inclination enhances the velocity
3. The radiation enhances the velocity and temperature, and reduces the concentration.
4. The radiation enhances the local and average skin-friction, and local and average Sherwood number, and reduces the local and average Nusselt number.

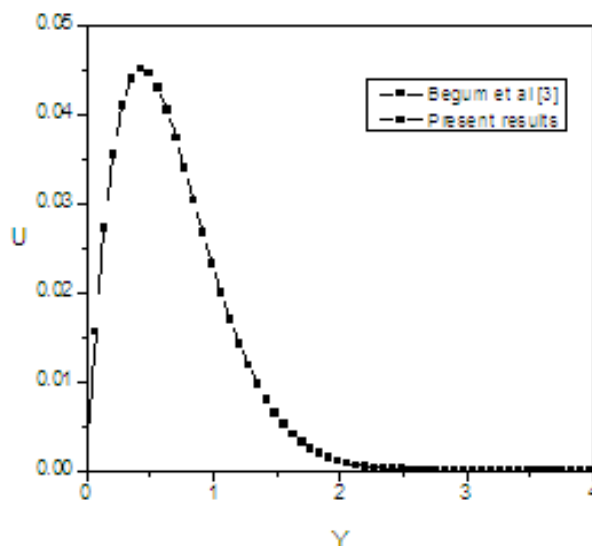


Fig. 1 Comparison of velocity for $t=0.40$, $Pr=0.72$ and $\alpha=60^\circ$

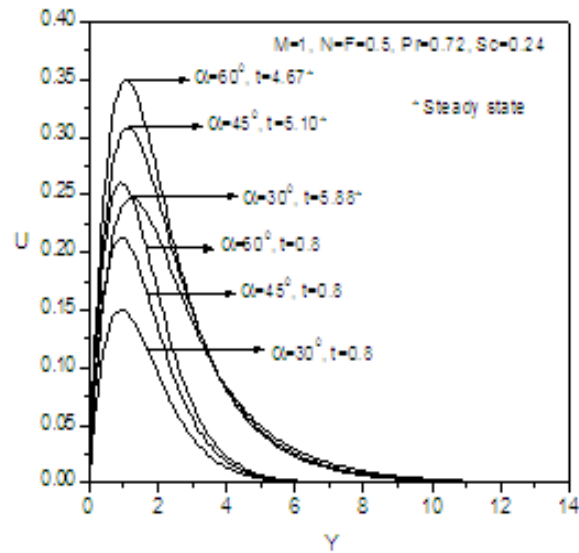


Fig 2 Transient velocity at $X=1.0$ for the different values of α .

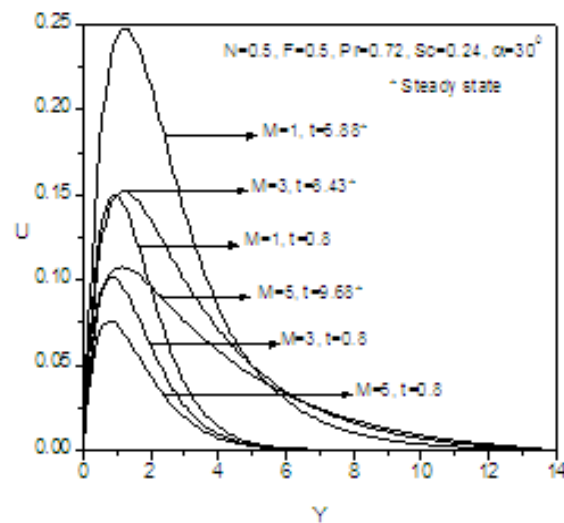


Fig 3 Transient velocity at $X=1.0$ for the different values of M .

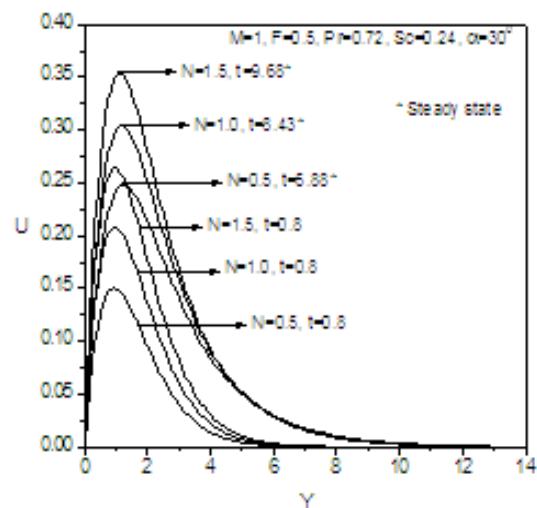


Fig 4 Transient velocity at $X=1.0$ for the different values of N .

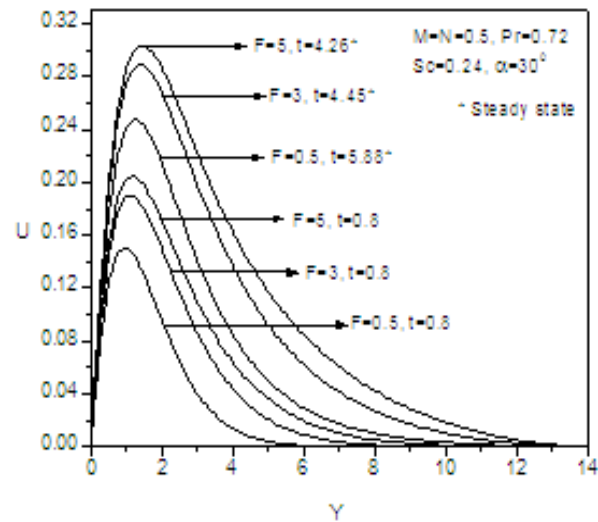


Fig 5 Transient velocity for at X=1.0 the different values of F.

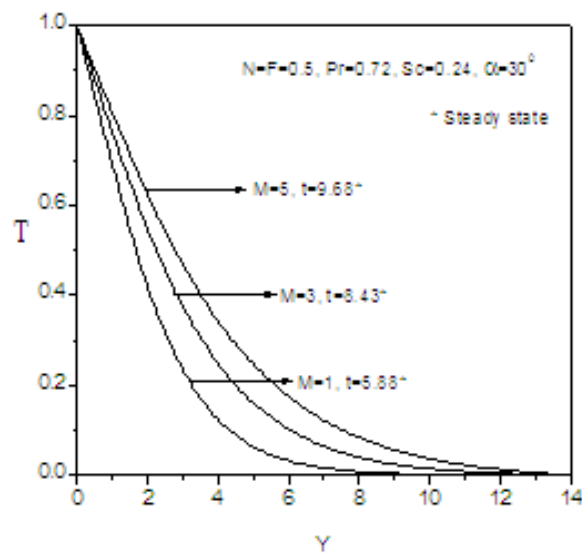


Fig 6 Steady state temperature for different values of M at X=1.0.

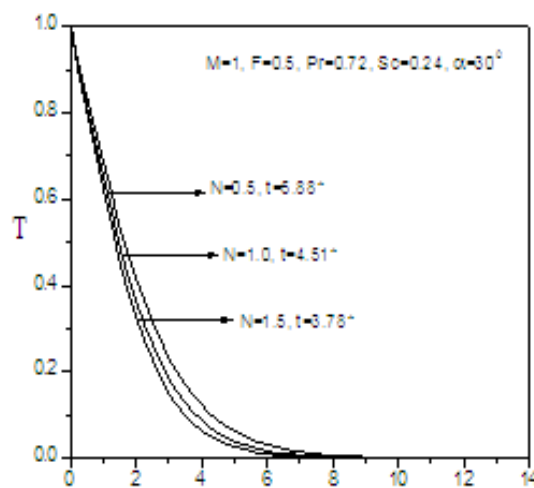


Fig 7 Steady state temperature for different values of N at X=1.0.

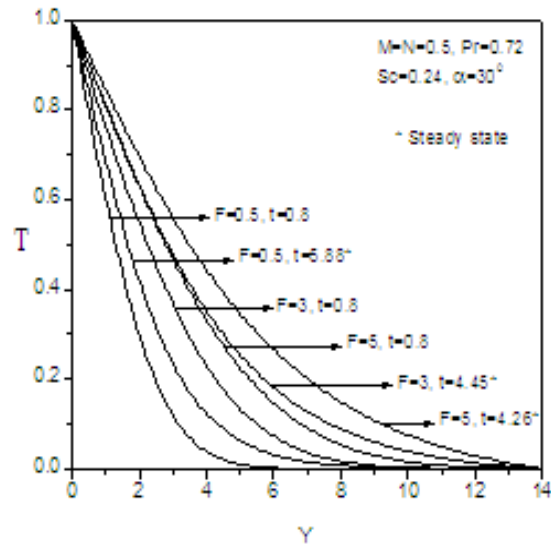


Fig 8 Transient temperature at $X=1.0$ for different values of F .

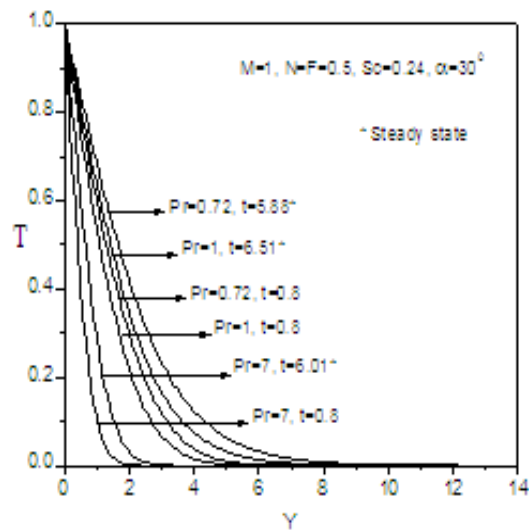


Fig 9 Transient temperature at $X=1.0$ for different values of Pr .

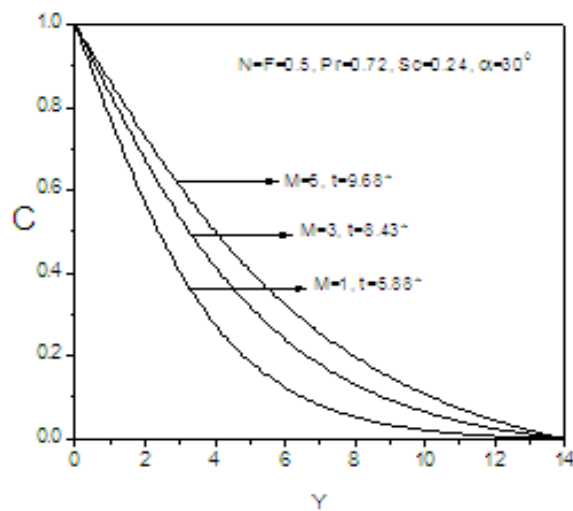


Fig 10 Steady state concentration for different values of M at $X=1.0$.

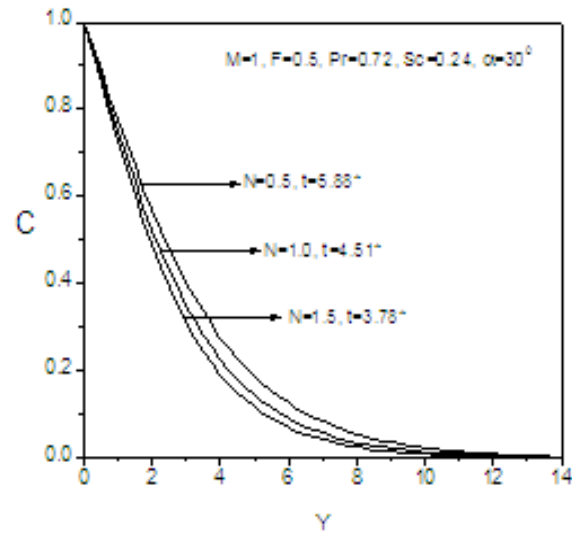


Fig 11 Steady state concentration for different values of N at $X=1.0$.

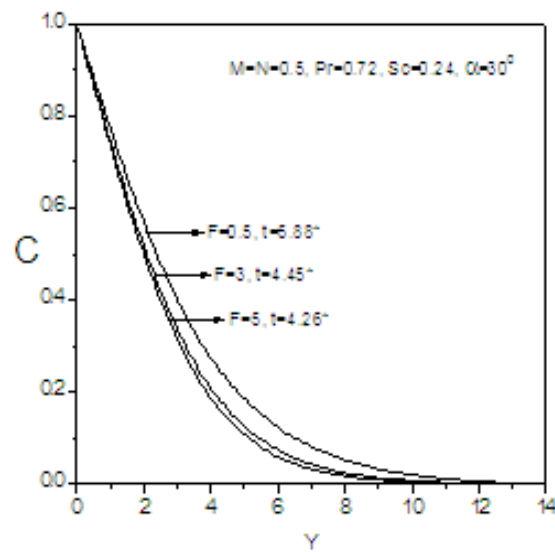


Fig 12 Steady state concentration for different values of F at $X=1.0$.

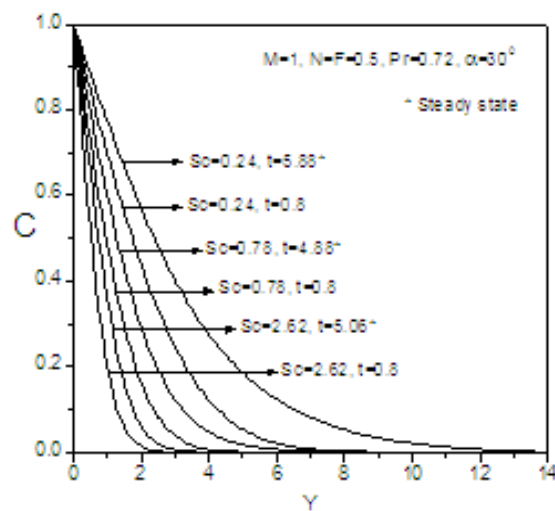


Fig 13 Transient concentration at $X=1.0$ for the different values of Sc .

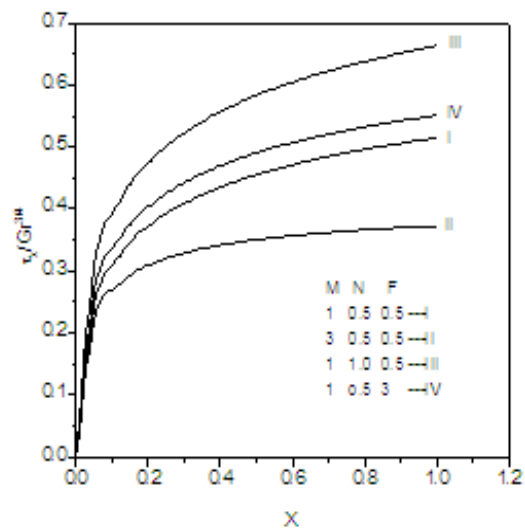


Fig 14 The effects of M , N and F on local skin friction.

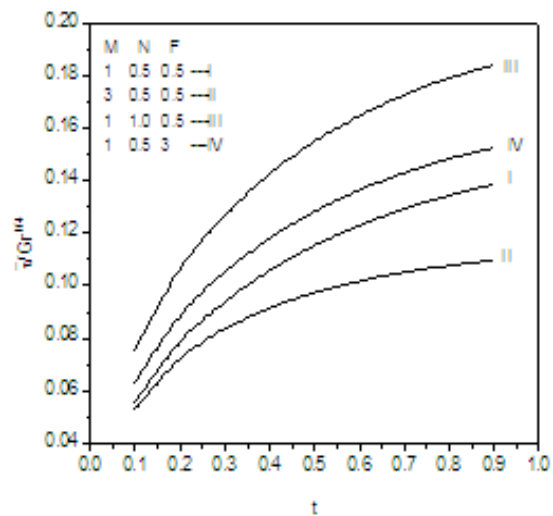


Fig 15 The effects of M , N and F on average skin friction.

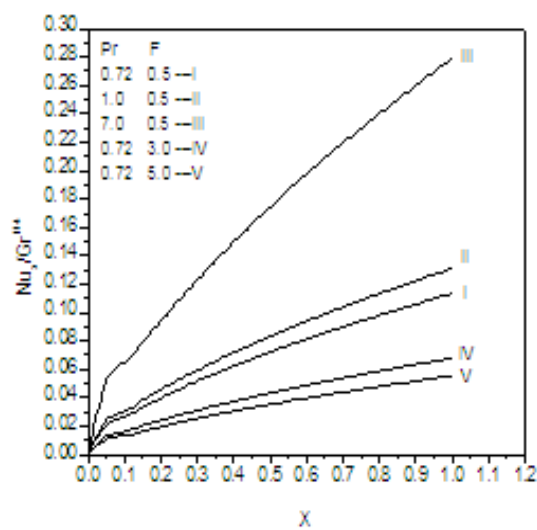


Fig 16 The effects of Pr and F on local Nusselt number.

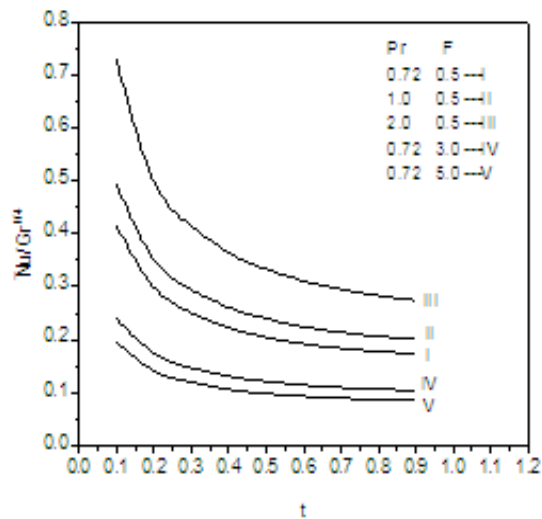


Fig 17 The effects of Pr and F on average Nusselt number.

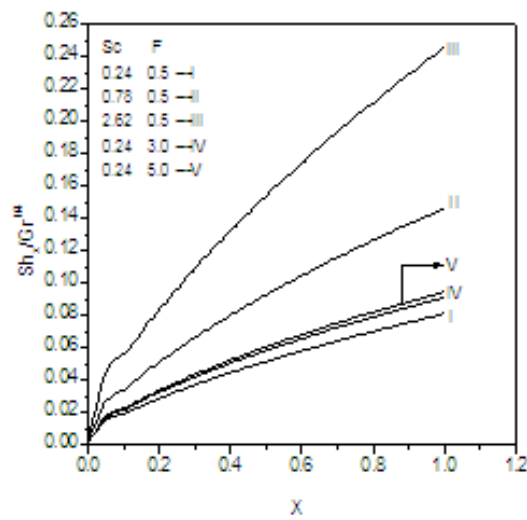


Fig 18 The effects of Sc and F on local Sherwood number.

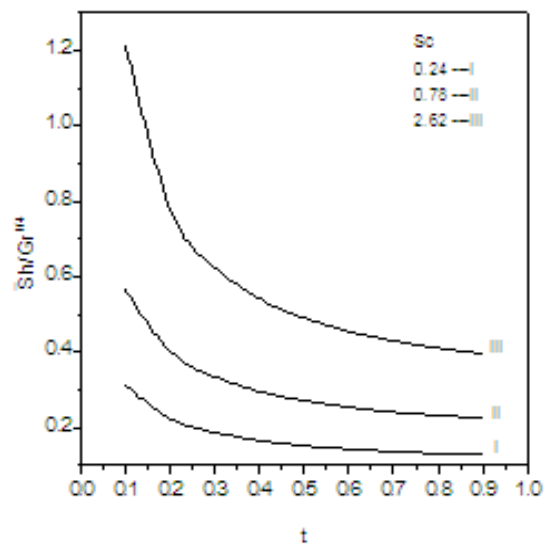


Fig 19 The effect of Schmidt number on average Sherwood number.

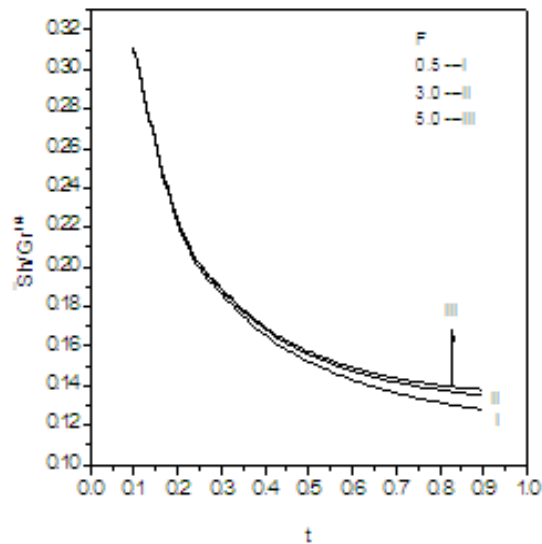


Fig 20 The effect of R on average Sherwood number.

REFERENCES

- [1]. Callahan, G. D. and Marner, W.J., (1976), Transient free convection with mass transfer on an isothermal vertical flat plate, *Int. J. Heat and Mass transfer*, Vol.19, pp. 165-174.
- [2]. Soundalgekar, V.M. and Ganesan, P., (1980), Transient free convection flow on a semi-infinite vertical plate with mass transfer, *Reg. J. Energy Heat Mass Transfer*, Vol.2, pp. 83-91.
- [3]. Asma Begum, Abdul Maleque, Md., Ferdows, M., and Masahiro Ota, (2012), Finite Difference Solution of Natural Convection Flow over a Heated Plate with Different Inclination and Stability Analysis, *Applied Mathematical Sciences*, Vol.6, No.68, pp.3367-3379.
- [4]. Callahan, G. D. and Marner, W. J. (1976), *Int. J. Heat and Mass Trans.*, pp 149-165.
- [5]. Soundalgekar, V. M., and Ganesan, P., (1985) Finite difference analysis of transient free convection with mass transfer on an isothermal vertical flat plate., *Int. J. Engg Sci.* 19, pp 757-770.
- [6]. Marner, W. J. and Callahan, G. D., (1976), *Int. J. Heat and Mass Trans.*, pp 19,165.
- [7]. Chamkha, A. J., Rahim, A. and Khalid, A., (2001), *Heat and Mass trans.*, Vol.37, pp.117.
- [8]. Ganesan, P. and Palani, G., (2003), Free convection effects on the flow of water at 4°C past a semi-infinite inclined plate, *Heat and mass Transfer*, Vol.39, pp.785-789.
- [9]. Huges, W.F. and Young, F.J., (1966), *The Electro-Magneto Dynamics of fluids*, John wiley and sons, New York.
- [10]. Raptis, A., (1986), Flow through a porous medium in the presence of magnetic field, *Int. J. Energy. Res.*, Vol.10, pp. 97-101.
- [11]. Helmy, K.A., (1998), MHD unsteady free convection flow past a vertical porous plate, *ZAMM*, Vol.78, pp. 255-270.
- [12]. Elabashbeshy, E.M.A., (1997), Heat and Mass transfer along a vertical plate with variable surface temperature and concentration in the presence of the magnetic field, *Int. J. Eng Sci.*, Vol.34, pp. 515- 522.
- [13]. Cess, R.D., (1964), Radiation effects upon boundary layer flow of an absorbing gas, *ASME. J. Heat Transfer*, Vol.86c, pp.469-475.
- [14]. Mosa, M.F., (1979), Radiative heat transfer in horizontal MHD channel flow with buoyancy effects and an axial temperature gradient, Ph.D. thesis, Mathematics Department, Bradford University, England, U.K.,.
- [15]. Nath, O., Ojha, S.N. and Takhar, H.S., (1991), A study of stellar point explosion in a radiative MHD medium, *Astrophysics and Space Science*, Vol.183, pp.135-145.
- [16]. Takhar H.S., Gorla R.S.R. and Soundalgekar, V.M., (1996), Radiation effects on MHD free convection flow of a gas past a semi-infinite vertical plate, *Int. J. Numer. Methods Heat Fluid Flow*, Vol.6(2), pp77.
- [17]. Gamal El-Din., Azzam, A., (2002), Radiation effects on the MHD mixed free-forced convection flow past a semi-infinite moving vertical plate for high temperature difference, *Phys. Scripta*, Vol.66, pp71.
- [18]. Brewster, M.Q., (1992), *Thermal radiative transfer and properties*, John Wiley & Sons, New York.

Analysis of Genomic and Proteomic Sequence Using Fir Filter

P.Saranya¹, V.Harigopalkrishna², D.Murali³, M.Ravikumar⁴, M.Sujatha⁵
^{1,2,3,4,5}ECE, LIET, INDIA

ABSTRACT: Bioinformatics is a field of science that implies the use of techniques from mathematics, informatics, statistics, computer science, artificial intelligence, chemistry, and biochemistry to solve biological problems usually on the molecular level. Digital Signal Processing (DSP) applications in genomic sequence analysis have received great attention in recent years. DSP principles are used to analyse genomic and proteomic sequences. The DNA sequence is mapped into digital signals in the form of binary indicator sequences. Signal processing techniques such as digital filtering is applied to genomic sequences to identify protein coding region. Frequency response of genomic sequences is used to solve many optimization problems in science, medicine and many other applications. The aim of this paper is to describe a method of generating Finite Impulse Response (FIR) of the genomic sequence. The same DNA sequence is used to convert into proteomic sequence using transcription and translation, and also digital filtering technique such as FIR filter applied to know the frequency response. The frequency response is same for both gene and proteomic sequence.

Keywords: DSP, FIR, Frequency response, Genomic sequence, Proteomic sequences

I. INTRODUCTION

This paper represents a method for generating the response of genomic sequence using fir filter. Genomics is a highly cross-disciplinary field that creates paradigm shifts in such diverse areas as medicine and agriculture. It is believed that many significant scientific and technological endeavours in the 21st century will be related to the processing and Interpretation of the vast information that is currently revealed from sequencing the genomes of many living organisms, including humans. Genomic information is digital in a very real sense; it is represented in the form of sequences of which each element can be one out of a finite number of entities. Such sequences, like DNA and proteins, have been mathematically represented by character strings, in which each character is a letter of an alphabet. In the case of DNA, the alphabet is size 4 and consists of the letters A, T, C and G; in the case of proteins, the size of the corresponding alphabet is 20. Biomolecular sequence analysis has already been a major research topic among computer scientists, physicists, and mathematicians.

The main reason that the field of signal processing does not yet have significant impact in the field is because it deals with numerical sequences rather than character strings. The possibility of finding a wide application of DSP techniques to the analysis of genomic sequences arises when these are converted appropriately into numerical sequences, for which several rules have been developed. Notice that genomic signals do not have time or space as the independent variable, as occur with most physical signals. However, if we properly map character string into one or more numerical sequences, then digital signal processing (DSP) provides a set of novel and useful tools for solving highly relevant problems. Even the process of mapping DNA into proteins and the interdependence of the two kinds of Sequences can be analyzed using simulations based on digital filtering. The principles of DSP techniques are used to analyze both DNA and protein sequences.

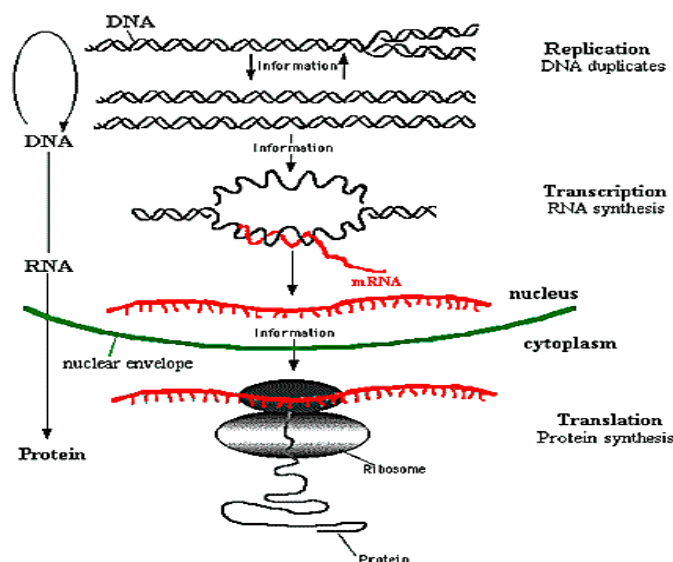
DSP techniques such as FIR filter are applied to find the frequency response. This response is used to identify protein coding region. When the DNA sequence is converted into protein sequence with the applications of DSP techniques, the structure of DNA and PROTEIN sequence will be approximately same. The frequency response of DNA and converted protein sequence can be obtained with the help of DSP algorithms. Among the different DSP algorithms digital filters are one of technique used for the analysis of DNA and PROTEIN sequences. With the use of FIR filter the response of these sequences can be obtained. Using the Kaiser window the linear phase application will be stable. These DSP-based approaches result in alternative mathematical formulations and may provide improved computational techniques for the solution of useful problems in genomic information science and technology. As DNA sequences are character strings, for DSP techniques to be applicable to these data, methods converting DNA sequences to numerical sequences are required. the generated numerical sequences are then processed using DSP techniques.

II. CONCEPTS OF MOLECULAR BIOLOGY

2.1 Central Dogma Of Molecular Biology

The Central dogma of molecular biology is that DNA codes for RNA and RNA codes for proteins. Thus the production of a protein is a two-stage process, with RNA playing a key role in both stages.

Transcription is the process by which the information contained in a section of DNA is transferred to a newly assembled piece of messenger RNA(mRNA). It is facilitated by RNA polymerase and transcription factors. In eukaryotic cells the primary transcript pre-mRNA must be processed further in order to ensure translation. This normally includes a 5' cap a poly-A tail and splicing. Alternative splicing can also occur, which contributes to the diversity of proteins any single mRNA can produce.



The Central Dogma of Molecular Biology

Eventually, this mature mRNA finds its way to a ribosome, where it is translated. In prokaryotic cells, which have no nuclear compartment, the process of transcription and translation may be linked together. In eukaryotic cells, the site of transcription the cell nucleus is usually separated from in the site of translation the cytoplasm), so the mRNA must be transported out of the nucleus into the cytoplasm, where it can be bound by ribosome. The mRNA is read by the ribosome as triplet codon, usually beginning with an AUG (adenine-Uracil-guanine), or initiator methionine codon downstream of the ribosome binding site. As the amino acids are linked into the growing peptide chain, they begin folding into the correct conformation. Translation ends with a UAA, UGA, or UAG stop codon. The nascent polypeptide chain is then released from the ribosome as a mature protein.

2.2 Dna

A single strand of DNA is a bio molecule consisting of many linked, smaller components called nucleotides. Each nucleotide is one of four possible types designated by the letters A, T, C, and G and has two distinct ends, the 5' end and the 3'end, so that the 5' end of a nucleotide is linked to the 3' end of another nucleotide by a strong chemical bond (covalent bond), thus forming a long, one-dimensional chain (backbone) of a specific directionality. Therefore, each DNA single strand is mathematically represented by a character string, which, by convention specifies the 5' to 3' direction when read from left to right. Single DNA strands tend to form double helices with other single DNA strands. Thus, a DNA double strand contains two single strands called complementary to each other because each nucleotide of one strand is linked to a nucleotide of the other strand by a chemical bond (hydrogen bond), so that A is linked to T and vice versa, and C is linked to G and vice versa. Each such bond is weak (contrary to the bonds forming the backbone), but together all these bonds create a stable, double helical structure. The two strands run in opposite directions, as shown in Figure, in which we see the sugar-phosphate chemical structure of the DNA backbone created by strong (covalent) bonds, and that each nucleotide is characterized by a base that is attached to it. The two strands are linked by a set of weak (hydrogen) bonds. The bottom left diagram is a simplified, straightened out depiction of the two linked strands.

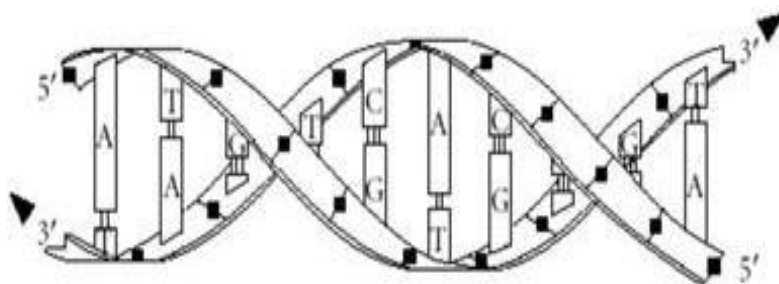
For example, the part of the DNA double strand shown in Figure is

5' - C-A-T-T-G-C-C-A-G-T - 3'

3' - G-T-A-A-C-G-G-T-C-A - 5'

Because each of the strands of a DNA double strand uniquely determines the other strand, a double-stranded DNA molecule is represented by either of the two character strings read in its 5' to 3' direction. Thus, in the example above, the character strings CATTGCCAGT and ACTGGCAATG can be alternatively used to describe the same DNA double strand, but they specify two different single strands which are complementary to each other. DNA strands that are complementary to themselves are called self-complementary, or palindromes. For example AATCTAGATT is a palindrome. DNA molecules store the digital information that constitutes the genetic blueprint of living organisms. This digital information has been created and reliably stored throughout billions of years of evolution during which some vital regions of DNA sequences have been remarkably preserved, despite striking differences in the body plans of various animals.

A DNA sequence can be separated into two types of regions: genes and intergenic spaces. Genes contain the information for generation of proteins. Each gene is responsible for the production of a different protein. Even though all the cells in an organism have identical genes, only a selected subset is active in any particular family of cells.



2.3 Rna

Ribonucleic acid (RNA) is a chemical similar to a single strand of DNA. Together with DNA, RNA comprises the nucleic acids, which, along with proteins, constitute the three major macromolecules essential for all known forms of life. Like DNA, RNA is assembled as a chain of nucleotides, but is usually single-stranded. Cellular organisms use messenger RNA (mRNA) to convey genetic information often notated using the letters G, A, U, and C for the nucleotides guanine, adenine, Uracil and cytosine that directs synthesis of specific proteins, while many viruses encode their genetic information using an RNA genome.

Some RNA molecules play an active role within cells by catalyzing biological reactions, controlling gene expression, or sensing and communicating responses to cellular signals. One of these active processes is protein synthesis, a universal function whereby mRNA molecules direct the assembly of proteins on ribosome. This process uses transfer RNA (tRNA) molecules to deliver amino acids to the ribosome, where ribosomal RNA (rRNA) links amino acids together to form proteins

2.4 Protiens

Proteins are large biological molecules, or macromolecules, consisting of one or more chains of amino acid residues. Proteins perform a vast array of functions within living organisms, including catalyzing metabolic reactions, replicating DNA, responding to stimuli, and transporting molecules from one location to another. Proteins differ from one another primarily in their sequence of amino acids, which is dictated by the nucleotide sequence of their genes, and which usually results in folding of the protein into a specific three-dimensional structure that determines its activity. Like other biological macromolecules such as polysaccharides and nucleic acids, proteins are essential parts of organisms and participate in virtually every process within cells. Many proteins are enzymes that catalyze biochemical reactions and are vital to metabolism. Proteins also have structural or mechanical functions, such as actin and myosin in muscle and the proteins in the cytoskeleton, which form a system of scaffolding that maintains cell shape. Other proteins are important in cell signalling, immune responses, cell adhesion, and the cell cycle. Proteins are also necessary in animals' diets, since animals cannot synthesize all the amino acids they need and must obtain essential amino acids from food. Through the process of digestion, animals break down ingested protein into free amino acids that are then used in metabolism.

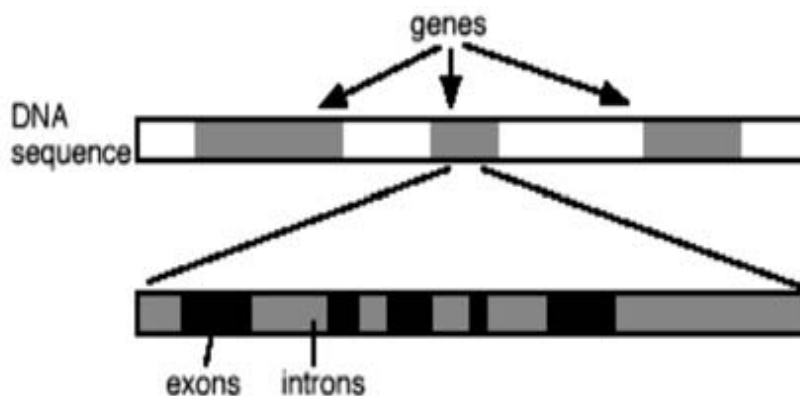
2.5 GENETIC CODE

Protein synthesis is governed by the genetic code which maps each of the 64 possible triplets (codons) of DNA characters into one of the 20 possible amino acids. Fig. shows the genetic code in which the 20 amino acids are designated by both their one-letter and three-letter symbols. A particular triplet, ATG, serves as the START codon and it also codes for the M amino acid (methionine); thus, methionine appears as the first amino acid of proteins, but it may also appear in other locations. We also see that there are three STOP codons indicating termination of amino acid chain synthesis, and the last amino acid is the one generated by the codon

preceding the STOP codon. Coding of nucleotide triplets into amino acids can happen in either the forward or the reverse direction based on the complementary DNA strand. Therefore, there are six possible reading frames for protein coding DNA regions.

		SECOND POSITION OF CODON					
		T	C	A	G		
F I R S	T	TTT Phe (F)	TCT Ser (S)	TAT Tyr (Y)	TGT Cys (C)	T C A G	T H I R
		TTC Phe (F)	TCC Ser (S)	TAC Tyr (Y)	TGC Cys (C)		
		TTA Leu (L)	TCA Ser (S)	TAA (STOP)	TGA (STOP)		
		TTG Leu (L)	TCG Ser (S)	TAG (STOP)	TGG Trp (W)		
P O S I T I O N	C	CTT Leu (L)	CCT Pro (P)	CCT Pro (P)	CGT Arg (R)	T C A G	T R D P
		CTC Leu (L)	CCC Pro (P)	CCC Pro (P)	CGC Arg (R)		
		CTA Leu (L)	CCA Pro (P)	CCA Pro (P)	CGA Arg (R)		
		CTG Leu (L)	CCG Pro (P)	CCG Pro (P)	CGG Arg (R)		
S I T E	A	ATT Ile (I)	ACT Thr (T)	AAT Asn (N)	AGT Ser (S)	T C A G	T O S I T E
		ATC Ile (I)	ACC Thr (T)	AAC Asn (N)	AGC Ser (S)		
		ATA Ile (I)	ACA Thr (T)	AAA Lys (K)	AGA Arg (R)		
		ATG Met (M)	ACG Thr (T)	AAG Lys (K)	AGG Arg (R)		
S I T E	G	GTT Val (V)	GCT Ala (A)	GAT Asp (D)	GGT Gly (G)	T C A G	T I O N
		GTC Val (V)	GCC Ala (A)	GAC Asp (D)	GGC Gly (G)		
		GTA Val (V)	GCA Ala (A)	GAA Glu (E)	GGA Gly (G)		
		GTG Val (V)	GCG Ala (A)	GAG Glu (E)	GGG Gly (G)		

The total number of nucleotides in the protein coding area of a gene will be a multiple of three, that the area will be bounded by a START codon and a STOP codon, and that there will be no other STOP codon in the coding reading frame in between. However, given a long nucleotide sequence, it is very difficult to accurately designate where the genes are. Accurate gene prediction becomes further complicated by the fact that, in advanced organisms, protein coding regions in DNA are typically separated into several isolated sub regions called exons. The regions between two successive exons are called introns. When DNA is copied into mRNA during transcription, the introns are eliminated by a process called splicing. The same gene can code for different proteins. This happens by joining the exons of a gene in different ways. This is called alternative splicing. Alternative splicing seems to be one of the main purposes for which the genes in eukaryotes are split into exons. The mRNA obtained after splicing is uninterrupted and is used for making proteins.



III. SIGNAL PROCESSING FOR DNA SEQUENCES

3.1 Collection of Input Data

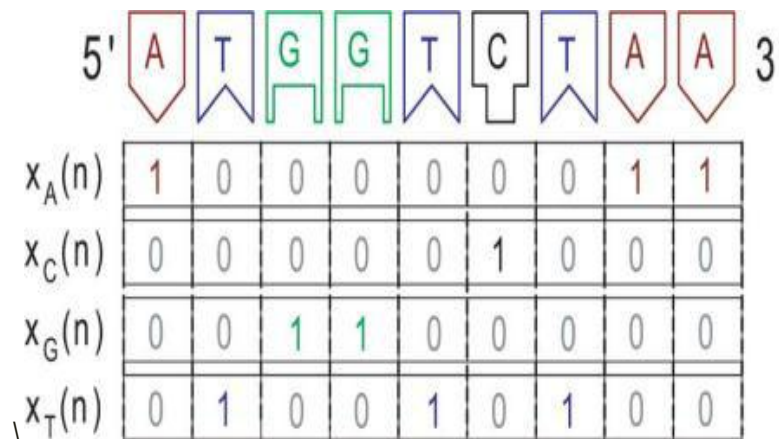
Most of the identified genomic data is publicly available over the Web at various places worldwide, one of which is the entrez search and retrieval system of the National Center for Biotechnology Information (NCBI) at the National Institutes of Health (NIH). The NIH nucleotide sequence database is called GenBank and contains all publicly available DNA sequences. For example, one can go to <http://www.ncbi.nlm.nih.gov/entrez> and identify the DNA sequence with Accession Number AF324494 and AF320294; choose Nucleotide under Search and then fill out the other entry by typing: [Accession Number] and pressing "Go." Clicking on the resulting accession number will show the annotation for the genes as well as the whole nucleotide sequence in the form of raw data. Similarly, *Entrez* provides access to databases of protein sequences as well as 3-D macromolecular structures, among other options. As another example, a specialized repository for the processing

and distribution of 3-D, macromolecular structures can be found in Public databases. The collected nucleotide sequences from such databases are such as AF324494 and AF320294.

3.2 Mapping of DNA Strand into Digital Signals

As explained Genomic information is in the form of alphabets A, T, C and G. Signal processing deals with numerical sequences. Hence character strings have to be mapped into one or more numerical sequences. Then signal processing techniques can be applied for analysis of DNA sequences.

In a DNA sequence we have to assign numbers to the characters A, T, C, G, respectively. A proper choice of the numbers *can* provide potentially useful properties to the numerical sequence. The first approach to convert genomic information in numerical sequences was given by Voss with the definition Of the indicator sequences, defined as binary sequences for each base, where 1 at position k indicates the presence of the base at that position, and 0 its absence.



For example, given the DNA sequence

ACTTAGCTACAGA...

The binary indicator sequences X for each base A, T, C and G are respectively:

$X_A [K] = 1000100010101...$

$X_T [K] = 0011000100000...$

$X_C [K] = 0100001001000...$

$X_G [K] = 0000010000010...$

The main advantages of the indicator sequences are their simplicity, and the fact that they can provide a four dimensional representation of the frequency spectrum of a character string, by means of computing the DFT of each one of the indicator sequences. The binary indicator sequences of both DNA and PROTEIN structure can be obtained. This can be applied to the digital filters in order to obtain the frequency response of sequences

3.3 Digital Filters

Digital filters that incorporate *digital-signal-processing* (DSP) techniques have received a great deal of attention in technical literature in recent years.

A digital filter is a discrete system capable of realizing some transformation to an input discrete numerical sequence. There are different classes of digital filters namely linear, nonlinear, time-invariant or adaptive digital filters. Digital filters are characterized by numerical algorithms that can be implemented in any class of digital processors. The system transfer function relates the input and output sequences $x[n]$ and $y[n]$, through their respective Z transforms $X[z]$ and $Y[z]$. A variety of digital filter design techniques allow to obtain any desired magnitude response with frequency selectivity properties. Digital Filters can be very complicated devices, but they must be able to map to the difference equations of the filter design. This means that since difference equations only have a limited number of operations available (addition and multiplication), digital filters only have limited operations that they need to handle as well. There are only a handful of basic components to a digital filter, although these few components can be arranged in complex ways to make complicated filters. A digital filter computes a quantized time-domain representation of the convolution of the sampled input time function and a representation of the weighting function of the digital filter. They are realized by an extended sequence of multiplications and additions carried out at a uniform spaced sample interval. In particular, LTI digital filters can pertain to one of two categories, according to the duration of their response to the impulse, or Dirac delta function, when it is used as the input signal: infinite (IIR) or finite (FIR) impulse

response. A variety of digital filter design techniques allow to obtain any desired magnitude response with frequency selectivity properties, whereas it is desired that the phase response be a linear function of ω , in order to have low distortion .

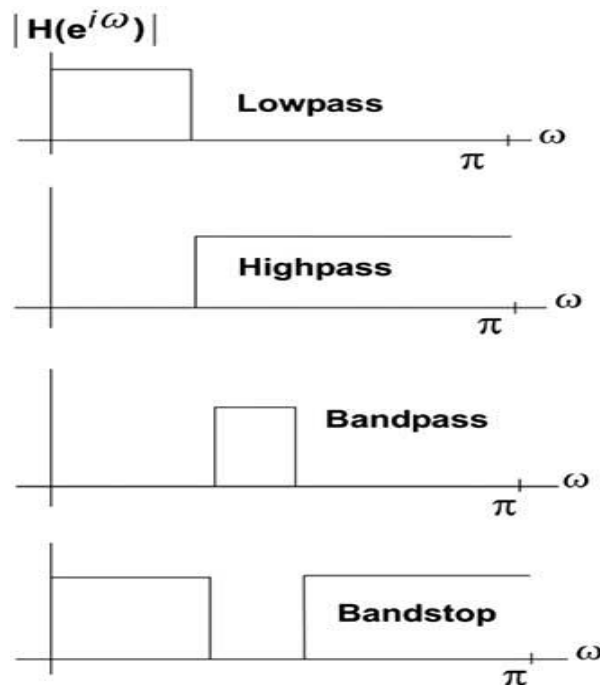
3.3.1 Fir Filter

In signal processing, a finite impulse response (FIR) filter is a filter whose impulse response (or response to any finite length input) is of *finite* duration, because it settles to zero in finite time. The impulse response of an Nth-order discrete-time FIR filter lasts for $N + 1$ samples, and then settles to zero. An FIR filter is based on a feed-forward difference equation

FIR digital filters are characterized by a discrete convolution operation of the form

$$y[n] = \sum_{m=0}^{N-1} h[m]x[n - m]$$

In this equation, $h[m]$ is the impulse response of the filter, which has a length of N samples. On the other hand, a property of FIR digital filters is that they can exhibit a perfect linear phase response under certain conditions of symmetry in their impulse response. This has been a motivation for the use of digital FIR filters in many applications. According to the frequency interval (band) transmitted, the magnitude of the basic ideal prototype filter frequency responses, can be *low pass*, *high pass*, *band pass* and *band stop*.



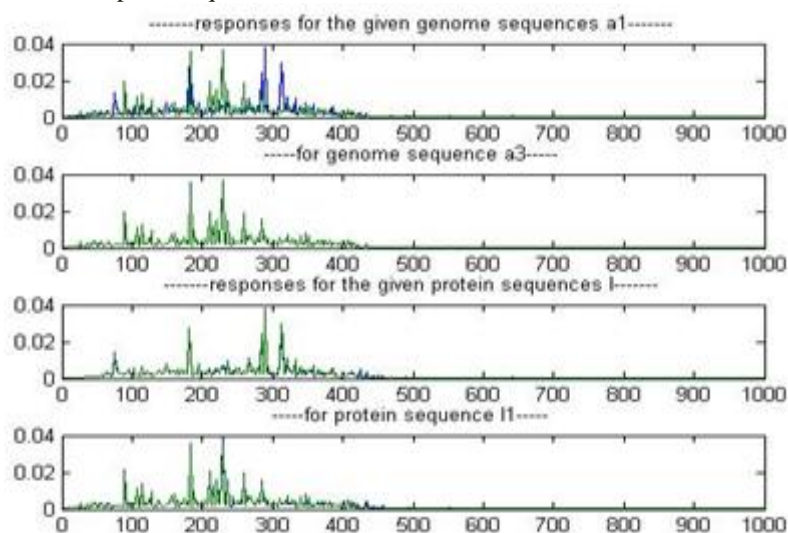
They can easily be designed to be linear phase by making the coefficient sequence symmetric. This property is sometimes desired for phase-sensitive applications the response of DNA sequence and protein sequence are generated using the FIR filter.FIR has different Types of implementations but this paper is implemented using the Kaiser Windowing technique.

3.3.2 Kaiser Window

The Kaiser window is an approximation to the prolate-spheroidal window, for which the ratio of main lobe energy to the side lobe energy is maximised. For a Kaiser window of particular length, the parameter β controls the side lobe height. For a given β , the side lobe height is fixed with respect to window length. As β increases the side lobe height decreases and the main lobe width increases. Kaiseord returns filter order n and beta parameter to specify a Kaiser window for use with the fir1 function. Given a set of specifications in the frequency domain, Kaiseord estimates the minimum FIR filter order that will exactly meet the specifications. Kaiseord converts the given filter specifications into pass band and stop band ripples and converts cut-off frequencies into the form needed for windowed FIR filter design.kaiser window method is constrained to produce filters with minimum deviation in all of the bands. The Kaiser window is a kind of adjustable window function which provides independent control of the main lobe width and ripple ratio. But the Kaiser window has the disadvantage of higher computational complexity due to the use of Bessel functions.

Results

The frequency response for the genomic and proteomic sequences are generated using fir filter are shown below. The peaks represent the exons which help in predicting the cancer cells. This can be useful for many genetic applications using different dsp techniques.



IV. CONCLUSION

The application of Digital Signal Processing in Genomic Sequence Analysis has received great attention in the last few years, providing a new insight in the solution of various problems. The responses for the DNA and genomic sequences when compared with the ideal characteristics of those sequences, provides the information regarding sequences. This help in developing new diagnostic tools, therapeutic procedures and pharmacological drugs for applications like cancer classification and prediction.

REFERENCES

- [1]. D. Anastassiou, —Genomic signal processing,|| *IEEE Sign Proc Mag*, vol. 18, no. 4, pp. 8-20, 2001.
- [2]. D. Anastassiou, —DSP in genomics processing and frequency-domain analysis of character strings,|| in *Proc. IEEE International Conference on Acoustics, Speech, and Signal Processing*, 2001, pp. 1053-1056.
- [3]. J. V. Lorenzo-Ginori, A. Rodriguez-Fuentes, R. G. Abalo, and R. S. Rodriguez, —Digital signal processing in the analysis of genomic sequences,|| *Current Bioinformatics*, vol. 4, pp. 28 – 40, 2009.
- [4]. D. L. Brutlag, —Understanding the human genome,|| in *Scientific American: Introduction to Molecular Medicine*, P. Leder, D. A. Clayton, and E. Rubenstein, Eds., New York NY: Scientific American Inc. 1994, pp. 153-168,.
- [5]. A. Khare, A. Nigam, and M. Saxena, —Identification of DNA sequences by signal processing tools in protein-coding regions,|| *Search & Research*, vol. 2, no. 2, pp. 44-49, 2011.
- [6]. J. Tuqan and A. Rushdi, —A DSP approach for finding the codon bias in DNA sequences,|| *IEEE J Select Topics Sign Proc*, vol. 2, pp. 343- 356, 2008.
- [7]. R. K. Deergha and M. N. S. Swamy, —Analysis of genomics and proteomics using DSP techniques,|| *IEEE Transactions on Circuits and systems—I: Regular papers*, vol. 55, no. 1, pp. 370-379, 2008.
- [8]. E. N. Trifonov, —3-, 10.5-, 200- and 400-base periodicities in genome sequences,|| *Physica A* , vol. 249, pp. 511-516, 1998.
- [9]. D. Kotlar and Y. Lavner, —Gene prediction by spectral rotation measure: a new method for identifying protein-coding regions,|| *Genome Res* , vol. 13, pp. 1930-1937, 2003.
- [10]. T. W. Fox and A. Carreira, —A digital signal processing method for gene prediction with improved noise suppression,|| *EURASIP J Appl Sign Proc*, vol. 1, pp. 108-111, 2004.
- [11]. S. Datta and A. Asif, —DFT based DNA splicing algorithms for prediction of protein coding regions,|| in *Proc. IEEE Conference Record of 38th Asilomar Conference on Signals, Systems and Computer*, 2004, vol. 1, pp. 45-49.
- [12]. P. P. Vaidyanathan and B. J. Yoon, —The role of signal-processing concepts in genomics and proteomics,|| *J Franklin Inst* , vol. 341, pp. 111-35, 2004.
- [13]. J. Tuqan and A. Rushdi, —A DSP perspective to the period-3 detection problem,|| in *Proc. IEEE International Workshop on Genomic Signal Processing and Statistics*, 2006, pp. 53-54.
- [14]. A. Rushdi and J. Tuqan, —Trigonometric transforms for finding repeats in DNA sequences,|| in *Proc. IEEE International Workshop on Genomic Signal Processing and Statistics*, 2008, pp. 1-4.
- [15]. S. S. Sahu and G. Panda, —A DSP approach for protein coding region identification in DNA sequence,|| *International Journal of Signal and Image Processing*, vol. 1, no. 2, pp. 75-79, 2010.

Speech Recognition for Agriculture based Interactive Voice Response System

Santosh Gaikwad¹, Bharti Gawali², Suresh Mehrotra³

*(Department of Computer Science and Information Technology
Dr. Babasaheb Ambedkar Marathwada University, Aurangabad Maharashtra, India

ABSTRACT: *Speech is the most desirable medium of communication between humans. The goal of speech processing is to provide natural interfaces to human –computer interaction through speech input and speech output capabilities in Regional languages. Speech being a natural mode of communication among human beings has the potential of being primary as well as convenient mode of interaction with computers. It is desirable to have a human computer dialogue in audio mode to take place in local language. Marathi is one of most widely used language in Maharashtra. The Interactive Voice response system is well known application of speech processing. This paper explores a new approach of IVRS system for agricultural assistance to farmers in Marathi.*

Keywords: *IVRS, Speech Recognition, CSL*

I. Introduction

The prevalent mode of human computer interaction is via a keyboard or a pointing device for input and visual display unit or a printer for output. In this age the machine oriented interfaces restrict the usage to minuscule fraction of the population, who are both computer literate and conversant with written English. This calls for human oriented interfaces with machines. Speech occupies a prominent role in human interaction. Thus, it is natural that people are expecting speech interfaces with computers [1]. It is possible that a computer speech interface permits spoken dialogue in one's native language. The advantage of this is that the majority of people can be benefit from this technology, when they are able to interact with computers in their native language. This advantage emerged with the automatic interactive voice response system (IVRS). There is various IVR systems for automated Attendants, ACD Systems, Call Distribution, Alerts & Reminders, Card Activation, Hotlines and Helpdesk etc [2].

The purpose of IVRs is mostly to make the initial process of answering and routing a call more efficient. Instead of talking to a live person, the caller is greeted by a pre-recorded voice coupled with technology that is capable of Understanding words the caller speaks or selections he/she makes using the phone keypad. When implemented correctly, an IVR can help people perform transactions or get answers over the phone faster than they would by speaking to a live representative. Many people, , appreciate the ability to quickly check the balance on a bank account, book a flight reservation with an airline, or refill a medical prescription. Most consumers are familiar with the well-established IVR that uses keypad selections to direct callers through a series of pre-recorded menus. Most advanced systems now include voice recognition, allowing callers to speak commands rather than punching in numbers. This type of advanced solution is most appropriate labeled "interactive voice response," since it involves not only the voice of the pre-recorded message, but also what the caller says. Early speech-recognition features for IVR systems weren't very sophisticated, but they have been greatly improved in the past few years. These systems can now understand not just words like "yes" and "no" but names and strings of numbers as well with a high degree of accuracy. Yet another technology, text-to-speech (TTS), is now being coupled with speech recognition to make IVR systems more flexible. Customized text — such as details of a bank account balance or specifics for an airline ticket — can be created, and then read to the customer by a computerized voice. This removes the limits placed by having to pre-record all information presented to the caller. Thus this paper focuses on the use of speech recognition technology for interactive voice response system for agriculture assistance to farmers.

The rest of the paper is organized as follows. The creation of Marathi speech database related to agricultural application is presented in section 2. A concept of AGRO IVRS is presented in section 3. An account of Experimental analysis is detailed in section 4. Section 5 presents results and conclusion. This paper focuses on the use of an IVRS system for an agricultural assistance.

II. Marathi Speech Database

For accuracy in the speech recognition, we need a collection of utterances, which are required for training and testing[3,4]. The Collection of utterances in proper manner is termed as database. The generation of a corpus for Marathi sentences as well as the collection of speech data for AGRO IVRS is given below. In this application, we maintained three set of database. One database corresponds to the names of the crops, second for queries regarding the infection symptoms of crops and third with the name of the disease and its solution. For testing the age group of speakers selected for the collection of database ranges from 20 to 30. Mother tongue of speakers was Marathi. The total number of speakers was 35 out of which 17 were Females and 18 were Males.

The vocabulary size of the database consists of:

- Database with the names of the crop = $5 * 35 = 175$ samples
- Database with the infection symptoms = $5 \text{ crops} * 2 \text{ symptoms} * 35 = 350$ samples
- Names of the disease = $2 \text{ disease} * 5 \text{ crops} = 10$ samples
- Solution database as sentences = $5 \text{ crops} * 2 \text{ solution} = 10$ samples

To achieve a high audio quality the recording took place in the 10 X 10 rooms without noisy sound and effect of echo. The Sampling frequency for all recordings was 11025 Hz in the Room temperature and normal humidity. The speaker were Seating in front of the direction of the microphone with the Distance of about 12-15 cm [5]. The speech data is collected with the help of Computerized speech laboratory (CSL) using the single channel. The CSL is most advanced analysis system for speech and voice. It is a complete hardware and software system with specifications and performance. It is an input/output recording device for a PC, which has special features for reliable acoustic measurements [6].

III. Agro Interactive Voice Response System

Agriculture has been the primary occupation of human being. Agriculture in India is the means of livelihood of almost two thirds of the work force in the country. It has always been INDIA'S most important economic sector. Generally farmers do not have the scientific information about diseases of crops and their solutions. Farmers don't wish to go to the Agro information Centre or visit the agro web site for their queries related to the crops. Even they have the problem with understanding language and typing. To facilitate the farmer having information regarding the solution with the crop diseases through their phones (land line or mobile), we propose a model with voice response in Marathi language. This model will be advantageous in following conditions: People with disabilities that prevent them from typing.

- Illiteracy of farmer that keep him away from the automatics systems.
- Lack of source to get the information.
- To save the time to find the information.
- For visually impaired users when it is not possible or convenient to use a Braille keyboard,

Today, many IVR systems are based on voice extensible markup language (VXML). This system has five main components: [7]

- a) A phone network (PSTN or VoIP) through which calls are routed, a TCP/IP network for Internet/intranet connectivity,
- b) A VXML phone server which acts as an interpreter between the caller and the information they're accessing, a Web/application server to house the IVR software applications,
- c) And a database from where information is accessed by the IVR applications.

The unique point of voice interfaces is the ability to access an information system remotely. The ubiquitous telecommunication system enables one to access information on an "anytime anywhere" basis [8]. The proposed model of AGRO IVRS is shown in figure 1. A Computer Telephonic card will be used to setup data collection environment. Once the farmer comes online, working of IVRS systems starts, which is as follows:

1. The call will be connected to IVRS.
2. The System will prompt user to tell the name of the crop.
3. The System will prompt user to tell the symptoms regarding the crops.
4. The searching time will be communicated to the user (i.e. User will hold for some time)
5. Depending on the symptoms the database will be searched in IVRS database and the result will revert back to the user.

6. The Agro IVRS will prompt for the continuation, if user want to continue with other symptoms the system will start by step 3 else it will thank the user and terminate.

The proposed IVRS model will be advantageous to farmers as it will provide, in--hand solution for the diseases of the crops on 24/7 basis.

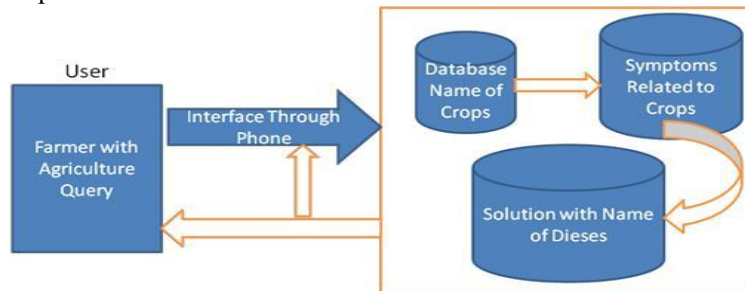


FIGURE 1 MODEL OF AGRO IVRS

IV. Experimental Analysis

The Experiment of Agriculture based Interactive Voice Response System is based on Speech Recognition. In this the query from farmer is given to the system for recognition .the time for training comes to one minute forty second ,where for testing (recognition) one minutes for 260 continuous sentences .The process is divided into two parts, first parts is identification of keywords from query and second part is recognizing the sentences using the keywords. The performance of system in term of recognition is done using word error rate. The recognition performance for accuracy is shown in table 1.

Word error rate can then be computed as

$$WER = \frac{S + D + I}{N}$$

Where

- S is the number of substitutions,
- D is the number of the deletions,
- I is the number of the insertions, N is the number of words in the reference

When reporting the performance of a speech recognition system, sometimes word recognition rate (WRR) is used instead.

$$WRR = 1 - WER = \frac{N - S - D - I}{N} = \frac{H - I}{N}$$

Where

- H is N-(S+D), the number of correctly recognized words

Table 1: Recognition performance for accuracy

Sr. No	Gender	Sentences Passed	Sentences Recognize	Accuracy
1	Male	50	46	92. %
2	Female	100	90	90%

V. Results and Conclusion

We presented an account of creation of Marathi language speech database with respect to agriculture. When tested it is been observed that the overall recognition rate of system comes to be 91%. We tried to use the created database for the prototype application of AGRO IVRS system. The corresponding application should be valuable for training speaker independent, continuous speech recognition systems for Marathi language as well as the IVRS model can further be extended to various sectors related to agriculture.

REFERENCE

- [1]. K Samudravijaya “Speech input/output systems in Hindi “ Tata Institute of Fundamental Research , Homi Bhabha road,Mumbai 400005
- [2]. The Interactive Voice System [online]http://www.hjelectronics.com/ivr_intrective_voice_response_system.html viewed on 1 Jan 2011.
- [3]. Santosh Gaikwad ,Bharti Gawali ,Pravin Yannawar “ A review on speech recognition Technique” International Journal of Computer Applicatin Bharti Gawali, Santosh Gaikwad, Pravin Yannawar, Suresh Mehrotra “ Marathi isolated word Recognition system using MFCC & DTW features” ACEEE Dec 2010.
- [4]. The website for The Disordered Voice Database Available [online]<http://www.kayelemetrics.com/Product%20Info/CSL%20Family/4500/4500.htm> viewed on Jan 2011.
- [5]. Burkhardt, A. Paeschke, M. Rolfes, W. Sendlmeier, B. Weiss, “A database of German Emotion Speech”, INTERSPEECH 2005, September, 4-8, Lisbon, Portugal
- [6]. IVRS Article [online] <http://www.tmcnet.com/channels/ivr/articles/43969-introduction-ivr.htm> viewed on 2 Jan 2011.
- [7]. Samudravijay K “Marathi speech database by samudravijaya” Tata Institute of Fundamental Research , Homi Bhabha Road, Mumbai.

Identifying the Coding and Non Coding Regions of DNA Using Spectral Analysis

R. Vijayashree¹, D. Naresh Kumar², P. Madhuri³, S. K. Asha Begum⁴,
P. Sumanth⁵

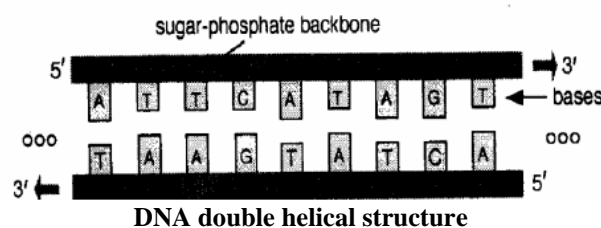
^{1, 2, 3, 4, 5} Dept. of ECE, Lendi Institute of Engineering and Technology, Affiliated to JNTUK, Vizianagaram

Abstract: This paper presents a new method for exon detection in DNA sequences based on multi-scale parametric spectral analysis. Identification and analysis of hidden features of coding and non-coding regions of DNA sequence is a challenging problem in the area of genomics. The objective of this paper is to estimate and compare spectral content of coding and non-coding segments of DNA sequence both by Parametric and Non-parametric methods. In this context protein coding region (exon) identification in the DNA sequence has been attaining a great interest in few decades. These coding regions can be identified by exploiting the period-3 property present in it. The discrete Fourier transform has been commonly used as a spectral estimation technique to extract the period-3 patterns present in DNA sequence. Consequently an attempt has been made so that some hidden internal properties of the DNA sequence can be brought into light in order to identify coding regions from non-coding ones. In this approach the DNA sequence from various Homo Sapiens genes have been identified for sample test and assigned numerical values based on weak-strong hydrogen bonding (WSHB) before application of digital signal analysis techniques.

I. Introduction

The enormous amount of genomic and proteomic data that are available in public domain inspires scientists to process this information for the benefit of the mankind. The genomic information is present in the strands of DNA and represented by nucleotide symbols (A, T, C and G). The segments of DNA molecule called gene is responsible for protein synthesis and contains code for protein in exon regions within it. When a particular instruction becomes active in a cell, the corresponding gene is turned on and the DNA is converted to RNA and then to protein by slicing up to exons (protein coding regions of gene). Therefore finding coding regions in a DNA strand involves searching of many nucleotides which constitute the DNA strand. As the DNA molecule contains millions of nucleotide element, the problem of finding the exons in it is really a challenging task. It is a fact that the base sequences in the protein coding regions of DNA molecules exhibit a period-3 pattern because of the non uniform distribution of the codons in recent past many traditional as well as modern signal processing techniques have been applied to process and analyze these data have used DFT for the coding region prediction.

The DFT based spectrum estimation methods produce the windowing or data truncation artifacts when applied to a short data segment. The Parametric spectral estimation methods, such as the autoregressive model, overcome this problem and can be used to obtain a high-resolution spectrum. But rapidly acquiring the genomic data demands accurate and fast tools to analyze the genomic sequences. In this paper we propose an alternate but efficient and cost effective technique for the identification of the protein coding regions exhibiting period-3 behaviour. These new methods employ the adaptive AR modelling which require substantially less computation and yield comparable performance than the conventional approaches



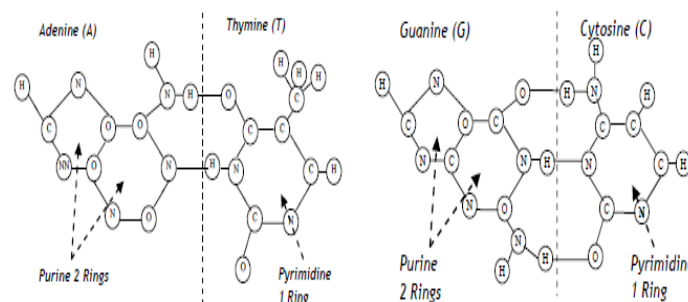
Only around 1.2 % of human DNA is known to be coding for proteins. Our knowledge of the role and location of other elements is limited and new types of sequences unknown function are still discovered. Recently, several sets of highly conserved non coding sequences have been identified in vertebrate genomes. A combination of comparative genomic studies and laboratory experiments has shown that these conserved non-coding elements (CNEs), most of which are more conserved than protein-coding exons.

Most of these sequences are located in and around developmental regulation genes and when some of them were tested in the laboratory, they appeared to drive tissue-specific gene expression in early development.

Genome sequences contain the genetic information of living organisms. This information, which is common to all life, is coded in the deoxyribonucleic acid (DNA) sequences. Understanding the codes will enable us to understand the life processes of a particular organism. As such, even with the genome sequence in hand, much work remains to be done to lay open the genetic secrets of a particular species.

II. DSP Techniques For Spectral Estimation Of DNA Sequences

Decoding the meaning of the nucleotide characters A, T, C, and G is becoming even more pressing with the final release of the sequencing of the human genome.



Double hydrogen bond Triple Hydrogen bond A=T signifies weak bond c=g signifies strong bond

Gene identification is of great importance in the study of genomes, to determine which open reading frames (ORFs) in a given sequence are coding sequences for prokaryotic, and to determine the exons and introns, and the boundaries between them in a given gene for eukaryotic DNA sequences. There are a number of identification methods being used, either with training datasets, or without any database information. Gene scan use a semi-hidden Markov model, and FEX use a linear discriminant function to determine genes, are examples of gene or exon finding algorithms based on database information.

Examples of algorithms without database information are statistical correlation analysis statistical regularity to detect coding regions and Fourier analysis.

For example a DNA sequence of length N:

$$X [n] = [A T G C C T T A G G A T](1)$$

After mapping:

$$X_{sw} [n] = [2 2 3 3 3 2 2 2 3 3 2 2]$$

Among the various methods, the most prominent distinctive feature of coding and non-coding regions is the 3 base pairs (bp) periodicity or 1/3 frequency, which has been shown to be present in coding sequences? The periodicity is caused by the coding biases in the translation of codons into amino acids.

The Fourier transform analysis has been widely used for sequence processing. However, Fourier transform contains the problems of windowing or data truncation artifacts and spurious spectral peaks, and thus, the spectral obtained using the Fourier transform will exhibit the same problems. This problem has been studied extensively in digital signal and image processing, where autoregressive (AR) models are used to achieve a high spectral resolution. The AR model or linear prediction (LP) process is a relatively new approach to spectral analysis to overcome the limitation of Fourier methods.

III. Non-Parametric Analysis of DNA Sequence

To perform the gene prediction based on period-3 property the total DNA sequence is first converted into four indicator sequences, one for each base. The DNA sequence $D(n)$ is mapped into binary signals $uA(n)$, $uC(n)$, $uG(n)$ and $uT(n)$

Which indicate the presence or absence of these nucleotides at location n.

For example the binary signal $u_A(n)$, attributed to nucleotide A takes a value of 1 at $n = n_0$ if $D(n_0) = A$, else $u_A(n_0)$ is 0. Suppose the DNA sequence is represented as

$D(n) = [AT\ GAT\ CGCAT]$

Then its numerical representation is given by

$u_A(n) = [1001000010]$

$u_C(n) = [0000010100]$

$u_G(n) = [0010001000]$

$u_T(n) = [0100100001]$

Thus $u_A(n) + u_C(n) + u_G(n) + u_T(n) = 1$

Non-parametric technique of spectrum estimation is based on the idea of first estimating the auto-correlation of data sequence and then taking its Fourier Transform to obtain its Power Spectral Density (PSD). This method also known as Periodogram method. Although periodogram is easy to compute it is limited in its ability to produce an accurate estimate of the power spectrum, particularly for short data records. For improvement of statistical property of periodogram method a variety of modifications have been proposed such as Barlett's method, Welch's method and the Blackman-Tukey method. In periodogram method PSD is estimated directly from signal itself.

IV. Parametric Analysis of DNA Sequence

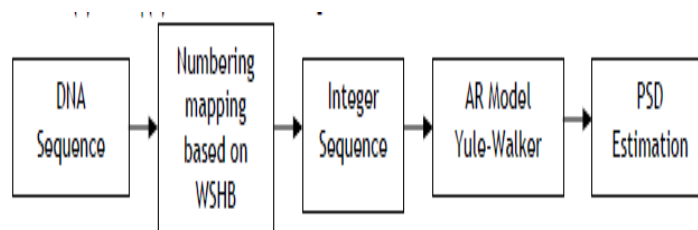
Parametric analysis can yield higher resolutions than nonparametric analysis in cases when the signal length is short. These methods use a different approach to spectral estimation; instead of trying to estimate the PSD directly from the data, they model the data as the output of a linear system driven by white noise, and then attempt to estimate the parameters of that linear system.

The most commonly used linear system model is the all-pole model, a filter with all of its zeroes at the origin in the z -plane. The output of such a filter for white noise input is an autoregressive (AR) process. For this reason, these methods are sometimes referred to as AR methods of spectral estimation.

The AR methods tend to adequately describe spectra of data that is "peaky," that is, data whose PSD is large at certain frequencies. The data in many practical applications (such as speech) tends to have "peaky spectra" so that AR models are often useful. In addition, the AR models lead to a system of linear equations which is relatively simple to solve. The Parametric method uses a different approach to Spectral estimation. Instead of estimating PSD from data directly as is done in non-parametric method, it models the data as output of a linear system driven by white noise and attempts to estimate parameters of this linear system.

$$P_{AR}(e^{j\omega}) = \frac{|b(0)|^2}{|1 + a_p(k)e^{-j\omega k}|^2}$$

The output of such a filter for white noise input is an AR process, known as AR method of spectral estimation. There are different types of AR methods such as Burg method, Covariance and Modified Covariance method, Yule-Walker (auto-correlation) method etc.



Block diagram realization of an AR model PSD estimation system

The advantage of Yule-Walker Autoregressive method is that it always produces a stable model. Parametric methods can yield higher resolution than non-parametric methods when the signal length is short. For achieving on line prediction of gene and exon the computational time needs to be reduced. Further the fixed AR method requires all data to be available simultaneously which is not always feasible. With a motive to alleviate these limitations an adaptive AR model based approach is suggested in this section for efficient prediction. The AR process can be viewed as an adaptive prediction error filter. which uses two bases out of the four DNA nucleotides by ignoring the base order, there are six combinations: AC, AC, AG, TC, TG, and CG. The power spectrum as constructed using can be given by $|P(f)|^2$.

4.1 BURG METHOD:

Another type of parametric method is Burg method. The Burg method for AR spectral estimation is based on minimizing the forward and backward prediction errors while satisfying the Levinson-Durbin recursion. In contrast to other AR estimation methods, the Burg method avoids calculating the autocorrelation function, and instead estimates the reflection coefficients directly.

The primary advantages of the Burg method are resolving closely spaced sinusoids in signals with low noise levels, and estimating short data records, in which case the AR power spectral density estimates are very close to the true values. It is always a stable model.

In addition, the Burg method ensures a stable AR model and is computationally efficient.

The accuracy of the Burg method is lower for high-order models, long data records, and high signal-to-noise ratios which can cause **line splitting**, or the generation of extraneous peaks in the spectrum estimate. The spectral density estimate computed by the Burg method is also susceptible to frequency shifts (relative to the true frequency) resulting from the initial phase of noisy sinusoidal signals. This effect is magnified when analyzing short data sequences.

Main characteristics of Burg method is Does not apply window to data, Minimizes the forward and backward prediction errors in the least squares sense, with the AR coefficients constrained to satisfy the L-D recursion.

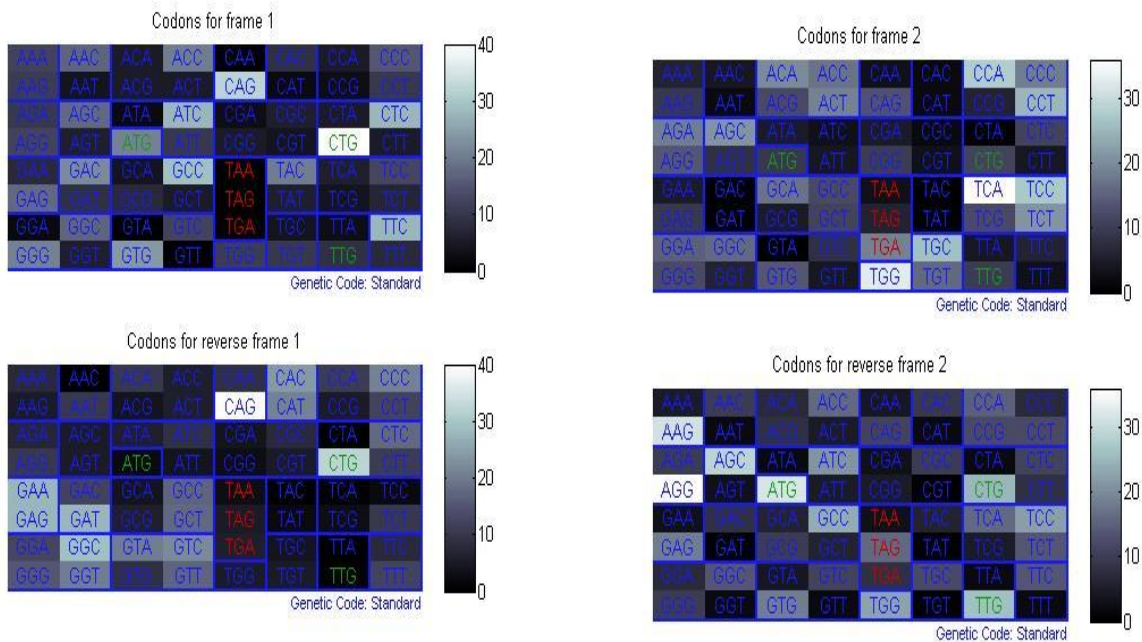
4.2 Covariance and Modified Covariance Methods:

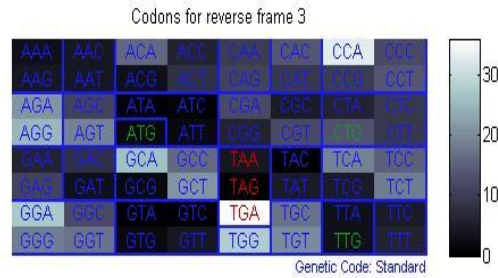
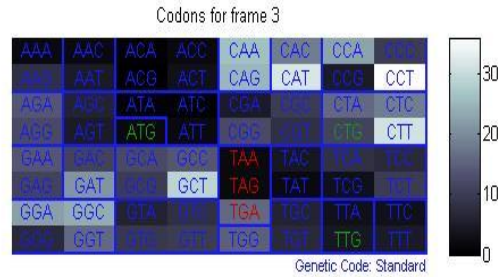
The covariance method for AR spectral estimation is based on minimizing the forward prediction error. The modified covariance method is based on minimizing the forward and backward prediction errors. Does not apply window to data. Major advantages of these methods are better resolution than Y-W for short data records (more accurate estimates). Able to extract frequencies from data consisting of p or more pure sinusoids.

V. Genomic Sequence for Protein

The protein sequences can be developed from DNA to codon and then protein codon sequences & reverse codon sequences are shown in fig (a,b,c).

If we assign numerical values to the four letters in the DNA sequence, we can perform a number of signal processing operations such as Fourier transformation, digital filtering, power spectrum estimations.





Some of the amino acids with nucleotide code can be represented by

For example:

Alanine (A) is GCT, GCC, GCA, GCG;

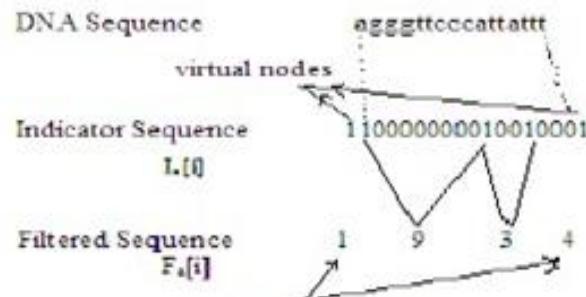
Arginine(R) is CGC, CGA, CGG, AGA, AGG;

Asparagines(N) is ATT,AAC

Part of a protein sequence could be

...PPVACATDEEDAF GGAYPO..

Similarly the gap sequence can be taken as DNA gap sequence...similarly indicator sequence developed for protein sequences as same as indicator sequence of Genomic sequences...



The relation between DNA sequence, the indicator sequence, and the filtered gap sequence

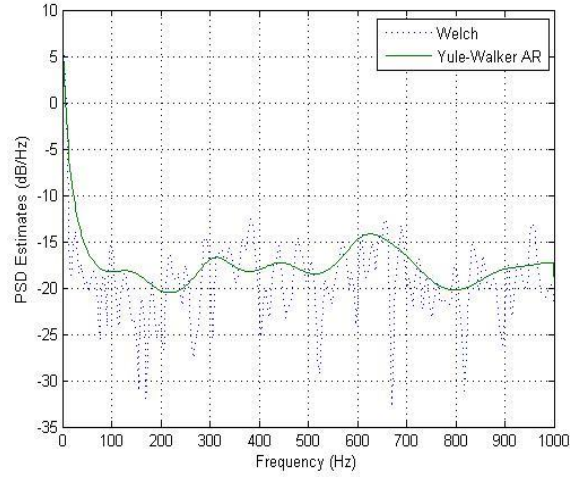
A short analysis frame may detect short exons and introns, but causes more statistical fluctuations. A larger window size may miss the short exons and introns, but cause fewer false negatives and false positives.

Thus, we make use of multiple window sizes, with the aim of reinforcing the advantages of both short and long window sizes but overcome the disadvantages that are caused by them We select the window size within the range of 60bp-360bp The P_{ratio} combination of the windows.

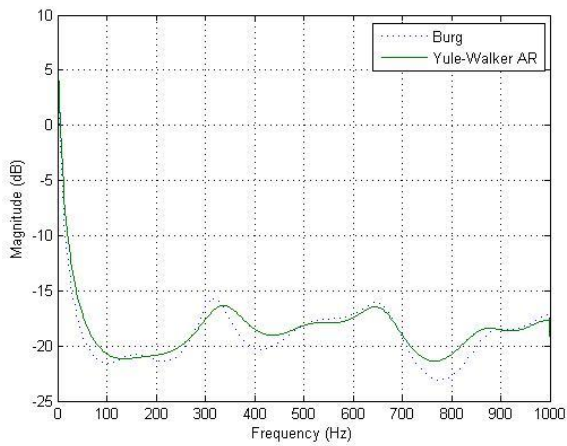
VI. Results and Discussions

6.1 Graphical Representation of Parametric Methods:

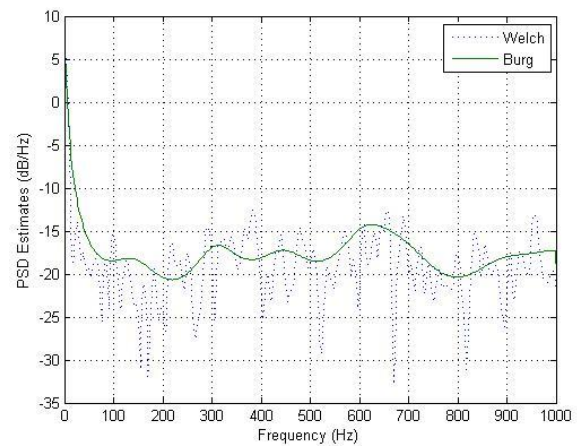
(1) Welch –Yule walker AR



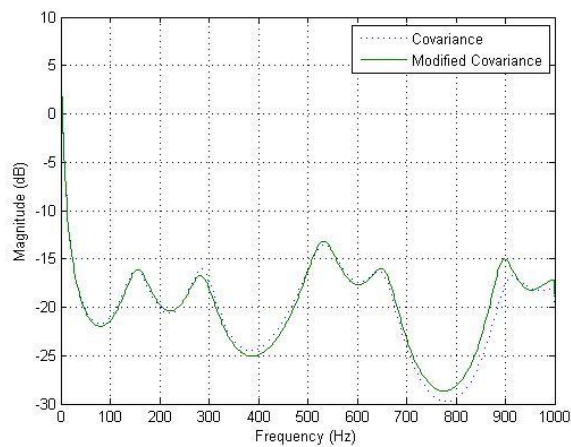
(2) Burg-Yule walker AR



(3) Welch-Burg



(4) Covariance-modified covariance



VII. Conclusion

We are well aware that stochastic or random signals have information bearing Power Spectral Density. Parameterization of a stochastic signal for efficient representation of this information is already in use for speech coding and various other biomedical signal processing applications. In this Paper we have applied parametric as well as non-parametric power spectrum estimation techniques to coding and non-coding regions of DNA sequence taken from Homo Sapiens genes. A comparative study has been organized in order to distinguish coding from non-coding regions. The non-parametric Power Spectral estimation method is methodologically straight forward and computationally simple among several parametric models available, AR models presented here are popular because they provide accurate estimation of PSD by solving linear equations. Data sets from various Homo Sapiens genes have been investigated.

It has been observed from the plots of average PSD for low order Auto Regressive Yule Walker method that the spectral signatures of exons bear a significant pattern as compared to that of introns after finding the exons used to convert DNA to protenic sequences. To find similar segments between gap sequences of DNA.

The normalized variance values show strong periodicities in case of exons for parametric and non-parametric methods where as introns do not reveal any such property. Future course of investigation may be steered towards other parametric methods such as Burg, Covariance, and Maximum Entropy etc. Genes from other species may also be taken into consideration.

REFERENCES

- [1] Anastassiou D., "Frequency-domain analysis of biomolecular sequences", *Bioinformatics* 16, 1073-1081.
- [2] Anastassiou D., "DSP in genomics: Processing and frequency domain analysis of character strings," *IEEE*, 0-7803-7041-2001.
- [3] Chakrabarty Nirranjan, Spanias A., Lesmidis L.D. and Tsakalis K., "Autoregressive Modelling and Feature Analysis of DNA Sequences", *EURASIP Journal on Applied Signal Processing* 2004:I, 13-28.
- [4] Ficket J.W. and Tung C.S., "Recognition of protein coding regions in DNA sequences", *Nucleic Acids Research*, Vol.10, No.17, pp.5303-5318, July 1982.
- [5] Ficket J.W. and Tung C.S., "Assessment of protein coding regions in DNA sequences", *Nucleic Acid Res*, 10, 5303-5318, 2000.
- [6] Hayes M.H., "Statistical digital signal processing and modelling", John Wiley & Sons, Inc., New York, USA, 1996.

Modeling, Simulation And Implementation Of Adaptive Optical System For Laser Jitter Correction

Anjesh Kumar, Devinder Pal Ghai, A.K Maini

Laser Science and Technology Centre, DRDO, Metcalfe House, Delhi-110054, India

ABSTRACT: Adaptive Optical System (AOS) for correction of beam jitter in a high power laser source is described. The jitter in a high power laser may results from platform vibrations and dynamically varying in-homogeneities in the lasing medium. The effect of beam jitter on the performance of high power laser in directed energy weapon (DEW) system is discussed. Simulation studies have been carried out to optimize parameters of jitter correction system. An experimental arrangement to stabilize a high power laser beam is described and results are presented.

Keywords: Adaptive optics, Laser beam jitter, Tip-tilt mirror, Directed energy weapon.

I. Introduction

Adaptive Optical System (AOS) has emerged as an integral part of optical systems that find applications in various fields such as astronomy, industry, laser communication, medical diagnostics and defence. In astronomy, adaptive optics is an indispensable part of optical systems meant for imaging of variety of stars and other science object of interest. In industry, AO system helps in generation of stable and diffraction limited laser spot for precise cutting, marking or drilling of objects. In free space communication, adaptive optics is used mainly for correction of beam wander to stabilize the laser spot in the receiver plane. Recently, satellite to submarine communication has emerged as another potential application that needs adaptive optics for establishment of effective communication link. Adaptive optics has also been used in ophthalmology for taking clear images of retina for medical analysis related to the eye related problems. In defence, Directed Energy Weapons (DEW) systems find direct use of adaptive optical system to concentrate brute laser power on the target to cause structural or sensor damage. Stabilization of laser beam is also important for beam pointing and tracking the target.

High power lasers system has inherent jitter and aberrations which severely degrade the performance of these systems. The effect of jitter becomes more pronounced as the target range increases. The lethality of a laser based system can be improved considerably by correction of beam jitter inherently present in HPL sources and beam wander resulting from atmospheric turbulence. The source jitter occurs because of mechanical vibrations of laser cavity and the platform supporting various optical components of beam delivery system. Low frequency jitter (beam drift) results from in-homogeneities in the lasing medium. In solid state lasers, in-homogeneities results from the thermal gradients in the lasing rods. In a chemical or a gas dynamic laser, the in-homogeneities results from non uniform mixing of the reacting species. The source jitter can be treated at the point of its origin, itself. Source jitter resulting from platform instabilities can be corrected to some extent by passive means such as using a vibration free table. However, laser source jitter resulting from laser cavity vibrations and in-homogeneities of lasing medium cannot be corrected by these methods. In such situations, adaptive optical jitter correction system is the only solution to correct the laser beam jitter and stabilize the laser beam, in real time.

II. Effect Of Beam Jitter

Small beam jitters result in large beam displacements as the distance from laser source increases. These beam displacements have very detrimental effect on the performance of a DEW system. On the source end the beam displacements severely affect the tracking range and accuracy of gimble stabilized beam delivery system. On the target end beam displacements adversely affect the lethality of the DEW system. The beam displacements in the target plane results in decreasing its power density. Large beam displacements also raise the probability of missing the target. The effect of jitter can be visualized with the help of Fig.1. A Laser beam is focused to a spot of area A on the target at a distance R . Due to jitter in the beam, the position of the spot is not stable at the target but keeps varying with time. If α is the maximum angular jitter then the maximum linear movement of the spot on the target is $R\alpha$. If this displacement is larger than the the size of the target or the

desired region of the target then there are chances of the laser beam mis-hitting the target or the desired location of the target. Even if, the beam displacements are not so large as to cause mis-hit, it definitely reduces the power density of the laser beam, thereby reducing the lethality of the DEW system.

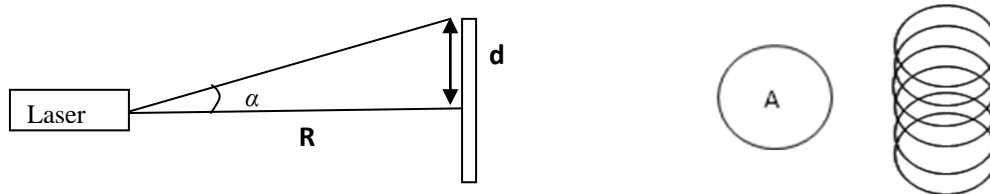


Fig. 1 Effect of beam jitter

If P_r is the power received in the target plane, the power density at the target in the absence of beam jitter would be P_r / A . In the presence of beam jitter at the source end, the displacement of the beam in the target plane increases the effective area. If A' is the effective area of the laser spot due to tilt errors, the effective power density reduces to P_r / A' . As a rule of thumb, the beam jitter correction should be such that there is at least 50% overlap of the laser spots resulting from residual tilt errors. This will reduce the power density to half of its value obtained in the absence of any tilt errors. This power density should be more than the threshold power required to incorporate structural damage to the target or incapacitate its sensor unit. A higher degree of jitter correction at the source end would increase the region of overlap of the laser spots on the target plane and thus improve the lethal power of the DEW system. Alternately, it would require lesser laser power at the source end to inflict the same damage to the target. In this entire discussion, the effect of beam wander resulting from atmospheric turbulence has not been taken into account. Effect of beam wander is indeed small for shorter target ranges or when atmospheric turbulence is low particularly for large laser wavelengths. However, for higher degree of atmospheric turbulence and for longer ranges, a separate adaptive optical jitter correction system is invariably required for correcting beam wander, in real time.

III. Simulation of Jitter Correction System

A jitter correction system has been designed using Tip-tilt mirrors (TTMs) and pyro-electric quadrant detectors for real time correction of a CO₂ laser beam. Correction algorithm sums up the current error sample with the previous one to obtain overall jitter error. Fig. 2 depicts block diagram of complete error correction system. The control loop is simulated using LABVIEW control module as shown in Fig. 3.

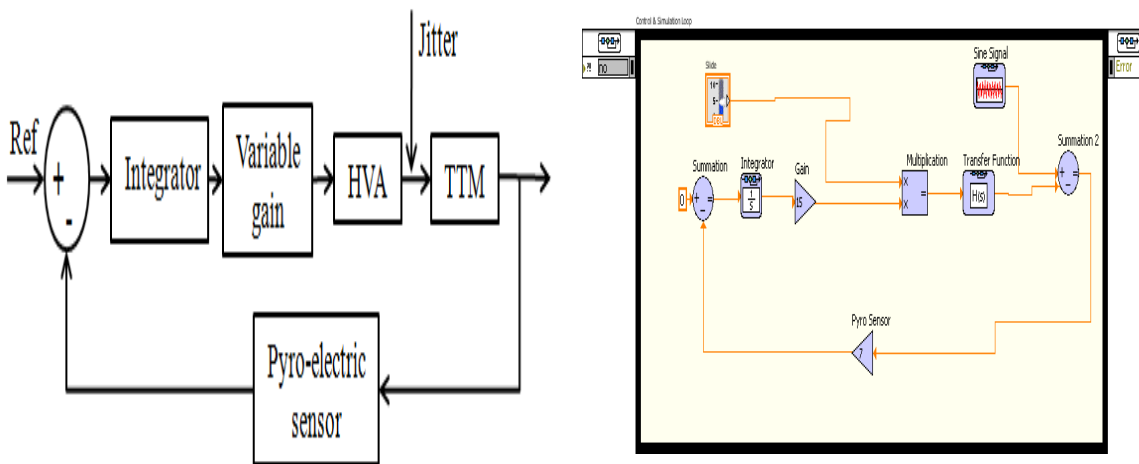


Fig. 3 Control loop simulation

TTM is modeled as a second order system with the transfer function as $4769856 / (S^2 + 1747S + 4769856)$ and resonant frequency 1800 rad/sec (~287 Hz). Bode plot of the TTM is depicted in Fig. 4. The plot shows an infinite Gain Margin (GM) at infinite phase crossover frequency and ~ 69 as Phase Margin (PM) at 2547.1 rad/s Gain crossover frequency Bode Plot of overall closed loop system is depicted in Fig.5. The closed loop system has a Gain Margin of 22 at 2184 rad/s phase crossover frequency and Phase Margin of 87.1 at 135.5 rad/s gain crossover frequency. Simulation results clearly indicate that the close loop system is stable.

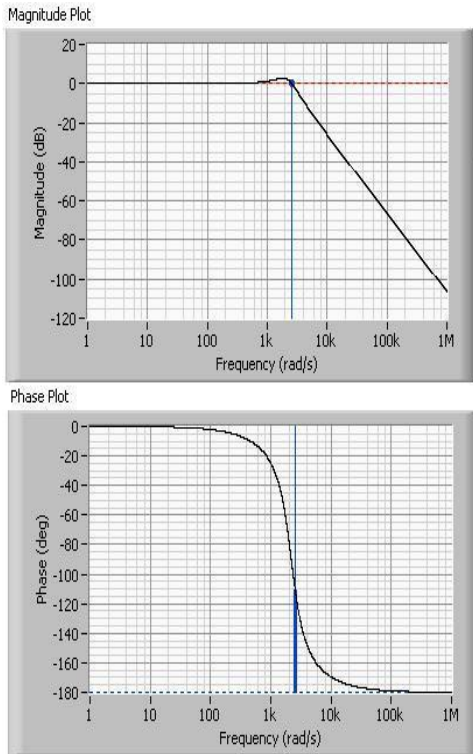


Fig. 4 Bode plot of the TTM

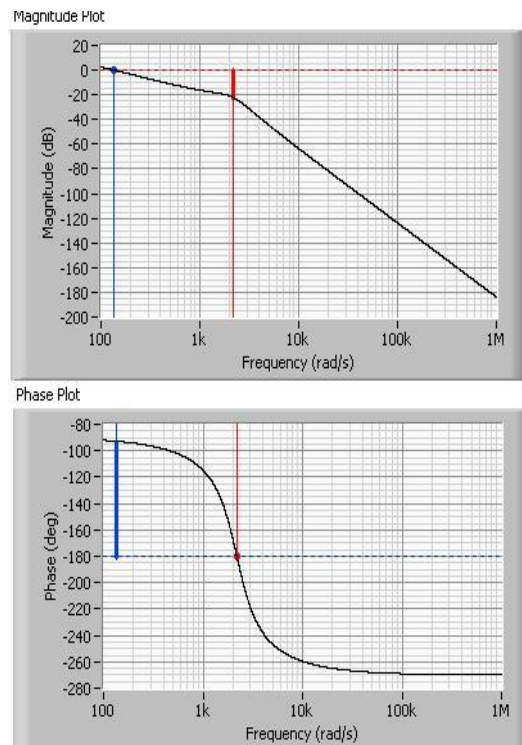


Fig. 5 Bode plot of closed loop system

IV. Experimental Arrangement

Schematic of closed loop jitter correction system is shown in Fig. 6. The system uses a pair of tip-tilt mirrors, pyro-electric quadrant detectors and the control electronics for online correction of laser beam jitter. A tip tilt mirror TTM1 is used to incorporate tilt errors of desired amplitude and frequency. The other two TTMs, TTM2 and TTM3 dynamically adjust themselves to ensure that the beam jitter is corrected without altering initial optical axis of the laser beam. A He-Ne laser (632.8 nm) is co-aligned with the CO₂ laser beam (10.6 μm) for ease of optical alignment. A part of CO₂ laser beam is sampled using a beam splitter and is made to incident on pyro quad detectors. Output of pyro-quad detectors is processed in a quadrant detector electronics unit to generate electrical signals corresponding to source beam jitter. The electrical signals are then digitized and processed in the controller to generate desired correction signals. Equivalent analogue voltages are generated through D/A converters interfaced with the controller. The analogue voltages are then suitably amplified using high voltage amplifiers and fed to TTMs to nullify the effect of source jitter. In close loop modeling, only one TTM is used to correct the jitter but practically two TTMs are, in general, employed to correct the jitter all along length of laser beam. Alignment of pyro-quad detectors is bit tricky as these detectors respond only to temperature variations.

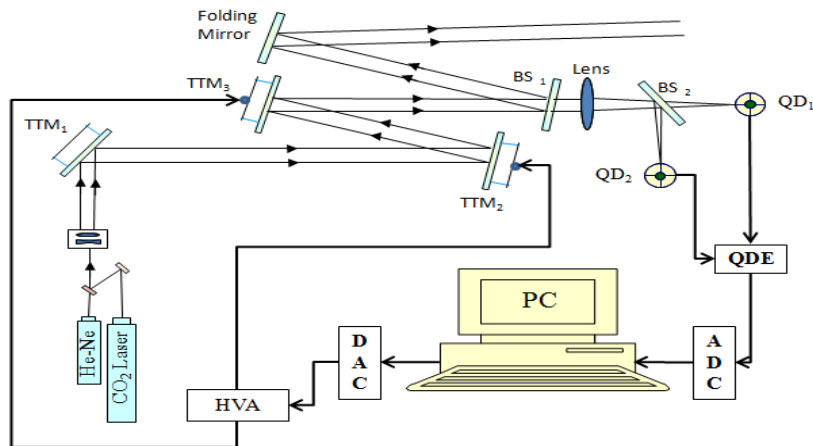


Fig. 6 Schematic of jitter correction system

V. Results

Results of closed loop jitter correction, using adaptive optical system described herein, are shown in Fig. 8. Experimental system has maximum jitter correction of 94% and closed loop bandwidth 25Hz. Regeneration effect at higher system gain as shown in simulation results was verified experimentally.

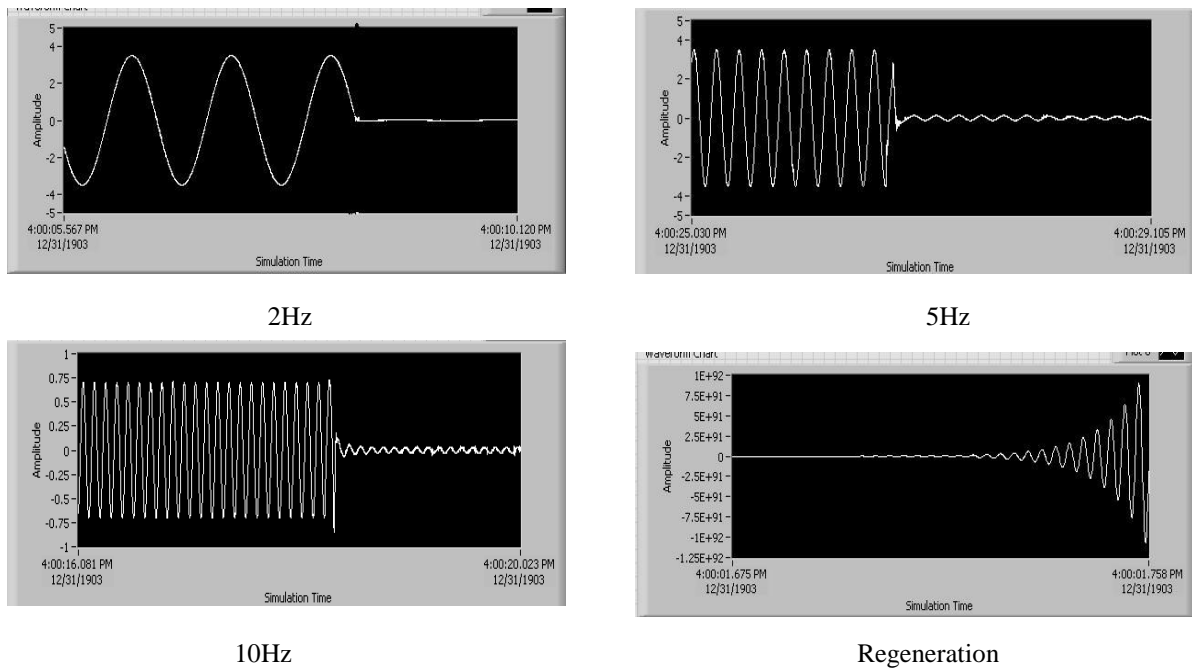


Fig. 7 depicts the results of simulated jitter correction at different frequencies

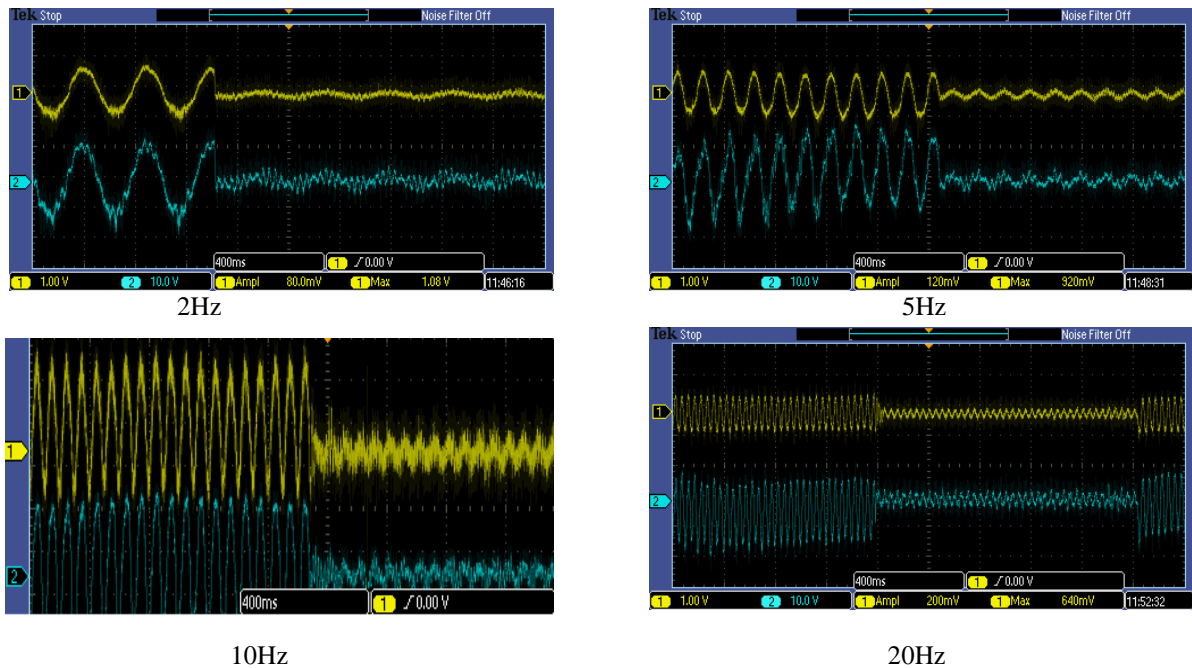


Fig. 8 Experimental jitter correction at different frequencies

VI. Conclusions

A closed loop jitter correction system has been developed using a pair of tip tilt mirrors and pyroelectric quadrant detectors. The system has been successfully used to correct beam jitter in a 100 watt CO2 laser. The control loop was simulated using LABVIEW control module. Simulated jitter correction results at various frequencies were found to be very close to actual experimental results.

REFERENCES

- [1] Gregory C Loney. Design of a small-aperture steering mirror for high bandwidth acquisition and tracking. Opt Eng, 1990, 29(11), 1360-1365.
- [2] Robert K. Tyson. Principles of Adaptive Optics, Taylor & Francis Group, CRC Press, 2011.
- [3] Devinder Pal Ghai*, Anuya Venkatesh, Het Ram Swami, and Anjesh Kumar, Large Aperture, Tip Tilt Mirror for Beam Jitter Correction in High Power Lasers, Defence Science Journal, Vol. 63, No. 6, November 2013, pp. 606-610.
- [4] Corley, C.M.S., Nagashima, M. & Agrawal, B.N, Beam control and a new laboratory testbed for adaptive optics in a maritime environment", IEEE Aerospace Conference. Big Sky, Montana, USA 2010.
- [5] Tapos, F.M.; Edinger, D.J.; Hilby, T.R.; Ni, M.S.; Holmes, Buck C. & Stubbs, David M. High bandwidth fast steering mirror. Optomechanics, Proc. SPIE, 2005, 5877, pp. 60-73.
- [6] Patel, B.. Flexure design for a fast steering scanning mirror. U.S. Patent 5550669. 27 August 1996.

Range Query on Big Data Based on Map Reduce

Zhang Tingting¹, Qu Haipeng²

¹(College of Information Science and Engineering, Ocean University of China, China)

²(Corresponding Author, College of Information Science and Engineering, Ocean University of China, China)

Abstract: Range query in P2P system is mainly made by establishing index, such as B+ tree or DST. However when the number of nodes in the system and the amount of data in a single node increases significantly, the above traditional index will become extremely large so it will affect the query efficiency. In the present, enterprises require effective data analysis when making some important decisions, such as user's consumption habits deriving from analyzing user data. This paper aims at optimization of range query in big data. This algorithm introduces MapReduce in P2P system and organizes files by P-Ring in different nodes. When making range query we use P-Ring to find the corresponding files and then search data in the file by B+ tree.

Keywords: Range query, Big Data, Map Reduce, P-Ring, B+ tree

I. Introduction

Today, the amount of data in various fields is increasing. Traditional data processing is transforming to big data. Big data which is firstly put forward by Viktor Mayer-Schönberger [1] is a data set whose content can't be crawled, managed and processed through conventional software tools within a certain time. It has four characteristics which are Volume, Variety, Velocity and Value [2]. Google deals with data through large-scale cluster and MapReduce software and the amount of data processed every month is over 400PB [3]. Cloud computing platform of Yahoo! has 34 clusters and more than 30000 computers. Its total storage capacity is over 100PB [4]. The traditional query algorithm is unable to meet the needs of enterprises. How to quickly find qualified data in such a flood of information becomes a major problem of enterprises.

Traditional range query is mainly based on establishing ordered indexes. Reference [5] presented a range query algorithm in P2P system. Firstly it creates a B+ tree index for each numerical attributes of the file and the index information of the file is only stored in the leaf nodes. When making range the original range is divided into sub-ranges according to the data stored in the root node of the B + tree. Each sub-query is made along the corresponding child node until the leaf node is reached. Then the queried results are returned. However, the performance of this algorithm extended to big data environment is to be improved. Reference [6] proposed a global index structure based on Map Reduce to optimize range query. Firstly sort the indexed attributes. Then the original index table is divided into a number of sub-tables sequentially and these sub-tables are assigned to different nodes of the cluster. Each sub-table of global index stores the location list of files. When making range query the range condition is split to different nodes and each sub-condition is parallel executed. But performance of this algorithm is limited to the speed of the global index.

The main difficulty of data queries on big data environment lies in how to extend the traditional query algorithm to massive data environment while query efficiency is not affected. Establishing a global index will lead to index being algorithm bottleneck of large data environment. Therefore, we need to get rid of the limitations of traditional centralized structure algorithm.

Map Reduce precisely is a model for large-scale data sets. It includes two functions Map and Reduce. Users only need to define these two functions without considering how to achieve the distribution of the underlying system. So this model facilitates programmer to run program in distributed system under the circumstance of not familiar with distributed programming. This model is frequently used to process large-scale distributed systems [7].

This paper presents a range query algorithm processing big data based on Map Reduce and P-Ring **Error! Reference source not found.** Files on each node are organized by P-Ring and then nodes of distributed system are organized by Map Reduce. Range query is divided into two steps: search files and query data.

The rest of this paper is organized as follows, section II surveys related work. Section III introduces dual-index. Section IV presents basic idea of the algorithm. Section V concludes this paper.

II. Related Work

Range query is achieved mainly based on building ordered indexes. But the index will become very large in big data. So what we need to do is to try to simplify the index structure. At present, the main index structure for range queries is B+ tree. It can sort files according to one attribute so that it is convenient for range query.

In order to simplify the index structure, this paper combines P-Ring and B+ tree to build a dual-index structure. This structure avoids the shortcoming of index being too large caused by establishing B+ tree directly among documents. This paper establishes a P-Ring for files in different nodes of distributed system. The algorithm complexity of exact search by P-Ring is $O(\log N)$. **Error! Reference source not found.** N is the number of nodes in P-Ring. Then create a B+ tree for a file based on attribute in the query condition and query data inside a file. This method effectively reduces the height of the B + tree and takes full advantage of the characteristics of P-Ring and B + tree.

At present P-Ring is mainly used in large-scale distributed P2P systems to search data. At present index structures of range query about P2P have some defects in a certain extent. P-trees can only handle a single data item per peer, and hence, are not well-suited for large data sets. The index proposed by Gupta et al. [0] only provides approximate answers to range queries and can miss results. Mercury [4] and P-Grid [0] provide probabilistic (as opposed to absolute) guarantees on search and load-balancing, even when the P2P system is fully consistent. Reference [0] pointed out that the main advantage of P-Ring relative to existing index structures of range query is high accuracy and it can be extended to environment where there are a large number of nodes and data.

III. Dual-Index

The index structure proposed in this paper firstly indexes to the file by improved P-Ring, and then to specific data by B+ tree.

A. Defect of current P-Ring

Traditional P-Ring mainly index to data. Under the environment of big data, data is distributed different nodes by the unit of file. So if we want to execute range query, the file including corresponding data must be found. In this circumstance traditional P-Ring can't meet our needs.

B. Improved P-Ring Index

P-Ring is an index based on sort. Data on P-Ring is strictly sequential. Each node stores a value and the location between two nodes stores values ranging from previous node to next one. In P-Ring every node saves hierarchically information about its successor node and the value of hierarchy is differentials of value between successor node and current node. Improved P-Ring is improved to index by files through creating index for ranges of attribute values in a file. Value segment between two nodes can store the index information for one or more files.

The index structure proposed in this article organizes files between different nodes by improved P-Ring. Every node stores one value according to ranges of attributes in file. Different nodes are arranged sequentially and everyone stores a table of index information named infoTable. The infoTable stores range segments, file name and file address of corresponding files of these segments.

The following are examples of file data:

Table 1 File information of node 1

File name	Range of attribute value	File address	Node of P-Ring
F1	10-15	A1	P0
F2	5-10	A2	P1
F3	6-8	A3	P1
F4	10-18	A4	P0
F5	1-8	A5	P1,P2

Table 2 File information of node 2

File name	Range of attribute value	File address	Node of P-Ring
F6	2-10	A6	P1,P2
F7	13-15	A7	P0
F8	4-6	A8	P1,P2
F9	2-10	A9	P1,P2
F10	16-20	A10	P3

Process of establishing P-Ring index on the above documents is as follows.

- 1) Store F1. Firstly define two nodes P0 and P1 on the ring, respectively stores 10 and 15. Then save the address and attribute ranges of F1 in infoTable of P0. Assuming the name of range is R, R0=(10,15);
- 2) Store F2. Because attribute range of F2 is 5 ~ 10, it is not included in the scope of R0, so create a new node P storing value 5. Because 5 is smaller than 10 stored in P0, so the P0 and P1, respectively, plus 1 to P1 and P2. The newly inserted node is P0. Save the address and attribute ranges R2=(5,10) of F2 in infoTable of P0;
- 3) Store F3. The attribute range of F3 is 6~8, so its name and address is stored in P0 and divide the range of P0 which is R2 into r21=(5,6), r22=(6,8) and r23=(8,10). Then corresponding files of every sub range are stored its infoTable. In this example the corresponding file of r21, r22 and r23 is respectively F2, F2 and F3, F2;
- 4) Store F4. The procedure is similar to 3). When storing file address we need to save the corresponding machine number or address of file;
- 5) Follow this step to store the remaining files.

The P-Ring created in accordance with above steps using files in Table1 and Table2 is as shown below.

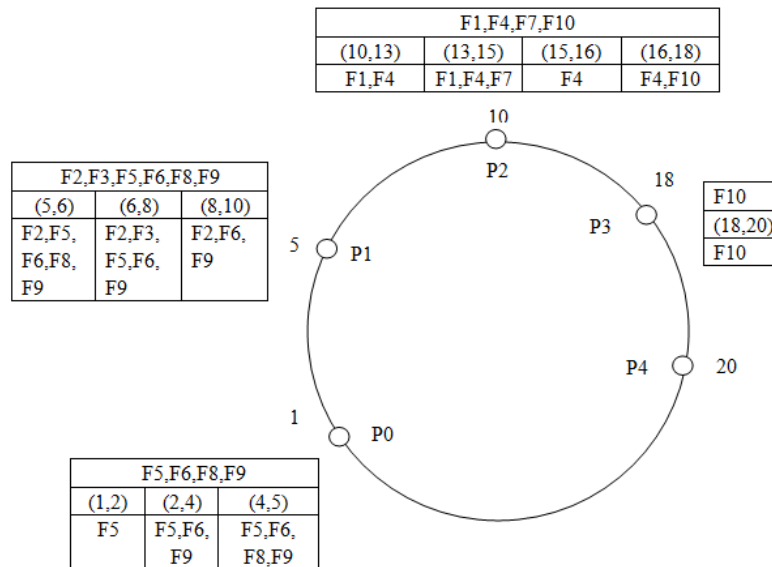


Figure 1 P-Ring index based on files

The first line of info Table in the above Fig.1 stores file name and file address. The second line stores every sub ranges. Corresponding file name of every range is stored in third line. Node of this ring can be Map of Map Reduce.

The central issue of P2P is routing. So after index structure is completed, we need to build the routing table for nodes. Traditional P-Ring structure uses hierarchical routing algorithm and the value difference of successor node and the current node in level n is 2^{n-1} . This article draws lessons from hierarchical algorithm and improves it on the basis of current one. Specific algorithm is as follows:

Routing of every node includes its predecessor and successor node. The definition of level is same to traditional P-Ring. As the number of levels in traditional P-Ring is $\lceil \log_2 N \rceil$ and in this article predecessor nodes are also indexed as similar with successor nodes so the number of levels is smaller than traditional P-Ring. It is $\lceil \log_2 \frac{N}{2} \rceil$. N is the number of nodes.

Routing table of nodes in Fig.1 according to above algorithm is as Fig.2.

Because the query complexity of current P-Ring is $\log N$. In the modified routing algorithm predecessor and successor nodes respectively index half of all nodes in the ring. So as long as traversing $\lceil \log_2 \frac{N}{2} \rceil$ nodes we can find information we need. Therefore query complexity of this algorithm is $\log \frac{N}{2}$.

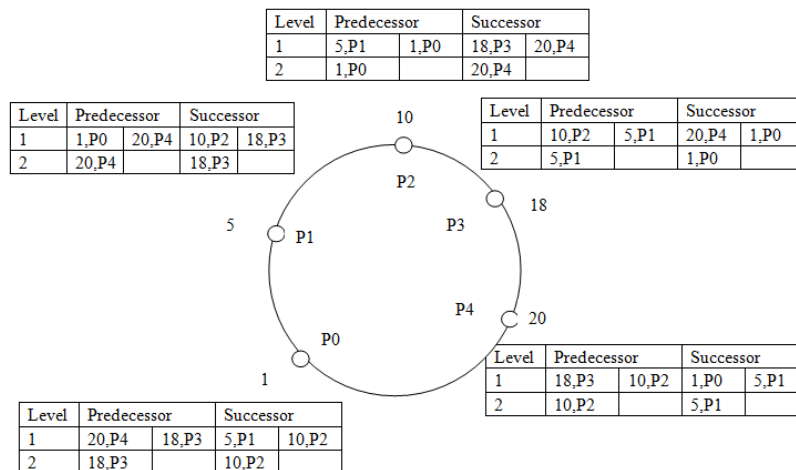


Figure 2 Routing table of nodes

When a range query is coming firstly we need to determine whether the scope of query contains sub ranges. If a range is split into several sub-ranges we can firstly record corresponding file name of each sub-range, and then merge them.

For example supposing that P4 receives a query whose attribute range is 1~8. Firstly find the minimum value 1 in the infoTable of P4. It is located in P0. Because stored values of range in every node of P-Ring are no smaller than the value of this node. As 8 is smaller than 10 which is the value of P2 so the maximum value 8 of the query range is located in P1. Then the search goes on in P2 and P1. The locating based on nodes in this example needs only once.

When completing locating nodes we need concretely search based on values in located nodes. In the above example we firstly query P0. Since the range stored in P0 is 1~5 and our query range is 1~8 which includes all values in P0. So all files stored in P0 need be queried in detail which are F5, F6, F8 and F9. Then query P1 to find files meeting with 5~8. There are two sub ranges in P1 meeting conditions which are (5, 6) and (6, 8). So record corresponding files of these two ranges and they are F2, F3, F5, F6, F8 and F9. Summarizing files meeting with query condition of the above two ranges (The repeated files in two ranges don't need to search twice.). The final results are that F2, F3, F5, F6, F8 and F9 need to be searched in detail. According to index information in infoTable find corresponding files to query concretely based on attribute values. That is B+ tree index.

C. B+ tree index

After finding corresponding files, we need to seek data meeting the condition in each file. Such search based on data requires building a B+ tree. That is to say the logical organization structure among data is B + tree. This paper takes F4 as an example. Assuming that data stored in F4 shows as the following table.

Table 3 Data in F4

Order Number	Attribute	Order Number	Attribute
1	43	11	54
2	46	12	58
3	51	13	43
4	44	14	46
5	42	15	52
6	50	16	56
7	55	17	59
8	48	18	57
9	49	19	47
10	41	20	60

B+ trees established based on attribute of this file show as follow.

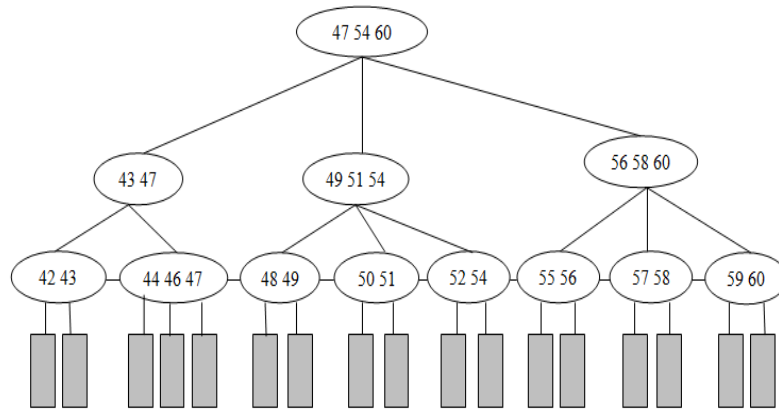


Figure 3 B+ tree based on attribute of file 4

In B+ tree only leaf nodes store keywords (In this paper they refer to data in the table). Non-leaf nodes store index only containing the biggest keyword of its sub-tree.

In the dual-index proposed in this paper, files found in Chord consist of information about B+ tree pointed to these files. For example, when the query range is $47 < a < 51$ F4 is the found file in Chord and then next step is making specific search in B+ tree of F4. Query results are 48, 49, 50, 51.

B+ tree index is created before the first query and the following queries can use it directly unless data is update.

D. Map Reduce

The Master node needs to know about information stored on each node so as to avoid sending query to a node which will return null results. That will affect query efficiency. Therefore each node needs to send its own ID, the range of fileID in this node and numeric attributes (Before receiving the query which attribute will be searched is not determined.) in each file to Master node which stores these index information. When deciding Map node we can choose nodes which don't execute query.

When Master node receives query request it firstly checked index information stored in it. Then Master node sends this request to a node containing this queried attribute. The chord will retrieve files containing the query attribute and attributes whose values range meets the query condition.

IV. Range Query Processing

When one query comes the Master node of Map Reduce decides which Map node the query will be sent to. After Determining queried node the search based on file begins in each node to find qualified files. Then search data inside the file. Finally data found is sent to the Reduce node to merge results.

The concrete steps show as following:

1. The query is sent firstly to the Master node. As the Master node stores attributes value range of files of the other nodes. It maintains a P-Ring index including all files in other nodes. So the Master node can determine which one or more nodes the query will be executed in. In this article we use P-Ring to organize nodes of MapReduce. Every node under query is Map.
2. When Master receives query it firstly needs to determine which node the maximum and minimum value of range is located in. Files in the node which storing values meeting with query range. There are following circumstances.
 - 1) The maximum and minimum value is exactly the value of node. If this happens, infoTable of all nodes (including node which minimum value is located in) between these two nodes need to be searched concretely;
 - 2) The minimum value is exactly equal to one node assuming it is P1 and the maximum value is between two nodes assuming P0 and P3. We need to determine which sub range of infoTable of P0 the maximum value is located in. So all files in P1 and files which are located in range from the first sub range of P0 to sub range includes the maximum need to be query.
 - 3) The maximum value is exactly equal to one node or two values of query range are between two nodes in ring. Locate files according to step 2) and return file name and address needing to search concretely. If two values of query range are between two nodes we can search files in two Map nodes at the same time using the parallelism of MapReduce.

1. Query B+ tree of each file in parallel in the list of found files according to file name and file address in infoTable. The search begins with root node of B+ tree. If child nodes fit with query condition the search will continue from this branch until the query arrives at leaf nodes. Finally results are returned to Reduce nodes designated by Master.
2. On the end of each Map node query, it sends a message to the Master node. Master decides which Reduce node to merge these results will send to.

V. Conclusion

This paper proposed a range query algorithm mainly based on big data which applies dual- index structure. In order to simplify B + tree we combined P-Ring with it. Files are stored in different nodes. The range between two nodes is corresponding to files containing these values. MapReduce dispatches tasks among nodes. The time complexity of this algorithm is finding files in P-Ring adding up to finding data in B+ tree. That is $\log_2 \frac{N}{P} + \log P$. N is the number of nodes in P-Ring and P is the maximum number of items in one file.

REFERENCES

- [1] Viktor Mayer-Schönberger, Big Data: A Revolution That Will Transform How We Live, Work, and Think.
- [2] Wang Dan, Li Maozeng, A Range Query Model based on DHT in P2P System, 2009 International Conference on Networks Security, Wireless Communications and Trusted Computing.
- [3] Hui Zhao, Shuqiang Yang, Zhikun Chen, Songcang Jin, Hong Yin, Long Li, MapReduce model-based optimization of range queries, 2012 9th International Conference on Fuzzy Systems and Knowledge Discovery (FSKD 2012).
- [4] Adina Crainiceanu, Prakash Linga, Ashwin Machanavajjhala, P-Ring: An Efficient and Robust P2P Range Index Structure, SIGMOD '07 Proceedings of the 2007 ACM SIGMOD international conference on Management of data Pages 223-234 New York 2007 .
- [5] A. R. Bharambe, M. Agrawal, and S. Seshan. Mercury: supporting scalable multi-attribute range queries. SIGCOMM Comput. Commun. Rev., 34(4), 2004.
- [6] Michael Cardosa, Chenyu Wang, Anshuman Nangia, Abhishek Chandra, Jon Weissman, Exploring MapReduce efficiency with highly-distributed data, MapReduce '11 Proceedings of the second international workshop on Map Reduce and its applications, Pages 27-34 , New York 2011.
- [7] Samet Ayhan, Johnathan Pesce, Paul Comitz, Gary Gerberick, Steve Bliesner, Predictive analytics with surveillance big data, BigSpatioal'12 Proceedings of the 1st ACM SIGSPATIAL International Workshop on Analytics for Big Geospatial Data, Pages 81-90, New York 2012.
- [8] Edward Z. Yang, Robert J. Simmons, Profile Jeff Dean: Big data at Google, XRDS: Crossroads, The ACM Magazine for Students - Big Data, Volume 19 Issue 1, fall 2012, Pages 69-69
- [9] Jens Dittrich, Jorge-Arnulfo Quiane-Rioz, Efficient big data processing in Hadoop MapReduce, Proceedings of the VLDB Endowment, Volume 5 Issue 12, August 2012 , Pages 2014-2015.
- [10] A. Gupta, D. Agrawal, and A. El Abbadi. Approximate range selection queries in peer-to-peer systems. In CIDR, 2003.
- [11] A. Datta, M. Hauswirth, R. John, R. Schmidt, and K. Aberer. Range-queries in trie-structured overlays. In P2P Comp. 2005.
- [12] P. Ganesan, M. Bawa, and H. Garcia-Molina. Online balancing of range-partitioned data with applications to peer-to-peer systems. In VLDB, 2004.

A Unique Application to Reserve Doctor Appointment by Using Wireless Application Protocol (WAP)

Adnan Affandi¹, Othman Abdullah saleh Al-Rusaini², Mubashshir Husain³

¹Professor, Dept., of Elect. & Comp. Eng., Faculty of Eng. King Abdul Aziz University Jeddah, KSA

²MS (Student), Dept., of Elect. & Comp. Eng., Faculty of Eng. King Abdul Aziz University Jeddah, KSA

³Lecturer, Dept., of Elect. & Comp. Eng., Faculty of Eng. King Abdul Aziz University Jeddah, KSA

Abstract: WAP is a standardized technology for cross-platform, distributed computing, very similar to the Internet's combination of Hypertext Markup Language (HTML) and Hypertext Transfer Protocol (HTTP). WAP could be described as a set of protocols that has inherited its characteristics and functionality from Internet standards and from standards developed for wireless services by some of the world's leading companies in the business of wireless telecommunications. This application will help patients, the normal doctor and the medical director. The patient can reserve an appointment. The normal doctor can view and print the lists of patient appointment under his responsibility. The medical director can add new departments, add new doctors, and also can change the password to access the database. He can also modify data and working schedules of doctors assigned. He can add new patients and can have privilege access to transfer any patient appointment to another doctor. This Application which has been developed by using WAP was the first of its kind here, where software has been developed.

Keywords: WAP, WML etc.

I. Introduction

Wireless Application Protocol (WAP) is a result of continuous work to define an industry-wide specification for developing applications that operate over wireless communication networks. The scope for the WAP Forum is to define a set of specifications to be used by service applications. WAP was developed by the WAP Forum as a standardized specification for technologies that operate over wireless networks. It is seen as an attempt to define the standard for how content from the Internet is filtered for wireless communications, thus bridging the gap between the mobile world and the Internet. The basic aim of WAP is to provide users with a web-like experience but over a handheld device rather than a PC, whilst accessing the content is readily available on the Internet. Most of the successful interactive services available on the Internet can be envisaged in a WAP environment too.

WAP is more than just a protocol specification, it also incorporates its own language called WML or Wireless Markup Language. WML is designed for low-power, resource-constrained devices. Developers starting to use WAP and WML to extend their Internet services quickly discover that wireless handheld devices differ significantly from the ordinary computer and must learn new ways of presenting information where the target medium is mobile devices. WAP is the set of rules governing the transmission and reception of data by computer applications on, or via, wireless devices like mobile phones. WAP is a standardized technology for cross-platform, distributed computing, very similar to the Internet's combination of Hypertext Markup Language (HTML) and Hypertext Transfer Protocol (HTTP).[1]

A. The Architecture and Workings of WAP

When people think of networks, they always think of the World-Wide-Web and the Internet. Generally people have a basic understanding of it, i.e. a two-tier architecture comprising clients (browsers) and servers which host the pages that are viewed (or the applications that produce pages on-the-fly). Well, WAP is essentially the same. The clients are now the wireless handheld devices and the servers are still hosting the pages (and applications). The main difference between a WAP network and the Internet is the interconnecting of the wireless network to the wired network, the basic view of the WAP network is shown in Figure 1.

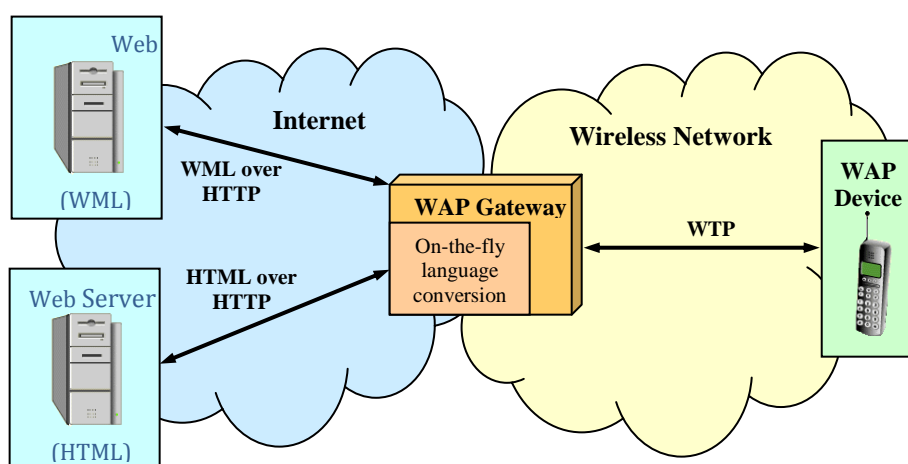


Figure 1: Basic View of the WAP Network

B. WAP standard

As much as possible, WAP uses existing Internet standards for the basis of its own architecture and is designed to allow standard Internet servers to provide services to wireless devices. However, Internet standards such as HTML, HTTP, TLS, and TCP, which require large amounts of mainly text-based data to be sent, are inefficient over wireless networks. So Internet standards such as HTML, HTTP, TCP, and TLS are not appropriate for the restrictions associated with wireless networks.

WAP does, however, use many other Internet standards such as eXtensible Markup Language (XML), User Datagram Protocol (UDP), and Internet Protocol (IP) to communicate with wireless devices. So WAP is based on familiar standards such as HTTP and TLS, but has been optimized for the constraints of the wireless environment. For example, a WAP gateway is required to communicate with other Internet nodes using HTTP, and the WAP specification requires devices to use standard URL addressing to request services.

So WAP has been optimized with the restrictions of the wireless environment in mind. It is designed for low bandwidth and long latency, and uses binary transmission for greater compression of data. WAP sessions deal with intermittent coverage and operate using IP over a large variety of wireless transports whenever possible.

It is important that WAP standards complement existing standards. For example, instead of the WAP specification designating how data is transmitted over the air interface, it is designed to sit on top of existing standards so that the bearer's standard is used with the WAP protocol.

The WAP Forum works closely with the World Wide Web Consortium and other bodies such as the European Telecommunications Standards Institute (ETSI), the Cellular Telecommunications Industry Association (CTIA), and the Internet Engineering Task Force (IETF) to ensure that the future versions of HTML, HTTP, and TCP take the special needs of wireless devices into account and can be supported in the WAP framework. The WAP Forum also works closely with these bodies and others as they become members of the Forum.

When the WAP Forum identifies a new area of technology with no existing standards specification, it works to submit its specification to related standards groups, believing that active participation leads to the best standards. With this approach, the WAP Forum hopes to produce open, not proprietary, standards through industry consensus and with no one vendor receiving favorable treatment.[2][3]

C. WAP Architecture

WAP architecture was designed to provide a scalable and extensible environment for application and content development. This is achieved through layered design of the entire protocol stack with many of the protocols used analogous to those used in existing Internet technology, but optimised for the constraints imposed by narrowband handheld devices and wireless networks, as shown in Figure 2. Each of these protocols for WAP 1.X and WAP 2.0 (WAP versions presented in section 3.8) will be discussed in turn.

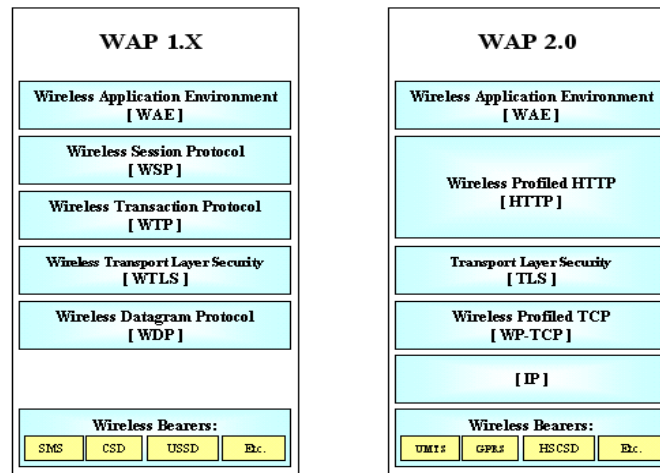


Figure 2: The WAP Protocol Stack for WAP 1.X and WAP 2.0

II. Developing a WAP Application

A. Defining a template

```
<wml>
  <template>
    <do type="goBack" name="goBack" label="Back">
      <prev/>
    </do>
  </template>
  <card id="init" newcontext="true">
  </card>
</wml>
```

The snippet of WML results in the Back option being displayed on each card in the deck. It uses the <do> element to associate the label Back with the <prev> task. Whenever the user selects the Back option as shown in Figure 3, the microbrowser will navigate to the previous card:



Figure 3: Back option

B. Defining a Card

```
<wml>
  <card id="init" newcontext="true">
    <p align="center">
      <b>Portfolio Service</b><br/>
    </p>
  </card>
</wml>
```

This code snippet just shows a simple WML card. It includes some formatting elements to influence how the text is laid out by the microbrowser. The card is shown in Figure 4:



Figure 4: Defining a card

C. Using anchors

```
<wml>
<card id="MainMenu" title="Main Menu">
  <p>
    <anchor>1. Market Indices
      <go href="#MarketIndices"/>
    </anchor><br/>
    <anchor>2. Portfolio Valuation
      <go href="#PortfolioValuation"/>
    </anchor><br/>
    <anchor>3. Current Fund Prices
      <go href="#CurrentFundPrices"/>
    </anchor><br/>
    <anchor>4. Buy/Sell
      <go href="#BuySell"/>
    </anchor><br/>
  </p>
</card>
</wml>
```

Anchors are used to link to other cards, as shown in the code snippet above and the screen shot here. Each anchor element is bound to a <go> task that references another card in the deck as shown in Figure 5



Figure 5: Using anchors

D. Using input fields

```
<wml>
<card id="Login" title="Client Login">
  <p>
    Please enter:<br/>
    Account No
    <input type="text" name="txtAccountNo"/><br/>
    Security Code
    <input type="password" name="txtSecurityCode"/><br/>
  </p>
  <do type="goMainMenu" label="Main Menu">
    <go href="#MainMenu"/>
  </do>
</card>
</wml>
```

Input fields are used to allow the user to enter data. The code snippet above creates two input fields, one of which takes some text, the other of which takes a password. The password will be obscured by asterisks as it is rendered on the screen as shown in Figure 4.5. The card is also bound to a <go> task, which links it to the main menu, by a <do> element.



Figure 6: Using input fields

E. Using tables and graphics

```
<wml>
<card id="init" newcontext="true">
  <p align="center">
    <table columns="1">
      <tr><td>
        <br/>
      </td></tr>
    </table>
    <b>Portfolio Service</b><br/>
  </p>
  <do type="goLogin" label="Login">
    <go href="#Login"/>
  </do>
</card>
</wml>
```

A table containing one column is created using the <table> element. The <p> element is used to align the table in the center of the screen. Within the table a <tr> element creates a single row that contains a single cell, created by the <td> element. Inside the cell the element creates a link to an image, with some alternate text associated with it for use in the event that the image cannot be displayed. A <do> element binds the card to a <go> task that links to the login card within the deck, that shown in Figure 7.



Figure 7: Using tables and graphics

This application is designed to help the patients, the normal doctor and the medical director. The patient can reserve an appointment date with the doctor. The doctor can view and print the lists of patient appointment under his responsibility. The medical director can add new departments, add new doctors, and also can change the password to access the database. He can also add/modify data and working schedules of doctors assigned. He can add new patients and can have privilege access to transfer any patient appointment to another doctor.

III. Results & Discussion

A. APPLICATION PAGES

The application home page can be seen in fig.8. The home page contains several links like new request, Inquiries about request, doctors, etc. Doctor can enter into login page by clicking on link “Doctors”. On login page they have to enter user name and password. After clicking on enter button , doctor can enter into another page named “Doctors Menu”, where he can see his name , patients name report link and option for changing password. He can anytime reach to home page by clicking on home page link. By clicking on “Patients Names Report” , he can come to new page containing information about patients. That page containing patients names , date & time of appointment.



Figure 8 : The application home page

By clicking on “New Request” link, patient enters into another page . On this page patient can select clinic , Doctor , date,etc. “New Request” page cab be seen in fig 9.



Figure 9: “New appointment request” page

After filling all the information in “ New Request “ page and pressing enter , the patient will move into new page containing booking informations like patient name , clinic , appointment date , appointment time, appointment day,etc. Patient can print this page and can be used as appointment slip.Confrmed appointment page can be seen in fig.10



Figure 10: “Confirmed appointment” page

Through this application medical director has authority to access Doctors data, clinic data , doctors unavailable dates , doctors’s patient transfer, patient data ,etc. By clicking on link “Doctors and clinic data” , medical director can modify clinics data and also modify doctors data like shifts working time,etc. By clicking on link “ Doctor’s patients transfer” , director can transfer patient to another doctor of same speciality.Medical director menu page can be seen in fig.11.

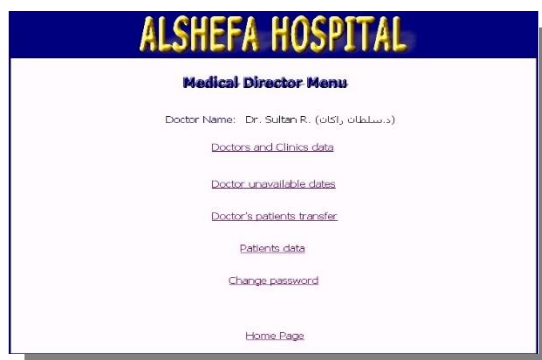


Figure 11: “Medical director menu” page

IV. Conclusion

In this paper, a Reserve Doctor Appointment Application using WAP has been developed. The WAP successfully protocol is designed using the best of the existing protocol and then was optimized to suite the wireless end-client. It was also found that WAP uses less than half the number of packets that the standard HTTP/TCP/IP stack uses to deliver the same content. This improvement is essential for the end-user to experience an acceptable transfer rate of data. To further enhance the browsing experience of HTML web pages through a thin mobile client a network element was added – the WAP gateway. Through the gateway infrastructure deployed in mobile operator's network it enables low capacity wireless devices to access web servers of the Internet. Indeed, the use of the gateway and compression in the network interface reduces the processing load at the handheld device so that an inexpensive CPU can be used and helps reducing power consumption and extends battery life. Hence, the gateway has increased the functionality in the communication subsystem, making the wireless clients much less flexible but making it possible to pleasantly view html content of the web on the run.

Acknowledgment

This article was funded by Deanship of Scientific Research (DSR), King Abdulaziz University, Jeddah. The authors, therefore, acknowledge with thanks DSR technical and financial support.

REFERENCES

- [1] Adnan Affandi1, Abdullah Dobaie2, Mubashshir Husain3, “WAP- Mobile Personal Assistant Application” , International Journal of Modern Engineering Research (IJMER), ISSN: 2249-6645 Vol. 3, Issue. 4, Jul - Aug. 2013 pp-2048-2055
- [2] Stuckmann, P. and Hoymann, C., “Performance Evaluation of WAP-based Applications over GPRS”, IEEE, pp. 3356, 2002.
- [3] Leavitt, N., “Will WAP Deliver the Wireless Internet?”, IEEE Computer, pp. 16-20, May 2000.

Improvement of Plant Layout by using 5S technique-An industrial case study

Dinesh B. Shinde¹, Prashant N. Shende²

¹(Department Of Mechanical Engineering, DMIETR Wardha, India)

²(Department Of Mechanical Engineering, YCCE Nagpur, India)

Abstract: 5S is one of the most widely adopted techniques from the lean manufacturing toolbox. Along with Standard Work and Total Productive Maintenance, 5S is considered a "foundational" lean concept, as it establishes the operational stability required for making and sustaining continuous improvements. The primary objective of 5S is to create a clean, orderly environment- an environment where there is a place for everything and everything is in its place. Beyond this, many companies begin their lean transformation with 5S because it exposes some of the most visible examples of waste it also helps establish the framework and discipline required to successfully pursue other continuous improvement initiatives.

Keywords: 5S, Continuous improvement, discipline, productivity.

I. Introduction

5S – A simple, but effective, lean manufacturing methodology that helps organizations to simplify, clean, and sustain a productive work environment. 5S is a system to reduce waste and optimize productivity through maintaining an orderly workplace and using visual cues to achieve more consistent operational results. Implementation of this method "cleans up" and organizes the workplace basically in its existing configuration, and it is typically the first lean method which organizations implement. The 5S pillars, Sort (*Seiri*), Set in Order (*Seiton*), Shine (*Seiso*), Standardize (*Seiketsu*), and Sustain (*Shitsuke*), provide a methodology for organizing, cleaning, developing, and sustaining a productive work environment. In the daily work of a company, routines that maintain organization and orderliness are essential to a smooth and efficient flow of activities. This lean method encourages workers to improve their working conditions and helps them to learn to reduce waste, unplanned downtime, and in-process inventory. A typical 5S implementation would result in significant reductions in the square footage of space needed for existing operations. It also would result in the organization of tools and materials into labeled and color coded storage locations, as well as "kits" that contain just what is needed to perform a task. 5S provides the foundation on which other lean methods, such as TPM, cellular manufacturing, just-in-time production, and six sigma can be introduced.

II. Types of 5S

2.1 Sort

The first S, Sort, calls for the elimination of unnecessary items that have collected around work areas. As debris and unused objects build up, productivity often takes a turn for the worse. In unproductive workspaces, frustrations mount when workers find that they are unable to satisfactorily finish the task at hand. Therefore, it is vital to implement a workplace sorting system. The effective visual method of identifying unneeded items is called "Red Tagging".

2.2 Set in order

Now that your workplace has been sorted, it is time to implement a more comprehensive system of organization. While sorting is an effective method, used by it, it is only a preliminary measure. Set in Order (*Seiton*) focuses on effective storage and organization methods, with the end goal of developing an environment that resists clutter and aids long-term productivity.

2.3 Shine

Once you have eliminated the clutter in your work area, it is important to thoroughly clean that area and the equipment in it. Leaks, squeals and vibrations involving clean equipment can often be easily detected, but a

dirty workplace tends to be distracting and equipment faults go unnoticed. Clean workplace conditions are also important to employee health, morale, and safety.

2.4 Standardize

Cleaning and organization systems implemented without established standards tend to lose effectiveness with time. Allow your employees to participate in the development of standards that improve workplace conditions. Ask for feedback as you find the best way to balance employee morale with production concerns.

2.5 Sustain

This is by far the most difficult S to implement and achieve. People tend to resist change and even the most well structured 5S plan will fail if not constantly reinforced. Fortunately, there are effective methods of sustaining positive growth.

III. Company Information

Name of Industry:- Metalfab Hightech Private Limited, Nagpur. (unit II)

Address: L-2, M.I.D.C., Hingna road, Nagpur (M.S.)

Establishment:- Company was established in year 1981 as M/S.METALFAB INDUSTRIES up to 1995, subsequently later known as M/s. METALFAB HIGHTECH PVT. LTD on Day 17th April 1996. ISO-9001-2000 certified company. The owner of this company is Mr. Hukumchand C. Jain.

Company Client:-BHEL-Bharat heavy electrical limited

L & T – Larson and Turbo

Company Product:-General Fabrication work “I section beam”

Raw Material: - M.S.Plate, M.S.Angle, M.S.Channel etc.

Labor:-50 (2 shift).

3.1 Plant Layout

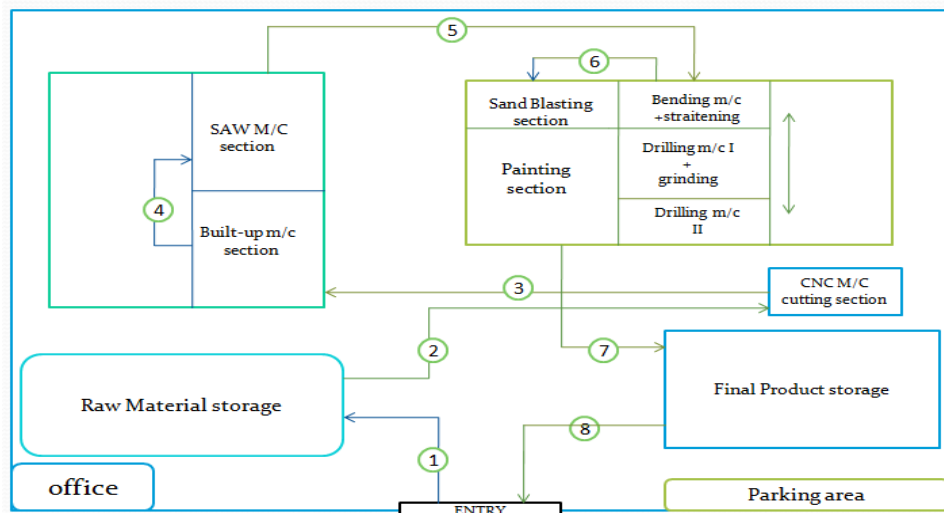


Fig 1. Plant Layout

3.2. Process

This is small industry. In which M.S.Plate is used as raw material and this raw material is converted into the finish good. The process for the I section beam is given below.

- 1) When raw material comes into the company, it is store in the storage by using fork left (Manually)
- 2) After stage of storing material the quality inspector check the raw material visually. If any problem found in the raw material then these raw materials send back or salvage it.
- 3) Then this raw material comes in CNC department where cutting operation perform as per requirement.
- 4) Built-up Machine fit the beam as per dimension.
- 5) After that Process next stage is welding for that submerged arc welding is used for welding purpose.
- 6) After that this product going to straightening department where straightening the beam operation are performed
- 7) After that this product is going to grinding machine where cleaning the beam is perform.
- 8) After that this product is going to sand blasting machine where super finishing is done.
- 9) After that Painting the beam and finally goes to the Final product store area.

3.3 Material flow of I section beam (Before improvement)

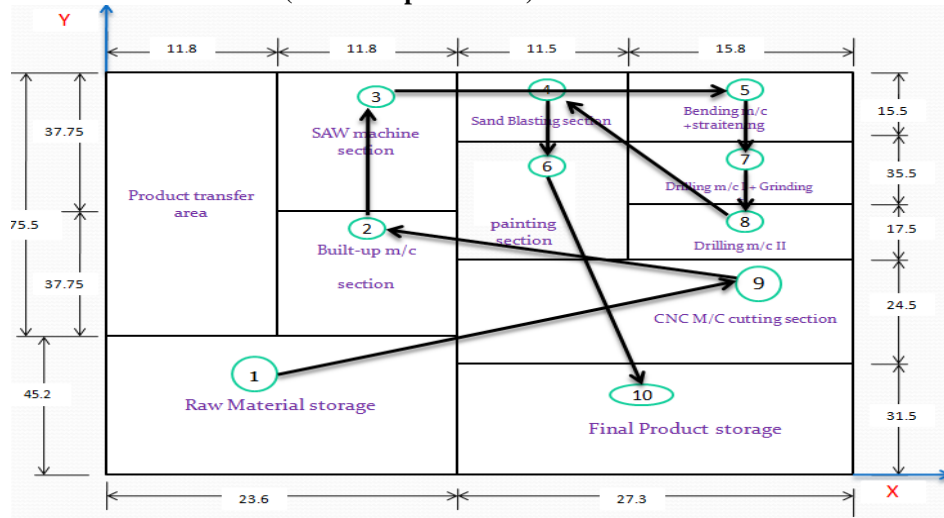


Fig 2. Material flow of I section beam

3.4. Department area

DEPARTMENT	AREA	
Raw material storage	23.6x45.2	1066.72 sq.mt
Material transfer section	75.5 x 11.8	890.9 sq.mt
Built-up machine section	37.75 x 11.8	445.45 sq.mt
SAW Machine section	37.75 x 11.8	445.45 sq.mt
Sand Blasting section	11.5 x 15.5	178.25 sq.mt
Painting section	11.5 x 53	609.5 sq.mt
Bending and straitening section	15.8 x 15.5	244.9 sq.mt
Drilling I and Grinding section	15.8 x 35.5	560.9 sq.mt
drilling II section	15.8 X 17.5	276.5 sq.mt
CNC cutting section	27.3 x 24.5	668.85 sq.mt
Final product storage section	27.3 X 31.5	859.95 sq.mt

Table 1. Department area

MACHINES	AREA	
Built-up Machine	6.5 x 4.8	31.2 sq.mt
SAW Machine	8.2 x 7.6	62.32 sq.mt
CNC Machine	18.8 x 17.6	330.88 sq.mt
Drilling machine I	2.3 x 1.3	2.99 sq.mt
Drilling machine II	4.9 x 1.4	6.86 sq.mt
Plate bending	6.9 x 1.4	9.66 sq.mt

Table 2. Machine area

3.5 Operation Process chart (Before improvement)

Operations	Product-I section beam						
	Material grade-E350BR						
	distance (Meter)	Time (Min)	○	→	D	□	▽
Laying raw material from storage							
Travel to CNC Machine	22.59	4.22					
Marking and Cutting		16.4					
Travel to built-up machine	19.85	3.35					
Await for Beam		3.83					
Fit up the Beam		20.14					
Checking the beam		1.45					
Travel to SAW Machine	37.75	5.15					
Welding the beam		26.5					
Checking the beam		1.13					
Travel to straitening	20.15	3.4					
Straightening the beam		31.12					
Travel to grinding m/c	18.86	3.2					
Grinding the Beam		34.32					
Checking the beam		1.4					
Travel to Drilling	17.8	3.12					
Marking and Drilling(6 hole)		38.81					
Travel to Sand blasting m/c	38.5	5.25					
Await for Beam		3.64					
Superfinishing the Beam		40.42					
Travel to paint section	27.86	5.13					
Primer and Paint		20.15					
Inspection		1.4					
Travel to storage	16.89	3.01					
Product storage							

Table 3. Operation process chart

IV. Area Of Study

- 1) Proper utilization of storage space more prominently.
- 2) Arrangement of departments in desired sequence.

4.1. Objective of study

Objectives of improve the plant layout are,

- 1) Minimize waiting time between straitening and grinding the beam .
- 2) Minimum material handling and related travelling cost.
- 3) Minimizing travelling distance in material flow.
- 4) Minimizing total time in process.
- 5) No backtracking moves.
- 6) Standard material flow pattern.
- 7) Better utilization of available space.

4.2 Problem Identification

- 1) More waiting time between straitening and grinding the beam .
- 2) More travelling distance and related time in material flow.
- 3) Material flow pattern is not standard.
- 4) Backtracking moves.
- 5) Scrap storage bins are located inside the industry which occupies extra space and material flow become difficult.

V. Comparison Of Existing Layout And Improved Layout

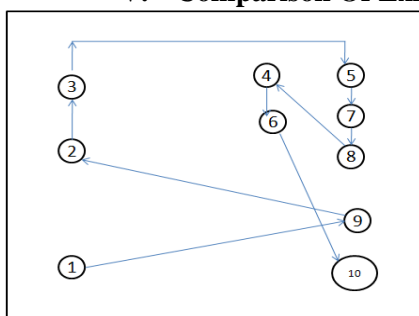


Fig 3 a. Existing material flow

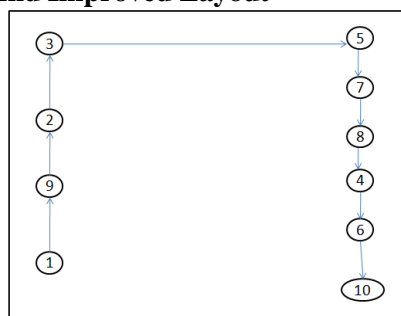
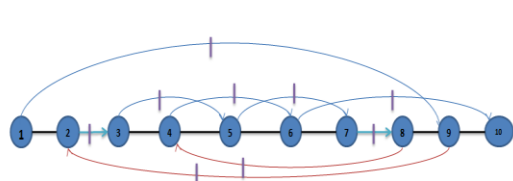


Fig 3 b. Proposed material flow

1. Raw material 2. Built-up machine 3. SAW machine 4.Sand blasting machine 5.Staritening 6. Painting 7.Grinding 8. Drilling machine 9. CNC Machine 10. Product storage

5.1 performances Measure of Material Flow Sequence



Total moves	In-sequence moves	Backtracking moves	Bypassing moves
09	02	02	05

Percentage of in-sequence moves = $2/9 = 0.22 = 22\%$

Percentage of backtracking moves = $2/9 = 0.22 = 22\%$

Percentage of bypassing moves = $5/9 = 0.56 = 56\%$

Fig 4a. Before Implementation



Total moves	In-sequence moves	Backtracking moves	Bypassing moves
09	09	00	00

Percentage of in-sequence moves = $9/9 = 1.00 = 100\%$

Percentage of backtracking moves = $0/9 = 0.00 = 00\%$

Percentage of bypassing moves = $0/9 = 0.00 = 00\%$

Fig 4 b. After Implementation

VI. Implementation of 5s Techniques

6.1 Sorting Out: Separate the necessary from the unnecessary and get rid of unnecessary

All unneeded tools, parts and supplies are removed from the area. The company layout is fixed according to process but the company does not consist of a systematic arrangement for various material handling and storage.

6.2 Set in Order: A place for everything and everything is in its place.



Fig 5. Set in order

6.3 Shine: The area is cleaned as the work is performed.



Fig 6. Shine

6.4 Standardize: Cleaning and identification methods are consistently applied.



Fig 7. Standardize

6.5 Sustain: 5S is a habit and is continually improved the company culture.

VII. Benefits

1. The production rate will increase due to systematic arrangement.
2. The space utilization will increase.
3. The atmospheric conditions will improve.
4. Clean and hygienic condition is achieved.
5. It is convenient to handle and operate each and every material.
6. Moral support of the operators and workmen's are improved.

7. Storage space is increased within the same area.

VIII. Conclusion

By using “5s” technique improved visibility of problem conditions, improved safety, reduced waste, improved morale, an increased sense of ownership of the workspace, improved productivity, improved quality, improved maintenance, shorter lead times, and a better impression on customers. More fundamentally, a well-implemented 5S program helps the culture develop a new sense of discipline and order that carries over into all activities.

REFERENCES

- [1] Mohd Nizam Ab Rahman, Nor Kamaliana Khamis, Rosmaizura Mohd Zain, Baba Md Deros and Wan Hasrulnizam Wan Mahmood. “*Implementation of 5S Practices in the Manufacturing Companies: A Case Study*”. “*American Journal of Applied Sciences* 7 (8): 1182-1189, 2010 ISSN 1546-9239”
- [2] R.T. Salunkhe, G.S. Kamble, Prasad Malage. “*Inventory Control and Spare Part Management through 5S, KANBAN and Kaizen at ABC Industry* “. “*IOSR Journal of Mechanical and Civil Engineering (IOSR-JMCE) ISSN:2278-1684, PP:43-47*”
- [3] Boca D. Gratiela. “*Study case: yellow tag vs quality management*” *Procedia - Social and Behavioral Sciences* 62 (2012) 313 – 318.
- [4] Alireza Anvari.ed “*Evaluation of Approaches to Safety in Lean Manufacturing and Safety Management Systems and Clarification of the Relationship Between Them*” *World Applied Sciences Journal* 15 (1): 19-26, 2011 ISSN 1818-4952.
- [5] Marko Milosevic.ed. “*implementation of the 5s system as a factor for improving the quality management*” 7th International Quality Conference May 24th 2013 Center for Quality, Faculty of Engineering, University of Kragujevac.
- [6] Raid A. Al-Aomar “*Applying 5S Lean technology: An infrasture for continuous process improvement*” *World academy of science ,Engineering and Technology* 59 2011
- [7] Alireza Anvari ed. “*Evaluation of Approaches to safety in lean manufacturing and safety management system and clarification of the Relationship between them*” *World Applied science journal* 15(1); 19-26, 2011 ISSN 1818-4952.

Denoising and Edge Detection Using Sobel method

P. Sravya¹, T. Rupa devi², M. Janardhana Rao³, K. Sai Jagadeesh⁴,
K. Prasanna Kumar⁵

^{1,2,3,4} IV-ECE, Lendi institute of engineering and Technology

⁵ Assistance professor, Lendi institute of engineering and Technology

ABSTRACT: The main aim of our study is to detect edges in the image without any noise, In many of the images edges carry important information of the image, this paper presents a method which consists of sobel operator and discrete wavelet de-noising to do edge detection on images which include white Gaussian noises. There were so many methods for the edge detection, sobel is the one of the method, by using this sobel operator or median filtering, salt and pepper noise cannot be removed properly, so firstly we use complex wavelet to remove noise and sobel operator is used to do edge detection on the image. Through the pictures obtained by the experiment, we can observe that compared to other methods, the method has more obvious effect on edge detection.

Keywords: sobeloperator, complexwaveletdenoising, white gaussian noise.

I. Introduction

Image processing is any form of signal processing, in which the input is an image such as a video, photograph, the output of an image processing may be either an image or set of characteristic related to the image. Edge detection is one of the foremost techniques in image processing. Edges carry important information of the image, it contains a wealth of internal information of the image. Therefore edge detection is one of the key research works in the image processing. Edge detection is the name for a set of mathematical methods which aim at identifying points in a digital image at which the image brightness changes sharply. The point at which image brightness changes sharply are typically organized into a set of curved line segments termed edges. In the ideal case, the result of applying an edge detector to an image may lead to a set of connected curves that indicate the boundaries of objects, the boundaries of surface markings as well as curves that correspond to discontinuities in surface orientation. Thus, applying an edge detection algorithm to an image may significantly reduce the amount of data to be processed and may therefore filter out information that may be regarded as less relevant, while preserving the important structural properties of an image.

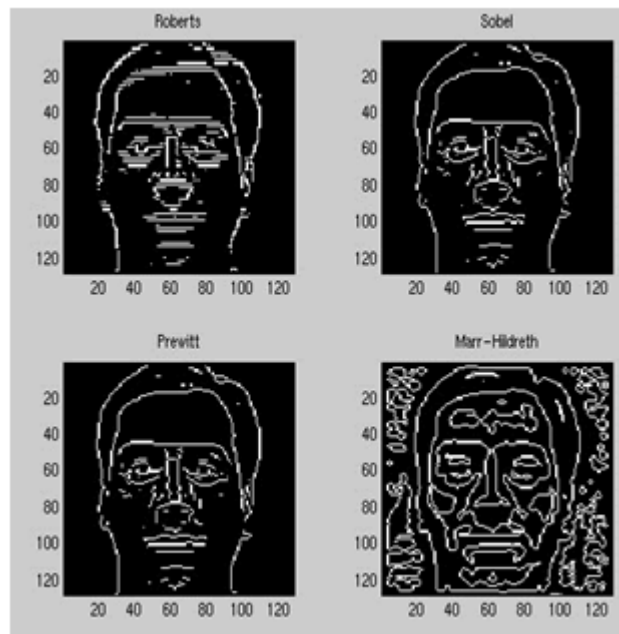
II. Edge Detection Methods

Edge widely exists between objects and backgrounds, objects and objects, primitives and primitives. The edge of an object is reflected in the discontinuity of the gray. Therefore the general method of edge detection is to study the changes of a single image pixel in a gray area, edge detection is mainly the measurement, detection and location of the changes in image gray. Suppose in an image if there were two pictures in an image which were attached or side by side, difference in these two will be identified by the edge, therefore edge extraction is the important technique.

There are many ways to perform edge detection. However, the most may be grouped into two categories, gradient and laplacian. The gradient method detects the edges by looking for the maximum and minimum in the first derivative of the image. The laplacian method searches for zero crossings in the second derivative of the image to find edges. This first figure shows the edges of an image detected using the gradient method (Roberts, Prewitt, Sobel) and the Laplacian.

III. Principal of Edge Detection

The basic idea of edge detection is as follows: First, use edge enhancement operator to highlight the local edge of the image. Then, define the pixel "edge strength" and set the threshold to extract the edge point set. However, because of the noise and the blurring image, the edge detected may not obtained edge point set into be continuous. So, edge detection includes two contents. First is using edge operator to extract the edge point set. Second is removing some of the edge points from the edge point set, filling it with some another and linking the obtained edge point set into lines. in this paper we use sobel operator.



IV. Sobel Operator

Compared to other edge operator, Sobel has two main advantages:

Since the introduction of the average factor, it has some smoothing effect to the random noise of the image. Because it is the differential of two rows or two columns, so the elements of the edge on both sides have been enhanced, so that the edge seems thick and bright. A way to avoid having the gradient calculated about an interpolated point between the pixels which is used 3 x 3 neighborhoods for the gradient calculations

$$G_x = \begin{bmatrix} +1 & 0 & -1 \\ +2 & 0 & -2 \\ +1 & 0 & -1 \end{bmatrix} * A \quad \text{and} \quad G_y = \begin{bmatrix} +1 & +2 & +1 \\ 0 & 0 & 0 \\ -1 & -2 & -1 \end{bmatrix} * A$$

Since the Sobel kernels can be decomposed as the products of an averaging and a differentiation kernel, they compute the gradient with smoothing. For example,

G_x Can be written as

$$\begin{bmatrix} +1 & 0 & -1 \\ +2 & 0 & -2 \\ +1 & 0 & -1 \end{bmatrix} = \begin{bmatrix} 1 \\ 2 \\ 1 \end{bmatrix} \begin{bmatrix} +1 & 0 & -1 \end{bmatrix}$$

The x-coordinate is defined here as increasing in the "right"-direction, and the y-coordinate is defined as increasing in the "down"-direction. At each point in the image, the resulting gradient approximations can be combined to give the gradient magnitude, using:

$$G = \sqrt{G_x^2 + G_y^2}$$

Using this information, we can also calculate the gradient' direction:

$$\Theta = \text{atan2}(G_y, G_x)$$

Where, for example, Θ is 0 for a vertical edge which is darker on the right side. Sobel operator is a kind of orthogonal gradient operator. Gradient corresponds to first derivative, and gradient operator is a derivative operator. For a continuous function $f(x, y)$, in the position (x, y) , its gradient can be expressed as vector (the two components are two first derivatives which are along the X and Y direction respectively

$$\nabla f(x, y) = [G_x \quad G_y]^T = \left[\frac{\partial f}{\partial x} \quad \frac{\partial f}{\partial y} \right]$$

The magnitude and direction angle of the vector are:

$$mag(\nabla f) = |\nabla f_{(2)}| = [G_x^2 \quad G_y^2]^{1/2}$$

$$\phi(x, y) = \arctan\left(\frac{G_x}{G_y}\right)$$

Every point in the image should use these two kernels to do convolution. One of the two kernels has a maximum response to the vertical edge and the other has a maximum response to the level edge. The maximum value of the two convolutions is used as the output bit of the point, and the result is an image of edge amplitude.

-1	-2	-1
0	0	0
1	2	1

(a) Convolution template S1

-1	0	-1
-2	0	2
-1	0	1

(b) Convolution template S2

Their convolution is as follows:

$$g_1(x, y) = \sum_{k=-1}^1 \sum_{l=-1}^1 S_1(k, l) f(x+k, y+l) \quad (4)$$

$$g_2(x, y) = \sum_{k=-1}^1 \sum_{l=-1}^1 S_2(k, l) f(x+k, y+l) \quad (5)$$

$$g(x, y) = g_1^2(x, y) + g_2^2(x, y) \quad (6)$$

If $g_1(x, y) > g_2(x, y)$, it means that there is an edge with a vertical direction passing through the point (x, y) . otherwise, an edge with a level direction will pass through the point. If the pixel value of the point (x, y) is $f(x, y)$, and this point is judged as an edge point if $f(x, y)$ Satisfy one of the following two conditions

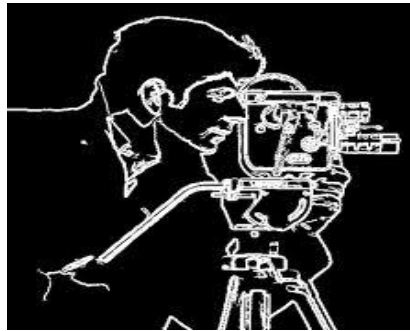
- 1) (1) $g(x, y) > 4 \times \frac{\sum_{i=1}^{row} \sum_{j=1}^{list} g^2(i, j)}{row \times list}$
- (2) $g_1(x, y) > g_2(x, y)$
- (3) $g(x, y-1) \leq g(x, y)$
- (4) $g(x, y) \geq g(x, y+1)$

$$2) (1) g(x, y) > 4 \times \frac{\sum_{i=1}^{row} \sum_{j=1}^{list} g^2(i, j)}{row \times list}$$

$$(2) g_1(x, y) > g_2(x, y)$$

$$(3) g(x-1, y) \leq g(x, y)$$

$$(4) g(x, y) \leq g(x+1, y)$$



V. Image Denoising

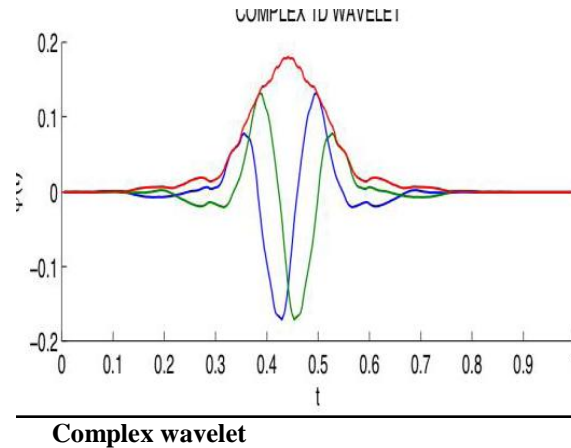
Information is important while processing an image that means it should not be lost. Due to noise we couldn't get the required information. . It is important to reduce noise before trying to extract features from a noisy image. so before we give a short introduction to wavelets.. Many filters have been developed to improve image quality .Recently there has been considerable interest in using wavelet transform as a powerful tool for recovering data from noisy data. But wavelet transform we have some problems to achieve this problems we use complex wavelets'.

VI. Complex wavelets

The complex wavelets have difficulty in designing complex filters which satisfy perfect reconstruction. To overcome this, Kingsbury proposed a dual tree implementation of the complex wavelet transform (DT CWT) which uses 2 trees of real filters to generate the real and imaginary parts of the wavelet coefficients separately. In our method we used dual tree complex wavelet transform

VII. Dual Tree Complex Wavelet Transform

The dual-tree complex DWT of a signal x is implemented using two critically-sampled DWTs in parallel on the same data, as shown in the figure. The transform is 2-times expansive because for an N -point signal it gives $2N$ DWT coefficients [2][4]. If the filters in the upper and lower DWTs are the same, then no advantage is gained. However, If the filters are designed in a specific way, then the sub band signals of the upper DWT can be interpreted as the real part of a complex wavelet transform, and sub band signals of the lower DWT can be interpreted as the imaginary part. One of the advantages of the dual-tree complex wavelet transform is that it can be used to implement 2D wavelet transforms that are more selective with respect to orientation than is the separable 2D DWT. 2-D dual-tree DWT of an image x is implemented using two critically-sampled separable 2-D DWTs in parallel. Then for each pair of sub bands we take the sum and difference. The wavelet coefficients w are stored as a cell array. For $j = 1 \dots J$, $k = 1 \dots 2$, $d = 1 \dots 3$, $w\{j\}\{k\}\{d\}$ are the wavelet coefficients produced at scale j and orientation (k,d) The six wavelets associated with



VIII. Denoising

In an image like bacteria the information (micro cells) are very important, if it is corrupted with noise it will be difficult to segment the number of cells. Hence denoising may be useful for improving the SNR. By improving the SNR the segmentation is related to SNR. Thus the probability of detecting the number of cells may be improved. One technique for denoising is wavelet thresholding (or "shrinkage"). [8] When we decompose the data using the wavelet transform, some of the resulting wavelet coefficients correspond to details in the data set (high frequency sub-bands). If the details are small, they might be omitted without substantially affecting the main features of the data set. The idea of thresholding is to set all high frequency sub-band coefficients that are less than a particular threshold to zero. These coefficients are used in an inverse wavelet transformation to reconstruct the data set.

IX. Algorithm

The advantage of Sobel edge operand is its smoothing effect to the random noises in the image. And because it is the differential separated by two rows or two columns, so the edge elements on both sides have been enhanced and make the edge seem thick and bright. Sobel operator is a gradient operator. The first derivative of a digital image is based on a variety of two-dimensional gradient approximation, and generates a peak on the first derivative of the image, or generates a zero-crossing point on the second derivative. Calculate the magnitude and the argument value of the image horizontal and vertical first-order or second-order gradients, at last calculate modulus maxima along the angular direction and obtain the edge of the image. But when the image has lots of white Gaussian noises, it is very difficult to get the peak value of the first derivative; the reason is because that the noise points and the useful signals mix up. Therefore this paper combines soft-threshold wavelet de-noising and Sobel operator. The core idea of the algorithm of de-noising and Sobel operator:

1. The standard test images like bacteria, Lena are considered and are corrupted by additive White Gaussian Noise. It is given as $x = s + g$ where s is original image, x is noisy image corrupted by additive white Gaussian noise g of standard deviation σ . Both s and x are of same sizes
2. The dual tree complex wavelet transform uses 10 tap filters for analysis at different stages. The reconstruction filters are obtained by simply reversing the alternate coefficients of analysis filters.
3. Perform the 2D Dual tree DWT to level $J = 4$. During each level the filter bank is applied to the rows and columns of an image.
4. A different threshold value with soft Thresholding is applied for each sub band coefficients.
5. The inverse DT DWT is performed to get the Denoised image
6. The quantitative measures, Mean Square Error and Peak Signal to Noise Ratio are determined for different thresholds.
7. Do wavelet decomposition to the image matrix and get the wavelet coefficients with noises.
8. Process the wavelet coefficients HL, LH and HH obtained by the decomposition, and keep the low frequency coefficients unchanged.
9. Select an appropriate threshold to remove Gaussian white noise signals.
10. Do inverse wavelet transformation to the image matrix and get the image matrix after de-noising.
11. Custom template edge coefficient according to the Sobel operator template showed in Figure 1.
12. After given Sobel edge detection operator template, convolute on every pixel of the image using this template, get the gradient of this point, and the gradient amplitude is the output of this point. At last we get the edge detection image.

X. Results

The original image



complex wavelet denoising



Sobel operator image



XI. Conclusion

As edges carry most important part of the information, here we used sobel operator and dual transform wavelet on white Gaussian noise images. By using the denoising wavelet, image is noise free after that sobel operator is applied to detect edges. By using this method we will obtain the edges thick and dark which we can identify accurately.

References

- [1]. Chang S G, Bin Yu, Vetlerti M. Adaptive wavelet threshold for image denoising and compression [J]. IEEE Trans Image Processing, 2000,
- [2]. Donoho D L. De-noising by soft-threshold [J]. IEEE Trans Information Theory 1995,41: 613-627.
- [3]. Xiaoguang Zhang Digital Media Department. Communication of University of china, ICICT 2010 Beijing, China zxcgpc 1988@yahoo.cn M. Young, The Technical Writer's Handbook. Mill Valley, CA: University sciences, 1989.
- [4]. Ostu N.A. Threshold Selection Method from Gray - Level Histograms[J]. IEEE Trans on Systems. Man and Cybernetics, SMC - 9, 1979, 9(1):62-66
- [5]. International Journal of Engineering and Innovative Technology (IJEIT) Volume 2, Issue 7, January 2013
- [6]. Kenneth R. Castleman. Digital Image Processing. Beijing : Tsinghua university press, 1998
- [7]. Azzalini A, Farge M, Schneider K. Nonlinear wavelet threshold : A recursive method to determine the optimal denoising threshold[J]. Appl. Comput. Harmon. Anal., 2005, 18: 177-185

Stakeholders' Perception of the Causes and Effect of Construction Delays on Project Delivery

P. S. Gandhak¹, Prof. Syed Sabihuddin²

¹ P. G. Student, PRMCE, Amravati,

² HOD, Dept. of Civil Engg., PRMCE, Amravati,

ABSTRACT: Indian Construction industry is large, volatile, and requires tremendous capital outlays. Typically, the work offers low rates of return in relation to the amount of risk involved. A unique element of risk in the industry is the manner in which disputes and claims are woven through the fibre of the construction process. Delay is generally acknowledged as the most common, costly, complex and risky problem encountered in construction projects. Because of the overriding importance of time for both the Owner and the Contractor, it is the source of frequent disputes and claims leading to lawsuits. The growing rate of delays is adversely affecting the timely delivery of construction projects. Presently construction industries are facing a lot of problems, considering that a paper assess construction stakeholder's perception to the causes of delays and its effects on project delivery. And also one case study is considered in this paper to elicit responses from construction stakeholders. The primary aim of this paper is to identify the perceptions of the different parties regarding causes of delays, the allocation of responsibilities and the types of delays, and method of minimizing the construction delays.

Keywords: Delay, Project Delivery, Stake Holders, Cost overrun.

I. Introduction

The problem of delays in the construction industry is a global phenomenon, Delays and disruptions are the challenges faced in the course of executing construction projects. The purpose of this paper is to assess causes and effects and disruptions in construction projects. The growing rate of delays is adversely affecting the timely delivery of construction projects. This paper therefore assesses stakeholders' perception of the causes of delays and its effects on project delivery in a bid to proper solution in minimizing the occurrences of delays. Questionnaire survey was conducted to elicit responses from stakeholders, On the other hand, time overrun, cost overrun, negative social impact, accumulation of interest rates, idling resources and disputes are the main effects of delays and disruptions. The study concludes that there still exist a number of causes of delays and disruptions and their effects put construction projects at great risk that have an effect on their performance.

Now a day's construction industries are facing the problem of Delays and Disruptions while executing the construction project

II. Delay

In construction, the word "delay" refers to something happening at a later time than planned, beyond the date that the parties agreed upon for the delivery of a project. Delay is defined as the slowing down of work without stopping construction entirely and that can lead to time overrun beyond the date that the parties have agreed upon for the delivery of the project. Delays are classified into non-excusable delays, excusable non-compensable delays, excusable compensable delays and concurrent delays

Tables, figures, mathematics, acknowledgements, appendixes, notations are optional contents for papers. When the figures and tables are added, all contents need to be numbered correctly.

Types of Delay

Delays can be grouped in the following four broad categories according to how they operate contractually:

- I. Non-excusable delays
- II. Excusable non-compensable delays
- III. Excusable compensable delays
- IV. Concurrent delays

Non-excusable Delays

Non-excusable delays are delays, when the contractor is responsible for the cause of the Delay; these delays might be the results of underestimates of productivity, inadequate Scheduling or mismanagement,

construction mistakes, weather, equipment breakdowns, Staffing problems. The contractor cannot obtain a time extension for non-excusable delays. The contractor is also liable for damages incurred by the owner as a result of the non-excusable delay. These delays are within the control of the Contractor.

Non-compensable Excusable Delays:

When a delay is caused by factors that are beyond the Contractor's control and not attributable to the Contractor's fault, it called as "Excusable delay". This term has the implied meaning that neither party is at fault under the Terms of the contract and has agreed to share the risk and consequences when excusable events occur. The Contractor will not receive compensation for the cost of delay, but he will be entitled for an additional time to complete his work and is relieved from any contractually imposed liquidated damages for the period of delay.

Concurrent Delays

Concurrent delays occur when both Owner and the Contractor are responsible for the delay. Generally, if neither the Contractor can be held responsible for the delay (forced to accelerate, or be liable for liquidated damages) nor can he recover the delay damages from the Owner. Until the development of CPM schedule analysis, there was no reliable method to differentiate the impact of Contractor caused delays from Owner-caused delays. With the sophisticated computerized techniques now available, however, it has become possible to segregate the impacts of apparently concurrent Owner and Contractor delays.

Causes of delays:

One of the most important problems in the Construction industry is delay. Delays occur in every construction project and the magnitude of these delays varies considerably from project to project. Some projects are only a few days behind the schedule; some are delayed over a year. So it is essential to define the actual causes of delay in order to minimize and avoid the delays in any construction project. There is a wide range of views for the causes of time delays for engineering and construction projects. The successful execution of construction projects and keeping them within estimated cost and prescribed schedules depend on a methodology that requires sound engineering judgment. Delays can be minimized only when their causes are identified. Knowing the cause of any particular delay in a construction project would help avoiding the same.

There are two kinds of causes for delays in construction projects: external and internal causes. Internal causes of delays include the causes, which come from four parties involved in that project. These parties include the Owner, Designers, Contractors, and Consultants. Other delays, which do not come from these four parties, are based on external causes for instance from the government, material suppliers, or weather.

In this step, all the causes for delays that may be encountered in a construction project were identified and the causes of delays are classified into six broad categories depending on their nature and mode of occurrence. Based on the findings, the delays checklist is as follows:

TABLE I

DELAYS CHECKLIST

Sr. No.	Causes	Sub Causes
a	Acts of god	<i>Flood Hurricane Fire Wind Damage</i>
b	Design – related	<i>design development change order decision during development stage changes in drawings</i>
c	Construction-related	<i>inspections subsurface soil conditions material procurement poor subcontractor performance equipment availability</i>
d	Financial/economica l	<i>financial process financial difficulties delayed payments economic problems</i>
e	Management/admini strative	<i>labour dispute and strike inadequate planning inadequate scheduling</i>

f		<i>staffing problems</i>
	Code-related	<i>building permits approval process changes in laws and regulations safety rules</i>

Effects of delay:

Construction delays occur either as a liability on part of the client and his team, liability on part of the contractor and his team, social political issues through the changes bye-laws, statues etc. The effects of these delays is always debilitating on construction project performance. Studies conducted on the effect of delay on project delivery have revealed that delays are associated with time and cost overruns as well as litigation and project abandonment.

The followings are some of the possible effects of delays that the construction industry is facing now a days are:

- Extension of time on the project
 - Cost overruns due to inflation and fluctuations
 - Accumulations of interest rate on the capital to finance the project
 - Wastage and under-utilization of man-power resources
 - Claims on the disturbance of regular progress of work by the main contractor
 - Under-utilization of equipment and plant purchased for the project
 - Loss of confidence on the contract, thereby jeopardizing the reputation of the contractor in the case of future tendering chances
 - Late returns of income (Private developers)
 - Dispute between the parties involved.
 - Additional insurance charges
 - Extra taxes and dues due to delay
 - In solvency of the contractor.
 - Arbitration/ Litigation
 - Total Abandonment of project
- Method to minimize delays and its effects:*

A. Research Design

This survey was carried out base on the review of relevant literatures and questionnaire surveys. Data used for the survey were primary and secondary. The primary data are the responses of the three main classifications of construction stakeholders of clients, consultants and contractors. Information regarding causes and effects of delays were extracted from above study and domesticated to the study population.

Data for this research were primarily gathered through a structured questionnaire. The questionnaire was designed with three major parts; the first part seeks for the general information about the respondents. The second part obtains the information on factors that contribute to the causes of delay in construction projects while in the final part, respondents were asked to rank the individual causes of delay in construction project based on frequency of occurrence according to their own judgment and working experience as clients' contractors or consultants.

B. Population and Sample

The population of the research was drawn from the practitioners of the construction industry where High concentration of construction works is prevalent in this areas. Judgmental sampling technique was adopted in chosen respondents; construction clients, consultants and contractors were identified to provide their perceptions and opinions on the causes and effects of delays on project delivery based on their experience.

C. Characteristics of Respondents

Following Table presents the characteristics of respondents with respect to their organization types. From the table, 16% of the respondents are professionals that work in clients' organization, while 39% and 45% represent respondents working in contracting and consulting organizations respectively.

TABLE II
CHARACTERISTICS OF RESPONDENTS

Type of Organization	No.	Percent (%)
Client Organization	6	16

Contracting Organization	15	39
Consulting Organization	17	45
Total	30	100

III. Case Study

The preliminary data for this Case study was collected through a literature review and the use of a questionnaire survey targeted at Contractors in the State of Florida.

Detailed Literature Review

I

Questionnaire Survey

I

Florida's construction Contractors

I

Analysis

I

Conclusions & Recommendations

In this step, all the causes for delays that may be encountered in a construction project were identified through a detailed review of published technical papers, recent magazines, newspapers and via Internet. The causes of delays are classified into six broad categories depending on their nature and mode of occurrence, as early seen in the delays checklist.

Questionnaire:

The questionnaire survey was developed to identify:

- The type of delay:

A=Non-Excusable

B=Excusable Non-Compensable

C=Excusable Compensable

D=Concurrent

- Chance of occurrence:

1-Unlikely = 20 % probability to happen.

2-As likely as not = 40 %

3-Likely = 60 %

4-Almost certain = 80 %

5-Certain = 100 % probability to happen

- Responsibility

Own=Owner

Cont=Contractor

Cons=Consultant

Gov=Government

Shared=Shared

Results of Case Study

This deals with the analysis of the information gathered from the questionnaire survey and includes the identification of the critical causes of delays, responsibilities and types of delays based on the delays checklist outlined in the methodology section of the report.

Questionnaire Response Rate:

A detailed questionnaire was prepared and sent to the different companies specially General Contractors in the State of Florida by regular mail and also via Internet. The survey was carried out over the period from October 2001 to March 2002, and the response rate is as shown in the Table III:

TABLE III

RESPONSE RATE

Questionnaire Sent	Regular Mail	Via Internet	Total
No. of Participant	200	180	380
No. of Companies Responding	23	12	35
Response Rate	11.5%	6.67%	9.21%

Identification of the Key Delays:

The key causes of delays are presented in tables IV – IX. Each table categorizes the different causes of delays (Acts of God, Design-Related Delays, Construction-Related Delays, Financial/Economical Delays, Management/Administrative Delays and Code-Related Delays) based on the chance of occurrence. The chance of occurrence was rated on a scale of 1 to 5 with 1 having the lowest frequency of occurrence and 5 is the highest. The number in the filled cells indicates the number of respondents who chose that option. The last cell in each category shows the average of the responses while the far most right column indicates the selection of the key causes of delays, which were selected as those having a value of 2.5 or higher indication at least a 50% chance of occurrence.

TABLE IV
KEY DELAYS – ACTS OF GOD

Acts of God	1	2	3	4	5	Avg. of Responses	Key Delay
Flood	20	4	3	0	0	1.37	
Hurricane	5	10	9	1	0	2.24	
Fire	11	11	3	0	0	1.68	
Wind Damage	7	11	7	0	0	2.00	
Total of Key Delay							0

TABLE V
KEY DELAYS – DESIGN RELATED

Design-Related	1	2	3	4	5	Avg. of Responses	Key Delay
Change Order	0	3	5	12	6	3.81	✓
Decision in development stage	0	5	11	6	4	3.35	✓
Changes in Drawings	0	3	6	10	6	3.76	✓
Changes in Specifications	2	4	8	8	5	3.37	✓
Shop Drawings Approval	0	5	10	4	3	3.23	✓
Incomplete Documents	0	4	8	5	7	3.63	✓
Design Development	1	4	12	7	2	3.19	✓
Total of Key Delay							7

TABLE VI
KEY DELAYS – FINANCIAL/ECONOMICAL

Financial/Economical	1	2	3	4	5	Avg. of Responses	Key Delay
Financial Process	4	10	8	2	0	2.33	
Financial Difficulties	5	10	8	1	0	2.21	
Delayed Payments	2	8	8	5	0	2.70	✓
Economic Problems	4	11	7	2	0	2.29	
Total of Key Delay							1

TABLE VII
KEY DELAYS – CONSTRUCTION RELATED

Construction Related	1	2	3	4	5	Avg.of Responses	Key Delay
Lack of Inspections	0	4	12	4	5	3.40	✓
Subsurface Soil Conditions	4	10	10	3	0	2.44	
Material/Fabrication Delays	1	7	14	3	2	2.93	✓
Material Procurement	1	13	6	5	1	2.69	✓
Lack of Qualified Craftsmen	4	8	9	3	2	2.65	✓
Poor Subcontractor Performance	2	9	8	5	2	2.85	✓
Construction Mistakes	5	9	6	2	3	2.56	✓
Total of Key Delay							6

TABLE VIII
KEY DELAYS – MANAGEMENT AND ADMINISTRATIVE

Management and Administrative	1	2	3	4	5	Avg.of Responses	Key Delay
Labor Dispute and Strike	12	4	6	1	0	1.74	
Inadequate Planning	5	9	7	3	0	2.33	
Inadequate Scheduling	4	9	7	2	0	2.32	
Contract Modifications	2	7	5	2	1	2.91	✓
Staffing Problems	4	10	7	2	0	2.30	
Lack of coordination On-site	5	9	8	1	0	2.22	
Transportation Delays	3	11	7	1	0	2.27	
Total of Key Delay							1

TABLE IX
KEY DELAYS - CODE RELATED

Code Related	1	2	3	4	5	Avg. of Responses	Key Delay
Building Permits Approval Process	1	2	6	5	9	3.83	✓
Changes in Laws and Regulations	1	7	8	4	3	3.04	✓
Safety Rules	3	8	9	0	2	2.65	✓
Florida Building Code	1	7	9	3	3	3.00	✓
Building Regulations in Coastal Regions	0	10	9	1	3	2.87	✓
Coastal Construction Control Line Permit	3	4	9	3	3	2.95	✓
Florida Administrative Code	4	6	6	4	2	2.73	✓
National Flood Insurance program	5	7	5	3	2	2.55	✓

OSHA Regulations	2	11	5	3	2	2.65	✓
Total of Key Delay							9

After analysing tables IV through IX, based on their chance of occurrence the main key delays ranked from the highest to the lowest in each category affecting the Florida Construction Industry are shown in highlighting.

Figures II through VII are briefly explained below:

Basic structure of the flow diagram as it relates to delays:



Figure I
Basic Structure Of Delay Showing Causes And Responsibilities

Acts of God:

There is no key delay in this category. The most likely to happen is a hurricane with a 44.8% (2.24 from table IV) chance of occurrence which is less than 50% to be considered as a key delay. In the event a delay occurs due to Acts of God, the responsibility is borne by the Owner and the type of delay is an excusable compensable

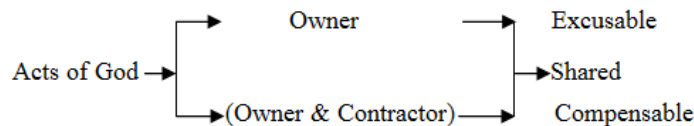


Figure II. Acts Of God

Design Related:

This is one of the most critical categories among the six because all of the causes were identified as key delays, which means that a delay is most likely to happen due to a design related problem. In fact there is a 76.2% chance (3.81 from table V) that a delay occurs due to a change order, which is very high in number. According to the survey, Design-Related Delays are considered as excusable compensable delays.

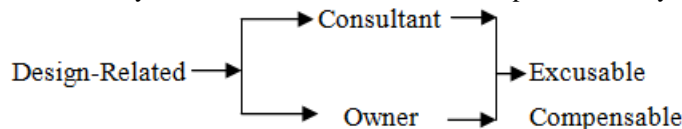


Figure III. Design Related

Construction Related:

Basically in construction stage, the contractor will always have the responsibility and the construction company will get no time or money if a delay occurs. However, if a delay occurs because of Subsurface Soil Conditions or Different Site Conditions, the responsibility would be shared between the contractor and the owner and the type of delay in this situation would be considered excusable compensable. Delays due to lack of inspections with 68% (3.40 from table VII) are the most common in this stage

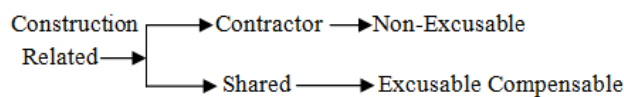


Figure IV. Construction Related

Financial/Economical:

A delayed payment (2.70) was selected as the only Key Delay. According to the results, it seems that delays rarely occur because of Financial/Economical reasons. The owner of the project will always have the responsibility, which means that the delay will be excusable compensable.



Figure V. Financial and Economical

Management/Administrative:

Similar to the above category (Financial/Economical), this also has just one key delay; Contract Modifications (2.91). However there are two parties involved (Owner and Contractor) that have to carry the responsibility depending on the cause of the delay and the type of delay is also depending on what caused the delay.

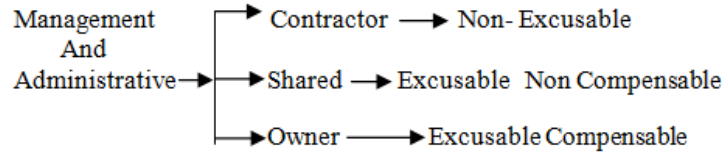


Figure VI, Management and Administrative

Code Related:

This is the category that influences the most in delays, especially on projects built on the coastal areas. Very often (77.7%), the government is responsible for it and in this case they are excusable compensable delays. However, there is a chance of 22.3% that the Contractor be responsible for it in which the delays are Non-Compensable.

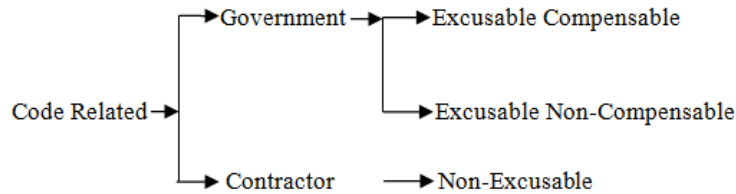


Figure VII. Code Related

IV. Conclusions For Case Study

Based on the results of the questionnaire survey and information gathered, the following conclusions were drawn.

Generally, whether a delay is determined to be excusable or non-excusable, a contractor is not entitled to an extension of time or to an upward adjustment in costs without Understanding the full context of the contract.

➤ Code-Related Delay is ranked as the most critical category followed by Design-Related Delays, Construction-Related Delays, and so on, as shown below:

1. Code-Related Delays
2. Design-Related Delays
3. Construction-Related Delays
4. Financial/Economical Delays
5. Management/Administrative Delays
6. Acts of God

➤ In general, the ten (10) most critical causes (across the six sub-headings given above) of delays are:

1. Building Permits Approval (3.83)
2. Change order (3.81)
3. Changes in Drawings (3.76)
4. Incomplete Documents (3.63)
5. Inspections (3.40)
6. Changes in Specifications (3.37)
7. Decision during Development Stage (3.35)
8. Shop Drawings Approval (3.23)
9. Design Development (3.19)
10. Changes Laws - Regulations (3.04)

➤ Based on the overall results, we can conclude that the following is the ranking of Responsibilities of the contractual from the most responsible (1) to the least (5):

1. Contractor = 44%
2. Owner = 24%

3. Government = 14%
4. Shared = 12%
5. Consultant = 6%

➤ It can be said that the most common type of delays are
Excusable Compensable at 48%,
Non-Excusable delays with 44%
Excusable Non - Compensable Delays with 8%.

In most of the cases, it is found that when the contractor has the responsibility, the type of delay respectively is Non-Excusable; when the responsibility is the owner's or the consultant's it is an Excusable Compensable Delay; and when the government is responsible, the delay is considered an Excusable Compensable. The consultants play a very important role in Design-Related Delays because as they are in charge of the design process in conjunction with the owner of the project. On the other hand, the government plays the most important role in Code-Related Delays. The contractor has the major responsibility for delays in Construction-Related Delays. Delays due to Financial/Economical Causes as well as Management/Administrative Causes share an intermediate position of importance, just presenting one Key Delay –Delayed Payments. These categories do not have the same negative impact on project Completion times as other factors considered in this study such as code, design and construction related issues.

V. Conclusion

Construction clients demand the timely completion of projects without delay or additional cost. The findings from the views of construction stakeholders is that financial related delays such as financial / cash flow difficulties faced by clients, contractors and public agencies, design changes, delays in payment to contractors, information delays, funding problems, poor project management, compensation issues and disagreement are the top significant causes of delay in construction project delivery. Cost and time overruns and interest accumulation on capital are the most frequent effects of delay in the construction industry although the effects are slightly more on time overruns than cost overruns. Arbitration/litigation and total abandonment of projects were no longer seen to be the usual effects of delays. However, it is therefore recommended that adequate construction budget, timely issuing of information, finalization of design and project management skills should be the main focus of the parties in project procurement process. Sufficient planning and the establishment of sufficient quality control mechanisms should be put in place to avoid design changes. Appropriate time should be allocated to careful production of designs and complete tender documents, so as to improve the quality of contract documents with minimum errors and discrepancies and reduce delay during the construction stages.

REFERENCES

- [1] Olusegun Emmanuel Akinsiku, Akintunde Akinsulire "Stakeholders' Perception of the Causes and Effects of Construction Delays on Project Delivery", KICEM journal of Construction Engineering and Project Management.
- [2] Semple, F.T. Hartman, G. Jergeas, "Construction claims and disputes: Causes and cost/time overruns", Journal of Construction Engineering and Management, vol. 120, no. 4, pp. 785-795, 1994.
- [3] Michael Ashworth, Planning Consultant, State of Florida, Department of community Affairs "Construction Delays in Florida: An Empirical Study"
- [4] A.H. Al-Momani, "Construction delay: a qualitative analysis", International Journal of Project Management, vol. 18, no. 1, pp. 51-59, 2000.
- [5] Y. W. Soon, M. Sambasivan, "Causes and effects of delays in Malaysian construction industry", International Journal of Project Management, vol. 25, no. 5, pp.517-526, 2007.
- [6] N.R. Mansfield, O. Ugwu, T. Doran, "Causes of delay and cost overruns in Nigerian construction projects", International Journal of Project Management, vol. 12, no. 4, pp. 254-260, 1994.

Optimal Allocation of FACTS Device with Multiple Objectives Using Genetic Algorithm

G. Sasank Das¹, B. Mohan²

¹Department of EEE, PVP Siddhartha Institute of Technology, A.P, INDIA

²Department of EEE, PVP Siddhartha Institute of Technology, A.P, INDIA

ABSTRACT: In this paper Multi objective functions are simultaneously considered as the indexes of the system performance minimize total generation fuel cost and maximize system load-ability within system security margin. To find the optimal location and optimal value for Thyristor Controlled Series Compensator (TCSC) using optimization technique Genetic Algorithm (GA) to maximize system load-ability and minimize the system losses considering multi objectives optimization approach. A GA based Optimal Power Flow (OPF) is proposed to determine the type of FACTS (Flexible AC Transmission system) controllers, its optimal location and rating of the devices in power systems. The value of TCSC and line losses is applied as measure of power system performance. The type of FACTS controllers are used and modeled for steady-state studies: TCSC, minimize total generation fuel cost and maximize system load-ability within system security margin. Simulations will be carrying on IEEE30 bus power system for type of FACTS devices.

Keywords: FACTS Device, Genetic algorithm, Optimal Power Flow (OPF), Loss minimization.

I. Introduction

Deregulated power systems suffer from congestion management problems. Also they cannot fully utilize transmission lines due to excessive power loss that it could cause. FACTS devices such as Thyristor-controlled series compensators (TCSC) can, by controlling the power flow in the network, help reducing the flows in heavily loaded lines. Also they can minimize the power loss of the systems. However, because of the considerable cost of FACTS devices, it is important to minimize their number and obtain their optimal locations in the system [1].

The TCSC is one of the series FACTS devices. It uses an extremely simple main circuit. In this FACTS device a capacitor is inserted directly in series with the transmission line to be compensated and a Thyristor-controlled inductor is connected directly in parallel with the capacitor, thus no interfacing equipment, like high voltage transformers, are required. This makes the TCSC much more economic than some other competing FACTS technologies [2].

In [3], the TCSC may have one of the two possible characteristics: capacitive or inductive, respectively to decrease or increase the overall reactance of the line XL. It is modeled with three ideal switched elements connected in parallel: a capacitor, an inductor and a simple switch to short circuit both of them when they are not needed in the circuit. The capacitor and the inductor are variable and their values are dependent on the reactance and power transfer capability of the line in series with which the device is inserted. In order to avoid resonance, only one of the three elements can be switched at a time. Moreover, in order to avoid overcompensation of the line, the maximum value of the capacitance is fixed at $-0.8 XL$. For the inductance, the maximum is $0.2 XL$. The TCSC model is presented in [3] is shown in Fig. 1.

In [4], the TCSC is a capacitive reactance compensator which consists of a series capacitor bank shunted by a thyristor-controlled reactor to provide a smooth control of the series capacitive reactance. Model of the TCSC presented in [4] is shown in Fig. 2.

Another TCSC model has been used in [5]. According to this model a variable reactance is inserted in series with the line to be compensated. This model is used in this paper and the reactance is assumed to vary in the range from $-0.3 XL$ to $-0.7 XL$.

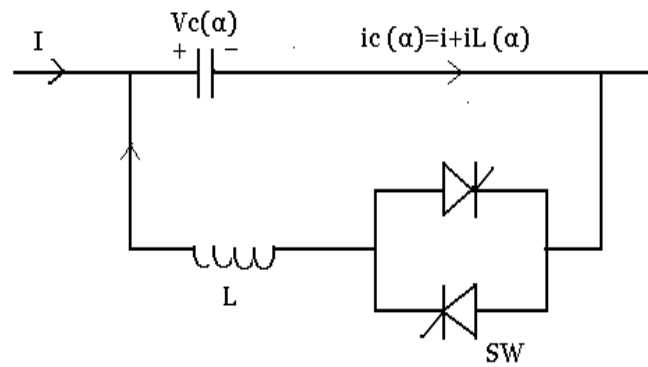


Figure.1. Thyristor controlled-series capacitor

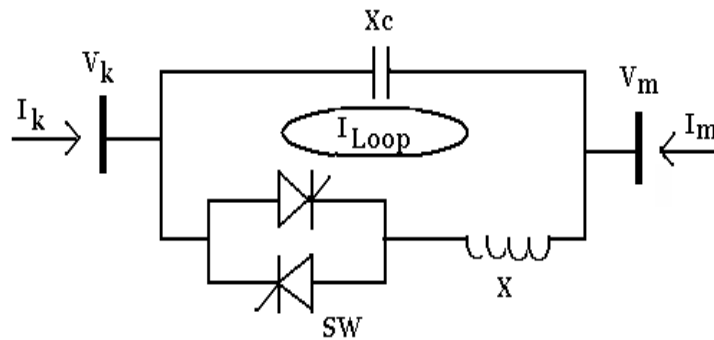


Figure.2. TCSC Model

Several research works are carried out to solve the optimal location problem of the TCSC. Optimization techniques applied in most of these works cannot be accepted as general optimization techniques as they used a fixed pre-specified number of FACTS devices. Some other works did not select the proper type or the proper working range of FACTS devices used in the optimization problem. Power system can, in general, be measured by system load-ability and/or system losses at a condition that nodal voltage magnitudes are kept within acceptable limits and thermal constraints of system elements are not violated.

According to such optimization problem can be solved by using heuristic methods such as genetic algorithms [6,7]. GA is integrated with conventional optimal power flow (OPF) [8] to select the best control parameters to minimize the total generation fuel cost and keep the power flows within the security limits. In proposed optimal choice and allocation of FACTS devices [9] in multi-machine power systems using genetic algorithm. The objective is to achieve the power system economic generation allocation and dispatch in a deregulated electricity market.

The objective is to achieve the power system economic generation allocation and dispatch in a deregulated electricity market. In implementation of the proposed real genetic algorithm has performed well when it is used to determine the location and compensation level of TCSC with the aim of maximizing the Total Transfer Capability (TTC) [10] of the system. The location of FACTS devices and the setting of their control parameters are optimized by a Bacterial Swarming Algorithm (BSA) [11] to improve the performance of the power network. Two objective functions are simultaneously considered as the indices of the system performance: maximization of system load-ability in system security margin and minimization of total generation fuel cost.

In this paper, an approach to find the optimal location of TCSC in the power system to improve the load-ability of the lines and minimize the total loss using GA is presented. The proposed approach aims to find the optimal number of devices and their optimal ratings with taking into consideration the thermal and voltage limits. Examination of the proposed approach is carried out on IEEE30-bus system.

II. The Proposed Optimization Technique

The problem is to find the optimum numbers, locations and reactance of the TCSC devices to be used in the power system. This problem is a nonlinear multi-objective one. The GA method will be used in this paper where it only uses the values of the objective function and less likely to get trapped at a local optimum.

Minimize the total losses without taking into consideration on the number of devices. That is it is required to minimize the objective function. Total system losses are equal to Sum of real losses of all system lines. Total loss and real losses are founded using MATPOWER [12].

New reactance = Old reactance + X_{TCSC} . Power flows are calculated before and after placing TCSC's.

TCSC Modeling

Thyristor controlled series compensation (TCSC) is shown in figure 3.

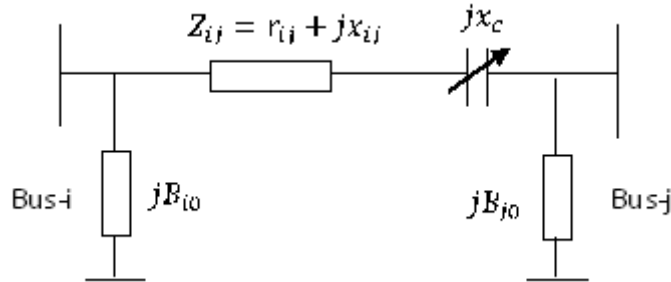


Figure.3 Thyristor controlled series compensation

Where x_{ij} is the reactance of the line , r_{ij} is the resistance of the line, B_{i0} and B_{j0} are the half-line charging susceptance of the line at bus-i and bus-j. The difference between the line susceptance before and after the addition of TCSC can be expressed as:

$$\Delta y_{ij} = y'_{ij} - y_{ij} = (g'_{ij} + jb'_{ij}) - (g_{ij} + jb_{ij}) \tag{1}$$

$$g_{ij} = \frac{r_{ij}}{\sqrt{r_{ij}^2 + x_{ij}^2}} \tag{2}$$

$$b_{ij} = -\frac{x_{ij}}{\sqrt{r_{ij}^2 + x_{ij}^2}} \tag{3}$$

$$g'_{ij} = \frac{r_{ij}}{\sqrt{r_{ij}^2 + (x_{ij} + x_c)^2}} \tag{4}$$

$$b'_{ij} = -\frac{r_{ij} + x_c}{\sqrt{r_{ij}^2 + (x_{ij} + x_c)^2}} \tag{5}$$

$$Y'_{BUS} = Y_{BUS} + \begin{bmatrix} 0 & 0 & 0 & \dots & 0 & 0 & 0 \\ 0 & \Delta y_{ij} & 0 & \dots & 0 & -\Delta y_{ij} & 0 \\ 0 & 0 & 0 & \dots & 0 & 0 & 0 \\ \dots & \dots & \dots & \dots & \dots & \dots & \dots \\ 0 & 0 & 0 & \dots & 0 & 0 & 0 \\ 0 & -\Delta y_{ij} & 0 & \dots & 0 & \Delta y_{ij} & 0 \\ 0 & 0 & 0 & \dots & 0 & 0 & 0 \end{bmatrix} \tag{6}$$

III. Problem Formulation

Problem Variables

Optimal power system operation seeks to optimize the steady state performance of a power system in terms of an objective function while satisfying several equality and inequality Constraints [7]-[9]. Generally, Optimal Power Flow is formulated an optimization problem as follows:

Minimize $J(x,u)$

Subject to

$$g(x, u) = 0 \tag{7}$$

$$h(x, u) \leq 0 \quad (8)$$

u : Vector of problem control variable

x : Vector of system state variables

$J(x, u)$: Objective function to be minimized

$g(x, u)$: Equality Constraints represents non-linear load flow equations.

$h(x, u)$: Inequality Constraints i.e. system functional operating constraints.

Where u is a vector of control variables consisting of generator voltages V_G , generator real power outputs P_G except at slack bus P_{G1} , transformer tap settings T and shunt VAR compensation Q_c .

Hence u can be expressed as:

$$u^T = [V_{G_1} \dots V_{G_{NG}}, P_{G_2} \dots P_{G_{NG}}, T_1 \dots T_{NT}, Q_{C_1} \dots Q_{C_{NC}}] \quad (9)$$

Objective Functions

J is the objective function to be minimize, which is one of the following:

Fuel cost minimization

It seeks to find the optimal active power outputs of the generation plants so as to minimize the total fuel cost.

This can be expressed as

$$J = \sum_{i=1}^{NG} f_i \left(\frac{\$}{hr} \right) \quad (10)$$

Where f_i is the fuel cost curve of the i th generator and it is assumed here to be represented by the following quadratic function:

$$f_i = a_i + b_i P_{G_i} + c_i P_{G_i}^2 \left(\frac{\$}{hr} \right) \quad (11)$$

Where a_i, b_i , and c_i are the cost coefficients of the i^{th} generator.

Active power loss minimization

The objective function J is considered as active power loss of the system.

$$J = f_c(x, y) = \sum_{i=1}^{n_{line}} Loss_i \quad (12)$$

Where n_{line} is the number of branches.

Problem Constraints

Equality constraints: The equality constraints that are the power flow equations corresponding to both real and reactive power balance equations, which can be written as:

$$P_{G_i} - P_{D_i} - P_i(V, \delta) = 0 \quad (13)$$

$$Q_{G_i} - Q_{D_i} - Q_i(V, \delta) = 0 \quad (14)$$

$$P_i = \sum V_i V_j (G_{ij} \cos \delta_{ij} + B_{ij} \sin \delta_{ij}) \quad (15)$$

$$Q_i = \sum V_i V_j (B_{ij} \cos \delta_{ij} - G_{ij} \sin \delta_{ij}) \quad (16)$$

Inequality constraints: The inequality constraints are the system operating limits. The inequality constraints that are real power outputs, reactive power outputs and generator outputs.

$$\begin{aligned} P_{G_i}^{min} &\leq P_{G_i} \leq P_{G_i}^{max} && i \in N_G \\ Q_{G_i}^{min} &\leq Q_{G_i} \leq Q_{G_i}^{max} && i \in N_G \\ |S_k| &\leq S_k^{max} && k \in N_E \\ V_i^{min} &\leq V_i \leq V_i^{max} && i \in N_B \end{aligned} \quad (17)$$

IV. Results And Discussions

The proposed approach has been tested on the standard IEEE 30 bus test system. In order to show the effectiveness of proposed method, a developed program in MATLAB environment is used.

Case Study: IEEE 30 bus system [12]:

IEEE 30 bus system is taken as a test system. That the system consists of 30 buses, 41 branches and 5 generators. The range of TCSC is taken as -30% to -70% from line reactance as in [13] and the power flow is carried out before and after allocating the TCSCs to determine their benefits. The cost coefficients of IEEE 30 bus system is as shown in below table.1.

Table.1 a,b,c constants for generators

Generator No	a	b	c
1	0	2	0.00375
2	0	1.75	0.0175
3	0	1	0.0625
4	0	3.25	0.002075
5	0	3	0.025
6	0	3	0.025

Table.2 Generator Voltages, Pg and Cost values

Unit No	Bus no	Voltage Before TCSC	Voltage After TCSC	Pgen Before TCSC	Pgen After TCSC	Cost Before TCSC	Cost After TCSC
1	1	1.050000	1.050000	176.35828	175.01343	469.34998	464.88824
2	2	1.038235	1.039999	50.342983	49.727625	132.45249	130.29798
3	5	1.045077	1.005882	20.435657	21.315960	46.536663	49.714096
4	8	1.027835	1.005882	23.680715	22.166740	81.639197	76.139884
5	11	1.008730	1.059999	10.854663	12.632362	35.509582	41.886502
6	13	1.055293	1.045294	12.047861	12.252980	39.772357	40.512329

Table.3 Fuel Cost

Before TCSC	After TCSC
804.144360 \$/hr	802.936280\$/hr
problem converged in 47 iterations	problem converged in 52 iterations

Voltage magnitudes of IEEE30-bus system without TCSC

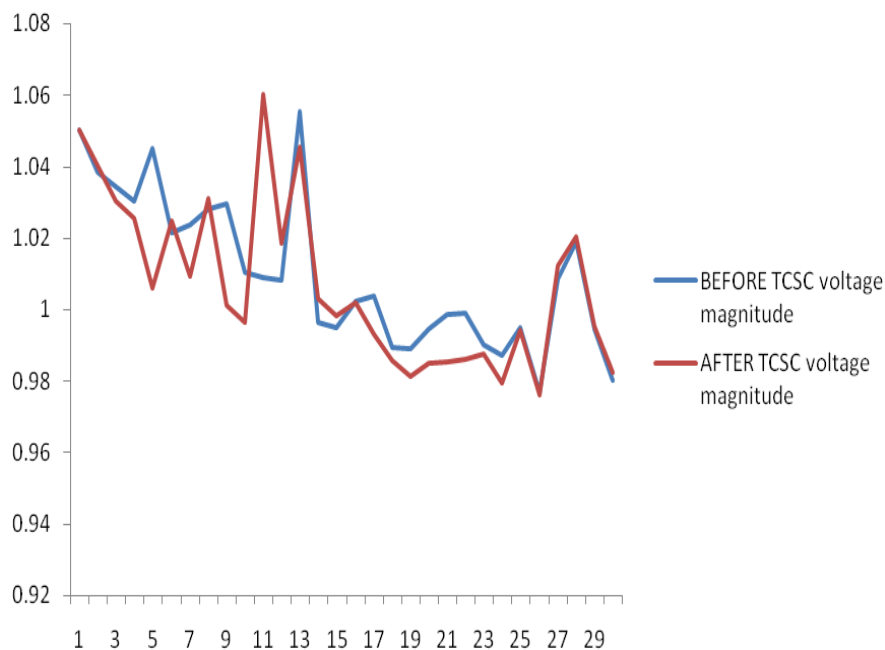


Figure 4. Voltage magnitudes before and after placement of TCSC

Active power loss and Reactive power loss of IEEE30-bus system with and without TCSC

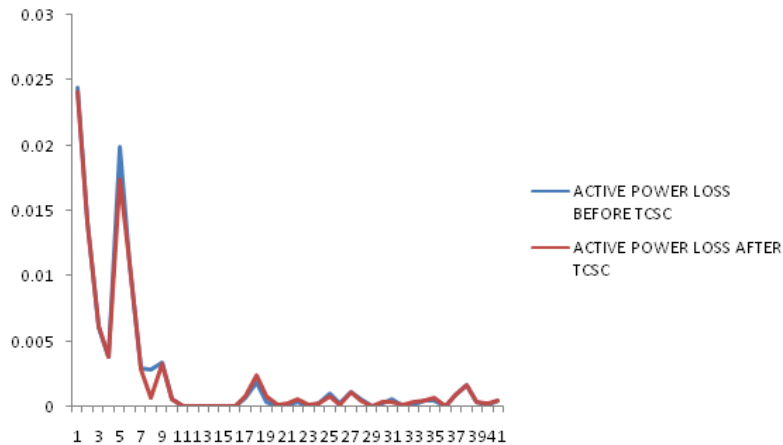


Figure 5. Active Power Loss before and after placement of TCSC

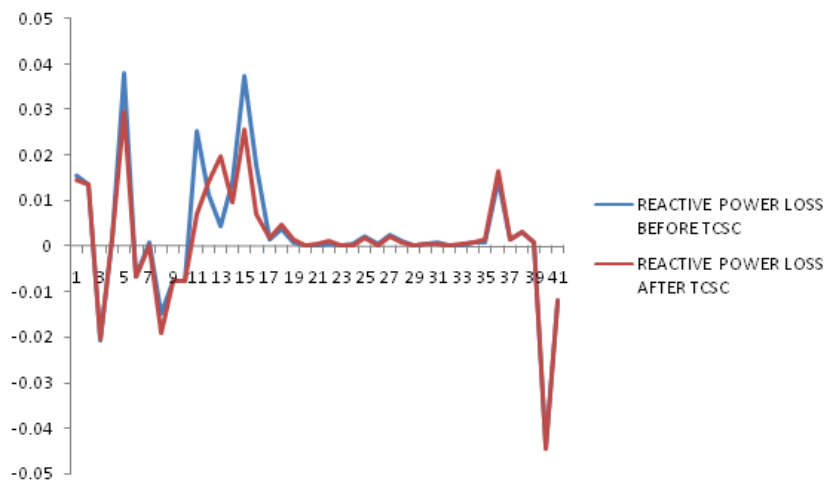


Figure 6. Reactive Power Loss before and after placement of TCSC

V. Conclusion

Optimal location of TCSC is placed in line number 20 and rating of TCSC is -0.084375(Reactance value) using GA is proposed in this paper. TCSC in a power system is improved the load-ability of its lines and minimize its total loss. The proposed technique minimizes the real power loss and reactive power loss. And also it improved the voltage profile. The fuel cost also reduced from 804.144360\$/hr to 802.936280\$/hr. The power angles of nodal voltages are increased. A MATLAB program for optimal allocation and rating of TCSC using GA results are presented.

REFERENCES

- [1] A. Y. Abdelaziz, M. A. El-Sharkawy, M. A. Attia "Optimal Allocation of TCSC Devices Using Genetic Algorithms" Proceedings of the 14th International Middle East Power Systems Conference, Cairo University, Egypt, December 19-21, 2010.
- [2] S. Meikandasivam, Rajesh Kumar Nema and Shailendra Kumar Jain, "Behavioral Study of TCSC Device - A Matlab/Simulink Implementation," World Academy of Science, Engineering and Technology, Vol. 45, 2008, pp. 694-699.
- [3] Stéphane Gerbex, Rachid Cherkaoui, and Alain J. Germond, "Optimal Location of Multi-Type FACTS Devices in a Power System by Means of Genetic Algorithms," IEEE Transactions on Power Systems, Vol. 16, No. 3, August 2001, pp. 537-544.
- [4] R. Narmatha Banu and D. Devaraj, "Genetic Algorithm Approach for Optimal Power Flow with FACTS Devices," 4th International IEEE Conference Intelligent Systems, Varna, September 2008.

- [5] M. Saravanan, S. M. R Slochanal, P. Venkatesh and J. P. S. Abraham, "Application of Particle Swarm Optimization Technique for Optimal Location of FACTS Devices Considering Cost of Installation and System Loadability", *Electric Power Systems Research*, Vol. 77, No. 3/4, 2007 , pp. 276-283.
- [6] S. M. Sait and H. Youssef, "Iterative Computer Algorithms with Application in Engineering: Solving Combinatorial Optimization Problems," IEEE Computer Society Press, 1999.
- [7] D. E. Goldberg, "Genetic Algorithms in Search Optimization and Machine Learning", Addison-Wesley Publishing Company, 1989.
- [8] T. S. Chung and Y. Z. Li, "A Hybrid GA Approach for OPF with Consideration of FACTS Devices," *IEEE Power Engineering Review*, August 2000, Vol. 20, Issue 8, pp. 54-57.
- [9] L. J. Cai, I. Erlich and G. Stamsis, "Optimal Choice and Allocation of FACTS Devices in Deregulated Electricity Market Using Genetic Algorithms," in *Proceeding of the IEEE Power Systems Conference and Exposition*, October 2004, Vol. 1, pp. 201-207.
- [10] W. Feng and G. B. Shrestha, "Allocation of TCSC Devices to Optimize Total Transmission Capacity in a Competitive Power Market," *Proceedings of the IEEE Power Engineering Society Winter Meeting*, Columbus, OH, Vol. 2, 2001, pp. 587-593.
- [11] Z. Lu., M. S. Li, L. Jiang and Q. H. Wu, "Optimal Allocation of FACTS Devices with Multiple Objectives Achieved by Bacterial Swarming Algorithm," *IEEE Power and Energy Society 2008 General Meeting: Conversion and Delivery of Electrical Energy in the 21st Century*, Pittsburg, PA, July 2008, pp. 1-7.
- [12] Ray D. Zimmerman and E. Carlos Murillo-Sanchez, "Matpower A Matlab™ Power System Simulation Package Version 3.2", User's Manual, September 21, 2007. <http://www.Pserc.Cornell.Edu/Matpower/>
- [13] G. Y. Yang, G. Hovland, R. Majumder and Z. Y. Dong, "TCSC Allocation based on Line Flow Based Equations Via Mixed-Integer Programming," *IEEE Transactions on Power Systems*, Vol. 22, No. 4, November 2007, pp. 2262-2269.
- [14] W. Shao and V. Vittal, "LP-based OPF for corrective FACTS control to relieve overloads and voltage violations," *IEEE Transactions on Power Systems*, vol. 21, no. 4, pp. 1832–1839, Dec., 2006.
- [15] S. Gerbex, R. Cherkaoui, and A. J. Germond, "Optimal location of multi type facts devices in a power system by means of genetic algorithms," *IEEE Transactions on Power Systems*, vol. 16, no. 3, pp. 537–544, Aug., 2001.
- [16] N.G.Hingorani and L.Gyugyi, "Understanding FACTS", the Institution of Electric and Electronics Engineers, 1998.

BIOGRAPHIES



G. Sasank Das received the B. Tech degree in Electrical and Electronics Engineering from DMS SVH College of Engineering Machilipatnam in the year 2010. At present Pursuing M. Tech (Power Systems Control and Automation) in PVP Siddhartha Institute of Technology, A.P, INDIA.



B. Mohan received the B. Tech degree in Electrical and Electronics Engineering from JNTU Hyderabad in the year 2009 and M. Tech in Power Systems Engineering from NIT Warangal in the year 2011. From July 2011-May 2012 he worked as an Assistant Professor at S.V.C.E.T, Hyderabad, India and since May 2012 he is working as an Assistant Professor at P.V.P.S.I.T, Vijayawada, India. His research interests include Power Systems, Power Systems Deregulation, HVDC, FACTS and Power Electronics and Drives.

Analysis of Coiled-Tube Heat Exchangers to Improve Heat Transfer Rate With Spirally Corrugated Wall

Prof. Pravin R. Ingole¹, Prof. Swapnil L. Kolhe²

¹(Department Of Mechanical Engg., D.M.I.E.T.R, Wardha, India)

²(Department Of Mechanical Engg., D.M.I.E.T.R, Wardha, India)

ABSTRACT: Steady heat transfer enhancement has been studied in helically coiled-tube heat exchangers. The outer side of the wall of the heat exchanger contains a helical corrugation which makes a helical rib on the inner side of the tube wall to induce additional swirling motion of fluid particles. Numerical calculations have been carried out to examine different geometrical parameters and the impact of flow and thermal boundary conditions for the heat transfer rate in laminar and transitional flow regimes. Calculated results have been compared to existing empirical formula and experimental tests to investigate the validity of the numerical results in case of common helical tube heat exchanger and additionally results of the numerical computation of corrugated straight tubes for laminar and transition flow have been validated with experimental tests available in the literature. Comparison of the flow and temperature fields in case of common helical tube and the coil with spirally corrugated wall configuration are discussed. Heat exchanger coils with helically corrugated wall configuration show 80–100% increase for the inner side heat transfer rate due to the additionally developed swirling motion while the relative pressure drop is 10–600% larger compared to the common helically coiled heat exchangers. New empirical Co-relation has been proposed for the fully developed inner side heat transfer prediction in case of helically corrugated wall configuration.

Keywords: Heat exchanger, swirling motion, corrugated, regimes, boundary condition

I. Introduction

Helically coiled-tube heat exchangers are one of the most common equipment found in many industrial applications ranging from solar energy applications, nuclear power production, chemical and food industries, environmental engineering, and many other engineering applications. Heat transfer rate of helically coiled heat exchangers is significantly larger because of the secondary flow pattern in planes normal to the main flow than in straight pipes. Modification of flow is due to the centrifugal forces (Dean roll cells) caused by the curvature of the tube. Several studies have been conducted to analyze the heat transfer rate of coiled heat exchangers in laminar and turbulent flow regimes. Numerical study of laminar flow and forced convective heat transfer in a helical square duct has been carried out by Jonas Bolinder and Sunden. Many authors investigated experimentally the turbulent heat transfer in helical pipes. Further enhancement of heat transfer rate in coiled pipes has great importance in several industrial applications mainly where the flow regime is in the laminar or transitional zone like hot water solar energy applications. There are basically two different concepts to increase the rate of heat transferred, the first one is the active and the other one is the passive method. Many different active techniques exist to increase the heat transfer rate mostly for straight pipes. In case of passive techniques heat transfer enhancement by chaotic mixing in helical pipes has great importance and investigated by Kumar and Nigam and Acharya et al. Helical screw-tape inserts have been investigated in straight pipes experimental by Sivashanmugam and Suresh. There is considerable amount of work reported in the literature on heat transfer augmentation in straight pipes with different corrugation techniques; helical tape Experimental investigation of thermosyphon solar water heater with twisted tape inserts has been carried out by Jaisankaretal. According to the author's knowledge a few examinations are considered in helically coiled tubes with different passive heat transfer augmentation techniques like inside wall corrugation, helical tape inserts and this question is not studied numerically at all in the available literature. Experimental investigations have been conducted in a helical pipe tube possibly increases the heat transfer rate because of the developed swirling motion. Basic aim of this study is to investigate the impact of different geometrical parameters of the corrugation for the inner side heat transfer rate in case of helical tube.

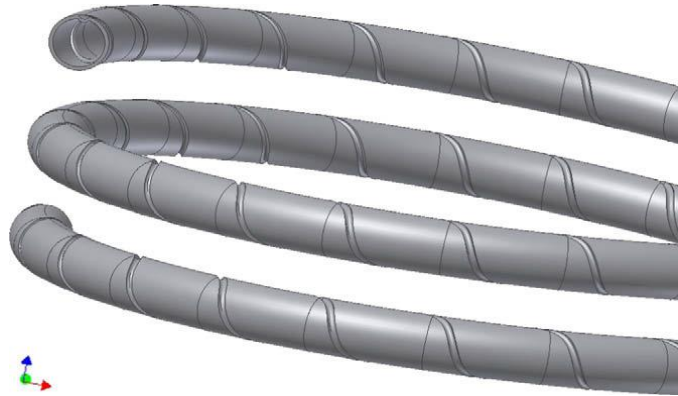


Fig1. Schematic figure of the corrugated coiled-tube heat exchangers with the following geometrical parameters $d_p = 20$ mm, $p_c = 40$ mm, $p = 44.5$ mm and $h = 2$ mm

II. Mathematical Formulation

This section provides the basic equations that must be solved to describe the velocity field and the temperature distribution inside the heat exchanger coils. It is well known that, the transition from laminar to turbulent flow in curved pipes occur much higher critical Reynolds number(Re) than in straight pipes. The critical Reynolds number for smooth helical pipes can be estimated by the following formula found in. $Re_{crit} = 2100(1 + 12\sqrt{\delta})$.

2.1. Conservation equations

The following set of partial differential equations for U_1, U_2, U_3, P and T as functions of x, y, z describes the flow and temperature field inside a helically coiled heat exchanger. The conservation equations are formulated in the Cartesian coordinate system because the applied flow using the Cartesian system to formulate the conservation equations for all quantities. Description of the entire geometry of the studied problem is incorporated into the generated unstructured numerical grid.

2.1.1. Continuity equation

The continuity equation is formulated in the following manner in Cartesian coordinate system $\frac{\partial}{\partial x} (\rho U_i) = 0$.

2.1.2. Momentum equations

The following equation system is the representation of the momentum equations in Cartesian coordinate system where $I, j \in \{1, 2, 3\}$,

$$\frac{\partial}{\partial x} \rho U_j U_i = -\frac{\partial p}{\partial x_i} + \frac{\partial p}{\partial x_i} \left(n \left(\frac{\partial U_i}{\partial X_i} \right) \right)$$

μ is the dynamic viscosity and ρ is the density of the working fluid.

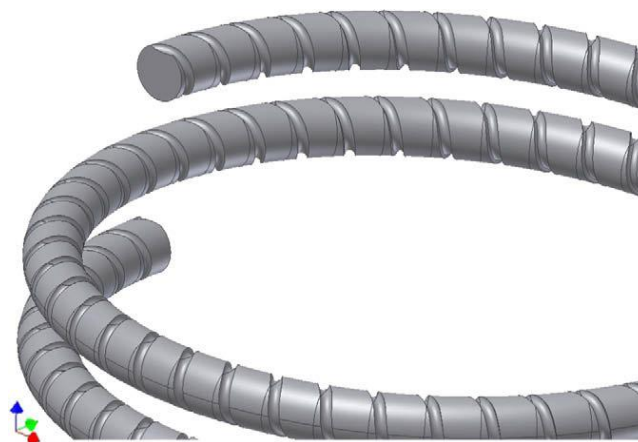


Fig 2. Computational domain with parameters $d_p = 25$ mm, $p_c = 40$ mm, $p = 22.25$ mm and $h = 2.5$ mm.

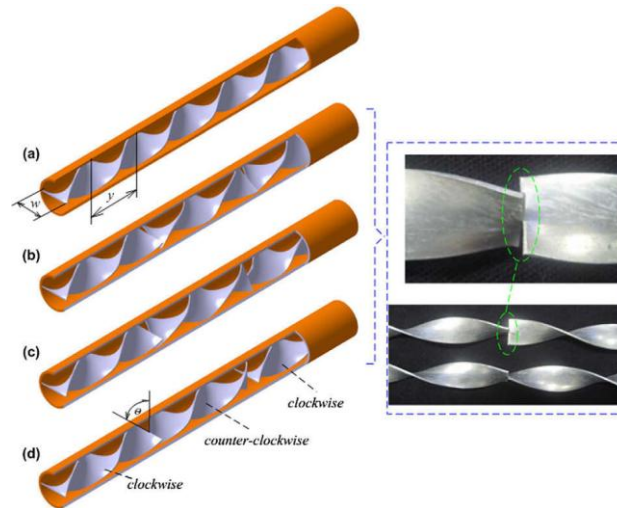


Fig2 (a): horizontal pipes with different tapes

2.1.3. Heat transport equation

The following form of the energy equation is solved to calculate the temperature field

$$\frac{\partial p}{\partial x_i} (p c_p U_i T) = \frac{\partial}{\partial x_i} \left(\lambda \left(\frac{\partial T}{\partial x_i} \right) \right)$$

Where are the thermal conductivity function and the function of the working fluid at constant?

Fig. 3a shows the generated grid near the outlet region of the corrugated pipe. Fig. 3b presents an enlarged view of the generated grid at the bottom zone of the outlet Diag.

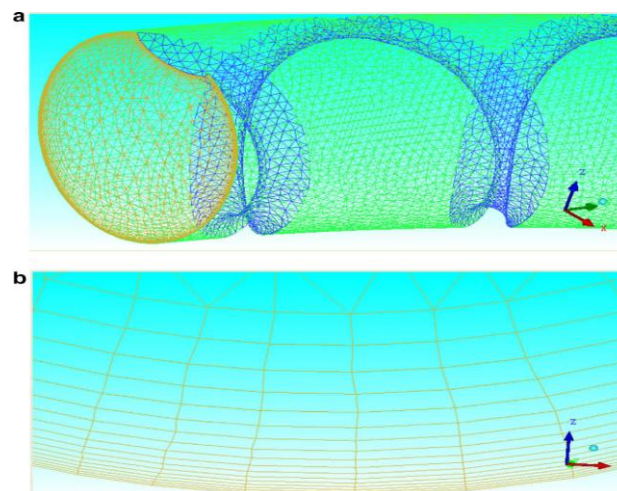


Fig3. One of the applied grids for the calculations and an enlarged view at the bottom of the outlet side of the corrugated coil.

2.5. Calculation of the dimensionless quantities

Representing calculated results the following dimensional and nondimensional quantities have been used. In case of Re number calculations the value of the density and dynamic viscosity of the working fluids have been calculated by averaging for the entire fluid volume. The thermal conductivity of the fluid K (avgas) has been calculated at a specific cross section. It is important to note that the modification of the thermal conductivity between the tube inlet and outlet is not more than 1–2% because of the variation of the fluid temperature.

$$Re = \frac{d_p \rho \bar{v}}{\eta}, \quad Nu = \frac{d_p q_w}{k_{avg}(T_w - T_m)},$$

$$q_w = \frac{1}{A_{wall\ section}} \int \int_A q dA_{wall\ section},$$

$$T_w = \frac{1}{A_{wall\ section}} \int \int T dA_{wall\ section},$$

$$T_m = \frac{1}{\bar{v} A_{wall\ section}} \int \int \bar{v} T dA_{cross\ section}.$$

III. Model Validation

Two completely different problems have been tested based on measurements available in the literature. All of the necessary ingredients of the calculations are investigated to extend the validity of the numerical results to the corrugated helical tubes.

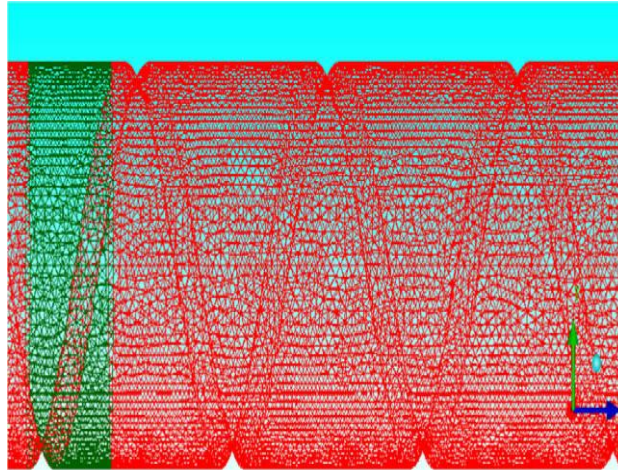


Fig4a. An unstructured grid of a corrugated straight tube with pitch of corrugation $p = 15.95$ mm and corrugation depth $h = 1.03$

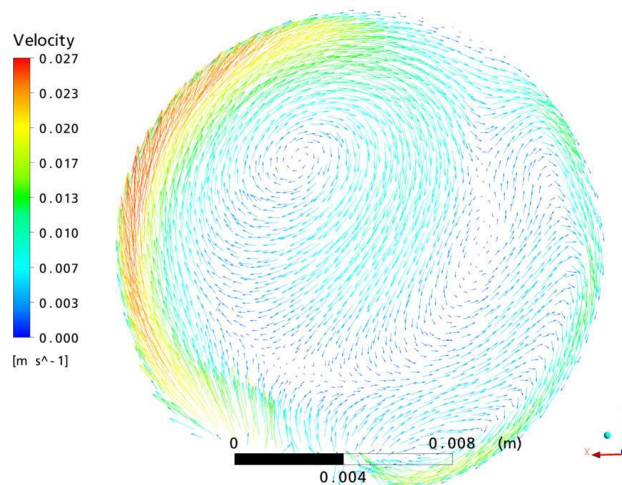


Fig.4 (b): Secondary flow field inside a corrugated straight tube with corrugation parameters ($p = 15.95$ mm, $h = 1.03$ mm).

IV. Result

Several geometrical parameters of the studied heat exchanger configuration have been investigated numerically. Length of the coil has been specified according to the assumption that the velocity and temperature field is fully developed near the end of the first turn. For this reason 2 turns configuration of the corrugated helical coil has been investigated because it should be enough to test the development of the peripherally averaged Nusselt number of $d_{ip} = 20$ mm the depths are $h = \{1, 1.5, 2\}$ mm and in case of $d_{ip} = 25$ mm the corrugation depths are $h = \{1.25, 1.875, 2.5\}$ mm.

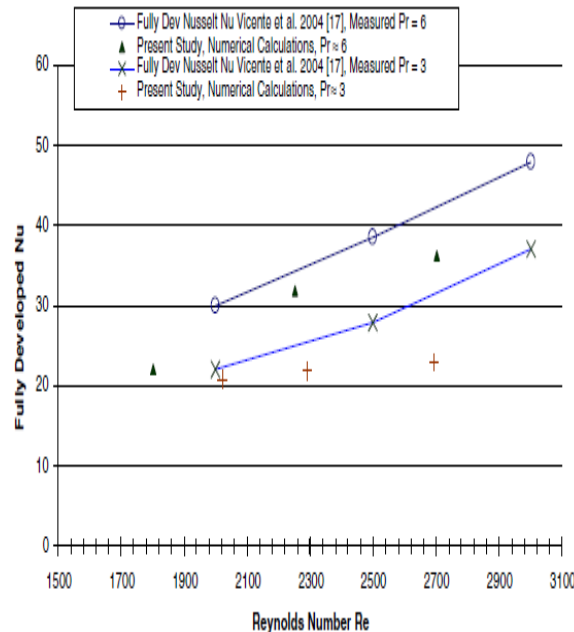


Fig (5): Comparison of the numerical results of a corrugated straight pipe ($p = 15.95$ mm, $h = 1.03$ mm) with eased in the numerical calculations

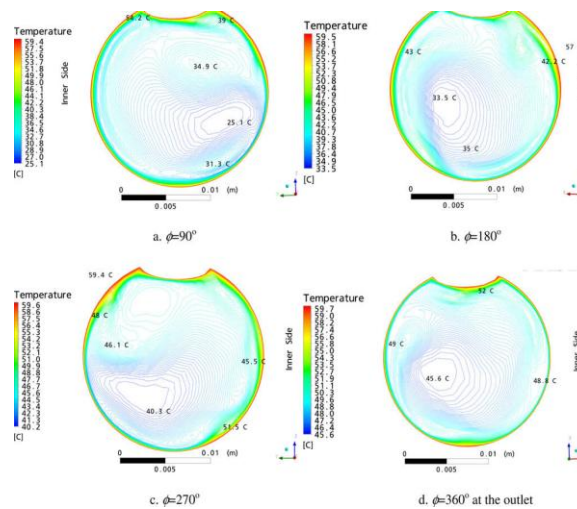


Fig5 (b): Temperature isotherms at different location of a corrugated coiled heat exchanger configuration for $De = 1120$.

In some cases higher and lower surface temperatures are examined but it was found that the different surface temperatures does not significantly modify the heat transfer rate of the studied heat exchangers. The presented results are valid in laminar and transitional flow regime in the Dean number range $30 < De < 1400$ and Prandtl number range $3 < Pr < 30$. Fig. presents temperature isotherms at different axial location of a corrugated helically coiled heat exchanger. comparison of the isotherms presented in Fig. With the isotherms of a smooth tube coiled heat exchanger indicates the substantial difference between the two temperature fields. It can be concluded that the temperature field of the corrugated case is far more homogeneous than the smooth tube case helical coil case. This process further increase the cross sectional mixing of the temperature field.

$$Nu = 0.5855 De^{0.6688} Pr^{0.408} \left(\frac{h}{d}\right)^{0.166} \left(\frac{p}{d}\right)^{-0.192}$$

The formula was obtained via curve-fitting of heat transfer results for the corrugated helical coils. The presented formula is applicable in the following Dean and Prandtl number ranges $30 < De < 1400$,

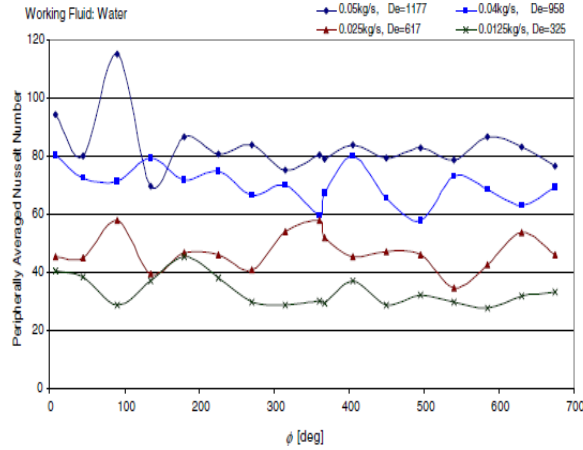


Fig6 (a): Development of the peripherally averaged Nusselt number along the axial direction in case of geometrical parameters $dp = 25$ mm, $p = 22.25$ mm, $h = 2.5$ mm and $Pr \cong 5$.

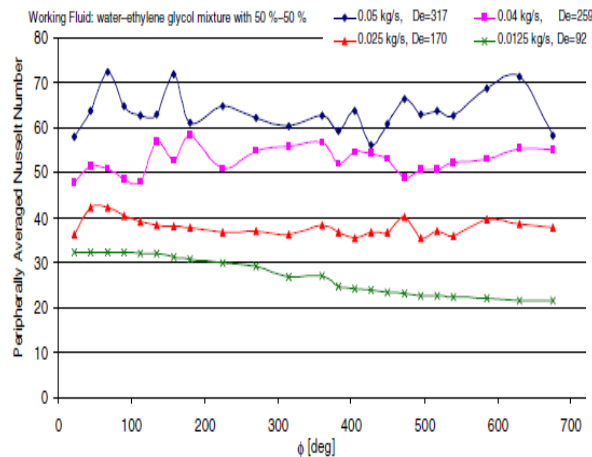


Fig6(b): Development of the peripherally averaged Nusselt number along the axial direction in case of geometrical parameters $dp = 20$ mm, $p = 22.25$ mm, $h = 2$ mm and $Pr \cong 15$.

A. Zachár/International Journal of Heat and Mass Transfer xxx (2010) xxx-xxx

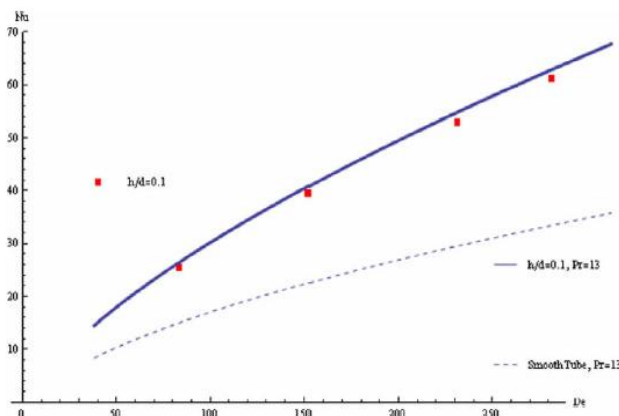


Fig. 14. Nusselt number versus Dean number in case of water-ethylene glycol mixture.

V. Conclusion

Different geometrical parameters of helical corrugation on the outer surface of helically coiled-tube heat exchangers are examined to improve the inside heat transfer rate. Several different in flow rates and temperatures have been studied to test the impact of flow parameters for the efficiency of the heat exchanger. It can be concluded that the heat transfer rate is almost independent from the inlet temperature and the outer surface temperature. As it was expected the volumetric flow rate significantly influences the performance of coiled-tube heat exchangers with and without outer helical corrugation. An empirical formula has been suggested to indicate the dependency of the Nusselt number from the Dean and Prandtl numbers... The presented results show that the ratio of the helical pitch and tube diameter (p/d) and the ratio of the corrugation depth and the tube diameter (h/d) nearly increase or decrease in the same way the heat transfer rate of the studied heat exchangers. The results also show that a spirally corrugated helical tube with corrugation parameters ($p/d = 1$, $h/d = 0.1$) can increase the heat transfer rate nearly 100% larger than a smooth helical pipe in the Dean number range $30 < De < 1400$.

REFERENCES

- [1] W.R.Dean, Notes on the motion of fluid in a curved pipe, *Philos. Mag.* 4 (1927) 208–223.
- [2] B. Zheng, C.X. Lin, M.A. Ebdian, Combined laminar forced convection and thermal radiation in helical pipe, *Int. J. Heat Mass Transfer* 43 (2000) 1067–1078.
- [3] C.X. Lin, M.A. Ebdian, Developing turbulent convective heat transfer in helical pipes, *Int. J. Heat Mass Transfer* 40 (1997) 3861–3873.
- [4] J.J.M. Sillekens, C.C.M. Rindt, A.A. Van Steenhoven, Developing mixed convection heat in coiled heat exchanger, *Int. J. Heat Mass Transfer* 41 (1998) 61–72.
- [5] C.E. Kalb, J.D. Seader, Heat and mass transfer phenomena for viscous flow in curved circular tubes, *Int. J. Heat Mass Transfer*.

An Energy Audit of Hindustan Machine Tools, Pinjore - A Case Study

Jyoti Saraswat

Asst. Professor, department of Electrical Engineering Baddi University

Abstract: The scope for electrical energy conservation is gigantic and if properly harnessed can take the organization to the path of opulence. Energy Audit becomes all the more important in the view of the energy conservation Act 2001 enacted by govt. of India. This paper contains the findings and analysis of the results obtained from energy audit program employed in an industrial unit "Hindustan Machine Tools". Electrical audit was carried out under two major heads, i) Motor load based energy audit, ii) Harmonic analysis at PCC. Readings were taken under these heads, analyzed to find the scope of electrical energy conservation opportunities in the selected test case industrial unit.

Keywords: Energy audit, point of common coupling, power harmonic analyzer, energy conservation.

I. Introduction

An energy audit identifies where energy is consumed and how much energy is consumed in an existing facility, building or structure. Information gathered from the energy audit can be used to introduce energy conservation measures (ECM). An energy audit, therefore, is a detailed examination of a facility's energy uses and costs that generates recommendations to reduce those uses and costs by implementing equipment and operational changes [1]. The energy audit is an organized approach through which the energy wastage can be easily identified also determine how this waste can be eliminated at a reasonable cost and within a suitable time frame.

In developing countries like India, where electrical energy resources are scarce and production of electricity is very costly, energy conservation studies are given great importance. The primary objective of energy audit is to determine ways to reduce energy consumption per unit of product output or to lower operating costs. Energy audit gives a positive orientation to the energy cost reduction, preventive maintenance and quality control programs which are vital for production and utility activities [2]. Under the energy audit program the first head is the Electrical Motor Energy Audit, which is performed during the Facility Assessment process which involves a visit to the plant in order to identify eligible motors for the Energy Conservation process.

Second head under which the energy audit program was performed is harmonics analysis. Harmonics reflect the distortion of the wave form and deteriorate the quality of the power this leads to increased transformer heating and transmission losses. Harmonics can be defined as periodic, steady-state distortion of voltage or may be current waveform in a power system. These distortions are produced by devices which exhibit non-linear relationship between current and voltage.

II. Electrical Motor Energy Audit

Normally, motors are operated more efficiently at 75% of rated capacity as compared to the motors operated lower than 65% of rated capacity, because they were chosen in big capacity, performing inefficiently, and due to reactive current increase, power factors are also decreased. These kinds of motors do not consume the energy efficiently because they have been chosen in big power, not according to the need.

Three phase, 4 pole, 1470 rpm induction motors of Kirloskar make are being used for various production processes in the plant. During the energy audit the focus area were the Light Machine shop and the Foundry. Motors having rated capacity above 5 HP were analyzed and assessed. Table 1 represents the motors which were under analysis during motor load based energy audit, table consists of the rated capacity of each motor, the rated voltage, rated power factor (PF), rated capacity i.e true power (KW), rated speed in rpm and the manufacturer of the respective motor.

Table 1: Motor load analysis

	<i>Identity of motor</i>	<i>Rated Power</i>	<i>Rated efficiency</i>	<i>Voltage</i>	<i>Current</i>	<i>PF</i>	<i>Output Power (kW)</i>	<i>Motor loading %</i>
1	FAY	45 (60)	92	396	55	.64	24	53
2	Riveting	30 (40)	92	398	45	.82	27	90
3	STC-02	30 (40)	92	398	28	.76	15	50
4	RTV	22 (30)	91	397	31	.71	16	72
5	FN2	18.5 (25)	90.5	398	23	.81	13	70
6	M900	12.5 (18)	88.4	396	15	.78	8	64
7	S-Pilot	11 (15)	88.4	398	15	.86	9	81
8	L200	7.5 (10)	87	398	14	.84	5.63	75

During the survey and measurement process it has been observed that some of the motors are under-loaded.

- Two 60 HP (45 kW) motors has been running at 53% of the rated capacity.
- Two 40HP (30 kW) motors has been running at 50% of the rated capacity.
- One 18HP (12.5 kW) motor running at 65% of the rated capacity.

There are some problems with under loaded motors, under- loading increases motor losses and reduces motor efficiency and the power factor. Under- loading is the most common cause of inefficiency of motor performance due to following reasons:

- Equipment manufacturers tend to use a large safety factor when selecting the motor.
- Equipment is often under-utilized. For example, machine tool equipment
- Manufactures provide for a motor rated for the full capacity, resulting in under- loaded operation most of the time.
- d)

1.1 Energy Efficient Motors

High efficiency electric motors have been designed especially to increase operating efficiency compared to standard electric motors. Efficiencies are 5% to 9% higher compared with standard motors. Figure1 describes the improvement opportunities that are often used in the design of energy efficient motors.

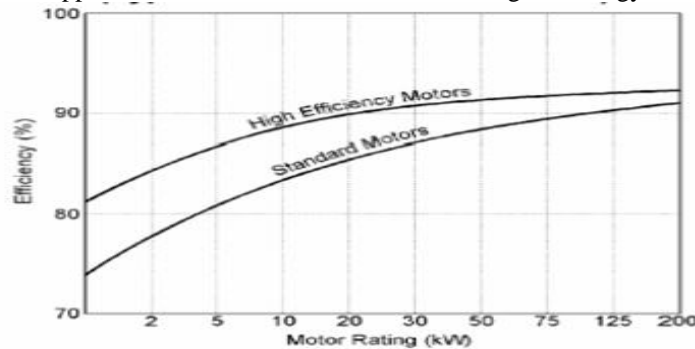


Fig 1: comparison between high efficiency and standard motor [6].

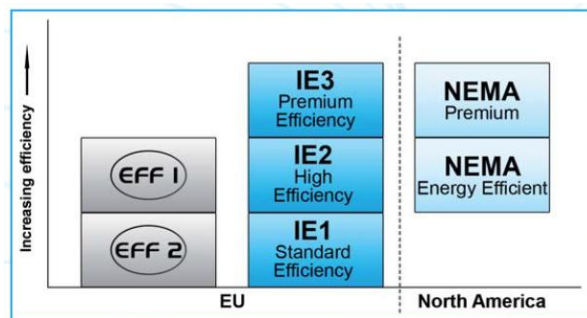


Fig 2 the new energy efficiency classes [4]

1.2 Energy Efficient Motors performance

Energy-efficient motors now available in India operate with efficiencies that are typically 5 to 7% points higher than standard motors. In keeping with the demand of the BIS, energy-efficient motors are designed to operate without loss in efficiency at loads between 75% and 100% of rated capacity. Energy-efficient motors have lower operating temperatures and noise levels, greater ability to accelerate higher-inertia loads, and are less affected by supply voltage fluctuation.

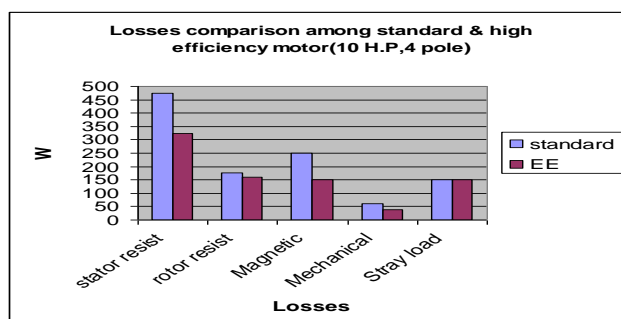


Fig 3 Losses comparison among standard & high efficiency motors [7]

1.3 Payback Period

Table 2: Payback period

No. of hrs of usage/yr	Std (45 kW) loss kWh/yr	Std (30 kW) loss kWh/yr	EE (30 kW) loss kWh/yr	Cost @ 5.77 std (45 kW)	Cost @ 5.77 std (30 kW)	Cost @ 5.77 EE (30 kW)	Savings for 30 kW std	Savings for 30 kW EE	Payback period (years)	Payback period (years)
16 hr/day	45,360	15840	11,520	2,61,727	91,397	66,470	1,70,330	1,95,257	0.5	0.4
12 hrs/day	34,020	11,880	8640	1,96,295	68,548	49,853	1,27,747	1,46,442	0.7	0.6
10 hrs/day	28,350	9,900	7200	1,63,580	57,123	41,544	1,06,457	1,22,036	0.8	0.7
8 hrs/day	22,680	7920	5760	1,30,863	45,698	33,235	85165	97,628	1.04	0.9

III. Harmonic Analysis

The usage of non-linear electric load and automation in industries is being increased as compared to the early days, with this increase poor power quality due to harmonics has come up as a serious issue.

To tackle the problem of increasing harmonic distortion in power distribution network government has issued guidelines for various large scale and medium scale industrial units of the state to get current and voltage harmonic content evaluated at their premises at the point of common coupling (PCC), and if the current and voltage harmonic content are not within the limits as stipulated by IEEE-519-1992 Standard then it is under guidelines to undertake remedial filtering solutions.

The goal of harmonic studies is to quantify the distortion in current and voltage waveforms in the power system of industrial units. The results of the harmonic analysis are useful for evaluating corrective measures and troubleshooting harmonic related problems.

2.1 Effects of harmonics on the network [5]

- Overloading of neutral conductor
- Reduced efficiency of motors.
- Poor power factor of the total system due to introduction of distortion factor.
- Overloading of power factor capacitors
- Malfunctioning of control equipment

2.2 Harmonic Measurements at the industry under Energy Audit

The harmonic spectrum of LT currents in three phase distribution system of plant recorded with the help of Power and Harmonic Analyzer is indicated in table 3.

2.3 Verification of IEEE Limit Compliance.

From the data provided by the electrical division of the plant, per unit impedance of transformer is 0.103. The maximum demand current (I_L) is 980 amperes. The short circuit current (I_{SC}) calculated at Point of Common Coupling (PCC) is 4273.64 amperes and Short-Circuit ratio is 4.4 amperes [Table 3]. The industrial consumer under study falls in the category of short-circuit ratio lying in range <20 for which the maximum allowable THD value is 4% (up to 11th harmonics).

It is seen that THD value at PCC of HMT,Ltd is within limit. Further calculations of TDD at PCC are also within limit as per IEEE-519-1992 Std.

Table3: Values of LT currents as shown by Harmonic Analyzer

$\frac{I_{sc}}{I_L}$	<11	11 ≤ h < 17	17 ≤ h < 23	23 ≤ h < 35	35 ≥ h	TDD
<20	4.0	2.0	1.5	0.6	0.3	5.0
20-50	7.0	3.5	2.5	1.0	0.5	8.0
50-100	10.0	4.5	4.0	1.5	0.7	12.0
100-1000	12.0	5.5	5.0	2.0	1.0	15.0
>1000	15.0	7.0	6.0	2.5	1.4	20.0

Table 4 Current Distortion Limit of IEEE-519-1992 Standard [8]

Currents	RMS Current (A)	Total Harmonic Distortion (THD)	Total Demand Distortion (TDD)
I_1	750 A	4%	3%
I_2	486 A	4.5%	2.2%
I_3	469 A	4.6%	2.29%

References

- [1] Guide Books for the National Certificate Examination for Energy Managers and Energy Auditors, Book I General Aspect of Energy Management and Energy Auditing Book, Book II Energy Efficiency in Electrical Utilities, <http://www.energymanagertraining.com>
- [2] Detailed information and case studies on energy audits, Monitoring equipment & Energy Audit Report of MLA. Hostel (Nagpur). <http://www.energymanagertraining.com>
- [3] Guide for electrical energy conservation, "Proprietary Method for Energy Conservation in Electric Induction Motors".
- [4] New standards and legal requirements, "Information about IE2, IE3 and NEMA motor changeover".
- [5] "IEEE recommended practice for electric power systems in commercial buildings", Recognized as an American National Standard (ANSI) IEEE Standard, pp.241, 1990
- [6] Energy Efficiency Guide for Industry in Asia – www.energyefficiencyasia.org
- [7] Cassio T. C. Andrade, Ricardo S. T, "THREE-PHASE INDUCTION MOTORS ENERGY EFFICIENCY STANDARDS -A CASE STUDY". Pontes Electrical Engineer Department Ceará Federal University.
- [8] "IEEE STANDARD IEEE-519-1992".
- [9] RC Dugan, "Electrical Power Systems Quality", 2nd edition, Tata McGraw-Hill, 2004.
- [10] AtifZaman Khan." Electrical Energy Conservation andits Application to a Sheet Glass Industry" Member IEEE Department of Electrical Engineering King Fahd University of Petroleum & Minerals Dhahran, Saudi Arabia *IEEE Transactions on Energy Conversion*, Vol. 11, No. 3, September 1996
- [11] Putri Zalila Yaacoh and Dr. Abdullah Asuhainu Mohd. Zin "Electrical Energy Management in Small and Medium Size Industries", Faculty of Electrical Engineering University Tekmlogi, Malaysia Jalan Semarak 54100 Kuala Lumpur, IEEE TENCON 1993/Beijing.
- [12] R.Saidur, A review on electrical motors energy use and energy savings. "Renewable and sustainable energy reviews", university of Malaysia, 50603 Kuala Lumpur, Malaysia. www.elsevier.com
- [13] H. K. Wong, C.K. Lee , "Applications of Energy Audit in Buildings and A CASE STUDY", Electrical and Mechanical Services Department, HONG KONGIEEE 2nd InternationalConference on Advances in Power System Control, Operation and Management, December 1993, Hong Kong.
- [14] D.P.Kothari, I.J Nagrath, "Modern Power System Analysis", Tata McGraw-Hill, 2002.

Using of Dynamic Voltage Restorer (DVR) to Mitigate Sag & Swell Voltage during Single Line to Ground & Three-Phase Faults

¹Rasool M. Imran, ²Jyoti Srivastava

^{1,2}Department of Electrical & Electronics Engineering, Sam Higginbottom Institute of Agriculture, Technology & Sciences, Allahabad-India

ABSTRACT: The power quality (PQ) requirement is one of the most important issues for power system. The main problems of the power quality like voltage sags/swells in low voltage distribution systems and on the transmission side due to sensitive loads. There are different methods to compensation of voltage sag and swell, one of the most popular methods of sag and swell compensation is Dynamic Voltage Restorer (DVR), The Dynamic Voltage Restorer (DVR) is series-connected power electronics based device. It provides advanced and economic solution to compensate voltage sag and swell. This device can be implemented to protect a group of medium or low voltage consumers. The new configuration of DVR has been proposed using improved d-q-0 controller. This study presents compensation of sags and swells voltage during single line to ground (SLG) and three-phase faults. Simulation results carried out by Matlab/Simulink verify the performance of the proposed method.

Keywords: Dynamic Voltage Restorer, Voltage Sags, Voltage Swells, Single Line to Ground & three phase faults.

I. Introduction

As well known, quality of the power is facing a various problems such as voltage sags/swells, surge, flicker, voltage imbalance, interruptions and harmonic distortion, Voltage sags/swells can occur more frequently than other Power quality problems, also these sags/swells are the most severe power quality disturbances in the power distribution system. One of the most important custom power devices that have been created to improve the performance of power quality is Dynamic Voltage Restorer (DVR). The DVR maintains the load voltage at a nominal magnitude and phase by compensating the voltage sag/swell and voltage unbalance at the point of common coupling (PCC). These systems are able to compensate voltage sags by increasing the appropriate voltages in series with the supply voltage, and therefore prevent loss of power [5].

Voltage sags/swells caused by unsymmetrical line-to-line, single line-to-ground (SLG), double line-to-ground and symmetrical three phase faults. the DVR injects the independent voltages to restore and maintained sensitive to its nominal value The injection power of the DVR with zero or minimum power for compensation purposes can be achieved by choosing an appropriate amplitude and phase angle [10]. Voltage sags can occur at any instant of time, with amplitudes ranging from 10-90% and a duration lasting for half a cycle to one minute. Voltage swell, on the other hand, is defined as an increase in rms voltage for durations from 0.5 cycles to 1 minute. Typical magnitudes are between 1.1 and 1.8 up. IEEE 519 1992 and IEEE 1159-1995 describe the voltage sags/swells as shown in Figure 1.

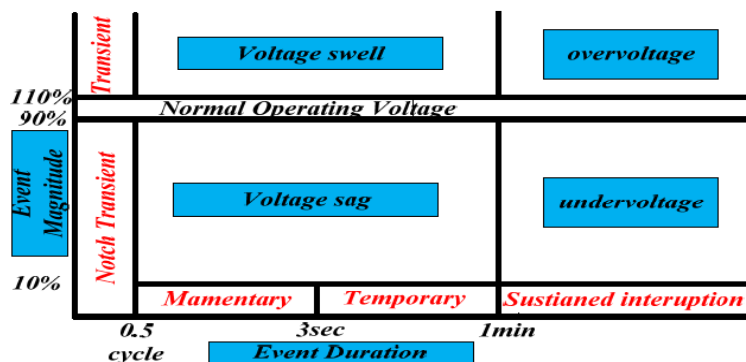


Figure (1) Voltage reduction standard of IEEE 1159-1995

Due to the fact that voltage swells are less common in distribution systems, they are not as important as voltage sags. Voltage sag and swell can cause sensitive equipment (such as found in semiconductor or chemical plants) to fail, or shutdown, as well as create a large current unbalance that could blow fuses or trip breakers. These effects can be very expensive for customers, ranging from minor quality variations to produce downtime and equipment damage [4].

II. Dynamic Voltage Restorer

In 1994, L. Gyugyi proposed a device and a method for dynamic voltage restoration of utility distribution network. This method uses real power in order to inject the faulted supply voltages and is commonly known as the Dynamic Voltage Restorer [15]. In this paper, a DVR design essentially contains a voltage source inverter (VSI), an injection transformer connected between the AC voltage supply and the sensitive load, a DC energy storage device, and a control system as shown in Figure 2.

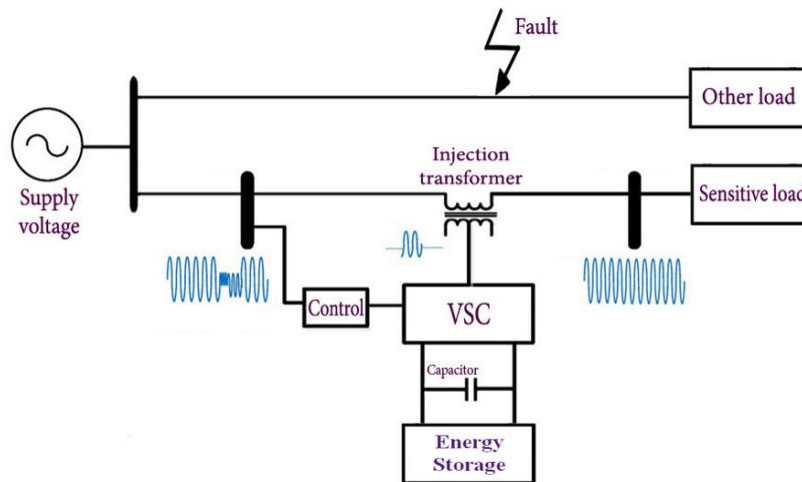


Figure (2) Basic DVR topology

The main function of the DVR is the protection of sensitive loads from voltage sags/swells coming from the network.

The DVR is connected in series between the source voltage or grid and sensitive loads through injection transformer. There are several types of energy storage that has been used in the DVR such as battery, capacitance and superconducting coil. These types of energy storages are very important in order to supply active and reactive power to the DVR. The controller is an important part of the DVR for switching purposes. The switching converter is responsible to do conversion process from DC to AC and to make sure that's only the swell or sag voltage is injected to the injection transformer.

The three-phase transformers connection used in the three-phase DVR can be configured either in delta/open or star/open connection. In case of asymmetrical fault in the high voltage side, the zero sequence current flowing almost zero, if the distribution transformer connection in Δ -Y with the grounded neutral. As such connection, the DVR only mitigates the positive and negative sequence components [15].

III. Compensation Methods in DVR

The type of the compensation strategy mainly depends upon the limiting factors such as DVR power ratings, various conditions of load, voltage sag type. Some loads are sensitive towards phase angle jump and some are sensitive towards change in magnitude and others are tolerant to these [16]. Therefore, the control strategies depend upon the type of load characteristics; there are three different methods of DVR voltage injection which are:

- (a) Pre-sag compensation method
- (b) In-phase compensation method
- (c) Voltage tolerance method with minimum energy injection

(a) Pre-Sag/Dip Compensation Method

The pre-sag method tracks the supply voltage continuously and if it detects any disturbances in supply voltage it will inject the difference voltage between the sag or voltage at PCC and pre-fault condition, so that the load voltage can be restored back to the pre-fault condition. Compensation of voltage sags in the both phase angle

and amplitude. Sensitive loads would be achieved by pre-sag compensation method as shown in Figure 3. In this method the injected active power cannot be controlled and it is determined by external conditions such as the type of faults and load conditions. The voltage of DVR is given below:

$$V_{DVR} = V_{pre\ fault} - V_{sag}$$

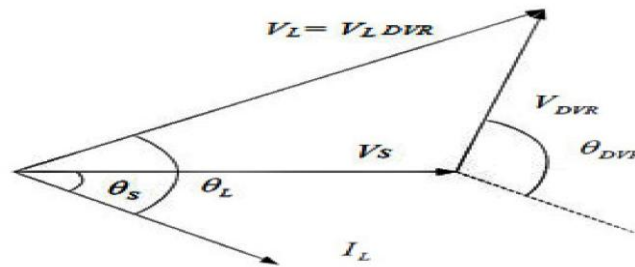


Figure (3) phasor diagram of pre-sag/dip method

(b) In-Phase Compensation Method

In this method the injected voltage is in phase with the supply side voltage irrespective of the load current and pre-fault voltage as shown in Figure 4. The phase angles of the pre-sag and load voltage are different but the most important criteria for power quality that is the constant magnitude of load voltage are satisfied. The load voltage is given below:

$$|V_L| = |V_{pre-fault}|$$

One of the advantages of this method is that the amplitude of DVR injection voltage is minimum for certain voltage sag in comparison with other strategies. Practical application of this method is in non-sensitive loads to phase angle jump.

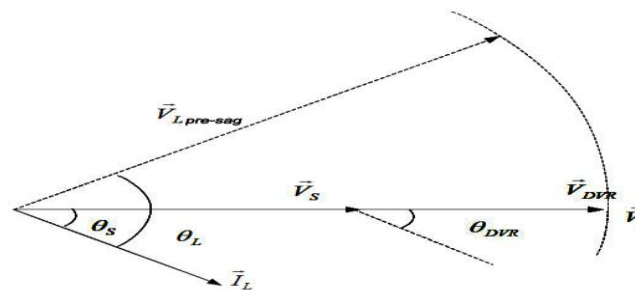


Figure (4) phasor diagram of in phase method

(c) Voltage Tolerance Method with Minimum Energy Injection

A small drop in voltage and small jump in phase angle can be tolerated by the load itself. If the voltage magnitude lies between 90%-110% of nominal voltage and phase angle variations between 5% -10% of nominal state that will not disturb the operation characteristics of loads. Both magnitude and phase are the control parameter for this method which can be achieved by small energy injection. In this method, the phase angle and magnitude of corrected load voltage within the area of load voltage tolerance are changed. The small voltage drop and phase angle jump on load can be tolerated by load itself. The sensitivity of loads to phase angle jump and voltage magnitude is different.

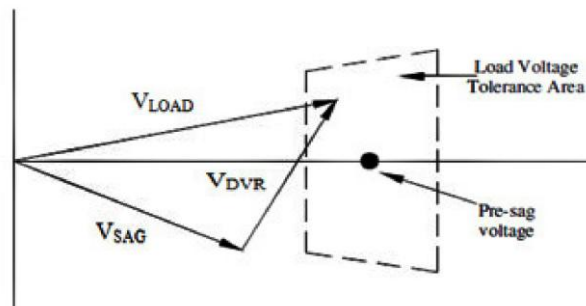


Figure (5) voltage tolerance method with minimum energy injection

IV. Propose Control Technique

The control system of a DVR plays an important role, with the requirements of fast response when voltage sag/swells are occur. When voltage sag/swells are detected, the DVR should react as fast as possible and injects AC voltage to the grid. It can be implemented using a Space Vector PWM control technique based on the voltage reference and instantaneous values of supply and load voltage. There are various basic rules of a controller in a DVR: detection of the voltage sag/swell occurrences in the system; calculation of the compensating voltage, generation of the trigger pulses of PWM inverter and stop triggering pulses when the occurrence has passed. The dq0 method gives the information of the depth (d) and phase shift (q) of voltage sag with start and end time. The load voltage is transformed to V_D , V_Q and V_0 based on park transformation according equations (1), (2) & (3).

$$\vec{V}_d = \frac{2}{3} [V_a \cos \omega t + V_b \cos(\omega t - \frac{2\pi}{3}) + V_c \cos(\omega t - \frac{2\pi}{3})] \quad (1)$$

$$\vec{V}_q = \frac{2}{3} [V_a \sin \omega t + V_b \sin(\omega t - \frac{2\pi}{3}) + V_c \sin(\omega t - \frac{2\pi}{3})] \quad (2)$$

$$\vec{V}_0 = [V_a + V_b + V_c] / 3 \quad (3)$$

Phase locked loop (PLL) is used to generate unit sinusoidal wave in phase with main voltage. The abc components are given to generate three phase pulses using PWM technique. Proposed control technique block is shown in Figure 6. The flow chart of the DVR operation is shown in Figure 7.

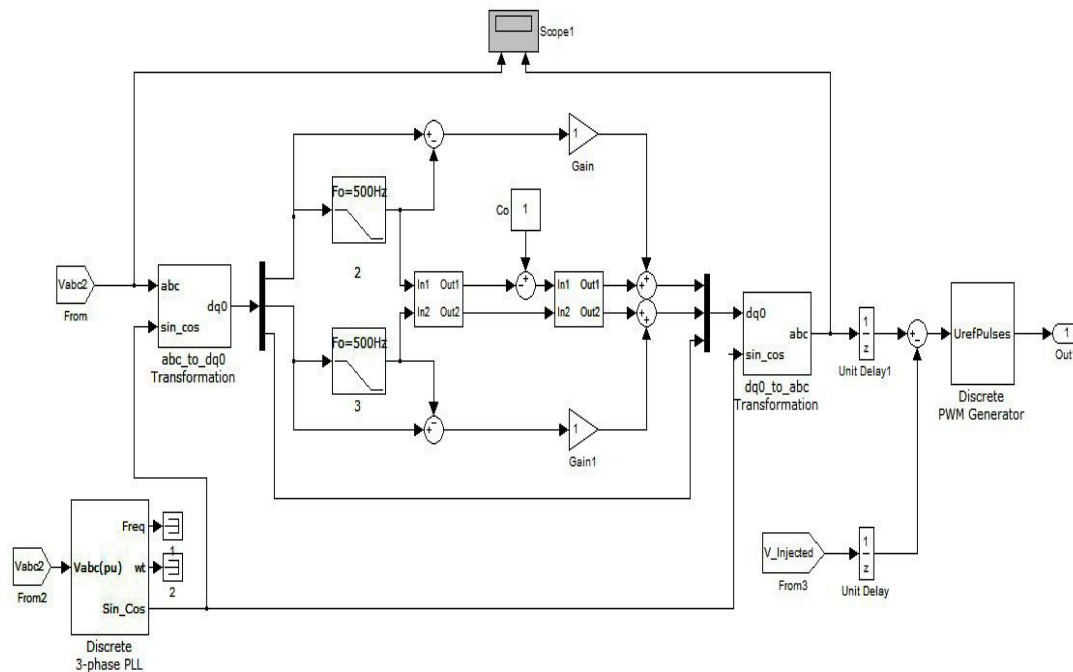


Figure (6) Block diagram control scheme of DVR

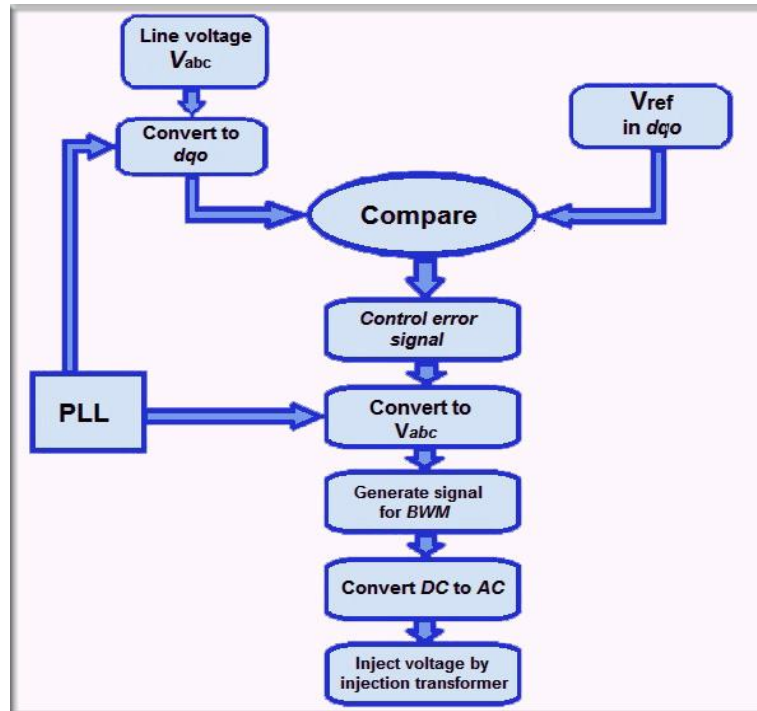


Figure (7) Flow chart of DVR operation

V. Simulations and Results

Investigation on the DVR performance can be observed through testing under various disturbances condition on the source voltage. The proposed control algorithm was tested for balanced and unbalanced voltages sags/swells in low voltage distribution system.

The first simulation shows the single phase voltage sag. The simulation started with the supply voltage 50% sagging as shown in Figure 9 (a). The Figure 9 (a) also shows a 50% voltage sag initiated at 0.1 sec and it is kept until 0.2 sec, with total voltage sag duration of 0.1 sec. Figure 9 (b) illustrates the voltage injected by the aid of DVR and (c) shows the corresponding load voltage with compensation. As a result of the DVR, the load voltage is kept at 1 PU, and the Figure 10 shows the occurrence of 50% three phase voltage sag on utility grid, also the injected voltage and load voltage are shown.

The second simulation shows the DVR performance during a voltage swell condition. In case of balance voltage swell, the source voltage has increased about 20- 25% of its nominal value. The simulation results of the balance three phase voltage swell as shown in Figure 12(a). Figures 12(b) and (c) show the injected and the load voltage respectively. The swells voltages occur at the time duration of 0.1 sec and after 0.2 sec the voltage will restore back to its normal value. As can be seen from the results, the load voltage is kept at the nominal value with help of the DVR. Figures 11 (a), (b), and (c) show the single phase voltage swell, injected voltage by the DVR and the load voltage respectively.

In addition, as a result of SLG fault. An unbalanced voltage sag is created immediately after the fault as shown in Figure 13(a), the supply voltage with two of the phase voltages dropped down to 60-80%. The DVR injected voltage and the load voltage are shown in Figure 13(b) and (c) respectively.

In case of unbalance voltage swells, this phenomenon caused due to single phase to ground fault. One of the phase of voltage swells has increased around 20-25% with duration time of swells is 0.1 sec. The swells voltage will stop after 0.2 sec as shown in Figure 14(a). At this stage the DVR will injects the missing voltage in order to compensate it and the voltage at the load will be protected from voltage swells problem. The injected voltage that is produced by the DVR in order to correct the load voltages and the load voltages maintain at the constant level are shown in Figures 14(b) and (c), respectively.

The Figure 8 shows the Matlab/Simulink of power system grid under the fault condition connected to the Dynamic Voltage Restorer. The table 1 summarizes the specification of the simulation of the DVR.

Supply voltage per phase	400V
Source voltage	22KV
Series transformer turn ratio	1:1

DC bus voltage	150
Source resistance	0.8Ω
Line frequency	50
Line impedance	L = 1mH, R = 0.01Ω
Filter inductance	7mH
Filter capacitance	10μF

Table (1) System parameters and constant values

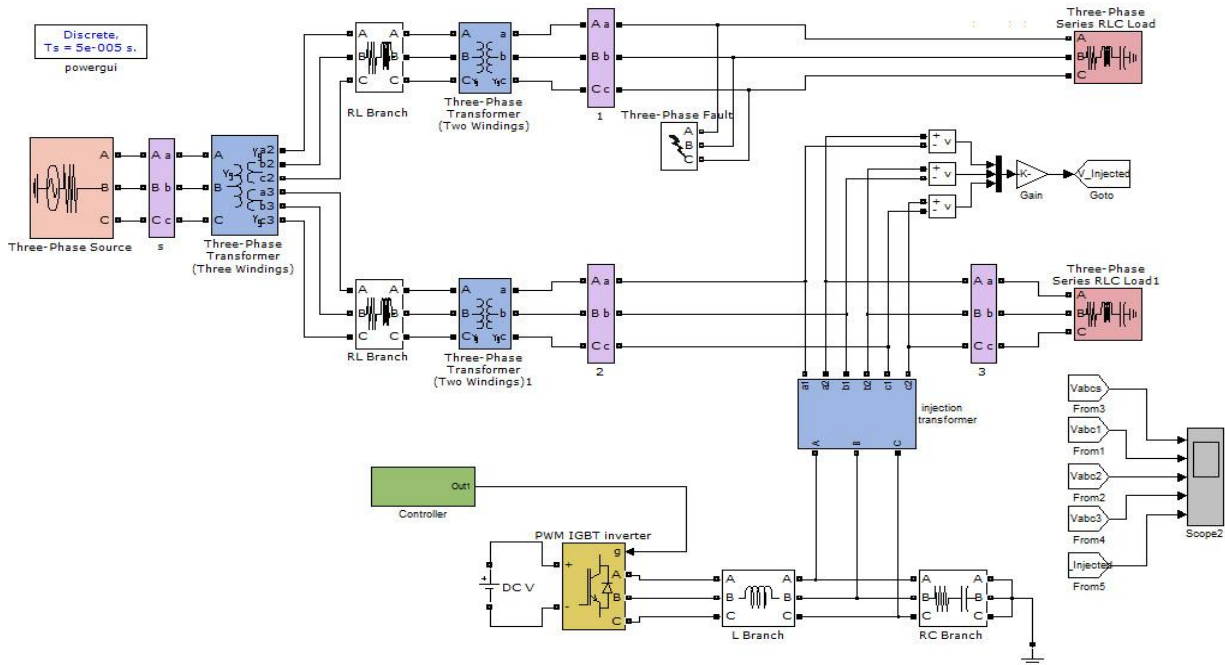
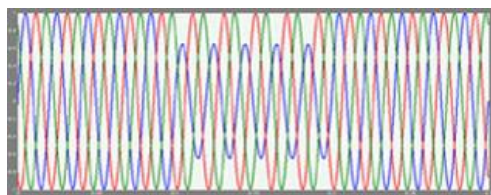
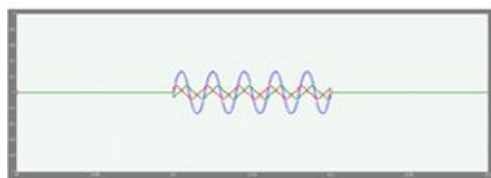


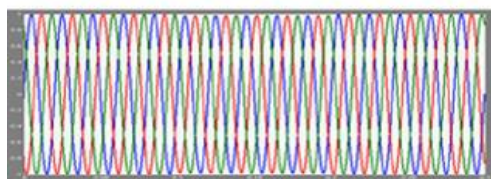
Figure (8) Matlab model of the DVR connected system



(a)

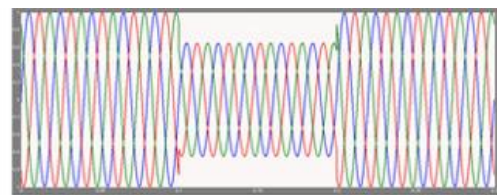


(b)

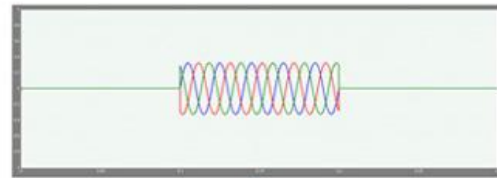


(c)

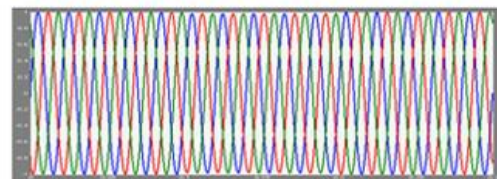
Figure (9) Single phase voltage sag
a) Source voltage b) Injected voltage c) Load voltage



(a)



(b)



(c)

Figure (10) Three phase voltage sag
a) Source voltage b) Injected voltage c) Load voltage

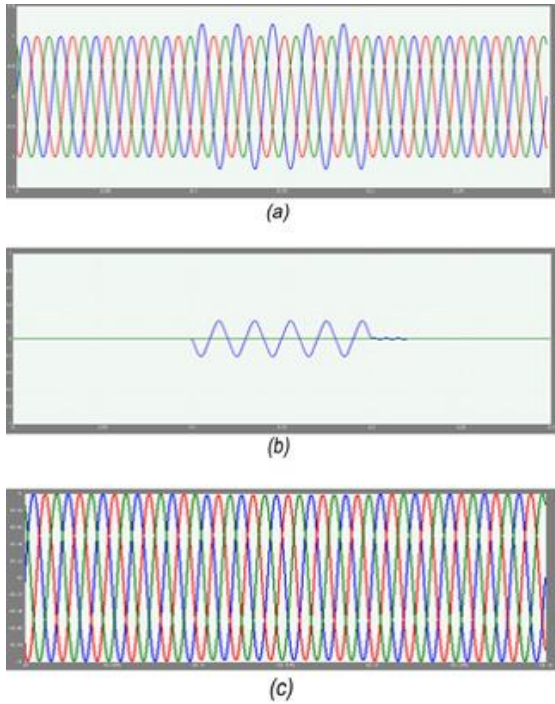


Figure (11) Single phase voltage swell
a) Source voltage b) Injected voltage c) Load voltage

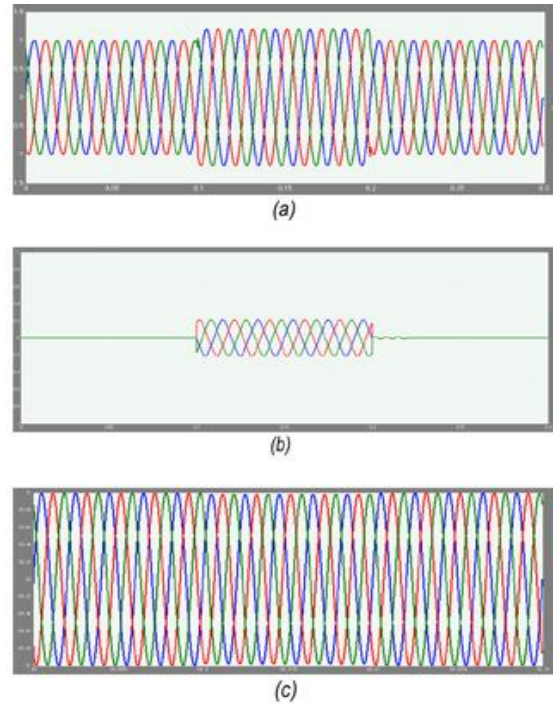


Figure (12) Three phase voltage swell
a) Source voltage b) Injected voltage c) Load voltage

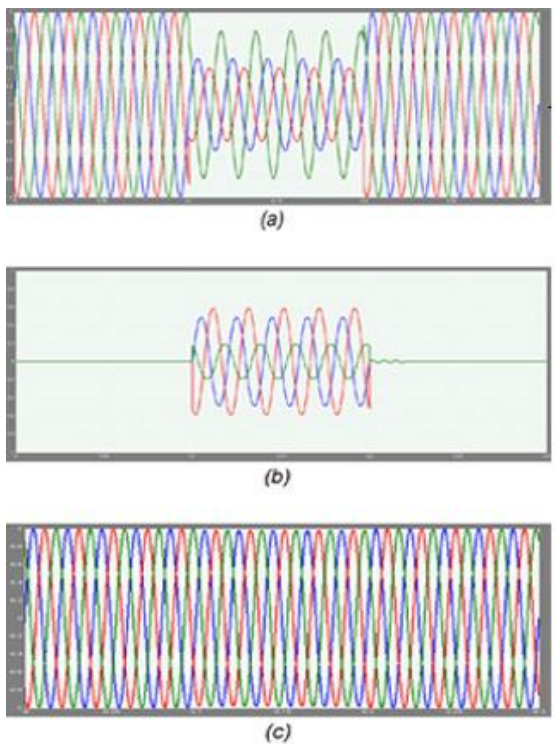


Figure (13) Unbalanced voltage sag
a) Source voltage b) Injected voltage c) Load voltage

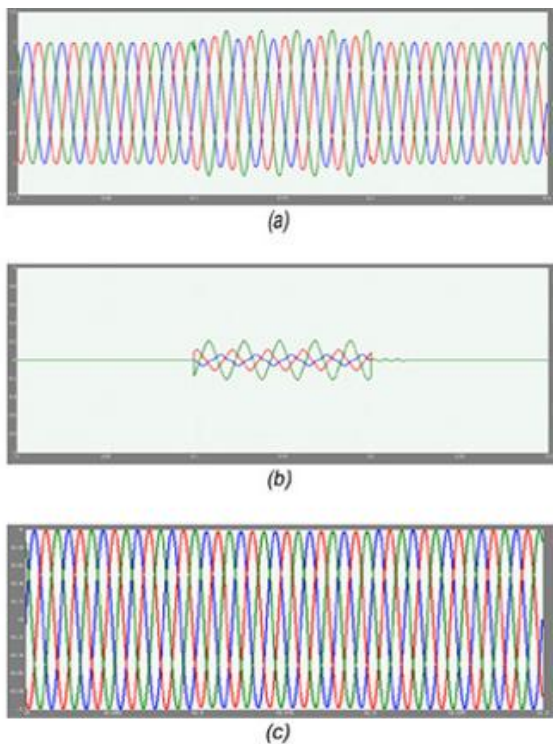


Figure (14) Unbalanced voltage swell
a) Source voltage b) Injected voltage c) Load voltage

V. Conclusions

A comprehensive study of a DVR as a powerful custom power device has been shown with aid of matlab/Simulink. The main advantages of DVR are low cost, simpler implementation, require less computational efforts and its control is simple as compared to other methods. The control system is based on dq0 technique which is a scaled error between source side of the DVR and its reference for compensating sags and swells. The simulation shows that the DVR performance is efficient in mitigation of voltage sags and swells. The DVR handles both balanced and unbalanced situations without any difficulties. It injects an appropriate voltage component to correct any anomaly rapidly in the supply voltage; in addition, it keeps the load voltage balanced and constant at the nominal value.

REFERENCES

- [1] A.A.D.R. Perera, D.M. Vilathgamuwa, S.S. Choi, "Voltage Sag Compensation with Energy Optimized Dynamic Voltage Restorer", IEEE Trans. on Power Del., Vol. 11, No. 3, pp. 928-936, July 2003.
- [2] V. Salehi, S. Kahrobaee, S. Afsharnia, "Power Flow Control and Power Quality Improvement of Wind Turbine Using Universal Custom Power Conditioner", IEEE Conference on Industrial Electronics, Vol. 4, pp. 1688-1892, July 2002.
- [3] B.H. Li, S.S. Choi, D.M. Vilathgamuwa, "Design Considerations on the Line-Side Filter Used in the Dynamic Voltage Restorer", IEE Proc. Gener. Transmission Distrib., Issue 1, Vol. 148, pp. 1-7, Jan. 2001.
- [4] H.P. Tiwari, Sunil Kumar Gupta, "DC Energy Storage Schemes for DVR Voltage Sag Mitigation System" International Journal of Computer Theory and Engineering, Vol. 2, No. 3, June, 2010.
- [5] P. Boonchiam, N. Mithulananthan, "Understanding of Dynamic Voltage Restorers through Matlab Simulation" Thammasat Int. J. Sc. Tech., Vol. 11, No. 3, July-Sept. 2006.
- [6] M.R. Banaei, S.H. Hosseini, S. Khanmohamadi, G.B. Gharehpetian, "Verification of a New Control Strategy for a Dynamic Voltage Restorer by Simulation", Elsevier Simulation Modeling Practice and Theory, Vol. 14, pp. 112-125, March 2006.
- [7] B.J. Quirl, B.K. Jhonson, H.L. Hess, "Mitigation of Voltage Sags with Phase Jump Using a Dynamic Voltage Restorer", 38th Power Symposium, Carbondal, IL, North American, pp. 647-654, Sept. 2006.
- [8] Yash Pal, A. Swarup, Senior Member, IEEE, and Bhim Singh, Senior Member, IEEE "A Review of Compensating Type Custom Power Devices for Power Quality Improvement" IEEE Power India Conference, pp. 1-8, 2008.
- [9] S.S. Mahesh, M.K. Mishra, B.K. Kumar, V. Jayashankar, "Rating and Design Issues of DVR Injection Transformer", Power Electronics Conference and Exposition, pp. 449-455, Feb. 2008.
- [10] A. Ramasamy, V.K. Ramachandaramurthy, R.K. Iyer, Z.L. Liu, "Control of Dynamic Voltage Restorer Using TMS320F2812", Electrical Power Quality and Utilisation Conference, pp. 1-6, Oct. 2007.
- [11] H. Toodeji, S.H. Fathi. "Cost Reduction and Control System Improvement in Electrical Arc Furnace Using DVR", IEEE Conference on Industrial Electronics and Applications, pp. 211-215, Tehran, Iran, May 2009.
- [12] V.K. Ramachandaramurthy, A. Arulampalam, C. Fitzner, C. Zhan, M. Barnes, N. Jenkins, "Supervisory Control of Dynamic Voltage Restorers", IEEE Proc. Gener. Transm. Distrib, Issue 1, Vol. 151, pp. 509-516, July 2004.
- [13] L. Gyugyi, C.D. Schauder, C.W. Edwards, M.Sarkozi, "Apparatus and Method for Dynamic Voltage Restoration of Utility Distribution Networks", U.S. Patent, Issue 1, Vol. 5, pp. 329-222, 1994.
- [14] A.O. Ibrahim, T.H. Nguyen, D.C. Lee, "A Fault Ride-Through Technique of DFIG Wind Turbine Systems Using Dynamic Voltage Restorers", IEEE Transaction Energy Conversion, Vol. 26, No. 3, pp. 871- 882, Sept. 2011.
- [15] C. Fitzner, M. Barnes, P. Green, "425V Voltage Sag Detection Technique for a Dynamic Voltage Restorer", IEEE Transactions on Industry application, Issue 1, Vol. 40, pp. 203-212, Feb. 2004.
- [16] John Godsk Nielsen, Frede Blaabjerg, "Control Strategies for Dynamic Voltage Restorer Compensating Voltage Sags with Phase Jump", Applied Power Electronics Conference and Exposition, IEEE, vol. 2, pp. 1267-1273, 2001.
- [17] S. Deepa, S. Rajapandian, "Voltage Sag Mitigation Using Dynamic Voltage Restorer System by Modified Z-Source Inverter", 2nd International Conference on Electrical, Electronics and Civil Engineering (ICEECE'2012), pp. 1-4, April 2012.
- [18] M. Karimian, A. Jalilian, "Proportional Repetitive Control of a Dynamic Voltage Restorer (DVR) for Power Quality Improvement", International Journal on Technical and Physical Problems of Engineering (IJTPE), Issue 11, Vol. 4, No. 2, pp. 18-23, June 2012.
- [19] Mokhtarpour, H.A. Shayanfar, S.M.T. Bathaee, "Extention of Fourier Transform for Very Fast Reference Generation of UPQC", International Journal on Technical and Physical Problems of Engineering (IJTPE), Issue 9, Vol. 3, No. 4, pp. 120-126, Dec. 2011.
- [20] A.Teke, K.Bayindir, M.Tumay, Department of Electrical and Electronics Engineering, Cukurova University, Adana, Turkey "Fast sag/swell detection method for fuzzy logic controlled dynamic voltage restorer" generation transmission and distribution IET, vol. 4, pp. 1-12, 2010.

BIOGRAPHIES



Rasool Mohammed Imran: Born in Iraq/Karbala in 1989. He received B.Sc. degree (electrical engineering) from technical college of al-musaib in Iraq in 2011. He is currently working toward the M. tech degree in electrical and electronics engineering (power system) in SHIATS, Allahabad India.



Dr. Jyoti Srivastava: has done her graduation in electrical engineering and her post-graduation in design of heavy electrical equipment at present she is serving as an Senior Assistant Professor in Electrical Engineering Department at college of engineering and technology SHIATS Allahabad India She has several international and national paper to her credit Her field of interest and research are power system control and operation and condition monitoring of heavy electrical equipment her research aims to increase Transmission & Distribution systems capacity and enhancing system reliability.

Integrated Geo-spatial ICT Solution for Scientific Planning & Monitoring of MGNREGS works in Gujarat

Paru Thakkar¹, Manoj Pandya², Leena Patel³, Rajiv Kanzaria⁴, Yogiraj Shete⁵,
V. Kanagasabapathy⁶

¹ (Project Manager, BISAG, Gandhinagar, Gujarat, India)

² (Project Manager, BISAG, Gandhinagar, Gujarat, India)

³ (Project Manager, BISAG, Gandhinagar, Gujarat, India)

⁴ (Project Scientist, BISAG, Gandhinagar, Gujarat, India)

⁵ (Subject Expert (GIS), MGNREGS, Commissionerate of Rural Development, Govt. of Gujarat)

⁶ (M&E Consultant State Resource Centre, (Managed by TRIOS development support (p) Ltd., MGNREGS)

ABSTRACT: Mahatma Gandhi National Rural Employment Guarantee Scheme (MGNREGS), aims at enhancing livelihood security of households in rural areas by providing at least one hundred days of guaranteed wage employment in a financial year to every household whose adult members volunteer to do unskilled manual work. Its auxiliary objectives are strengthening natural resource management through works that address causes of chronic poverty like drought, deforestation and soil erosion and to encourage sustainable development. The objective of this paper is to illustrate the function and benefits of the mobile based Geo-Information Communication Technology solution to monitor works performed in MGNREGS. Use of Geo-ICT initiative enhances the effective management of the works undertaken in MGNREGS and supports to better governance.

Keywords: MGNREGS, GIS, Geo ICT, Planning, cadastral map, Cell phone, GPS.

I. Introduction

MGNREGS marks a paradigm shift from all preceding wage employment programmes. Significant aspects of this paradigm shift include a rights-based framework for wage employment. Employment is dependent on the worker exercising the choice to apply for registration, obtain a Job Card, and seek employment for the time and duration that the worker wants. The need to act within a time limit necessitates advance planning. Timely generation of employment within 15 days with the assurance of the quality in design and selection of works are the key concerns. Gram Panchayat prepares yearly development plan and maintain various works under MGNREGS. After taking approval from Gram Sabha the proposed works are forwarded to the Block Panchayat for scrutiny and for preliminary approval prior to their commencement in the year in which the work is proposed. After obtaining approvals, at various levels of the Government hierarchy, a set of pre approved works are kept ready, to be initiated as and when the demand is registered at the Gram Panchayat.

II. Methodology

Satellite Images obtained from National Remote Sensing Center (NRSC) with 1:10,000 to 1:5,000 variable scales are used as a base maps for the geo-spatial database creation. Other departmental geo-data sets (spatial & non-spatial data) generated over the years were also collected and superimposed on the Baseline map to create composite village map. Revenue Department data & LISS IV Satellite images were used to digitize the village local boundaries. Recently the village local boundary had been revised with 2011 village census codes. Locations of ongoing works of rural natural resource development had also been captured to maintain digital Geo-asset inventory on a real time basis. By overlaying these layers, composite map was generated for every village in Gujarat state.

Technical Assistants facilitated the community participation in the Gram Sabha to plan the works that could be undertaken in the financial year 2013-14. Thus the Composite Maps were used to prepare the 2014-14 - MGNREGS Labour Budget for the entire state.

II Use of natural resources

Natural Resources	Features	Source
Land	Land use	Satellite Data
	Landform (hill, Alluvial, Coastal areas etc)	Satellite Data
	Soil type	Soil and Land Use Survey of India, National Bureau of Soil Survey & Land Use Planning, Agri. Dept.
	Slope/Elevation	Satellite Data & Open Source
Water	Surface Water Bodies	Satellite Data
	Ground Water condition	GWRDC, CGWB
	Wells	Revenue Department
	Check Dam	Departmental Data
Vegetation	Agriculture	Agriculture Department, Satellite Data
	Forest	Forest Department, Satellite Data
Village	Socio-Economic Facilities, SC & ST data , Actual Wages, Drinking Waters, % of SF & MF, % Poverty Index	Department of Rural Development, Bureau of Economic & Statistics
	Village Map	Computerized maps from Revenue Department
Infrastructure	Roads, Canals, Water Supply	Line Departments
Ownership Details	Forests, Government, Panchayat, Private	Revenue Department
Others	Sanctuaries, Mining areas	Line Departments

Table 1: Overview of natural resources and its features mapped for Geo-ICT initiative at village level

In addition, the requirement of the beneficiaries are also prepared and used along with the maps. The composite village maps were provided to all MGNREGS Technical Assistants for use as a planning tool.

III Use of composite village maps

Composite Village Map used during Participatory Planning in Gram Sabha. Budgeted work plan of MGNREGS had been digitised and a mobile application had been developed based on the budget. The Mobile application is installed in the cost effective GPS enabled mobile devices. Each Technical Assistant uses the mobile application for submission of current status of the proposed work in the labour budget. Apart from that, the weekly work progress information is reported from the work site through SMS based reporting system. SMS received with GPS coordinates provides the real time report for the supervisors and administrative functionaries to act upon.

Other than the above described mobile application, additional two mobile applications were also developed and used in the Geo-ICT initiative. With respect to the additional two applications, the first application is used by the Technical Assistants for validating the MGNREGS assets created in the previous financial years. The second one is used by Works manager for supervisory reporting. The information received through the SMS reporting system is stored in the centralized server.

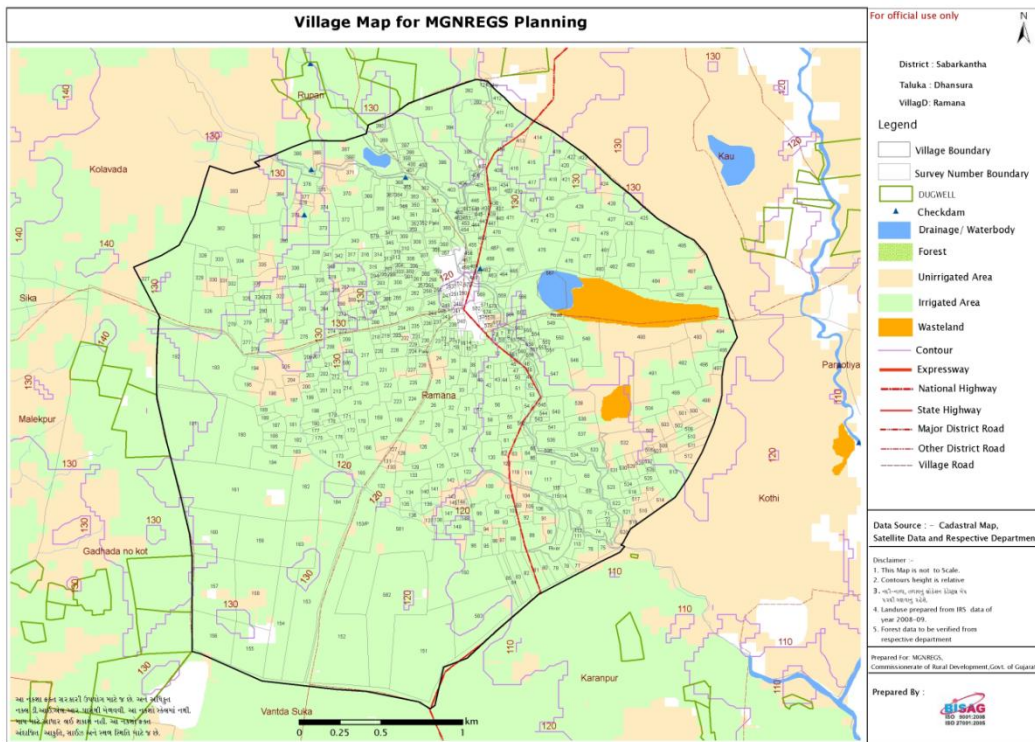


Fig 1: Composite village map for District: sabarkantha, taluka: Dhansura and village: Ramanna

For each mobile application a corresponding modem and Gateway application had been developed for running the application on internet. Refer the information flow diagram, the modem/ gateway applications 1, 2 & 3 are prepared to link the input mobile application information to the GIS website. The modem/ gateway applications 4, 5 & 6 are developed to generate reports to the different supervisory officials. Access to the server database and maps are provided to all the District and Block level officials through the web link accessible through Gujarat State Wide Area Network (GSWAN) and in later phase it is available through live internet access. Alerts on the MGNREGS performance variations are also displayed on the website. Customized alerts are also sent to the State, District & Block level officials on a daily/weekly basis using the modem application 4, 5 & 6 respectively. These facilities are useful for taking real time decisions. The work progress information captured in GIS website is linked with the NREGAssoft MIS. Following flow diagram depicts the technical overview of information flow in Geo-ICT initiative.

II.II MGNREGS – Gujarat, information flow in Geo-ICT initiative

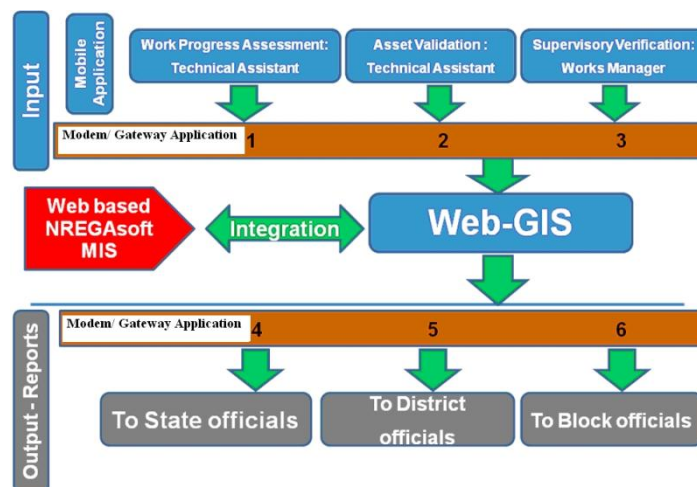


Fig 2: A framework for the integration of Web GIS and NREGA Soft and Gateway/ Modem Application

II.III Technology used in Geo-ICT initiative of MGNREGS, Gujarat

Hardware	Software
<ul style="list-style-type: none"> ✓ 1 High End Server ✓ 1 GSM MODEM at Server side or SMS Gateway service ✓ Mobile Devices having GPS/ A-GPS 	<ul style="list-style-type: none"> ✓ In house GIS Engine ✓ Microsoft© Visual studio 2005 ✓ Microsoft© SQL Server 2005

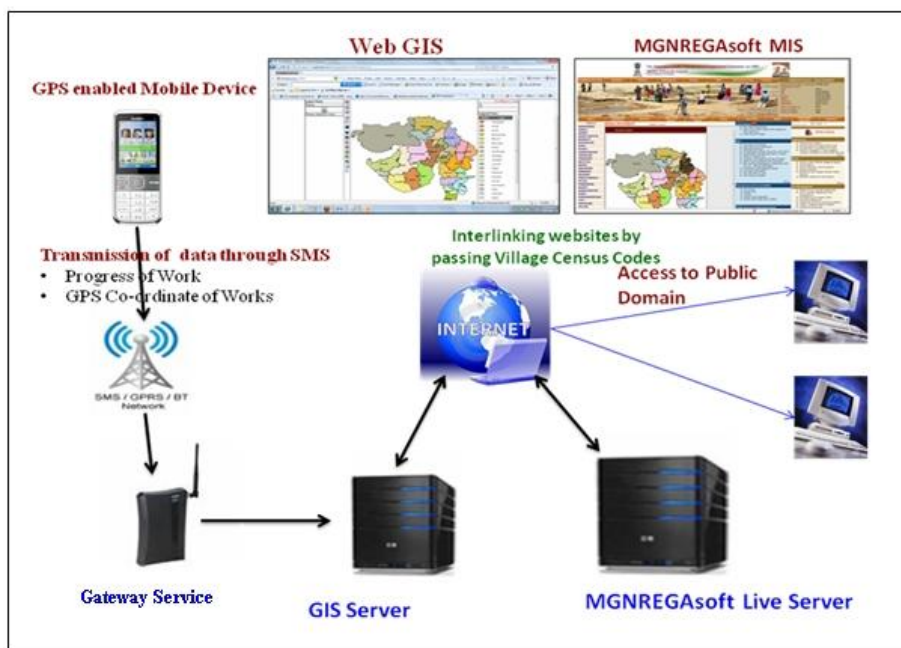


Fig 3: Information flow diagram after integration of Web-GIS & NREGAsoft MIS

Integration of Web-GIS with NREGAsoft MIS through web interface: In order to comprehensively track the MGNREGS progress, Geo-ICT tools have been integrated with NREGAsoft MIS at various levels. Database-level integration has led to MIS and GIS sharing a common database; data changes in one reflects in the other i.e., if there is a change in the MIS, the other system (GIS) automatically changes the visual interpretation on the maps. Data sent over the mobile phones is transmitted to the central server which facilitates map creation for monitoring before, during and post implementation phases of the project. SMS from the work sites sent by the Technical Assistants are received in the Central server located at State Data Center through Gateway service. The received data updates the GIS database which in turn updates the GIS maps & also the NREGAsoft MIS.

III. Conclusion

Mobile based SMS reporting system for tracking MGNREGS work progress are useful to the supervisors & administrators to take decisions on near-real time basis. From the geo-asset directory the composite village maps are generated and used for the scientific planning. This also helps to reduce the duplication of works most efficiently. Gujarat’s Geo-ICT initiative is unique in its approach. It goes one step ahead than all other initiatives in using the Geo-reference tracking system by measuring the GPS coordinates (Latitude-Longitude) of all work sites. With the encouraging results from the piloting exercise, the full fledged implementation of Geo-validation and near real time monitoring of the works have been achieved. The Geo-ICT initiative enhances the effective management of the works undertaken in MGNREGS, Gujarat. It also increases the transparency, accountability, and therefore credibility of the Program.

Acknowledgements

Authors are thankful to the officials working in Commissionerate of Rural Development, District Rural Development Agency, Block Panchayat, Ministry of Rural Development, Government of India, National Informatics Center, New Delhi, National Institute of Rural Development, C-GARD and TRIOs Development Support (P) Ltd. for various roles in implementation of Geo-ICT initiative in MGNREGS, Gujarat.

We are sincerely thankful to Shri T. P. Singh, director, Bhaskaracharya Institute for space Applications and Geo-Informatics (BISAG) for his encouragement and support in carrying out this task.

REFERENCES

- [1] The National Rural Employment Guarantee Act 2005 (NREGA), Operational Guidelines, 2008 – 3rd Edition published by Ministry Of Rural Development, Department Of Rural Development, Government Of India, New Delhi
- [2] NREGAsoft : Strengthening National Rural Employment Guarantee Scheme (NREGS) (<http://nrega.nic.in>) implementation article written by Madhuri Sharma, Technical Director (NIC)
- [3] Documentation of best practice SMS based monitoring system, October 2010, researched & documented by one world.net, one world foundation India.
- [4] Human Resource Management System (HRMS), Documentation of best practice, February 2011, researched & documented by one world.net, one world foundation India.
- [5] Documentation of best practice, Computerised Treasury Management Information System, December 2010, researched & documented by one world.net, one world foundation India
- [6] C. P. Lo & Albert K.W. Yeung (2004) “Concepts and Techniques of Geographic Information Systems”, PHI
- [7] P. Paneeravel (2005) “E-Governance, a change management tool”, Rawat Publications
- [8] Subhash Bhatnagar, Robert Schware (2000) “Information and Communication technology in development - cases from India”, Sage Publications

Evaluation of Biodiesel as an Alternate Fuel to Compression Ignition Engine and To Study Its Effect on Performance and Emission Characteristics

Santosh Kumar S.

(Department of Mechanical Engineering, Raja Reddy Institute of Technology, India)

ABSTRACT: To meet increasing energy requirements, there has been growing interest in alternate fuels like biodiesel to provide a suitable diesel oil substitute for internal combustion engines. Biodiesel offer a very promising alternate to diesel oil since they are renewable and have similar properties. Further it can be used with/without any modifications to the engine. It is an oxygenated fuel and emissions of carbon monoxide are less unlike fossil fuels, the use of biodiesel does not contribute to global warming as CO₂ emitted is once again absorbed by the plants grown for vegetable oil/biodiesel production, thus CO₂ balance is maintained. In the present work the Honge and Jatropha Curcas oil (Biodiesel) at various blends is used with pure diesel to study its effect on performance and emission characteristics of the engine. The performance of the engine under different operating conditions and blends are compared by calculating the brake thermal efficiency and brake specific fuel consumption by using pure diesel and adding various blends of Honge and Jatropha Curcas oil to diesel. The exhaust gas analyzers and smoke meters are used to find the percentage of carbon monoxide (CO), carbon dioxide (CO₂), Hydrocarbons (HC) and oxides of nitrogen (NO_x) emissions.

Keywords: Biodiesel, Brake thermal efficiency, Brake specific fuel consumption Honge, Jatropha.

I. Introduction

Petroleum crude is expected to remain main source of transport fuels at least for the next 20 to 30 years. The petroleum crude reserves however, are declining and consumption of transport fuels particularly in the developing countries is increasing at high rates. Severe shortage of liquid fuels derived from petroleum may be faced in the second half of this century. Energy security is an important consideration for development of future transport fuels. Recently, more and more stringent environmental regulations being enacted in the USA and EUROPE have led to research and development activities on clean alternate fuels. A number of liquid and gaseous fuels are among the potential fuel alternatives. most important among them are alcohols, ethanol and methanol, natural gas, liquefied petroleum gas (LPG), hydrogen, biodiesel and biogas etc. the large increase in number of automobiles in recent years has resulted in great demand for petroleum products with crude oil reserves estimated to last only for few decades; there has been an active search for alternate fuels. The depletion of crude oil would cause a major impact on the transportation sector. of the various alternate fuels under consideration, biodiesel, derived from vegetable oils, is the most promising alternative fuel to conventional diesel fuel (derived from fossil fuels; hereafter just “diesel”) due to the following reasons [1]. A lot of research work has been carried out using vegetable oil both in its neat form and modified form. Studies have shown that the usage of vegetable oils in neat form is possible but not preferable [2]. The high viscosity of vegetable oils and the low volatility affects the atomization and spray pattern of fuel, leading to incomplete combustion and severe carbon deposits, injector choking and piston ring sticking. Methods such as blending with diesel, emulsification, pyrolysis and transesterification are used to reduce the viscosity of vegetable oils. Among these, the transesterification is the most commonly used commercial process to produce clean and environmentally friendly fuel. a large number of studies on performance, combustion and emission using raw vegetable oils and methyl/ethyl esters of sunflower oil [3], rice bran oil, palm oil [4], mahua oil, Jatropha oil, Karanja oil [5], Soybean oil, rapeseed oil and rubber seed oil have been carried out on compression ignition(CI) engines. The purpose of this paper is to review previous studies that look into the effect of bio-diesel on CI engine from the viewpoint of performance, combustion and emissions.

1.1 Biodiesel

Biodiesel is methyl or ethyl ester of fatty acid made from virgin or used vegetable oils (both edible and non edible) and animal fats. Neat (100%) biodiesel contains no petroleum, but it can be blended at any level with

diesel to create biodiesel blends. Just like diesel, biodiesel operates in compression ignition (diesel) engine, which essentially requires very little or no engine modifications as biodiesel as properties similar to that of diesel fuels. It can be stored just like diesel fuel and hence does not require a separate infrastructure. The use of biodiesel in conventional diesel engines results in substantial reduction of unburned hydrocarbons, carbon monoxide and particulate matter emissions. Biodiesel is considered a clean fuel since it has no sulfur no aroma has about 10% oxygen content, which helps it to burn fully. Its higher Cetane Number (CN) improves the ignition quality even when blended with diesel [6].

II. Properties of Biodiesel

2.1 Density/Specific gravity

Biodiesel is slightly heavier than conventional diesel fuel (specific gravity 0.88 compared to 0.84 for diesel fuel). This allows the use of splash blending by adding biodiesel on top of diesel fuel for making blends [6].

2.2 Cetane Number

Cetane number is indicative of its ignition characteristics. The higher is the Cetane Number; the better is its ignition properties. The Cetane Number affects a number of engine performance parameters like combustion, stability, drivability, white smoke, noise and emissions of CO and HC. Biodiesel has a high Cetane Number than conventional diesel fuel. This results in higher combustion efficiency and smoother combustion [6].

2.3 Viscosity

In addition to lubricating of fuel injection system components, fuel viscosity controls the characteristics of the injection from the diesel injector (droplet size, spray characteristics etc). The viscosity of biodiesel can reach very high levels and hence it is important to control it within an acceptable level to avoid negative impact on the performance of the fuel injection system. Therefore, the viscosity specifications proposed are same as that of the diesel [6].

2.4 Flash Point

The flash point of a fuel is defined as the temperature at which it will ignite when exposed to a flame or a spark. The flash point of biodiesel is higher than the petroleum-based diesel fuel. Thus, in storage, biodiesel and its blends are safer than conventional diesel. The flash point of biodiesel is around 160°C [6].

2.5 Cloud Point

Cloud point is the temperature at which a cloud or haze of crystals appears in the fuel under test conditions and thus it is important for low temperature operations. Biodiesel generally has higher cloud point than diesel [6].

2.6 Distillation Characteristics

The distillation characteristics of biodiesel are quite different from that of diesel fuel. Biodiesel does not contain highly volatile components; the fuel evaporates only at high temperatures. This is the reason that sometimes the dilution of sump lubrication oil is observed in many tests. Boiling point of biodiesel generally ranges between 330-357°C [6].

Table I: Properties of Jatropha Curcas oil and Diesel

<i>Sl No</i>	<i>Blend</i>	<i>Kinematic Viscosity at 40°C (mm²/s)</i>	<i>Flash Point (°C)</i>	<i>Calorific Value (KJ/Kg)</i>
1	J10	4.9	59	43647
2	J20	5.2	64	43093
3	J30	5.4	78	42207
4	Diesel	4	50	44755

Table II: Properties of Honge oil and Diesel

<i>Sl No</i>	<i>Blend</i>	<i>Density at 40°C(Kg/m³)</i>	<i>Flash Point (°C)</i>	<i>Calorific Value (KJ/Kg)</i>
--------------	--------------	--	-------------------------	--------------------------------

1	H10	832	102	43647
2	H20	839	104	43093
3	H30	840	106	42207
4	Diesel	829	50	44755

III. Method of Bio-Diesel Production

There are so many investigations on bio-diesel production of non-conventional feed stocks of oils have done in last few years. Ramadhas *et al.* [1] described various methods by which vegetable oils technology development of bio-diesel as an energy alternative 5 can be used in CI engines. Overview of transesterification process to produce biodiesel was given for introductory purpose. It is reported that enzymes, alkalis, or acids can catalyze process. Alkalis result in fast process. Barnwal and Sharma [7] give theoretical knowledge of catalyzed and supercritical method of transesterification process to produce biodiesel. It is mentioned that catalyzed process is easy but supercritical method gives better result. Usta *et al.* [8] produced a methyl ester bio-diesel from a hazelnut soap stock (45-50% free fatty acids) and waste sunflower oil mixture using methanol, sulphuric acid and sodium hydroxide in a two stage process and found satisfactory results. Adaptation of the vegetable oil as a CI engine fuel can be done by four methods [1, 14]; Pyrolysis, Micro emulsification, Dilution, and Transesterification.

3.1 Pyrolysis

The pyrolysis refers to a chemical change caused by the application of thermal energy in the absence of air or nitrogen. The liquid fractions of the thermally decomposed vegetable oils are likely to approach diesel fuels. The pyrolyzate had lower viscosity, flash point, and pour point than diesel fuel and equivalent calorific values. The Cetane Number of the pyrolyzate was lower. The pyrolyzed vegetable oils contain acceptable amounts of sulfur, water and sediments and give acceptable copper corrosion values but unacceptable ash, carbon residual and pour point. Depending on the operating conditions, the pyrolysis process can be divided into three subclasses: conventional pyrolysis, fast pyrolysis and flash pyrolysis. The mechanism of pyrolysis of triglycerides was given by Schwab *et al* [9].

3.2 Micro-Emulsification

The formation of micro emulsion is one of the potential solutions for solving the problem of vegetable oil viscosity. Micro emulsions are defined as transparent, thermodynamically stable colloidal dispersion. The droplet diameters in micro emulsions ranges from 100 to 1000 Å. Micro emulsion can be made of vegetable oils with an ester and dispersant (co solvent), or of vegetable oils, and alcohol and a surfactant and a Cetane improver, with or without diesel fuels. All micro emulsions with Butanol, Hexanol and Octanol met the maximum viscosity requirement for diesel fuel. The 2-octanol was found to be an effective amphiphile in the Micellar Solubilization of methanol in Triolein and soybean oil [10].

3.3 Dilution

The dilution of vegetable oils can be accomplished with such material as diesel fuels, solvent or ethanol. Dilution results in reduction of viscosity and density of vegetable oils. The addition of 4% ethanol to diesel fuel increases the brake thermal efficiency, brake torque and brake power, while decreasing the brake specific fuel consumption. Since the boiling point of ethanol is less than that of diesel fuel, it could assist the development of the combustion process through an unburned blend spray [11].

3.4 Transesterification

The transesterification is the method of biodiesel production from oils and fats and can be carried out by two ways [12].

3.4.1 Catalytic Transesterification.

3.4.2 Supercritical Methanol Transesterification.

3.4.1 Catalytic Transesterification

The "Catalytic Transesterification" process is the reaction of a triglyceride (fat/oil) with an alcohol in the presence of some catalyst to form esters and glycerol. A triglyceride has a glycerin molecule as its base with three long chain fatty acids attached. The characteristics of the oil/fat are determined by the nature of the fatty acids attached to the glycerin. The nature of the fatty acids can in turn affect the characteristics of the bio-diesel. A successful transesterification reaction is signified by the separation of the ester and glycerol layer after the

reaction time. The heavier, co-product, glycerol settles out and may be sold as it is or it may be purified for use in other industries, e.g. the pharmaceutical, cosmetics etc.

3.4.2 Super Critical Transesterification

The simple transesterification processes discussed above are confronted with two problems, i.e. the processes are relatively time consuming and needs separation of the catalyst and saponified impurities from the biodiesel. The first problem is due to the phase separation of the vegetable oil/ alcohol mixture, which may be dealt with by vigorous stirring. These problems are not faced in the supercritical method of transesterification. This is perhaps due to the fact that the tendency of two phase formation of vegetable oil/alcohol mixture is not encountered and a single phase is found due to decrease in the dielectric constant of alcohol in the supercritical state (at 340°C and 43 MPa). As a result, the reaction was found to be complete in a very short time within 2-4 min. Further, since no catalyst is used, the purification on biodiesel is much easier, trouble free and environment friendly.

IV. Effect of Biodiesel on Engine Performance

4.1 Brake Thermal Efficiency

Thermal efficiency is the true indication of the efficiency with which the chemical energy input in the form of fuel is converted into useful work. Much work has been done at many research institutes to examine the potential of biodiesel engines for achieving high thermal efficiency. Researchers such as Tsolakis [13], Senatore et al. [14], Shaheed and Swain [15], Graboski et al. [16], Canakci [17], reported no improvement in thermal efficiency when using different types of biodiesel fuels. A small number of experiments, however, have reported some improvement in thermal efficiency when using biodiesel fuels. Kaplan et al. [18] explained their observed increase in efficiency by means of improved combustion, giving no further reasoning. Agarwal and Das [19] tested linseed-oil biodiesel blended with high sulfur diesel fuel in a single cylinder 4 kW portable engine widely used in the agricultural sector and showed increases in thermal efficiency, especially at low loads. A few studies report small improvements in efficiency with biodiesel, or even synergic blending effects, which could be caused by reductions in friction loss associated with higher lubricity.

4.2 Fuel Consumption

Brake-specific fuel consumption (BSFC) is the ratio between mass of fuel consumption and brake effective power, and for a given fuel, it is inversely proportional to thermal efficiency. If the latter is unchanged for a fixed engine operation mode, the specific fuel consumption when using a biodiesel fuel is expected to increase by around 14% in relation to the consumption with diesel fuel, corresponding to the increase in heating value in mass basis. In other words, the loss of heating value of biodiesel must be compensated for with higher fuel consumption. Researchers such as Graboski et al. [16] and Canakci [17] have reported increases in BSFC ranging from 2% to 10%. Most of the authors have explained these increases by the loss of heating value, although some others attributed them to the different densities of biodiesel and diesel fuels.

V. Effect of Biodiesel on Emissions

Biodiesel mainly emits unburned hydrocarbons, carbon monoxide, oxides of nitrogen, sulphur oxides and particulates. A brief review has made of these pollutants emitted from biodiesel-fuelled engines.

5.1 Unburned Hydrocarbon

Most Researchers results show a sharp decrease in unburned hydrocarbon emissions when substituting conventional diesel fuel with biodiesel fuels [20-22]. The US Environmental Protection Agency (EPA) review [23] shows a 70% mean reduction with pure biodiesel with respect to conventional diesel as shown in Fig. 3. Most of the authors have attributed this to better combustion in biodiesel fuelled engines. Since biodiesel is an oxygenated fuel, it promotes combustion and results in the reduction of UBHC emissions. However, a few studies show no significant differences [24-25] or increases [25] in UBHC emissions when fuelling diesel engines with biodiesel instead of conventional diesel.

5.2 Carbon Monoxide (CO)

Some researchers [22-23], found a decrease in CO emissions when substituting diesel fuel with biodiesel shown in Fig. 4. Most of the authors have explained this to better combustion in biodiesel fuelled engine. Since biodiesel is an oxygenated fuel, it promotes combustion and results in reduction in CO emissions. Nevertheless, other authors found no differences between diesel and biodiesel [25], and even noticeable increases when using biodiesel [26].

5.3 Nitrogen Oxides (NO_x)

NO_x is formed by chain reactions involving Nitrogen and Oxygen in the air. These reactions are highly temperature dependent. Since diesel engines always operate with excess air, NO_x emissions are mainly a function of gas temperature and residence time. Most of the earlier investigations show that NO_x emissions from biodiesel engines are generally higher than that in conventional diesel fueled engines. Also earlier investigations revealed that NO_x emissions increase with an increase in the biodiesel content of diesel as shown in Fig. 5. They say this is due to higher combustion temperatures and longer combustion duration [23]. The investigation of Schumacher et al. [27] and Marshall et al. [28] report an increase in the biodiesel engine NO_x emissions and concluded that diffusion burning was the controlling factor for the production of NO_x . An almost equal number of investigations report a declining trend in the level of emissions of NO_x e.g. Hamasaki et al. [26].

5.4 Smoke and Particulates (PM)

It might be expected that biodiesel engines would produce less smoke and particulates than standard engines for reasons such as high gas temperatures and high temperatures of the combustion chamber wall. Although some authors have occasionally reported some increases in PM emissions when substituting diesel fuel with biodiesel [29-30], a noticeable decrease in PM emissions with the biodiesel content can be considered as an almost unanimous trend [20-21].

VI. Experimental Setup

The below figure (1) shows the schematic of four stroke diesel engine of variable compression ratio type. The main components of the computerized diesel engine test rig are:

[1] PT Combustion Chamber Pressure Sensor. [2] F1 Liquid fuel flow rate. [3] PTF Fuel Injection Pressure Sensor. [4] F2 Air Flow Rate. [5] FI Fuel Injector. [6] F3 Jacket water flow rate [7]. FP Fuel Pump. [8] F4 Calorimeter water flow rate. [9] T1 Jacket Water Inlet Temperature. [10] LC Load Cell. [11] T2 Jacket Water Outlet Temperature. [12] CA Crank Angle Encoder. [13] T3 Inlet Water Temperature at Calorimeter. [14] EGC Exhaust Gas Calorimeter. [15] T4 Outlet Water Temperature at Calorimeter. [16] T5 Exhaust Gas Temperature before Calorimeter. [17] T6 Exhaust Gas Temperature after Calorimeter.

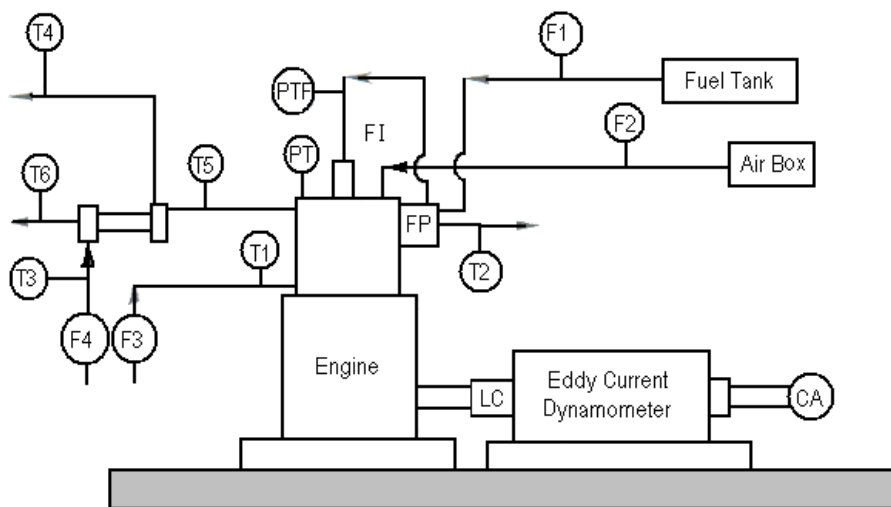


Figure 1: Schematic Diagram of the Experimental Set-up.

VII. Results and Discussion

The performance evaluation is carried out on the diesel engine at various blends of Honge and Jatropha Curcas oil. The present work shows no significant improvement in thermal efficiency (Refer Fig 2 & 3). At blend (B30) both Honge and Jatropha Curcas oil exhibits little increase in brake thermal efficiency and decrease in brake specific fuel consumption (Refer Fig 2, 3, 5 & 6). The results shows that the emission parameters such as Carbon monoxide (CO), Carbon dioxide (CO_2), Hydrocarbons (HC) and oxides of nitrogen (NO_x) decreases with increase in blends and load (Refer Fig 7 to 13). A significant decrease is observed in emission parameters in particular oxides of nitrogen and carbon monoxide and Hydrocarbons; hence the biodiesel proves to be most promising alternate fuel at higher blends.



Figure 4: Maximum Brake Thermal Efficiency v/s Blends

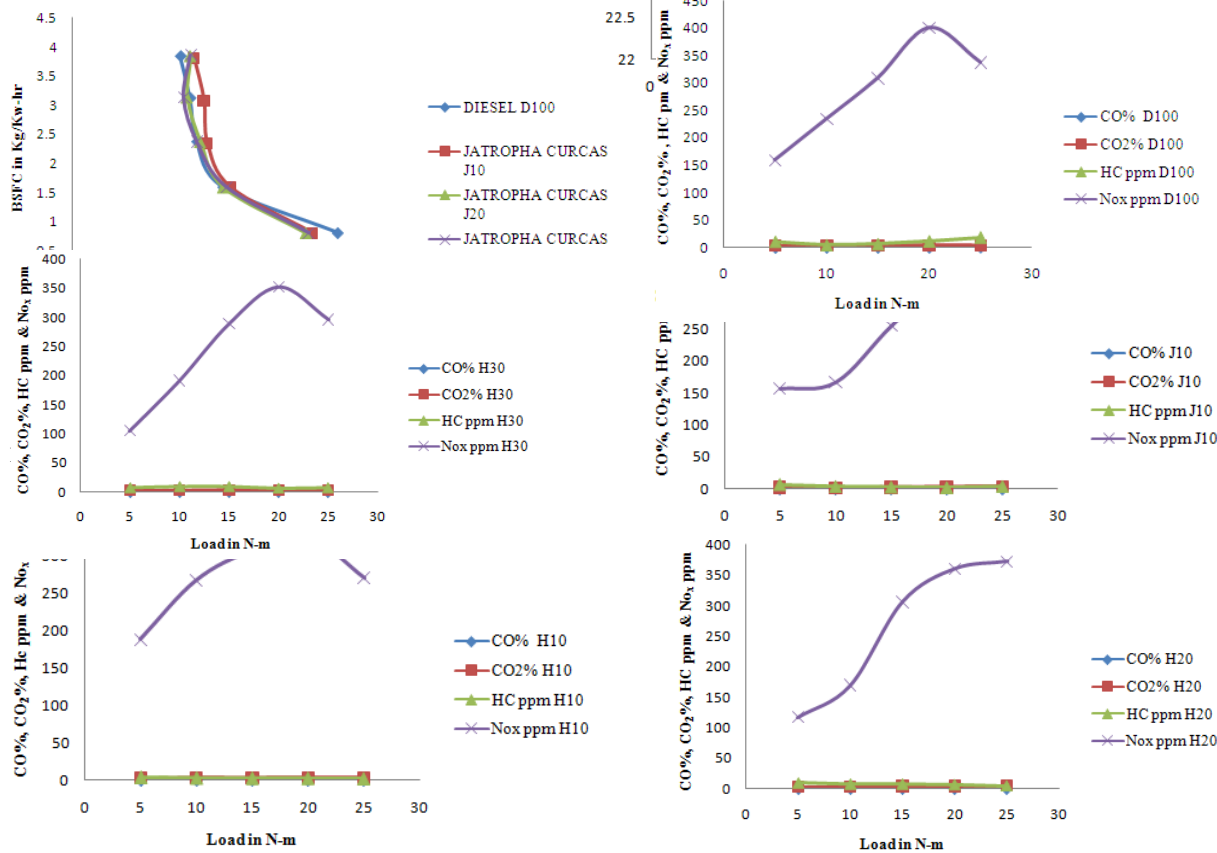


Figure 10: Emission Constituents v/s Load.

Figure 11: Emission Constituents v/s Load.

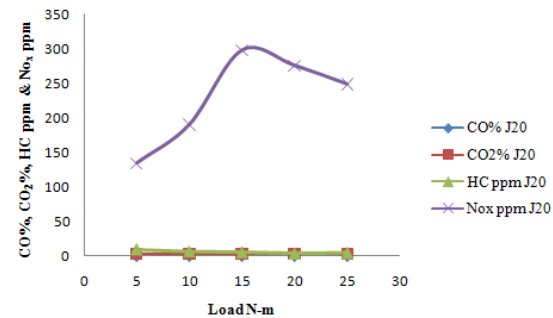


Figure 12: Emission Constituents v/s Load.

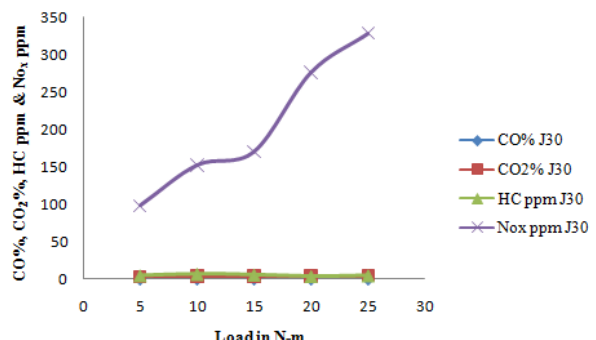


Figure 13: Emission Constituents v/s Load.

REFERENCES

- [1] RAMADHAS A.S, JAYARAJ S, MURALEEDHARAN C, Use Of Vegetable Oils As I.C. Engine Fuel, *A Review Renewable Energy*, 29 (2004), 727-742.
- [2] BARI C.W.YU, LIM T.H, Performance Deterioration and Durability Issues While Running a Diesel Engine with Crude Palm Oil, *Proc. Instn. Mech. Engrs Part - J. Automobile Engineering* 216 (2002), 785-792.
- [3] KAUFMAN KR, ZIEJEWSKI M, Sunflower Methyl Esters for Direct Injected Diesel Engines, *Trans. ASAE* 27 (1984), 1626-1633.
- [4] KALAM MA, MASJUKI H, Biodiesel from Palm Oil-An Analysis of Its Properties and Potential, *Biomass and Bioenergy* 23 (2002), 471-479.
- [5] RAHEMAN H PHADATARE A.G, Diesel Engine Emissions and Performance from Blends of Karanja Methyl Ester and Diesel, *Biomass and Bioenergy* 27 (2004), 393-397.
- [6] M.L. MATHUR AND R.P SHARMA, Internal Combustion Engines Dhanpat Rai Publications, New Delhi, 2010
- [7] BARNWAL B.K AND SHARMA M.P, Aspects of Biodiesel Production from Vegetable Oils in India, *Renewable and Sustainable Energy Reviews*, (2004), 1-16.
- [8] USTA N, OZTURK E, CAN O, CONKUR E.S, NAS S, ÇON A.H, CAN A.C, AND TOPCU M, Combustion of Biodiesel Fuel Produced From Hazelnut Soapstock/Waste Sunflower Oil Mixture in A Diesel Engine, *Energy Conversion and Management*, (2005), 46, 741-755.
- [9] SCHWAB A.W, DYKSTRA G.J., SELKE E, SORENSON S.C, PRYDE EH, *Diesel Fuel from Thermal Decomposition of Soybean oil*, JAOCS 1988; 65:1781-6.
- [10] SCHWAB A.W, BAGBY M.O, FREEDMAN B, Preparation and Properties of Diesel Fuels from Vegetable Oils, *Fuel* (1987), (66), 1372-8.
- [11] BILGIN A, DURGUN, SAHIN Z, The Effects of Diesel-Ethanol Blends On Diesel Engine Performance, *Energy Sources*,(2002), (24), 431-40.
- [12] P.MAHANTA AND A. SHRIVASTAVA, Technology Development of Biodiesel as an Energy Alternative, *Department of Mechanical Engineering*, IIT Guwhati.
- [13] TSOLAKIS A, Effects On Particle Size Distribution from the Diesel Engine Operating on RME-Biodiesel with EGR, *Energy Fuels* 10 (2006) 1021/Ef050385c.
- [14] SENATORE A, CARDONE M, ROCCO V, PRATI M.V, A Comparative Analysis of Combustion Process in D.I. Diesel Engine Fueled With Biodiesel and Diesel Fuel, *SAE Paper* (2000) 2000-01-0691.
- [15] SHAHEED A, SWAIN E, Combustion Analysis of Coconut Oil and Its Methyl Esters in a Diesel Engine, *Proc I MECH E Part A J Power Energy* 213/5 (1999) 417-425.
- [16] GRABOSKI MS, ROSS JD, MCCORMICK RL, Transient Emissions from No. 2 Diesel and Biodiesel Blends in a DDC Series 60 Engine, *SAE Paper* (1996) 961166.
- [17] CANAKCI M, Performance and Emissions Characteristics of Biodiesel from Soybean Oil, *Proc I MECH E Part D J Automob Eng D7* (2005) 915-922.
- [18] KAPLAN C, ARSLAN R, SURMEN A, Performance Characteristics of Sunflower Methyl Esters as Biodiesel, *Energy Sources*, Part A 28 (2006) 751-755.
- [19] AGARWAL AK, DAS LM, Biodiesel Development and Characterization for Use as a Fuel in Compression Ignition Engines, *Trans ASME J Eng Gas Turbine Power* 123 (2001) 440-447.
- [20] MONYEM A, VAN GERPEN JH, The Effect of Biodiesel Oxidation on Engine Performance and Emissions, *Biomass and Bioenergy*, 20 (2001) 317-325.
- [21] PINTO AC, GUARIEIRO LLN, REZENDE MJC, RIBEIRO NM, TORRES EA, LOPES WA, DE P PEREIRA PA, DE ANDRADE JB, Biodiesel: An Overview, *J Braz Chem Soc* 16/6B (2005) 1313-1330.
- [22] Assessment and Standards Division (Office of Transportation and Air Quality of the US Environmental Protection Agency), A Comprehensive Analysis of Biodiesel Impacts on Exhaust Emissions, (2002) EPA420- P-02001.
- [23] LABECKAS G, SLAVINSKAS S, The Effect of Rapeseed Oil Methyl Ester on Direct Injection Diesel Engine Performance and Exhaust Emissions, *Energy Conversion Management* 47 (2006) 1954-1967.
- [24] SERDARI A, FRAGIOUDAKIS K, TEAS C, ZANNIKOS F, STOURNAS S, LOIS E, Effect of Biodiesel Addition To Diesel Fuel on Engine Performance and Emissions, *J Propul Power* 15/2 (1999) 224-231.
- [25] HAMASAKI K, KINOSHITA E, TAJIMA H, TAKASAKI K, MORITA D, Combustion Characteristics of Diesel Engines with Waste Vegetable Oil Methyl Ester, In: *The 5th International Symposium on Diagnostics and Modeling of Combustion in Internal Combustion Engines* (2001) (COMODIA 2001).
- [26] SCHUMACHER LG, BORGELT SC, HIRES WG, FOSSEEN D, GOETZ W, Fueling Diesel Engines with Blends of Methyl Ester Soybean Oil and Diesel, *Fuel*, (1994).
- [27] MARSHALL W, SCHUMACHER LG, HOWELL S, Engine Exhaust Emissions Evaluation of a Cummins L10E When Fuelled With A Biodiesel Blend, *SAE Paper* (1995) 952363.
- [29] Munack A, SCHRODER O, KRAHL J, BUNGER J, Comparison of Relevant Gas Emissions from Biodiesel And Fossil Diesel Fuel, *Agricultural Engineering International: The CIGR Journal of Scientific Research and Development* 3 (2001) Manuscript EE 01 001.



International Journal of Modern Engineering Research (IJMER)

Volume : 4 Issue : 2 (Version-2)

ISSN : 2249-6645

February - 2014

Contents :

Journey from Six Sigma to Lean Six Sigma: A Literature Review <i>Tapan Vora, Prof. P. M. Ramanan</i>	01-03
Probabilistic Modeling and Performance Analysis of A 2(K)-Out-Of-3(N) System with Inspection Subject To Operational Restriction <i>G. S. Mokaddis, Y. M. Ayed, H. S. Al-Hajeri</i>	04-11
Propabilistic Analysis of a Man-Machine System Operating Subject To Different Physical Conditions <i>G. S. Mokaddis, Y. M. Ayed, H. S. Al-Hajeri</i>	12-22
Absorption of Nitrogen Dioxide into Sodium Carbonate Solution in Packed Column <i>Dr. Jafar Ghani Majeed</i>	23-35
Some Operation Equation and Applications <i>Ning Chen, Jiqian Chen</i>	36-45
Implementation of Lean Manufacturing Principles in Foundries <i>Praveen Tandon, Dr. Ajay Tiwari, Shashikant Tamrakar</i>	46-50
Review of crosstalk free Network <i>Ramesh Kumar, Vedant Rastogi</i>	51-54
Data and Information Integration: Information Extraction <i>Varnica Verma</i>	55-62
Simulink Model for Cost-effective Analysis of Hybrid System <i>Raja Sekhar Gorthi, K. Giri Babu, Dr. S. Shiv Prasad</i>	63-71
Parking Management System <i>S. B. Baglane, M. S. Kulkarni, S. S. Raut, T. S. Khatavkar</i>	72-77

Journey from Six Sigma to Lean Six Sigma: A Literature Review

Tapan Vora¹, Prof. P. M. Ramanan²

^{1,2}(Department of Production Engineering, VJTI/ Autonomous (affiliated to Mumbai University), India

ABSTRACT : This paper reviews the published literature related to six –sigma and lean six-sigma. The paper shows that how the methodology changes with changing trend and competition. Nowadays, the pressure of competition from multi-national companies had increased and among them is the automotive industry. It is the impact when the level of competition is intensifying as the manufactured vehicles shifts from being national to global. As a part of competition, the important of understanding the implementation of LSS concept is really useful to be a good competitor. The review gives why the industries fail to implement as well how they can overcome it.

Keywords: Six Sigma, Lean, LSS (Lean Six Sigma), DPMO (Defects Per Million Opportunities)

I. Introduction

What is Six Sigma? Imagine yourself as a head of management of an organization. Ask yourself, what is it that your organization produces using different processes. Are the requirements tested? Are the customers satisfied? Is everything working as per desired? There are so many questions that might pop up but crunching all of them to one single answer is not easy. For a successful business, it is essential to keep track of all processes involved and take adequate actions that satisfy the end user and helps maintain an everlasting relationship.

1.1 Six sigma

Motorola engineers expanded on the term in the 1980s when they decided that the traditional quality levels (measuring defects in thousands of opportunities) were inadequate. Instead, they wanted to measure the defects per million opportunities. By using statistical analysis to minimize variation, Six Sigma enables data-based process improvements, but gained momentum after its adoption by General Electric in the mid-1990s. Motorola developed Six Sigma to drive defects to zero, but did not explicitly address the elimination of unnecessary tasks. *Six Sigma* is a data-driven process improvement methodology used to achieve stable and predictable process results, reducing process variation and defects. Snee (1999) defined it as: ‘a business strategy that seeks to identify and eliminate causes of errors or defects or failures in business processes by focusing on outputs that are critical to customers’. Six Sigma methodology is to accelerate the company’s rate of improvement in quality and productivity. *Our conclusions are that Six Sigma is only a distant second to Lean in terms of popularity.*

In one research out of the 17 surveys examined, it was possible to estimate the percentage of organizations implementing Six Sigma based on only eight studies. Based on the four large sample studies we could conclude that the uptake of Six Sigma among organizations has been low, ranging from 5.0% to 15.5%.

Barriers to implement six sigma are that it is too complex to use, difficulty in collecting data, etc. In recent years, companies have begun using Six Sigma Methodology to reduce errors, excessive cycle times, inefficient processes, and cost overruns. The goal of the project was to streamline and standardize the establishment and maintenance of costing and planning for all business activities.

1.2 Lean

The first applications of Lean were recorded in the Michigan plants of Ford in 1913, and were then developed to perfection in Japan (within the Toyota Production System). Lean manufacturing inspects the process by analyzing each task or activity to determine whether it is value-added, is not value-added but necessary, or is not value-added. A value-added activity is something for which the customer is willing to pay. An example of a value-added activity is the maintenance of a satellite operations center. If a contractor was maintaining this center, then an example of a non-value added but necessary activity is an invoice payment. Activities that neither add value nor are necessary should be eliminated.

II. Methodology

2.1 DMAIC (Six Sigma)

Six Sigma as a whole can function primarily in three different mannerisms: As a metric, management system, and methodology. As a metric, Six Sigma can be a scale of how good a company's quality is. To have "Six Sigma" quality standard, a company must only have 3.4 DPMO. As a management system Six Sigma pulls in the concepts of Six Sigma into a corporate business strategy. As a methodology, Six Sigma is represented by the DMAIC model (Goodman, 2012). DMAIC method is applicable in both manufacturing and non-manufacturing industries. DMAIC is defined as follows:

Define – To identifies the problems.

Measure – Gather the right data to accurately assess a problem.

Analyze – Use statistical tools to correctly identify the root causes of a problem.

Improve – Correct the problem (not the symptom).

Control – Put a plan in place to make sure problems stay fixed and sustain the gains.

2.2 Waste elimination process (Lean)

Lean similarly is an approach for improvement in an organization focusing on waste elimination. This waste is of seven types: (1) Overproduction, (2) Waiting, time in queue, (3) Transportation, (4) Non-value-adding processes, (5) Inventory, (6) Motion, and (7) Costs of quality: scrap, rework, and inspection (Pande and Holpp, 2002). In short it is all about maximizing the added value to the customer.

III. Results

Lean is clearly the most popular performance improvement programme with 36% to 40% of the respondents implementing this programme. Six Sigma is the second most popular performance improvement programme with just over 15% of the respondents implementing it. As already mentioned in the introduction, Six Sigma techniques focus on reducing the variation in a process, making them the ideal tools for tackling an incapable but stable process, whereas Lean tools focus more on the elimination of waste and would be the first port of call for streamlining an unstable process. Priority should be given to unstable processes, using Lean tools to eliminate the waste and simplify the process. Once it has stabilized, more advanced statistical tools from the Six Sigma toolbox, can be used to reduce variation and make the process capable. Thus, Lean-Six Sigma came to exist so that we can take the benefits of both of them.

3.1 Lean Six sigma

The management of the company will always be looking for opportunities that will enhance the effectiveness of the company's processes. Lean Six Sigma is one of the significant methodologies of quality management, this seeks to increase productivity and improve quality of process outputs. It emphasizes that imperfection is an opportunity for improvement.

Lean Six Sigma is rooted in the manufacturing industry as well LSS starts with top management. Lean Six Sigma (LSS) is a combination of historical methods for process improvement that focuses on the bottom line and critical-to-customer requirements and that takes both suppliers and customers into account. Lean Six Sigma is a business improvement methodology that aims to maximize shareholders' value by improving quality, speed, customer satisfaction, and costs. It has been widely adopted widely in manufacturing and service industries.

The benefits of Lean Six Sigma in the industrial world (both in manufacturing and services) have been highlighted extensively in the literature and include the following:

1. Ensuring services/products conform to what the customer needs ('voice of the customer').
2. Removing non-value adding steps (waste) in critical business processes.
3. Reducing the cost of poor quality.
4. Reducing the incidence of defective products/transactions.
5. Shortening the cycle time.
6. Delivering the correct product/service at the right time in the right place.

Every customer expects quality, speed and low cost so LSS provide these by DMAIC (Define, Measure, Analyze, Improve, and Control) project management methodology and various lean tools are utilized to streamline processes and enhance productivity. The companies that are the strongest proponents of LSS include General Electric Co., Sony Corporation, Honeywell, TRW Inc., Bombardier, Johnson and Johnson, The Dow Chemical Company, Exxon Mobil Corp., J.P. Morgan Chase & Co., Citibank, GMAC Mortgage Corporation, and John Deere.

Lean Six Sigma combines the principles of both the reduction of the seven types of wastes as well as the reduction of defects in manufacturing operations. The DMAIC cycle (Design, Measure, Analyze, Implement and Control) assists the researchers in reducing the various types of waste throughout the corporation being assessed along with the organization performing the assessment.

Why has the government largely ignore it?

Air Force Base, was recently quoted as saying, "I will tell you that in virtually every one of our major programs we are out of control on cost and schedule" [2]. LSS is designed for process improvement, but its principles can help maintain both cost and schedule control.

A total of 135 organizations were contacted, of which only approximately 10% reported the application of Lean Six Sigma. This is considered quite a negative phenomenon, because the success and prosperity of organizations largely depends on appropriate methods applied for their improvement. Lean Six Sigma does not require the application of new methods and techniques, but expects effective application of proven methods, consistently and correctly. It can bring dramatic improvements and building and developing corporate culture.

The barriers in health care to implement LSS are 1. Measurement: It is often difficult to identify processes, which is required to find out defects. 2. Psychology of workforce: It is particularly important to not use jargonistic language, as this has a high chance of being rejected or accepted with cynicism by medical professionals.

3.2 Critical success factors

Successful LSS application requires committed leadership, education, and institutionalization. Regardless of future names and improvements LSS requires each of the following activities: (1) focusing on what is critical to the customer, (2) emphasizing the bottom line, (3) validating any claims of success, and (4) institutionalizing the process through extensive training programs and certification of expertise.

IV. Conclusion

Lean Six Sigma is an approach that learns from past failures, one of them is insufficient support of management.

Focus on customer, processes, employee characterize the lean Six Sigma as a method of building and developing a new corporate culture and providing organizations with a tool for a competitive advantage.

The integration of this two principles is logical and practical which can bring dramatic improvements. It is not possible to achieve lean processes without statistical control of variables, since it is not possible to achieve a 6 Sigma process level without optimal flows and elimination of waste. However, there are no. of barriers of LSS in services, such as innate characteristics of services, as well as manufacturing origins of LSS that have conditioned service managers to consider them as physical products only.

Journal Papers

- [1] Kenneth D. Shere, Ph.D., Lean Six Sigma: How Does It Affect The Government?, The Journal of Defence Software Engineering, March-2003, 8-11.
- [2] A. Ansari, Seattle University, Diane Lockwood, Seattle University, Emil Thies, Zayed University, Batoul Modarress, Zayed University and Jessie Nino, Seattle University, Application of Six-Sigma in finance: a case study, Journal of Case Research in Business and Economics.
- [3] Nabeel Mandahawia, Rami H. Fouad*,a, Suleiman Obeidata, An Application of Customized Lean Six Sigma to Enhance Productivity at a Paper Manufacturing Company, Jordan Journal of Mechanical and Industrial Engineering, 6(1), Feb. 2012, 103-109.
- [4] Boyer, K. K. (1996), An assessment of managerial commitment to lean production, International Journal of Operation Management, 16 (9), 48-59
- [5] Alessandro Laureani, Lean Six Sigma in the service industry, Advanced topic in Applied Operations Mangement
- [6] Elliot Boldt and Matthew Franchetti, Total Sustainability Assesments for Manufacturing Operations Using the Lean Six Sigma Approach, Science Journal of Environmental Engineering Research, ISSN:2276-7495,201

Probabilistic Modeling and Performance Analysis of A 2(K)-Out-Of-3(N) System with Inspection Subject To Operational Restriction

G. S. Mokaddis¹, Y. M. Ayed², H. S. Al-Hajeri³

¹Ain shams University, Department of Mathematics, Faculty of Science, Cairo, Egypt.

²Suez University, Department of Mathematics, Faculty of Science, Suez, Egypt

³Kuwait University, Faculty of Science, Kuwait

ABSTRACT: In repairable redundant the failed units can either be repaired or replaced by identical standby to reduce the system down time. The failed units are inspected for repair/replacement. In this paper, one stochastic model for 2(k)-out-of-3(n) redundant system of identical units with repair and inspection are examined stochastically. The system is considered in up-state only if 2(k)-out-of-3(n) units are operative in this model. Normally, the server either attends the system promptly or may take some time, after failure. The system is studied under an operational restriction on the inspection i.e. in case when system has only one unit in operational mode the server has to attend the system for inspection. Semi- Markov processes and regenerative point technique is adopted to obtain the expressions for measures of system effectiveness such as transition probabilities, mean sojourn times, to system failure , steady state availability, busy period, expected number of visits etc. Cost-analysis is also carried out for the system model.

Keywords: Probabilistic modeling, performance analysis, regenerative point, semi-Markov process, mean sojourn times, availability, busy period.

I. Introduction

Redundancy techniques are widely used to improve system performance in terms of reliability and availability. Among various redundancy techniques standby is the simplest and commonly accepted one. In general there are three types of standby; cold, worm and hot standby. Hot standby implies that the redundant (spare) unit or component has same failure rate as when it is in operation mode where as in case of cold standby the failure rate of the redundant unit or component is zero and it can't fail in standby mode. Between hot and cold there is an intermediate case known as worm standby. In this case the failure rate of redundant unit lies in between that of hot and cold standby.

In order to reduce the down time redundancy is necessary. In literature, many researchers have been discussed the reliability and availability of standby systems in detail by considering different cases and strategies such as by considering weather conditions [2] , replacement policy with spares [3], dissimilar unit system with perfect or imperfect switch [4].

In this paper a probabilistic model of a 2(k)-out-of-3 (n) worms standby systems are examined stochastically. Such system found applications in various fields including the process industry, network design and many more. For such a system when an operating unit fails the standby unit becomes operative after repaired and the system works if at least 2k-out-of-3(n) units are in operative mode. In this model , server attends the system promptly whenever needed and first inspects the failed unit to see the practicability of its repair. If repair of the unit is not practicable, it is replaced by new one so that unnecessary expanses on repair can be avoided. In real life, it is not always possible for the server to attend the system swiftly when required may because of his pre-occupation. In such a situation server may be allowed to take some time to reach the system. But it is urgently required that the server must arrive at the system promptly in case of urgent situation. In this model, the standby server do not takes time to arrive at the system when 2(k)-out-of 3(n) units are operative. While in case when the system has only one unit in operational mode the server has to attend the system swiftly for inspection due to operational restriction imposed on it, so that the down time of the system may be reduced. Failure time follows negative exponential distribution while repair and inspection times follow arbitrary distributions. All the random variable are mutually independent and un-correlated. The expressions for

various measures of system performances such as transition probabilities, sojourn times, MTSF (mean time of system failure), availability, busy period of server and profit function are down for steady state.

II. Notations

- N_0 Units in normal mode and operative.
- $\overline{N_0}$ Units in normal mode but not working.
- S_i i^{th} transition state.
- a/b Probability that repair is useful/not useful.
- c/d Probability that repair is useful/not useful of the standby unit.
- λ Constant failure rate of an operative unit.
- α Constant failure rate of an warm standby unit.
- $q_{ij}(t)/Q_{ij}(t)$ pdf/cdf of first passage time from a regenerative state i to a regenerative state j or to a failed state without visiting any other regenerative state in (0,t].
- $q_{ij.kr}(t)/Q_{ij.kr}(t)$ pdf/cdf of first passage time from a regenerative state i to a regenerative state j or to a failed state j visiting states k, r once in (0,t].
- h(t)/H(t) pdf/cdf of inspection time.
- g(t)/G(t) pdf/cdf of repair time of the server.
- $F_{wi}/F_{WI}/F_{ui}/F_{UI}$ Unit is completely failed and waiting for inspection/ waiting for inspection continuously from previous state/ under inspection/ under continuous inspection from previous state.
- F_{ur}/F_{UR} Unit is completely failed and under repair/ under repair continuously from previous state.
- $p_{ij}/p_{ij.kr}$ Probability of transition from regenerative state i to state j without visiting any other state in (0,t]/ visiting state k,r once in (0,t].
- */ & Laplace/ laplace-stiltje's transform.

III. Transition States

The following are the possible transition states of system. The state S_0, S_1, S_2, S_3, S_4 are regenerative states while states $S_5, S_6, S_7, S_8, S_9, S_{10}$ are failed and non-regenerative stat.

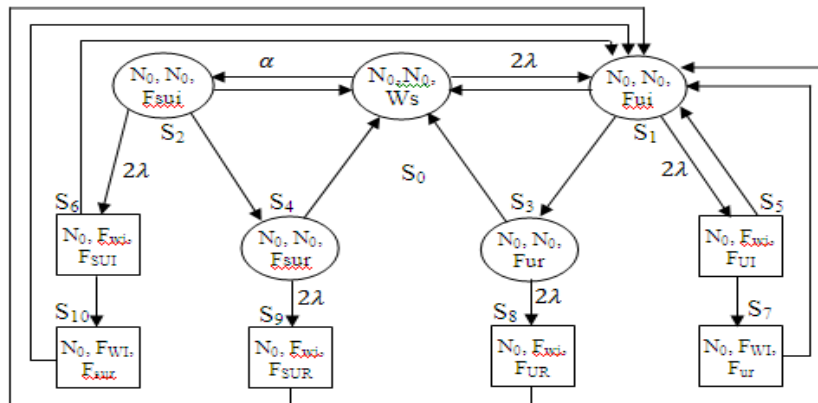


Figure. 1 : State Transition diagram

○ Up state □ Down state

Transition states:-

- $S_0(N_0, N_0, W_s)$: two units are operative and the other unit is kept as worm standby
- $S_1(N_0, N_0, F_{ui})$: two units are operative and the other unit is under inspection

- $S_2(N_0, N_0, F_{sui})$: two unit are operative and the standby unit is under inspection
 $S_3(N_0, N_0, F_{ur})$: two units are operative and the other unit is under repair
 $S_4(N_0, N_0, F_{sur})$: two units are operative and the standby unit is under repair
 $S_5(\bar{N}_0, F_{wi}, F_{UI})$: one unit is normal but not working , the second unit is wait for inspection and the third unit is still under inspection
 $S_6(\bar{N}_0, F_{wi}, F_{SUI})$: one unit is normal but not working , the second unit is wait for inspection and the standby unit is still under inspection
 $S_7(\bar{N}_0, F_{WI}, F_{ur})$: one unit is normal but not working , the second unit is still wait for inspection and the third unit is under repair
 $S_8(\bar{N}_0, F_{wi}, F_{UR})$: one unit is normal but not working , the second unit is wait for inspection and the third unit is still under repair
 $S_9(\bar{N}_0, F_{wi}, F_{SUR})$: one unit is normal but not working , the second unit is wait for inspection and the standby unit is still under repair
 $S_{10}(\bar{N}_0, F_{WI}, F_{sur})$: one unit is normal but not working , the second unit is still wait for inspection and the standby unit is under repair

IV. Transition Probabilities

1. We shall consider the state transition from state S_0 , there are two transitions one to state S_1 and one to S_2 . Therefore,

$$P_{01} = \int_0^{\infty} 2\lambda e^{2\lambda t} e^{-\alpha t} dt = \frac{2\lambda}{2\lambda + \alpha}, P_{02} = \int_0^{\infty} \alpha e^{2\lambda t} e^{-\alpha t} dt = \frac{\alpha}{2\lambda + \alpha}$$

Thus, it can easily regarded that

$$P_{01} + P_{02} = 1.$$

2. In state S_1 , there are three transitions one to state S_0 , one to state S_3 , and one to state S_5 . Therefore,

$$P_{10} = b \int_0^{\infty} h(t) e^{-2\lambda t} dt, \quad P_{13} = a \int_0^{\infty} h(t) e^{-2\lambda t} dt, \quad P_{15} = 2\lambda \int_0^{\infty} e^{-2\lambda t} \bar{H}(t) dt,$$

Thus, it can easily regarded that

$$P_{10} + P_{13} + P_{15} = 1$$

3. In state S_2 , there are three transitions one to state S_0 , one to state S_4 , and one to state S_6 . Therefore,

$$P_{20} = c \int_0^{\infty} h(t) e^{-2\lambda t} dt, \quad P_{24} = d \int_0^{\infty} h(t) e^{-2\lambda t} dt, \quad P_{26} = 2\lambda \int_0^{\infty} e^{-2\lambda t} \bar{H}(t) dt,$$

Thus, it can easily regarded that

$$P_{20} + P_{24} + P_{26} = 1.$$

4. In state S_3 , there are two transitions one to state S_0 , one to state S_8 . Therefore,

$$P_{30} = \int_0^{\infty} g(t) e^{-2\lambda t} dt, \quad P_{38} = 2\lambda \int_0^{\infty} e^{-2\lambda t} \bar{G}(t) dt,$$

Thus, it can easily regarded that

$$P_{30} + P_{38} = 1.$$

5. In state S_4 , there are two transitions one to state S_0 , one to state S_9 . Therefore,

$$P_{40} = \int_0^{\infty} g_s(t) e^{-2\lambda t} dt, \quad P_{49} = 2\lambda \int_0^{\infty} e^{-2\lambda t} \overline{G}_s(t) dt,$$

Thus, it can easily regarded that

$$P_{40} + P_{49} = 1.$$

6. In state S_5 , there are two transitions one to state S_1 , one to state S_7 . Therefore,

$$P_{51} = b \int_0^{\infty} h(t) dt, \quad P_{57} = a \int_0^{\infty} h(t) dt,$$

Thus, it can easily regarded that

$$P_{51} + P_{57} = 1.$$

7. In state S_6 , there are two transitions one to state S_1 , one to state S_{10} . Therefore,

$$P_{61} = c \int_0^{\infty} h(t) dt, \quad P_{610} = d \int_0^{\infty} h(t) dt,$$

Thus, it can easily regarded that

$$P_{61} + P_{610} = 1.$$

8. In state S_7 , there is one transition to state S_1 . Therefore,

$$P_{71} = \int_0^{\infty} g(t) dt$$

9. In state S_8 , there is one transition to state S_1 . Therefore,

$$P_{81} = \int_0^{\infty} g(t) dt$$

10. In state S_9 , there is one transition to state S_1 . Therefore,

$$P_{91} = \int_0^{\infty} g_s(t) dt$$

11. In state S_{10} , there is one transition to state S_1 . Therefore,

$$P_{101} = \int_0^{\infty} g_s(t) dt$$

The mean sojourn times μ_i , in state S_i is given by: -

$$\mu_0 = \int_0^{\infty} e^{-2\lambda t} e^{-\alpha t} dt, \quad \mu_1 = \int_0^{\infty} \overline{H}(t) e^{-2\lambda t} dt, \quad \mu_2 = \int_0^{\infty} \overline{H}(t) e^{-2\lambda t} dt,$$

$$\mu_3 = \int_0^{\infty} \overline{G}(t) e^{-2\lambda t} dt, \quad \mu_4 = \int_0^{\infty} \overline{G}_s(t) e^{-2\lambda t} dt.$$

(4.1)

V. MTSF Analysis

On the basis of arguments used for regenerative processes, we obtain the expressions for cdf ($\phi_i(t)$) of first passage times from regenerative state i to a failed states

$$\phi_i(t) = \sum_{ij} \phi_{ij}(t) \& \phi_{ij}(t)$$

Their for

$$\begin{aligned} \pi_0(t) &= Q_{01}(t) \& \pi_1(t) + Q_{02}(t) \& \pi_2(t), \\ \pi_1(t) &= Q_{10}(t) \& \pi_0(t) + Q_{13}(t) \& \pi_3(t) + Q_{15}, \\ \pi_2(t) &= Q_{20}(t) \& \pi_0(t) + Q_{24}(t) \& \pi_3(t) + Q_{26}, \\ \pi_3(t) &= Q_{30}(t) \& \pi_0(t) + Q_{38}(t), \\ \pi_4(t) &= Q_{40}(t) \& \pi_0(t) + Q_{49}(t). \end{aligned} \tag{5.1}$$

Taking Laplace-Stieltjes transform for this equations and solving for $\tilde{\pi}_0(0)$ we get the Mean Time to System Failure (MTSF) which is given by

$$\left. \frac{-d}{ds} \tilde{\pi}_0(s) \right|_{s=0} = \frac{(D_1'(0) - N_1'(0))}{D_1(0)}, \tag{5.2}$$

where,

$$\text{MTSF} = \frac{\mu_0 + P_{01}\mu_1 + P_{02}\mu_2}{1 - P_{01}P_{10} + P_{02}P_{20}}. \tag{5.3}$$

VI. Availability Analysis

The following probabilistic arguments

$$\begin{aligned} M_0(t) &= e^{-2\lambda t} e^{-\alpha t}, & M_1(t) &= e^{-2\lambda t} \bar{H}(t), \\ M_2(t) &= e^{-2\lambda t} \bar{H}(t), & M_3(t) &= e^{-2\lambda t} \bar{G}(t), \\ M_4(t) &= e^{-2\lambda t} \bar{G}_s(t). \end{aligned} \tag{6.1}$$

Can be used in the theory of regenerative process in order to find the point wise availabilities $A_i(t)$ as shown in following recursive relations:-

$$\begin{aligned} A_0(t) &= M_0(t) + Q_{01}(t) \odot A_1(t) + Q_{02}(t) \odot A_2(t), \\ A_1(t) &= M_1(t) + Q_{10}(t) \odot A_0(t) + Q_{13}(t) \odot A_3(t) + Q_{11}^5(t) \odot A_1(t) \\ &\quad + Q_{11}^{57}(t) \odot A_1(t), \\ A_2(t) &= M_2(t) + Q_{20}(t) \odot A_0(t) + Q_{24}(t) \odot A_4(t) + Q_{21}^6(t) \odot A_1(t) \\ &\quad + Q_{21}^{610}(t) \odot A_1(t), \\ A_3(t) &= M_3(t) + Q_{30}(t) \odot A_0(t) + Q_{31}^8(t) \odot A_1(t), \\ A_4(t) &= M_4(t) + Q_{40}(t) \odot A_0(t) + Q_{41}^9(t) \odot A_1(t). \end{aligned} \tag{6.2}$$

Using Laplace transform for equations and solving for $A_0^*(s)$ we can calculate the steady state availability such that

$$A_0 = \lim_{s \rightarrow 0} sA_0^*(s) = \frac{N_2(0)}{D_2'(0)} \tag{6.3}$$

$$D_2'(0) = \mu_0(p_{10} + p_{13}p_{30}) + \mu_1(1 - p_{02}(p_{20} + p_{24}p_{40})) + \mu_2(p_{02}(p_{10} + p_{13}p_{30})) + \mu_3p_{13}(1 - p_{02}(p_{20} + p_{24}p_{40})) + \mu_4p_{02}p_{24}(p_{10} + p_{13}p_{30}).$$

$$N_2 = \mu_0(1 - p_{11}^5 - p_{13}p_{31}^8 - p_{11}^{57}) + \mu_1(p_{01} + p_{02}(p_{21}^6 + p_{24}p_{41}^9 + p_{21}^{610})) + \mu_2(p_{02}(1 - p_{11}^5 - p_{13}p_{31}^8 - p_{11}^{57})) + \mu_3p_{13}(p_{01} + p_{02}(p_{21}^6 + p_{24}p_{41}^9 + p_{21}^{610})) + \mu_4p_{02}p_{24}(1 - p_{11}^5 - p_{13}p_{31}^8 - p_{11}^{57}).$$

VII. Busy Period Analysis

The following probabilistic arguments

$$W_1(t) = e^{-2\lambda t} \overline{H}(t), \quad W_2(t) = e^{-2\lambda t} \overline{H}(t),$$

$$W_3(t) = e^{-2\lambda t} \overline{G}(t), \quad W_4(t) = e^{-2\lambda t} \overline{G}_s(t). \tag{7.1}$$

Can be used in the theory of regenerative process in order to find the busy period analysis for the expert repairman $B_i(t)$ (the probability that the operative unit is under repair at time t) as shown in following recessive relations:-

$$B_0(t) = Q_{01}(t) \& B_1(t) + Q_{02}(t) \& B_2(t),$$

$$B_1(t) = W_1(t) + Q_{10}(t) \& B_0(t) + Q_{13}(t) \& B_3(t) + Q_{11}^5(t) \& B_1(t) + Q_{11}^{57}(t) \& B_1(t),$$

$$B_2(t) = W_2(t) + Q_{20}(t) \& B_0(t) + Q_{24}(t) \& B_4(t) + Q_{21}^6(t) \& B_1(t) + Q_{21}^{610}(t) \& B_1(t),$$

$$B_3(t) = W_3(t) + Q_{30}(t) \& B_0(t) + Q_{31}^8(t) \& B_1(t),$$

$$B_4(t) = W_4(t) + Q_{40}(t) \& B_0(t) + Q_{41}^9(t) \& B_1(t). \tag{7.2}$$

After using Laplace transform for equations and solving for $B_0^*(s)$ we can calculate the busy period analysis steady such that

$$B_0 = \lim_{s \rightarrow 0} s\tilde{B}_0(s) = \frac{N_3(0)}{D_2'(0)} \tag{7.3}$$

where,

$$N_3 = \mu_1(p_{01} + p_{02}(p_{21}^6 + p_{24}p_{41}^9 + p_{21}^{610})) + \mu_2(p_{02}(1 - p_{11}^5 - p_{13}p_{31}^8 - p_{11}^{57})) + \mu_3p_{13}(p_{01} + p_{02}(p_{21}^6 + p_{24}p_{41}^9 + p_{21}^{610})) + \mu_4p_{02}p_{24}(1 - p_{11}^5 - p_{13}p_{31}^8 - p_{11}^{57}). \tag{7.4}$$

VIII. The Expected Profit Gained In (0, T]

Profit = total revenue in (0,t]- total expenditure incurred in (0,t] i.e.

At steady state the net expected profit per unit of time is:

$$\text{Profit} = \lim_{t \rightarrow \infty} G(t)/t = C_1A_0 - C_2B_0, \tag{8.1}$$

where,

C_1 : is revenue per unit uptime by the system.

C_2 : is per unit repair cost.

IX. Special Cases

The failure and repair times are exponential distributions

$$G(t) = 1 - e^{-\beta t}, \quad G_s(t) = 1 - e^{-\theta t}, \quad H(t) = 1 - e^{-\gamma t}. \quad (9.1)$$

3.10- GRAPHICAL REPRESENTATION

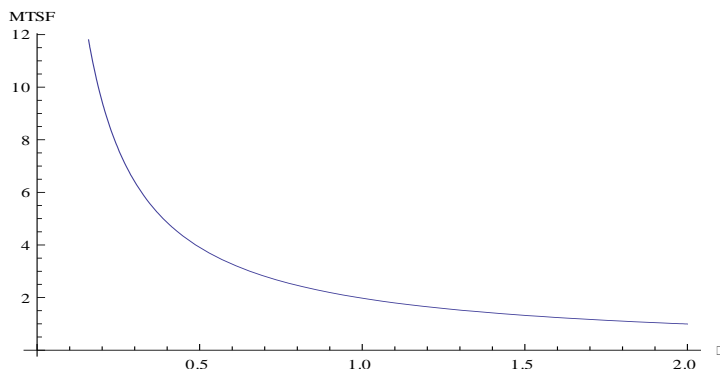


Fig. 2 MTSF vs. failure rate λ

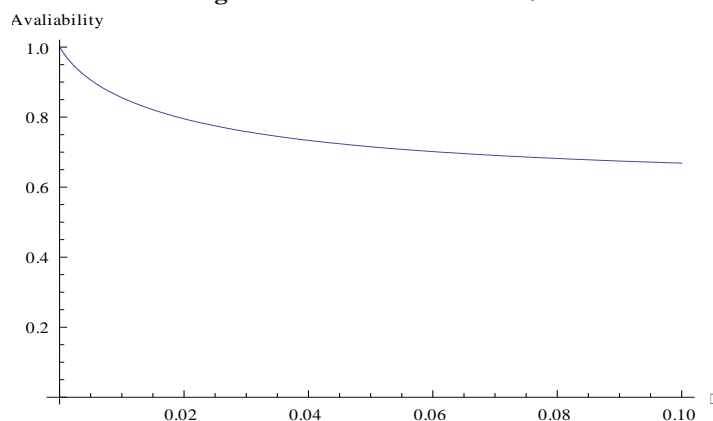


Fig. 3 Availability vs. failure rate λ

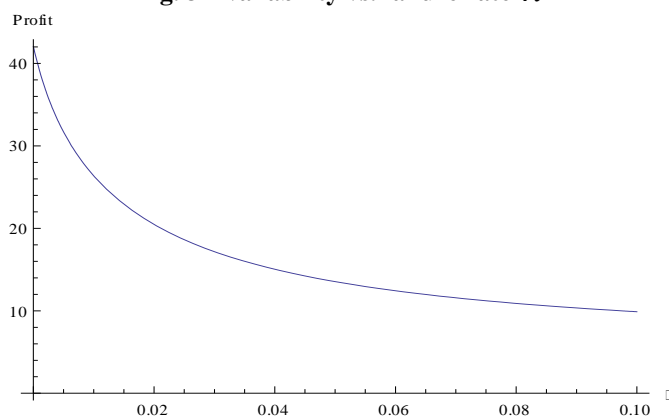


Fig. 4 Profit vs. failure rate λ

X. Summary

A 2(k)-out-of-3(n) worm standby system of identical units with arbitrary distribution of repair and inspection under operational restrictions is studied. Expressions for various system performance characteristics are drawn by using semi-Markov processes and re-generative point technique. By using these expressions, the analytical as well numerical solutions of measures of performance can be obtained for the system in transient and steady states.

In each figure we vary the parameter in question and fix the rest for consistency. It is evident from figures 2 – 4 that the increase in deterioration or failure rates induces decrease in MTSF, availability and profit.

REFERENCES

- [1]. Barlow, R E. and Proschan, F. *Mathematical Theory of Reliability*, John Wiley, New York (1965).
- [2]. Goel, L. R., Sharma, G. C., and Gupta, P., "Cost analysis of a two unit standby system under different weather conditions", *Microelectron. Reliab.*, Vol. 25, No. 4, pp. 655-659, (1985).
- [3]. Nakagawa, T. "A replacement policy maximizing MTTF of a system with several spare units", *IEEE Transactions on Reliability*, 38(8), p. 1277-1287, (1989).
- [4]. Mokaddis G.S., Labib S.W. and El Said M.K.H. two models for two dissimilar-unit standby redundant system with three types of repair facilities and perfect or imperfect switch, *Micro electron. Reliab.*, 34(7), pp. 1239–1247,(1994).
- [5]. Singh, S.K. Profit evaluation of a tow- unit cold standby system with random appearance and disappearance time of the service facility. *Microelectron. Reliab.*, 29, p. 705-709, (1989).
- [6]. Yadavalli V.S.S., Both M. and Bekker, A. Asymptotic confidence limits for the steady state availability of a tow – unit parallel system with "preparation time" for the repair facility, *Asia Pac J Oper Res*,19(2),p.249-256,(2002).

Probabilistic Analysis of a Man-Machine System Operating Subject To Different Physical Conditions

G. S. Mokaddis¹, Y. M. Ayed², H. S. Al-Hajeri³

¹Ain shams University, Department of Mathematics, Faculty of Science, Cairo, Egypt.

²Suez University, Department of Mathematics, Faculty of Science, Suez, Egypt

³Kuwait University, Faculty of Science, Kuwait

ABSTRACT: This paper deals with the stochastic behavior of a single unit of man-machine system operating under different physical conditions. Assuming that the failure, repair and physical conditions (good - poor) times are stochastically independent random variables each having an arbitrary distribution. The system is analyzed by the semi-Markov process technique. Some reliability measures of interest to system designers as well as operations managers have been obtained. Explicit expressions for the Laplace-Stieltjes transforms of the distribution function of the first passage time, mean time to system failure, pointwise availability, and steady state availability of the system are obtained. Busy period by the server, expected number of visits by the server and the cost per unit time in steady state of the system are also obtained. Several important results have been derived as particular cases.

Keywords: Availability. Failure rate. Cost function. Busy period.

I. Introduction and Description of The System

Many authors have studied the single-unit system under different conditions and obtain various reliability parameters by using the theory of regenerative process, Markov renewal process and semi-Markov process [2, 3].

This paper investigates the model of a single-unit operating by a person who may be in good or poor physical condition. The failure, physical conditions and repair times are stochastically independent random variables each having an arbitrary distribution. The unit may fail in one of three ways, the first is due to hardware failure, the second is due to human error when operator is in good physical condition and the third is due to human error when operator is in poor physical condition. The operator reports to work in good physical condition which may change to poor is generally distributed. He can revive to good physical condition with another arbitrary distribution. It is assumed that when the system is down and the operator is in good physical condition, it can't determine as he is supposed to be at rest. Repair time distributions for the three types of failure are taken arbitrary. Repair facility is always available with the system to repair the failed unit and after repair of the unit becomes like new. Using the semi-Markov process technique, and the results of the regenerative process, several reliability measures of interest to system designers are obtained as the distribution time to the system failure. The mean time to system failure, pointwise availability and steady state availability, busy period by the server, expected number of visits by the server and the cost per unit time in a steady state of the system are also obtained. The results obtained by [5,6] are derived from the present paper as special cases. In this system the following assumptions and notations are used to analysis the system.

- (1) The system consists of a single unit which can operate by a person in good or poor physical condition.
- (2) The unit fails in one of three ways; the first is due to hardware failure, the second is due to human error when operator is in good physical condition and the third is due to human error when operator is in poor physical condition.
- (3) Failure, physical conditions and repair times are stochastically independent random variables each having an arbitrary distribution.
- (4) The operator reports to work in good physical condition which may change to poor and vice versa are stochastically independent random variables each having an arbitrary distribution.
- (5) When the system is down and the operator is in good physical condition, it cannot deteriorate as he is supposed to be at rest.
- (6) There is a single repair facility with the system to repair the failed unit.
- (7) On repair of the failed unit, it acts like a new unit.
- (8) All random variables are mutually independent.

II. Notations and States of the System

E_0	state of the system at epoch $t = 0$,
E	set of regenerative states; $\{ S_0, S_1, S_2, S_3, S_4, S_5 \}$, as in fig. 1,
\bar{E}	set of non-regenerative state; $\{ S_6, S_7 \}$, as in fig. 1
$f(t), F(t)$	pdf and cdf of failure time of the unit due to hardware failure,
$f_1(t), F_1(t)$	pdf and cdf of failure time of the unit due to human error; where, the operator is in good physical condition,
$f_2(t), F_2(t)$	pdf and cdf of failure time of the unit due to human error; where, the operator is in poor physical condition,
$l(t), L(t)$	pdf and cdf of change of physical condition from good mode to poor mode,
$h(t), H(t)$	pdf and cdf of change of physical condition from poor mode to good mode,
$g(t), G(t)$	pdf and cdf of time to repair the unit from hardware failure,
$g_1(t), G_1(t)$	pdf and cdf of time to repair the unit from human error; where the operator is in good physical condition,
$g_2(t), G_2(t)$	pdf and cdf of time to repair the unit due to human error; where the operator is in poor physical condition,
$q_{ij}(t), Q_{ij}(t)$	pdf and cdf of first passage time from regenerative state i to a regenerative state i or to a failed state j without visiting any other regenerative state in $(0, t]$; $i, j \in E$,
$q_{ij}^{(k)}(t), Q_{ij}^{(K)}(t)$	pdf and cdf of first passage time from regenerative state i to a regenerative state j or to a failed state j without visiting any other regenerative state in $(0, t]$; $i, j \in E, K \in \bar{E}$,
p_{ij}	one step transition probability from state i to state j ; $i, j \in E$,
p_{ij}^k	probability that the system in state i goes to state j passing through state k ; $i, j \in E, K \in \bar{E}$
$\pi_i(t)$	cdf of first passage time from regenerative state i to a failed state,
$A_i(t)$	probability that the system is in upstate at instant t given that the system started from regenerative state i at time $t = 0$,
$M_i(t)$	probability that the system having started from state i is up at time t without making any transition into any other regenerative state,
$B_i(t)$	probability that the server is busy at time t given that the system entered regenerative state i at time $t = 0$,
$V_i(t)$	expected number of visits by the server given that the system started from regenerative state i at time $t = 0$,
μ_{ij}	contribution mean sojourn time in state i when transition is to state j is $-\tilde{Q}_{ij}(0) = q_{ij}^*(0)$,
μ_i	Mean sojourn time in state i , $\mu_i = \sum_j [\mu_{ij} + \sum_k \mu_{ij}^{(k)}]$,
\sim	Symbol for Laplace-Stieltjes transform, e.g. $\tilde{F}(s) = \int e^{-st} dF(t)$,
$*$	Symbol for Laplace transform, e.g. $f^*(s) = \int e^{-st} f(t) dt$,
\textcircled{S}	Symbol for Stieltjes convolution, e.g. $A(t) \textcircled{S} B(t) = \int_0^t B(t-u) dA(u)$,

© Symbol for ordinary convolution, e.g. $a(t) \otimes b(t) = \int_0^t a(u) b(t-u) du$

For simplicity, whenever integration limits are $(0, \infty)$, they are not written.

Symbols used for the state

- o Operative unit,
- d The physical condition is good,
- p The physical condition is poor,
- \mathcal{R} The failed unit is under repair when failed due to hardware failure,
- \mathcal{R}_1 The failed unit is under repair when failed due to human error; where the operator is in good physical condition,
- \mathcal{R}_2 The failed unit is under repair when failed due to human error; where the operator is in poor physical condition,
- \mathcal{R} The unit is in continued repair; where the failure is due to hardware failure,
- \mathcal{R}_2 The unit is in continued repair when failed due to human error; where the operator is in poor physical condition.

Considering these symbols, the system may be in one of the following states at any instant where the first letter denotes the mode of unit and the second corresponds to physical condition

- $S_0 \equiv (o, d)$, $S_1 \equiv (o, p)$, $S_2 \equiv (r, d)$, $S_3 \equiv (r_1, d)$,
- $S_4 \equiv (r, p)$, $S_5 \equiv (r_2, p)$, $S_6 \equiv (\mathcal{R}, d)$, $S_7 \equiv (\mathcal{R}_2, d)$.

Stated and possible transitions between them are shown in Fig. 1.

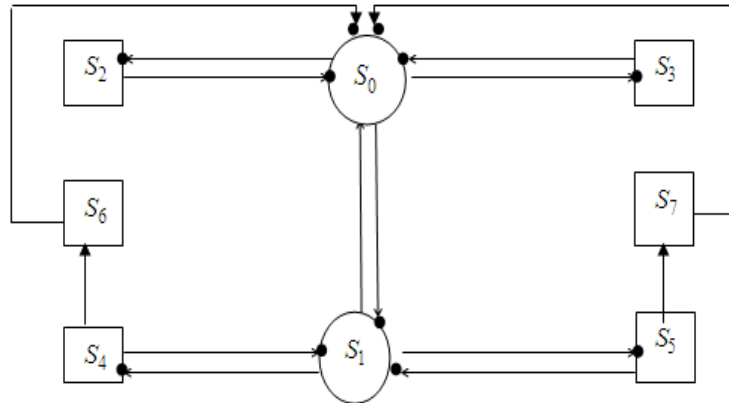
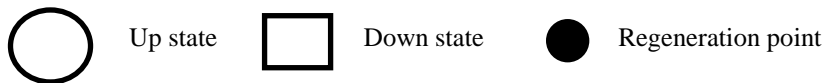


Fig.1 state transition diagram



III. Transition Probabilities And Mean Sojourn Times

It can be observed that the time points of entry into $S_i \in E, i=0,1,2,3,4,5$ are regenerative points so these states are regenerative. Let $T_0 (\equiv 0), T_1, T_2, \dots$ denote the time points at which the system enters any state $S_i \in E$ and X_n denotes the state visited at the time point T_{n+1} , i.e. just after the transition at T_{n+1} , then $\{X_n, T_n\}$ is a Markov-renewal process with state space E and

$$Q_{ij} = P [X_{n+1} = j, T_{n+1} = T_n < t | X_n = i]$$

is a semi-Markov kernel over E. The stochastic matrix of the embedded Markov chain is

$P = (p_{ij}) = (Q_{ij}(\infty)) = Q(\infty)$ and the nonzero elements p_{ij} are

$$p_{01} = \int \ell(t) \bar{F}(t) \bar{F}_1(t) dt, \quad p_{02} = \int f(t) \bar{L}(t) \bar{F}_1(t) dt,$$

$$\begin{aligned}
 p_{03} &= \int f_1(t) \bar{L}(t) \bar{F}(t) dt, & p_{10} &= \int h(t) \bar{F}(t) \bar{F}_2(t) dt, \\
 p_{14} &= \int f(t) \bar{F}_2(t) \bar{H}(t) dt, & p_{15} &= \int f_2(t) \bar{F}(t) \bar{H}(t) dt, \\
 p_{20} = p_{30} &= 1, & p_{41} &= \int g(t) \bar{H}(t) dt, \\
 p_{46} &= \int h(t) \bar{G}(t) dt, & p_{40}^{(6)} &= \iint h(u) g(t) \bar{L}(t-u) dt du, \\
 p_{51} &= \int g_2(t) \bar{H}(t) dt, & p_{57} &= \int h(t) \bar{G}_2(t) dt, \\
 p_{50}^{(7)} &= \iint h(u) g_2(t) \bar{L}(t-u) du dt. \tag{3.1}
 \end{aligned}$$

The mean sojourn times μ_i in state S_i are

$$\begin{aligned}
 \mu_0 &= \int \bar{F}(t) \bar{F}_1(t) \bar{L}(t) dt, & \mu_1 &= \int \bar{F}(t) \bar{F}_2(t) \bar{H}(t) dt, \\
 \mu_2 &= \int \bar{G}(t) \bar{L}(t) dt, & \mu_3 &= \int \bar{G}_1(t) \bar{L}(t) dt, \\
 \mu_4 &= \int \bar{G}(t) \bar{H}(t) dt, & \mu_5 &= \int \bar{G}_2(t) \bar{H}(t) dt, \tag{3.2}
 \end{aligned}$$

IV. Mean Time To System Failure

Time to system failure can be regarded as the first passage to failed states S_6, S_7 which are considered as absorbing. By probabilistic arguments, the following recursive relations for $\pi_i(t)$ are obtained

$$\begin{aligned}
 \pi_0(t) &= Q_{02}(t) + Q_{03}(t) + Q_{01}(t) \odot \pi_1(t), \\
 \pi_1(t) &= Q_{14}(t) + Q_{15}(t) + Q_{10}(t) \odot \pi_0(t) \tag{4.1}
 \end{aligned}$$

Taking Laplace-Stieltjes transforms of equations (4.1) and solving for $\tilde{\pi}_0(s)$, dropping the argument “s” for brevity, it follows

$$\tilde{\pi}_0(s) = N_0(s) / D_0(s), \tag{4.2}$$

where

$$\begin{aligned}
 N_0(s) &= \tilde{Q}_{02} + \tilde{Q}_{03} + \tilde{Q}_{01}(\tilde{Q}_{14} + \tilde{Q}_{15}) \\
 \text{and} \\
 D_0(s) &= 1 - \tilde{Q}_{01}\tilde{Q}_{10}. \tag{4.3}
 \end{aligned}$$

The mean time to system failure with starting state S_0 is given by

$$\text{MTSF} = N_0 / D_0, \tag{4.4}$$

where

$$\begin{aligned}
 N_0 &= \mu_0 + p_{01} \mu_1 \\
 \text{and} \\
 D_0 &= 1 - p_{01} p_{10}. \tag{4.5}
 \end{aligned}$$

V. Availability Analysis

Elementary probability arguments yield the following relations for $A_i(t)$

$$\begin{aligned}
 A_0(t) &= M_0(t) + q_{01}(t) \odot A_1(t) + q_{02}(t) \odot A_2(t) + q_{03}(t) \odot A_3(t), \\
 A_1(t) &= M_1(t) + q_{10}(t) \odot A_0(t) + q_{14}(t) \odot A_4(t) + q_{15}(t) \odot A_5(t), \\
 A_2(t) &= q_{20}(t) \odot A_0(t), \\
 A_3(t) &= q_{30}(t) \odot A_0(t), \\
 A_4(t) &= q_{41}(t) \odot A_1(t) + q_{40}^{(6)}(t) \odot A_0(t),
 \end{aligned}$$

$$A_5(t) = q_{51}(t) \odot A_1(t) + q_{50}^{(7)}(t) \odot A_0(t). \quad (5.1)$$

where

$$M_0(t) = \bar{F}(t) \bar{F}_1(t) \bar{L}(t) \quad , M_1(t) = \bar{F}(t) \bar{F}_2(t) \bar{H}(t) \quad . \quad (5.2)$$

Taking Laplace transforms of equations (5.1) and solving for $A_0^*(s)$, it gives

$$A_0^*(s) = A_1(s) / D_1(s). \quad (5.3)$$

where

$$N_1(s) = M_0^*(1 - q_{14}^* q_{41}^* - q_{15}^* q_{51}^*) + M_1^* q_{01}^*$$

and

$$D_1(s) = (1 - q_{02}^* q_{20}^* - q_{03}^* q_{30}^*) (1 - q_{14}^* q_{41}^* - q_{15}^* q_{51}^*) - q_{01}^* (q_{10}^* + q_{14}^* q_{40}^{(6)*} + q_{15}^* q_{50}^{(7)*}), \quad (5.4)$$

The steady state availability of the system is

$$A_0(\infty) = N_1 / D_1, \quad (5.5)$$

where

$$N_1 = \mu_0 (1 - p_{14} p_{41} - p_{15} p_{51}) + \mu_1 p_{01}$$

and

$$D_1 = (1 - p_{01}) (\mu_{14} p_{41} + p_{14} \mu_{41} + p_{15} \mu_{51} + \mu_{15} p_{51}) + (1 - p_{14} p_{41} - p_{15} p_{51}) (\mu_{02} + p_{02} \mu_{20} + p_{03} \mu_{30} + \mu_{03}) + \mu_{01} (p_{10} + p_{14} p_{40}^{(6)} + p_{15} p_{50}^{(7)}) + p_{01} (\mu_{10} + \mu_{14} p_{40}^{(6)} + p_{14} \mu_{40}^{(6)} + p_{15} \mu_{50}^{(7)} + \mu_{15} p_{50}^{(7)}) . \quad (5.6)$$

VI. Busy Period Analysis

Elementary probability arguments yield the following relations for $B_i(t)$

$$B_0(t) = q_{01}(t) \odot B_1(t) + q_{02}(t) \odot B_2(t) + q_{03}(t) \odot B_3(t),$$

$$B_1(t) = q_{10}(t) \odot B_0(t) + q_{14}(t) \odot B_4(t) + q_{15}(t) \odot B_5(t),$$

$$B_2(t) = V_2(t) + q_{20}(t) \odot B_0(t),$$

$$B_3(t) = V_3(t) + q_{30}(t) \odot B_0(t) ,$$

$$B_4(t) = V_4(t) + q_{41}(t) \odot B_1(t) + q_{40}^{(6)}(t) \odot B_0(t) ,$$

$$B_5(t) = V_5(t) + q_{51}(t) \odot B_1(t) + q_{50}^{(7)}(t) \odot B_0(t) , \quad (6.1)$$

where

$$V_2(t) = \bar{G}(t) \bar{L}(t) \quad , \quad V_3(t) = \bar{G}_1(t) \bar{L}(t) \quad ,$$

$$V_4(t) = \bar{G}(t) \bar{H}(t) \quad , \quad V_5(t) = \bar{G}_2(t) \bar{H}(t) \quad .$$

Taking Laplace transforms of equations (6.1) and solving for $B_0^*(s)$, it gives

$$B_0^*(s) = N_2(s) / D_1(s) \quad , \quad (6.2)$$

where

$$N_2(s) = (q_{02}^* V_2^* + q_{03}^* V_3^*) (1 - q_{14}^* q_{41}^* - q_{15}^* q_{51}^*) + q_{01}^* (q_{14}^* V_4^* + q_{15}^* V_5^*) , \quad (6.3)$$

and

$$D_1(s) \text{ is given by (5.4).}$$

In long run the fraction of time for which the server is busy is given by

$$B_0(\infty) = N_2 / D_1 , \quad (6.4)$$

where

$$N_2 = (p_{02} \mu_2 + p_{03} \mu_3) (1 - p_{14} p_{41} - p_{15} p_{51}) + p_{01} (p_{14} \mu_4 + p_{15} \mu_5) \quad (6.5)$$

and

$$D_1 \text{ is given by (5.6).}$$

The expected busy period of server facility in $(0, t]$ is

$$\mu_b(t) = \text{expected busy time of the repairman in } (0, t] .$$

The repairman may be busy during $(0, t]$ starting from initial state S_0 .

Hence

$$\mu_b(t) = \int_0^t B_0(u) du ,$$

so that

$$\mu_b^*(s) = B_0^*(s) / s .$$

Thus one can evaluate $\mu_b(t)$ by taking inverse Laplace transform of $\mu_b^*(s)$.

Expected idle time of the repairman in $(0, t]$ is

$$\mu_1(t) = 1 - \mu_b(t) .$$

VII. Expected Number of Visits by The Repairman

Elementary probability arguments yield the following relations for $B_i(t)$

$$\begin{aligned} V_0(t) &= Q_{01}(t) \otimes [1 + V_1(t)] + Q_{02}(t) \otimes [1 + V_2(t)] + Q_{03}(t) \otimes [1 + V_3(t)] , \\ V_1(t) &= Q_{10}(t) \otimes [1 + V_0(t)] + Q_{14}(t) \otimes [1 + V_4(t)] + Q_{15}(t) \otimes [1 + V_5(t)] , \\ V_2(t) &= Q_{20}(t) \otimes V_0(t) , \\ V_3(t) &= Q_{30}(t) \otimes V_0(t) , \\ V_4(t) &= Q_{41}(t) \otimes V_1(t) + Q_{40}^{(6)}(t) \otimes V_0(t) , \\ V_5(t) &= Q_{51}(t) \otimes V_1(t) + Q_{50}^{(7)}(t) \otimes V_0(t) , \end{aligned} \tag{7.1}$$

Taking Laplace-Stieltjes transforms of equations (7.1) and solving for $V_0^*(s)$, dropping the argument “s” for brevity, it follows

$$V_0^*(s) = N_3(s) / D_2(s) , \tag{7.2}$$

where

$$N_3(s) = (1 - \tilde{Q}_{01} + \tilde{Q}_{02} + \tilde{Q}_{03})(1 - \tilde{Q}_{14}\tilde{Q}_{41} - \tilde{Q}_{15}\tilde{Q}_{51}) + \tilde{Q}_{01}(\tilde{Q}_{10} + \tilde{Q}_{14} + \tilde{Q}_{15})$$

and

$$\begin{aligned} D_2(s) &= (1 - \tilde{Q}_{02}\tilde{Q}_{20} - \tilde{Q}_{03}\tilde{Q}_{30})(1 - \tilde{Q}_{14}\tilde{Q}_{41} - \tilde{Q}_{15}\tilde{Q}_{51}) \\ &\quad - \tilde{Q}_{01}(\tilde{Q}_{10} + \tilde{Q}_{14}\tilde{Q}_{40}^{(6)} + \tilde{Q}_{15}\tilde{Q}_{50}^{(7)}) \end{aligned} \tag{7.3}$$

In steady state, number of visits per unit is given by

$$V_0(\infty) = N_3 / D_2 , \tag{7.4}$$

where

$$N_3 = 1 + p_{01} - p_{14}p_{41} - p_{15}p_{51}$$

and

$$D_2 = p_{01} [1 - p_{10} - p_{14}(p_{41} + p_{40}^{(6)}) - p_{15}(p_{51} + p_{50}^{(7)})] .$$

VIII. Cost Analysis

The cost function of the system obtained by considering the mean-up time of the system, expected busy period of the server and the expected number of visits by the server, therefore, the expected profit incurred in $(0, t]$ is

$$\begin{aligned} C(t) &= \text{expected total revenue in } (0, t] \\ &\quad - \text{expected total service cost in } (0, t] \\ &\quad - \text{expected cost of visits by server in } (0, t] \\ &= K_1 \mu_{up}(t) - K_2 \mu_b(t) - K_3 V_0(t) . \end{aligned} \tag{8.1}$$

The expected profit per unit time in steady-state is

$$C = K_1 A_0 - K_2 B_0 - K_3 V_0 \tag{8.2}$$

where K_1 is the revenue per unit up time, K_2 is the cost per unit time for which system is under repair and K_3 is the cost per visit by repair facility.

IX. Special Cases

9.1. The single unit with failure and repair exponentially distributed :

Let

α failure rate of the unit due to hardware failure ,

- β failure rate of the unit due to human error; where the operator is in good physical condition ,
- γ failure rate of the unit due to human error; where the operator is in poor physical condition ,
- δ change of physical condition rate from good mode to poor mode ,
- θ change of physical condition rate from poor mode to good mode ,
- ω repair rate of the unit from hardware failure ,
- λ repair rate of the unit from human error; where the operator is in good physical condition ,
- ε repair rate of the unit from human error; where the operator is in poor physical condition .

Transition probabilities are

$$p_{01} = \delta / (\delta + \alpha + \beta) \quad , \quad p_{02} = \alpha / (\delta + \alpha + \beta), \quad p_{03} = \beta / (\delta + \alpha + \beta), \quad p_{10} = \theta / (\theta + \alpha + \gamma),$$

$$p_{14} = \alpha / (\theta + \alpha + \gamma) \quad , \quad p_{15} = \gamma / (\theta + \alpha + \gamma), \quad p_{41} = \omega / (\omega + \theta), \quad p_{46} = \theta / (\omega + \theta),$$

$$p_{51} = \varepsilon / (\varepsilon + \theta) \quad , \quad p_{57} = \theta / (\varepsilon + \theta) \quad , \quad p_{40}^{(6)} = \theta \omega / (\theta + \omega) (\omega + \delta),$$

$$p_{50}^{(7)} = \theta \varepsilon \omega / (\theta + \varepsilon) (\varepsilon + \delta).$$

The mean sojourn times are

$$\mu_0 = 1 / (\alpha + \beta + \delta), \quad \mu_1 = 1 / (\alpha + \gamma + \theta), \quad \mu_2 = 1 / (\omega + \delta), \quad \mu_3 = 1 / (\lambda + \delta),$$

$$\mu_4 = 1 / (\omega + \theta), \quad \mu_5 = 1 / (\varepsilon + \theta) \quad .$$

$$MTSF = \hat{N}_2 / \hat{D}_1 \quad \text{where} \quad \hat{N}_0 = \frac{1}{(\delta + \alpha + \beta)} \left[1 + \frac{\delta}{(\alpha + \gamma + \theta)} \right] \quad , \quad \hat{D}_0 = 1 - \frac{\delta \theta}{(\alpha + \beta + \delta)(\alpha + \gamma + \theta)}$$

in this case, $\hat{M}_i(t)$ are

$$\hat{M}_0(t) = e^{-(\alpha + \beta + \delta)t} \quad , \quad \hat{M}_1(t) = e^{-(\alpha + \gamma + \theta)t}$$

The steady state availability of the system is

$$\hat{A}_0(\infty) = \hat{N}_1 / \hat{D}_1 \quad \text{where,} \quad \hat{N}_1 = \frac{1}{(\delta + \alpha + \beta)} \left\{ 1 - \frac{1}{(\alpha + \gamma + \theta)} \left[\frac{\alpha \omega}{(\omega + \theta)} + \frac{\gamma \varepsilon}{(\varepsilon + \theta)} \right] + \frac{\delta}{(\alpha + \gamma + \theta)} \right\},$$

$$\hat{D}_1 = \frac{1}{(\alpha + \gamma + \theta)} \left[1 - \frac{\delta}{(\alpha + \beta + \delta)} \right]$$

$$\left\{ \frac{\alpha \omega}{(\omega + \theta)} \left[\frac{1}{(\alpha + \gamma + \theta)} + \frac{1}{(\omega + \theta)} \right] + \frac{\gamma \theta}{(\varepsilon + \theta)} \left[\frac{1}{(\alpha + \gamma + \theta)} + \frac{1}{(\omega + \theta)} \right] \right\}$$

$$+ \frac{1}{(\alpha + \beta + \delta)} \left\{ 1 - \frac{1}{(\theta + \alpha + \delta)} \left[\frac{\alpha \omega}{(\omega + \theta)} + \frac{\gamma \varepsilon}{(\varepsilon + \theta)} \right] \right\}$$

$$\left[\frac{(\alpha + \beta)}{(\alpha + \beta + \delta)} + \frac{\alpha}{\omega} + \frac{\beta}{\lambda} \right] + \frac{\delta \theta}{(\alpha + \beta + \delta)^2 (\alpha + \gamma + \theta)}$$

$$\left\{ \left[1 + \frac{\alpha \omega}{(\theta + \omega)(\omega + \delta)} + \frac{\gamma \varepsilon}{(\theta + \varepsilon)(\varepsilon + \delta)} \right] + 2(\delta + \theta) \left[\frac{\alpha \omega^2}{(\omega + \theta)^2 + (\omega + \delta)^2} + \frac{\gamma \varepsilon^2}{(\theta + \varepsilon)^2 (\delta + \varepsilon)^2} \right] \right\},$$

in this case $\hat{V}_i(t)$ are

$$\hat{V}_2(t) = e^{-(\omega + \delta)t} \quad , \quad \hat{V}_3(t) = e^{-(\lambda + \delta)t}$$

$$\hat{V}_4(t) = e^{-(\omega + \theta)t} \quad , \quad \hat{V}_5(t) = e^{-(\varepsilon + \theta)t}$$

In long run, the function of time for which the server is busy is given by

$$\hat{B}_0(\infty) = \hat{N}_2 / \hat{D}_1 \quad ,$$

where

$$\hat{N}_2 = \frac{1}{(\delta + \alpha + \beta)} \left[\frac{1}{(\omega + \delta)} + \frac{1}{(\lambda + \delta)} \right] \left\{ 1 - \frac{1}{(\theta + \alpha + \gamma)} \left[\frac{\alpha \omega}{(\omega + \theta)} + \frac{\gamma \varepsilon}{(\varepsilon + \theta)} \right] \right\}$$

$$+ \frac{\delta}{(\delta + \alpha + \beta)(\theta + \alpha + \gamma)} \left[\frac{\alpha}{(\omega + \theta)} + \frac{\gamma}{(\varepsilon + \theta)} \right]$$

In steady state, number of visits per unit is given by

$$\hat{V}_0(\infty) = \hat{N}_3 / \hat{D}_2, \text{ where, } \hat{N}_3 = 1 + \frac{\delta}{(\delta + \alpha + \beta)} - \frac{1}{(\theta + \alpha + \gamma)} \left[\frac{\alpha\omega}{(\omega + \theta)} + \frac{\gamma\varepsilon}{(\varepsilon + \theta)} \right],$$

$$\hat{D}_2 = \frac{\delta}{(\delta + \alpha + \beta)} \left\{ 1 - \frac{\theta}{(\theta + \alpha + \gamma)} - \frac{\alpha\omega}{(\theta + \alpha + \gamma)(\omega + \theta)} \left[1 + \frac{\theta}{(\omega + \theta)} \right] - \frac{\gamma\varepsilon}{(\theta + \alpha + \gamma)(\varepsilon + \theta)} \left[1 + \frac{\theta}{(\varepsilon + \delta)} \right] \right\}$$

The expected profit per unit time in steady state is

$$\hat{C} = K_1 \hat{A}_0 - K_2 \hat{B}_0 - K_3 \hat{V}_0$$

9.2 Numerical Example :

Let $K_1 = 2000, K_2 = 100, K_3 = 50, \beta = 0.3, \gamma = 0.7, \theta = 0.5, \omega = 0.6, \lambda = 0.4, \varepsilon = 0.1$

Table 1

α	C		
	$\delta = 0.3$	$\delta = 0.5$	$\delta = 0.8$
0.1	1024.2690	1298.3750	1564.9260
0.2	826.5411	1075.1180	1322.3090
0.3	639.8087	890.6446	1123.4460
0.4	476.2774	734.9694	957.9896
0.5	330.6919	601.2720	818.3685
0.6	199.2988	484.7160	698.9977
0.7	100.3174	381.7681	595.7105
0.8	51.9091	189.7883	505.3575
0.9	23.8333	206.7642	425.5283

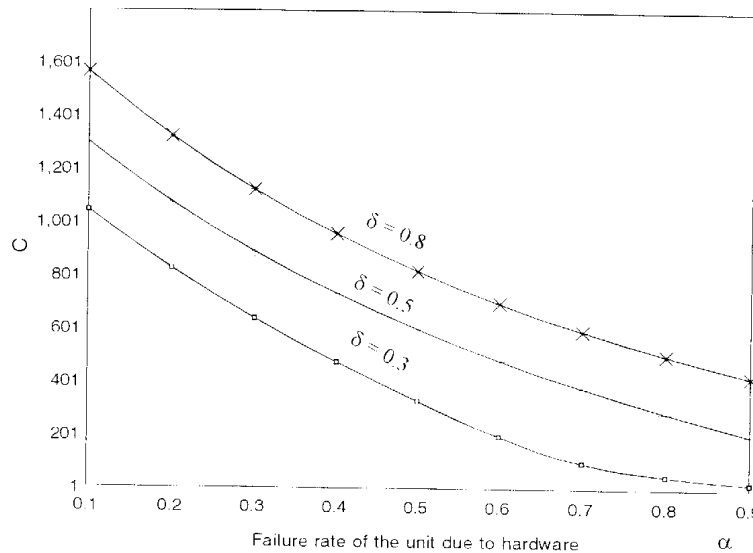


Fig. 2

Relation between the failure rate of the unit due to hardware failure and the cost per unit time.

Let $K_1 = 2000, K_2 = 100, K_3 = 50, \alpha = 0.5, \gamma = 0.4, \theta = 0.5, \omega = 0.6, \lambda = 0.5, \varepsilon = 0.1$

Table 2

β	C		
	$\delta = 0.4$	$\delta = 0.6$	$\delta = 0.8$
0.1	998.1833	1226.7330	1401.331
0.2	785.9746	1014.0950	1183.079
0.3	612.1279	842.9411	1008.1970
0.4	464.8877	700.7023	863.8236
0.5	336.9454	579.4864	741.7718
0.6	223.4917	474.0720	636.5713
0.7	121.2211	380.8579	544.4236
0.8	27.7779	297.2745	462.6036
0.9	10.5644	221.4357	389.1040

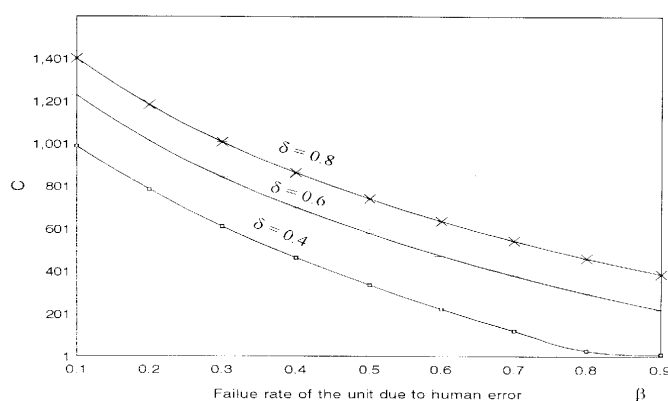


Fig. 3

Relation between the failure rate of the unit due to human error ; where the operator is in good physical condition and the cost per unit time

Let $K_1 = 5000$, $K_2 = 150$, $K_3 = 20$, $\alpha = 0.3$, $\beta = 0.1$, $\delta = 0.7$, $\omega = 0.1$, $\lambda = 0.1$, $\epsilon = 0.1$

Table 3

γ	C		
	$\theta = 0.2$	$\theta = 0.4$	$\theta = 0.6$
0.1	1884.574	1657.749	1479.912
0.2	1808.792	1628.560	1474.749
0.3	1754.425	1603.204	1466.649
0.4	1717.041	1582.434	1458.143
0.5	1693.305	1566.145	1450.294
0.6	1680.808	1553.974	1443.551
0.7	1677.841	1545.511	1438.081
0.8	1673.205	1540.367	1433.920
0.9	1669.083	1538.083	1431.036

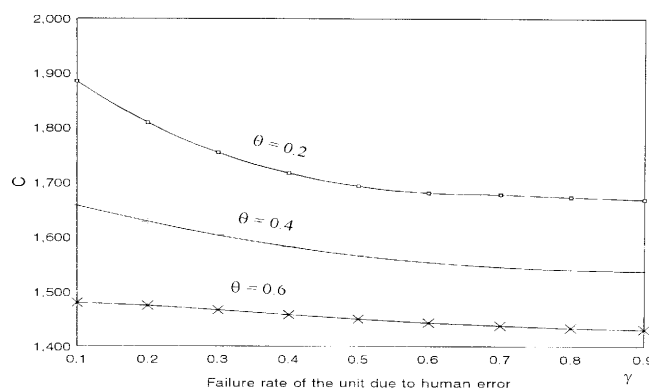


Fig. 4

Relation between the failure rate of the unit due to human error ; where the operator is in poor physical condition and the cost per unit time.

Let $\beta = 0.3$, $\gamma = 0.7$, $\theta = 0.5$.

Table 4

α	MTSF		
	$\delta = 0.2$	$\delta = 0.5$	$\delta = 0.8$
0.1	2.2059	1.9565	1.8103
0.2	1.8182	1.6522	1.5493
0.3	1.5455	1.4286	1.3529
0.4	1.3433	1.2575	1.2000
0.5	1.1875	1.1224	1.0776
0.6	1.0638	1.0132	0.9774
0.7	0.9633	0.9231	0.8940
0.8	0.8800	0.8475	0.8235
0.9	0.8099	0.7831	0.7632

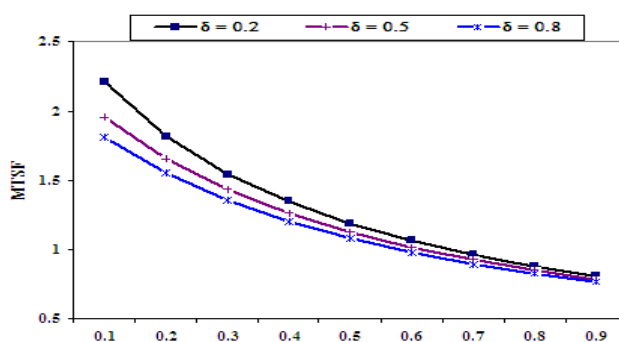


Fig. 5.

α

Relation between the failure rate of the unit due to hardware failure and the mean time to system failure.

Let $\alpha = 0.3$, $\gamma = 0.9$, $\theta = 0.5$.

Table 5

β	MTSF		
	$\delta = 0.2$	$\delta = 0.5$	$\delta = 0.8$
0.1	2.0652	1.7188	1.5244
0.2	1.7431	1.5172	1.3812
0.3	1.5079	1.3580	1.2626
0.4	1.3287	1.2291	1.1628
0.5	1.1875	1.1224	1.0776
0.6	1.0734	1.0329	1.0040
0.7	0.9794	0.9565	0.9398
0.8	0.9005	0.8907	0.8834
0.9	0.8333	0.8333	0.8333

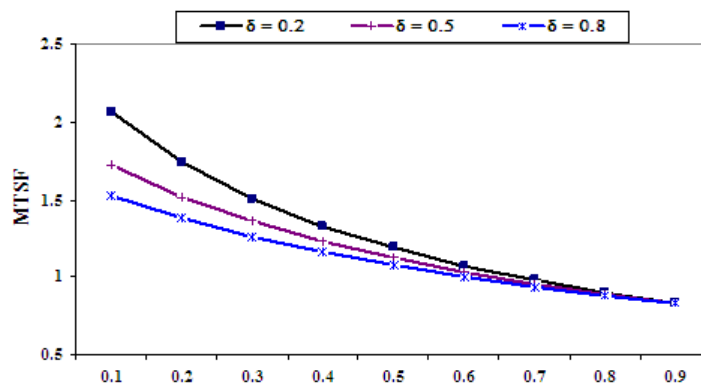


Fig. 6.

β

Relation between the failure rate of the unit due to human error ; where the operator is in good physical condition and the mean time to system failure.

Let $\alpha = 0.2$, $\beta = 0.9$, $\delta = 0.1$.

Table 6

γ	MTSF		
	$\theta = 0.1$	$\theta = 0.4$	$\theta = 0.7$
0.1	1.0638	1.000	0.9735
0.2	1.0169	0.9783	0.9600
0.3	0.9859	0.9615	0.9489
0.4	0.9639	0.9483	0.9396
0.5	0.9474	0.9375	0.9317
0.6	0.9346	0.9286	0.9249
0.7	0.9244	0.9215	0.9189
0.8	0.9160	0.9146	0.9137
0.9	0.9091	0.9091	0.9091

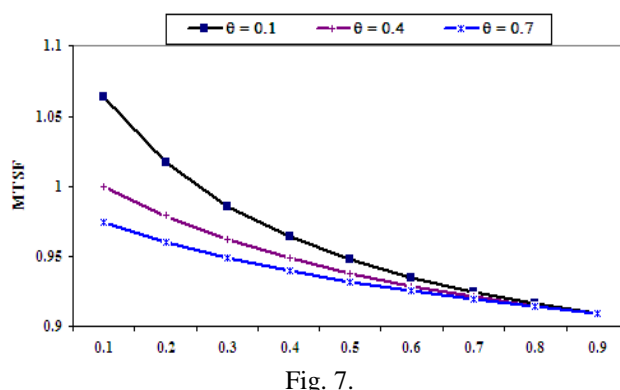


Fig. 7.

Relation between the failure rate of the unit due to human error ; where the operator is in poor physical condition and the mean time to system failure.

X. Summary

Expressions for various system performance characteristics are drawn by using semi-Markov processes and regenerative point technique. By using these expressions, the analytical as well numerical solutions of measures of performance can be obtained for the system in transient and steady states.

In each figure we vary the parameter in question and fix the reset for consistency. It is evident from figures 2-7 that the increase in failure rates (hardware failure and human error where the operating is in good /bad physical condition) induces decrease in MTSF, and cost profit.

REFERENCES

- [1]. Barlow, R.E And Proschan, F., "Mathematical Theory Of Reliability", New York, John Wiley, 1965.
- [2]. Dhillon, B.S., "Stochastic Models For Producing Human Reliability", Microelectron. Reliab., 22, 491, 1982.
- [3]. Dhillon, B.S., "On Human Reliability Bibliography", Microelectron. Reliab., 20, 371, 1980.
- [4]. Feller, W., "An Introduction To Probability Theory And Its Applications", Col. 2, New York, John Wiley, 1957.
- [5]. Goel, L.R., Kumar, A., Rastogi, A.K., "Stochastic Behaviour Of Man-Machine Systems Operating Under Different Weather Conditions", Microelectron. Reliab., 25, No. 1, 87-91, 1985.
- [6]. Mokaddis, G.S., Tawfek, M.L., El-Hssia, S.A.M., "Reliability Analysis Of Man-Machine System Operating Subject To Physical Conditions", Has Been Accepted For Publication In "Microelectronics And Reliability", England, 1996.

Absorption of Nitrogen Dioxide into Sodium Carbonate Solution in Packed Column

Dr. Jafar Ghani Majeed

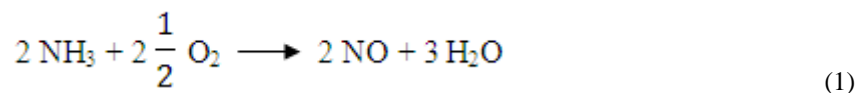
Department of Materials Engineering College of Engineering Al-Mustansiriyah University, Baghdad, Iraq

ABSTRACT: Absorption of nitrogen dioxide (NO₂) gas from (NO₂/Air or NO₂/N₂) gas mixture into sodium carbonate (Na₂CO₃) alkaline solution was performed using packed column in pilot scale. The aim of the study was to improve the Absorption efficiency of this process, to find the optimal operation conditions, and to contribute to the application of this process in the industry. Absorption efficiency (η) was measured by using various operating parameters: gas mixture flow rate (QG) of 20-30 m³/h, nitrogen dioxide inlet concentration (YNO₂) of 500-2500 ppm, experimental temperature (T) of 30-50 °C, Na₂CO₃ solution concentration (CNa₂CO₃) of 10-30 wt %, and liquid holdup in the column (VL) of 0.02-0.03 m³ according to experimental design. The measured η was in the range of $\eta = 60.80-89.43$ %, and of $\eta = 60.10-91.50$ % respectively depending on the operating parameters investigated. Computer program (Statgraphics/Experimental Design) was used to estimate the fitted linear models of η in terms of (QG, YNO₂, CNa₂CO₃, T, and VL), and the economic aspects of the process. The accuracy of η models is ± 2.3 %. The linear models of η were adequate, the operating parameters were significant, and the interactions were negligible. Results of η obtained reveal that a negligible influence of oxidation with a maximum deviation of 2.2 %.

Keywords: Packed column, NO₂ absorption, Na₂CO₃ solution, Absorption efficiency.

I. Introduction

The most important gas- purification is the chemical absorption in which one or more soluble components of a gas mixture are dissolved in the solution. The sources of emissions of toxic gases to atmospheric air are chemical factories as a result of certain chemical reactions or producing different chemical products [1, 2]. Absorption of toxic gases from gas mixtures into chemical solutions is very important task for environment protection. Nitrogen oxides belong to the most troublesome gaseous components polluting atmospheric air. Among several nitrogen oxides (N₂O₃, NO₃, N₂O₃, NO₂, N₂O₄, N₂O₅), the most common in atmospheric air are nitrogen mono oxide (NO) and nitrogen dioxide (NO₂) [1, 3, 4]. In combustion techniques, the total content of (NO + NO₂ converted to NO₂) is marked with a common symbol NO_x [1, 3]. Those pollutions are heavily toxic for human environment. In concentrated nitric acid producing plant, the colorless nitrogen mono oxide (NO) is one of the emissions gases of nitrogen oxides (NO_x) to atmospheric air. The NO gas produces commercially by oxidizing of ammonia gas by air as shown in the chemical equation (1):



Oxidation of nitrogen mono oxide (NO) gas by pure oxygen in presence platinum as catalyst producing brown color gas nitrogen dioxide (NO₂) as seen in the equation (2):



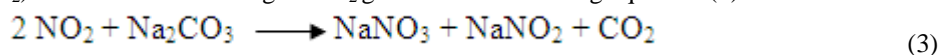
The applied methods of absorption of nitrogen oxides from flue gases in recent years belong to following groups [1, 5]:

- * Catalytic reduction (non-selective catalytic reduction (NSCR), and selective catalytic reduction (SCR).
- * Adsorption.
- * Absorption (acid and alkaline).

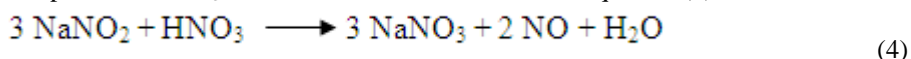
Catalytic reduction is an efficient but very expensive method of gas treatment. It used mainly in highly industrialized countries to neutralize nitrogen oxides from energetic exhaust fumes and from industrial flue gases, which formed during production of nitric acid [1, 5]. Absorption methods exploiting traditional adsorbents have not been commonly used in installation for absorption nitrogen oxides from industrial flue

gases, mainly for economical reasons and because of difficulties connected with regeneration of adsorbent or its utilization. Methods of absorption of nitrogen oxides in solutions belong to the earliest ones in technology of industrial flue gases treatment. Those methods are based on fundamental properties of nitrogen oxides present in gases: their solubility in water [1] or in solutions of nitric acid [6] and sulphuric acid [7] as well as their ability to form appropriate salts, nitrates, and nitrites in reactions with substrate of alkaline character [8]. Application of the alkaline absorption to protect environment is determined by physicochemical properties of nitrogen oxides. Nitrogen dioxide has sufficiently high solubility and reactivity with water and with aqueous alkaline solutions, and as such it can be absorbed in solutions [8-10]. Generally, the methods of absorption are characterized by a simplified technological outlines and simple, typical apparatuses.

In present work alkaline solution of sodium carbonate (Na_2CO_3) is used to absorb nitrogen dioxide (NO_2) from NO_2/Air and NO_2/N_2 gas mixtures separately. Solution of Na_2CO_3 will react with NO_2 gas to produce ($\text{NaNO}_3 + \text{NaNO}_2$) solution with evolving of CO_2 gas as in the following equation (3):



It was difficult in this work to separate NaNO_3 and NaNO_2 solutions from each other, dilute nitric acid of (5-7 wt % HNO_3) is added to produce NaNO_3 solution and could be seen in the equation (4):



NaNO_3 solution and NO gas send to HNO_3 producing factory for further treatment operations.

NO_2 gas is more toxic than NO gas according to OSHA standard. The allowable concentrations for exposure time of 8 hours for NO and NO_2 gases are 25 ppm. and 1 ppm. respectively, where (1 ppm. $\text{NO} = 1.227 \text{ mg/m}^3$, while 1 ppm. $\text{NO}_2 = 1.882 \text{ mg/m}^3$). Many processes have been developed for NO_2 removal from flue gases [11-14] which are based on absorption in aqueous solutions of soluble alkali metal compound. Sodium compounds are preferred over potassium or the other alkali metals strictly on the basis of cost.

II. Experimental Work

2.1 Experimental apparatus:

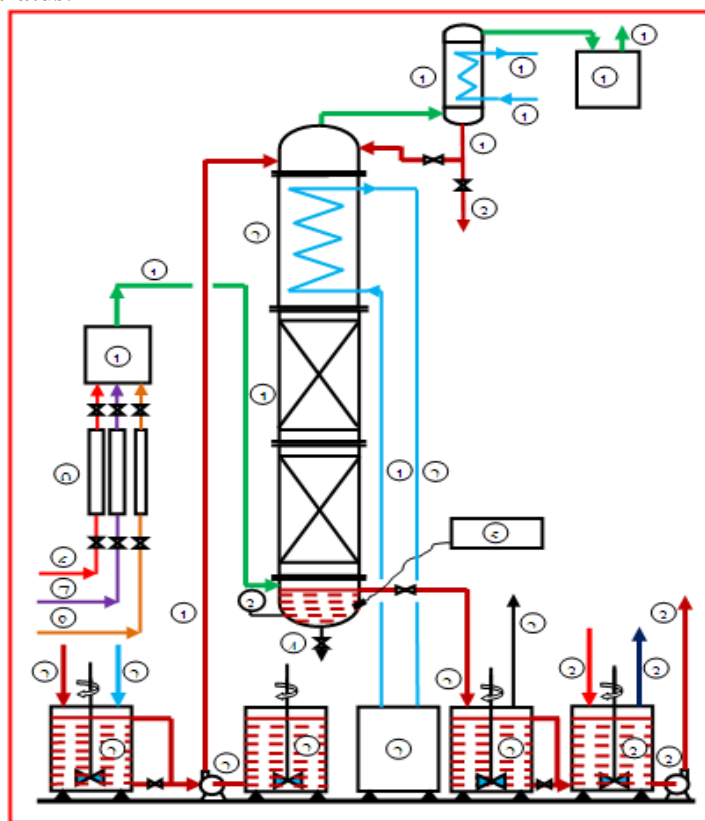


Figure 1: Schematic diagram of the experimental apparatus for NO_2 gas absorption from gas mixture into Na_2CO_3 solution in packed column.

The main equipment of the experimental apparatus as shown in Figure 1 is the packed column (1), and its heat exchanger (2), the size to gather of 3.5 m height and 0.150 m in diameter. The main complementary apparatus and pipe lines are as follows: Temperature gage (3), discharge point (4), digital pH- meter (5), compressed nitrogen in (6), compressed air in (7), nitrogen dioxide gas in (8), nitrogen gas, air, and nitrogen dioxide gas rotameters respectively (9), mixing chamber (10), gas mixture in (11), gas mixture out (12), Na₂CO₃ solution in (13), liquid recycle to top of the column (14), condenser (15), cold water in (16), cold water out (17), NO₂ gas analyzer (18), water to heat exchanger from thermostat (19), water from heat exchanger to thermostat (20), solid Na₂CO₃ (21), process water (22), mixing tank to prepare Na₂CO₃ solution (23), feeding pump of Na₂CO₃ solution to packed column (24), Na₂CO₃ solution tank (25), thermostat water bath (26), (Na₂NO₃, and Na₂NO₂) solution tank (27), (Na₂NO₃, and Na₂NO₂) solution from bottom of column (28), CO₂ gas out (29), stirred tank for reaction of NaNO₂ solution and (5-7 wt %) HNO₃ acid (30), (5-7 wt %) HNO₃ acid in (31), NO gas to nitric acid plant (32), discharge pump of Na₂NO₃ solution (33), Na₂NO₃ solution to sub plant at nitric acid plant for producing powder Na₂NO₃ (34), and drain line (35).

2.2 Operating parameters:

The preliminary experiments were carried out to absorb of NO₂ gas from gas mixture into Na₂CO₃ solution in pilot scale packed column by using experimental apparatus as shown in Figure 1 to find the proper operating parameters could be used in this work. Operating variable parameters were as follows:

- * Gas mixture flow rate (Q_G): 20-30 m³/h.
- * NO₂ gas inlet concentration (Y_{NO_2}): 500-2500 ppm.
- * Na₂CO₃ solution concentration ($C_{Na_2CO_3}$): 10-30 wt %.
- * Experimental temperature (T): 30-50 °C.
- * Liquid holdup in the column (V_L): 0.02-0.03 m³.

2.3 Absorption of NO₂ gas from NO₂/Air gas mixture into Na₂CO₃ solution:

Sodium carbonate (Na₂CO₃) solution and NO₂/Air gas mixture were prepared in the following manners:

2.3.1. Preparation of Na₂CO₃ solution:

Solid Na₂CO₃ (21) and process water (22) are added to mixing tank (23) to prepare Na₂CO₃ solution in the proper concentration range of (10-30) wt % which are required to perform present study.

2.3.2. Preparation of NO₂/Air gas mixture:

The valves of compressed air line (7) and NO₂ gas line (8) are opened in order to measured their volumetric flow rates by using calibrated air and NO₂ rotameters (9), valves in compressed nitrogen line (6) is closed before and after nitrogen rotameter in this case. The NO₂/Air gas mixture (11) is prepared to proper required gas mixture flow rate in the range of (20-30) m³/h, NO₂ gas inlet concentrations in the range of (500-2500) ppm by using the valves before their rotameters, and by mixing them in mixing chamber (10). Volume percent used to determine NO₂ gas inlet concentration in the gas mixture (0.05 v/v % = 500 ppm.).

Experiments of absorption of NO₂ gas from NO₂/Air gas mixture into Na₂CO₃ solution have been carried out using the mentioned various operating parameters by using experimental apparatus as shown in Figure 1, according to experimental design plan seen in Table 1. The gas mixture (11) enters the packed column (1) from lower part, while Na₂CO₃ solution from solution tank (25) by feeding pump (24) enters the upper part of the column. The heat exchanger (2) is maintain the desired temperature constant in packed column (1) during the all experiments runs by circulation water [(19), and (20)] from and to thermostat water bath (26) through the heat exchanger (2). Gas mixture from the top of column enters the condenser (15) to condense any liquid drops with it by cold water (16). The liquid (14) returns back to upper part of the column as recycle liquid or drain out from drain line (35). The NO₂ gas concentration in dry outlet gas mixture is measured by NO₂-gas analyzer (18), then the gas mixture (12) to atmosphere air with few traces of NO₂ gas. In the column, the liquid temperature measured by temperature gage (3), while the pH of the liquid is measured by digital pH-meter (5), the value was in the range of (pH = 6.8- 7.3). The liquid (28) contains (NaNO₃ + NaNO₂) solution from downer part of column sent to solution tank (27).The CO₂ gas (29) evolves to atmosphere air. In stirred tank (30) there is (NaNO₃and NaNO₂) solution, it is difficult to separate them from each other, for that reason (5-7 wt %) HNO₃ acid (31) is added to the stirred tank (30). In the tank, the dilute HNO₃ acid reacts with NaNO₂ solution to produce NaNO₃ solution and NO gas. The NO gas (32) sends to HNO₃ concentrated acid production plant to oxides it to NO₂ gas in presence of platinum as catalyst. The NO₂ gas used to producing nitric acid, while the NaNO₃ solution (34) from tank (30) is transfer by using solution pump (33) to sub plant belongs to HNO₃ acid plant for concentration, crystallization, draying, and milling to produce powder NaNO₃, which is demand product.

2.4. Absorption of NO₂ gas from NO₂/N₂ gas mixture into Na₂CO₃ solution:

In order to check the effect of oxidation on the Absorption efficiency of NO₂ gas absorption into Na₂CO₃ solution in packed column, experiments were performed by using NO₂/N₂ gas mixture instead of NO₂/Air gas mixture according to experimental design plan seen in Table 1, and by using the same experimental apparatus shown in Figure 1.

2.4.1. Preparation of Na₂CO₃ solution:

Na₂CO₃ solution in the concentration range of (10-30) wt % is prepared by the same manner mentioned in section 2.3.1.

2.4.2. Preparation of NO₂/N₂ gas mixture:

From nitric acid plant, compressed nitrogen gas (N₂) and nitrogen dioxide gas (NO₂) are coming to experimental apparatus via lines (6) and (8) respectively after their valves are opening and closing the valve of compressed air line (7). Volumetric flow rates of N₂ gas and NO₂ gas are measured by using their calibrated rotameters. The amount of volumetric flow rates of N₂ gas and NO₂ gas are regulated by valves fixed on their lines before the rotameters. The NO₂/N₂ gas mixture flow rate in line (11) and the inlet NO₂ gas concentration are obtained by mixing the required amounts of flow rates of N₂ gas and the NO₂ gas in mixing chamber (10) by volume relation. The gas mixture flow rate and NO₂ gas inlet concentration in gas mixture were in the range of (20-30) m³/h and (500-2500) ppm. respectively.

Table 1: Experimental design plan for absorption of NO₂ gas from gas mixture into Na₂CO₃ solution.

Run No.	Gas mixture flow rate (Q _G)	NO ₂ gas inlet concentration (Y _{NO2})	Na ₂ CO ₃ solution concentration (C _{Na2CO3})	Experiment temperature (T)	Liquid holdup in the column (V _L)
	(m ³ /h)	(ppm)	(wt %)	(°C)	(m ³)
1	20	500	30	50	0.020
2	20	2500	10	50	0.020
3	30	2500	10	50	0.030
4	25	1500	20	40	0.025
5	30	500	10	30	0.020
6	30	500	30	30	0.020
7	20	500	30	50	0.030
8	25	1500	20	40	0.025
9	20	2500	10	30	0.030
10	20	500	10	50	0.020
11	20	2500	30	30	0.030
12	30	2500	30	50	0.030
13	20	500	10	30	0.030
14	20	500	10	30	0.020
15	30	2500	30	50	0.020
16	30	500	30	30	0.030
17	30	2500	10	30	0.020
18	25	1500	20	40	0.025
19	20	500	30	30	0.030
20	30	1500	10	30	0.030
21	30	500	30	50	0.020
22	20	2500	30	50	0.030
23	30	500	10	50	0.030
24	20	2500	10	50	0.030
25	20	2500	30	50	0.020
26	30	2500	30	30	0.020
27	30	500	30	50	0.030
28	30	500	10	50	0.020
29	30	2500	10	50	0.020

30	30	2500	30	30	0.030
31	20	2500	30	30	0.020
32	20	500	30	30	0.020
33	30	500	10	30	0.030
34	20	500	10	50	0.030
35	20	2500	10	30	0.020

III. Results and Discussion

The absorption of NO₂ gas from NO₂/Air gas mixture (*a*) into sodium carbonate (Na₂CO₃) solution were carried out according to experimental design plan in Table 1 with the variation of gas mixture flow rate (*Q_G*), NO₂ gas inlet concentration (*Y_{NO2}*), experimental temperature (*T*), Na₂CO₃ solution concentration (*C_{Na2CO3}*), and liquid holdup in the column (*V_L*).

In order to check the influence of oxidation on the Absorption efficiency (*η*) of NO₂ gas, experiments were performed by using NO₂/N₂ gas mixture (*b*) instead of NO₂/Air gas mixture (*a*) using the same experiment design plan presented in Table 1

3.1 Definition of Absorption efficiency:

The NO₂ Absorption efficiency (*η*) was defined as [2, 15]:

$$\eta = \frac{Y_{NO2,in} - Y_{NO2,out}}{Y_{NO,in}} \times 100 \tag{5}$$

Where,

η = Absorption efficiency in (%).

Y_{NO2,in} = NO₂ gas inlet concentration in gas mixture in (ppm).

Y_{NO2,out} = NO₂ gas outlet concentration in gas mixture in (ppm).

Absorption efficiency (*η*) was calculated by using equation (5). The Absorption efficiency of NO₂ gas absorption from gas mixture (*a*) was in the range of *η* = **60.80- 89.43 %**, and the Absorption efficiency of NO₂ gas absorption from gas mixture (*b*) was in the range of *η* = **60.10-91.50 %**. The results of Absorption efficiency are summarized in Table 2 and Table 3. The *η* increased with the increase in *Y_{NO2,in}*, *C_{NaCO3}* and *V_L*, and decreased with an increase in *Q_G*, and *T*. The biggest effect of operating parameters on Absorption efficiency was the gas mixture flow rate (*Q_G*), and smallest one was the liquid holdup in the column (*V_L*).

Table 2: Data base of experimental design and results of NO₂ gas absorption from gas mixture (NO₂/Air) into Na₂CO₃ solution.

Run No.	Gas mixture flow rate (<i>Q_G</i>)	NO ₂ Gas inlet concentration (<i>Y_{NO2}</i>)	Na ₂ CO ₃ solution concentration (<i>C_{Na2CO3}</i>)	Experiment temperature (<i>T</i>)	Liquid holdup in the column (<i>V_L</i>)	Absorption efficiency (<i>η</i>)
	(m ³ /h)	(ppm)	(wt %)	(°C)	(m ³)	(%)
1	20	500	30	50	0.020	75.39
2	20	2500	10	50	0.020	79.72
3	30	2500	10	50	0.030	81.55
4	25	1500	20	40	0.025	76.83
5	30	500	10	30	0.020	63.90
6	30	500	30	30	0.020	72.20
7	20	500	30	50	0.030	76.60
8	25	1500	20	40	0.025	75.12
9	20	2500	10	30	0.030	85.78
10	20	500	10	50	0.020	62.52

11	20	2500	30	30	0.030	89.43
12	30	2500	30	50	0.030	81.30
13	20	500	10	30	0.030	70.20
14	20	500	10	30	0.020	68.33
15	30	2500	30	50	0.020	79.10
16	30	500	30	30	0.030	72.44
17	30	2500	10	30	0.020	79.32
18	25	1500	20	40	0.025	74.10
19	20	500	30	30	0.030	77.77
20	30	1500	10	30	0.030	81.55
21	30	500	30	50	0.020	65.55
22	20	2500	30	50	0.030	83.38
23	30	500	10	50	0.030	62.90
24	20	2500	10	50	0.030	81.67
25	20	2500	30	50	0.020	86.16
26	30	2500	30	30	0.020	80.13
27	30	500	30	50	0.030	68.70
28	30	500	10	50	0.020	60.80
29	30	2500	10	50	0.020	77.92
30	30	2500	30	30	0.030	82.50
31	20	2500	30	30	0.020	88.40
32	20	500	30	30	0.020	74.92
33	30	500	10	30	0.030	65.80
34	20	500	10	50	0.030	64.86
35	20	2500	10	30	0.020	83.62

Table 3: Data base of experimental design and results of NO₂ gas absorption from gas mixture (NO₂/N₂) into Na₂CO₃ solution.

Run No.	Gas mixture flow rate (Q_G)	NO ₂ gas inlet concentration (Y_{NO_2})	Na ₂ CO ₃ solution concentration ($C_{Na_2CO_3}$)	Experiment temperature (T)	Liquid holdup in the column (V_L)	Absorption efficiency (η)
	(m ³ /h)	(ppm)	(wt %)	(°C)	(m ³)	(%)
1	20	500	30	50	0.020	75.20
2	20	2500	10	50	0.020	80.01
3	30	2500	10	50	0.030	81.02
4	25	1500	20	40	0.025	77.20
5	30	500	10	30	0.020	68.70
6	30	500	30	30	0.020	69.90
7	20	500	30	50	0.030	77.20
8	25	1500	20	40	0.025	74.90
9	20	2500	10	30	0.030	91.50
10	20	500	10	50	0.020	60.10

11	20	2500	30	30	0.030	90.10
12	30	2500	30	50	0.030	80.90
13	20	500	10	30	0.030	71.20
14	20	500	10	30	0.020	68.10
15	30	2500	30	50	0.020	78.10
16	30	500	30	30	0.030	75.80
17	30	2500	10	30	0.020	79.90
18	25	1500	20	40	0.025	73.93
19	20	500	30	30	0.030	78.11
20	30	1500	10	30	0.030	81.20
21	30	500	30	50	0.020	63.10
22	20	2500	30	50	0.030	82.88
23	30	500	10	50	0.030	63.20
24	20	2500	10	50	0.030	81.21
25	20	2500	30	50	0.020	86.90
26	30	2500	30	30	0.020	80.30
27	30	500	30	50	0.030	68.80
28	30	500	10	50	0.020	61.20
29	30	2500	10	50	0.020	80.00
30	30	2500	30	30	0.030	81.98
31	20	2500	30	30	0.020	86.00
32	20	500	30	30	0.020	75.10
33	30	500	10	30	0.030	65.23
34	20	500	10	50	0.030	64.55
35	20	2500	10	30	0.020	83.42

3.2 Correlation models of Absorption efficiency:

Computer program (Statgraphics/Experimental Design) were used to estimate the fitted linear models of Absorption efficiency (η) of NO₂ gas absorption from different gas mixtures into Na₂CO₃ solution in packed column in terms of operating parameters: Q_G , Y_{NO_2} , T , $C_{Na_2CO_3}$, and V_L .

The model of η in case of NO₂ gas absorption from NO₂/Air gas mixture is:

$$\eta = 73.091 - 0.152 T - 0.454 Q_G + 180.937 V_L + 0.263 C_{Na_2CO_3} + 0.007 Y_{NO_2} \quad (6)$$

While, the model of η in case of NO₂ gas absorption from NO₂/N₂ gas mixture as follows:

$$\eta = 74.229 - 0.194 T - 0.452 Q_G + 242.813 V_L + 0.218 C_{Na_2CO_3} + 0.007 Y_{NO_2} \quad (7)$$

The validity range for the models in equation (6) and equation (7) are:

- $30 \leq T \leq 50$ °C
- $20 \leq Q_G \leq 30$ m³/h
- $0.02 \leq V_L \leq 0.03$ m³
- $10 \leq C_{Na_2CO_3} \leq 30$ wt %
- $500 \leq Y_{NO_2} \leq 2500$ ppm

The accuracy of the η models is ± 2.3 %.

The linear models in equation (6) and equation (7) were adequate, and the operating parameters were significant and were in ordered of $Y_{NO_2} > C_{Na_2CO_3} > Q_G > T > V_L$, and in ordered of $Y_{NO_2} > Q_G > C_{Na_2CO_3} > T > V_L$ respectively. The interactions of operating parameters were negligible.

3.3. Comparison of Absorption efficiencies:

The Pareto Chart of Absorption efficiency (η) of NO₂ gas absorption from NO₂/Air gas mixture (a), and from NO₂/N₂ gas mixture (b) could be seen in Figure 2 and Figure 3.

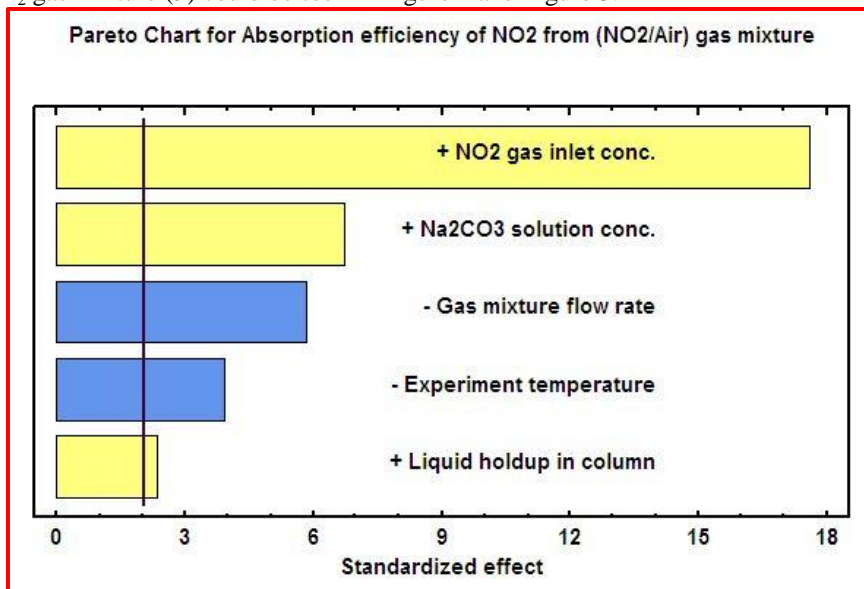


Figure 2: Effects of operating parameters on Absorption efficiency of NO₂ gas

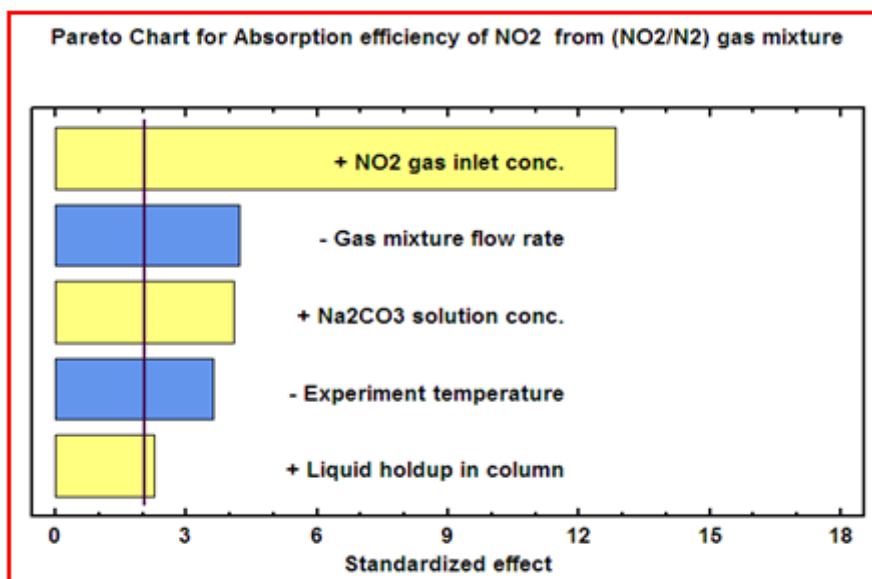


Figure 3: Effects of operating parameters on Absorption efficiency of NO₂ gas

The main effects of operating parameters on Absorption efficiency of NO₂ gas absorption from gas mixers NO₂/Air (a) and from NO₂/N₂ (b) are seen in following Figures (4, 5):

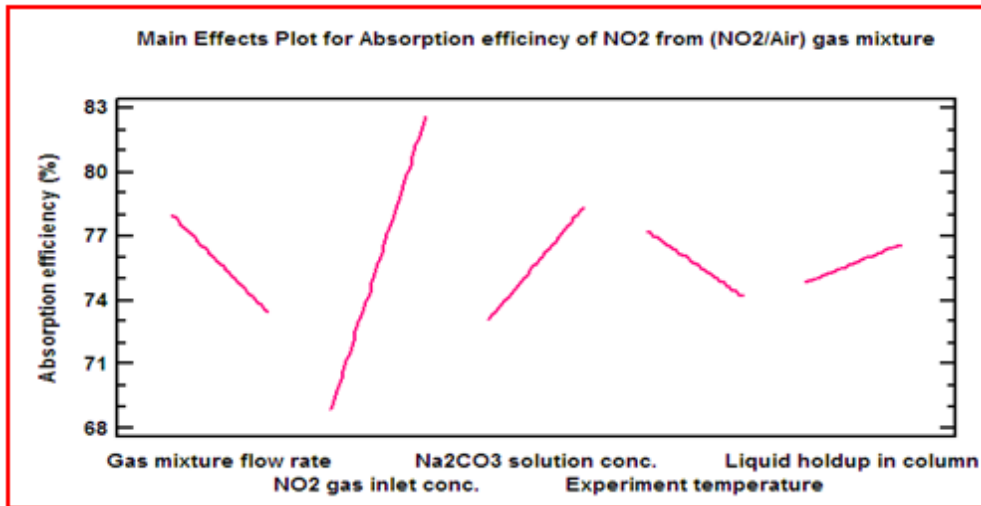


Figure 4: Main effects of operating parameters on Absorption efficiency of NO_2

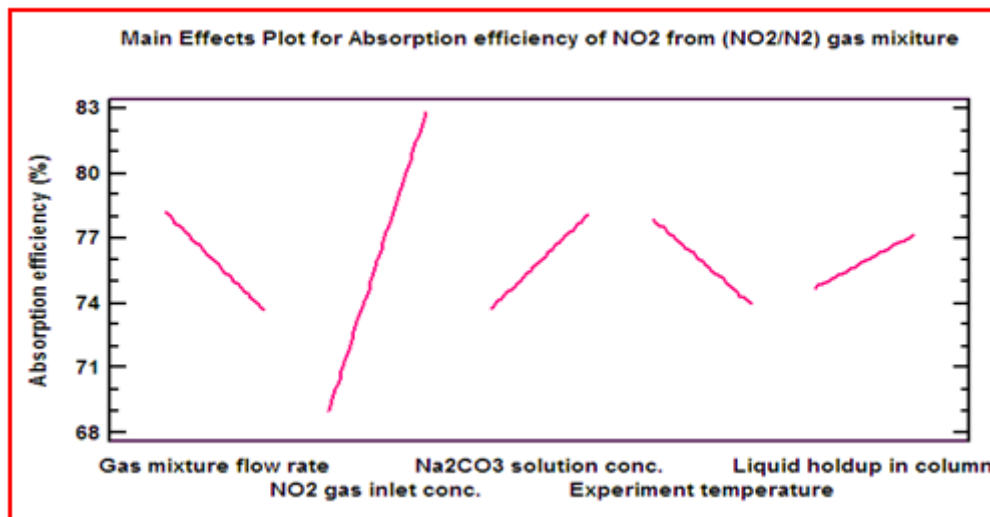


Figure 5: Main effects of operating parameters on Absorption efficiency of NO_2

The observed and predicted Absorption efficiency of NO_2 gas absorption from (NO_2/Air and NO_2/N_2) gas mixture are represent in following Figures (6, and 7) respectively:

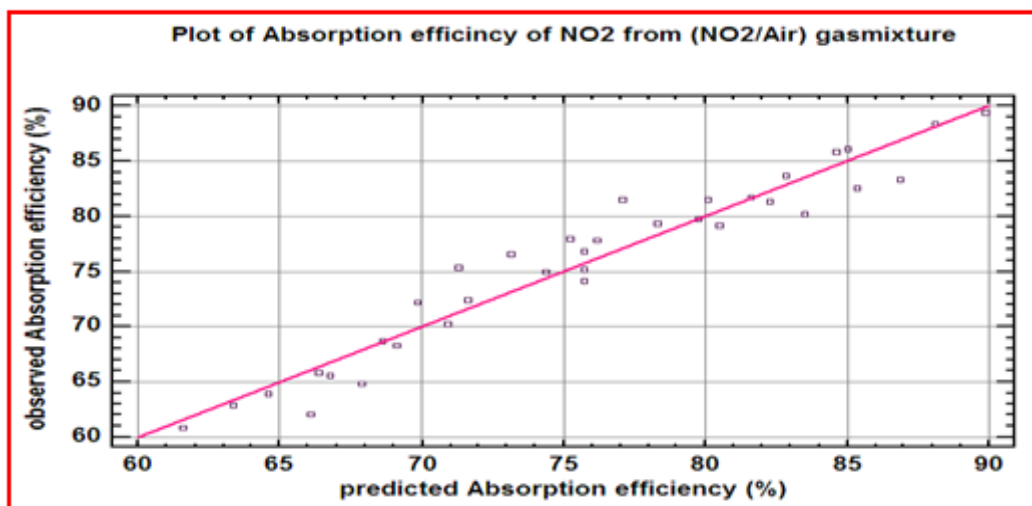


Figure 6: Observed vs. predicted Absorption efficiency of NO_2 gas.

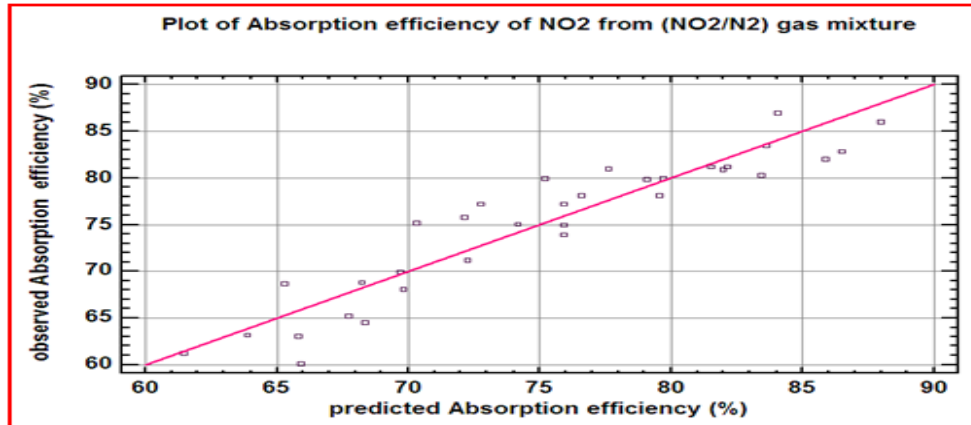


Figure 7: Observed vs. predicted Absorption efficiency of NO₂ gas.

Effects of (Q_G , Y_{NO_2} , T , C_{NaCO_3} , and V_L) on Absorption efficiency (η) of NO₂ gas from NO₂/Air gas mixture (a), and gas NO₂/N₂ gas mixture (b) as shown in Figures (8, 9):

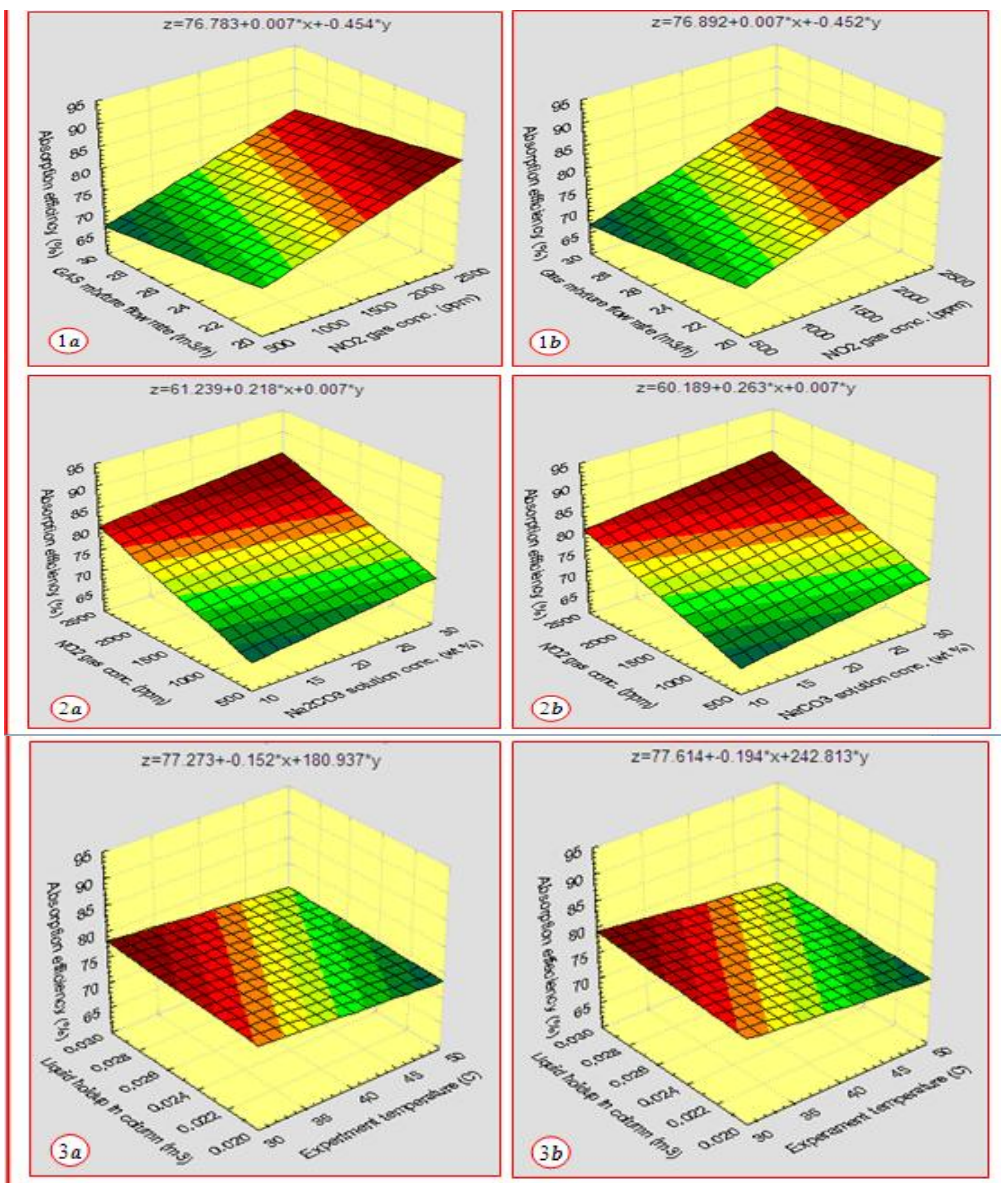


Figure 8: Effects of operating parameters on Absorption efficiency of NO₂

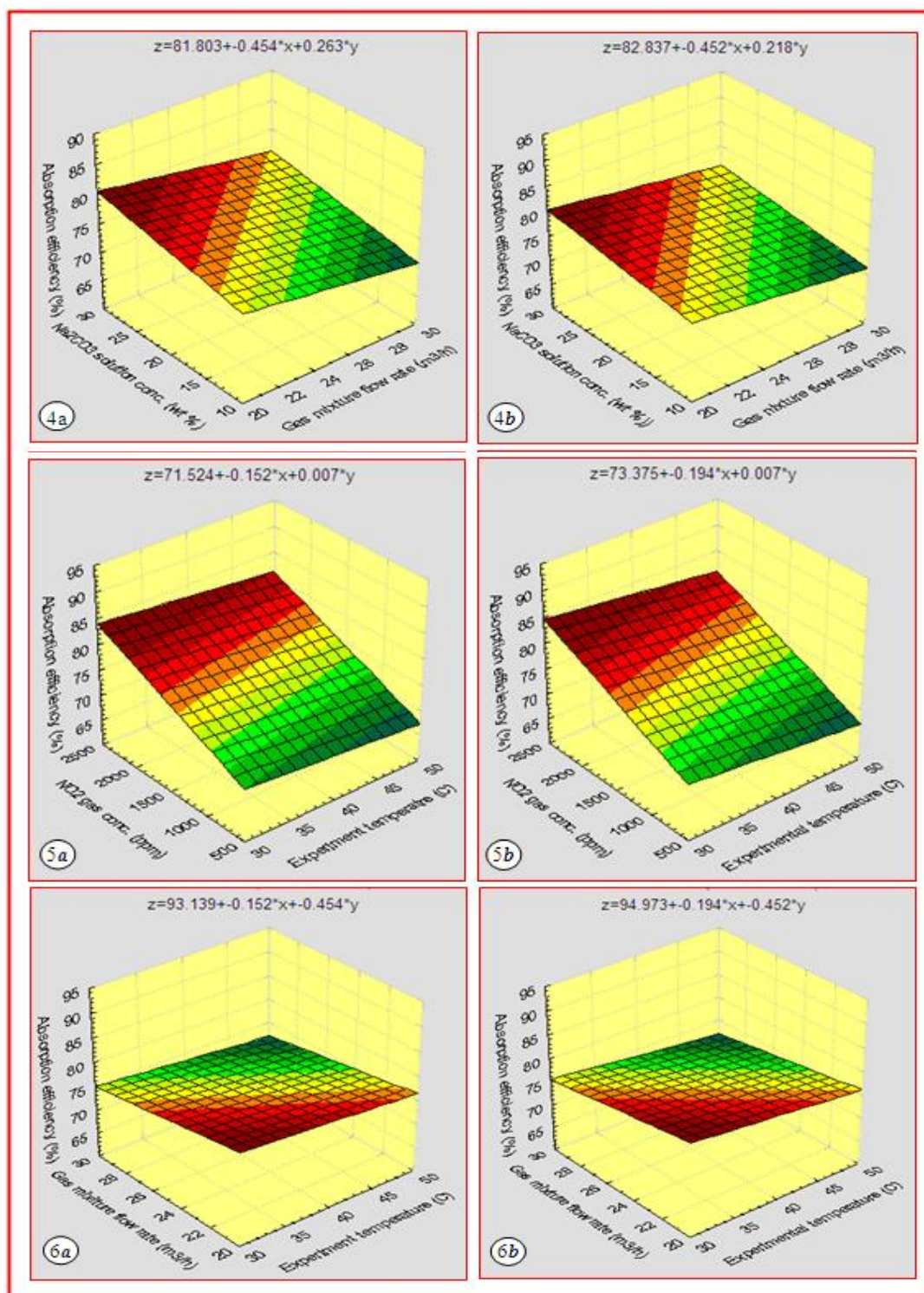


Figure 9: Effects of operating parameters on Absorption efficiency on of NO₂

Figures (8, and 9) are represent the influences of operating parameters (Q_G , Y_{NO_2} , C_{NaCO_3} , T , and V_L) on Absorption efficiency (η) of NO₂ gas absorption from gas mixtures (a and b). In general the η increases with increasing in (Y_{NO_2} , C_{NaCO_3} , and V_L), and decreases with increasing of (Q_G , and T),

3.4. Optimal Response:

The optimum operating parameters for present work were obtained using the computer program to analyze the experimental results. The goal of optimizing was to maximize the Absorption efficiency (η) of NO₂ gas absorption from different gas mixtures. The results of optimizing were summarized in Table 4:

Table 4: Optimum operating parameters and optimum Absorption efficiency of NO₂ gas.

Operating parameters	Low value	High value	Optimum value
Gas mixture flow rate (m ³ /h):	20	30	20
NO ₂ gas inlet conc. (ppm):	500	2500	2500
Na ₂ CO ₃ solution conc. (wt %):	10	30	30
Experimental temperature (°C):	30	50	30
Liquid hold up in column (m ³):	0.02	0.03	0.03
Absorption efficiency of NO ₂ gas from NO ₂ /Air gas mixture (%):			89.88
Absorption efficiency of NO ₂ gas from NO ₂ /N ₂ gas mixture (%):			90.38

IV. Conclusions

* Absorption of NO₂ gas from (NO₂/Air or NO₂/N₂) gas mixture into Na₂CO₃ solution was carried out in pilot scale packed column. The Absorption efficiency (η) of NO₂ gas was measured at various operating conditions (Q_G , Y_{NO_2} , T , C_{NaCO_3} , and V_L) according to experimental design. The measured Absorption efficiency was in the range of $\eta = 60.80$ - 89.43 %, and of $\eta = 60.10$ - 91.50 % respectively. The η could be improved and increases by increasing in the Y_{NO_2} , C_{NaCO_3} , and V_L and with decreasing of Q_G and T .

* A negligible influence of oxidation on Absorption efficiency was observed in this work with a maximum deviation of **2.2** %. For economical reasons we conclude to absorb NO₂ gas from gas mixture by using **Air** as carrier gas instead of N₂ in the gas mixture.

* A computer program (Statgraphics/Experimental Design) was used to estimate the linear fitted models of Absorption efficiency (η) in terms of operating conditions (Q_G , Y_{NO_2} , T , C_{NaCO_3} , and V_L). Both linear fitted models of η were adequate, and operating parameters were significant, while the interactions were negligible. The accuracy of Absorption efficiency models is ± 2.3 %.

* Using the same computer program the optimum operating conditions were obtained with values of $Q_G = 20$ m³/h, $Y_{NO_2} = 2500$ ppm, $C_{NaCO_3} = 30$ wt %, $T = 30$ °C, and $V_L = 0.03$ m³. The optimum Absorption efficiency (η) was in values of **89.88** % and **90.38** % respectively.

* On the base of results of measured Absorption efficiency, we conclude to scaling up the size of the pilot plant used in this study by 3-4 times to commercial size plant and using the optimum operating parameters obtained in future work.

REFERENCES

- [1]. Kurooka J., "Removal of nitrogen oxides from flue gases in a packed column", Environment Protection Engineering, Vol. 37 (1), 2011, pp. 13-22.2.
- [2]. Majeed J.G., Korda B., and Bekassy-Molnar E., "Comparison of the efficiencies of sulfur dioxide absorption using calcium carbonate slurry and sodium hydroxide solution in an ALT reactor", Gas Sep.Purif., Vol. 9 (2),1995, pp. 111-120.
- [3]. Ishibe T.,Santo T.,Hyhashi T., Kato N., and Hata T., "Absorption of nitrogen dioxide and nitric oxide by soda lime", "Journal of Anaesthesia, Vol. 75, 1995, pp. 330-33.
- [4]. Fowler D., Flechard C., Skiba U., Coyle M., and Cape J.N., "The atmospheric budget of oxidized nitrogen and its role in ozone formation and deposition", New Phytol., Vol. 139, 1998, pp. 11-23.
- [5]. Jakubiak M. P., and Kordylewski W. K., "Pilot-scale studies on NO_x removal from flue gas via NO ozonation and absorption into NaOH solution", Chem. Process Eng., Vol. 33 (3), 2012, pp. 345-358.
- [6]. Weisweiler W., "Absorption of NO₂/N₂O₄ in nitric acid", Chem. Eng. Technol., Vol. 13 (1), 1990, pp. 97-101.
- [7]. Lefers J. B., and Berg P. G., "The oxidation and absorption of nitrogen oxides in nitric acid in relation to the tail gas problem of nitric acid plants", Chem. Eng. Sci., Vol. 35 (1-2),1980, pp. 145-159.
- [8]. Glowiski J., Biskupski A., Slonka T., and Ttlus W., "Absorption of nitrogen oxides at the final stage of ammonium nitrate production" Chem. Process Eng., Vol. 30 (2), 2009, pp. 217-229.
- [9]. Lodder P., and Lefers, J. B., "The effect of natural gas, C₂H₆ and CO on the homogeneous gas phase reduction of NO_x by NH₃", Chem. Eng. Journal, Vol. 30 (3), 1985, pp. 161-167.
- [10]. Chanq MB., Lee HM.,Wu F., and Lai CR., "Simultaneous removal of nitrogen oxide/nitrogen dioxide/Sulfur dioxide from gas streams by combined plasma scrubbing technology", J. Air waste Manaq Assoc., Vol. 54 (8), 2004, pp. 941-949.
- [11]. Chu H., Chien T., and Twu B., "Simultaneous Absorption of SO₂ and NO in a stirred Tank Reactor with NaClO₂/NaOH Solutions" Water, Air, and Soil Pollution, Vol. 143 (1-4), 2003, pp. 337-350.
- [12]. Jakubiak M., and Kordylewski W., "Effectiveness of NO_x removal from gas via preoxidation of NO with ozone and absorption in alkaline solution", Chem. Process Eng., Vol. 31 (4), 2010, pp. 699-709.13.
- [13]. Barbooti M. M., Ibraheem N. K., and Ankosh A. H., "Removal of Nitrogen Dioxide and Sulfur Dioxide from Air Streams by Absorption in Urea Solutions" Journal of Environmental Protection, Vol. 2 (2), 2011, pp. 175-185.

- [14]. Modlinski N. J., Kordylewski W. K. , and Jakubiak M. P., “**Numerical Simulation of O_3 and Reacting in Tubular Flow Reactor**”, Chem. Process Eng., Vol. 3 (3), 2013, pp. 361-375.
- [15]. Bekassy-Molnar E., Marki E., and Majeed J.G.,”**Sulphur dioxide absorption in air-lift-tube absorbers by sodium citrate buffer solution**”, Chem. Eng. Processing, Vol. 44, 2005, pp.1059-1046.

Some Operation Equation and Applications

Ning Chen¹, Jiqian Chen²

¹(College of Scienc , Southwest University of Science and Technology, Mianyang 621010, PR China)

²(College of Scienc , Southwest University of Science and Technology, Mianyang 621010, PR China)

ABSTRACT: In this paper, we give several new fixed point theorems to extend results [3]-[4], and we apply the effective modification of He's variation iteration method to solve some nonlinear and linear equations are proceed to examine some a class of integral-differential equations and some partial differential equation, to illustrate the effectiveness and convenience of this method(see[7]). Finally we have also discussed Berge type equation with exact solution.

Keywords: Semi-closed 1-set-contractive operator, Topology degree, Modified variation iteration method, Integral-differential equation, Partial Differential Equation

I. Introduction And Preliminaries

The introduction of the paper should explain the nature of the problem, previous work, purpose, and the contribution of the paper. The contents of each section may be provided to understand easily about the paper. In recent years, the fixed point theory and application has rapidly development.

The topological degree theory and fixed point index theory play an important role in the study of fixed points for various classes of nonlinear operators in Banach spaces (see [1-2],[3]and[4],[7],etc.). The new conclusions of main theorems: Theorem 2.1 and theorem 2.4, theorem 2.6 and theorem 2.7, theorem 3.1 and theorem 4.1. Next, the effective methods of variation iterative method to combine some integral-differential equation and partial differential equations with He's iterative method. First, we need following some definitions and conclusion (see [3]).

Let E be a real Banach space, Ω a bounded open subset of E and θ the zero element of E If $A: \bar{\Omega} \rightarrow E$ is a complete continuous operator, we have some well known theorems for needing Lemma 1.1 as follows (see [3-4]).
Lemma 1.1 (see Corollary 2.1 [3]) Let E be a real Banach Space, Ω is a bounded open subset of E and $\theta \in \Omega$. If $A: \bar{\Omega} \rightarrow E$ is a semi-closed 1-set-contractive operator such that satisfies the Leray-Schauder boundary condition $Ax \neq tx$, for all $x \in \partial\Omega$ and $t \geq 1$, then $\deg(I - A, \Omega, \theta) = 1$, and so A has a fixed point in Ω .

II. Several fixed point theorems

In recent years, some new types fixed point theory and application to study the differential-integral equations in the physic and mechanics fields. Therefore, some application has rapidly development. First, we extended some results as follows. For convenience, we give out following Theorem 2.1.

Theorem2.1 Let E be a real Banach Space, Ω is a bounded open subset of E and $\theta \in \Omega$. If $A: \bar{\Omega} \rightarrow E$ is a semi-closed 1-set-contractive operator such that

$$\|Ax + (m^2 + 1)x\|^{n(\alpha+\beta)+\gamma} \leq \|Ax + mx\|^{n\alpha+\gamma} \|Ax\|^{n\beta} + \|x\|^{n(\alpha+\beta)+\gamma}, \text{ for all } x \in \partial\Omega. \quad (2.1)$$

(where $\alpha > 1, \beta \geq 0, \gamma \geq 0, m, n$ - positive integer)

Then $\deg(I - A, \Omega, \theta) = 1$, if A has no fixed points on $\partial\Omega$ and so A has a fixed point in $\bar{\Omega}$.

Proof By lemma 1.1, we can prove theorem 2.1 .Suppose that A has no fixed point on $\partial\Omega$. Then assume it is not true, there exists $x_0 \in \partial\Omega, \mu_0 \geq 1$ such that $Ax_0 = \mu_0 x_0$.

It is easy to see that $\mu_0 > 1$. Now, consider the function defined by

$$f(t) = (t + (m^2 + 1))^{n(\alpha+\beta)+\gamma} - (t + m)^{n(\alpha+\beta)+\gamma} - 1, \text{ for any } t \geq 1.$$

Since $f'(t) = (n\alpha + n\beta + \gamma)[(t + (m^2 + 1))^{n(\alpha+\beta)+\gamma-1} - (t + m)^{n(\alpha+\beta)+\gamma-1}] > 0, t \geq 1$ and $f'(t) > 0$.

So, $f(t)$ is a strictly increasing function in $[1, +\infty)$, and $f(t) > f(1)$ for $t > 1$. Thus,

Consequently, noting that $\|x_0\| \neq 0, \mu_0 > 1$, we have

$$\begin{aligned} \|Ax_0 + (m^2 + 1)x_0\|^{n(\alpha+\beta)+\gamma} &> [(\mu_0 + m)^{n(\alpha+\beta)+\gamma} + 1]\|x_0\|^{n(\alpha+\beta)+\gamma} \\ &= \|Ax_0 + mx_0\|^{n\alpha+\gamma} \|Ax_0\|^{n\beta} + \|x_0\|^{n(\alpha+\beta)+\gamma}, \end{aligned}$$

which contradicts (2.1), and so the condition $(L-S)$ is satisfied. Therefore, it follows from lemma 1.1 that the conclusion of theorem 2.1 holds.

Corollary 2.2. Let $m = 1$, we get theorem 2.3 [3].

Corollary 2.3. If $\|Ax + (m^2 + 1)x\|^{n(\alpha+\beta)+\gamma} \leq \|Ax + mx\|^{n\alpha+\gamma} \|Ax\|^{n\beta}$, then $\text{deg}(I - A, \Omega, \theta) = 1$ by similar proof method.

In fact, $\|Ax + mx\|^{n\alpha+\gamma} \|Ax\|^{n\beta} \leq \|Ax + mx\|^{n\alpha+\gamma} \|Ax\|^{n\beta} + \|x\|^{n(\alpha+\beta)+\gamma}$, it satisfies condition of theorem 2.1.

In the same reason, we extend some theorem [3] as follows.

Theorem 2.4 Let E be a real Banach Space, Ω is a bounded open subset of E and $\theta \in \Omega$. If $A: \overline{\Omega} \rightarrow E$ is a semi-closed 1-set-contractive operator such that satisfies condition:

$$\|Ax - kx\|^3 + k\|Ax + x\|^3 \neq (k + 1)[\|Ax\|^3 + 3\|Ax\| \cdot \|x\|^2 + (1 - k^2)\|x\|^2], \text{ for all } x \in \partial\Omega \quad (2.4)$$

Then $\text{deg}(I - A, \Omega, \theta) = 1$

Proof Similar as above stating, we shall prove that the L-S condition is satisfied. That is there exists $x_0 \in \partial\Omega, \mu_0 \geq 1$ such that $Ax_0 = \mu_0 x_0$, and $\mu_0 > 1$. Now, consider it by (2.4), we have that

$$(\mu_0 - k)^3 + k(\mu_0 + 1)^3 \neq (k + 1)(\mu_0^3 + k^3 \mu_0).$$

This is a contradiction. By lemma 1.1, then $\text{deg}(I - A, \Omega, \theta) = 1$ that A has a fixed point in $\overline{\Omega}$. We complete this proof.

Theorem 2.5. Let E, Ω, A be the same as theorem 2.7. Moreover, if substituting (2.4) into that inequality:

$$\|Ax - x\|^4 + \|Ax + x\|^4 \neq 2\|Ax\|^4 + 6\|Ax\|^2 \|x\|^2 + \|x\|^4, \text{ for all } x \in \partial\Omega \quad (2.5)$$

Then $\text{deg}(I - A, \Omega, \theta) = 1$, then the A has at least one fixed point in $\overline{\Omega}$.

Proof Similar as the proof of theorem 2.4. If we suppose that A has no fixed point on $\partial\Omega$. Then we shall prove that the L-S condition is satisfied. We assume it is not true, there exists $x_0 \in \partial\Omega, \mu_0 \geq 1$ such that $Ax_0 = \mu_0 x_0$, and $\mu_0 > 1$.

Now, consider it by (2.5), we have that $(\mu_0 - 1)^4 + (\mu_0 + 1)^4 = 2(\mu_0^4 + 6\mu_0^2 + 1)$.

By (2.5) we have that $(\mu_0 - 1)^4 + (\mu_0 + 1)^4 \neq 2(\mu_0^4 + 6\mu_0^2 + 1)$. Thus, this is a contradiction,

then by lemma 1.1 that we get the conclusions of theorem 2.5.

Therefore, we shall consider some higher degree case as follow (Omit similar proof).

Theorem 2.6 Let E be a real Banach Space, Ω is a bounded open subset of E and $\theta \in \Omega$. If $A: \overline{\Omega} \rightarrow E$ is a semi-closed 1-set-contractive operator such that satisfies condition:

$$\begin{aligned} \|Ax - x\|^{2n+1} + \|Ax + x\|^{2n+1} &\neq 2[\|Ax\|^{2n} + C_{2n}^2 \|Ax\|^{2n-2} \|x\|^2 \\ &+ C_{2n}^4 \|Ax\|^{2n-4} \|x\|^4 + \dots + C_{2n}^{2n-4} \|Ax\|^4 \cdot \|x\|^{2n-4} + C_{2n}^{2n-2} \|Ax\|^2 \cdot \|x\|^{2n-2} + \|x\|^{2n}], \text{ for every } x \in \partial\Omega \end{aligned} \quad (2.6)$$

Then $\text{deg}(I - A, \Omega, \theta) = 1$, then if A has no fixed points on $\partial\Omega$ and so A has at least one fixed point in $\overline{\Omega}$.

Theorem 2.7 Let E be a real Banach Space, Ω is a bounded open subset of E and $\theta \in \Omega$. If $A: \overline{\Omega} \rightarrow E$ is a semi-closed 1-set-contractive operator such that satisfies condition:

$$\begin{aligned} \|Ax - x\|^{2n} + \|Ax + x\|^{2n} &\neq 2[\|Ax\|^{2n} + C_{2n}^2 \|Ax\|^{2n-2} \|x\|^2 \\ &+ C_{2n}^4 \|Ax\|^{2n-4} \|x\|^4 + \dots + C_{2n}^{2n-4} \|Ax\|^4 \cdot \|x\|^{2n-4} + C_{2n}^{2n-2} \|Ax\|^2 \cdot \|x\|^{2n-2} + \|x\|^{2n}] \text{ for all } x \in \partial\Omega \end{aligned} \quad (2.7)$$

Then $\text{deg}(I - A, \Omega, \theta) = 1$, then if A has no fixed points on $\partial\Omega$ and so A has at least one fixed point in $\overline{\Omega}$ (We omit the similar proof of above Theorems).

III. Some Notes For Altman Type Inequality

It is well known we may extend that boundary condition inequality as bellow case:

$$\|Ax - mx\|^2 \geq \|Ax\|^2 - \|mx\|^2 \text{ for all } x \in \partial\Omega, m > 0. \quad (3.1)$$

then the semi-closed 1-set-contractive operator A must have fixed point in $\bar{\Omega}$.

In fact, there exists $x_0 \in \partial\Omega, \mu_0 \geq 1$ such that $Ax_0 = \mu_0 x_0$, and $\mu_0 > 1$. By (3.1), we have that $(\mu_0 - m)^2 \geq \mu_0^2 - m^2, 2m^2 - 2\mu_0 m \geq 0$.

Then $\Delta = \mu_0^2 > 1 > 0$, this is a contradiction.

By Lemma 1.1, we obtain $\deg(I - A, \Omega, \theta) = 1$, then operator A must have fixed point in $\bar{\Omega}$.

We can extend this Altman's inequality into the determinant type form (also see [3]-[5], [6] etc):

$$\|Ax - mx\|^2 \geq \|Ax\|^2 - \|mx\|^2 = \frac{\|A(x)\|, \|mx\|}{\|mx\|, \|A(x)\|} = D_2$$

that we consider these general case: D_n for n-order determinant. Similar Corollary (2) satisfy condition bellow:

$\|Ax\|^2 + \|Ax - B_i x\|^2 \leq \|Ax - mx\|^2 + \|mx\|^2 (i=1,2,\dots,l)$. Then if these semi-closed operators B_1, B_2, \dots, B_l have not common fixed point each other, then S have at least l numbers fixed points. Now, we write n-order determinant type form

$$D_n = \begin{vmatrix} \|Ax + x\| & \|x\| & \cdots & \|x\| \\ \|x\| & \|Ax + x\| & \cdots & \|x\| \\ \vdots & \ddots & \ddots & \vdots \\ \|x\| & \|x\| & \cdots & \|Ax + x\| \end{vmatrix}.$$

Then by simple calculation, $D_n = (\|Ax + x\| + (n-1)\|x\|)(\|Ax + x\| - \|x\|)^{n-1}$.

Moreover, in the similar discussion along this direction, we extend Corollary 2.6 in [3] with as following Theorem 3.1

Theorem 3.1 Let E, Ω, A be the same as in lemma 1.1. Moreover, if there exists n-positive integer such that $(n \geq 2)$,

$$\|Ax\|^{2(n+1)} \geq D_n D_{n+2}, \text{ for all } x \in \partial\Omega, \tag{3.2}$$

Then $\deg(I - A, \Omega, \theta) = 1$, if A has no fixed points on $\partial\Omega$, and so A has at least one fixed point in $\bar{\Omega}$.

Proof Noting the determinant by $D_n, D_{n+2} = (\|Ax + x\| + (n+1)\|x\|)(\|Ax + x\| - \|x\|)^{n+1}$.

By (3.2), we have

$$\|Ax\|^{2(n+1)} \geq (\|Ax + x\| + (n-1)\|x\|)(\|Ax + x\| + (n+1)\|x\|)(\|Ax + x\| - \|x\|)^{2n}.$$

In fact, there exists $x_0 \in \partial\Omega, \mu_0 \geq 1$ $x_0, x_0 \in \partial\Omega, \mu_0 \geq 1$ such that $Ax_0 = \mu_0 x_0$. It is easy to see that $\mu_0 > 1$.

Now, we have the inequality

$$\mu_0^{2n+2} \geq [(\mu_0 + (n-1))][\mu_0 + (n+1)]\mu_0^{2n} > \mu_0^{2n+2}.$$

Hence, $(\|Ax_0 + x_0\| + (n-1)\|x_0\|)(\|Ax_0 + x_0\| + (n+1)\|x_0\|)(\|Ax_0 + x_0\| - \|x_0\|)^{2n} > \|Ax_0\|^{2n+2}$,

Which is a contradiction to (3.2), and so the boundary condition of Leray-Schauder condition is satisfied. Therefore, it follows from lemma 1.1 that the conclusion of Theorem 3.1 holds.

Theorem 3.2 Let be the same as in lemma 1.1. Moreover, if there exists n - positive integer such that $(n \geq 2)$,

$$D_{n+1}^2 \neq D_n D_{n+2}, \text{ for all } x \in \partial\Omega, \tag{3.3}$$

Then $\deg(I - A, \Omega, \theta) = 1$, if A has no fixed points on $\partial\Omega$, and so A has at least one fixed point in $\bar{\Omega}$. (Omit this similar proof).

Theorem 3.3 Let E, Ω, A be the same as in lemma 1. And, if there exists n - positive integer such that $(n \geq 2)$.

$$\|Ax - x\|^{3(n+1)} \geq D_n D_{n+1} D_{n+2}, \text{ for all } x \in \partial\Omega, \tag{3.4}$$

Then $\deg(I - A, \Omega, \theta) = 1$, if A has no fixed points on $\partial\Omega$, and so A has at least one fixed point in $\bar{\Omega}$.

Proof Notice the determinant D_n , then $D_{n+1} = (\|Ax + x\| + n\|x\|)(\|Ax + x\| - \|x\|)^n$, and

$D_{n+2} = (\|Ax + x\| + (n+1)\|x\|)(\|Ax + x\| - \|x\|)^{n+1}$, similar as in above way that we omit the similar proof of

Theorem 3.2. In fact, on the contrary, there exists $x_0 \in \partial\Omega, \mu_0 \geq 1$ such that $Ax_0 = \mu_0 x_0$. It is easy to see that

$\mu_0 > 1$. It is well know by (3.4), we easy obtain that there is a contraction for this inequality. So A has at least one fixed point in $\bar{\Omega}$.

Theorem 3.4 Suppose that same as Theorem 3.3, satisfy follows form:

$$\|Ax - x\|^{2(n+3)} \geq D_n D_{n+1} D_{n+2} D_{n+3}, \text{ for all } x \in \partial\Omega, \tag{3.5}$$

Then $\deg(I - A, \Omega, \theta) = 1$, if A has no fixed points on $\partial\Omega$ and so A has at least one fixed point in $\bar{\Omega}$. (Omit this similar proof of Theorem 3.4).

Remark Notes that new case of non-symmetry form with D_n for n-order determinant are given with more conclusions.

IV. solution of integral equation by vim

To ensure a high-quality product, diagrams and lettering MUST be either computer-drafted or drawn using India ink. Recently, the variation iteration method (VIM) has been favorably applied to some various kinds of nonlinear problems, for example, fractional differential equations, nonlinear differential equations, nonlinear thermo-elasticity, nonlinear wave equations.

They have wide applications in mechanics, physics, optimization and control, nonlinear programming, economics, and engineer sciences.

In this section, we apply the variation iteration method (simple writing VIM) to Integral-differential equations bellow (see [3] and [4-6] etc.). To illustrate the basic idea of the method, we consider:

$$L[u(t)] + N[u(t)] = g(t),$$

where L is a linear operator, N is a nonlinear operator and $g(t)$ is a continuous function.

The basic character of the method is to construct functional for the system, which reads:

$$u_{n+1}(x) = u_n(x) + \int_0^x \lambda(s) Lu(L\bar{u}_n + Nu_n - g(s)) ds,$$

where λ is the Lagrange multiplier which can be identified optimally via variation theory, u_n is the nth approximate solution, and \bar{u}_n denotes a restricted variation, $\delta\bar{u}_n = 0$. There is an iterative formula:

$$u_{n+1}(x) = f(x) + \lambda \int_a^b k(x,t) u_n(t) dt$$

of this integral equation.

Theorem 4.1 ([4, theorem 4.1]). Consider the iteration scheme $u_0(x) = f(x)$, and the

$$u_{n+1}(x) = f(x) + \lambda \int_a^b k(x,t) u_n(t) dt. \tag{4.1a}$$

Now, for $n = 0, 1, 2, \dots$, to construct a sequence of successive iterations that for the $\{u_n(t)\}$ to the solution of integral equation (4.1). In addition, we assume that $\int_a^b \int_a^b k^2(x,t) dx dt = B^2 < \infty$, and assume that $f(x) \in L^2_{[a,b]}$, if $|\lambda| < 1/B$, then the above iteration converges in the norm of $L^2_{[a,b]}$ to the solution of integral equation (4.1).

Corollary 4.2 If $k(x,t) = \sum_{i=1}^m a_i(x) b_i(t)$, and $\int_a^b \int_a^b k^2(x,t) dx dt = B^2 < \infty$, then assume $f(x) \in L^2_{[a,b]}$,

if $|\lambda| < 1/B$, the above iteration converges in the norm of $L^2_{[a,b]}$ to the solution of integral equation (4.1).

Corollary 4.3 If $k(x,t) = k_1(x,t) + k_2(x,t)$, and $\int_a^b \int_a^b k^2(x,t) dx dt = B^2 < \infty$, then assume $f(x) \in L^2_{[a,b]}$,

if $|\lambda| < 1/B$, the above iteration converges in the norm of $L^2_{[a,b]}$ to the solution of integral equation (4.1).

Example 4.1. Consider that integral equation

$$u(x) = x^\alpha + x^3 + x^2 + \lambda \int_0^1 (xt + t) u(t) dt. \tag{4.2}$$

Where $u_0(x) = x^\alpha + x^3 + x^2$, ($0 < \alpha < 1$), let $\gamma = (\alpha + 2)^{-1} + 5^{-1} + 4^{-1}$ and that

$$u_{n+1}(x) = x^\alpha + x^3 + x^2 + \lambda \int_0^1 (xt+t)u_n(t)dt \tag{4.2a}$$

Where $\int_a^b \int_a^b k^2(x,t)dxdt = \int_0^1 \int_0^1 (xt+t)^2 dxdt = 9^{-1} + 3^{-1} + 3^{-1} = 7/9 = B^2 < \infty$, if $|\lambda| < 3/\sqrt{7}$, then the iterative (4.1a) is convergent to the solution of equation (4.2). Substituting $u_0(x)$ in to (4.2a), it is that (writing $P_\alpha(x) = x^\alpha + x^3 + x^2$)

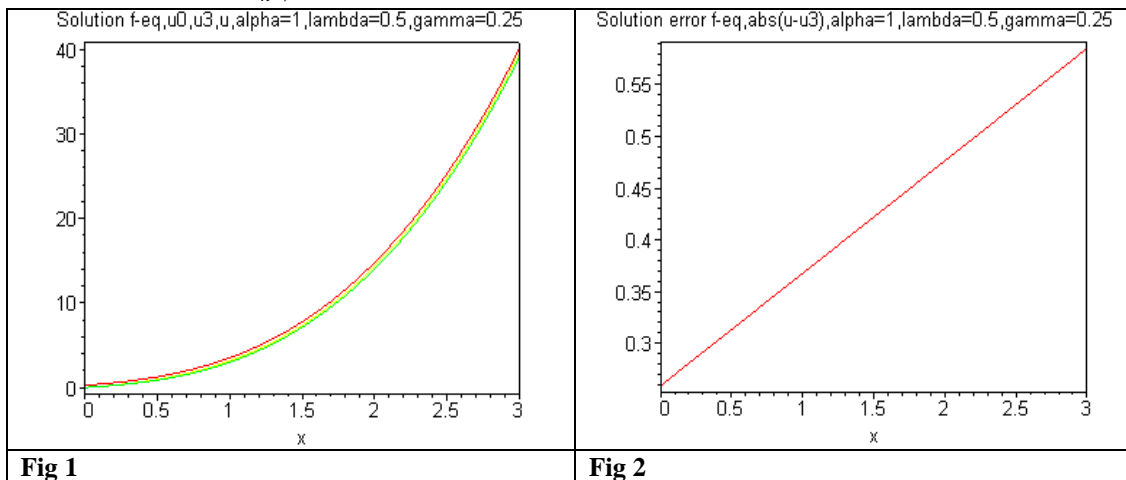
$$u_1(x) = x^\alpha + x^3 + x^2 + \lambda \int_0^1 (xt+t)u_0(t)dt = x^\alpha + x^3 + x^2 + \lambda\gamma(x+1),$$

$$u_2(x) = P_\alpha(x) + \lambda \int_0^1 (xt+t)u_1(t)dt = P_\alpha(x) + \lambda \int_0^1 (x+1)t(t^\alpha + t^3 + t^2 + \lambda\gamma(t+1))dt \\ = P_\alpha(x) + 2\gamma(x+1)(\lambda + \lambda^2/4)$$

$$u_3(x) = P_\alpha(x) + 2\gamma(x+1)(\lambda + \lambda^2/4) + \lambda \int_0^1 (x+1)t \cdot u_2(t)dt = P_\alpha(x) + 2\gamma(x+1)(\lambda + (\lambda/3)^2 + (\lambda/3)^3)$$

By inductively, $u_{n+1}(x) = P_\alpha(x) + \lambda\gamma x(1 + \lambda/3 + (\lambda/3)^2 + \dots + (\lambda/3)^n)$

Then the solution: $u(x) = \lim_{n \rightarrow \infty} u_n(x) = P_\alpha(x) + 3\lambda\gamma x / (3 - \lambda)$. (See Fig 1 and Fig 2)



Example 4.2 Consider that integral equation (positive integer $k \geq 1$)

$$u(x) = x^\alpha + x^{k+2} + x^k + \lambda \int_0^1 (x^k t)u(t)dt \tag{4.3}$$

Where $u(0) = 0$, and $u_0(x) = x^\alpha + x^{k+2} + x^k$ ($0 < \alpha < 1$)

From that $u_n(x) = x^\alpha + x^{k+2} + x^k + \lambda \int_0^1 (x^k t)u_{n-1}(t)dt$

By theorem 4.1 and by simple computation, we obtain again that

$$\int_a^b \int_a^b k^2(x,t)dxdt = \int_0^1 \int_0^1 (x^k t)^2 dxdt = 1/3(2k+1) = B^2 < \infty,$$

then if $|\lambda| < \sqrt{3(2k+1)}$, then iterative

$$u_n(x) = x^\alpha + x^{k+2} + x^k + \lambda \int_0^1 (x^k t)u_{n-1}(t)dt,$$

which is convergent the solution of integral equation (4.3). We may omit the detail calculating (Let $\gamma = (\alpha + 2)^{-1} + (k + 4)^{-1} + (k + 2)^{-1}$).

$$u_{n+1}(x) = x^\alpha + x^{k+2} + x^k + \lambda x^k \gamma (1 + (\lambda / (k + 2)) + (\lambda / (k + 2))^2 + \dots + (\lambda / (k + 2))^n).$$

$$u_n(x) = x^\alpha + x^{k+2} + x^k + \lambda \int_0^1 (x^k t)u_{n-1}(t)dt,$$

which is convergent the solution of integral equation (4.3). We may omit the detail calculating (Let $\gamma = (\alpha + 2)^{-1} + (k + 4)^{-1} + (k + 2)^{-1}$).

$$u_{n+1}(x) = x^\alpha + x^{k+2} + x^k + \lambda x^k \gamma \left(1 + (\lambda / (k+2)) + (\lambda / (k+2))^2 + \dots + (\lambda / (k+2))^n \right).$$

The solution $u_{n+1}(x) = x^\alpha + x^{k+2} + x^k + \lambda x^k \gamma (k+2) / (k+2-\lambda)$.

Theorem 4.2 (see theorem 3 in [5]) Let D be a bounded open convex subset in a real Banach space X and $\theta \in D$; Suppose that $A: D \rightarrow E$ is a semi-closed 1-set-contractive operator and satisfies the following condition:

$$\|Ax - x_0\| \leq \|x - x_0\| \text{ for every } x \in \partial D \text{ and } x_0 \in D. \tag{4.4}$$

Then the operator equation $Ax = x$ has a solution in D (omit the proof)

To illustrate the application of the obtained results, we consider the examples.

Example 4.3 Similar as example 1, we consider integral equation:

$$\int_0^x \left((1/7)^{-1} \sin |t| + (1/11)^{-1} \cos |t| \right) dt - x + 2.1 = 0, \forall x \in [-\pi, \pi] \tag{4.5}$$

It is easy to prove that this equation has a solution in $[-\pi, \pi]$.

In fact, let $Ax = \int_0^x \left((1/7) \sin |t| + (1/11) \cos |t| \right) dt + 2.1, \forall x \in [-\pi, \pi]$, and that $D = [-\pi, \pi], \partial D: x = \pm\pi$. We write $\|y\| = |y|$, for every $y \in R$. Thus, we have

$$|A(-\pi) - 2.1| = \left| \int_0^{-\pi} \left((1/7)^{-1} \sin |t| + (1/11)^{-1} \cos |t| \right) dt \right| \leq \int_{-\pi}^0 \left((1/7)^{-1} + (1/11)^{-1} \right) dt = 18\pi/77 < |-\pi - 2.1| = \pi + 2.1$$

And

$$|A(\pi) - 2.1| = \left| \int_0^{\pi} \left((1/7)^{-1} \sin |t| + (1/11)^{-1} \cos |t| \right) dt \right| = 18\pi/77 < |\pi - 2.1| = \pi - 2.1.$$

It follows that $|Ax - 2.1| \leq |x - 2.1|$, for every $x \in \partial D$. Meanwhile, A is semi-closed 1-set-contractive operator similar example 1 by theorem 4.2 that we obtain the $Ax = x$ has a solution in $[-\pi, \pi]$. That is, Eq. (4.5) has a solution in $[-\pi, \pi]$.

V. Effective Modification of He's variation iteration

In this section, we apply the effective modification method of He's VIM to solve some integral-differential equations [7]. In [7] by the variation iteration method (VIM) simulate the system of this form

$$Lu + Ru + Nu = g(x).$$

To illustrate its basic idea of the method, we consider the following general nonlinear system

$$Lu + Ru + Nu = g(x), \tag{5.1}$$

Lu shows the highest derivative term and it is assumed easily invertible, R is a linear differential operator of order less than L , Nu represents the nonlinear terms, and g is the source term. Applying the inverse operator L_x^{-1} to both sides of equation (*), then we obtain $u = f - L_x^{-1}[Ru] - L_x^{-1}[Nu]$.

The variation iteration method (VIM) proposed by Ji-Huan He (see [5], [7] has recently been intensively studied by scientists and engineers. the references cited therein) is one of the methods which have received much concern. It is based on the Lagrange multiplier and it merits of simplicity and easy execution. Unlike the traditional numerical methods. Along the direction and technique in [9], we may get more examples bellow.

We notice that an effective iterative method and some examples

Example5.1 Consider the following integral-differential equation

$$u''(x) = e^{\alpha x} - (4/3)x + \lambda \int_0^1 xt \cdot u(t) dt,$$

Where $u(0) = 1, u'(0) = 1 + \alpha, u''(0) = \alpha^2$ with exact solution $u(x) = x + e^{\alpha x}$.

In fact, we check $f_0(x) = x + e^{\alpha x}, f_1(x) = -7x/4$, to divide f in tow parts for $f(x) = f_0(x) + f_1(x)$, and writing $\delta = (1/\alpha - 1/\alpha^2)e^\alpha + 1/\alpha^2$.

$$L_x^{-1} \left(\int_0^1 xt u_0(t) dt \right) = L_x^{-1} \left(x \int_0^1 t(t + e^{\alpha t}) dt \right) = L_x^{-1} (x/3 + \delta x) = \int_0^1 \left((x/18) + (\delta x^3 / 6) \right) dx$$

$$= ((1 + 3\delta) / 18) \int_0^x x^3 dx = (1 + 3\delta) x^4 / 72.$$

By $u_{n+1}(x) = x + e^{\alpha x} - (1/4)((1 + 3\delta) / 18) x^4 + L_x^{-1} \left(\int_0^1 xtu_n(t) dt \right)$. Then, we have

$$u_1(x) = x + e^{\alpha x} - ((1 + 3\delta) / 72) x^4 + L_x^{-1} \left(\int_0^1 xtu_0(t) dt \right) = x + e^{\alpha x},$$

$$u_2(x) = x + e^{\alpha x} - ((1 + 3\delta) / 72) x^4 + L_x^{-1} \left(\int_0^1 xtu_1(t) dt \right) = x + e^{\alpha x}, \dots, \text{ and we have that}$$

$u_n(x) = x + e^{\alpha x}$ Therefore, this is a closed form $u(x) = x + e^{\alpha x}$, shows that the method is a very convenient and only one iterative leads to the exact solution.

Example5.2 Consider the following integral-differential equation

$$u^{(6)}(x) = e^{\alpha x} - (4/3)x + \int_0^1 xtu(t)dt, \tag{5.2}$$

where $u(0) = 1, u'(0) = 1 + \alpha, u''(0) = \alpha^2, u^{(3)}(0) = \alpha^3, u^{(4)}(0) = \alpha^4, u^{(5)}(0) = \alpha^5$

In similar example1, we easy have it.(We may omit it)

where $L_x^{-1}(\cdot) = \int_0^x \int_0^x \int_0^x \int_0^x \int_0^x \int_0^x (\cdot) dt dt dt dt dt dt, u_0(x) = f_0(x) = x + e^{\alpha x},$

$$f_1(x) = f(x) - f_0(x) = (e^{\alpha x} - (4/3)x) - (x + e^{\alpha x}) = -7x/3, f(x) = f_0(x) + f_1(x),$$

and writing $\delta = (1/\alpha - 1/\alpha^{-2})e^{\alpha} + 1/\alpha^{-2}.$

$$\begin{aligned} L_x^{-1} \left(\int_0^1 xtu_0(t) dt \right) &= L_x^{-1} \left(x \int_0^1 t(t + e^{\alpha t}) dt \right) = L_x^{-1} (x/3 + \delta x) \\ &= \int_0^x \int_0^x \int_0^x \left(\int_0^x ((x^3/18) + (\delta x^3/6)) dx \right) dx dx dx, \\ &= ((1 + 3\delta) / 18) \int_0^x \int_0^x \int_0^x (x^4/4) dx = ((1 + 3\delta) / 18) x^7 / 7!. \end{aligned}$$

$$u_1(x) = x + e^{\alpha x} - ((1 + 3\delta) / 3) x^7 / 7! + L_x^{-1} \left(\int_0^1 xtu_0(t) dt \right) = x + e^{\alpha x}, \dots,$$

and so on,

$$u_{n+1}(x) = x + e^{\alpha x} - ((1 + 3\delta) / 3) x^7 / 7! + L_x^{-1} \left(\int_0^1 xtu_n(t) dt \right) = x + e^{\alpha x}.$$

By simple operations, we have that

$$u_0(x) = x + e^{\alpha x}, u_1(x) = x + e^{\alpha x}, \dots, u_n(x) = x + e^{\alpha x}, n \geq 1.$$

Therefore, the exact solution in a closed form $u(x) = x + e^{\alpha x}$, shows that the method

is a very convenient. The exact solution $u(x) = x + e^{\alpha x}$ is only one iterative. (See Fig 3, $\theta = 0.75$ and $\theta = 1.25$).

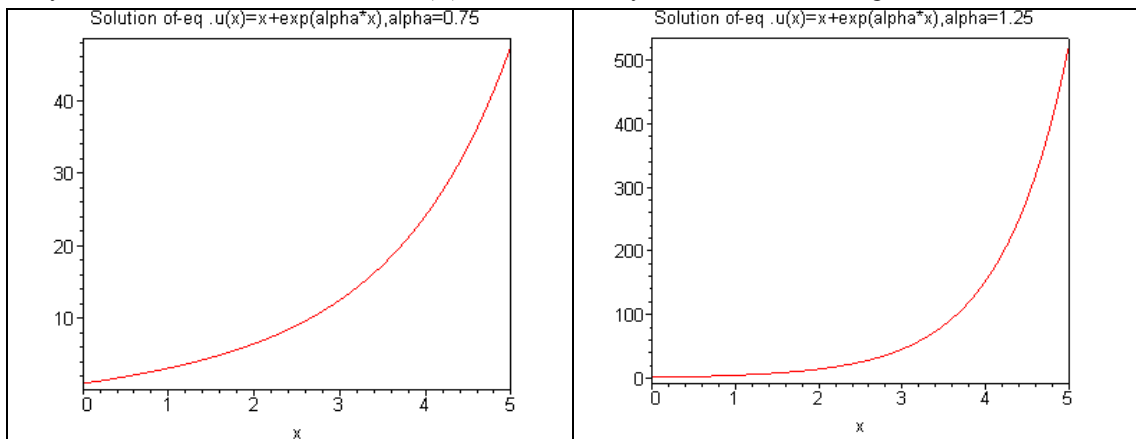


Fig 3

VI. Some Notes of Burger's Equation

We shall consider the exact and numerical solutions for Burger's equation ,which has attracted much attention .Solving this equation has been an interesting tasks for mathematicians

VI.1 One-dimensional Burger's equation

. Consider the following one-dimension Berger's equation with initial and boundary conditions:

Example 6.1 Consider the following equation (similar as example 1 [15]):

$$\begin{cases} \frac{\partial u}{\partial t} + u \frac{\partial u}{\partial x} = \frac{\partial^2 u}{\partial x^2}, \\ u(x, 0) = 3x, t > 0. \end{cases} \tag{6.0}$$

According the direction of [2] and method for this example, then it can be written as by iterative formula (6) [2]:

$$u_{n+1}(x, t) = u_n(x, t) + \int_0^x \lambda(\eta) \left(\frac{\partial u_n}{\partial \xi}(x, \xi) + u_n \frac{\partial u_n}{\partial x}(x, \xi) - v \frac{\partial^2 u_n}{\partial x^2} \right) d\xi. \tag{6.1}$$

Starting with $u_0(x, t) = 3x$.

The following reads can be derived from iterative formula (6.1)

$$\begin{aligned} u_1(x, t) &= 3x - 6xt, \\ u_2(x, t) &= 3x - 6xt + 12xt^2 - 24xt^3, \\ u_3(x, t) &= 3x - 6xt + 12xt^2 - 24xt^3 + 48xt^4 - 96xt^5 + 192xt^6 - 384xt^7, \dots \end{aligned}$$

Thus, we have that

$$\begin{aligned} u(x, t) &= \lim_{n \rightarrow \infty} u_n(x, t) \\ &= 3x(1 - 2t + 4t^2 - 8t^3 + 16t^4 - 32t^5 + 64t^6 - 128t^7 + \dots) \\ &= \sum_{n=0}^{\infty} (-1)^n 2^n (3x)t^n \\ &= 3x/(1 + 2t). \end{aligned}$$

This is an exact solution.

Remark Starting with $u_0(x, t) = (a + 1)x$, $u(x, t) = \lim_{n \rightarrow \infty} u_n(x, t) = (a + 1)/(1 + 2t)$.

As $a > 0$ (as special case: $a = 1$ that is example 1 [15], $a = 2$, this is example 1 in this paper). Notice that $u_0(x, t) = ax + b$ or $u_0(x, t) = x^2 + x$ (similar polynomial case). More form.

$$\begin{aligned} u(x, t) &= \lim_{n \rightarrow \infty} u_n(x, t) \\ &= (x^2 + x)(1 - 2t + 4t^2 - 8t^3 + 16t^4 - 32t^5 + 64t^6 + \dots) \\ &= \sum_{n=0}^{\infty} (-1)^n 2^n (x^2 + x)t^n \\ &= (x^2 + x)/(1 + 2t). \end{aligned}$$

This is an exact solution.

Or $u_0(x, t) = x^k + x^{k-1} + x$ (similar polynomial case).more form.

$$u(x, t) = \lim_{n \rightarrow \infty} u_n(x, t) = (x^k + x^{k+1} + x)/(1 + 2t).$$

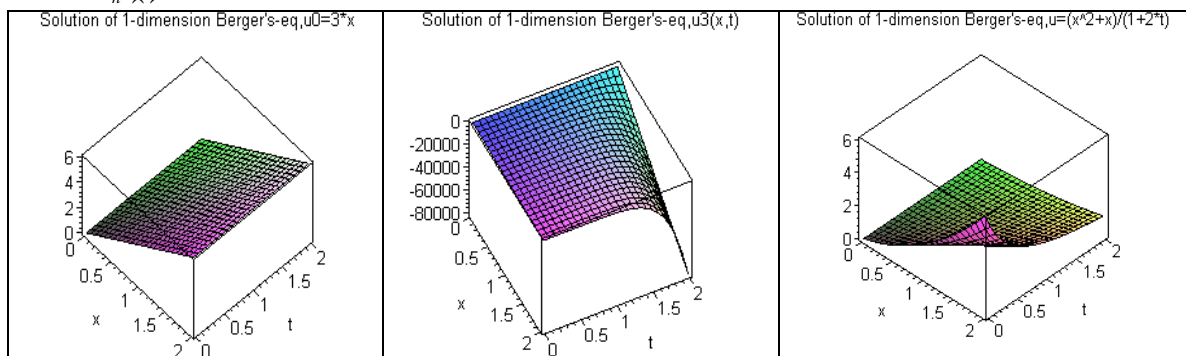


Fig 4

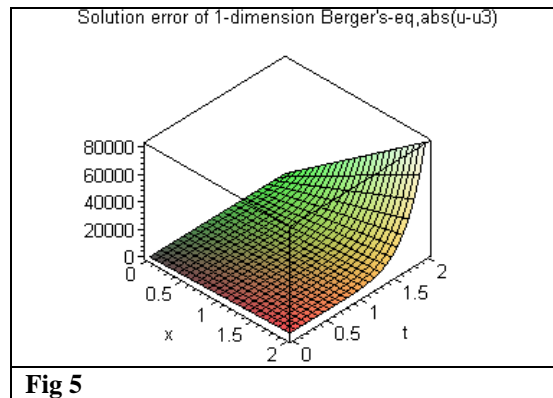


Fig 5

Example 6.2 Consider the following equation (similar as example 1 [15]):

$$\begin{cases} \frac{\partial u}{\partial t} + u \frac{\partial u}{\partial x} = \frac{\partial^2 u}{\partial x^2}, \\ u(x, 0) = 10x, t > 0. \end{cases} \quad (6.2)$$

For this example, by above Example 6.1, can be written as $a = 9$. Starting with $u_0(x, t) = 10x$. Thus, we have that an exact solution.

$$u(x, t) = \lim_{n \rightarrow \infty} u_n(x, t) = 10x / (1 + 2t).$$

VI-2 Two-dimensional Burger's equation

Similar as example 3 [15], we get following example 2 for two-dimension case.

Example 6.3 Consider the system of Burger's equation in the following equation (similar as example 3 [15]):

$$\frac{\partial u}{\partial t} + u \frac{\partial u}{\partial x} + v \frac{\partial u}{\partial y} = \frac{1}{R} \left(\frac{\partial^2 u}{\partial x^2} + \frac{\partial^2 u}{\partial y^2} \right), \quad \frac{\partial v}{\partial t} + u \frac{\partial v}{\partial x} + v \frac{\partial v}{\partial y} = \frac{1}{R} \left(\frac{\partial^2 v}{\partial x^2} + \frac{\partial^2 v}{\partial y^2} \right). \quad (6.3)$$

with initial conditions: $u_0(x, y, 0) = x + y, v_0(x, y, 0) = x - y$. We have by iterative [15]:

$$\begin{aligned} u_{n+1}(x, y, t) &= u_n(x, y, t) - \int_0^t \left[\frac{\partial u_n}{\partial \tau} + u_n \frac{\partial u_n}{\partial x} + v_n \frac{\partial u_n}{\partial y} - \frac{1}{R} \left(\frac{\partial^2 u_n}{\partial x^2} + \frac{\partial^2 u_n}{\partial y^2} \right) \right] d\tau, \\ v_{n+1}(x, y, t) &= v_n(x, y, t) - \int_0^t \left[\frac{\partial v_n}{\partial \tau} + u_n \frac{\partial v_n}{\partial x} + v_n \frac{\partial v_n}{\partial y} - \frac{1}{R} \left(\frac{\partial^2 v_n}{\partial x^2} + \frac{\partial^2 v_n}{\partial y^2} \right) \right] d\tau. \end{aligned} \quad (6.4)$$

Consider the initial approximations $u_0(x, y, 0) = x + y, v_0(x, y, 0) = x - y$. and applying VIM formula (6.4), other term of the sequence are computed as follows:

$$\begin{aligned} u_1(x, y, t) &= x + y - 2xt, v_1(x, y, t) = x - y - 2yt. \\ u_2(x, y, t) &= x + y - 2xt + 2xt^2 + 2yt^2 - (4/3)xt^3, \\ v_2(x, y, t) &= x - y - 2yt + 2xt^2 - 2yt^2 - (4/3)yt^3. \\ u(x, y, t) &= \lim_{n \rightarrow \infty} u_n(x, y, t) \\ &= x(1 + 2t^2 + 4t^4 + \dots) + y(1 + 2t^2 + \dots) - 2xt(1 + 2t^2 + \dots) \\ &= (x + y - 2xt) / (1 - 2t^2). \\ v(x, y, t) &= \lim_{n \rightarrow \infty} v_n(x, y, t) \\ &= x(1 + 2t^2 + 4t^4 + \dots) - y(1 + 2t^2 + \dots) - 2yt(1 + 2t^2 + \dots) \\ &= (x + y - 2xt) / (1 - 2t^2), \end{aligned}$$

which are exact solutions ($|t| < \sqrt{1/2}$). We omit the detail stating for this results.

VII. Conclusion

In this Letter, we apply the variation iteration method to integral-differential equation ,and extend some results in [3]- [4]-[5]. The obtained solution shows the method is also a very convenient and effective for various integral-differential equations, only one iteration leads to exact solutions.

Acknowledgements

This work is supported by the Natural Science Foundation (No.11ZB192) of Sichuan Education Bureau and the key program of Science and Technology Foundation (No.11Zd1007) of Southwest University of Science and Technology.

REFERENCES

- [1]. D. Guo, V. Lashmikantham, Nonlinear Problems in abstract Cones(Academic Press, Inc., Boston, New York, 1988).
- [2]. S.Y. Xu, New fixed point theorems for 1-set-contractive operators in Banach spaces, *Nonlinear Anal.*67,2007,938-944.
- [3]. N. Chen, and J.Q. Chen, New fixed point theorems for 1-set-contractive operators and variation iteration method, *Jp Journal of fixed point theory and application*,Vol.6(3),2011,147-162.
- [4]. N. Chen, J.Q. Chen, Operation equation and application variation iteration method, *Applied Mathematics*,3(8),2012,857-863.
- [5]. N.Chen , J.Q.Chen, Some approximation in cone metric space and variation iterative method, *Applied Mathematics*, 3(12),2012,2007-2018.
- [6]. C. X. Zhu, Generalization of Krasnoselski's theorem and Petrsbyn's theorem, *Applied mathematics letters* 19,2006, 628-632.
- [7]. Asghar Ghorbani, Jafar Sabaeri-Nadjafi, An effective modification of He's variational iteration method, *Nonlinear Analysis: Real World Application*10,2009, 2828-2833.
- [8]. Abdul-Majid Wazwaz, The variational iterative method :A reliable analytic tool for solving linear and nonlinear wave equations, *Computers & mathematics with applications* ,54,2007,926-932.
- [9]. S.Q.Wang,Ji-Huan He, Variational iterative method for solving integro-differential equations, *Physics Letters A* 367,2007,188-191.
- [10]. J. Biazr, H. Ghazvini, He's iterative method for forth-order parabolic equation,An international Journal of computers and mathematics with applications,54,(2007,1047-1054.
- [11]. N. Chen, Baodan Tian and Jiqian Chen, A class of new fixed point theorems and for 1-set -contractive operators and some variation iterative method,[J]. *Physics Procedia* 33,2012,1932-1938.
- [12]. Yousry S. Hanna, On Approximate solutions of second-order linear partial differential equations, *Applied Mathematics*,3,2012,1001-1007.
- [13]. Elcin Yusufoglu, The variation iteration method for studying the Klein-Gordon equation., *Applied Mathematics Letters*,21,2008,669-674.
- [14]. Z.L.Yang, Nontrivial solutions of systems of nonlinear Hammerstein integral equations and applications, *Acta Mathematica Scientia*, 26(A2),2006,233-240.
- [15]. A. Saandatmandi, and M. Dehghan, He's iterative method for solving a partial differential equation arising in modeling of water waves, *Zeitschrift fur naturfoschung* ,64,2009,783-787.

Implementation of Lean Manufacturing Principles in Foundries

Praveen Tandon¹, Dr. Ajay Tiwari², Shashikant Tamrakar³

¹(Mechanical Engineering Department, RCET /CSVT University, INDIA)

²(Mechanical Engineering Department, REC /CSVT University, INDIA)

³(Mechanical Engineering Department, RCET /CSVT University, INDIA)

ABSTRACT : *It is the general perception that the foundry industries are inherently more efficient and have a relatively less requirement for major improvement activities. Managers and engineers have also been hesitant to implement lean manufacturing tools and techniques to the continuous sector because of typical and identical characteristics that sector. These include costly and special purpose inflexible machines, options of modifications in machines are limited, long setup times, and the general difficulty in producing in small batches.*

Lean manufacturing technology when applied appropriately in a process industry, can help in eliminating waste, enhance the quality of product, attain better and smooth control on operations and thereby reducing the production cost and production time.

Keywords : *casting shakeout, Lean manufacturing, Takt time, production line.*

I. Introduction

Lean manufacturing (LM) is seen as major breakthrough process and is widely used by major industries all over the world. In a continuous process industry like casting the main approach of implementing the lean manufacturing is to reduce the production cost by eliminating the non value added activities. A basic concept of LM is pull production in which the flow on the factory floor is driven by demand from downstream pulling production upstream as opposed to traditional batch-based production in which production is pushed from upstream to downstream based on a production schedule. In a recent survey, approximately 36% of US-based manufacturing companies have implemented lean or are in the process of implementing lean.

An LM facility is capable of producing product in only the sum of its value added work content time. The significance of a LM model include: production of only one unit at a time; non-value added time eliminated; production of the job within time pre decided; relocation of required resources to the point of usage; and all processes must be completed within same Takt time, therefore it provide the smooth production of the complete job. The rate at which work progresses through the shop floor is called Takt. The available production time divided by customer demand. The objective of takt time is to measure the production with respect to demand. It sets the rate for production so that production cycle times can be matched to customer demand rate.

II. Principle

Jerry Kilpatrick^[1] stated that “Lean” operating principles began in manufacturing environments and are known by a variety of synonyms; Lean Manufacturing, Lean Production, Toyota Production System, etc. It is commonly believed that Lean started in Japan (Toyota, specifically), but Henry Ford had been using parts of Lean as early as the 1920’s, as evidenced by the following quote:

“One of the most noteworthy accomplishments in keeping the price of Ford products low is the gradual shortening of the production cycle. The longer an article is in the process of manufacture and the more it is moved about, the greater is its ultimate cost.” Henry Ford 1926

In order to set the groundwork for this paper, let’s begin with the definition of Lean, as developed by the National Institute of Standards and Technology Manufacturing Extension Partnership’s Lean Network:

“A systematic approach to identifying and eliminating waste through continuous improvement, flowing the product at the pull of the customer in pursuit of perfection.”

Keep in mind that Lean applies to the entire organization. Although individual components or building blocks of Lean may be tactical and narrowly focused, we can only achieve maximum effectiveness by using them together and applying them cross-functionally through the system.

III. Objective

The lean manufacturing will help reducing the waste, waiting time and balancing the production line. The major benefit is high productivity which is the need of the hour. Modification automation and effective utilisation of production resources ultimately serve the purpose. Lean Manufacturing is one such area having great potential to obtain higher productivity especially in foundry practice.

IV. Methodology

Collection of data through literature survey, interviews, group discussions, questionnaires, databases, seminars, conferences etc. Data analysis by using various tools like hypothesis testing, qualitative analysis, using relevant statistical software Mat Lab ,ANSYS etc.

John S. W. Fargher ^[2] suggested a method in his case study as follows:-

- The first step is to group products into families of similar production processes.
- The second step is to establish the Takt time. The Takt time is the demand rate and consequently the time between completion of each product off of the production line. It is first necessary to find the available capacity of the production line:

Available Capacity = Time Available x PFS x Utilization

Where:

Time Available = Hours / Time Period x Number of Employees

Personal, Fatigue, and Safety (PFS) = Standard Hours Produced / Hours Worked

Utilization = (Hours Available - Downtime) / Hours Available

- The third step is to review the work sequence by:
 - i. Observing the sequence of tasks each worker performs,
 - ii. Break operations into observable elements,
 - iii. Identify value added versus non value added elements and minimize or eliminate non value added operations, and Study machine capacity, cycle times and change over times
 - iv. In IE words, conduct methods and standards studies.
- The fourth step is to balance the line using the calculated Takt times found in step two.
- Step five is to design and construct the cell to:

Implement a “U” shaped line to assure one way flow and maximize visibility,
Provide a flexible layout to account for all members of the production family,

Decrease distance between operations and integrating process operations wherever possible for simplicity, minimizing both transportation and production lot sizes, integrate in point of use storage next to each assembly operation.

Minimize material handling by concentrating on value added motion

Establish replenishment procedures for point of use storage using the A-B-C rule

Assure the personnel understand their role and are cross trained to use their skills at a variety of tasks and work stations.

Provide visibility to allow operator decisions on problem solving, moving to where work needs to be performed, and focus management attention on production disruptions.

The objective of this practice is to achieve economies of scale by saving costs and making better use of assets. In addition, with a smaller number of employees (30 to 1000, as Toyota has in each plant), it is also easier for managers to motivate the workforce.

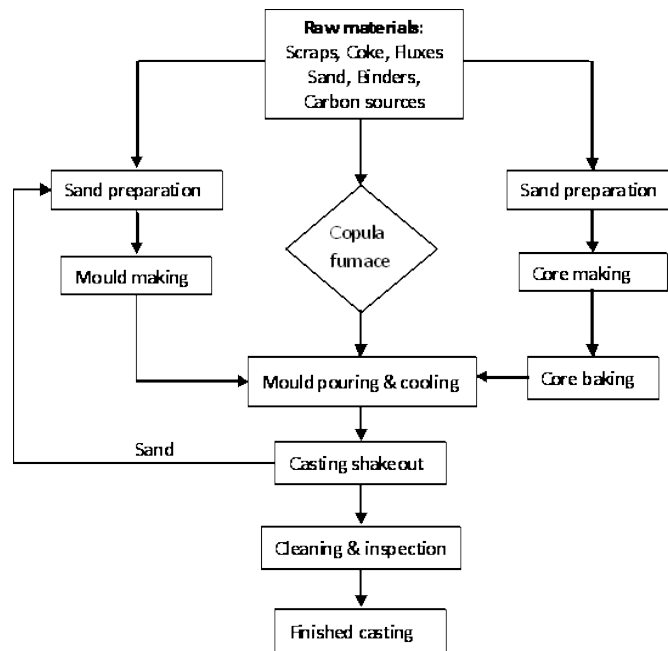


Fig. No. – 1: Flow chart of Foundry Practice

To carry out the proposed research work through data collection, small and medium sized foundries to be visited. Complexity of casting process and parameters need to be studied.

There are other lean practices to implement. If production flows perfectly, there is no inventory waiting to be worked on. Metal casters have helped minimize work-in-process by installing conveyor lines to keep castings moving right through to finished goods storage. This eliminated putting the castings in totes and the added handling. One low to medium volume gray/ductile iron jobbing foundry (casting weights under 50 pounds) we know now ships 30% of its production the same day and believes they can achieve 70% same day shipment. These standards aren't just for the high volume or dedicated metal casting companies any more.

“Autonomation” or “smart automation” is a part of lean manufacturing as well. Autonomation refers to automating the process so humans can focus on what humans do best. The objective here is to design the machine so it knows when it is working abnormally and alerts a human. The human no longer has to monitor normal production but can focus on abnormal or fault conditions. Removing routine and repetitive activity reduces the chance for error.

V. Case Study

A Case study on Application of Lean Manufacturing to Higher Productivity in the Apparel Industry in Bangladesh has been done and following outcomes have been observed :

5.1 Introduction

Generally in an industry more focus is given on profit. Though there are different issues involved in cost reduction internally spent by an industry through finding wastages, preventing and correcting defective work would result in huge savings [3]. The apparel industry faced considerable changes as a result of the removal of Multi Fiber Agreement in 2005 [4]. Delivering high quality garments at low cost in shorter lead times are the major challenges faced by the apparel manufacturers. Most of the apparel manufacturers are trying to achieve these challenges successfully. In 2008, global recession badly affected almost all the apparel manufacturing industries in the world [4]. Due to that demand for the low cost garments are increased by the customers. Suppliers are forced to deliver low cost garments. Because of many high cost factors in Bangladesh, most of the companies faced difficulties in getting orders and some companies were closed down. The companies are seeking ways to minimize their cost in order to meet the competition by other low cost countries such as China, India, Sri Lanka, and Pakistan and to survive. Lean Manufacturing can be defined as "A systematic approach to identify and eliminate waste through continuous improvement by flowing the product at the demand of the customer" (Introduction to Lean, 2010) [6]. Lean manufacturing helps to identify productive and non-productive activities. Group[5] located at, Gazipur, Bangladesh, to identify non productive activities so as to eliminate them for saving time, cost and improve productivity. By eliminating waste in the processes,

companies can achieve a shorter lead time, lower cost, highest quality and can understand a competitive advantage over the others.

5.2 Basic Research Approach

As shown in Fig. 1, a comprehensive literature review was carried out on Lean Manufacturing. After that effective suggestion and recommendations were made. The steps considered in the process are given below:-



Fig-1 Research approach- steps by steps process

5.3 Result of Case Study:

In Modern industries it is difficult to identify the key areas and practices, which can be used to eliminate waste in their processes. Based on the practical experiment conducted, it can be seen that lean manufacturing can be effectively applied to apparel industry as the key step of waste identification. Using this tool, it is possible to map the current status and subsequently analyze to achieve waste elimination. The case study presented in this paper, has shown that the wastes such as transport, inventory and defects, over processing, excess motion, over production etc can be reduced to a great extent which in turn improves the productivity of the organization. In order to accomplish this task, the managers of the case company have to implement approaches like 5S, one piece flow etc. Thus, lean manufacturing helps the organization to visualize the present level of wastes occurring in the organization and the future possibilities of reducing or eliminating them. In order to continuously reduce or eliminate waste, management of companies need to apply different Lean tools and techniques accordingly while giving adequate training to their employees. Therefore organizations of similar type can use the research outcomes as a knowledge base to identify their wastes and come up with suitable remedies. Findings of this research can be valuable to other organizations of Bangladesh, which expect to implement Lean Manufacturing in the near future.

VI. Conclusion

Expected outcome of the research to focus on the process of pouring metal inside the mould, cooling casting, shake-out, and transport to the finishing area, cleaning and cut burr processes. At the foundry industry where the research collected data, the scenarios simulated suggested to explore alternatives to reduce the time of pouring times through an improvement in industrial lay out and workload balancing including worker's multi skilling training. These procedures can lead to reduce the waste of time and reduce the queuing inside the processes, an agreement with lean manufacturing technology.

REFERENCES

- [1]. Jerry Kilpatrick, Lean Principles, *Utah Manufacturing Extension Partnership*, 2003, 1-5.
- [2]. John S. W. Fargher, "lean manufacturing and manufacturing Implementation tools" case study, April 2004, Missouri Enterprise, University of Missouri - Rolla
- [3]. Feld, M.W., (2000). Lean Manufacturing: Tools, Techniques, and how to use them. Boca Raton, London: The St. Lucie Press
- [4]. Kumar, S. A. (2008). Production and Operations Management. Daryaganj, Delhi, India: New Age International, p. 217-220.

- [5]. <http://www.viyellatexgroup.com>
- [6]. Shahidul, M. I. and Syed Shazali, S. T. Dynamics of manufacturing Productivity: *Journal of Manufacturing Technology Management* Vol. 22 No. 5, 2011, p. 664-678
- [7]. <http://www.opexgroup.com>
- [8]. Productivity Development Team, ed. *Cellular Manufacturing: (Portland, .Oregon: Productivity Press, 1999).*
- [9]. <http://www.sepalgroup.com>
- [10]. Saroj Bala, Factors Influencing Costing of Woven Fabrics, *The Indian Textile Journal, June 2003*
- [11]. Dr P Khanna: *Work study, time and motion study*, Dhanpat Rai and Sons, New Delhi, (pp 21).
- [12]. Romm, Joseph J. *Lean and Clean Management: How to Boost Profits and Productivity by Reducing. Pollution (New York: Kodansha International, 1994)*
- [13]. Abdulmalek, F.A. and Rajgopal, J. (2007). Analyzing the benefits of Lean Manufacturing and Value Stream Mapping via simulation: a process sector case study, *International Journal of Production Economics*, Vol. 107, pp. 223-36.
- [14]. Introduction to Lean (n.d.). Available from: http://www.mamtc.com/lean/intro_intro.asp (Accessed 10 May 2010)
- [15]. McBride, D. The 7 Manufacturing Wastes. Available from: <http://www.emsstrategies.com/dm090203article2.html> (Accessed 05 May 2010)
- [16]. Ohno, T. (1988). *Toyota Production System*, Productivity Press, New York, pp. ix
- [17]. Seth, D., Seth, N. and Goel, D. (2008). Application of Value Stream Mapping for minimization of wastes in the processing side of supply chain of cotton seed oil industry in Indian context, *Journal of Manufacturing Technology and Management*, Vol. 16 No. 4, pp. 529-50.

Review of crosstalk free Network

Ramesh Kumar, Vedant Rastogi

¹(CSE, IET ALWAR/ Rajasthan technical University Kota, India)

²(Department Computer Science, RTU University Kota Rajasthan, India)

ABSTRACT: Multistage interconnection networks (MIN) are among the most efficient switching architectures for the number of switching Element (SE). Optical crosstalk in optical multistage interconnection network on the omega network topology Switches are arranged in multiple stages. These switches also referred to as switching element (SEs) have two input and two output ports, interconnected to the neighboring stages in a shuffle exchange connected pattern message routing in such a network is determined by the interstate connection pattern.

Optical Multistage interconnection networks (OMIN) are advanced version of MINs. The main Problem with OMIN is crosstalk. The main purpose of this paper is to Present crosstalk free modified omega network, which is based on time domain approach. This paper presents the source and destination based Algorithm (SDBA) .SDBA does the scheduling for source and their respective destination addresses for the message routing. SDBA is compared with the crosstalk modified omega network (CFMON).CFMON also Minimizes the crosstalk. This paper is the modified form of the omega network.

Keywords: Omega network, Multistage Interconnections network, Optical Multistage interconnection network, Crosstalk, Time domain approach, Crosstalk Modified omega network.

I. Introduction

The multistage interconnection Network is an essential network for the Parallel computing applications .It contains N inputs to N outputs and is known as an $N \times N$ MIN. The parameter N is called the size of the network. In this paper we study the performance of optical multistage Interconnection network.

Omega network is a network configuration after used in parallel computing architecture .It is an indirect topology that relies on the Perfect Shuffle interconnection algorithm. The omega network is a highly blocking through one path can always be made from input to any output in free network. It connects N inputs to N outputs and is known as an $N * N$ MIN. Here N is the size of the network. In Omega network contains $N/2$ switches. An omega network is a $\log_2 N$ stage shuffle –exchange Interconnection network .Here multistage Omega network $N=8$ Multistage Interconnections network establishes a reliable communication between source and destination. But now a days electro optic technologies have built optical communication a reliable and fast network that fulfill the Increasing demands of users.

II. Analysis for the Network

Most of the interconnection network analysis related to identical processor And a uniform reference model. We shall analyze the performance of the n- stage Banyan network discussed.

1. Fixed size packets are generated by the modules at each source address
2. Arrival of packets at the network inputs are independent and identical.
3. A connection between two switches can carry the packet in each cycle.
4. If two packets arriving at two distinct network inputs require the use of common link between two stages, one of the packets is discarded.
5. The switches and links have no internal buffers to temporarily store an incoming packet that cannot be forwarded in the current.
6. There is no blocking at the output links of the network. This means that the output links have at least the same speed as the internal links.

Moreover, if the network is uniform, then for each stage in the network, the patterns of packet arrivals at the inputs of that stage have the same distribution. While Banyan networks are very attractive in their simplicity, other considerations such as performance or reliability sometimes dictate the use of more complicated

networks. We consider packet-switching networks built of 2×2 unbuffered switches with the topology of an n -stage square Banyan network. When several packets at the same switch require the same output, a randomly chosen packet is forwarded and the remaining packets are deleted. An 8×8 Banyan network is shown in Figure 1

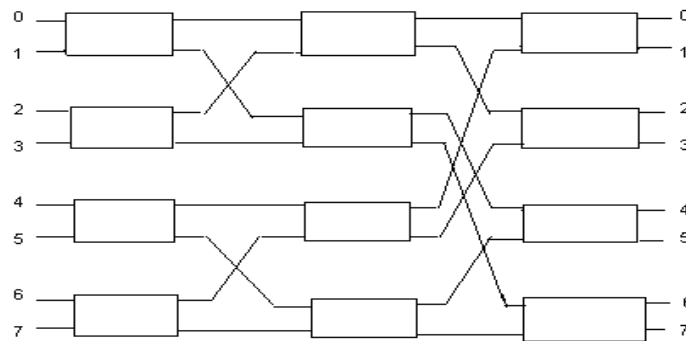


Figure 1. An 8x8 Banyan Network

Figure 1. An 8 x 8 Banyan network topology

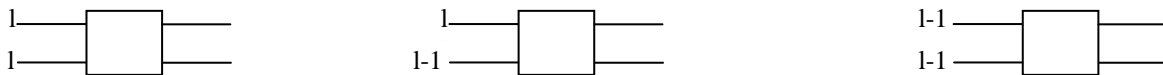
Since we are dealing with OMINs, at any instant of time we can only send one message through any switch to avoid the effect of crosstalk. But here in this paper for an $N \times N$ network we are allowing limited crosstalk's up to $C = (\log 2N - 1)$ (where 'C' is a parameter dependent on Technology). The number of stages for such a network is given by $n = \log 2^N$. Hence for the Banyan network shown in fig we can allow crosstalk in switches at two stages out of three stages in the network. Hence in this paper we can have switches where 0, 1 or 2 messages can be allowed at the same time. In other words a switch can be 2-active, 1-active or 0-active. Both 0-active and 1-active switches do not allow crosstalk whereas the 2-active switch produces optical conflicts. And hence could potentially contribute to crosstalk. We are most interested in analyzing the performance of a banyan network allowing limited cross-talk. For instance, one of the best ways for analyzing the performance is to calculate the bandwidth (BW) of the $N \times N$ Banyan network operating under a load l . Load is defined as the probability, that an input is active. Thus, the expected number of active inputs at load l for an $N \times N$ banyan network is Nl . We will derive some equations to find the BW of such a Banyan network built with 2×2 unbuffered switches. Let $P(j)$ be the probability that a request exists at an input link of a switch in stage j , and let $P(j+1)$ be the probability that an output link of this switch is used for routing a request. The analysis involves the iterative computation of $P(j+1)$ in terms of $P(j)$, starting with $P(1)$. For an n -stage network, the probability of acceptance, PA is given by $P(n)$. The crucial step in the analysis of each network is the recurrence relation to specify $P(j+1)$ in terms of $P(j)$. The recurrence relation depends on the network topology and the routing algorithm. Since we are dealing with a Banyan network with 2-active, 1-active or 0-active switches, we have the following equations.

For each stage ($1 \leq j \leq n$), we define

$P_2(j)$ = probability that a given switch is 2-active,

$P_1(j)$ = probability that a given switch is 1-active,

$P_0(j)$ = probability that a given switch is 0-active.



Various combination of load at stage 1

III. Optical Omega Network (Oon)

The OON has a shuffle exchange connection pattern. In this pattern the address is shifted one bit to the left circularly in each connection. This network connects the input to output nodes using n stages, where $n = \log 2^N$ with each stage containing 2^{n-1} SEs. When any source sends the communication signal to a destination then it has to pass through the OON. Each communication signal has a definite path from the given source to the given destination. Crosstalk occurs when two or more signals follow the same path in the same time period. In Fig. 1 the dotted black arrows show the switch conflict and the solid black arrows show the link conflict problem in OON.

The remainder of this paper is organized as follows. In the second section, related work and the theoretical about previously proposed algorithm is presented.

IV. Related Work

Using any one of the following three techniques we can minimize the crosstalk: the Space Domain Approach, the Wavelength Domain Approach, and the Time Domain Approach (TDA). The Time Domain Approach reduces the crosstalk problem by allowing only one source and its corresponding destination address to be active at a time within a SE in the network. The Window Method, the Improved Window Method, and many other TDA based approaches have come into limelight in recent years.

The aim of ASA is to select a particular source address that does not create conflict in the network in the first pass, and the remaining source address can be transmitted in the second pass. This algorithm is applicable for the 8 x 8 Optical Multistage Interconnection Networks. Initially, in this algorithm, the SA and DA are obtained sequentially. Next, the combination matrix of the source and corresponding destination address is obtained. Furthermore, transformation and row selection operations are applied on the combination matrix. In this way, two pairs of rows can be obtained. In the next step, addition and subtraction operations will be performed between the corresponding bits in each pair. Finally, some SAs and their DAs are selected for a current pass and again the ASA is applied to the rest of the addresses.

The routing process of RSA is little bit different from ASA. This algorithm emphasizes two operations (i.e., column selection and the construction of a conflict matrix table that is based on these columns). The rest of the operations of RSA is same as in ASA. Furthermore, providing crosstalk free routes in minimum passes is an exigent problem. For this problem, CFMON and its routing algorithm were proposed in. After going through, we found that the routing algorithm of CFMON does not provide the crosstalk-free routes in two passes in some exceptional cases. Hence, we have compared our research work with CFMON.

V. Conclusion

In this research work, we have analyzed the performance of an OMIN for crosstalk. The crosstalk is a challenging problem. Regarding this concern, we have proposed a new algorithm which is known as source destination based algorithm (SDBA). SDBA makes the cost effective and efficient for message transmission. In this result show minimum crosstalk and less time consume than the other CFMON. In the future research can be performed to analyze the performance of an OMIN with limited crosstalk under the bursty traffic, uneven and self-similar traffic conditions.

REFERENCES

- [1]. Nitin and Durg Singh Chauhan, "Stochastic Communication for Application Specific Networks-on-Chip," *Journal of Supercomputing*, 59 (2), DOI: 10.1007/s11227-010-0472-5, 2010, pp.779-810.
- [2]. Nitin, S. Garhwali and N. Srivastava, "Designing a Fault-tolerant Fully-chained Combining Switches Multi-stage Interconnection Network with Disjoint Paths," *Journal of Supercomputing*, 55 (3), DOI 10.1007/s11227-009-0336-z, 2009, pp.400-431.
- [3]. Nitin and Durg Singh Chauhan, "Comparative Analysis of Traffic Patterns on k-ary n-tree using Adaptive Algorithms based on Burton Normal Form," *Journal of Supercomputing*, 59 (2), DOI: 10.1007/s11227-010-0454-7, 2010, pp.569-588.
- [4]. Ved Prakash Bhardwaj and Nitin, "A New Fault Tolerant Routing Algorithm for Advance Irregular Augmented Shuffle Exchange Network, Proceedings of the 14th IEEE International conference on Computer Modeling and Simulation," Emmanuel College, Cambridge, UK, March 28-30, 2012, pp.505-509.
- [5]. J.C. Bernond, J.M. Fourneau, and A. Jean-Marie, "Equivalence of multistage interconnection networks," *Rapport LRI-217*, Univ. de Paris-Sud, France, May 1985.
- [6]. L.N. Bhuyan, and D.P. Agrawal, "Design and performance Of generalized interconnection networks," *IEEE Trans. Comput.*, Vol. C-32, no.12, pp.1081-1090, December 1983.
- [7]. Laxmi N. Bhuyan, Qing Yang, Dharma P. Agrawal, "Performance of Multiprocessor Interconnection Networks," *IEEE Computer* 22(2): 25-37, February 1989.
- [8]. M. Brenner, D. Tutsch, G. Hommel, "Measuring Transient Performance of a Multistage Interconnection Network Using Ethernet Networking Equipment," *Proceedings of the International Conference on Communications in Computing 2002 (CIC'02)*. Las Vegas, USA, 2002, pp. 211-216.
- [9]. S. Cheemalavagu, M. Malek, "Analysis and Simulation of Banyan Interconnection Networks with 2x2, 4x4 and 8x8 Switching Elements," *IEEE Real-Time Systems Symposium* 1982: 83-89.
- [10]. A. Verma and C.S. Raghvendra, "Interconnection Networks for Multiprocessors and Multi-computers: Theory and Practice", *IEEE Computer Society Press*, Los Alamitos, California, 1994.
- [11]. A.K. Katanga, Y. Pan and M.D Fraser, "Message Routing and Scheduling in Optical Multi-stage Networks Using Simulated Annealing", *International Proceedings of the Parallel and Distributed Processing Symposium (IPDPS)*, 2002

	<p>Ramesh Kumar was born on May 03, 1982, in Jehanabad (Bihar), India. He received the B. Engg in Computer Sc & Engineering from Rajasthan Institute of Engineering & Technology (RIET), Bhankrota jaipur in 2008 .In 2014, he received M. Tech in Computer Science and Engineering form Institute of Engineering & Technology (IET) Alwar Rajasthan India.</p>
	<p>Vedant Rastogi working as an Associate Professor in department of Computer Science & Engineering, I.E.T.,Alwar, Rajasthan. He received his M.Tech. from A.A.I. Deemed University, Allahabad (U.P.). He is pursuing his Ph.D. in Computer Science from K.L.University, Viajawada (A.P.). His research area are Speech recognition techniques, Image processing and Mobile Adhoc network. He has guided 9 M.Tech. Students in different research area.</p>

Data and Information Integration: Information Extraction

Varnica Verma¹

¹(Department of Computer Science Engineering, Guru Nanak Dev University, Gurdaspur Campus, Punjab, India)

ABSTRACT: Information extraction is generally concerned with the location of different items in any document, may be textual or web document. This paper is concerned with the methodologies and applications of information extraction. The field of information extraction plays a very important role in the natural language processing community. The architecture of information extraction system which acts as the base for all languages and fields is also discussed along with its different components. Information is hidden in the large volume of web pages and thus it is necessary to extract useful information from the web content, called Information Extraction. In information extraction, given a sequence of instances, we identify and pull out a sub-sequence of the input that represents information we are interested in.

Manual data extraction from semi supervised web pages is a difficult task. This paper focuses on study of various data extraction techniques and also some web data extraction techniques. In the past years, there was a rapid expansion of activities in the information extraction area. Many methods have been proposed for automating the process of extraction. We will survey various web data extraction tools. Several real-world applications of information extraction will be introduced. What role information extraction plays in different fields is discussed in these applications. Current challenges being faced by the available information extraction techniques are briefly discussed along with the future work going on using the current researches is discussed.

Keywords: DELA, HTML, IE, NLP, REES.

I. Introduction

Information Extraction (IE) is used to identify a predefined set of concepts in a specific domain, ignoring other irrelevant information, where a domain consists of a corpus of texts together with a clearly specified information need. In other words, IE is about deriving structured factual information from unstructured text. For instance, consider as an example the extraction of information on violent events from online news, where one is interested in identifying the main actors of the event, its location and number of people affected. Information extraction identifies class of pre-specified entities and relationships and their relevant properties. The main aim of information extraction is to represent the data in the database in structured view i.e., in a machine understandable form [6].

II. Literature Survey

According to Jakub Piskorski and Roman Yangarber [1], information extraction is an area of natural language processing that deals with finding information from free text. Sunita Sarawagi [2] studies the different techniques used for information extraction, the different input resources used and the type of output produced. She says that information extraction can be studied in diverse communities. Devika K and Subu Surendran [3] provide different tools for web data extraction. Jie Tang [5] details on the challenges in the field of information extraction.

2.1 Early Years: Knowledge Extraction Systems

In the early years, information extraction systems were developed using the knowledge engineering approaches where the creation of knowledge in the form of rules and patterns, for detecting and extracting the required information from the database, was done by human experts. Most of the early IE systems had a drawback that they showed a black-box character, which were not easily adaptable to the new scenarios. The aim of knowledge based systems is put efforts for general purpose information extraction systems and frameworks which are easier to adapt and learn by the new domains and languages [1]. Modularized approach was used for the development of such systems. Two examples of modular approach used are IE2 and REES. The

first one achieved the highest scores for all IE tasks and the second had been the first attempt for large scale events and relation extraction systems based on shallow text analysis methods.

2.2 Architecture: Components of Information Extraction System

Different IE systems are developed for performing different tasks but some components always remain the same. These components typically include core linguistic components-which are useful to perform NLP (natural language processing) tasks in general- and IE specific components which address the IE specific tasks. Also, domain-independent and domain specific components are also included [1].

The following steps are followed in order to extract information:-

2.2.1 Domain Independent Components

- ✚ Meta-Data Analysis: - Extracts the title, body, structure of the body and the date of the document i.e., the date when the document was created [1].
- ✚ Tokenization: - Text is segmented into different parts called tokens which constitute words with capital letters, punctuation marks, numbers used in the whole text etc. All the tokens are provided with different headings and the relevant data from the text is added to the respective tokens [1].
- ✚ Morphological Analysis: - In this step the information is extracted from the tokens [1].
- ✚ Sentence or Utterance Boundary Detection: - This performs the formation of sequence of sentences from the text, along with different items associated with it and their different features [1].
- ✚ Common Named-Entity Extraction: - Extraction of domain-independent entities is performed. These entities are represented with common names like number, currency, geographical references etc [1].
- ✚ Phrase Recognition: - Recognition of verbs, nouns, abbreviations, prepositional phrases etc. is performed in this step [1].
- ✚ Syntactic Analysis:-Structure for sentences is designed based on the sequence of different items being used in the sentence. The structure can be of two types: one is deep i.e. includes each and every detail of the items being consumed and second is shallow i.e. includes only the specific items and not their further properties or attributes. The structure can be like parse trees. The shallow structure fails to represent ambiguities (if any) [1].

2.2.2 Domain Specific Components

The core IE tasks are domain specific and are therefore implemented by domain specific components. Domain specific tasks can also be performed at lower level of database extraction. The following steps are applied:-

- ✚ Specific Named-Entity Recognition: - The text is extracted using some specifically highlighted terms from the text. For example, in domains related to medicine some specialized terms related to medicine are required whereas in case of a large enterprise there is no such requirement [1].
- ✚ Pattern Matching: - The entities and their key attributes are extracted. These must be relevant to the target relation or event. All the properties of each and every entity are detected from the text. The entities constitute different patterns according to the properties inherited by them [1].
- ✚ Co-Reference Resolution: - Implementation of inference rules is done in this step in order to create fully fledged relations or events [1].
- ✚ Information Fusion: - The entities with same attributes are combined to constitute one entity set. The related information is generally grouped together in different sentences and documents. All this data is collected and grouped together in the pattern of their properties so that a proper relation can be made [1].

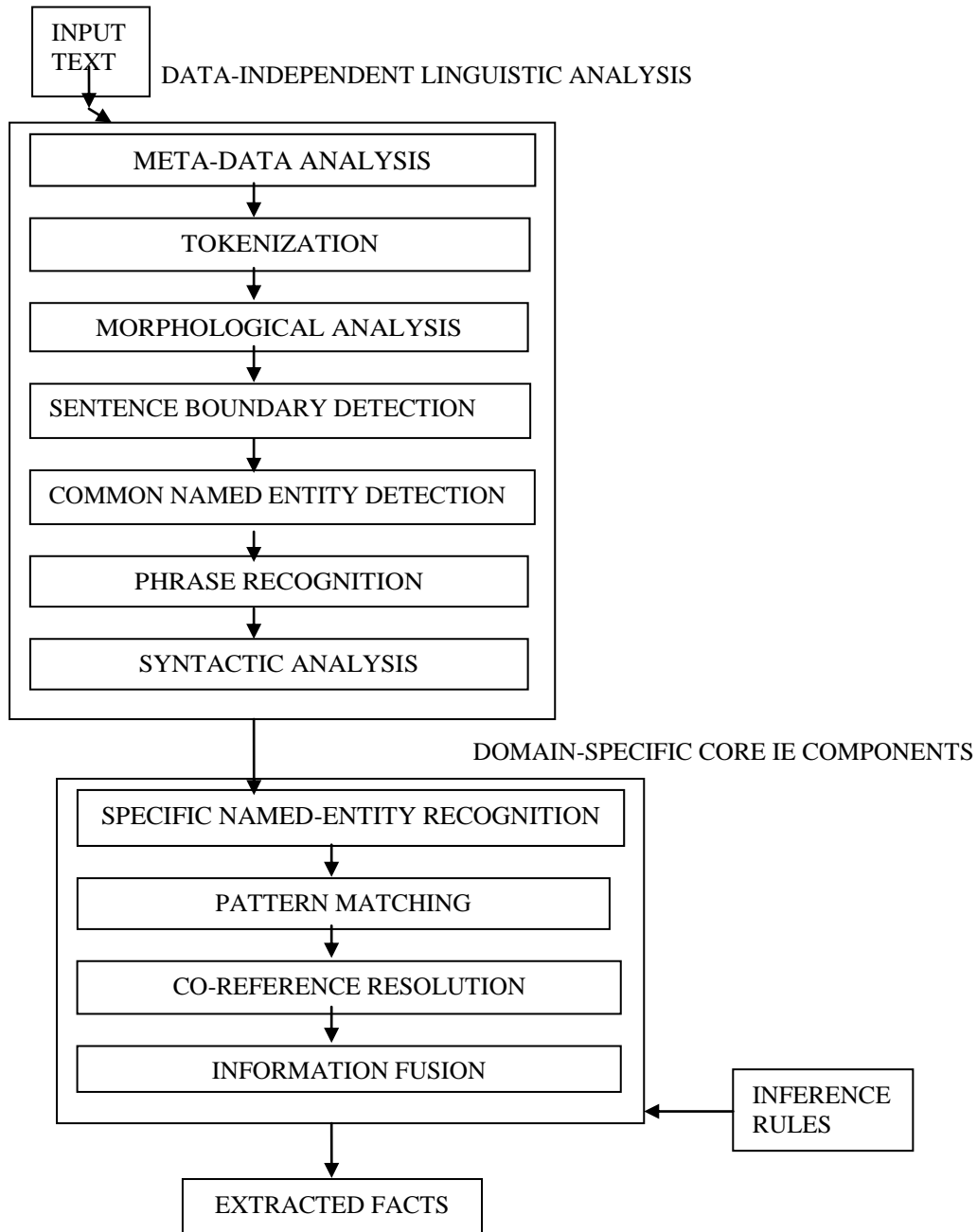


Figure: 1. Architecture of information extraction system

2.3 Knowledge Extraction Techniques

2.3.1 Rule Based Technique

The detection and extraction of information and data is performed by using some knowledge based rules. Human expertise plays an important role in this method [5].

Advantages:

- Fast
- Simple
- Easy to understand
- Easily implementable
- Can be implemented on different data standards [4].

Disadvantages:

- Ambiguity cannot be resolved
- Cannot deal with facts
- Mono-lingual technique

➤ Not easily adaptable on different platforms [4].

2.3.2 Pattern Learning Technique

This technique involves writing and editing patterns which requires a lot of skill. It also consumes a considerable amount of time. These patterns are not easily adaptable to new platforms used for different databases [4].

2.3.3 Supervised Learning Technique

This is pipeline style information extraction technique. In this method the task is split into different components and data annotation is prepared for these components. Several machine learning methods are used to address these components separately. Name tagging and relation extraction are some of the progress made using this field [4].

2.4 Web Data Extraction

Internet is a very powerful source of information. A lot many business applications depend on the internet for collecting information which plays a very crucial role in the decision making process. Using web data extraction we can analyze the current market trends, product details, price details etc. [7].

Web page generation is the process of combining data into a particular format. Web data extraction is the reverse process of web page generation. If multiple pages are given as input then the extraction target will be the page wide information and in case of a single page the extraction target will be record level information. Manual data extraction is time consuming and error prone [3].

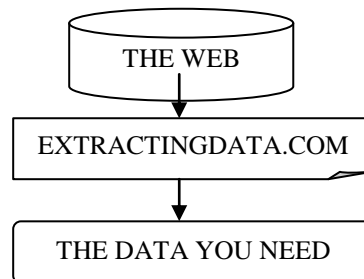


Figure: 2 web data extraction

2.4.1 WEB DATA EXTRACTION TOOLS

1) DELA (Data Extraction And Label Assignment For Web Databases)

DELA automatically extracts data from web site and assigns meaningful labels to data. This technique concentrates on pages that querying back end database using complex search forms other than using keywords [3].

DELA comprises of four basic components:-

- a. A form crawler
- b. Wrapper generator
- c. Data aligner
- d. Label assigner

❖ FORM CRAWLER

It collects labels of the website form elements. Most form elements contain text that helps users to understand the characteristics and semantics of the element. So, form elements are labeled by the descriptive text. These labels are compared with the attributes of the data extracted from the query-result page [3].

❖ WRAPPER GENERATOR

Pages gathered by the form crawler are given as input to the wrapper generator. Wrapper generator produces regular expression wrapper based on HTML tag structures of the page. If a page contains more than one instance of data objects then tags enclosing data objects may appear repeatedly. Wrapper generator considers each page as a sequence of tokens composed of HTML tags. Special token “text” is used to represent text string enclosed with in HTML tag pairs. Wrapper generator then extracts repeated HTML tag substring and introduces a regular expression wrapper according to some hierarchical relationship between them [3].

❖ **DATA ALIGNER**

Data aligner has two phases. They are data extraction and attribute separation [3].

➤ **DATA EXTRACTION**

This phase extracts data from web pages according to the wrapper produced by wrapper generator. Then it will load extracted data into a table. In data extraction phase we have regular expression pattern and token sequence that representing web page. A nondeterministic finite automation is constructed to match the occurrence of token sequences representing web pages. A data-tree will be constructed for each regular expression.

➤ **ATTRIBUTE SEPARATION**

Before attribute separation it is needed to remove all HTML tags. If several attributes are encoded in to one text string then they should be separated by special symbol(s) as separator. For instances "@", "\$", "." are not valid separator. When several separators are found to be valid for one column, the attributes strings of this column are separated from beginning to end in the order of occurrence portion of each separator.

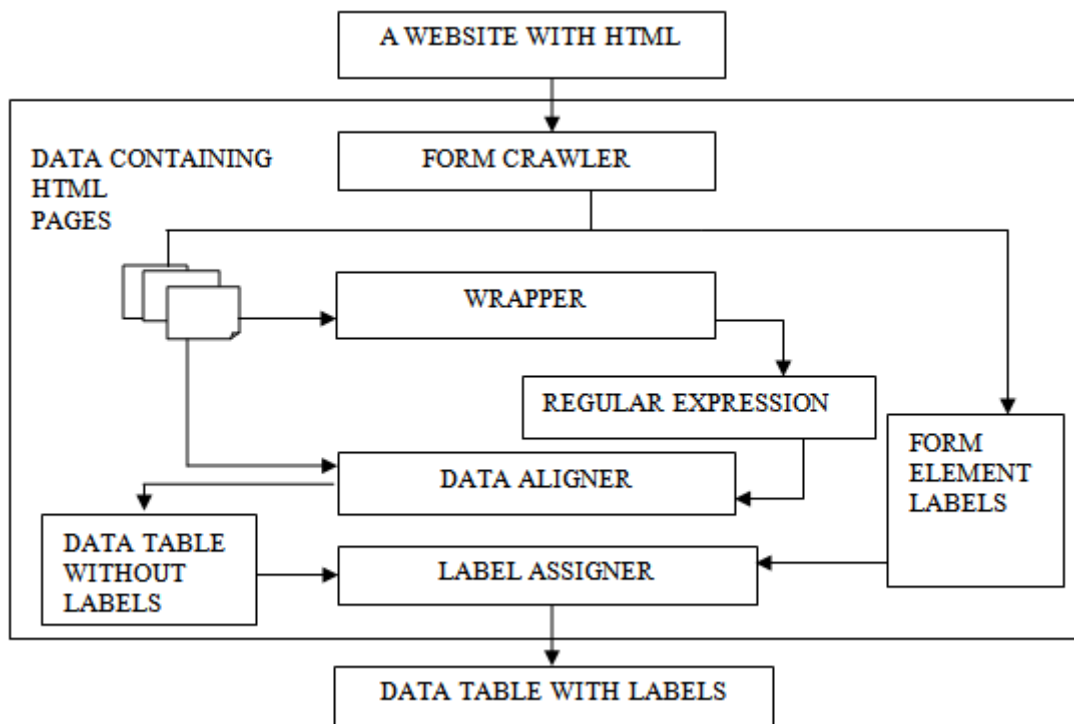


Figure: 3 DELA (Data extraction and label assignment for web data extraction)

2) **FIFA TECH**

Fifa Tech is a page level web data extraction technique. It comprises of two data modules through which data extraction is performed [3].

- First module takes DOM trees of web pages as input and merges all DOM trees into a structure called fixed/variant pattern tree.
- In the second module template and schema are detected from fixed/variant pattern tree.
- Peer node recognition: Peer nodes are identified and they are assigned same symbol.
- Matrix alignment: This step aligns peer matrix to produce a list of aligned nodes. Matrix alignment recognizes leaf nodes which represent data item.
- Optional node merging: This step recognizes optional nodes, the nodes which are which disappears in some column of the matrix.
- Schema detection: This module detects structure of the website i.e., identifying the schema and defining the template.

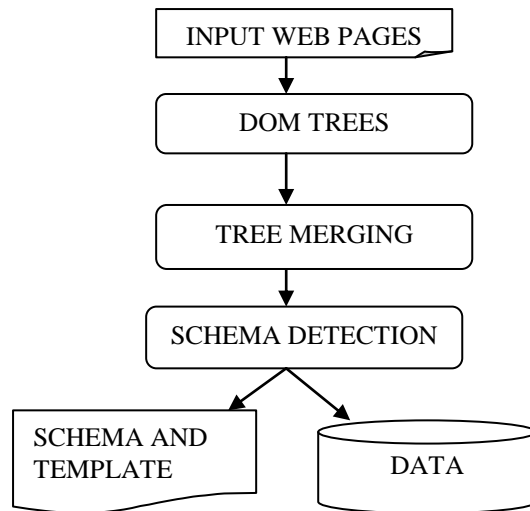


Figure: 4 Fifta tech for web data extraction

3) IEPAD

It is an information extraction system which applying pattern discovery techniques. It has three components, an extraction rule generator, pattern viewer and an extract module [3].

- Extraction rule generator accepts input web page and generate extraction rules. It includes a token translator, PAT tree constructor, pattern discoverer, a pattern validator and an extraction rule composer as shown in Fig.
- Pattern viewer is a graphical user interface which shows the repetitive pattern discovered.
- Extractor module extracts desired information from pages. [3]Translator generates tokens from input webpage. Each token is represented by a binary code of fixed length l.PAT tree constructor receives the binary file to construct a PAT tree. PAT tree is a PATRICIA tree (Practical Algorithm to Retrieve Information Coded in Alphanumeric). PAT tree is used for pattern discovery. Discoverer uses PAT tree to discover repetitive patterns called maximal repeats. Validator filters out undesired patterns from maximal repeats and generates candidate patterns.

HTML PAGE

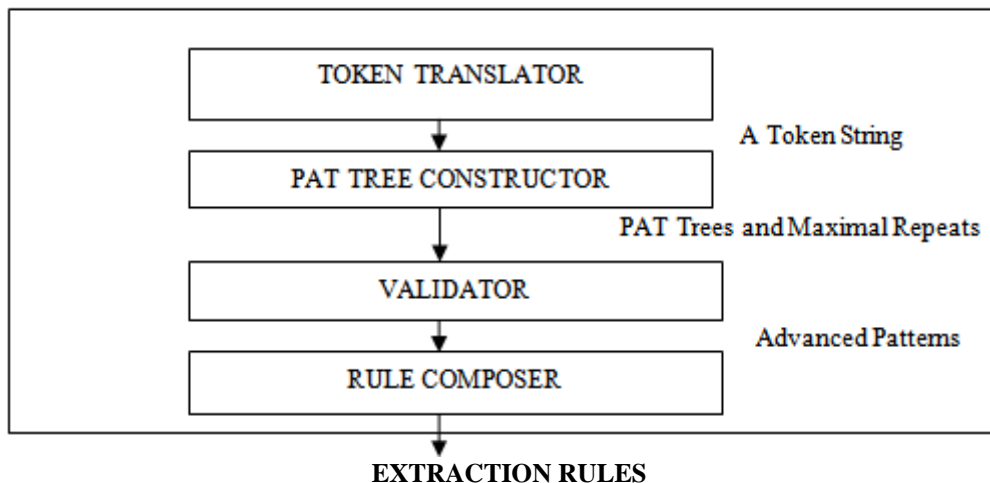


Figure: 5 IEPAD for web data extraction

III. Applications Of Information Extraction

Information extraction is used in different areas like business enterprises, personal applications, scientific applications etc. Information extraction plays a very important role in each and every field we work in. Various applications are listed as:-

3.1 Enterprise Applications

+ News Tracking

Information extraction plays a very important role in extracting information from different sources. There are two recent applications of information extraction on news articles: it integrates the data from videos and pictures of different events and entities of news articles and gathers background information on people, locations and companies [2].

+ Customer Care

A customer oriented enterprise requires to integrate itself with the customer requirements provided by them through mails and other means. This can be done by integrating customer interaction with the enterprise's own structured databases and business's ontologies [2].

+ Data Cleaning

Duplicacy of data needs to be removed from the databases. Data warehouse cleaning process is used to clean the information by keeping the similar data in same format at one place so that no redundancy arises. By dividing an entity into its properties it becomes easy to do the deduplication [2].

3.2 Personal Information Management

Personal information management systems aims to integrate the information provided in the form of e-mails, documents, projects and people in a structured format which links them with each other. Such systems are successful only if they are able to extract data from the predefined unstructured domains [2].

3.3 Scientific Applications

The rise in the field of bio-informatics has lead to the development of data extraction from terms like proteins and genes. Earlier it was not possible to extract the data from such biological terms but with the success in the field of information extraction and advancement in the techniques of data extraction it has become possible to extract data from various scientific entities and not stay limited only to the classical terms like people and companies [2].

3.4 Web Oriented Applications

+ Citation Databases

Many citation databases require different structure extraction steps for its creation. These are navigating websites for locating pages containing publication records, extracting individual publication records as per requirement of the database, extracting title, authors and references and segmenting all of them resulting in a structured database [2].

+ Opinion Databases

There is a lot of data available on the web related to any topic but in rough format. By using different structured techniques this data can be organized and all the reviews which lie behind the blogs, review sites, newspaper reports etc. can be extracted [2].

+ Community Websites

These are the websites which are created using data about researchers, conferences, projects and events which are related to a particular community. These structured databases require these steps for its creation: locating the talks of the departments, finding the title of the conference, collecting the names of the speakers and so on [2].

+ Comparison Shopping

Different websites are created listing the information of their products and their price details. Such websites are used when looking for any product and its data is extracted from these collectively in order to form a structured database [2].

IV. Challenges and Future

- + Traditionally the task of information extraction was carried out in only one language i.e., English. But with the growing textual data available in other languages there had become a need to extract data in all these languages [1].**
- + Designing information extraction techniques in different languages creates a difficulty in implementation. Hence, in order to remove this difficulty such techniques are designed which work for all languages [1].**
- + The different protocols to be used for information extraction are designed and formulated in such a way that all the textual data from different languages can be extracted easily [1].**
- + Thus, it is harder to implement information extraction using different languages and also the performance of non-English information extraction techniques is also lower [1].**

- ✦ Extracting different entities from database has become easy by the different methodologies being developed but the identification of the relationship among these is still a very challenging task to perform. Bunescu and Mooney (2005b) have introduced a Statistical Relational Learning model to deal with this complex problem and are trying to investigate and find results on this side [5].
- ✦ In current researches, emphasis is also laid on the characteristic of extracting information not only from one single source but from multiple sources [5].
- ✦ Extracting facts from multiple sources helps in defining them and understanding them more precisely and accurately. Many efforts are being laid in this aspect.
- ✦ As another future work, more emphasis is required to be laid on the applications of information extraction. Investigation on these applications will provide more sources of information extraction and can bring new challenges to this field. This is because different applications have different characteristics and different techniques are required to extract information from these fields.

V. Conclusion

This paper includes the study of information extraction systems in the past. Then comes the architecture of the knowledge extraction system and the different components included in it. It includes domain independent and domain specific components. Different knowledge extraction techniques are discussed like rule based technique, pattern learning technique and supervised learning technique. A method of data extraction, web data extraction, is detailed with its different tools. Tools like DELA (data extraction and label assignment), fifa tech and IEPAD have been discussed.

Extracting information from web plays a very important role in different business, personal and scientific applications. The next part of the paper includes the various applications of information extraction. The different techniques of information extraction helps in designing customer care applications, citation databases, news tracking applications etc. and is used for the purpose of data cleaning.

A vast progress has been made in this field but a more lot is still to be done. Researches continue in this field, emerging with new techniques with more efficiency and more performance. A model for information extraction system which acts as the base model for all the language dependent databases has been developed and removed the complex problem of developing a separate model for each database with different language as its base. A great future development is expected in this field with the researches continuing to move in more depth and bringing in new terms and techniques towards information extraction.

REFERENCES

- [1] Jakub Piskorski and Yoman Yangarber (2013), "*Information extraction- past, present and future*", The 4th Biennial International Workshop on Balto-Slavic Natural Language Processing, Multisource, Multilingual Information Extraction and Summarization, Publisher: Springer, ISBN: 978-3-643-28568-4.
- [2] Sunita Sarawagi (2008), "*Information extraction*", Foundations and trends in databases, Volume.1, Issue No. 3(2007), 261-377, DOI: 10.1561/9781601981899, E-ISBN: 978-1-60198-189-9, ISBN: 978-1-60198-188-2.
- [3] Devika K, Subu Surendran (April, 2013), "*An overview of web data extraction techniques*", International journal of scientific engineering and technology, Volume 2, Issue 4, pp: 278-287, ISSN: 2277-1581.
- [4] Heng ji (june 12,2012), "*Information extraction: techniques, advances and challenges*", North American Chapter of the Association for Computational Linguistics (NAACL) Summer School.
- [5] Jie Tang, Mingcai Hong, Duo Zhang, Bangyong Liang and Juanzi li (2007), "*Information extraction: Methodologies and applications*", Emerging Technologies of Text Mining: Techniques and Applications, pp: 1-33.
- [6] Douglas E. Appelt (1999), "*Introduction to information extraction*", Artificial Intelligence centre, SRI International, Menlo Park, California, USA, ISSN: 0921-7126.
- [7] Alexander Yates (2007), "*Information Extraction from the Web: Techniques and Applications*", University of Washington.

Simulink Model for Cost-effective Analysis of Hybrid System

Raja Sekhar Gorthi¹, K. Giri Babu², Dr. S. Shiv Prasad³

^{1,2,3}Department of Electrical & Electronics Engineering, JBIET, Hyderabad, A.P, India.

Abstract: Utilization of non conventional sources of energy to meet the present day energy requirement has become very much essential in the era of fossil fuel crises. The present paper discusses the importance of PV-Diesel hybrid system to meet electrical requirement in remote areas. A model of a photovoltaic array with diesel battery was designed by MATLAB simulink. In this paper, the cost-effective analysis which includes the fuel consumed, the energy obtained per gallon of fuel supplied, and the total cost of fuel. Simulations done for Diesel generator system, diesel-battery system and solar PV with diesel-battery system using a one-year time period. Based on simulation results energy payback period for PV array, the simple payback time for the PV module calculated. Simulation analysis includes the comparison of system cost, efficiency, and kWh per gallon with those predicted by Hybrid Optimization Model for Electric Renewables (HOMER).

Keywords: Energy payback period, simple payback time, hybrid system, HOMER.

I. Introduction

Hybrid power systems are intended for the generation of electrical power and are used in remote areas. Hybrid systems consists of a number of power generation devices such as photovoltaic, micro-hydro and/or fossil fuel (diesel) generators. Hybrid power systems range from 0.1kwh to 10 Mwh per day. Hybrid power systems to provide reliable power to the many remote areas in the developing countries where transportation costs of diesel fuel are very high. The use of non conventional power generation systems reduces the use of fossil fuels, allows for the cleaner generation and also improves the standard of living .The use of non conventional energy sources in remote areas could help reduce the operating cost through the reduction in fuel consumption, increase system efficiency, and reduce emissions[1],[2]. There are issues associated with storage of fuels. Therefore, photovoltaic and other renewable sources of energy are being integrated with DEGs to help reduce the fuel consumed by the DEGs.

The RTU provides the information for modeling of power system. Remote terminal unit processed by the simulink model. In this way, the RTU and the model can be used to optimize the performance of the hybrid power system.

MATLAB Simulink is used to model the system and distribute the electrical load distribution between the PV array and diesel-electric generator. Simulations are performed for three cases: 1) only diesel system 2) diesel with battery and 3) PV with diesel-battery system using a one-year time period. The Simulation results used to perform a cost-effective analysis and predict the ecological impacts of hybrid power system. The cost-effective part of the model calculates the fuel consumed, the energy obtained per gallon of fuel supplied, and the total cost of fuel. These results are then utilized to calculate the EPBT (Energy payback time), the SPBT (simple payback time) for the PV module.

II. Hybrid Systems Model

A hybrid system is a combination of one or more resources of renewable energy such as solar, micro or mini-hydropower and biomass with other technologies such as batteries and diesel generator. Particularly, the solar hybrid system developed with a combination of solar with battery and diesel generator. The hybrid system offers clean and efficient power that will in many cases be more cost-effective than individual diesel systems. As a result, renewable energy options have increasingly become the preferred solution for off-grid power generation. The system has been installed at the middle and top stations. Hybrid system supplies power for base load from non conventional energy resources whilst the peak load could be met via battery and diesel generator.

When two or more different power sources are connected to a common grid and operate hand in hand to give the desired load, the system becomes a hybrid electric power system. Simple block diagram of a hybrid power system is shown in Fig 2.1. The hybrid system consists of a diesel generator, a battery bank, a PV array. The diesel generator is the main source of power for many of the distant villages and around the world. The Diesel generator gives ac voltage as output, which supplies the load through transformer.

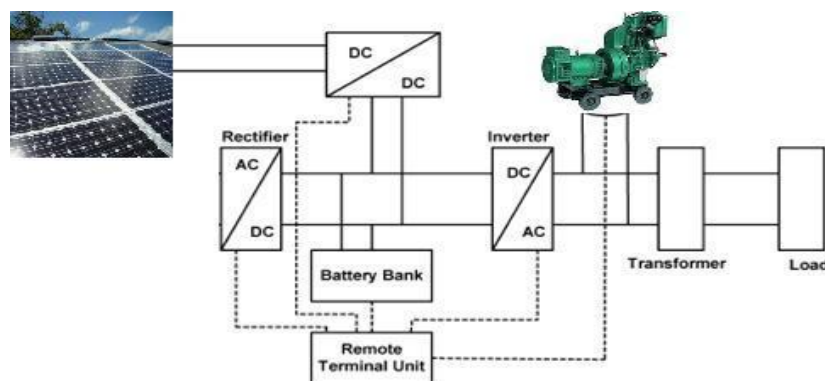


Fig.2.1

The battery bank, the PV array is interlinked through a dc bus. The RTU controls the flow of power to and from the different units, depending on the load. RTU plays main role in a hybrid power system to improve the performance of the system. The purpose of the RTU is to monitor and control the hybrid system. The RTU is interfaced with many sensors and control devices located at different locations within the hybrid system. The RTU processes the data from these sensors and transmits it to a control center.

In this paper, the hybrid power system consists of 21- and 35-kW diesel generators, 100 kWh of lead acid batteries, and a 12-kW PV array. The PV array consists of 8 kW and 4 kW solar panels. A 30-kVA bidirectional power controller is used to supply power to and from the batteries and from the PV array. The use of renewable energy in the form of a PV array combined with regulated battery storage helps in constraining the use of the diesel generator while optimizing the efficiency and economics of the system.

A hybrid power station typically includes (a) Inverter unit (b) Diesel engines, which are 1.5 times the inverter rating with diesel generator control system. A fully automatic diesel generator control system enables automatic operation and automatic selection of power sources (c) A battery storage system (d) A solar PV array and solar regulator (e) A microprocessor based controller unit to monitor and manage the system automatically.

The solar hybrid power system makes use of the solar PV to produce electricity that can be supplemented by diesel generators. The configuration of solar hybrid system is analyzed for various photovoltaic array sizes with respect to a diesel generator to operate in tandem with the battery system. The power controller unit will determine the AC conversion of the DC power in relation to optimum diesel generator operation following the load profile. The charge controller will charge the batteries with energy from solar modules as well as from the diesel generator. The main objective of solar hybrid system is to reduce the cost of operation and maintenance and cost of logistic by minimizing diesel runtime and fuel consumption. To achieve this generator only runs as needed to recharge the battery and to supply excess load. It is started when the battery reaches a preset discharge level and is run at full capacity until the battery is fully recharged and then shut down. During day time, Solar PV panels used to generate the electricity while the generator is off mode. The output of PV arrays i.e., DC power converts to AC power using inverter. The additional generated power is stored in battery system. During Night Time, battery supplies the energy to load while the generator and PV arrays are both off. The inverter again converts the battery output power to AC power for the load. The battery will supply the load to its maximum discharge level. During shortfall, the battery reaches its maximum discharge level and therefore, the generator is on. At this time, the generator serves the load as well as charges the battery. The battery charge rate is adjusted to maintain the generator at full output. The operations, which activate or deactivate generator set and charging or discharging battery are managed and done by a microprocessor-based controller unit. The controller unit monitors and manages the load demand and energy supplied.

III. Simulation Model

The simulation models for three cases are shown below viz., Fig 3.1, Fig 3.2 and Fig 3.3. The Simulation model consists of nine blocks. The Input Parameters block consists of data files obtained from the site. The model receives the information from the Remote terminal unit after installation. Sensors collect the information from the location which includes the amount of sunlight insolation, incident upon the PV arrays, charge and discharge level of the batteries, and operating parameters of the diesel generator and passed to signal conditioning devices. These signals are then transmitted to A/D converter for processing. The data is then saved within the memory of the RTU[3]. The data which includes solar insolation values, electrical load, and temperature are useful to develop the model and also to find out efficiency and the amount of fuel used for the Diesel generator. These parameters sufficient to analyze any hybrid power system.

The PV Model block is the model of the 12-kW PV array to calculate the power available from the PV array, based on the intensity of sunlight. The -function written in MATLAB performs the following tasks.

- 1) The total power available from the PV array (aligned due south and tilted at a 15 degrees) is calculated using the solar insolation values which are collected from NREL, the total area of the collector from the manufacturer data sheet, and the efficiency of the solar collector. In this project, a collector efficiency of 12% is assumed.
- 2) The model compares the calculated PV power to the required load.

The Battery Model block consists of the battery bank and controller. The -function in the Battery Model block performs the following tasks. The total battery voltage is calculated using the number of battery cells and the voltage per cell as follows:

$$\text{Battery volt} = n * \text{volt_per_cell}$$

Where volt per cell is obtained from the output of the Input Parameters block. The model then compares the required load with the rated capacity of the two generators. If the required load more than the capacity of the two generators, then the model displays the message that the load can't be supplied. If the load is less, then the Simulink model checks for the available energy and the mode (charging or discharging) of the battery bank. If the battery bank energy is greater than 20% and the battery is in the discharging state, then the battery energy will be supplied to the load. If the available energy of the battery bank is less than 20% of its rated kilowatt-hours or if the battery bank is in the charging stage, then the energy from the diesel generator will be used to supply the load and charge the battery bank simultaneously.

The Generator Model block contains parameters like efficiency of the electric generator. The input power to the generator can be calculated as

$$P_i = \frac{P_1}{\eta}$$

Where P_1 is the load on the diesel generator.

The Generator Model block is designed in such a way that the diesel generators are always operating at 95% of their kilowatt rating while operating in conjunction with the battery bank and the PV array.

The Fuel Consumption Model block calculates the amount of fuel required by the diesel engine to supply the load. The fuel consumed by the engine depends on the load and the electrical efficiency of the generator. The plot for the fuel consumption obtained from the manufacturer's data sheet can be mathematically interpreted as follows:

$$F_c = \frac{0.5 * P_i + 0.5}{7.1}$$

Fuel consumed

Where P_i is the input power to the generator given in kilowatts; 7.1 is the factor that converts pounds (lbs) to gallons.

The Error block calculates the difference between the powers (supplied and required). The error within the model is calculated by

$$\text{Error} = P_s + P_G + P_{p_v} - P_L - P_D$$

Where P_s is the power supplied by the battery bank, P_G is the power supplied by the diesel generators, P_{p_v} is the power supplied by the PV array, P_L is the power delivered to the load, and P_D is the power delivered to the dump load.

The rms value of error is given by

$$\text{Error (rms)} = \sqrt{\frac{\sum (\text{Ins tan tan eous value})^2}{n}}$$

The Other Parameters block calculates the parameters such as the total energy per gallon supplied by the generator, fuel consumed, the total cost of fuel (in U.S. dollars). The kilowatt-hours per gallon and total fuel cost are calculated as

$$\frac{\text{kwh}}{\text{gallon}} = \frac{\text{kwh}_{Gen}}{F_c}$$

$$\text{And Total cost (USD)} = F_c * \frac{\text{cost}}{\text{gallon}}$$

The Display Parameters block is used to display all the calculated parameters

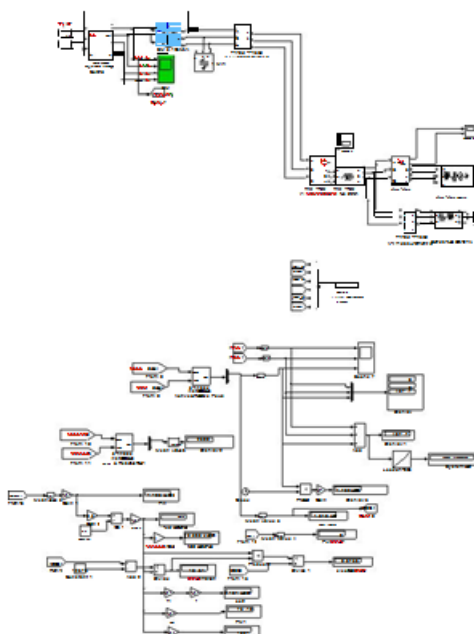


Fig 3.1 Remote diesel only System (Case-I)

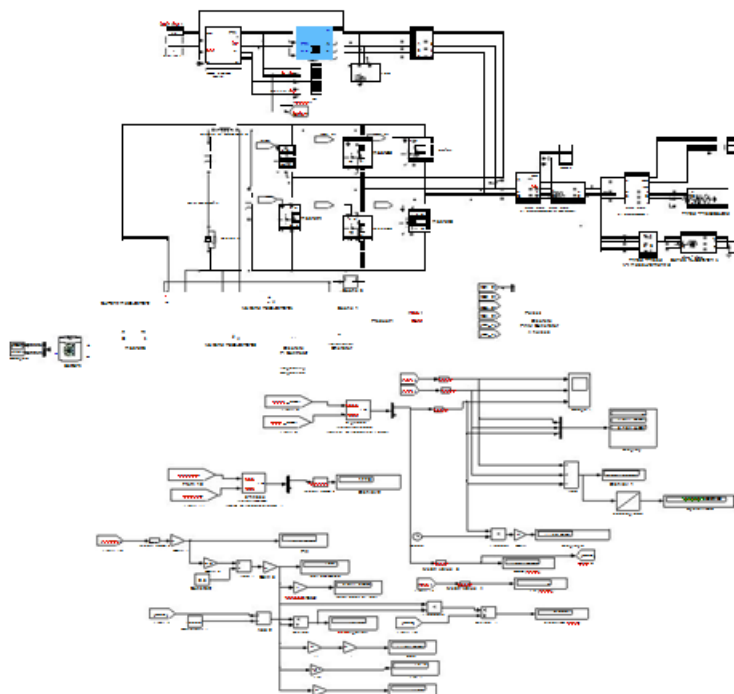


Fig 3.2 Remote diesel-battery System (Case-II)

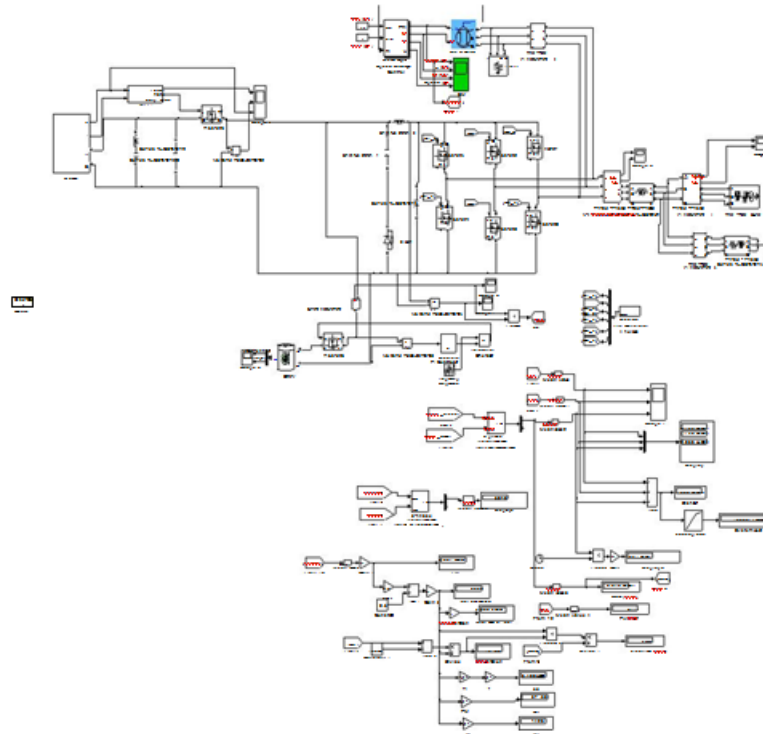


Fig 3.3 Remote PV diesel-battery System (Case-III)

IV. Simulations and Results

Simulations were performed for diesel system, diesel-battery system, and PV with diesel-battery system. The costs of the different components were obtained from the various manufacturers listed[4] in Table I. Due to the distance of the site, the cost for transporting the various components is relatively high.

Table II shows the results for diesel,diesel battery and pv with diesel battery cases. In this model, converters efficiency was considered as 90%. The solar collector efficiency for the PV array is assumed as 12%. As per HOMER, the density of fuel is assumed to be 840 Kg/m³ and the heating value of fuel is assumed to be 48.5 MJ/kg, and Simulation results were utilized to analyze cost-effective which includes the simple payback time and energy payback time. The cost-effective analysis part of the simulation model involves calculation of the simple payback time (SPBT) and energy payback time (EPBT) for the PV module and array respectively. Usually, battery banks are used as back-up sources for power. Therefore, the PV with diesel-battery system is compared to the diesel-battery system in the analysis of SPBT. The Simple payback time is expressed as

$$SPBT = \frac{\text{Excess cost of PV system}}{\text{Rate of saving}}$$

From table 2,

$$SPBT = 18.11 \text{ years}$$

In order to calculate the Energy payback time for the PV array, it is essential to know the energy required in the construction of the PV array is also called as embodied energy. In this method [5], the total energy required is the sum of energies required for raw materials and the energy required in the various processes involved to convert the raw materials into the PV array.

The embodied energy of a PV system is given by

$$\text{Embodied energy} = 5600 * \text{Rated power of PV}$$

And

$$EPBT = \frac{\text{Embodied energy}}{E}$$

$$EPBT = 7.11 \text{ years}$$

The PV array is rated to produce 12 kW, and from Table II, the value for is 9445 Wh/yr.

Table III shows the comparison of the results using the Simulink model with those predicted by HOMER. It was observed that the efficiency of the diesel generator is higher using the Simulink model. This is because in the Simulink model, the battery bank has a longer charge/discharge cycle. So, the life time of the battery bank is less in the Simulink model as compared to that of HOMER.

In HOMER, the energy generated by the diesel engine is higher because the battery bank is designed to cycle between 40% and 82% of its energy rating rather than between 20% and 95% in the Simulink model. The converters are operating with much less efficiency in HOMER as compared to the Simulink model (about 20% difference). In HOMER, the Diesel generator is loaded anywhere between 6.3–21 kW, with the average load of 13.4 kW, and, hence, operates with a lower electrical efficiency than in the Simulink model. In the Simulink model, the battery bank acts as a source of power. So whenever the Diesel generator is —on,|| it operates at 95% of its rated power—therefore, with a higher electrical efficiency. If the load on the DEG is less than 95% of its rated power, the excess power is utilized to charge the battery bank. It can also be observed that the efficiencies for the DEG-battery and PV-DEG-battery are the same in the Simulink analysis. In the above analysis, HOMER has the advantage with a higher net present value (NPV) due to the longer life of the battery bank over the Simulink model. The battery bank is the most expensive component of the system.

After conducting the simulations for the three cases, it was observed that pv with diesel hybrid system provided better results in terms of fuel consumption for the diesel generator .It was observed that the diesel generator operates most efficiently for case 3, while the diesel-battery system has the highest kilowatt-hours per gallon. In diesel only system the entire load was supplied without the PV array and the battery bank, leaving the load to be supplied by the diesel generator. Since the diesel generator operates with the lowest load for the diesel-only system, it is the least efficient system and has the lowest kilowatt-hours per gallon. In diesel battery system, when the battery bank is discharged, the diesel generator is used to charge the battery bank, so finally, the entire load is supplied with the help of the diesel generator. In case 3, part of the load was supplied using the PV array. As a result, there is substantial saving in the fuel consumption by the diesel generator due to use of the battery bank and the PV array with the diesel-only system.

Table I : Installation costs for 3 cases (Diesel, diesel-battery and PV with Diesel battery)

Item	Cost per unit	No. of units	Diesel-only system	Diesel-Battery system	PV with Diesel-Battery system
35 KW diesel generator	\$28,000	1	\$28,000	\$28,000	\$28,000
21KW diesel generator	\$18,500	1	\$18,500	\$18,500	\$18,500
Switch gear to automatic control of both diesels	\$16,000	1	\$16,000	\$16,000	\$16,000
Rectification/ Inversion	\$18,000	1	\$0	\$18,000	\$18,000
New absolyte IIP6-90A13 Battery bank	\$2,143	16	\$0	\$34,288	\$34,288
BP 275 Solar	\$329	105	\$0	\$0	\$34,545
Siemens M55 Solar	\$266	75	\$0	\$0	\$19,650
Engineering		1	\$3,000	\$3,500	\$4,000
Commissioning, Installation, Freight, Travel miscellaneous		1	\$13,000	\$14,000	\$16,000
		Total	\$78,500	\$1,32,288	\$1,88,983

Table II: Comparison results for 3 cases (Diesel,diesel-battery and PV with Diesel battery)

Parameter	Diesel-only system	Diesel-Battery system	PV with Diesel-Battery system
System cost	\$78,500	\$1,32,288	\$1,88,983
System efficiency (%)	26.22	29.94	29.96
KWh/gallons (KWh)	10.61	12.1	12.1
Fuel consumed(gallons)	8410	7367	6583
Total cost of fuel(USD)	\$33,640	\$29,470	\$26,340
System load(KWh)	89220	89220	89220
Energy supplied			

(a). DEG (KWh)	101900	100100	89500
(b). PV(KWh)	0	0	9455
Electrical efficiency of DEG (%)	87.56	89.13	90.17

Table III : Comparison of results with HOMER

Parameter	Simulink Model	HOMER
System efficiency	29.96	29
Fuel Consumed (gallons)	6,583	6,817
Kwh per gallon	12.1	11.84
Energy generated		
1) Diesel engine	82497	87064
2) Solar Panels	9445	9444
Energy Supplied to load (kwhr)	89220	89224
Operational life		
1) Generator(years)	5.4	4.62
2) Battery bank(years)	5.4	6.07
System Cost(USD)	188,983	188,983
Net present value(NPV) (USD)	547,322	585,012

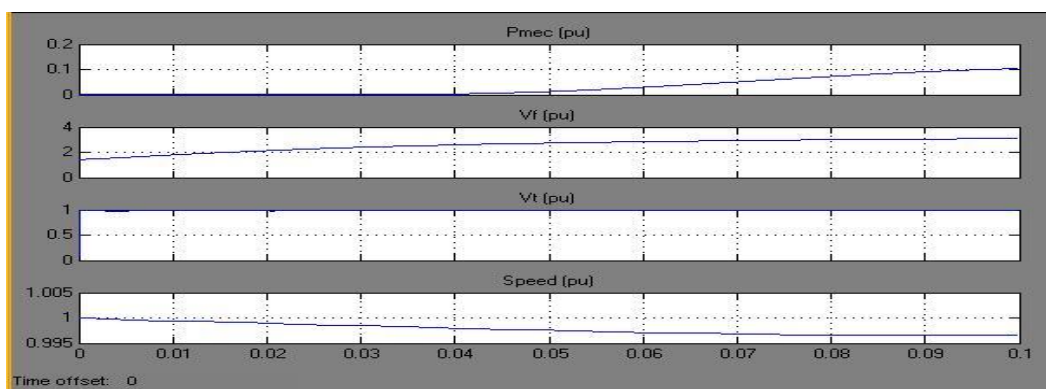


Fig 4.1 Diesel System output (Case-I)

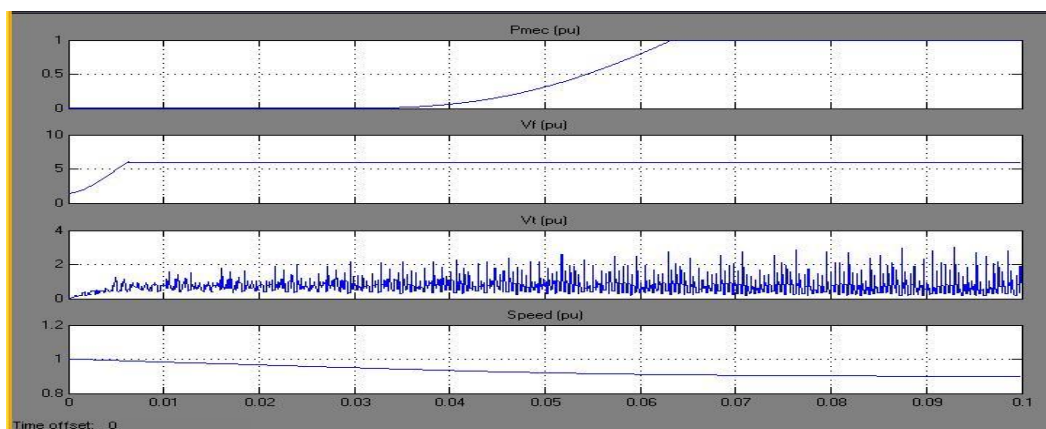


Fig 4.2 Diesel system output (Case-II)

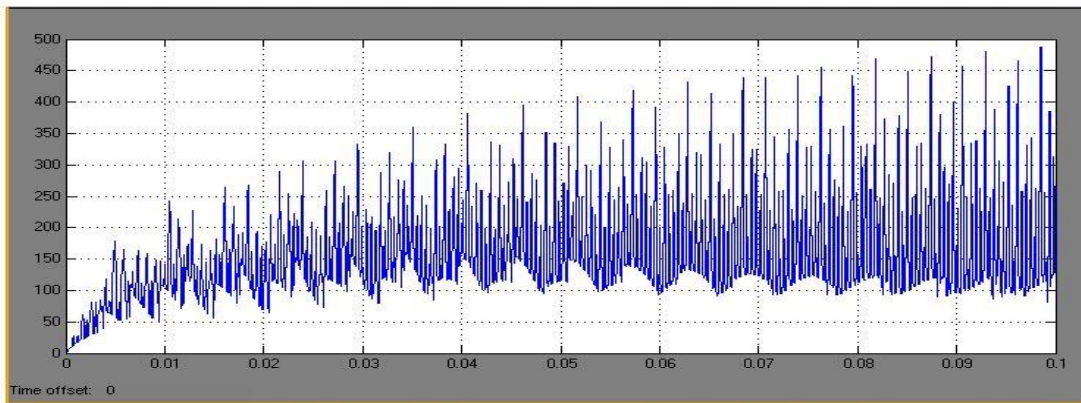


Fig 4.3 Battery system output voltage (Case-II)

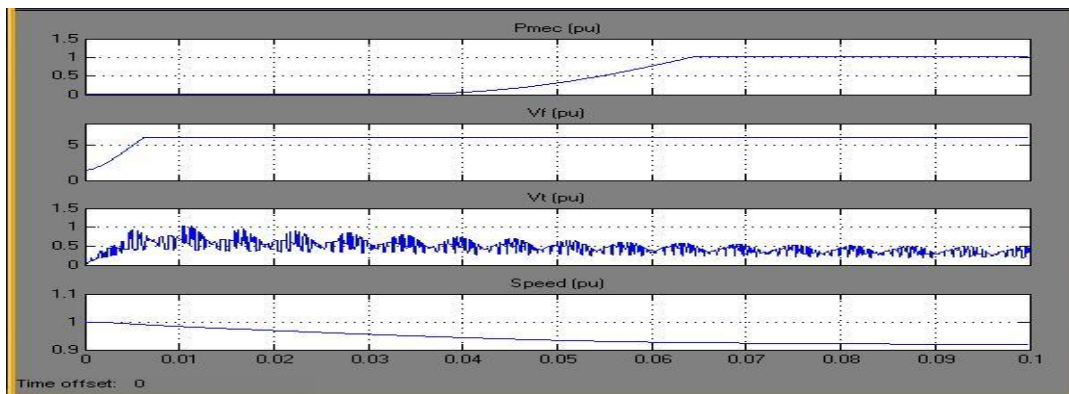


Fig 4.4 Diesel System Output (Case-III)

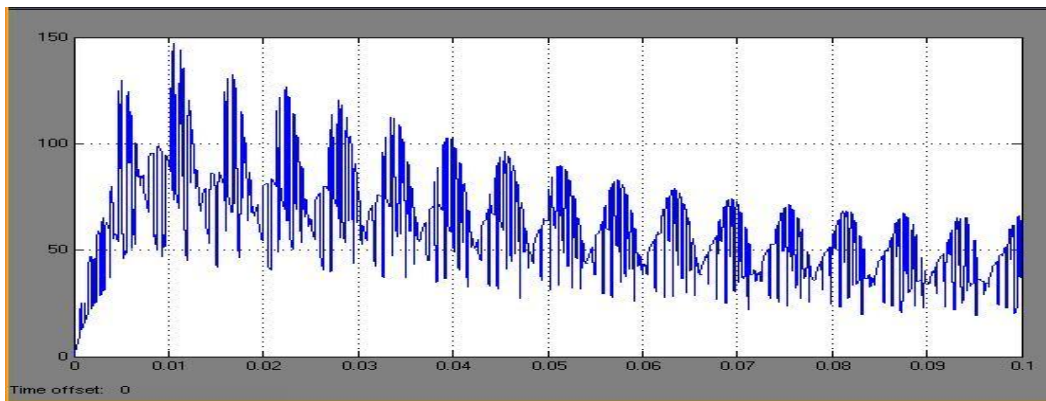


Fig 4.5 Battery Voltage (Case-III)

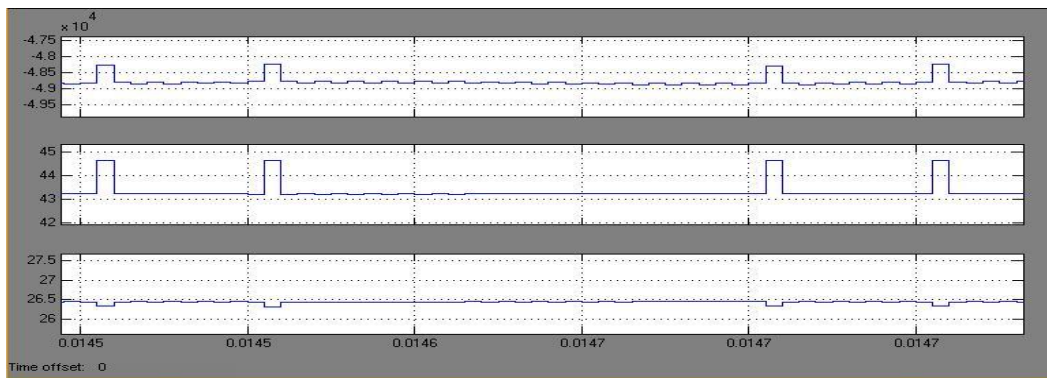


Fig 4.6 PV System Response (Case-III)

V. Conclusion

The preliminary results reported here demonstrate that the integration of a PV array into a diesel-battery stand-alone hybrid power system reduces the operating costs. A Simulink model of the PV with diesel-battery hybrid power system was developed in this project. The Simulink model can be used to study the performance of any PV with diesel-battery hybrid power system if the operating characteristics of the power system are known. With few modifications, the model can be extended to incorporate other renewable energy sources. The incorporation of additional renewable sources of energy, such as wind turbines in this system, could further reduce fuel consumption. The dynamic performance and the control system strategy of the power system can also be incorporated into the model. The model was validated by comparing the results for supplying an annual load profile with those predicted by HOMER. Although there is a significant capital investment to purchase a PV system for this application, the PV system may have acceptable 20-yr LCCs for many remote locations. Furthermore, over its life cycle, the PV hybrid power system will consume less fuel than the diesel-only system. If the external costs associated with emissions are taken into account, the PV system discounted payback period will further decrease. Hybrid energy systems, which result in more economical and efficient generation of electrical energy, would not only improve the capability of automated and precision generation systems, but would also help to extend the life of nonrenewable energy sources.

REFERENCES

- [1]. W. S. Fyfe, M. A. Powell, B. R. Hart, and B. Ratanasthien, —A globalcrisis: Energy in the future,|| Nonrenewable Resources, pp. 187–195,1993.
- [2]. F. P. Dawson and S. B. Dewan, —Remote diesel generator with photovoltaic cogeneration,|| in Proc. Solar Conf., Denver, CO, Sep. 1989, pp.269–274.
- [3]. Wales, Alaska High Penetration —Wind-Diesel Hybrid Power System:Theory of Operation|| , National Renewable Energy Laboratory, olden,CO, 2002.
- [4]. Lime Village Power System Alternative|| , Alaska Energy Authority, Anchorage, AK, 2001.
- [5]. National Renewable Energy Laboratory, Golden, CO. [Online], Available: http://rredc.nrel.gov/solarPV_payback, 2000.

Parking Management System

S. B. Baglane¹, M. S. Kulkarni², S. S. Raut³, T. S. Khatavkar⁴
PVG's College of Engineering & Technology, Pune, India

Abstract: The main objective of this project is to avoid the congestion in the car parking area by implementing a parking management system. Normally at public places such as multiplex theaters, market areas, hospitals, function-halls, offices and shopping malls, one experiences the discomfort in looking out for a vacant parking slot, though it's a paid facility with an attendant/ security guard. The parking management system is proposed to demonstrate hazard free parking for 32 cars, with 16 slots on each of the two floors. The proposed system uses 32 infrared transmitter-receiver pairs that remotely communicate the status of parking occupancy to the microcontroller system and displays the vacant slots on the display at the entrance of the parking so that the user gets to know the availability /unavailability of parking space prior to his/her entry into the parking place. In this system the users are guided to the vacant slot for parking using Bi-colored LEDs and the ultrasonic sensors enable the drivers to park the vehicle safely. The parking charges are automatically deducted from the user's account using RFID technology. From security point of view a daily log-book of entry/exit along with the vehicle details is also registered in the computer's memory. Implementation of concept of green communication and exception handling facility make the system concept unique and innovative.

Keywords: parking management system, RFID-tags, ultrasonic sensors, green communication.

I. Introduction

Now days in many public places such as malls, multiplex systems, hospitals, offices, market areas there is a crucial problem of car parking. The car-parking area has many lanes/slots for car parking. So to park a car one has to look for all the lanes. Moreover this involves a lot of manual labour and investment. So there is a need to develop an automated parking system that indicates directly the availability of vacant parking slots in any lane right at the entrance. The project involves a system including infrared transmitter-receiver pair in each lane and an LED/ LCD display outside the car parking gate. So the person desirous to park his vehicle is well informed about the status of availability of parking slot. Conventional parking systems do not have any intelligent monitoring system and the parking lots are monitored by security guards. A lot of time is wasted in searching vacant slot for parking and many a times it creates jams. Conditions become worse when there are multiple parking lanes and each lane with multiple parking slots. Use of parking management system would reduce the human efforts and time with additional comfort. In the proposed system, the display unit and the LEDs indicate the status of the parking lanes viz. a GREEN LED indicates a vacant slot and a RED LED indicates the unavailability. The system would not only save time but the software and hardware would also manage the Check-in and check-outs of the cars under the control of RFID readers/ tags with additional features of automatic billing, green communication, entry/exit data logging and obstacle indication during parking using ultrasonic sensors.

II. Literature Survey

The concept of the automated parking system is driven by two factors: need for parking space and scarcity of available land. The earliest use of an Automated parking system (APS) was in Paris, France in 1905 at the Garage Rue de Pontius [1]. The APS consisted of a groundbreaking multi-story concrete structure with an internal elevator to transport cars to upper levels where attendants parked the cars [2]. In the 1920s, a Ferris wheel-like APS (for cars rather than people) called a paternoster system became popular as it could park eight cars in the ground space normally used for parking two cars. Mechanically simple with a small footprint, the paternoster was easy to use in many places, including inside buildings. In 1957, 74 Bowser, Pigeon Hole systems were installed, and some of these systems remain in operation. However, interest in APS in the U.S. waned due to frequent mechanical problems and long waiting times for patrons to retrieve their cars [3]. Interest in APS in the U.S. was renewed in the 1990s, and there are 25 major current and planned APS projects (representing nearly 6,000 parking spaces) in 2012 [4]. While interest in the APS in the U.S. languished until the

1990s, Europe, Asia and Central America had been installing more technically advanced APS since the 1970s. In the early 1990s, nearly 40,000 parking spaces were being built annually using the paternoster APS in Japan. In 2012, there are an estimated 1.6 million APS parking spaces in Japan. The ever-increasing scarcity of available urban land and increase of the number of cars in use have combined with sustainability and other quality-of-life issues [1][5] to renew interest in APS as alternatives to multi-story parking garages, on-street parking and parking lots.

III. Objectives of Proposed Design

Proposed parking system would save time and provide comfortable hazard free parking experience to the users. Features of the parking management system are as listed below:

- Monitoring of parking space and updated indication of vacant parking slots.
- Assistance to the parking place via displays.
- Safe parking assistance using ultrasonic sensors.
- Automatic record of check-in and check-outs of the cars/vehicles under the control of RFID readers/ tags [6].
- Concept of Green Communication (for energy conservation) [7] i.e. need-based ON/OFF facility of parking floor light.
- Entry- exit log book.
- Printed receipt using thermal printer.
- Parking charges display.
- Automated payment of parking charges from the users account.

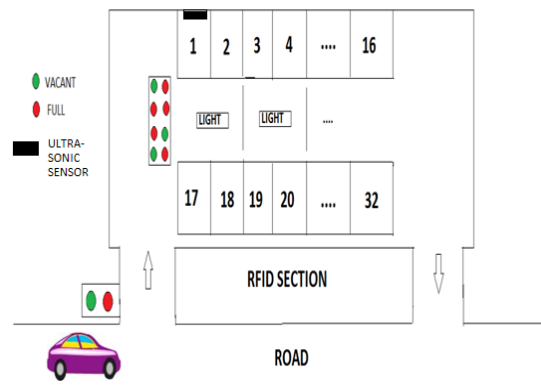


Fig.1 Proposed design layout of parking management system

IV. System Specifications

- Number of parking slots: 32
- Parking Floors : 2
- Green Communication: 6 lights (3/floor).
- Ultrasonic wall distance alarm for: <70 cm
- Data logging capacity/Parking Record- Data: Entry-Exit Log Book (Refresh rate: 1 month)

V. System Architecture

The system architecture, shown in figure 2 consists of 32 Infrared sensor(IR) array blocks at the input and output followed by the latch blocks to hold the signals received from the sensor array in terms of logic1 and logic0. If a vehicle is parked in a particular slot then RED indication is given and if the slot is vacant, GREEN indication is given. The RFID reader/tags will control the check-in and check-outs of vehicle. Output of the latch is given to receive and transmission lines using a microcontroller. At the exit section of the parking area, RFID section and the microcontroller based system would calculate the parking-space usage time and automatically deduct the parking charges from the owner's account and a receipt would be printed using thermal printers as shown in Fig.2. In case of exceptions that there is no balance in the user's account, alarm indication and manual payment provision is made.

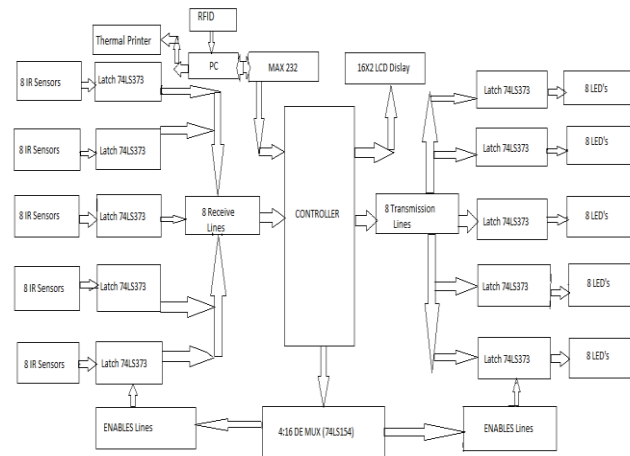


Fig.2 System Architecture

VI. Hardware Unit

The hardware unit consists of array of sensors, latches, De multiplexer, RFID tags/readers, thermal printer and ultrasonic sensors as shown in Fig.2. Each of the blocks are explained in this section.

Sensors: The proposed design consists of IR transmitters and IR receivers for each parking slot. The IR receivers are interfaced to a microcontroller. IR rays are obstructed when a car is parked in any parking slot. Thus AVR understands that the slot is occupied else it is free. The proposed system uses 40 IR sensors, 32 for parking slots and 8 for Green Communication.

Ultrasonic Sensors: These sensors are used for the obstacle detection. Sensors calculate the time interval between sending the signal and receiving the echo to determine the distance to an object.

Microcontroller: The proposed design uses Atmega32L microcontroller. It is a low power controller that provides support for high speed communications, with the ability to be programmed using AT commands. Record of vehicles coming in a month would also be recorded. When the vehicle passes the RFID Reader, the Reader reads the RFID Tag and sends the RFID tag information to the database system. The database notes the vehicle information. The Bi-colored LED mounted on the front panel at the parking entrance indicates the space availability status.

Latches: Latches are the simplest memory units, storing individual bits. The basic function of the latch in our project is that, when the output of the latch is high, implying the car is parked, then the red LED should glow else when the output of the latch is low, implying the parking slot is vacant, then the green LED should glow. In all, we are using 10 latches (5 at the transmitter and 5 at the receiver) in our design. For this we have selected 74LS 373.

RFID: The RFID detector is located at some distance from the car. As the driver will bring his preprogrammed RFID tag near the detector, the RFID Reader will read the time in and time out, car details, bank account number [6].

BI-COLOR LED: Bi means two, so this is an LED with two colors. This is typically two LED's in a single package, one of each color. They are wired back to back, so one glows for current in one direction, and the other glows for current in the other direction.

DEMULTIPLEXER: Single data input; n control inputs ("selects"); 2n outputs. Single input connects to one of 2n outputs. "Selects" or decides which output is connected to the input. When used as a decoder, the input is called an "enable". The proposed parking system uses 74LS154 IC.

MAX232: The MAX232 is an integrated circuit that converts signals from an RS-232 serial port to signals suitable for use in TTL compatible digital logic circuits.

RS 232 PROTOCOL:It is used for serial communication between Micro-controller to PC. In the proposed design the PC and the serial thermal printer is connected to Microcontroller via RS-232.

LCD:LCD is used in a project to display the output of the application. The design consists of 16x2 LCD which indicates 16 columns and 2 rows and can write 16 characters in each line. So, total 32 characters we can display on 16x2 LCD. The design consists of LCD is used to display the deducted amount and a ‘THANK YOU’ message.

THERMAL PRINTER:The function of thermal printers in proposed design is to print the receipt with car details-time-in and time-out, the parking charges per hour and total charges deducted.

VII. Flowchart

The parking management system functioning can be well understood from the flowchart shown in figure 3. The Flowchart of the proposed parking system is as shown

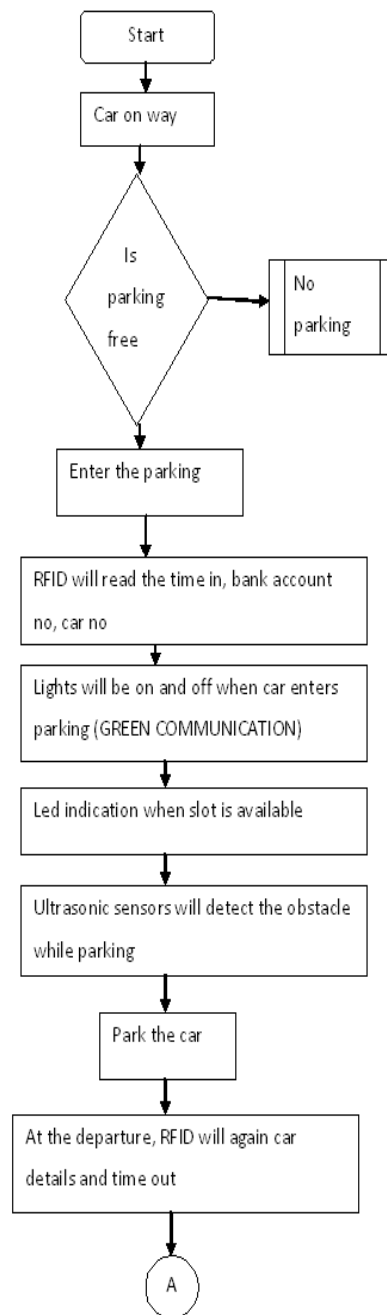


Figure 3: Flowchart 1

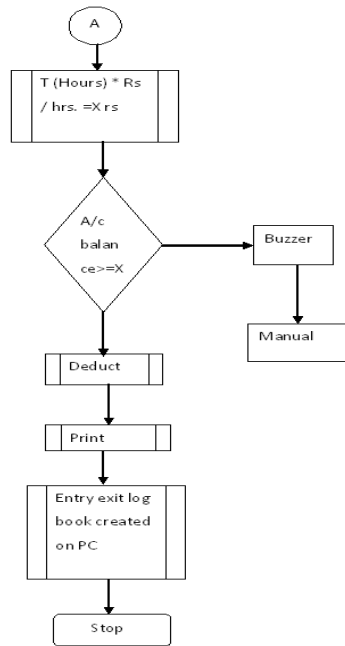


Fig.3 Flowchart of proposed system

VIII. Results

The hardware implementation and simulation results are discussed below.

[A] Simulation of IR sensor using Proteus software

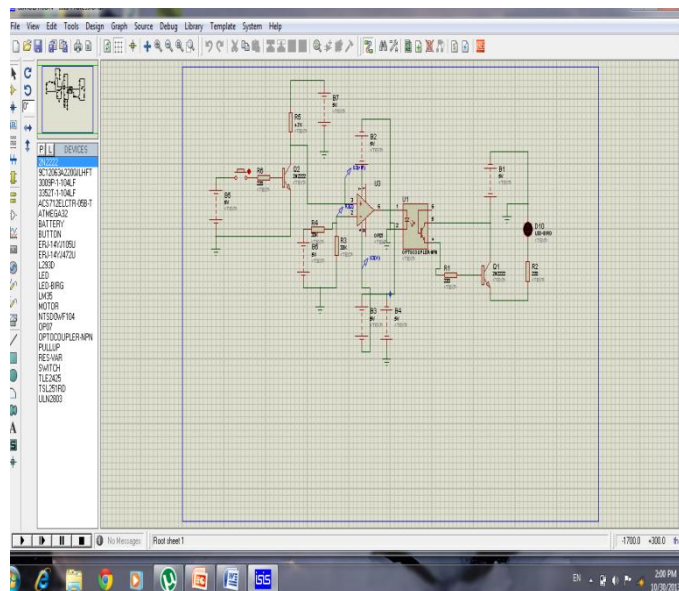


Figure 4: IR sensor simulation

[B] Ultrasonic sensor results: The hardware implementation of the ultrasonic sensor based anti-collision circuit was successfully done. While parking, when the distance between the car and the wall or any other obstacle reduces to 75 cm, the alarm indication turns ON, thus alerting the driver.

IX. Applications

The system can be installed at the

- Parking Lots of Offices
- Malls
- Toll plazas
- Underground parking areas in Metros
- Commercial buildings

X. Conclusion

The proposed parking management system takes into account all possible attributes that is expected from it. This system uses IR and ultrasonic sensors and RFID tags/readers to handle chaos-free and guided parking for 32 vehicles. This system can be expanded to accommodate increased number of vehicles by applying the concept to more number of floors and lanes and parking slots. The project can be customized to authenticating military gate-pass entrants & it could also be improvised with a voice guided system.

Acknowledgement

We would like to thank and acknowledge the support and guidance given by Prof. Mrs. Khatavkar T.S in the formulation and implementation of this project.

REFERENCES

- [1] Sanders McDonald, Shannon. "Car Parking and Sustainability", The Transportation Research Forum.
- [2] Hamelin, Ir. Leon J. (2011), "The Mechanical Parking Guide 2011", ISBN 1-466-43786-3.
- [3] Beebe, Richard S, "Automated Parking: Status in the United States", 2011.
- [4] Monahan, Don, "Man vs. Machine: Is Robotic Parking Right for Your Project?" International Parking Institute, September 2012.
- [5] Staff, GreenandSave, "Automated Parking and Garage Lights Take "Green" Garages to New Levels", 2012.
- [6] International Journal of Research in Engineering & Applied Sciences. [http:// www.euroasiapub.org](http://www.euroasiapub.org)
- [7] V.Sumathi "ENERGY EFFICIENT AUTOMATED CAR PARKING SYSTEM", TN 632014 India, and Volume 5 No 3 Jun-Jul 2013.



International Journal of Modern Engineering Research (IJMER)

Volume : 4 Issue : 2 (Version-3)

ISSN : 2249-6645

February - 2014

Contents :

Reliable Hydra SSD Architecture for General Purpose Controllers <i>Renjith G., Prof. R. Bijukumar</i>	01-07
A New approach for controlling the power flow in a transmission system using Unified Power Flow Controller <i>Ramasamy A., Vibin R., Gowdham Kumar S.</i>	08-14
Stability of Simply Supported Square Plate with Concentric Cutout <i>Jayashankarbabu B. S., Dr. Karisiddappa</i>	15-22
An Efficient Clustering Method for Aggregation on Data Fragments <i>Srivaishnavi D., M. Kalaiarasu</i>	23-28
Improving Distribution Feeders for Photovoltaic Generation by Loop Power Control Method <i>Husam Saad Abdulla, Surya Prakashline</i>	29-38
Multiple Optimization of Wire EDM Machining Parameters Using Grey Based Taguchi Method for Material HCHCR <i>Anwarul Haque, A. B. Amale, P. D. Kamble</i>	39-45
Minkowski Distance based Feature Selection Algorithm for Effective Intrusion Detection <i>Rm. Somasundaram, K. Lakshmanan, V. K. Shunmuganaathan</i>	46-50
Moving Object Detection for Video Surveillance <i>Abhilash K.Sonara, Pinky J. Brahmbhatt</i>	51-56
A production - Inventory model with JIT setup cost incorporating inflation and time value of money in an imperfect production process <i>R. Chakrabarty, T. Roy, K. S. Chaudhuri</i>	57-65
Wavelet Based Analysis of Online Monitoring of Electrical Power by Mobile Technology <i>P. Ram Kishore Kumar Reddy</i>	66-70

Reliable Hydra SSD Architecture for General Purpose Controllers

Renjith G.¹, Prof. R. Bijukumar²

¹PG Scholar, Dept. of Electronics and Communication Engg, TKM Institute of Technology, Kollam, Kerala, India

²Head of the Dept., Dept. of Electronics and Communication Engg, TKM Institute of Technology, Kollam, Kerala, India.

Abstract: The Solid State Disks (SSDs) had almost replaced the traditional Hard Disk Drives (HDDs) in modern computing systems. SSDs possess advanced features such as low power consumption, faster random access and greater shock resistance. In general, NAND Flash memories are used for bulk storage applications. This project focus on an advanced SSD architecture, called Reliable Hydra to enhance the SSD performance. Hydra SSDs overcomes the discrepancy between slow flash memory bus and fast host interfaces like SATA, SCSI, USB etc. It uses multiple high level memory controllers to execute flash memory operation without the intervention of FTL (Flash Translation Layer). It accelerates the processing of host write requests by aggressive write buffering. Memories are subjected to bit flipping errors, so this project also considers the incorporation of matrix code for increasing the reliability and hence yield of the system. The highly sophisticated controllers for real time systems in the industrial, robotics, medical and scientific applications require high performance and reliable memories. The aim of this project is to design Reliable Hydra SSD architecture for controller applications to enhance the performance. The design architecture is to be coded in VHDL using Xilinx ISE tools.

I. Introduction

Flash memories are widely used as a storage medium in modern computing devices because of its low power consumption, fast random access, and high shock resistance. Most of the conventional Hard Disk Drives (HDDs) are replaced with the Solid State Disk Drives (SSDs). Solid State Disk Drives (SSDs) are much better suited to embedded computers and the cost of flash memory still going decreases. The widely used Flash memories are NAND flash based solid state disks (SSDs) [2] because of flash memories are nonvolatile, less power consumable and shock resistant. A basic NAND flash memory chip consists of a set of blocks, each sub divided with a set of pages. Each page has a provision for data that stores the user data and a separate provision that stores metadata associated with the user data. HDDs can be overwritten data directly, but in flash memory it is difficult to perform in place updating. The flash memory to get wide acceptance as a storage device, it has to imitate the functionality of HDDs. The software layer that provides this imitation is called the flash translation layer (FTL) [1]. It hides the anomalies of flash memory and gives the illusion of an HDD. The reliability of the data is very much important while saving or reading, because the application may be scientific, real time or in medical field. Here this project designs a new model of SSD architecture called Reliable Hydra SSD, which exploits the parallelism of multiple NAND flash memory chips to enhance storage system performance and the matrix code for increasing the reliability of the data.

Discrepancy between the slow flash memory bus and the fast host interface is overcome by interleaving enough flash memory buses so that their effective bandwidth meets that that of the host interfaces. In addition to this bus-level interleaving, chip-level interleaving hides the flash read latency. Multiple high level flash memory controllers execute sequences of high level flash memory operations without any intervention by the FTL. One of these controllers is named as the foreground unit and the other is called background units, which have less priority. The foreground unit is used to accelerate the processing of host read requests for which processes in the host system are waiting. Aggressive write buffering accelerates.

The bus level and chip level interleaving of flash memory provides the parallelism and increase the transfer rate of the data. Most of the host controller transfers data in very high rate and a single chip memory cannot follow the transfer rate of the interface. So this superchip increases the fastness of the data read and write operations and it bring the speed up to the host controller. The flash translation layer (FTL) hides the anomalies

of flash memory and imitates the functionality of an HDD. The most important role of the FTL is to maintain a mapping between the logical sector address used by the host system and the physical flash memory address. In this project, a high level method for detection and correction of multiple faults using Matrix [3] code is presented. This code is a combination of Hamming codes and Parity codes in a matrix format which can correct multiple faults in memory. A memory chip protected with the Matrix Code technique, it possess high reliability than the Cyclic Redundancy Check (CRC), Hamming [3] or Reed-Muller codes. The overhead of Matrix Code is less than the overhead imposed by the Reed-Muller code. Note that, although Cyclic Redundancy Check (CRC), Hamming code has less overhead compared to the matrix Code method and Reed-Muller [3], it can detect only two errors and correct one error.

II. Related Works

Most of the modern computing devices have recently started replacing hard drives with NAND [2][8] flash based solid state disks (SSDs). An SSD communicates with the host computer through a standard interface, such as PATA (Parallel Advanced Technology Attachment), SATA (Serial Advanced Technology Attachment), SCSI (Small Computer System Interface) or USB (Universal Serial Bus), and behaves much like a standard hard drive. An SSD incorporates a controller and a flash memory array and the SSD controller firmware performs disk emulation. The read/write/erase behavior of flash memory is differing than that of other programmable memories, such as magnetic disks and volatile RAM (Random Access Memory).

In fact, flash memories come in two flavors, NOR and NAND, that are also entirely different from each other. In both types, write operations can only clear bits (change their value from 1 to 0). The only way to set bits (change their value from 0 to 1) is to erase an entire region of memory. These regions have fixed size in a given device, typically ranging from several kilobytes to hundreds of kilobytes and are called erase units. NOR flash memory, the older type for code storage, is a random access device that is directly addressable by the processor. NOR flash memory suffers from high erase times. NAND flash memory [9], the newer type for data storage, enjoys much faster erase times, but it is not directly addressable, access is by page (a fraction of an erase unit, typically 512 bytes) not by bit or byte, and each page can be modified only a small number of times in each erase cycle. That is, after a few writes to a page, subsequent writes cannot reliably clear additional bits in the page; the entire erase unit must be erased before further modifications of the page are possible. Because of these peculiarities, storage management techniques that were designed for other types of memory devices, such as magnetic disks, are not always appropriate for flash memory.

Since most operating systems does not support flash memory directly but it is possible with a thin software layer called FTL (Flash Translation Layer) is usually employed between OS and flash memory. The main role of FTL is to imitate the functionality of HDD, hiding the latency of erase operation as much as possible. FTL achieves this by redirecting each write request from OS to an empty location in flash memory that has been erased in advance, and by maintaining an internal mapping table to record the mapping information from the logical sector number to the physical location. The mapping schemes of FTL are classified into a page level mapping scheme into a block level or into a hybrid mapping scheme. In page level mapping, a logical page can be mapped to any physical page in flash memory. In block level mapping, only the mapping information between the logical block number (LBN) and the physical block number (PBN) is maintained. Hybrid mapping is a compromise between page level mapping and block-level mapping. Many FTL schemes are proposed to reduce the number of block erase and the data page copying in block level mapping.

The use of block level mapping in Hydra considerably simplifies wear leveling since block level mapping, unlike page level mapping, does not suffer from the complications that arise if wear leveling is coupled to garbage. Instead, Hydra uses two simple techniques borrowed from wear leveling in page mapping FTLs: one is implicit and the other explicit. In implicit wear-leveling [1] [10], when a merge operation is performed, the free physical superblock with the smallest erase count is used as the destination of the copy back superchip operation. In explicit wear leveling, when the SSD is idle, the physical superblock with the smallest erase count (among those mapped to logical superblocks) is swapped with the free physical superblock with the largest erase count, provided that the difference between the two counts is above a certain threshold.

Matrix Code is the combination of Hamming Code and the Parity Code. It can correct multiple faults in the memory. Concurrent Error Detection (CED) [3] is one of the major approaches for transient errors mitigation. In its simpler forms, CED allows only the detection of errors, requiring the use of additional techniques for error correction. Nevertheless, the implementation of CED usually requires sometimes the duplication of the area of circuit to be protected. One of the simpler examples of CED is called duplication with comparison, which duplicates the circuit to be protected and compares the results generated by both copies to check for errors. This technique imposes an area overhead higher than 100%, and when an error is detected the outputs of the circuit must be recomputed.

Hamming codes and odd weight codes are largely used to protect memories against SEU because of their efficient ability to correct single upsets with a reduced area and performance overhead. The Hamming

code implementation is composed by a combinational block responsible to code the data (encoder block), inclusion of extra bits in the word that indicate the Parity (extra latches or flip flops) and another combinational block responsible for decoding the data (decoder block). The encoder block calculates the parity bit, and it can be implemented by a set of two input XOR gates. The decoder block is more complex than the encoder block, because it needs not only to detect the fault, but it must also correct it.

The Reed–Muller [3] code is another protection code that is able to detect and correct more errors than a Hamming code and is suitable for tolerating multiple upsets in SRAM memories. Although this type of protection code is more efficient than Hamming code in terms of multiple error detection and correction, the main drawback of this protection code is its high area and power penalties (since encoding and decoding correcting circuitry in this code is more complex than for a Hamming code). Hence, a low overhead error detection and correction code for tolerating multiple upset is required.

III. System Architecture

The basic NAND flash based memories have single bus chip architecture and are constructed from an array of flash packages. Each SSD must contain host interface logic to support some form of physical host interface connection (USB [4], Fiber Channel, PCI Express, and SATA) and logical disk imitation, like a flash translation layer mechanism to enable the SSD [2] to mimic a hard disk drive. The bandwidth of the host interface is often a critical parameter on the performance of the device as a whole, and it must be matched to the performance available to and from the flash array.

A. Basic NAND flash Architecture

The basic NAND flash based memory architecture as the following figure 1. The architecture contains the NAND based flash memory chip, NAND flash controller, Cache buffer controller and SRAM etc.

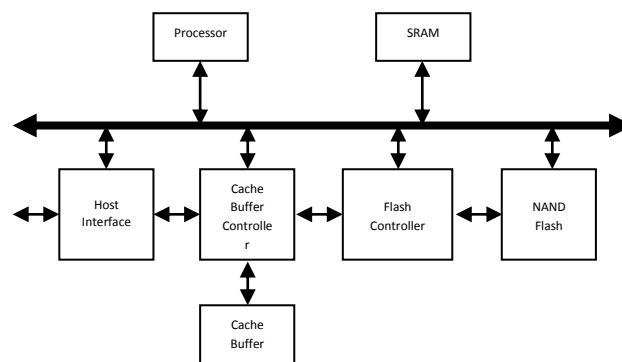


Figure: 1 Basic NAND flash Architecture.

One of the major disadvantages of the basic NAND flash based memory is the discrepancy between the transfer rate of the host interface and the flash memory. Most of the host controllers (SATA, SCSI, and USB [4] etc.) are operating at very high transfer rate because of the technology advantage. Operating systems use storage devices to provide file systems and virtual memory, and it is usually assumed that these devices have an HDD like interface. The software layer that provides this imitation is called the flash translation layer (FTL). It hides the anomalies of flash memory and gives the illusion of an HDD. The FTL needs a device driver installation for the particular storage volume. In the case of firmware it may not be feasible.

Another important parameter is the reliability of the data. In the basic NAND [10] flash based memories only a simple error check and correction mechanism like CRC. It only detects and corrects single bit errors. It cannot do the bulk data error check and correction. The disadvantages of basic NAND flash based memories are at a glance is

- 1 The discrepancy between slow flash memory bus and the fast host interface.
- 2 The intervention of Flash Translation Layer (FTL).
- 3 There is no efficient mechanism for the reliability of the data.

B. Reliable Hydra SSD Architecture

The Reliable Hydra [1] Solid State Disk (SSD) architecture is a new proposed model which over comes all the disadvantages of the conventional NAND flash based memories. The Hydra SSD architecture uses various techniques to achieve this goal. The discrepancy between the slow flash memory bus and the fast host is overcome by interleaving enough flash memory buses so that their effective bandwidth meets that of the host interface. In addition to this bus level interleaving, chip level interleaving hides the flash read latency.

Multiple high level flash memory controllers execute the operations of high level flash memory without any intervention by the FTL. One of these controllers is designated as the foreground unit and has priority over the remaining controllers, called background units. Aggressive write buffering expedites the processing of host write requests. More importantly, it also allows the parallelism in multiple flash memory chips to be exploited by multiple background units that perform materialization to flash memory in parallel on different interleaved units. By introducing Matrix Code [3] error detection and correction mechanism, which provides the reliability of the data while reading or writing it to the flash memory without make high overheads. In Figure 2, block MCE represents Matrix code encoder and block MCD represents Matrix code decoder.

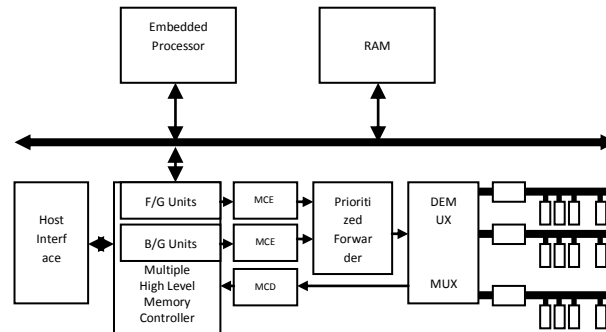


Figure: 2 Reliable Hydra SSD Architecture.

C. Chip level and bus level interleaving

The Hydra SSD uses interleaving over multiple flash memory buses to overcome the bandwidth limitation of the flash memory bus. In the bus level interleaving, each memory location within a superblock are distributed in a round robin manner. In Hydra, the set of flash memory chips that are related to each other by the bus level and chip level interleaving is called a superchip.

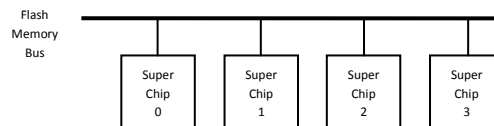


Figure: 3 Superchips.

D. Multiple high level memory controllers

The Hydra SSD architecture uses multiple high level flash memory controllers, consisting of one foreground unit and several background units. Each controller is capable of executing a sequence of high level flash memory operations, as the descriptors. In Hydra, a high level flash [9] memory operation is directed to a superchip, and it is to be designed to perform the read, write, erase and program the chip. The operation of the MHL memory controller is based on a counter FSM algorithm. Here two counters operate in parallel for the operation of the MHL counter algorithm, read count FSM and write count FSM.

E. Matrix Code error check and correction mechanism

Matrix Code [3] is the combination of Hamming Code and the Parity Code. It can correct multiple faults in the memory. By introducing Matrix Code error detection and correction mechanism, which provides the reliability of the data while reading or writing it to the flash memory without make high overheads. The Reed–Muller code is another protection code that is able to detect and correct more errors than a Hamming code and is suitable for tolerating multiple upsets in SRAM memories. Although this type of protection code is more efficient than Hamming code in terms of multiple error detection and correction, the main drawback of this protection code is its high area and power penalties (since encoding circuitry ,decoding and correcting circuitry in this code is more complex than for a Hamming code). Hence, a low-overhead error detection and correction code for tolerating multiple upset is required.

In order to improve the efficiency of repairing embedded memories, a novel redundancy mechanism to cope not only with defects but as well as with transients is required. The proposed technique, in comparison with the previous techniques, improves the overall systems reliability.

IV. Simulation Results

The design entry is modeled using VHDL in Xilinx ISE Design Suite 12.1 and the simulation of the design is performed using ModelSim SE 6.2c from Mentor Graphics to validate the functionality of the design. Chip structure for Super Chip flash memory module is designed as follows

1 Word	=	32 bit
1 Page	=	4 Words (Word 0, Word 1, Word 2, Word 3)
1 Block	=	2 Pages (Page 0, Page 1)
1 Chip	=	4 Blocks (Bus 0, Bus 1, Bus 2, Bus 3)
1 Super Chip	=	2 Chips (Chip 0, Chip 1)

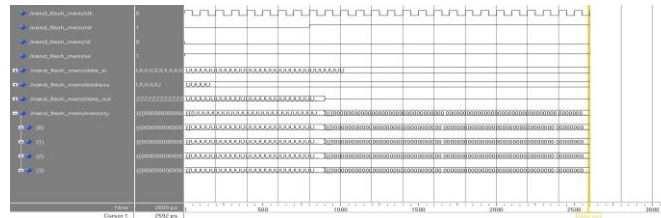


Figure: 4 Synchronous reset.

The input signals to the memory are the global clk, rst, rd, wr, address and data_in. Applying the global clk signal and run the simulation we can see that the flash memory is in high impedance state. After applying the rst signal high, rd low, wr high it can be see that the entire memory is reset to zero. Data out is also at high impedance state.

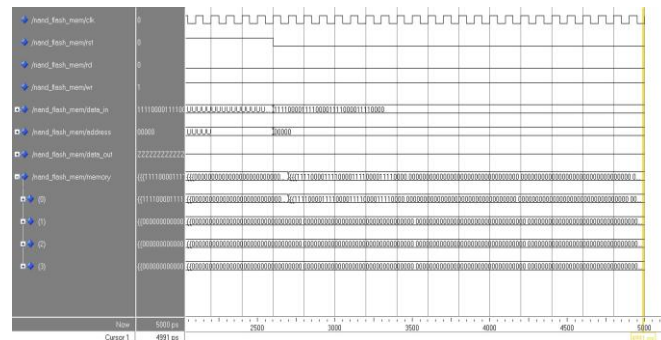


Figure: 5 Memory write operation.

For memory write operation the rst signal to low and make a particular data force to the data_in and also force the address signal to a particular address. Make the rd signal is low and wr signal is high then run the simulation it can see that the particular data is write to the particular memory.

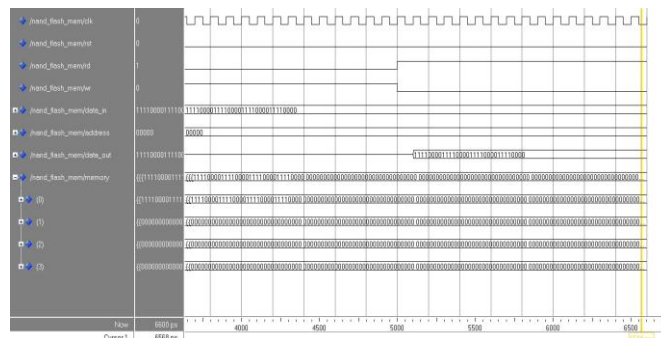


Figure: 6 Memory read operation.

For memory read operation the rst signal to low and make a particular data force to the data_in and also force the address signal to a particular address. Make the rd signal is high and wr signal is low then run the simulation it can see that the particular data is read from the particular memory address to the data out.

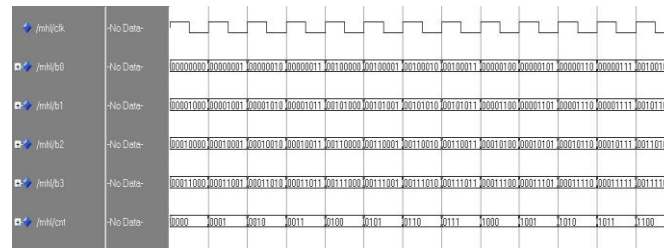


Figure: 11 MHL memory controller counter FSM.

REFERENCES

- [1] Yoon Jae Seong, Eyee Hyun Nam, Jin Hyuk Yoon, Hongseok Kim, Jin-Yong Choi, Sookwan Lee, Young Hyun Bae, Jaejin Lee, Member, *IEEE*, Yookun Cho, Member, *IEEE*, and Sang Lyul Min, Member, *IEEE*, "Hydra: A Block-Mapped Parallel Flash Memory Solid-State Disk Architecture", *IEEE Transactions on Computers*, Vol. 59, No. 7, July 2010, pp 905-921.
- [2] Li-Pin Chang, "A Hybrid Approach to NAND-Flash-Based Solid-State Disks", *IEEE Transactions on Computers*, Vol. 59, No. 10, October 2010, pp 1337-1349.
- [3] Costas Argyrides, Member, *IEEE*, Dhiraj K. Pradhan, Fellow, *IEEE*, and Taskin Kocak, "Matrix Codes for Reliable and Cost Efficient Memory Chips", *IEEE Transactions on Very Large Scale Integration (VLSI) Systems*, Vol. 19, No. 3, March 2011, pp 420-428.
- [4] Chung-Ping Young, Michael J. Devaney, Member, *IEEE*, and Shyh-Chyang Wang, "Universal Serial Bus Enhances Virtual Instrument-Based Distributed Power Monitoring", *IEEE Transaction on Instrumentation and Measurement*, Vol. 50, No. 6, December 2001, pp 1692-1696.
- [5] Jin Hyuk Yoon¹, Eyee Hyun Nam², Yoon Jae Seong², Hongseok Kim², Bryan S. Kim², Sang Lyul Min², and Yookun Cho³ School of Computer Science and Engineering, Seoul National University, Seoul, Korea, "Chameleon: A High Performance Flash/FRAM Hybrid Solid State Disk Architecture", *IEEE Computer Architecture Letters*, Vol. 7, No. 1, January-June 2008, pp 17-20.
- [6] Tao Xie, Member, *IEEE*, and Yao Sun, "Dynamic Data Reallocation in Hybrid Disk Arrays", *IEEE Transactions on Parallel and Distributed Systems*, Vol. 21, No. 9, September 2010, pp 1330-1341.
- [7] Dong Kim, Kwanhu Bang, Student Member, *IEEE*, Seung-Hwan Ha, Sungroh Yoon, Member, *IEEE*, and Eui-Young Chung, Member, *IEEE*, "Architecture Exploration of High-Performance PCs with a Solid-State Disk", *IEEE Transactions on Computers*, Vol. 59, No. 7, July 2010, pp 878-890.
- [8] Soojun Im and Dongkun Shin, Member, *IEEE*, "Flash-Aware RAID Techniques for Dependable and High-Performance Flash Memory SSD", *IEEE Transactions on Computers*, Vol. 60, No. 1, January 2011, pp 80-92.
- [9] Seung-Ho Park, Jung-Wook Park, Shin-Dug Kim, and Charles C. Weems, "Brief Contributions A Pattern Adaptive NAND Flash Memory Storage Structure", *IEEE Transactions on Computers*, Vol. 61, No. 1, January 2012, pp 134-138.
- [10] Sarah Boyd, Arpad Horvath, and David Dornfeld, "Life-Cycle Assessment of NAND Flash Memory", *IEEE Transactions on Semiconductor manufacturing*, Vol. 24, No. 1, February 2011, pp 117-12.

A New approach for controlling the power flow in a transmission system using Unified Power Flow Controller

Ramasamy A.¹, Vibin R.², Gowdham Kumar S.³

¹(Assistant Professor, Department of EEE, CMS College of Engineering and Technology/Anna University of Technology, Chennai, India)

²(Assistant Professor, Department of EEE, CMS College of Engineering and Technology/Anna University of Technology, Chennai, India)

³(Assistant Professor, Department of EEE, CMS College of Engineering and Technology/Anna University of Technology, Chennai, India)

ABSTRACT: Electrical power systems is a large interconnected network that requires a careful design to maintain the system with continuous power flow operation without any limitation. Flexible Alternating Current Transmission System (FACTS) is an application of a power electronics device to control the power flow and to improve the system stability of a power system. Unified Power Flow Controller (UPFC) is a new concept for the compensation and effective power flow control in a transmission system. Through common DC link, any inverters within the UPFC is able to transfer real power to any other and there by facilitate real power transfer among the line. In this paper a test system is simulated in MATLAB/SIMULINK and the results of the network with and without UPFC are compared and when the voltage sag is compensated, reactive power is controlled and transmission line efficiency is improved.

Keywords: FACTS, UPFC, Power flow, Real and reactive power, Matlab/simulink.

I. Introduction

The technology of power system utilities around the world has rapidly evolved with considerable changes in the technology along with improvements in power system structures and operation. The ongoing expansions and growth in the technology, demand a more optimal and profitable operation of a power system with respect to generation, transmission and distribution systems [1]. In the present scenario, most of the power systems in the developing countries with large interconnected networks share the generation reserves to increase the reliability of the power system. However, the increasing complexities of large interconnected networks had fluctuations in reliability of power supply, which resulted in system instability, difficult to control the power flow and security problems that resulted large number blackouts in different parts of the world. The reasons behind the above fault sequences may be due to the systematical errors in planning and operation, weak interconnection of the power system, lack of maintenance or due to overload of the network. The main objective of the power system operation is to match supply/demand, provide compensation for transmission loss, voltage and frequency regulation, reliability provision etc. The need for more efficient and fast responding electrical systems has given rise to innovative technologies in transmission using solid-state devices. These are called FACTS devices which enhance stability and increase line loadings closer to thermal limits [2]. FACTS have gained a great interest during the last few years, due to recent advances in power electronics. FACTS devices have been mainly used for solving various power system steady state control problems such as voltage regulation, power flow control, and transfer capability enhancement. The development of power semiconductor devices with turn-off capability (GTO, MCT) opens up new perspectives in the development of FACTS devices. FACTS devices are the key to produce electrical energy economically and environmental friendly in future. The latter approach has two inherent advantages over the more conventional switched capacitor- and reactor- based compensators. Firstly, the power electronics-based voltage sources can internally generate and absorb reactive power without the use of ac capacitors or reactors. Secondly, they can facilitate both reactive and real power compensation and thereby can provide independent control for real and reactive power flow [3]. Since then different kind of FACTS controllers have been recommended. FACTS controllers are based on voltage source converters and includes devices such as Static Var Compensators (SVC), static Synchronous Compensators (STATCOM), Thyristor Controlled Series Compensators (TCSC), Static Synchronous Series Compensators (SSSC) and Unified Power Flow Controllers (UPFC) [4]. Among them UPFC is the most versatile and efficient

device which was introduced in 1991. In UPFC, the transmitted power can be controlled by changing three parameters namely transmission magnitude voltage, impedance and phase angle.

II. Control of Power Systems

2.1 Power System Constraints

The limitations of the transmission system can take many forms and may involve power transfer between areas or within a single area or region and may include one or more of the following characteristics:

- Steady-State Power Transfer Limit
- Voltage Stability Limit
- Dynamic Voltage Limit
- Transient Stability Limit
- Power System Oscillation Damping Limit
- Inadvertent Loop Flow Limit
- Thermal Limit
- Short-Circuit Current Limit
- Others

Each transmission bottleneck or regional constraint may have one or more of these system-level problems. The key to solving these problems in the most cost-effective and coordinated manner is by thorough systems engineering analysis [5].

2.2 Controllability of Power Systems

To illustrate that the power system only has certain variables that can be impacted by control, we have considered here the power-angle curve, shown in Figure 2. Although this is a steady-state curve and the implementation of FACTS is primarily for dynamic issues, this illustration demonstrates the point that there are primarily three main variables that can be directly controlled in the power system to impact its performance [5]. These are:

- (1) Voltage
- (2) Angle
- (3) Impedance

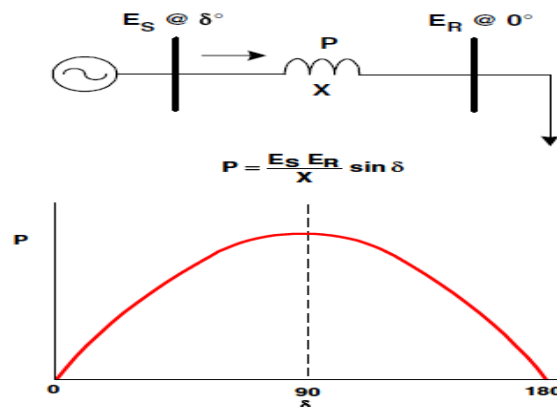


Fig.1 Illustration of controllability of power systems

2.3 Conventional Devices for Enhancing Power System Control

- (1) Series Capacitor -Controls impedance
- (2) Switched Shunt-Capacitor and Reactor -Controls voltage
- (3) Transformer LTC -Controls voltage
- (4) Phase Shifting Transformer -Controls angle
- (5) Synchronous Condenser -Controls voltage
- (6) Special Stability Controls-Focuses on voltage control but often include direct control of power.

2.4 FACTS Controllers for Enhancing Power System Control

- (1) Static Synchronous Compensator (STATCOM) -Controls voltage
- (2) Static VAR Compensator (SVC) -Controls voltage
- (3) Unified Power Flow Controller (UPFC)

- (4) Convertible Series Compensator (CSC)
- (5) Inter-phase Power Flow Controller (IPFC)
- (6) Static Synchronous Series Controller (SSSC)

2.5 Benefits of utilizing FACTS devices

The benefits of utilizing FACTS devices in electrical transmission systems can be summarized as follows [6]:

- (1) Better utilization of existing transmission system assets
- (2) Increased transmission system reliability and availability
- (3) Increased dynamic and transient grid stability and reduction of loop flows
- (4) Increased quality of supply for sensitive industries
- (5) Environmental benefits Better utilization of existing transmission system assets

III. Incorporation of UPFC in Power System

In real time applications the UPFC would have to manage the power flow control of a complex, transmission system in which the length, voltage, and capacity of the individual lines could widely differ. One of the attractive features of the UPFC is that it is inherently flexible to accommodate complex systems and several operating requirements. The UPFC is particularly advantageous when controlled series compensation or other shunt power flow control is already contemplated. Moreover, the single inverter of the UPFC can be operated as independent series reactive compensator. The operating areas of the individual inverter of the UPFC can differ significantly, depending on the voltage and power ratings of the individual ones and on the amount of compensation desired. The UPFC is an ideal solution to balance both real and reactive power flow in a transmission [7].

The basic operation of the unified power flow controller was described and the UPFC consists of two switching converters operated from a common dc link, as shown in Fig.1. Converter 2 (series converter) performs the main function of the UPFC by injecting an AC voltage with controllable magnitude and phase angle in series with the transmission line. The basic function of converter 1 (shunt converter) is to supply or absorb the active power demanded by converter 2 at the common dc link. This is represented by the current I_q . Converter 1 can also generate or absorb controllable reactive power and provide independent shunt reactive compensation for the line. This is represented by the current I_q . The open and closed loop modified system for UPFC shunt injected current is as shown in the Fig.1

3.1 Operation of UPFC System

This arrangement of UPFC ideally works as a ideal ac to dc power converter in which real power can freely flow in either direction between ac terminals of the two converters and each converter can independently generate or absorb reactive power at its own AC output terminal. The main functionality of UPFC provided by shunt converter by injecting an ac voltage considered as a synchronous ac voltage source with controllable phase angle and magnitude in series with the line. The transmission line current flowing through this voltage source results in real and reactive power exchange between it and the AC transmission system. The inverter converts the real power exchanged at ac terminals into dc power which appears at the dc link as positive or negative real power demand [8].

Series converter Operation: In the series converter, the voltage injected can be determined in different modes of operation: direct voltage injection mode, phase angle shift emulation mode, Line impedance emulation mode and automatic power flow control mode. Although there are different operating modes to obtain the voltage, usually the series converter operates in automatic power flow control mode where the reference input values of P and Q maintain on the transmission line despite the system changes [7]. Shunt converter operation: The shunt converter operated in such a way to demand the dc terminal power (positive or negative) from the line keeping the voltage across the storage capacitor V_{dc} constant. Shunt converter operates in two modes: VAR Control mode and Automatic Voltage Control mode. Typically, Shunt converter in UPFC operates in Automatic voltage control mode [7].

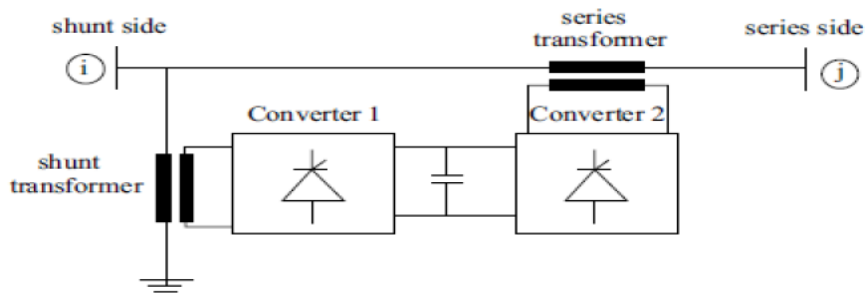


Fig.2 Block diagram arrangement of the UPFC system

3.2 The Controlling Parameters of UPFC System

Without UPFC shunt compensation, the line current, which is consisted of active and reactive components, made up of the following terms: (neglecting the dc and harmonic components).

$$i(t) = i_p(t) + i_q(t) \\ = I_p \sin(\omega t) + I_q \cos(\omega t) \quad (1)$$

Where,

$i_p(t)$ - in phase line active current of the transmission line

$i_q(t)$ - reactive current of the transmission line

To regulate the voltage at bus connected to the shunt converter of the UPFC, the only component that this bus should supply is the active current component. Using eqn(1), it can be noted that if the shunt converter of the UPFC supplies the reactive component, then the sending bus needs only to supply the active component as shown in figure.1. This can easily accomplished by subtracting the active current component from the measured line current [9].

$$I_q(t) = i(t) - I_p \sin(\omega t) \quad (2)$$

In eqn. (2), I_p is the magnitude of the in-phase current to be estimated and $\sin(\omega t)$ is a sinusoidal in phase with the line voltage. Consider the product of the line current of eqn. (2) and a sinusoid in phase with the line voltage.

IV. Simulation & Performance Analysis

4.1 Open Loop Model Based UPFC System

The overall simulation model of open loop UPFC incorporated to the test system is shown below in Fig. 3.

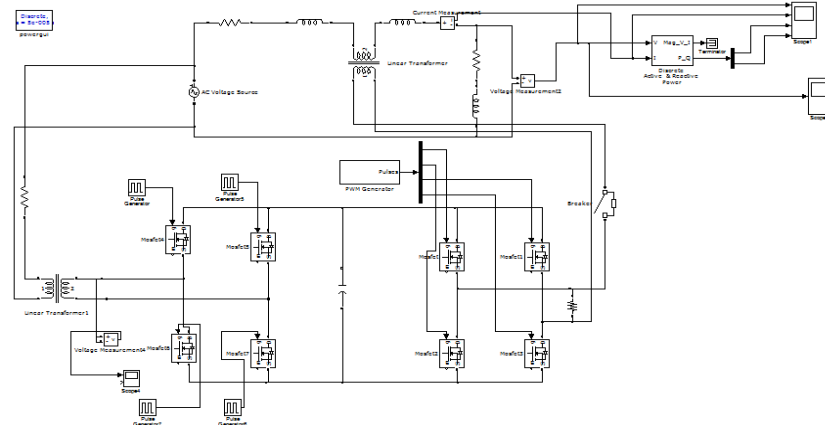


Fig.3 Open loop based UPFC model to the test system

The test system represented in Fig.3 consists of single phase 230V/50Hz AC source, delivering active and reactive power to non-linear load through a transmission system along with UPFC which is used to provide necessary compensation. Voltage measurement block is used to measure the source and load voltage and current measurement block is used to measure the instantaneous current flowing across the load. The active & reactive power measurement block in Matlab/simulink is used to measure the real power and reactive power across the non-linear load.

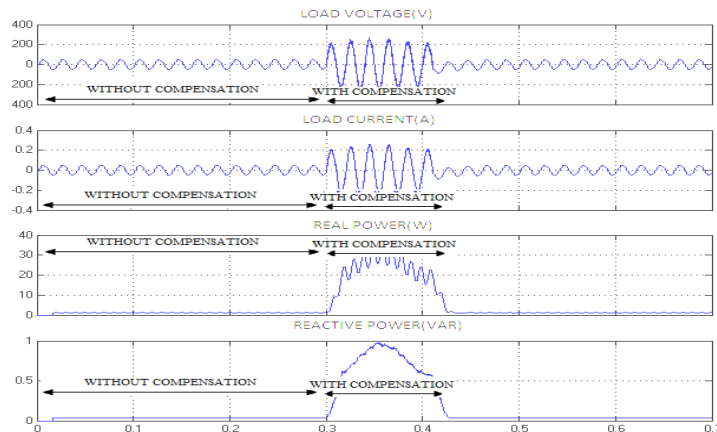


Fig.4 Output waveforms across the non-linear load

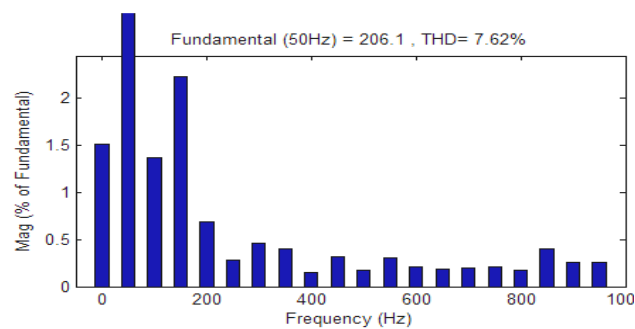


Fig.5 FFT Analysis for open loop UPFC

In Fig.4, the load voltage & current and real & reactive power of the system measured by the scope is shown. Here real and reactive power flow is obtained without any compensation. Here the active power (P) is 1kw and reactive power is 0.1kvar for uncompensated system model. So, it has to provide reactive power compensation in order to keep the system stable. Now for compensated system model, the real power observed is 20kw and reactive power is 0.4kvar.

Here for all three system models, generated waveforms are taken and calculations are done for the common parameter $C=1000\mu\text{F}$, sampling time $50e-6$ sec. The THD (Total Harmonic Distortion) block is used to measure the THD level of the system and the THD is around 7.62%.

4.2 Closed Loop Model Based UPFC System

The overall simulation model of closed loop UPFC incorporated to the test system is shown below in Fig. 6.

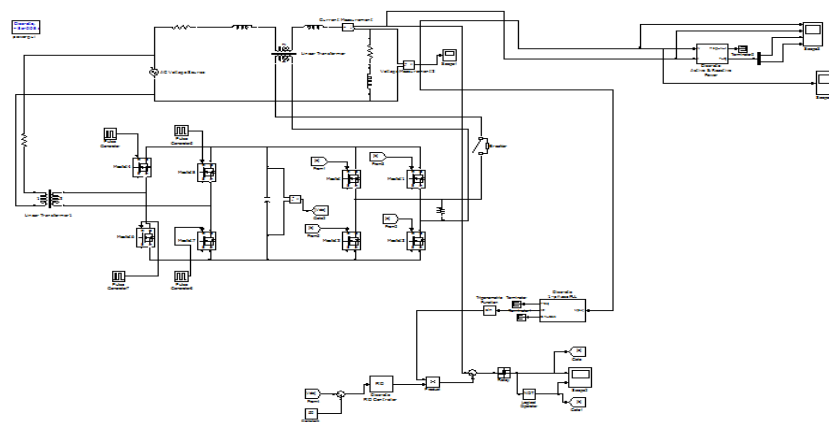


Fig.6 Closed loop based UPFC model to the test system

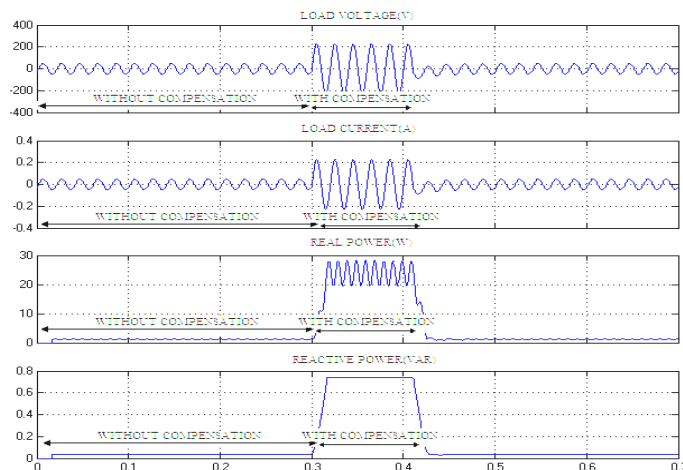


Fig.7 Output waveforms across the non-linear load

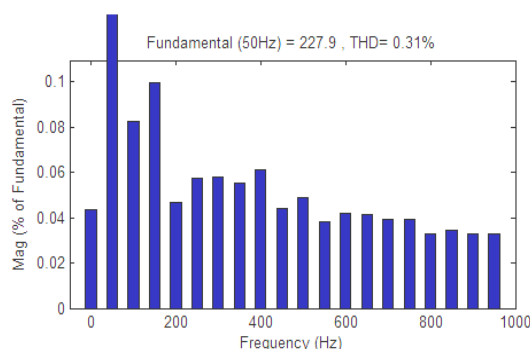


Fig.8 FFT Analysis for Closed loop UPFC

In Fig.7, the load voltage & current and real & reactive power of the system measured by the scope is shown. Here real and reactive power flow is obtained without any compensation. Here the active power (P) is 2kw and reactive power is 0.4kvar for uncompensated system model. So, it has to provide reactive power compensation in order to keep the system stable. Now for compensated system model, the real power observed is 30kw and reactive power is 0.7kvar and the THD is around 0.31%.

Here for all three system models, generated waveforms are taken and calculations are done for the common parameter $C=1000\mu\text{F}$, sampling time $50\text{e-}6$ sec. The THD (Total Harmonic Distortion) block is used to measure the THD level of the system.

Table.1 Performance analysis of UPFC

FACTS DEVICE	Open loop system		Closed loop system	
	Real power(kw)	Reactive power(kvar)	Real power(kw)	Reactive power(kvar)
Without UPFC	1	0.1	2	0.4
With UPFC	20	0.4	30	0.7

Table.2 FFT analysis of UPFC

FACTS Device	Open loop system	Closed loop system
With UPFC	7.62%	0.31%

V. Conclusion

In this paper performance analysis of UPFC are presented in SMIB system and MATLAB 2009a/simulink environment is used for this comparative study to model and simulate UPFC connected to a simple transmission line. Real power (P) and reactive power (Q) of the system is compared with and without the

presence of UPFC in the system for both open loop and close loop configuration. It is shown from the table.1 that power profiles are improved with the addition of the compensating devices with respect to uncompensated system model in each case.

In table.2 it is also shown with the help of FFT (Fast Fourier Transform) analysis that in open loop system the total harmonic distortion level % for UPFC are very low and it is further improving in case of close loop system.

REFERENCES

- [1] R. Billinton, L. Salvaderi, J. D. McCalley, H. Chao, Th. Seitz, R.N. Allan, J. Odom, C. Fallon, "Reliability Issues In Today's Electric Power Utility Environment", *IEEE Transactions on Power Systems*, Vol. 12, No. 4, November 1997.
- [2] Ch. Kiran Kumar, M. Sudheer Kumar, V. SriramBabu, S. Nagulmeera, "A comparative analysis of UPFC as a Power Flow controller with applications", *IOSR Journal of Electrical and Electronics Engineering*, Vol. 4, No. 6, April 2013.
- [3] N.G. Hingorani and L. Gyugyi "Understanding FACTS concepts and technology of flexible AC transmission systems", *IEEE Press*, New York, 2000.
- [4] L. Gyugyi, "Unified power-flow control concept for flexible ac transmission systems", *IEE Proceedings-C*, Vol. 139, NO.4, pp:323-33 I, July 1992.
- [5] Alok Kumar Mohanty, Amar Kumar Barik, "Power System Stability Improvement Using FACTS Devices", *International Journal of Modern Engineering Research (IJMER)*, Vol.1, Issue.2, pp-666-672.
- [6] Y. N. Yu, *Electric Power System Dynamics*. Academic Press, 1983.
- [7] Rishabh shah, Sarafraz Gandhi, Bhavin Trivedi, "Simulation and Performance Evaluation of UPFC and IPFC for Power System Performance Enhancement", *International Journal Of Engineering Development And Research*, ISSN: 2321-9939.
- [8] A.S. Kannan, R. Kayalvizhi, "Modeling and Implementation of d-q Control system for a unified power Flow controller", *International Journal of Engineering and Technology*, Vol.2 (6), 2010.
- [9] Rishabh Shah, Nehal Patel "Simulation Modeling & Comparison of Various FACTS Devices for Reactive Power Control In Power System", *emerging vistas of technology in 21st century 2013*.



A.Ramasamy received his B.E degree in Electrical and Electronics Engineering from Sri Subramanya College of Engineering and Technology, India in 2005 and M.E degree in Power systems from Annamalai University, India in 2007. His areas of interest include Control system, Electrical Machines and Power systems. He is a life member of ISTE and IAENG. Now he is currently working as an Assistant Professor in the Department of Electrical and Electronics Engineering, C.M.S College of Engineering and technology, Coimbatore, India.



R.Vibin received his B.E degree in Electrical and Electronics Engineering from V.L.B Janakiammal College of Engineering and Technology, in 2008 and honored M.E degree with university rank & gold medal in Power systems from S.N.S College of Technology, Coimbatore, India in 2012. His areas of interest include Electrical machines and Power systems. He is a life member of IAENG and now he is currently working as an Assistant Professor in the Department of Electrical and Electronics Engineering, C.M.S College of Engineering and technology, Coimbatore, India.



S.Gowdhankumar received his B.E degree in Electrical and Electronics Engineering from Bannari Amman Institute of Technology, in 2010 and M.E degree in Power electronics and drives from Sri Ramakrishna Engineering College, Coimbatore, India. His areas of interest include Electrical machines and Power electronics. He is a life member of IAENG and now he is currently working as an Assistant Professor in the Department of Electrical and Electronics Engineering, C.M.S College of Engineering and technology, Coimbatore, India.

Stability of Simply Supported Square Plate with Concentric Cutout

Jayashankarbabu B. S.¹, Dr. Karisiddappa²

¹(Civil Engineering Department, PES College of Engineering, Mandya/ VTU, India)

²(Civil engineering Department, Government college of Engineering, Hassan/ VTU, India)

ABSTRACT: The finite element method is used to obtain the elastic buckling loads for simply supported isotropic square plate containing circular, square and rectangular cutouts. ANSYS finite element software had been used in the study. The applied inplane loads considered are uniaxial and biaxial compressions. In all the cases the load is distributed uniformly along the plate outer edges. The effects of the size and shape of concentric cutouts with different plate thickness ratios and having all-round simply supported boundary condition on the plate buckling strength have been considered in the analysis. It is found that cutouts have considerable influence on the buckling load factor k and the effect is larger when cutout ratios greater than 0.3 and for thickness ratio greater than 0.15.

Keywords: Elastic buckling load, Finite element method, inplane compression loads, Plate thickness ratio, Plate with cutout

I. Introduction

Steel plates are often used as the main components of steel structures such as webs of plate girders, box girders, ship decks and hulls and platforms on oil rigs. Perforations are often included in the stressed skin cover of air plane wings. In plates cutouts are provided to decrease the self-weight, to provide access, services and even aesthetics. When these structures are loaded, the presence of cutouts will cause changes in the member mechanical properties, consequently there will be change in the buckling characteristics of the plate as well as on the ultimate load carrying capacity of the structure. The cutout shape and size, different plate thickness ratios and the type of load applied, influence the performance of such plates. However, though the cutouts are provided to achieve certain structural advantages, it is worth to mention here that they may inadvertently affect the stability of the plate component in the form of buckling. This always can be accomplished by thicker plate but the design solution will not be economical in terms of the weight of material used. It is possible to design an adequately strong and rigid structural plate element by keeping its thickness as small as possible. Hence the study of plate stability behavior is of paramount importance. Although much information is available regarding the buckling strength of perforated plate under simply supported boundary conditions, very little published information is available in the literature concerning the influence of different shape and size of cutout at centre and plate thickness on the elastic buckling strength of plates, this is because of the difficulties involved in determining the buckling strength of such plates by using classical methods of analysis. Owing to the complexity of the problem caused by plate thicknesses and the cutout, it appears that a numerical method such as the finite element method would be the most suitable for solving this problem.

The stability of plates under various compressive loading and boundary conditions has been the subject and studied by Herrmann and Armenkas [1], Timoshenko and Gere [2] and many others. Thin plate theory is based on several approximations, the most important of which is the neglect of transverse shear deformations. The errors of such a theory naturally increase as the thickness of plate increases, Srinivas and Rao [3]. Chiang–Nan Chang and Feung–Kung Chiang [4] observed the change of mechanical behaviors due to the interior holes cut from plate structures and proved the importance to study the buckling behaviors to avoid the structure instability. They used FEM and considering the incremental deformation concept to study the buckling behavior of Mindlin thick plate with interior cutout for different plate boundaries and different opening ratios. Christopher J. Brown, Alan L. Yettram and Mark Burnett [5] have used the conjugate load/displacement method to predict the elastic buckling load of square plate with centrally located rectangular holes under different types of loads. Shanmugam, Thevendran and Tan [6] have used FEM to develop a design formula to determine the ultimate load carrying capacity of axially compressed square plates with centrally located perforations, circular or square.

They concluded that the ultimate load capacity of the square perforated plate is affected significantly by the hole size and the plate slenderness ratios. Ultimate strength of square plate with rectangular opening under axial compression using non-linear finite element analysis was studied by Suneel Kumar, Alagusundaramoorthy and Sundaravadevelu [7]. El-Sawy and Nazmy [8] have used the FEM to investigate the effect of plate aspect ratio and hole location on elastic buckling of uniaxially loaded rectangular plates with eccentric holes with simply supported edges in the out-of-plane direction. The study concluded that the use of a rectangular hole, with curved corners, with its short dimension positioned along the longitudinal direction of the plate is better option than using a circular hole, from the plate stability point of view. A general purpose finite element software ANSYS was used for carrying out the study. Jeom Kee Paik [9] studied the ultimate strength of perforated steel plate under combined biaxial compression and edge shear loads for the circular cutout located at the centre of the plate. A series of ANSYS elastic-plastic large deflection finite element analysis has been carried out on perforated steel plates with varying plate dimension.

In the present paper it has been attempted to investigate the effect of the size and shape of concentric circular, square and rectangular cutouts and the impact of plate thickness on the buckling load of all-round simply supported isotropic square plate subjected to uniform inplane uniaxial and biaxial compression loadings. To carry out the study, ANSYS software has been used with 8SHELL93 element [10]. The finite element mesh used to model the plate has been decided upon carrying out a series of convergence tests and considered 10 x 10 mesh shows nearly the accurate results and hence considered in the analysis.

II. Problem Definition

The problem of elastic buckling of a square plate subjected to inplane compression loadings along its ends, Fig.1, having different cutouts such as circular, square and rectangular shapes with all-round simply supported boundary condition are considered. The plate has thickness h and dimensions A and B in x and y -directions, respectively and circular cutouts with diameter d , square and rectangular cutout of size $a \times b$. Here concentric cutout ratio is defined as the ratio of size of cutout to side of plate. The buckling load factor k is assessed with respect to the concentric cutout, vary between 0.1 to 0.6 for circular and square where as for rectangular cutout it is 0.1 to 0.5 and also with respect to the plate thickness ratios η , 0.01 to 0.3.

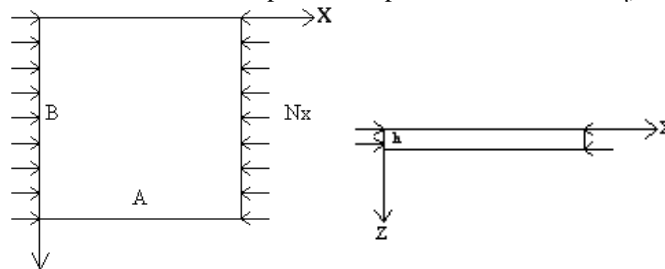


Fig.1: Plate coordinate system

III. Finite Element Analysis Procedure

The finite element software program ANSYS was employed in this study. 8SHELL93 element is used to model the perforated plate because it shows satisfactory performance in verification work previously described by El-Sawy [8]. The elastic SHELL93 element has eight nodes possessing six degrees of freedom per node. The material of the plate was assumed to be homogeneous, isotropic and elastic. The material properties for Young's modulus $E=210924\text{N/mm}^2$ and Poisson's ratio $\mu=0.3$, were used.

3.1 Buckling of Simply Supported Thick Plate under uniaxial compression

R.D. Mindlin in 1951, published the famous thick plate theory. This two dimensional theory of flexural motions of isotropic elastic plates is deduced from the three dimensional equations of elasticity. The theory includes the effects of rotary inertia and shear in the same manner as Timoshenko's one dimensional theory of bars [2]. The following assumptions are also applied.

1. The straight line that is vertical to the neutral surface before deformation remains straight but not necessarily vertical to the neutral surface after deformation.
2. Displacement is small so that small deformation theory can be applied.
3. Normal stress in the z -direction is neglected.
4. Body force is neglected.

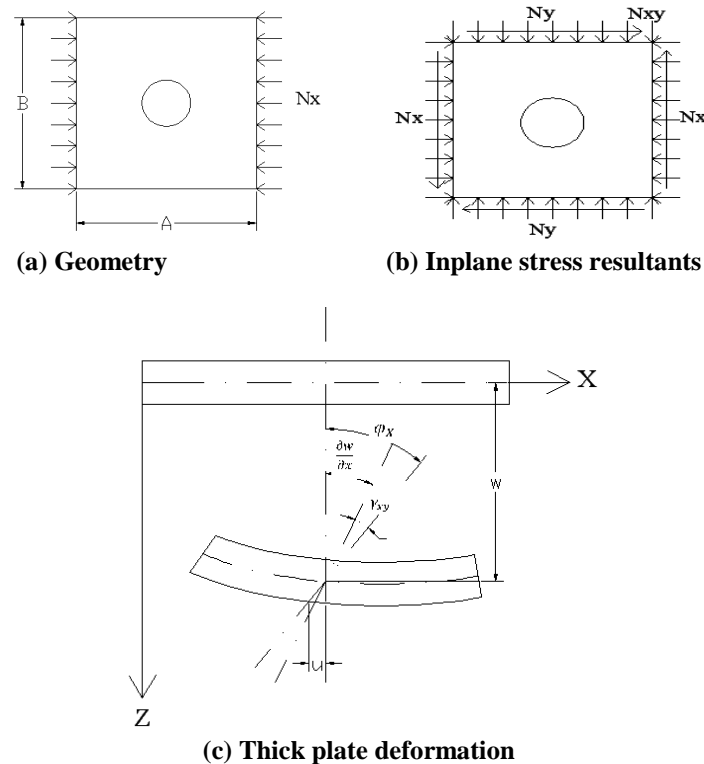


Fig.2: Plate with opening and inplane stress resultants.

A plate of size A and B subjected to a system of general external inplane loadings and the internal stress resultants at the edges of an element due to the external inplane loads be N_x , N_y and N_{xy} as depicted in Fig 2. The total potential energy of the plate due to flexure and the work done by the membrane stress resultants, taking the shear deformation into account may be written as:

$$\begin{aligned}
 U = & \frac{D}{2} \int_0^A \int_0^A \left\{ \left[\frac{\partial^2 w}{\partial x^2} + \frac{\partial^2 w}{\partial y^2} \right]^2 - 2(1-\mu) \left[\frac{\partial^2 w}{\partial x^2} + \frac{\partial^2 w}{\partial y^2} - \left(\frac{\partial^2 w}{\partial x \partial y} \right)^2 \right] \right\} dA + \frac{D}{2} \int_0^A \int_0^A \frac{6\chi(1-\mu)}{h^2} [\phi_x^2 + \phi_y^2] dA \\
 & + \frac{1}{2} \int_0^A \int_0^A \left[N_x \left\{ \left(\frac{\partial u}{\partial x} \right)^2 + \left(\frac{\partial v}{\partial x} \right)^2 + \left(\frac{\partial w}{\partial x} \right)^2 \right\} + N_y \left\{ \left(\frac{\partial u}{\partial y} \right)^2 + \left(\frac{\partial v}{\partial y} \right)^2 + \left(\frac{\partial w}{\partial y} \right)^2 \right\} + 2N_{xy} \left\{ \frac{\partial u}{\partial y} \frac{\partial u}{\partial z} + \frac{\partial v}{\partial z} \frac{\partial v}{\partial x} + \frac{\partial w}{\partial x} \frac{\partial w}{\partial y} \right\} \right] dA \quad (1)
 \end{aligned}$$

Where χ is the Reissner's shear correction factor, A_p is the area of the plate including the cutout, A_c is the area of the cutout, Φ_x , Φ_y are average shear strains, N_x , N_y , N_{xy} are inplane stress resultants and D is the flexural rigidity of the plate. The stiffness matrix [K] is the combination of $[K_b]$ and $[K_s]$ such that $[K] = [K_b] - [K_s]$, in which the former is due to flexure [4] and the later is due to the work associated with the inplane stress resultants. Thus static buckling equilibrium equation becomes,

$$[[K_b] - [K_s]] \{q\} = 0 \quad (2)$$

The stress resultants N_x , N_y and N_{xy} are functions of geometrical ordinates (X,Y) for the plate and depend upon the magnitude of the external inplane loads, $\{q\}$ is nodal displacement vector. Choosing a factor λ , by which the inplane stress resultants can be gradually increased, equation (2) may be written as.

$$[[K_b] - \lambda [K_\sigma]] \{q\} = 0, \text{ in which } [K_s] = \lambda [K_\sigma] \quad (3)$$

The Eigen values of the equation (3) give the critical loads λ_i of the plate under investigation. The lowest Eigen value correspond to the fundamental critical load ' λ_{cr} '

Let P_{cr} be the critical bucking load and by replacing λ by P_{cr} the governing equation for the static stability problem modified to

$$[[K_b] - P_{cr} [K_\sigma]] \{q\} = 0 \quad (4)$$

The general equation of stability given in equation (4) contain the structural properties in matrix form, viz., $[K_b]$ and $[K_s]$. The very basic assumption in the derivation of these equations is that the displacement model of the entire structure which satisfies the equilibrium equations and compatibility conditions. Developing such a true displacements model is a tedious exercise. In the present study an alternate method, using the finite element technique through ANSYS software, has been used.

IV. Results and Discussions

Results on the effect of shape and size of circular, square and rectangular cutout and plate thickness ratio on the buckling load factor k of the square plate having simply supported plate boundary conditions, subjected to inplane uniaxial and biaxial compression loading cases are presented and discussed in this section. Here, the concentric cutout ratio, defined as the ratio of side of the cutout to plate side, for circular β and square δ lies between 0.1 – 0.6 and for rectangular cutout it is 0.1–0.5, along x-direction γ and along y-direction γ' . The thickness ratio η , defined as the ratio of plate thickness to the plate side and varies from 0.01 - 0.3. The critical buckling load factor is non-dimensionalised and represented as follows:

$$k = \frac{(N_{cr})B^2}{\pi^2 D} \tag{5}$$

Where, k = Buckling load factor.

N_{cr} = Critical buckling load.

D = Plate flexural rigidity = $\frac{Eh^3}{12(1-\mu^2)}$

μ = Poisson’s ratio of isotropic plate.

h = Thickness of the plate.

4.1 Comparative Study

In order to verify the present analysis, a comparison with existing results in the literature on buckling of square plate with and without cutout has been performed. The results of present study with the available values are tabulated in Table 1 and 2. It can be observed that the results from the present work are in good agreement with the established work.

Table 1

Comparison of buckling load factor k for isotropic simply supported plate with concentric circular cutout subjected to inplane uniaxial compression load.

Sl. no	Cutout ratio, \square	Buckling load factor, k	
		Present study	Reference value
1	0.1	3.8434	3.80 ^[11]
2	0.2	3.5310	3.50 ^[11]
3	0.3	3.2642	3.20 ^[11]
4	0.4	3.1124	3.10 ^[11]
5	0.5	3.0460	2.99 ^[11]
6	0.6	2.8547	Present study

Table 2

Comparison of buckling load factor k for isotropic simply supported plate with concentric square cutout subjected to inplane biaxial compression load.

Sl. no	Ratio of size of hole to plate side $\square=b/A$	Buckling load factor, k	
		Present study	Reference value
1	0	1.9980	2.0 ^[2]
2	0.1	1.9051	Present study
3	0.2	1.7496	Present study
4	0.25	1.6986	1.65 ^[12]
5	0.3	1.6684	Present study
6	0.4	1.7028	Present study
7	0.5	1.8891	1.55 ^[12]
8	0.6	2.5182	Present study

4.2 Case of plate with simply supported boundary conditions

The results obtained are plotted as shown in Figs. 3 - 10 for plate with different cutout ratios and plate thickness ratios having simply supported plate boundary condition subjected to inplane uniaxial and biaxial compression loading cases. In all these Figs the variation of the buckling load factor k are plotted against

thickness ratio η and cutout ratios. It can be noticed in these figures that, stability of the square plate with cutout is greatly affected by increase in thickness ratios.

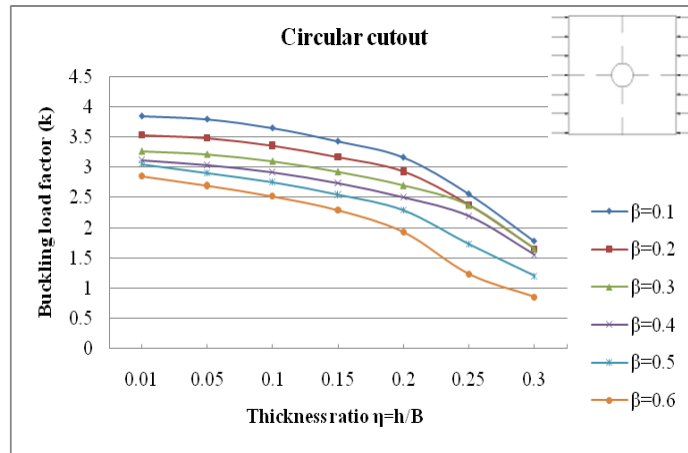


Fig.3: Variation of k with η and β for uniaxial compression.

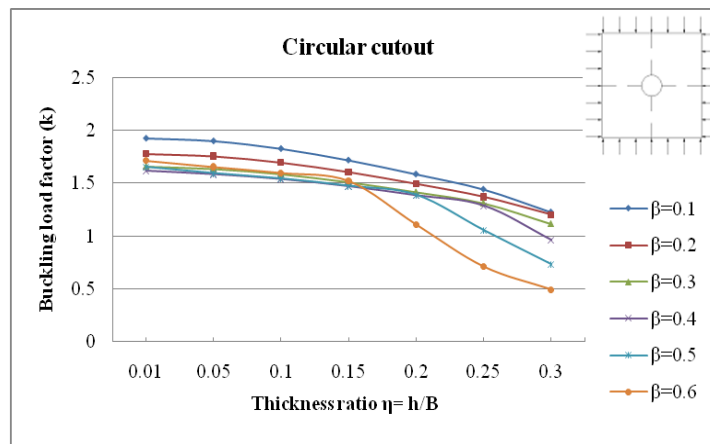


Fig.4 : Variation of k with η and β for biaxial compression

In Fig.3, buckling load factor k decreases gradually up to the thickness ratio $\eta < 0.2$ for all circular cutout ratios β and when $\eta > 0.2$, k reduction is in higher magnitude i.e., in the range of 25% to 52% as η increases from 0.01 to 0.3 for each cutout ratio. Fig.4 represents the variation of buckling load factor k for square plate having concentric circular cutout subjected to biaxial loading. In case of biaxial loading, k value is found to be almost 50% to that of uniaxial compression value. This may be due to stiffening of the plate in both x and y -directions. It is noticed that k always decreases with increase in η and β and this decrease is more steeper for $\beta > 0.3$ and $\eta > 0.15$, when $\beta = 0.6$ and $\eta = 0.3$, 60% of reduction in k is observed to that of $\beta = 0.1$.

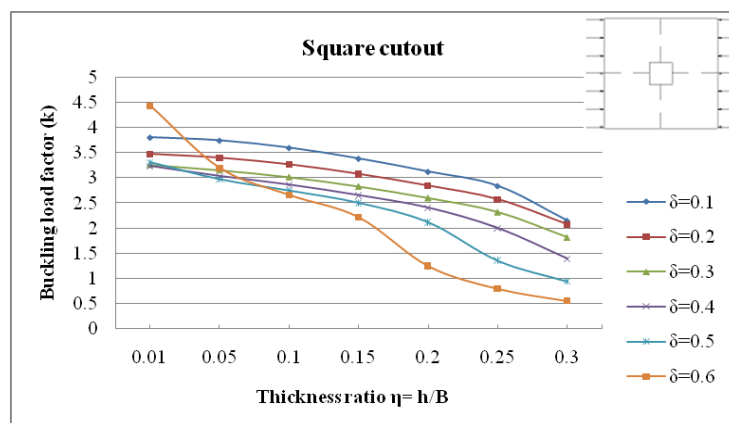


Fig. 5: Variation of k with η and δ for uniaxial compression

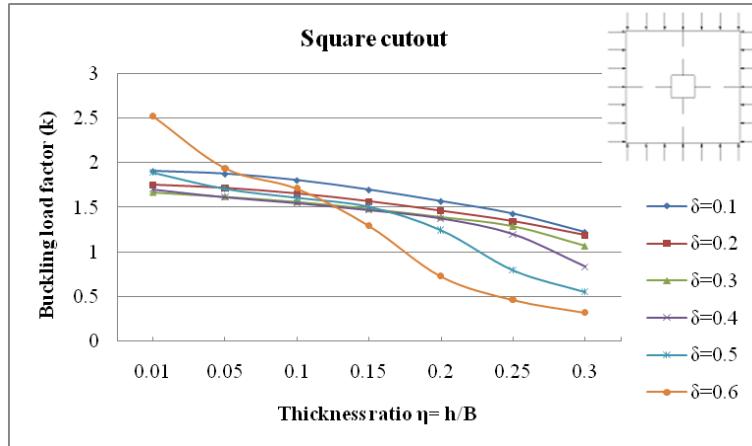


Fig. 6: Variation of k with δ and η for biaxial compression

Fig.5, represents the variation of buckling load factor k for square plate with concentric square cutout ratios δ , subjected to uniaxial loading. Here, the value of k is 10% less than that of circular cutout and k value decreases as δ and η increases, except at $\delta=0.6$ for $\eta=0.01$, where an increase of 16.33% in k value can be observed compared to $\delta=0.1$. This does not necessarily mean that the actual increase in buckling strength of the plate because the strength of the plate corresponds to less removal of plate material. When the cutout ratio becomes large and $\eta > 0.15$, the reduction is more rapid and it is up to 50% for $\delta \leq 0.3$ for all values of η and it is more than 50% for $\delta > 0.3$. Fig.6, represents the variation of buckling load factor k for square plate having concentric square cutout, subjected to biaxial loading. Here, k value is 50% compared to uniaxial loading case. It is noticed that the variation of k is very less for δ up to 0.3 with respect to η values, but high variation is noticed when $\delta > 0.3$. Decrease in buckling load factor k is unpredictable at $\delta=0.6$ and k reduction is noticed in the magnitude of 54%, 67% and 74% when $\eta=0.2, 0.25$ and 0.3 respectively.

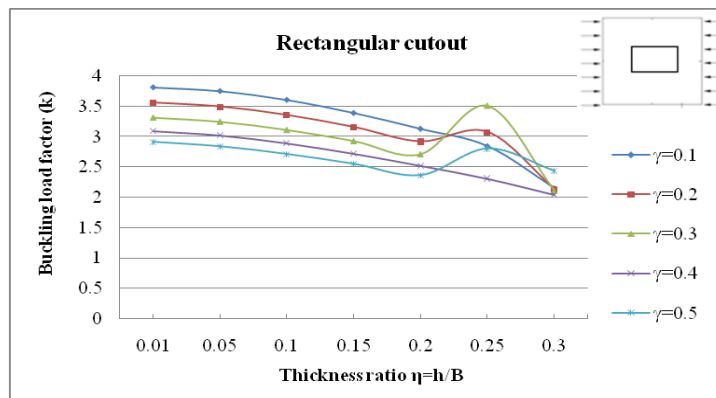


Fig.7: Variation of k with γ and η for uniaxial compression

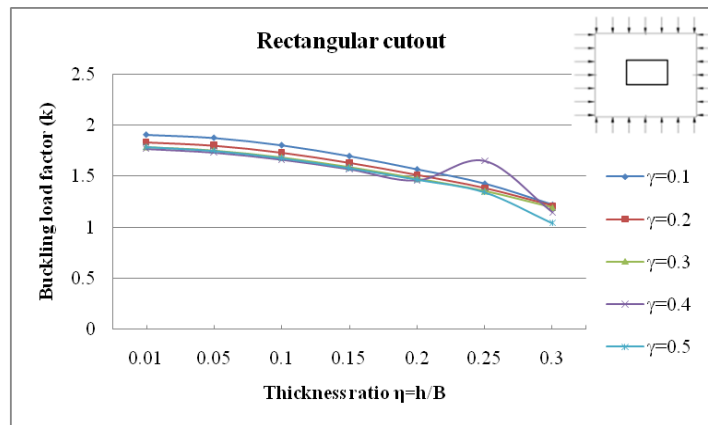


Fig.8 : Variation of k with γ and η for biaxial compression.

Fig.7 represents the variation of buckling load factor k for square plate having concentric rectangular cutout γ along x -direction, subjected to uniaxial loading. Here, the decrease in k is gradual when compared to circular and square cutout and k always decreases as η and γ increases except for η lies between 0.2 to 0.25 and $\gamma=0.2, 0.3$ and 0.5 , where a sudden variation in k value can be observed. Fig.8 and Fig.10 represents the variation of buckling load factor k for square plate having concentric rectangular cutout along x and y -directions γ and γ' respectively under biaxial loading. Here, the value of k is half of that of uniaxial loading case and the variation of k is very less as η and cutout ratios increases. In case of biaxial loading, rectangular cutout along x and y -directions, k reduces in slower manner. Fig.9 represents the variation of buckling load factor k for square plate having concentric rectangular cutout along y -direction subjected to uniaxial loading. Here, k increases with increase in the value of γ' and for η up to 0.15, beyond k reduces with the increase of γ' . It is noticed that as η increases k decreases and this decrease is significant when $\gamma' > 0.3$. The reduction of k is upto the range 43.5%, 51%, 60%, 69% and 76% with the increase of γ' from 0.1 to 0.5 with respect to $\eta=0.01 - 0.3$. It is also observed that, for small cutout ratios, there is a little effect of thickness ratio η upto 0.15. But when cutout ratio becomes larger, increasing the plate thickness ratio shows significant effect on the buckling strength of the plate.

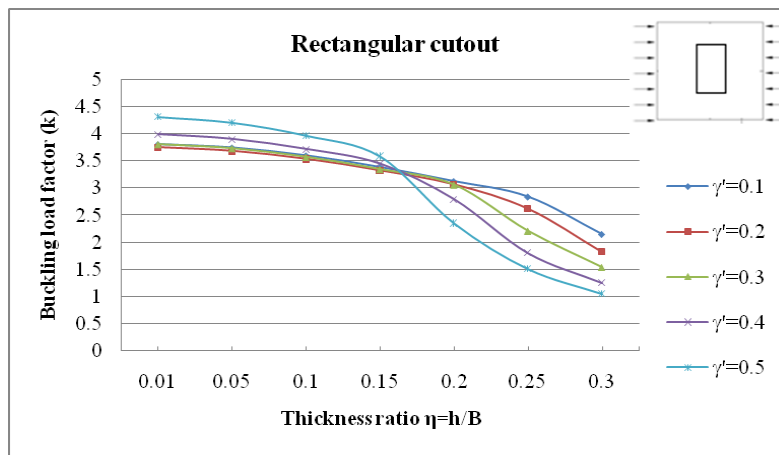


Fig.9 :Variation of k with η and γ' for uniaxial compression

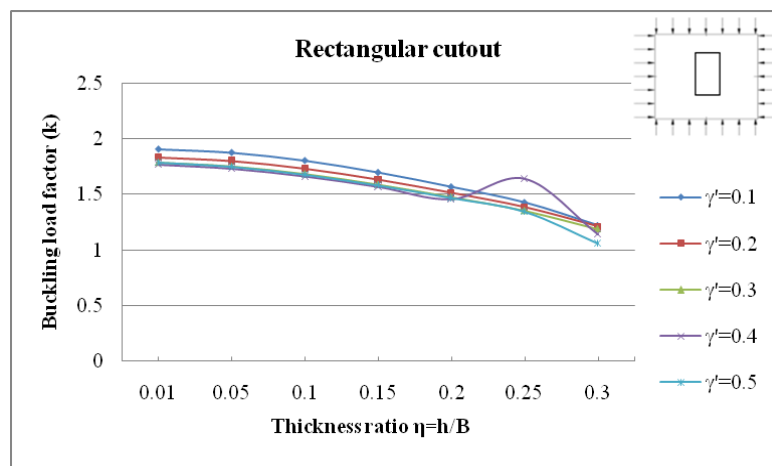


Fig.10 :Variation of k with η and γ' for biaxial compression

V. Conclusion

A study of buckling behavior of uniformly compressed isotropic square plate with different cutouts such as circular, square and rectangular are investigated using FEM. Simply supported square plate with wide ranges of concentric cutout ratios and plate thickness ratios are considered. Following conclusions are drawn.

1. Buckling is the critical mode of failure for the major portion of the compressed plate with cutout especially when its thickness is considerably small.
2. The cutouts have considerable influence on the buckling load factor k . The effect is larger in higher cutout ratios ≥ 0.3 and for thickness ratio ≥ 0.15 .
3. Square plates with circular cutouts and square cutouts have similar buckling loads, but, plate with circular

cutout is more efficient compare to plate with square cutout.

4. In the plate with circular cutout and square cutout, buckling load factor k decreases with the increase of thickness ratio and cutout ratios. The value of k is less by 10% in case of plate having square cutout compared to circular cutout.
5. Plate with concentric rectangular cutout, along x -direction, decrease in the buckling load factor k of the plate is 34-43%.
6. In case of biaxial loading, k value is found to be nearly 50% to that of uniaxial compression value.

In summary, buckling of simply supported plate with concentric cutout having different plate thickness ratio is important for optimizing the engineering design. The present study offers useful information for the researchers.

REFERENCES

- [1] G.Herrmann, and A.E.Armenakas, Vibration and stability of plates under initial stress, *Journal of Engineering Mechanics, ASCE*, 86(no.EM3), June 1960, 65-94.
- [2] S.P.Timoshenko, and James M. Gere., “*Theory of Elastic Stability*”, (second ed. McGraw- Hill company, Singapore, 1963) 348-389.
- [3] S.Srinivas, and A.K. Rao, Buckling of thick rectangular plates, *AIAA Journal*, 7, 1969, 1645 – 1647.
- [4] Chiang-Nan Chang, and Feung-Kung Chiang, Stability analysis of a thick plate with interior cutout, *AIAA Journal*, .28(7), 1990, 1285-1291.
- [5] Christopher J. Brown, Alan L. Yettram, and Mark Burnett, Stability of plates with rectangular cutouts, *Journal of Structural Engineering*, vol.113, no 5, 1987, 1111-1116.
- [6] N.E.Shanmugam, V. Thevendran, and Y.H. Tan, Design formula for axially compressed perforated plates, *Thin-Walled Structures*, 34(1), 1999, 1-20.
- [7] M.P.Suneel Kumar, Alagusundaramoorthy, R.Sundaravadivelu, Ultimate strength of square plate with rectangular opening under axial compression, *Journal of Naval Architecture and Marine Engineering*, 2007, 15-26.
- [8] El-Sawy K.M., Nazmy A.S., Effect of aspect ratio on the elastic buckling of uniaxially loaded plates with eccentric holes, *Thin Walled Structures*, 39, 2001, 983-998.
- [9] Jeom Kee Paik, Ultimate strength of perforated steel plate under combined biaxial compression and edge shear loads, *Thin-Walled Structures*, 46, 2008, 207-213.
- [10] ANSYS, User Manual, Version 10.0, Ansys Inc.
- [11] A.B. Sabir, and F.Y. Chow, Elastic buckling containing eccentrically located circular holes, *Thin-Walled Structures*, 4, 1986, 135-149.
- [12] A.L.Yettram, and C.J. Brown, The elastic stability of square perforated plates under biaxial loading, *Computers and Structures*, 22(4), 1986, 589-594.

An Efficient Clustering Method for Aggregation on Data Fragments

Srivaishnavi D., M. Kalaiarasu

PG Scholar (CSE), Sri Ramakrishna Engineering College, Coimbatore
Associate Professor, Dept. of IT(UG), Sri Ramakrishna Engineering College, Coimbatore

ABSTRACT: Clustering is an important step in the process of data analysis with applications to numerous fields. Clustering ensembles, has emerged as a powerful technique for combining different clustering results to obtain a quality cluster. Existing clustering aggregation algorithms are applied directly to large number of data points. The algorithms are inefficient if the number of data points is large. This project defines an efficient approach for clustering aggregation based on data fragments. In fragment-based approach, a data fragment is any subset of the data. To increase the efficiency of the proposed approach, the clustering aggregation can be performed directly on data fragments under comparison measure and normalized mutual information measures for clustering aggregation, enhanced clustering aggregation algorithms are described. To show the minimal computational complexity. (Agglomerative, Furthest, and Local Search); nevertheless, which increases the accuracy.

Key words: Clustering aggregation, Fragment based approach, point based approach.

I. Introduction

Clustering is a problem of partitioning data object into clusters that is object belongs to similar groups. Clustering becomes a problem of grouping objects together so that the quality measure is optimized. The goal of data clustering is to partition objects into disjoint clusters. Clustering is based on aggregation concepts.

The objective is to produce a single clustering that agrees m input clustering. Clustering aggregation is a optimization problem where there is a set of m clustering, To find the clustering that minimizes the total number of disagreement in the framework for problems related to clustering. It gives a natural clustering algorithm data. It detects outliers; clustering algorithm is used in machine learning, pattern recognition, bio informatics and information retrieval.

II. Related Works

Point-based clustering aggregation is applying aggregation algorithms to data points and then combining various clustering results. Apply clustering algorithms to data points increase the computational complexity and decrease the accuracy. Many existing clustering aggregation algorithms have a time complexity, decreases the efficiency, in the number of data points. Thus the Data fragments are considered. A Data fragment is any subset of the data that is not split by any of the clustering results. Existing model gives error rate due to lack of preprocessing of outliers. Non spherical clusters will not be split by using distance metric.

N.Nugen and R.Carunahave proposed each input clustering in effect votes whether two given data points should be in same clustering. Consensus clustering algorithms often generate better clustering, find a combined clustering unattainable by any single clustering algorithm; are less sensitive to noise, outliers or sample variations, and are able to integrate solutions from multiple distributed sources of data or attributes..

X.Z.Fern and C.E.Brodly, it proposes random projection for high dimensional data clustering Data reduction techniqueit does not use any “interestingness “criterion to optimize the projection. Random projections have special promise for high dimensional data clustering. High dimension poses two challenges; The drawback of random projection is that it is highly unstable and different random projection may lead to radically different clustering results.

Inclustering based similarity partitioning algorithm if two objects are in the same cluster then they are considered to be fully similar, and if not they are fully dissimilar. Define the similarity as a fraction of clustering's in which two objects are in the same clusters.TheHyper graph partitioning algorithmis a direct approach to cluster ensembles that re-partitions the data using the given clusters which indicates the strong bonds .The hyper edge separator that partitions the hyper graph into k unconnected components of same size. The main idea of Meta clustering algorithm is to group and collapse related hyper edges and assign object to the

collapsed hyper edge in which it participates more strongly. The three methods require the constructions of edge between each pair of points; all their complexities are atleast $O(N^2)$.

III. Proposed System

Fragment-based clustering aggregation is applying aggregation algorithms to data points and then combining various clustering results. Applying clustering algorithms to data points increases the time complexity and improves the quality of clustering. In this fragment –based approach, a data fragment is any subset of the subset of the data that is not split by any of the clustering results. The main aim of the fragment based clustering aggregation defines the problem of clustering aggregation and demonstrates the connection between clustering aggregation and correlation clustering.

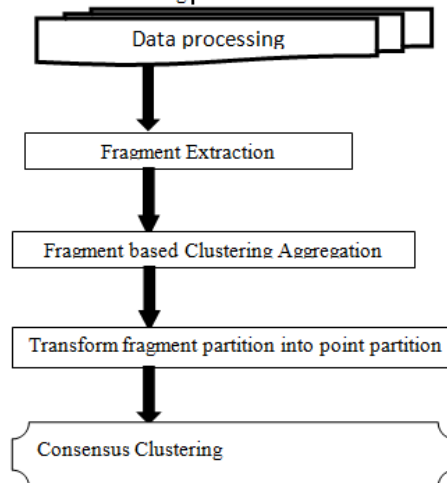


Fig.1. Architecture Diagram for Fragment Based Approach

Preprocess the datasets using the preprocessing technique then extract the data from the preprocessed data sets. The extracted data are fragmented using clustering aggregation. After these steps transform the fragment partition into point partition which results the consensus clustering.

IV. Implementation Details

In Fragment based extraction partitions the given data sets into a set of clusters. Each partition divides the data set into three clusters. Large data sets are split into one sentences and then extracted into a one word. The fragments can be represented as

$$F = \{F_1, \dots, F_2, \dots, F_z\}$$

Z-Represent the number of fragments

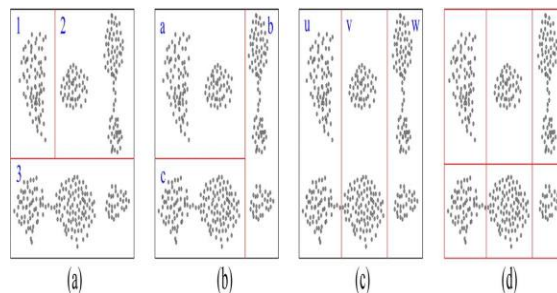


Fig.2. Sample Extraction for Data Fragment

(a), (b), and (c) are three input partitions; (d) shows the union of all the three solutions. Each data subset, enclosed by red lines and red borders in (d), is a data fragment. The number of fragments is six.

The clustering aggregation can be directly achieved on data fragments when either comparison measure or the NMI measure is used. This provides a theoretical basis to guarantee that the fragment based clustering aggregation is feasible.

Clustering Algorithm

4.1. F-Agglomerative

The Agglomerative algorithm is a standard bottom-up algorithm for the correlation clustering problem. It starts by placing every node into a singleton cluster. It then proceeds by considering the pair of clusters with the smallest average distance. The average distance between two clusters is defined as the average weight of the edges between the two clusters. If the average distance of the closest pair of clusters is less than 0.5 then the two clusters are merged into a single cluster. If there are no two clusters with average distance smaller than 0.5, then no merging of current clusters can lead to a solution with improved cost of class. The average distance between two clusters

$$\text{avg_dis}(\pi_{ik}, \pi_{jl}) = \frac{\sum_u \sum_v \text{DMP}(u, v) / (|\pi_{ik}| |\pi_{jl}|)}{|\pi_{ik}| |\pi_{jl}|} \dots 1.1$$

Where,

u,v-Edges of data point

Avg-Average

D-Distance

Since the proposed system is performed on fragments, the average distance between two clusters can be rewritten as then no merging of current clusters can lead to a solution with improved cost of class.

Algorithm 1

Input: $X = \{x_1, \dots, x_i, \dots, x_n\}$, $\Pi = \{\pi_1, \dots, \pi_i, \dots, \pi_n\}$

Output: Consensus clustering

Steps:

- 1) Extract data fragments based on input partitions
- 2) Calculate the distance matrix for fragments (DMF)
- 3) Place each fragment in a single cluster.
- 4) Calculate the average distance between each pair of clusters using formula, and choose the smallest average distance is below 0.5. otherwise, go to the next step.
- 5) Transform the obtained fragment partition into a data point partition, and return the new data point partition.

4.2. F-Furthest

Furthest algorithm is a top-down algorithm that's work on the correlation clustering problem. It is inspired by the first traversal algorithm, it uses centers to partition the graph in a top-down fashion.

It starts by placing all nodes into a single cluster. Its find the pair of nodes that are furthest apart and places them into different clusters. Then the nodes become the center of clusters.

The DMP distance is largest, and then makes each point the center of a new cluster. The remaining nodes are assigned to one or other of two clusters according to their distances to the two clusters centers. The procedure is repeated iteratively: at each step, the furthest data point from the existing centers is chosen and taken as a new center of singleton cluster; the nodes are assigned to the new cluster that leads to the least moving cost defined by formula. If the total moving cost is not smaller than 0, the algorithm stops their work. it moves the fragments instead of data points at each step .Equation and can be rewritten for fragment as

$$\text{cost}(F_{\zeta}, \pi_{ik} \rightarrow \pi_{il}) = \text{cost}(F_{\zeta}, \pi_{il}) - \text{cost}(F_{\zeta}, \pi_{ik}) \dots 1.2$$

Where

Cost-To calculate the value for data points

F_{ζ} -Total number of fragment

DMP-Distance matrix point

Then, the cost of moving F_{ζ} from cluster π_{ik} to π_{il} is

Algorithm 2

Steps of F-Furthest

Input: $X = \{x_1 \dots x_i \dots x_n\}$, $\Pi = \{\pi_1, \dots, \pi_i, \dots, \pi_n\}$

Output: Consensus clustering

Steps:

- 1) Extract data fragments based on the input partitions.
- 2) Calculate the distance matrix for fragments.
- 3) Place the entire fragment in a single cluster, then find the pair of fragments whose distance (DMF distance) is furthest, and make each of them the center of a singleton cluster.

- 4) Assign the rest of the fragments to one of the two clusters in order to achieve the minimum moving cost.
- 5) Choose the furthest fragment from the existing centers and make the fragment the center of a new singleton cluster.

4.3. F-Local search

Local search algorithm is an application of a local search heuristic to the problem of correlation clustering. The algorithm starts with some clustering of the nodes. The aim of the F-local search algorithm is to find a partition of a data set such that the data points with low DMP distances the values is less than 0.5, the data points are kept together.

Its start with initial clustering is given. The algorithm goes through the all the data point by considering a local movement of a point from a cluster to one another or creating a new singleton cluster with this node. For each local movement, calculate the moving cost by formula .If one data points yield a negative moving cost, it improves the goodness of the current clustering. Repeatedly the node is placed in the cluster that yields minimum moving cost .The algorithm iterates until all moving cots are not smaller than 0, Based on local search ,the steps of F-Local search are detailed in Algorithm 3.

The process is iterated until there is no move that can improve the cost .

4.4. Comparison and Analysis

Three algorithms are used to evaluate the performance analysis .The input to the algorithm are datasets which are evaluate using the following formula.

Entropy formula

$$E\chi(\pi_i) = \sum_{\varphi=1}^{\pi_i} (|\pi_i\varphi| - \mu_i\varphi) / N \dots\dots 1.3$$

Where

E-Entropy

P-Partition of data sets

N-Number of data sets

Average entropy formula

$$AE(\pi_i) = \sum_{j=1}^{\pi_i} |\pi_{ij}| / N \times (\sum_{k=1}^{|c|} -m_{ij} / |\pi_{ij}| \log_2 m_{ij} / |\pi_{ij}|) \dots\dots 1.4$$

Where

AE-Average Entropy

N-Total number of data points

The above formula computes the entropy values which are compared to plot out the performance. Based on the entropy values generated, the agglomerative algorithm has the best performance among the three algorithms

V. Results and Discussion

A graph is plotted to represent the sum of entropy values for three different algorithms. It is observed that the value of the sum of entropy is least for agglomerative compared to other two algorithms.

Table 5.1. Comparison of algorithms with respect to datasets

Data sets	F-Agglomerative	F-local search	F-Furthest search
Glass	30.84	37.38	32.3
Hayes	30.27	37.38	30.37
yeast	34.51	35.48	37.62

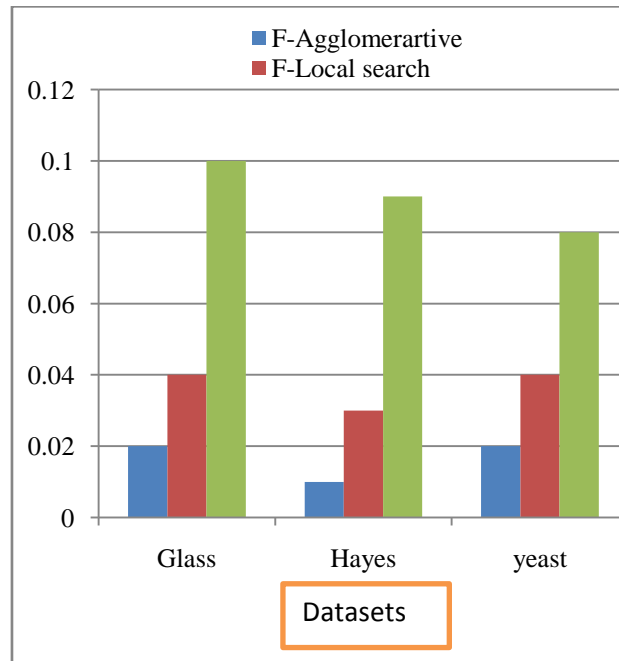


Fig .3. Datasets results using entropy

Table.5.3. Table Comparison of algorithm with respect to data sets

Datasets	F-agglomerative	F-Local search	F-furthest search
Glass	30.84	37.38	32.3
Hayes	30.27	37.38	30.37
yeast	34.51	37.62	71.6

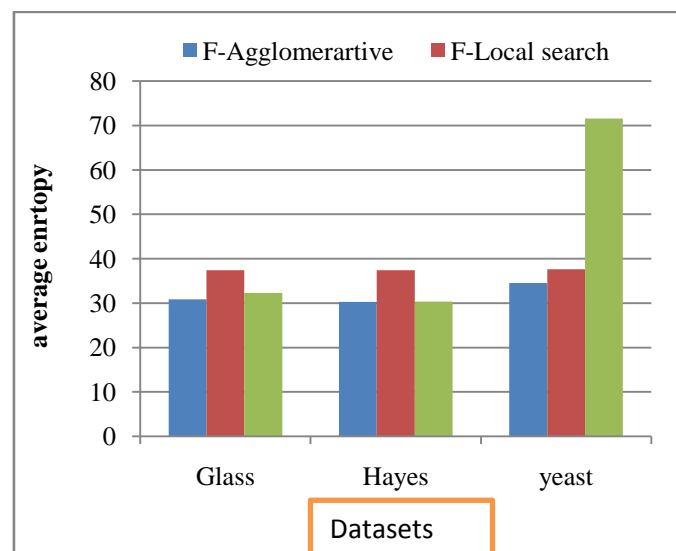


Fig.4. Datasets results using entropy

Another graph is plotted to represents the sum of average entropy for three different algorithm using the same algorithm. The results show that the agglomerative has the least value. Compared to other algorithms using different datasets.

Results on the magic sets

From the above table the lowest running time is F-agglomerative algorithm. Compared to other two algorithms F-agglomerative is efficient one.

VI. Conclusion

Proposed system has defined data fragments and proposed a new fragment-based clustering aggregation approach. This approach is based on the proposition that in an optimal partition each fragment is a subset of a cluster. Existing point-based algorithms can be brought into our proposed approach. As the number of data fragments is usually far smaller than the number of data points, clustering aggregation based on data fragments is very likely to have a low error rate than directly on data points. To demonstrate the efficiency of the proposed approach, three new clustering aggregation algorithms are presented, namely-Agglomerative, F-Furthest, and F-Local Search (based on three existing point-based clustering aggregation algorithms ones). Experiments were on three public data sets. The results show that the three new algorithms outperform the original clustering aggregation algorithms in terms of running time without sacrificing effectiveness.

VII. Future Enhancement

In our future work, we aim to solve the following problems:

The numbers of fragments increases when there are missing values or points with unknown clusters in the original clustering results. This leads to a lower efficiency.

Clustering validity measurement technique such as Davies Bouldin Index technique is used. In this Davies Bouldin Index technique, we determine the most similar cluster among the clusters has same similarity. If the fragment has similar cluster more than one clusters means then this technique is calculated the most similar cluster. The Davies – Bouldin index is based on similarity measure of clusters (R_{ij}) whose bases are the dispersion measure of a cluster (s_i) and the cluster dissimilarity measure (d_{ij}).

REFERENCES

- [1]. Ou Wu, *Member, IEEE*, Weiming Hu, *Senior Member, IEEE*, Stephen J. Maybank, *Senior Member, IEEE*, Mingliang Zhu, and Bing Li, vol. 42, no 3, june* 2012
- [2]. J. Wu, H. Xiong, and J. Chen, "A data distribution view of clustering algorithms," in *Encyclopedia of Data Warehousing and Mining*, vol. 1, J. Wang, Ed., 2nd ed. Hershey, PA: IGI Global, pp. 374–381, 2008.
- [3]. Gionis, A, Mannila, H, and Tsaparas, P, 'Clustering aggregation', *ACM Trans. Knowl. Discov. Data*, vol. 1, no. 1, pp. 1–30, Mar. 2007
- [4]. Z. Zhou and W. Tang, "Cluster ensemble," *Knowledge-Based Systems*, vol. 19, no. 1, pp. 77–83, Mar. 2006.
- [5]. Ailon, N, Charikar, M, and Newman, A, 'Aggregating Inconsistent Information: Ranking and Clustering', in *Proc. STOC*, New York, pp. 684–693, 2005.
- [6]. N. Nguyen and R. Caruana, "Consensus clustering," in *Proc. IEEE ICDM*, pp. 607–612, 2005.
- [7]. M. Meil'a, "Comparing clustering's—An axiomatic view," in *Proc. ICML*, pp. 577–584, 2005.
- [8]. A. P. Topchy, M. H. C. Law, A. K. Jain, and A. L. Fred, "Analysis of consensus partition in cluster ensemble," in *Proc. IEEE ICDM*, pp. 225–232, 2004.
- [9]. X. Z. Fern and C. E. Brodley, "Random projection for high dimensional data clustering: A cluster ensemble approach," in *Proc. ICML*, pp. 186–93, 2003.
- [10]. Fred, A. L. N and Jain, A. K, 'Robust data clustering', in *Proc. IEEE CVPR*, vol. 2, pp. II-128–II-133, 2002.
- [11]. D. R. Cox and P. A. W. Lewis, *The Statistical Analysis of Series of Events*. London: Methuen, 1966.
- [12]. [Online]. Available: <http://archive.ics.uci.edu/ml/>

Improving Distribution Feeders for Photovoltaic Generation by Loop Power Control Method

Husam Saad Abdulla¹, Surya Prakashline²

¹(Libyan Electricity Ministry/ University SHIATS, India)

²(Electrical Engineering Department, SHIATS, India)

ABSTRACT: Now a day's solar power plants are more reliable, because no fuel and reduced CO₂ emission. But the solar power generation system do not work in all weather conditions, it is power generated only solar radiation time .To overcome this problem by using (pv)). In fuel cell power generation there will be no problems, where as in fuel cell power distribution systems have some problems like overloading the distribution feeders. In this project to overcome this overloading by using Loop Power Controller (LPC).The loop power controller to control real power and reactive power flow by adjusting voltage ratio and phase shift. Daily loading unbalance is determined by analyzing (pv) power generation recording by using SCADA system and load profile based on Data Automation System (DAS).The loop power controller can improve controllability, operational flexibility and reduce power loss of the distribution system. The Loop Power Controller (LPC) is based on the MATLAB/ SIMULINK.

Keywords: Power, Distribution Grid, solar power, Loop Power Controller.

I. Introduction

Renewable energy resources such as wind turbines, hydrogen turbines and photovoltaic arrays are environmental friendly. This type of generations rapidly increasing around the world because they can increasing the demand of electric power and to decrease the green house gases. Penetration of wind power generation and PV power generation into distribution systems is expected to increase dramatically, which raises concerns about system impact by the intermittent power generation of DG [1]–[3]. Compared to large-scale wind power and conventional bulk generation, the generation cost of a PV system is relatively higher However, many countries offer significant financial subsidies to encourage customers to install PV systems. To achieve the goal of 1000 MW PV installed capacity by 2025, the Taiwan government has launched a promotion program to subsidize 50% of the PV installation cost and has increased the selling price of PV generation to 40¢/kWh [4]. Considerable efforts have been proposed in the previous works to solve the loading balance of distribution systems. The distribution static compensator (DSTATCOM) was considered for compensation of loading unbalance caused by stochastic load demand in distribution systems [6]. The control algorithm for static var compensation (SVC) has been developed for loading balance at any given power factor [7]. Fuzzy multi objective and Tabu search have been used to optimize the on/off patterns of tie switches and sectionalizing switches to achieve feeder loading balance in distribution systems with distributed generators [8]. A heuristic-expert system approach for network reconfiguration to enhance current balance among distribution feeders was presented by Reddy and Sydulu [9]. A Petri-Net algorithm has also been proposed for loading balance of distribution systems with open loop configuration by identifying open-tie switches [10]. For the distribution system with large capacity of PV installation, the feeder loading will be varied dramatically because the power injection by PV generation is varied with the intensity of solar radiation. The load transfer between feeders with an open-tie switch must be adaptively adjusted according to PV power generation. Due to the intermittent power generation by PV systems, it becomes very difficult to achieve loading balance with conventional network reconfiguration methods by changing the status of line switches. With the advancement of power electronics, the back-to-back (BTB) converters can be applied to replace the open-tie switch for better control of real power and reactive power load transfer by changing the voltage ratio and phase shift between two feeders according to the power unbalance at any time instant [11]. For the distribution system with high penetration of renewable energy sources, voltage profiles and loading balance have to be enhanced by improving the power exchange capability between feeders. This study pro- poses a loop power controller (LPC) [12], [13] to replace the conventional open-tie switch so that loading balance of distribution feeders can be obtained by power flow control in a more active manner. A transformer less converter with snubberless insulated gate bipolar transistor (IGBT) is applied to the proposed LPC using an active-gate-control (AGC) scheme. The AGC scheme can balance the collector

voltage of IGBTs connected in series and allow the converter to connect directly to distribution feeders with a high enough AC voltage output [14]. Additionally, LPC can reduce the voltage fluctuation and system power loss by enhancing reactive power compensation. In this paper, the three-phase balanced flow condition is assumed for both distribution feeders to perform the load transfer by LPC. The design of the LPC control strategy must consider intermittent power injection by PV generation and varying feeder loading so that the loading unbalance and system power loss can be minimized in each study hour. This paper is organized as follows. First, Section II introduces the distribution automation system with a loop power controller. Section III presents the feeder loading balance simulation and LPC control algorithm. In Section IV, the impact of the PV system on feeder loading balance and loss reduction of the distribution system is investigated. Finally, Section V gives conclusions.

II. Loop Power Controller In Distribution Automation System

The distribution automation system (DAS) as shown in fig .1 its take to reference from taipower station. The DAS consists master station (MS) with software application, remote terminal unit (RTU) and feeder terminal unit (FTU) in substation. The distribution feeders are connected as open loop configuration with one of the automatic line switches selected the open tie switch. In open loop configuration feeder having circuit breaker, when fault occurs in feeder the circuit breaker will be trips, the over current fault flags of all upstream FTUs are set due to large fault currents, after the all fault flags are received in master station. The master station sends command to open all line switches by using the open tie switches around the faulted location, after clearing the faults the feeder has to be recloses.

In DAS fault restoration effectively in taipower, but balance of loading is difficult in distribution system because the switching operation is required too frequently, to overcome the problem we are proposing the LPC, it is applied to replace open tie switch by adaptive power flow control for load transfer. The advantages of LPC in distribution feeder pair, 1) reduce the voltage fluctuations with fast compensate the reactive power. 2) The real power an reactive power is controlled. 3) In the distribution system controllability operation flexibility is improved. 4) Reduced power system losses with improved load balance of distribution system.

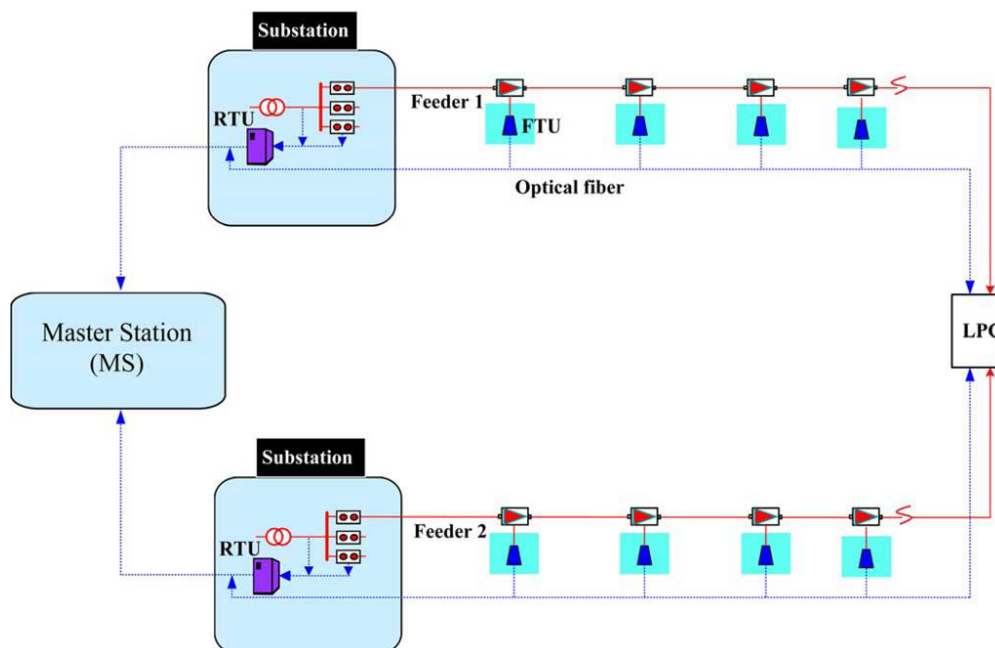


Fig .1: Distribution automation system with a loop power controller

III. Control Model of Loop Power Controller

To derive the voltage ratio and phase shift of LPC for the control of load transfer, the equivalent circuit model of LPC is proposed by considering the branch impedances of distribution feeders for the simulation of feeder loading balance. Fig. 2 shows the overall process to derive the LPC control algorithm to enhance loading balance of distribution feeders.

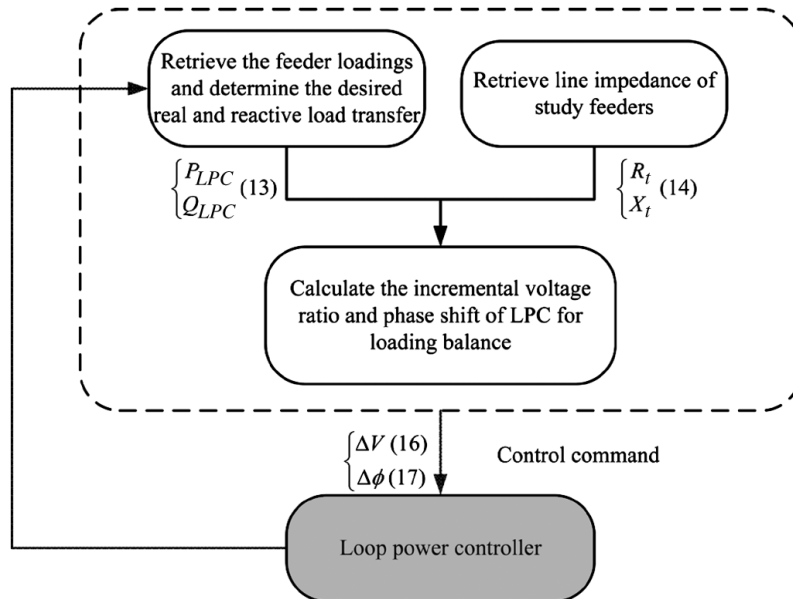


Fig2: Flowchart of LPC control algorithm.

A. simulation of feeder loading balance

In this study, the LPC is considered as the combination of tap changer and phase shifter with a circuit model as shown in Fig. 3. By adjusting the voltage ratio and phase shift between both sides of the LPC according to the branch impedance and loading unbalance of distribution feeders, the real and reactive power flows through the LPC can be controlled to achieve the loading balance. The equivalent circuit model can be represented as an ideal transformer with turn ratio of $1:n e^{j\theta}$ and a series admittance y .

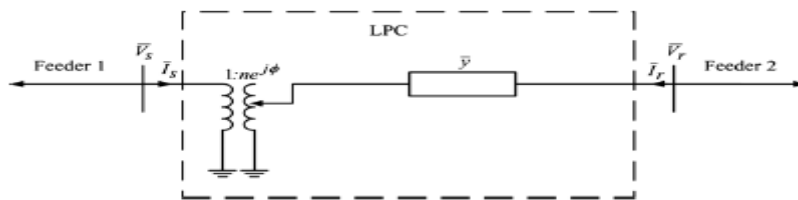


Fig3: Circuit model of loop power controller.

The mathematical model of LPC can be illustrated in (1) to represent the relationship between the node injection currents and voltages:

$$\begin{bmatrix} \bar{I}_s \\ \bar{I}_r \end{bmatrix} = \begin{bmatrix} |n|^2 \bar{y} & -\bar{n}^* \bar{y} \\ -\bar{n} \bar{y} & \bar{y} \end{bmatrix} \begin{bmatrix} \bar{V}_s \\ \bar{V}_r \end{bmatrix} \dots\dots(1)$$

where $\bar{n} = n e^{j\theta}$.

To simplify the process to determine the voltage ratio and phase shift of LPC, this paper proposes a modified equivalent circuit with dependent currents source and as shown in Fig. 4. Here, the dependent current sources are revised according to the adjustments of turn ratio and phase shift during the iteration process. To derive the injection currents due to the change of voltage ratio by LPC, the node currents are represented by assuming zero phase shifts as follows:

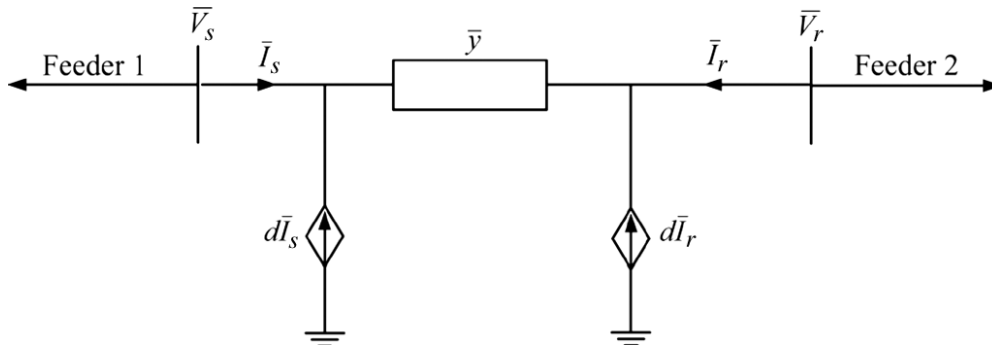


Fig4: Modified equivalent circuit model of LPC.

$$I_s = n^2 \bar{y} \bar{V}_s - n \bar{y} \bar{V}_r$$

$$= (n^2 - 1) \bar{y} \bar{V}_s + (1 - n) \bar{y} \bar{V}_r + \bar{y} (\bar{V}_s - \bar{V}_r) \dots\dots\dots(2)$$

$$I_r = -n \bar{y} \bar{V}_s + \bar{y} \bar{V}_r$$

$$= (1 - n) \bar{y} \bar{V}_s + \bar{y} (\bar{V}_r - \bar{V}_s) \dots\dots\dots(3)$$

The equivalent injection currents are solved as

$$dI'_s = - (n^2 - 1) \bar{y} \bar{V}_s - (1 - n) \bar{y} \bar{V}_r \dots\dots\dots(4)$$

$$dI'_r = - (1 - n) \bar{y} \bar{V}_s \dots\dots\dots(5)$$

To derive the injection current due to the change of phase shift by LPC, the node currents are represented by assuming a fixed voltage ratio of 1.0 as follows:

$$I_s = \bar{y} \bar{V}_s - \bar{y} e^{-j\phi} \bar{V}_r$$

$$= (1 - e^{-j\phi}) \bar{y} \bar{V}_r + \bar{y} (\bar{V}_s - \bar{V}_r) \dots\dots\dots(6)$$

$$I_r = (1 - e^{j\phi}) \bar{y} \bar{V}_s + \bar{y} (\bar{V}_r - \bar{V}_s) \dots\dots\dots(7)$$

The equivalent injection currents are solved as

$$dI''_s = - (1 - e^{-j\phi}) \bar{y} \bar{V}_r \dots\dots\dots(8)$$

$$dI''_r = - (1 - e^{j\phi}) \bar{y} \bar{V}_s \dots\dots\dots(9)$$

Therefore, the equivalent currents due to the change of both voltage ratio and phase shift by LPC in Fig. 4 are determined as follows:

$$dI_s = dI'_s + dI''_s \dots\dots\dots(10)$$

$$dI_r = dI'_r + dI''_r \dots\dots\dots(11)$$

$$\begin{bmatrix} d\bar{I}_s \\ d\bar{I}_r \end{bmatrix} = \begin{bmatrix} (1 - n^2) \bar{y} & (n + e^{-j\phi} - 2) \bar{y} \\ (n - 1) \bar{y} & (n + e^{j\phi} - 2) \bar{y} \end{bmatrix} \begin{bmatrix} \bar{V}_s \\ \bar{V}_r \end{bmatrix} \dots\dots\dots(12)$$

By this way, the network impedance matrix remains unchanged during the iteration process to solve the voltage ration and phase shift of LPC.

B. loop power control Algorithm

To illustrate the proposed control algorithm for LPC to achieve feeder loading balance, consider the two sample radial feeders connected with an LPC in Fig. 5. The desired real and reactive power flows through the LPC for feeder loading balance are defined as

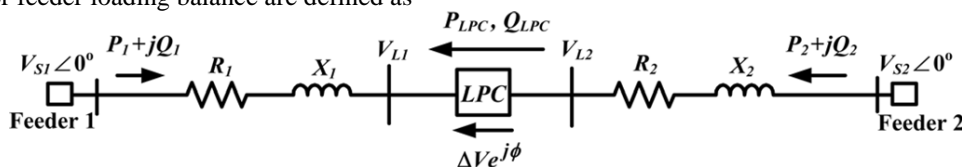


Fig. 5: Incremental circuit model of distribution feeders with LPC.

$$\begin{cases} P_{LPC} = \frac{P_1 - P_2}{2} \\ Q_{LPC} = \frac{Q_1 - Q_2}{2} \end{cases} \dots\dots\dots(13)$$

If the branch impedances of Feeder 1 and Feeder 2 are (R_1, X_1) and (R_2, X_2) , respectively, the total impedance of two feeders is defined as

$$\begin{cases} R_t = R_1 + R_2 \\ X_t = X_1 + X_2 \end{cases} \dots\dots\dots(14)$$

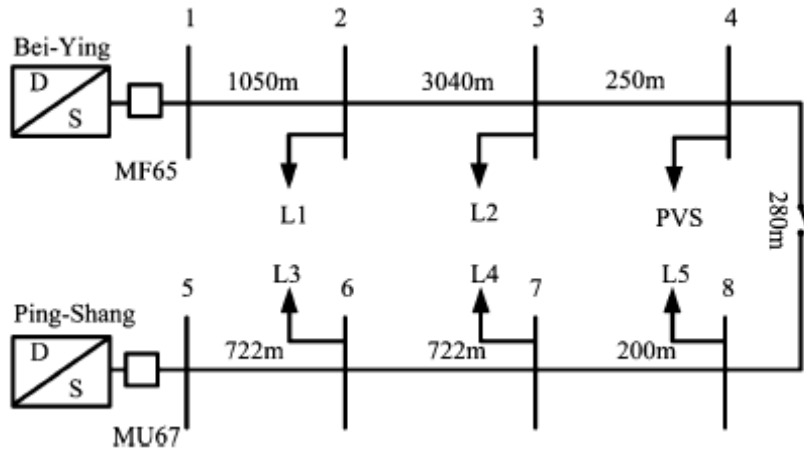


Fig. 6: Taipower distribution feeders for computer simulation.

In order to perform the LPC control strategy to have the proper load transfer between both feeders for loading balance, the terminal voltage V_{L1} at the primary side of LPC is assumed to have a fixed value of $1.0 \angle 0^\circ$. The terminal voltage at the secondary side of LPC is derived in (4.15):

$$\frac{|V'_{L2}|}{|V_{L1}|} = \sqrt{(1 + P_{LPC}R_t + Q_{LPC}X_t)^2 + (P_{LPC}X_t - Q_{LPC}R_t)^2} \dots\dots\dots(15)$$

The incremental terminal voltage ΔV and phase shift $\Delta\phi$ are therefore calculated as follows:

$$\Delta V = |V'_{L2}| - 1.0 \dots\dots\dots(16)$$

$$\Delta\phi = \tan^{-1} \frac{P_{LPC}X_t - Q_{LPC}R_t}{1 + P_{LPC}R_t + Q_{LPC}X_t} \dots\dots\dots(17)$$

IV. Loading Balance and Loss Analysis Using LPC In and Distribution Feeder

With the variation of customer loading profiles and the intermittent generation of PV systems, an adaptive LPC control algorithm is derived to adjust the voltage ratio and phase shift between both feeders according to the feeder loading and PV generation for each study hour. To illustrate the effectiveness of LPC for system loading balance, an LPC is assumed to be installed to replace the open-tie switch between Feeders.

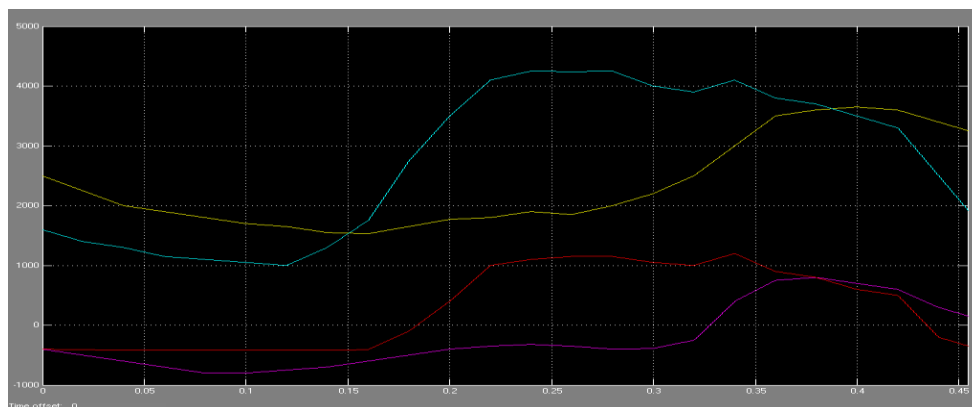


Fig.7:Balancing The Load Of Power Profile Of Feeder 1and 2 Without Photovoltaic System

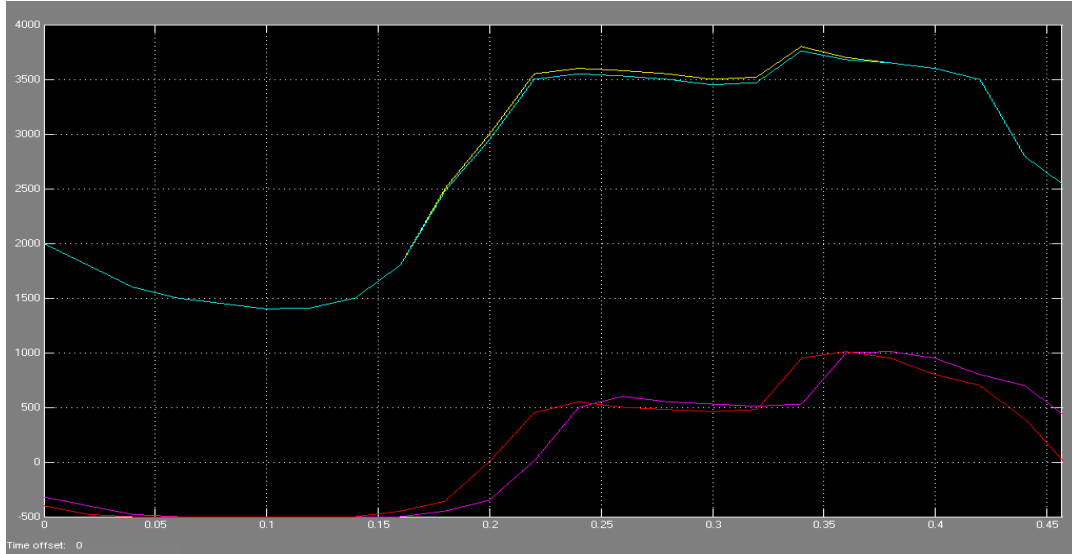


Fig 8: Balancing the Load of Both Feeders with the Control of LPC (W/O Photovoltaic System)

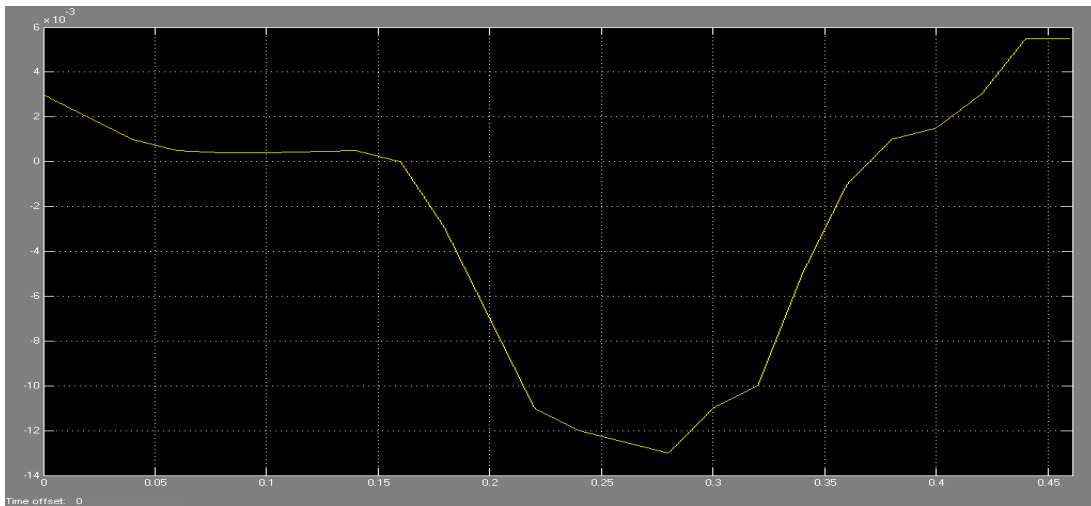


Fig 9: Voltage Ratio for power transfer With the Control of LPC (W/O The PV System)

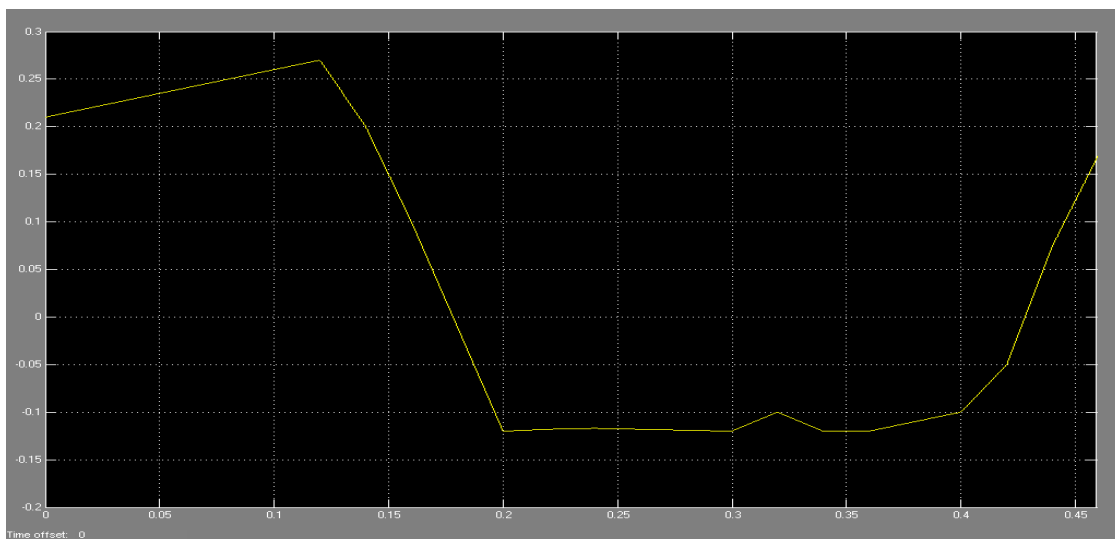


Fig 10: phase shift with the control of LPC (W/O The PV System).

after execution the real power and reactive power load profile of two feeders without PV system power as show in fig .8 , the distribution feeders to achieve the load balance using LPC only , the real power and reactive power difference between feeder MF65 and MU67 to be reduced from 1864KW/1715KVAR to 170KW/71KV after connecting LPC for power flow control. and the voltage ratio and phase shift also show in fig.9 and fig 10 respectively after connecting LPC.

V. Loading Balance When Using Both PV & LPC

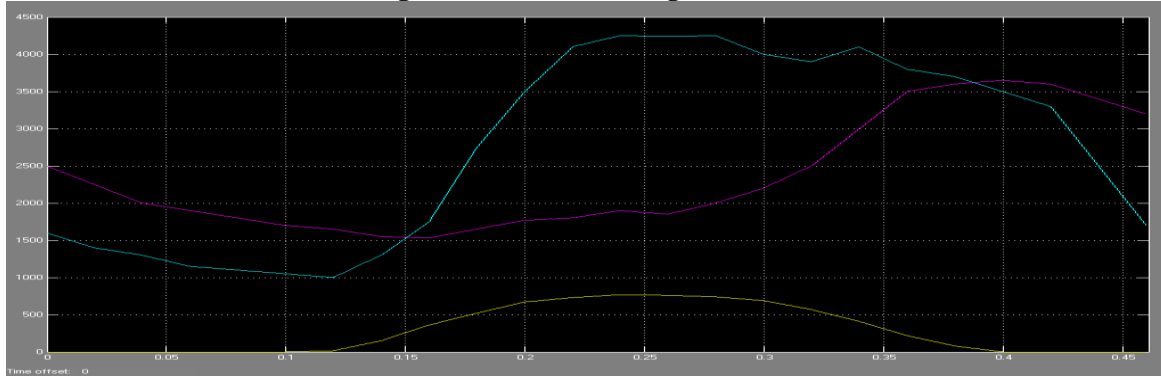


Fig 11: power profiles of feeder MF65 and MU67 for both PV&LPC.

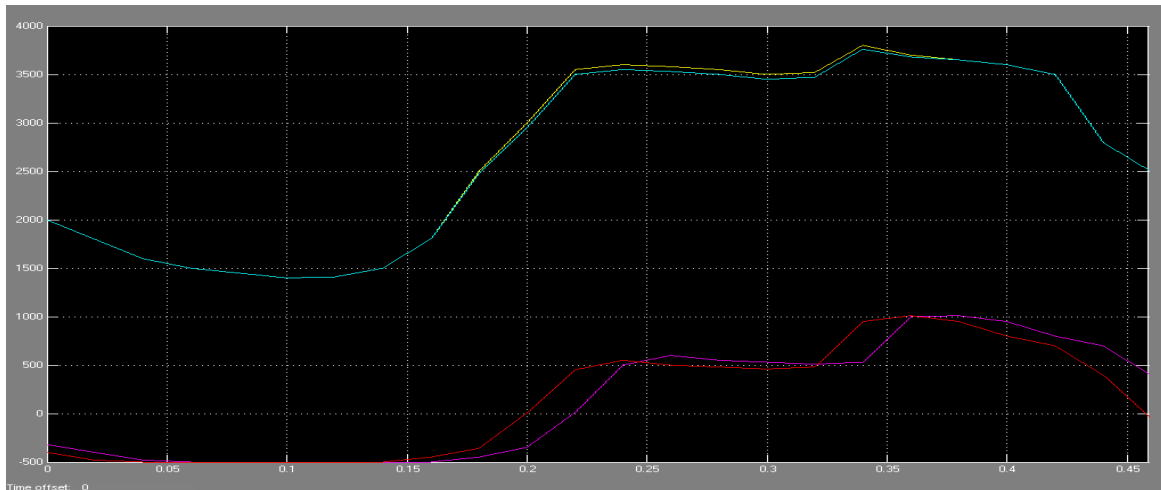


Fig 12: Loading balance of both feeders with the control of LPC & PV.

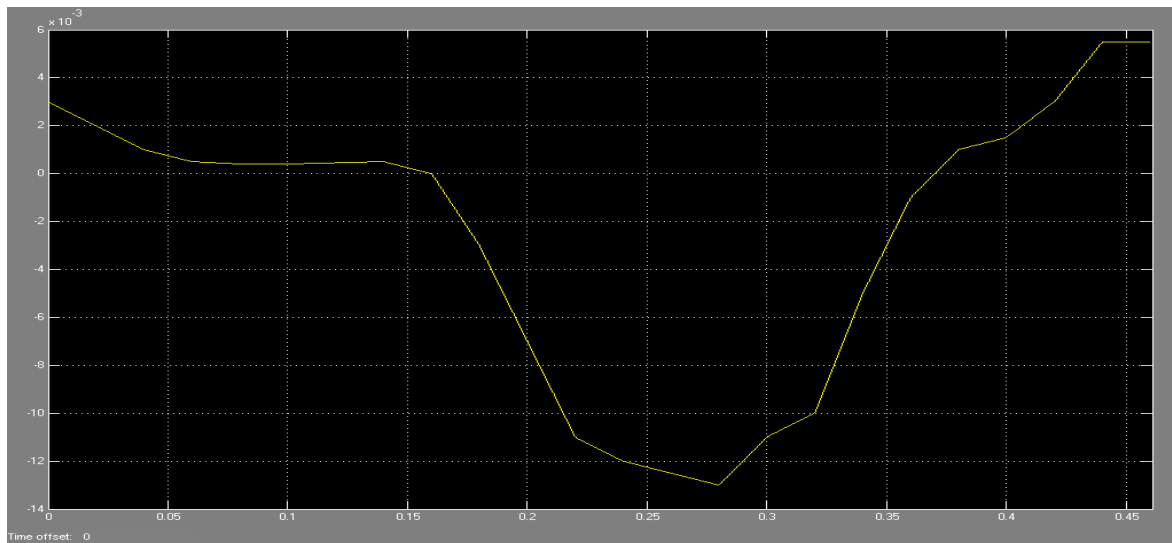


Fig13: Voltage ratio with the control of LPC & PV.

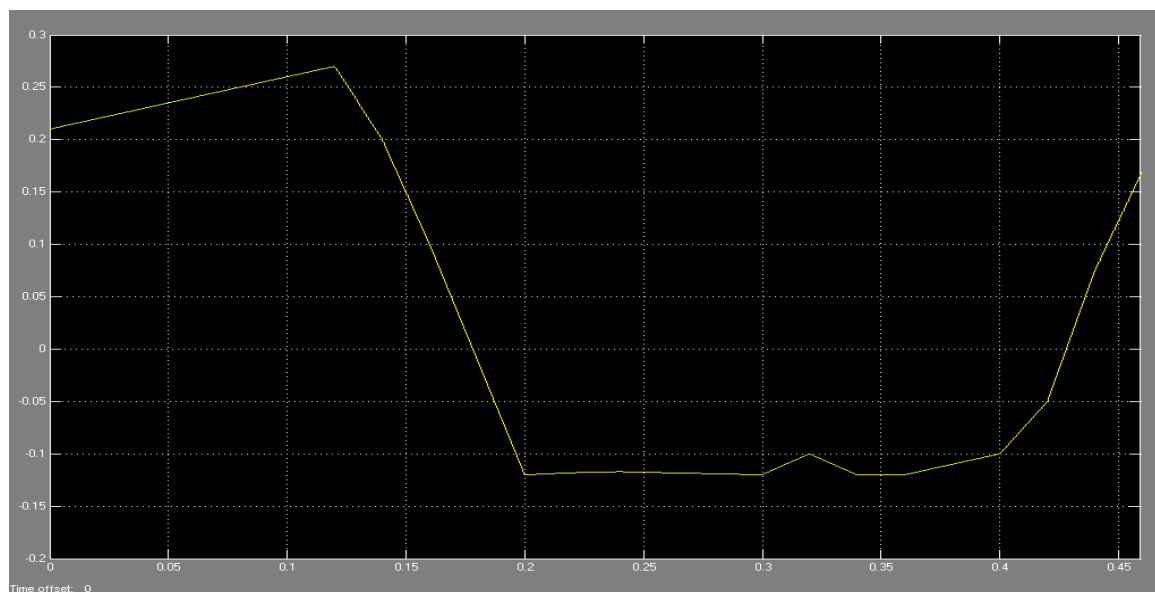


Fig 14: phase shift with control of LPC&PV.

Power load profile of two feeder after using both LPC and PV system as show in fig.11 and fig 12 it shows the real and reactive power after using the LPC and PV system, the differences of real and reactive power between feeders MF65and MU67 have been reduced from 1689KW/1589KVAR after implementing LPC and PV system and both of fig13 and fig14 as show voltage ratio and phase shift.

Distribution Feeder Loss Analysis

To investigate the effectiveness of LPC for the reduction of system power loss by loading balance, a three-phase power flow analysis is performed for both feeders MF65 and MU67 by considering the daily feeder power loading profiles before and after loading balance. Also, the loss incurred in LPC is assumed to be 1% of the power transfer by the LPC which has been included in the system loss analysis for each study hour. For the test distribution system with PV system, Fig. 15 shows the system power loss as percentages of feeder loading. Without applying the LPC for loading balance, the feeder power loss varies from 1.2% of the feeder loading during the light load period to 3.3% during the peak load period. The power loss over the daily period is reduced from 3457 kWh (2.8%) to 2970 kWh (2.3%) after loading balance by LPC. The system power loss reduction has therefore been obtained after implementing the LPC for loading balance.

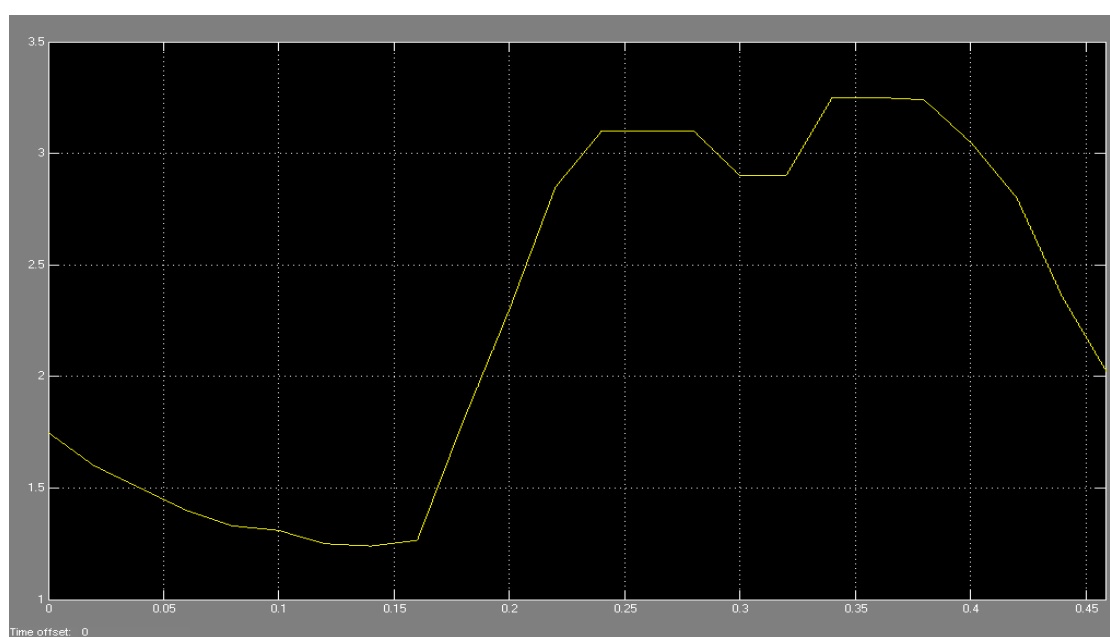


Fig 15: Percentage of system power loss with PV system (w/o LPC).

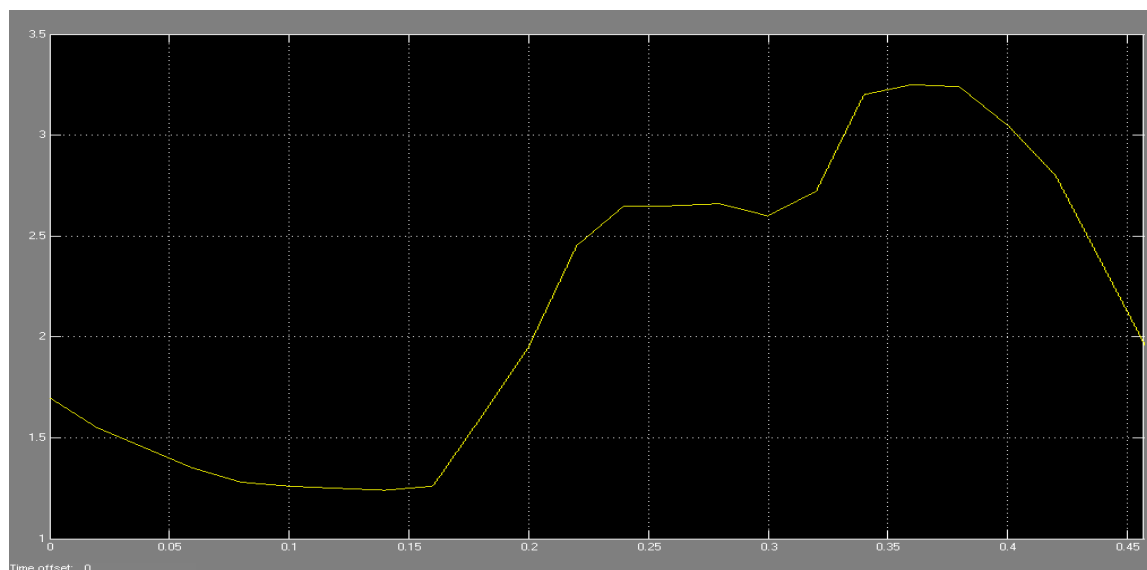


Fig 16: percentage of system power loss applying the LPC&PV.

VI. Conclusions

This study evaluates a power electronics-based loop power controller to replace the open-tie switch for the control of real power and reactive power transfer between distribution feeders to achieve loading balance of distribution system. The voltage ratio and phase shift adjusted by LPC are derived according to mismatches of real power and reactive power loadings between test feeders for each study hour. To demonstrate the effectiveness of LPC for the enhancement of loading balance, a Taipower distribution system consisting of two feeders with a large-scale PV system has been selected for computer simulation. The power loadings of the study feeders and the PV power generation have been recorded. By applying the control algorithm of LPC to adjust the voltage ratio and phase shift between both feeders, the proper amount of real power and reactive power can be transferred from the heavily loading feeder to the lightly loading feeder for each study hour. According to the computer simulation, it is concluded that the loading balance of distribution systems with intermittent PV power generation can be obtained effectively by the implementation of LPC to achieve adaptive control of load transfer between distribution feeders. The power loss reduction of test feeders after loading balance by LPC has also been derived in this paper.

REFERENCES

- [1] J.Bebic,R.Walling, K.O'Brien, andB.Kroposki,“The sun alsorises,” IEEE Power Energy Mag., vol. 7, no. 3, pp. 45–54, May./Jun. 2009.
- [2] T. Key, “Finding a bright spot,” IEEE Power Energy Mag., vol. 7, no. 3, pp. 34–44, May./Jun. 2009.
- [3] Y.ZhuandK.Tomsovic, “Adaptive power flow method for distribution systems with dispersed generation,” IEEE Trans. Power Del., vol. 17, no. 3, pp. 822–827, Jul. 2002.
- [4] 2008 Report of Long-Term Load Forecasting and Energy Development, Bureau of Energy, Ministry of Economic Affairs, Taiwan, Dec. 2008.
- [5] N. Okada, “A method to determine the distributed control setting of looping devices for active distribution systems,” in Proc. 2009 IEEE Bucharest Power Tech (POWERTECH), Bucharest, Romania, Jun. 2009, pp. 1–6.
- [6] B. Singh and J. Solanki, “A comparison of control algorithms for DSTATCOM,” IEEE Trans. Ind. Electron., vol. 56, no. 7, pp. 2738–2745, Jul. 2009.
- [7] S. A. Farouji, E. Bakhshizadeh, R. Kazemzadeh, and R. Ghazi, “The static var compensator equations development for loading balance at desired power factor based on load admittance parameters and instantaneous voltage and current values ,”in Proc.2009 Int. Conf. Elect.Power Energy Conversion Syst., Sharjah, United Arab Emirates, Nov. 10–12, 2009, pp. 1–6.
- [8] N. Rugthaicharoencheep and S. Sirisumrannukul, “Feeder reconfiguration with dispatch able distributed generators in distribution system by tabu search,” in Proc. 2009 44th Int. Universities Power Eng. Conf. (UPEC 1009), Glasgow, U.K., Sep. 1–4, 2009, pp. 1–5.
- [9] V. V. K. Reddy and M. Sydulu, “A heuristic-expert based approach for reconfiguration of distribution systems,” in Proc. 2007 IEEE Power Eng. Soc. General Meeting, Tampa, FL, Jun. 24–28, 2007, pp. 1–4.
- [10] C. H. Lin, “Distribution network reconfiguration for loading balance with a coloured petri net algorithm,” Proc. Inst. Elect. Eng., Gen., Transm., Distrib., vol. 150, no. 3, pp. 317–324, May 2003.

- [11] N. Okada, M. Takasaki, H. Sakai, and S. Katoh, "Development of a 6.6 kv–1 MVA transformerless loop balance controller," in Proc. IEEE 38th Annu. Power Electron. Specialists Conf., Orlando, FL, Jun. 17–21, 2007, pp. 1087–1091.
- [12] N. Okada, "Verification of control method for a loop distribution system using loop power flow controller," in Proc. 2006 IEEE PES Power Syst. Conf. Expo., Atlanta, GA, Oct./Nov. 2006, pp. 2116–2123.
- [13] N. Okada, H. Kobayashi, K. Takigawa, M. Ichikawa, and K. Kurokawa, "Loop power flow control and voltage characteristics of distribution system for distributed generation including PV system," in Proc. 3rd World Conf. Photovoltaic Energy Conversion, Osaka, Japan, May 12–16, 2003, pp. 2284–2287.
- [14] N. Okada, M. Takasaki, J. Narushima, R. Miyagawa, and S. Katoh, "Series connection of snubberless igbts for 6.6 kv transformerless converters," in Proc. 2007 Power Conversion Conf., Nagoya, Japan, Apr. 2007.
- [15] G. L. Ockwell, "Implementation of network reconfiguration for Taiwan power company," in Proc. 2003 IEEE Power Eng. Soc. General Meeting, Toronto, ON, Canada, Jul. 2003.



Husam Saad Abdulla ,1981,Libya,Sebha, Master of Technology in Electrical Engineering (Power System) , SHIATS, Allahabad , UP,India



Dr. Surya Prakash Belongs to Allahabad, DOB is 01.05.1971, Received his Bachelor of Engineering degree from The Institution of Engineers (India) in 2003, He obtained his M.Tech. In Electrical Engg. (Power System) from KNIT, Sultanpur. UP-India in 2009. Presently he is Pursuing Ph. D in Electrical Engg. (Power System). SSET, SHIATS (Formerly Allahabad Agriculture Institute, Allahabad-India). His field of interest includes power system operation & control, Artificial Intelligent control.

Multiple Optimization of Wire EDM Machining Parameters Using Grey Based Taguchi Method for Material HCHCR

Anwarul Haque¹, A. B. Amale², P. D. Kamble³

¹PG Student, Dept of Mechanical Engineering, YCCE, Nagpur, (India)

^{2,3}Asstt. Prof., Dept of Mechanical Engineering YCCE, Nagpur, 441110 (India)

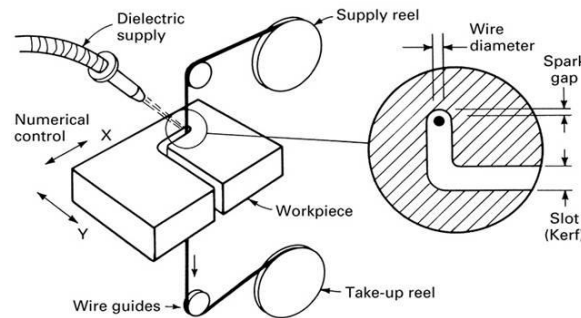
Abstract: Wire EDM is a non conventional machining process, which is used when the precision is prime importance. Multiple optimization (Grey based Taguchi) technique is used to find out the optimum machining setup for input parameter. This paper investigate the optimal set of process parameter such as Ton, Toff, Wp, Wf in wire EDM machining process to find out the variation in two output parameter such as material removal rate (MRR), and surface roughness (Ra) on material high chromium high carbon steel (HCHCr) using wire Brass/super alloy (coated). Experimentation was conducted on orthogonal array L-9 based on DOE. Analysis of experiment has been carried out using GRA. All the experimental data are fed into Minitab software, through which various tables, graphs & optimum values are obtained. The experimental result reveals that the optimum setting of input parameters significantly improves Wire EDM process.

Keywords: About five key words in alphabetical order, separated by comma.

I. Introduction

Wire electrical discharge machining (Wire-EDM) involves a series of complex heating and cooling process. Electrical discharging happens when work piece (anode) and wire-electrode (cathode) are very close (about 5--50 μm) with a gap voltage supplied. Good static and dynamic characteristic of machine are necessary to obtain optimal machining performance. In addition, machining parameters, including pulse-on time, pulse-off time, table-feed rate, flushing pressure, wire tension, wire velocity, etc., should be chosen properly. However, selection of appropriate machining parameters for Wire-EDM is difficult, and relies heavily on operators' experience.

The Grey theory can provide a solution of a system in which the model is unsure or the information is incomplete [1]. Besides, it provides an efficient solution to the uncertainty, multi-input and discrete data problem. The relation between machining parameters and performance can be found out with the Grey relational analysis. Also, the Grey relational grade will utilize the discrete measurement method to measure the distance. Some researches related to Wire-EDM machining-parameters setting were conducted. Kravet [2] proposed an estimating calculation method for a multi-cut Wire-EDM process. Scott, Boyina and Rajurkar [3] used a factorial design method to determine the optimal combination of control parameters in Wire-EDM. A number of 32 machining settings, which resulted in a better Metal removal rate and surface roughness, were determined from 729 experiments. Tarnag [4] applied neural network with simulated annealing (SA) algorithm to determine the optimal machining-parameters in Wire-EDM process. However, it cannot provide the optimal machining parameters for a desired surface roughness. Liao [5] presented an approach to determine optimal parameters setting based on the Taguchi Quality design method, analysis of variance, regression analysis and feasible direction method. Lin [6] presented the use of Grey relational grade to the machining parameters optimization of the electrical discharge machining (EDM) process. Optimal machining-parameters setting for Wire-EDM still has some difficulty: costly and time-consuming in conducting experiments, many machining parameters, and real mathematical models hard to be derived. The purpose of this paper is to present inefficient method to find the significant parameter affecting machining performance by integrating Grey relational analysis and statistical method. Also the optimal machining-parameters setting for maximum machining speed and minimum surface roughness can be obtained by applying Grey relational analysis. Furthermore, it is feasible to obtain optimal machining parameters for a desired surface roughness and maximum metal removal rate by the Grey relational analysis.



II. Grey Relational Analyses (GRA)

2.1 Data Preprocessing

In a Grey relational analysis, experimental data, i.e., measured features of the quality characteristics, are first normalized, ranging from zero to one. This process is known as Grey relational generation. Next, based on normalized experimental data, the Grey relational coefficient is calculated to represent the correlation between the desired and the actual experimental data. Then overall Grey relational grade is determined by averaging the Grey relational coefficient corresponding to selected responses 9. The overall performance characteristic of the multiple response process depends on the calculated Grey relational grade. This approach converts multiple-response process-optimization problem into a single-response optimization situation with the objective function of the overall Grey relational grade. The optimal parametric combination is then evaluated, which would result in the highest Grey relational grade. The optimal factor setting for maximizing the overall Grey relational grade can be performed using the Taguchi method.

In Grey relational generation, the normalized MRR and Ra corresponding to the smaller-the-better (SB) criterion which can be expressed as:

$$x_i(k) = \frac{\max y_i(k) - y_i(k)}{\max y_i(k) - \min y_i(k)} \quad (1)$$

MRR should follow the larger-the-better (LB) criterion, which can be expressed as:

$$x_j(k) = \frac{y_j(k) - \min y_j(k)}{\max y_j(k) - \min y_j(k)} \quad (2)$$

Where $x_i(k)$ and $x_j(k)$ are the value after the Grey relational generation for the SB and LB criteria, respectively. $\min y_i(k)$ is the smallest value of $y_i(k)$ and for the k th response, and $\max y_i(k)$ is the largest value of $y_i(k)$ for the k th response 9. An ideal sequence is $x_0(k)$ ($k=1, 2, \dots, m$) for the responses. The definition of the Grey relational grade in the course of the Grey relational analysis is to reveal the degree of relation between the 9 sequences [$x_0(k)$ and $x_i(k)$, $k = 1, 2, \dots, m$ and $i = 1, 2, \dots, 9$]. The Grey relational coefficient $\xi_i(k)$ can be calculated as:

$$\xi_i(k) = \frac{\Delta_{\min} - \Delta_{\max}}{\Delta_{0i}(k) + \psi \Delta_{\max}} \quad (3)$$

where $\Delta_{0i} = \|x_0(k) - x_i(k)\|$ is the difference of the absolute value $x_0(k)$ and $x_i(k)$; ψ is the distinguishing coefficient $0 \leq \psi \leq 1$; $\Delta_{\min}(k) = \forall j^{\min} \in i \forall k^{\min} \|x_0(k) - x_j(k)\|$ is the smallest value of Δ_{0i} ; and $\Delta_{\max}(k) = \forall j^{\max} \in i \forall k^{\max} \|x_0(k) - x_j(k)\|$ is the largest value of Δ_{0i} . After averaging the Grey relational coefficients, the Grey relational grade γ_i can be computed as:

$$\gamma_i = \frac{1}{n} \sum_{k=1}^n \xi_i(k) \quad (4)$$

Where n is the number of process responses. The higher value of the Grey relational grade corresponds to an intense relational degree between the reference sequence $x_0(k)$ and the given sequence $x_i(k)$. The reference sequence $x_0(k)$ represents the best process sequence; therefore, a higher Grey relational grade means that the corresponding parameter combination is closer to the optimal. The mean response for the Grey relational grade

with its grand mean and the main effect plot of the Grey relational grade are very important because the optimal process condition can be evaluated from this plot.

III. Experimental Procedures And Test Results

3.1 Experimental Details

The cutting experiments were carried out on an electronica 4-axes wire EDM using wire brass (super alloy coated) on material high chromium high carbon steel (HCHCr). The mechanical properties and percent of contains are shown in table 1

3.1.1 Surface roughness (SR):-

A Phynix TR-100 model surface-roughness tester was used to measure the surface roughness of the machined samples. No of reading was taken for getting average value of surface roughness. The multi-criteria optimization technique was chosen to find the optimum value.

3.1.2 Material removal rate (MRR):-

MRR (mm^3/min) was calculated using Eq. (5)

$$MRR = \frac{W_i - W_f}{\rho * t} \quad (5)$$

Where W_i =initial weight, W_f =final weight ρ =density of material (HCHCr) & t =time taken for machining.

3.2 Process Parameters and Test Results.

In full factorial design, the number of experimental runs exponentially increases as the number of factors, as well as their level increases. This results in a huge experimentation cost and considerable time periods. So, in order to compromise these two adverse factors and to search for the optimal process condition through a limited number of experimental runs Taguchi's L9 orthogonal array consisting of 9 sets of data was selected to optimize the multiple performance characteristics of the Wire EDM process.

Table 1, shows the chemical composition of material high chromium high carbon steel (HCHCr).

Table 2 shows the selected design matrix based on the Taguchi L9 orthogonal array consisting of 9 sets of coded conditions and the experimental results for the responses of, SR and MRR. All these data were utilized for the analysis and evaluation of the optimal parameter combination required to achieve the desired quality within the experimental domain.

Table 3 shows Ton Toff, W_f , W_p input parameter settings and its related output parameter values i.e. MRR & SR.

Table 4 shows the material removal rate MRR & Surface roughness SR.

Table 5 represents the calculation of ΔO_i (K), which is based upon the formula, ΔO_i (K) = $|x_0$ (K) - X_i (K)|

This helps to find out the value of Δ min & Δ max after calculation of ΔO_i (K) we calculate the value of grey relation coefficient with the help of equation no 4. Table no 6 shows the calculation of Grey Relational Coefficient.

Table 7 shows the value grey relation grade calculation with the help of equation no 4.

Table no 1 show the chemical composition of HCHCr steels.

Element	Content (%)
C	2.00-2.35
Mn	0.6
Si	0.6
Cr	11.00–13.50
Ni	0.3
W	1
V	1
P	0.03
S	0.03
Cu	0.25

Table no 2 Orthogonal Array L9

EXPERIMENTS	P1	P2	P3	P4
1	1	1	1	1
2	1	2	2	2
3	1		3	3
4	2	1	2	3
5	2	2	3	1
6	2	3	1	2
7	3	1	3	2
8	3	2	1	3
9	3	3	2	1

Table no 3 Experimental results

Runs	Ton (μ sec)	To ff (μ sec)	Wf (mm/sec)	Wp (mm3/min)	MRR(mm ³ /min)	SR (μ-sec)
1	120	63	5	5	3.71	3.325
2	120	58	10	7	3.89	8.935
3	120	53	15	10	2.22	8.511
4	122	63	10	10	4.08	9.822
5	122	58	15	5	4.26	5.321
6	122	53	5	7	4.267	7.588
7	123	63	15	7	3.89	10.427
8	123	58	5	10	3.71	9.172
9	123	53	10	5	4.267	3.932
MAX					4.267	10.427
MIN					2.22	3.325

Table no 4 shows the Normalization value

Table no 5: Calculation of Δ0i (K)

$$\Delta 0i (K) = |x0 (K) - Xi (K)|$$

NORMALIZATION	
NOR_MRR	NORM Ra
0.728	1.000
0.816	0.210
0.000	0.270
0.909	0.085
0.997	0.719
1.000	0.400
0.816	0.000
0.728	0.177
1.000	0.915

MRR	SR
1	1
0.272	0.000
0.184	0.790
1.000	0.730
0.091	0.915
0.003	0.281
0.000	0.600
0.184	1.000
0.272	0.823
0.000	0.085

Table 6. Grey Relational Coefficient:
(ψ = 0.33) COEFFICEINT FOR MRR & SR

Table 7 Grey relational grades. Grades

MRR	SR
1	1
0.548	1.000
0.642	0.295
0.248	0.311
0.783	0.265
0.990	0.540
1.000	0.355
0.642	0.248
0.548	0.286
1.000	0.794

0.774	0.191	0.03647
0.468	-0.115	0.013186
0.280	-0.303	0.092038
0.524	-0.059	0.003472
0.765	0.182	0.033064
0.677	0.094	0.008893
0.445	-0.138	0.019072
0.417	-0.166	0.027542
0.897	0.314	0.098644

A graphical representation of the S/N ratio for the overall grey relational grade is shown in figure. Figure 2 the center line is the value of total mean ratio.

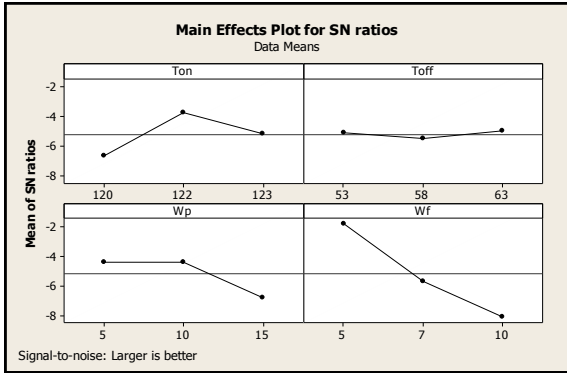


Figure 2. Main effects plot for SN ratios

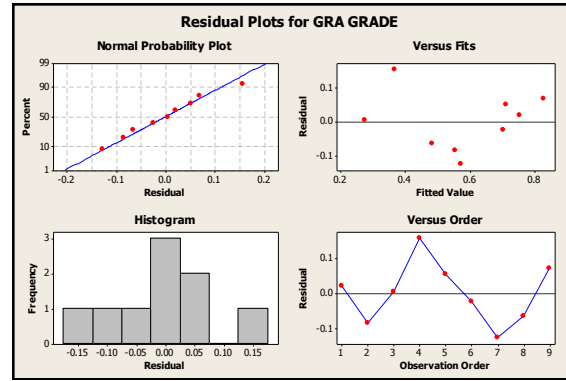


Figure 3. Residual plots for GRA Grade

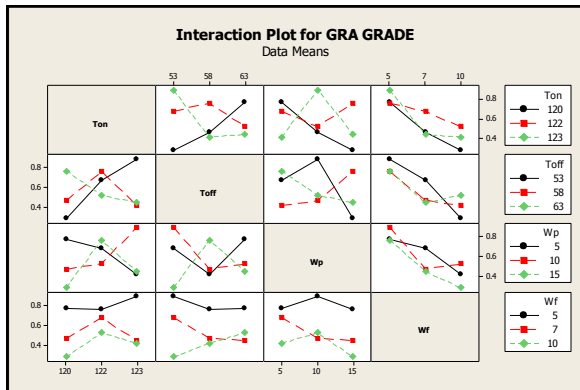


Figure 4. Interaction plot for GRA Grade

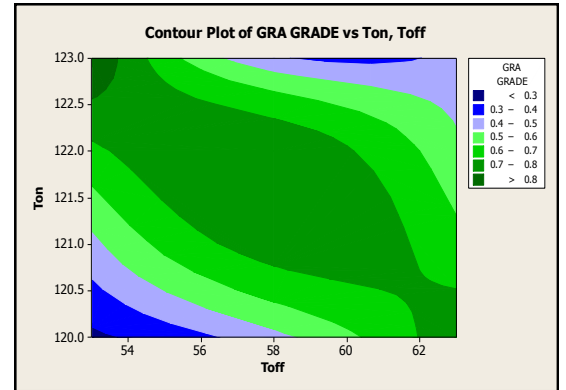
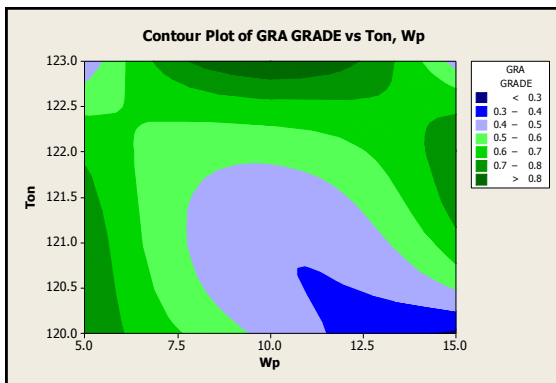


Figure 5. Contour plot of GRA Grade Vs Ton, Toff



6. Contour plot of GRA Grade Vs Ton, Wp

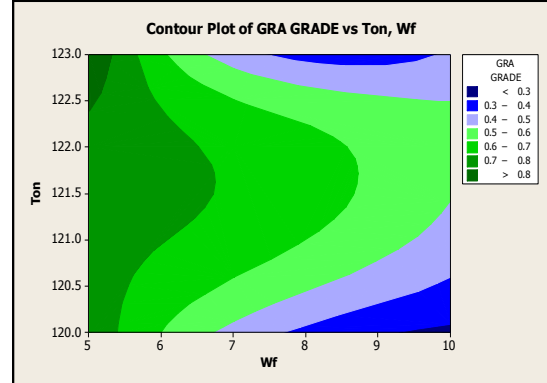


Figure 7. Contour plot of GRA Grade Vs Ton, Wf

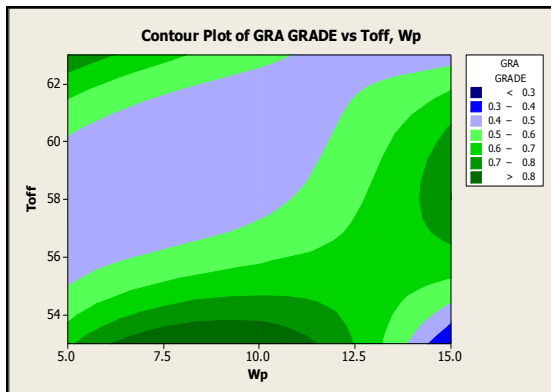


Figure 8. Contour plot of GRA Grade Vs Toff, Wp

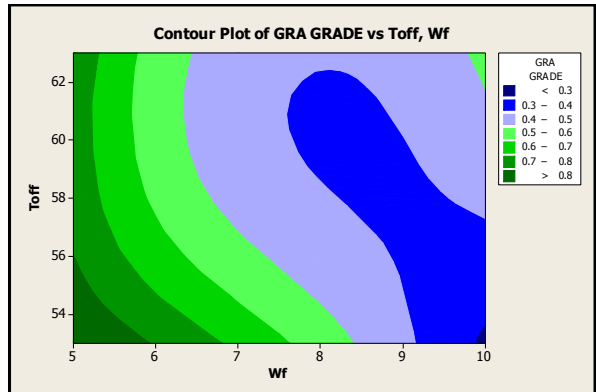


Figure 9. Contour plot of GRA Grade Vs Ton, Wf

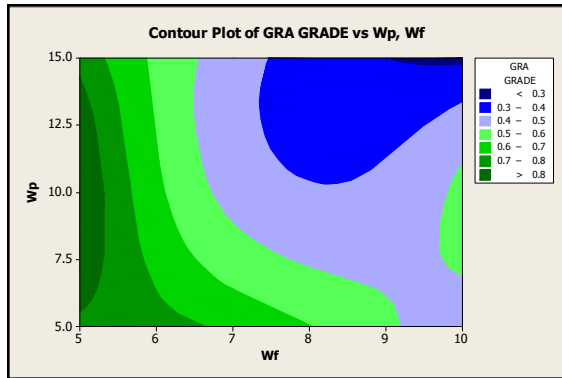


Figure 10. Contour plot of GRA Grade Vs Wp, Wf

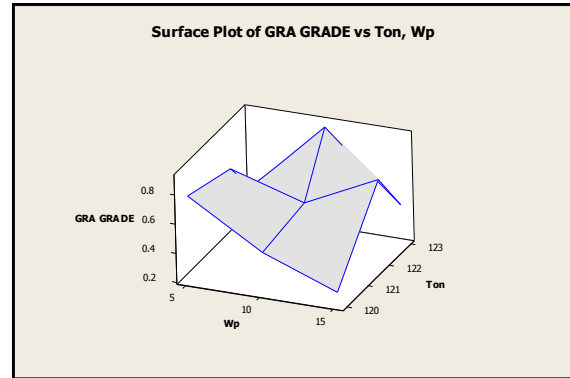


Figure 11. Surface Plot of GRA Grade Vs Ton, Wp

IV. Result and discussion

As indicated in Figure 2 the optimal condition for Wire EDM process for the parameter Ton 2, Toff 1, Wp 2, & Wf 1. As per the experiment performed on machine by taking the optimum values it is observed that machine performed effectively. The percent contributions of the input parameters on the material-removal rate, and the surface roughness are shown in Figure 2. The Main effects plot for SN ratios. Figure 3 shows the Residual plots for GRA Grades, It contain normal probability chart, versus fits, histogram, versus order. Figure 4 shows the Residual plots for GRA Grades i.e. interaction graph for GRA grades for the input parameter Ton, Toff, Wf, and Wp. Figure 5, 6, 7, 8, 9 Shows the Contour plot of GRA Grade simultaneously Vs (Ton, Toff), (Ton, Wp), (Ton, Wf), (Toff, Wp) and (Ton, Wf).

V. Analysis of Variance (ANOVA)

The purpose of the analysis of variance (ANOVA) is to investigate which turning parameters significantly affect the performance characteristics 8–10. This is accomplished by separating the total variability of the grey relational grades, which is measured by the sum of the squared deviations from the total mean of the grey relational grade, into contributions from each of the turning parameters and the error 9. Thus;

$$SS_T = SS_F + SS_E \tag{7}$$

$$SS_T = \sum_{j=1}^p (Y_j - Y_m)^2 \tag{8}$$

SST – Total sum of the squared deviations about the mean Y_j – Mean response for the j th experiment Y_m – Grand mean of the response

p – Number of experiments in the orthogonal array SSF – Sum of the squared deviations due to each factor SSE – Sum of the squared deviations due to error In addition, the F test was used to determine which input parameters have a significant effect on the per performance characteristic. Usually, the change of the input parameter has a significant effect on the performance characteristics when the F value is large. According to this analysis, the most effective parameters with respect to the material-removal rate and the surface roughness are the Ton, Toff, Wf, Wp. The percentage contribution indicates the relative power of a factor to reduce the variation. For a factor with a high percentage contribution, there is a great influence on the performance.

VI. Confirmation Test

After evaluating the optimal parameter settings, the next step is to predict and verify the enhancement of the quality characteristics using the optimal parametric combination 9. The estimated Grey relational grade Υ using the optimal level of the design parameters can be calculated as:

$$\Upsilon = Y_m + \sum_{i=1}^o (Y_i - Y_m) \tag{9}$$

Where Y_m is the total mean Grey relational grade, Y_i is the mean Grey relational grade at the optimal level, and o is the number of the main design parameters that affect the quality characteristics 9. Table 11 indicates the comparison of the predicted values of input parameter. Good agreement between the actual and the predicted results has been observed (the improvement in the overall Grey relational grade was found to be as 0.90). it shows the accuracy and effectiveness of the experiment

In the Taguchi method, the only performance feature is the overall Grey relational grade and the aim should be to search for a parameter setting that can achieve the highest overall Grey relational grade 9. The Grey relational grade is a representative of all the individual performance characteristics. In the present study, the objective functions were selected in relation to the parameters of the material-removal rate, and surface roughness. The importance weights of the material-removal rate, and the surface roughness were equally adjusted to be 0.33. The results show that using the optimal parameter setting (*Ton 2, Toff1, Wp2, Wf1*) causes lower surface roughness with a higher material removal rate and hence a better surface finish.

VII. Conclusions

In this study, the Grey-based Taguchi method was applied for the multiple performance characteristics of Wire EDM operations. A grey relational analysis of the material-removal rate, and the surface roughness obtained from the Taguchi method reduced from the multiple performance characteristics to a single performance characteristic which is called the grey relational grade. Therefore, the optimization of the complicated multiple performance characteristics of the processes can be greatly simplified using the Grey-based Taguchi method. As per the experimental result and graph it is clear that all the optimize values have significant effect on output parameter i.e. SR and MRR. Optimize values for a particular material to be machined is advantageous for the operator. As the repetition of the experiment causes delay in production and increases machining time. This paper will help to take input parameter for the material HCHCr. It is also shown that the performance characteristics of Wire WEDM operations, such as the material removal rate, and the surface roughness are greatly enhanced by using this method.

REFERENCES

- [1] Yan ,Mu-Tian & Chiang,Tsung-Liang , Design and experimental study of a power supply for micro-wire EDM, Int J Adv Manuf Technol (2009) 40.
- [2] Norliana Mohd Abbas, Darius G. Solomon, Md. Fuad Bahari, A review on current research trends in electrical discharge machining (EDM), International Journal of Machine Tools & Manufacture 47 (2007) .
- [3] K.H. Ho, S.T. Newman, State of the art electrical discharge machining (EDM),International Journal of Machine Tools & Manufacture 43 (2003).
- [4] D.T Pham, S.S Dimov,Bigot.S, A.Irvanov, K.Popov, Micro-EDM-recent developments and research issues., International Journal of Machine Tools & Manufacture 149(2004).
- [5] Y.S. Liao, Y.Y. Chu and M.T. Yan: Study of Wire Breaking Process and Monitoring Of WEDM, Int. J. Mach. Tools Manufact. Vol. 37, No. 4, pp.555-567,1997
- [6] R. E. Williams and K. P. Rajurkar, Study of wire electrical discharged machine surface characteristics, Journal of Materials Processing Technology,28(1991) pp. 127-138
- [7] S.S Mohapatra, Amar pattnaik,Optimization of WEDM process parameters using Taguchi method, International Journal of Advanced manufacturing Technology (2006)
- [8] P.J Ross. Taguchi Techniques for Quality Engineering. New York, McGraw- Hill, 1984 Page | 27
- [9] Y.S Liao, J.T.Huang, A study on the machining parameter optimization of WEDM, Journal of Material Processing Technology, 71(1997) pp. 487 493
- [10] Mohd Amri Lajis , H.C.D. Mohd Radzi, The Implementation of Taguchi Method on EDM Process of Tungsten Carbide, European Journal of Scientific Research ISSN 1450-216X Vol.26 No.4 (2009), pp.609-617
- [11] C.L.Lin, J.L.lin & T.C.Ko ,Optimization of the EDM process based on the Orthogonal Array with Fuzzy Logic and Grey Relational Analysis Method, International Journal of Advanced manufacturing Technology, 19(2002) pp. 271-277
- [12] Mu-Tian Yan, Hsing – Tsung Chien, Monitoring & Control of the micro wire–EDM process, International Journal of Machine Tools & Manufacture 47(2007) pp.148-157.
- [13] S.H.Lee, X.P Li ,Study of the effect of machining parameters on the machining characteristics in electrical discharge machining of tungsten carbide, Journals of Material Processing Technology 115 (2001) pp.344-358.

Minkowski Distance based Feature Selection Algorithm for Effective Intrusion Detection

Rm. Somasundaram¹, K. Lakshmanan², V. K. Shunmuganaathan³

¹(Dean, Computer Applications, SNS College of Engineering, Coimbatore, India)

²(Principal, Sri Durgadevi Polytechnic College, Chennai, India)

³(Principal, SNS College of Engineering, Coimbatore, India)

Abstract: Intrusion Detection System (IDS) plays a major role in the provision of effective security to various types of networks. Moreover, Intrusion Detection System for networks need appropriate rule set for classifying network bench mark data into normal or attack patterns. Generally, each dataset is characterized by a large set of features. However, all these features will not be relevant or fully contribute in identifying an attack. Since different attacks need various subsets to provide better detection accuracy. In this paper an improved feature selection algorithm is proposed to identify the most appropriate subset of features for detecting a certain attacks. This proposed method is based on Minkowski distance feature ranking and an improved exhaustive search that selects a better combination of features. This system has been evaluated using the KDD CUP 1999 dataset and also with EMSVM [1] classifier. The experimental results show that the proposed system provides high classification accuracy and low false alarm rate when applied on the reduced feature subsets.

Keywords: Feature Selection, Intrusion Detection, Minkowski Distance, Classification, EMSVM.

I. Introduction

With the rapid advancements in computer networks, the number of attacks by criminals on such computer networks also increases. Intrusion detection is an important technique which protects the computer network and hence is an essential tool for the network security [2]. According to the type of used pattern, intrusion detection techniques are classified into two categories namely misuse detection and anomaly detection [3][2]. Misuse detection is a rule-based approach and uses stored signatures of known attacks to detect intrusions. Therefore, this approach detects known intrusions reliably with low false positive rate. However, it fails to detect novel attacks when they occur. Moreover, the signature database must be updated manually at frequent intervals for future use when new attacks occur. On the other hand, anomaly detection uses normal patterns to model intrusions. In this model, any deviation from the normal behaviors is considered as anomalies [4]. However, it is very difficult to precisely model all normal behaviors. Therefore, it is easy to classify normal behaviors as attacks by mistake which results in high false positive rate. Therefore, the key consent of anomaly detection algorithm is to select an appropriate model to identify normal and abnormal behaviors.

Feature selection is the process of selecting relevant features by removing the irrelevant or redundant features from the original dataset. This method plays an important role in many different areas including statistical pattern recognition, machine learning, data mining and statistics [3]. Generally, feature selection and structure design are performed independently, i.e., one task is performed without considering another task [2][5]. However, since the subset of input features and the structure of neural network are interdependent, they provide a joint contribution to the performance of the classifier. Recently, a variety of new approaches for feature selection and classification have been proposed to solve the above problem [6][7], in which the input feature subset and the network structure are optimized simultaneously. In such a scenario, the relationship between input feature subset and neural network structure are considered resulting in the improvement of performance of the classifier.

In this paper, we propose a new Minkowski Distance and feature ranking based feature selection algorithm for detecting an effective intrusion detection system. This proposed method uses Minkowski distance for feature ranking and performs exhaustive search to choose a better combination of features. From the experiments conducted in this work, it is observed that the proposed feature selection provides optimal number of features and enhanced the classification accuracy to reduce false alarm rate with minimum time for classification.

The remainder of this paper is organized as follows: Section 2 describes the related works. Section 3 depicts the overall system architecture. Section 4 explains the proposed system. Section 5 provides the results and discussion. Section 6 gives the conclusion and future works.

II. Related Works

There are many research works on clustering approach for data analysis. K-means [8] is one of the simple partitioning algorithms available in the literature that solves the clustering problem. Moreover, the K-means algorithm provides a very simple and easy way to classify a given data set through a certain number of k clusters which are fixed in advance. A clustering algorithm that uses Self Organized Maps (SOM) and K-Means [9] for intrusion detection was proposed in the past which doing the SOM finish its training process, the K-means clustering refines the weights obtained by training, and when SOM finishes its cluster formation, K-means again refines the final result of clustering. A parallel clustering ensemble algorithm was proposed by Hongwei Gao et al [10] for IDS which achieves high speed, high detection rate and low false alarm rate. This parallel clustering ensemble is based on the evidence accumulation algorithm and hence combines the results of multiple clustering into a single data partition, and then detects intrusions with PEA algorithm.

Fengli Zhang and Dan Wang [3] proposed an effective wrapper feature selection approach based on Bayesian Networks for network intrusion detection. The authors evaluated the performance of the selected features using a detailed comparison between the wrapper approach and the other four feature selection methods namely Information Gain, Gain Ratio, ReliefF and ChiSquare using the NSL-KDD dataset. Their experimental results illustrate that the features extracted by their approach makes the classifier to achieve high classification accuracy than the other methods. Sannasi Ganapathy et al [2] proposed two new feature selection algorithms namely an Intelligent Rule based Attribute Selection algorithm and an Intelligent Rule-based Enhanced Multiclass Support Vector Machine for effective classification of intrusion data. These intelligent algorithms perform better feature selection and classification in the design of an effective intrusion detection system.

A hybrid learning approach was proposed by Muda et al [5] by using a combination of K-means and naive Baye's classification algorithm. This approach clusters the data to a corresponding group before applying the classification algorithm. A hybrid anomaly detection system was proposed in [11] which combine k-means clustering with two classifiers namely the k-nearest neighbor and naive Baye's classifier. First, it performs the feature selection from intrusion detection data set using an entropy based feature selection algorithm which selects the important attributes by removing the redundant attributes. Next, it performs cluster formation using the k-means clustering algorithm and then it classifies the results by using a hybrid classifier. Ganapathy et al [1] proposed an intelligent multi level classification technique for effective intrusion detection in Mobile Ad-hoc Networks. They use a combination of a tree classifier which uses a labeled training data and an Enhanced Multiclass SVM (EMSVM) algorithm for enhancing the detection accuracy.

III. System Architecture

This intrusion detection system proposed in this paper consists of five major components namely, KDD Cup Dataset, User Interface Module, Feature Selection Module, Classification Module and Decision Making module. The System Architecture is shown in figure 3.1.

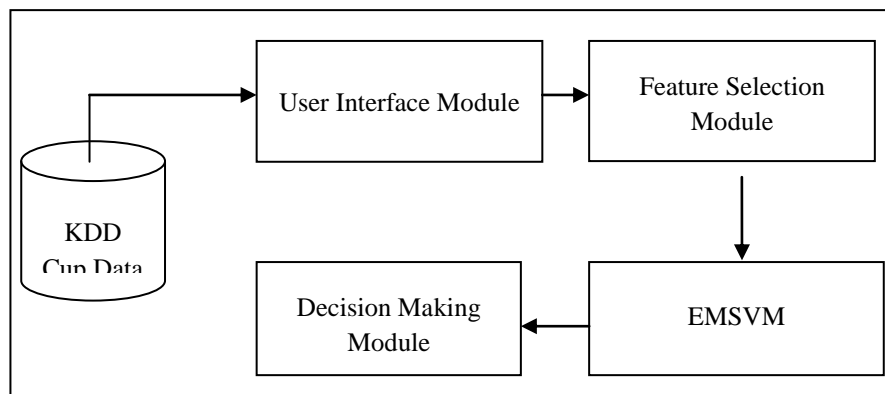


Figure: 3.1 System Architecture

The user interface module collects the necessary data from the KDD'99 Cup dataset. Feature selection module selects the important features using the proposed algorithm. The Classification module classifies the data by using the proposed classification algorithm. Finally, the Decision making module decides whether the particular data is normal or abnormal.

IV. Proposed Work

This section explains the proposed feature selection algorithm. The two important components of the algorithm namely, the feature ranking algorithm and the improved exhaustive search algorithm are examined in the following 2 subsections.

A. Minkowski Distance and Feature Ranking based Feature Selection Algorithm

Generally, feature ranking is performed in two stages, namely, ranking the individual features and ranking by evaluating the subsets of features. Moreover, feature selection is grouped according to the attribute evaluation measure is depending on the type (Filter or wrapper techniques). The filter model relies on common characteristics of the data to evaluate and select feature subsets without involving any mining algorithm. The wrapper model requires one fixed mining algorithm and uses its performance as the evaluation criterion. In this paper, we propose a new feature ranking algorithm based on Minkowski Distance using a single-feature ranking criteria with the filter model.

Phase 1: Feature Ranking Phase

Input : $K = [k_1, k_2, \dots, k_n]$ - the original feature set

Output: Ranking criterion function, c and ranked features $[l_1, l_2, \dots, l_n]$

1) Initialize: $K_i, i=1 \dots n$

2) Divide the feature sets into m groups.

3) For each feature $k_i \in K$

a) Compute the scalar Minkowski distance value ($D_{1,k}$) between the mean of a particular group A and the whole set of group, $D_{2,k}$ between the mean of a particular group B and the whole set of group.

b) Calculate and store merit scores f_k using the criterion. $f_k = D_{1,k} + D_{2,k}$

4) Rank features k_i to provide ranked feature set L where $L = [l_1, l_2, \dots, l_n]$

Phase 2: Exhaustive Search

Input: $L = [l_1, l_2, \dots, l_n]$ the ranked feature set

Output: Evaluation criterion function, $f(c, m)$ and optimal feature subsets R .

1) Initialize: $R = [PCR = [] ; MR = []]$.

2) Choose a reduced feature subsets which are greater than a threshold value: $F = [k_1, k_2, \dots, k_m], m < n$.

3) Perform a discriminate analysis with F using Minkowski distance in stepwise statistics. To obtain the output by the labeled data (group A and group B): $C =$ classification rate and $M =$ misclassification rate.

4) For each feature $k_i \in F$ and $k_j = \max(F_i)$

a) Select highest ranked feature and obtain: $R = \{R \cup F_k\} ; F = \{F - F_k\}$

b) Perform discriminate analysis with R using Minkowski distance in stepwise statistics. obtain the output by the labeled data from groups A and B using $c_k =$ current classification rate and $m_k =$ current misclassification rate.

c) Store c_k and m_k into PCR and MR separately.

5) End

6) Obtain the optimal feature subsets R based on evaluation criterion function $\min (f(c, m))$: $f(c, m) = \sqrt{((1 - c) \cdot 100 - m \cdot 100)}$

In [12], a modified greedy search algorithm is used to select the feature subset, which can reduce the iterations to some extent. However, the feature subset is not the optimal. In this work, the evaluation criterion function, which is a quadratic function with the minimum value and hence we can get the optimal feature subset based on the evaluation criterion function. The value range of the evaluation criterion function is between 0 and 100. The final output of this method provides important features for identifying every attack.

B. Enhanced Multiclass Support Vector Machine

In this work, we use the classification algorithm called Enhanced Multiclass Support Vector Machine (EMSVM) [1] for effective classification. In this technique, we test the proposed feature selection algorithm performance with classifier.

V. Results and Discussion

To evaluate our proposed feature selection method, we carried out the implementation of this algorithm by using WEKA software tool on KDD CUP 1999 dataset and calculated the classification rate and misclassification rate. In the experiments, we used Enhanced Multiclass Support Vector Machine (EMSVM) [1] for effective classification of the data set.

A. KDD Cup 1999 Data Set

In the International Knowledge Discovery and Data Mining Tools Competition, only "10% KDD" dataset is employed for the purpose of training [13]. We have selected "10% KDD" as the training data set and "Corrected KDD" as the test data set. Finally, we use EMSVM [1] classifier to validate the algorithm.

B. Experimental Result

The experiments have two phases namely selecting optimal feature subsets for every attack and then classifying the testing data. In the first phase, important attributes from training data of "Corrected KDD" are ranked by the feature ranking values and then an improved exhaustive search algorithm used to select the optimal feature subset. In the second phase, the training data of "10% KDD" was used to train EMSVM classifier and also for testing data of "Corrected KDD" using EMSVM classifier. This algorithm classified the data with full features and also with selected optimal feature subset separately to find the classification rates and false positive rates. Table I gives the optimal number of features selected in this work for all attack types after applying the proposed feature selection algorithm.

Attack Types	Selected Features
DoS	1,5,6,10,12, 23, 24, 26, 27, 28, 29, 30, 31,32,33, 34,35, 36, 40,41
Probe	1,5,6,11,12,23,24,31,32,33,34,36,37
R2L	10, 14,17, 19, 26,27,28,29,30,32,35,37,38, 40,41
U2R	1, 5,6,12,13, 23, 24, 27, 28, 30, 31,32,33, 41

Table I: List of Selected Features for Various types of attacks

Table II shows the performance analysis in terms of execution time taken for the proposed Feature Selection Algorithm with classification.

Attacks	Execution Time Taken (sec)	
	Malahanobis Distance + Feature Ranking	Minkowski Distance + Feature Ranking
Probe	4.2	2.71
DoS	12	8
Others	4.5	2.16

Table II: Performance of the Proposed Feature Selection Algorithm

From this table, it is observed that the classification accuracy is increased for all types of attacks. Moreover, the training and testing times are reduced for the all the types of attacks namely probe, DoS and others.

Table III shows the comparison of SVM and EMSVM with respect to classification accuracy when the classification is proposed with the selected features obtained from the proposed feature selection algorithms.

Exp. No.	SVM with Malahanobis Distance Feature Ranking			EMSVM with Minkowski Distance Feature Ranking		
	Probe	DoS	Others	Probe	DoS	Others
1	90.53	89.80	59.62	90.58	90.69	60.52
2	90.78	89.45	61.20	91.21	91.27	62.30
3	90.67	89.70	59.92	91.58	90.49	60.12
4	90.29	89.68	59.70	91.10	91.24	60.13
5	89.83	89.94	60.43	90.30	90.22	61.10

Table III: Detection Accuracy Comparisons with Feature Selection

From this Table, it is observed that the classification accuracy is increased in the proposed algorithm when it is compared with the existing algorithms for probe, DoS and others attacks. This is because proposed algorithm performs distance computation with Minkowski distance measures to produce optimal features leading to classification accuracy.

Figure 2 shows the false alarm rate comparison between the proposed feature selection with EMSVM and the existing feature selection with SVM Classifier.

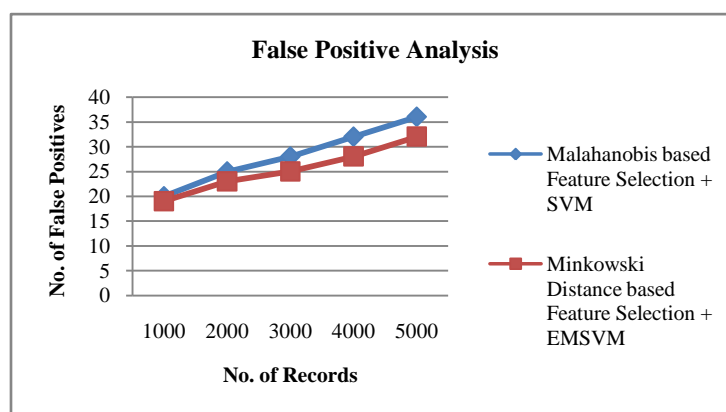


Figure 2: False Positive Analysis

From this figure, it is observed that the false alarm rate is reduced in the proposed model when it is compared with the existing model. This is due to the fact that in the proposed model, classification accuracy is improved by using Minkowski distance.

VI. Conclusion and Future Work

In this paper, we proposed a new intrusion detection system by combining the Enhanced Multiclass Support Vector Machine Algorithm [1] and newly proposed feature selection algorithm called Minkowski Distance and ranking based feature selection algorithm for effective decision making. The experimental results of proposed system provide better detection accuracy and reduced the false alarm rate. In future, the performance of the intrusion detection model can be improved further by adding temporal constraints.

REFERENCES

- [1] S.Ganapathy, P.Yogesh, A.Kannan, "An Intelligent Intrusion Detection System for Mobile Ad-Hoc Networks Using Classification Techniques", Computers and Communications and Information Systems, Vol. 148, pp. 117-121, 2011.
- [2] Sannasi Ganapathy, Kanagasabai Kulothungan, Sannasy Muthurajkumar, Muthusamy Vijayalakshmi, Palanichamy Yogesh, Arputharaj Kannan, "Intelligent Feature Selection and Classification Techniques for Intrusion Detection in Networks: A Survey", Journal on Wireless Communications and Networking, SprigerOpen, Vol. 271, pp. 1-16, 2013.
- [3] Fengli Zhang, Dan Wang, "An Effective Feature Selection Approach for Network Intrusion Detection", Eighth International IEEE Conference on Networking, Architecture and Storage, pp. 307-311, 2013.
- [4] Denning D E, "An Intrusion Detection Model", IEEE Transactions on Software Engineering, Vol. 51, no. 8, pp. 12-26, Aug. 2003.
- [5] Z. Muda, W. Yassin, M.N. Sulaiman, N.I. Udzir, "Intrusion Detection based on K-Means Clustering and Naïve Bayes Classification", In Proceedings of 7th IEEE International Conference on IT in Asia, 2011.
- [6] Guohua Geng, Na Li, Shangfu Gong, "Feature Selection Method for Network intrusion based on Fast Attribute Reduction of Fuzzy Rough Set", 2012 International Conference on Industrial Control and Electronics Engineering, pp. 530-534, 2012.
- [7] Janya Onpans, Suwanna Rasmeequan, Benchaporn Jantarakongkul, Krisana Chinnasarn, Annupan Rodtook, "Intrusion Feature Selection Using Modified Heuristic Greedy Algorithm of Itemset", 13th International Symposium on Communications and Information Technologies (ISCIT), pp. 627-632, 2013.
- [8] Yang Zhong, Hirohumi Yamaki, Hiroki Takakura, "A Grid-Based Clustering for Low-Overhead Anomaly Intrusion Detection", IEEE Conference on Grid Computing and Security, pp.17-24, 2011.
- [9] WANG Huai-bin, YANG Hong-liang, XU Zhi-jian, YUAN Zheng, "A clustering algorithm use SOM and K-Means in Intrusion Detection" In Proceedings of IEEE International Conference on E-Business and EGovernment, pp.1281-1284, 2010.
- [10] Hongwei Gao, Dingju Zhu, Xiaomin Wang, "A Parallel Clustering Ensemble Algorithm for Intrusion Detection System", In Proceedings of Ninth IEEE International Symposium on Distributed Computing and Applications to Business, Engineering and Science, pp.450-453, 2010.
- [11] Hari Om, Aritra Kundu, "A Hybrid System for Reducing the False Alarm Rate of Anomaly Intrusion Detection System", In Proceedings of First IEEE International Conference on Recent Advances in Information Technology, 2012.
- [12] Janya Onpans, Suwanna Rasmeequan, Benchaporn Jantarakongkul, Krisana Chinnasarn, Annupan Rodtook, "Intrusion Feature Selection Using Modified Heuristic Greedy Algorithm of Itemset", 13th International Symposium on Communications and Information Technologies (ISCIT), pp. 627-632, 2013.
- [13] KDD Cup 1999 Data, Information and Computer Science, University of California, Irvine.

Moving Object Detection for Video Surveillance

Abhilash K.Sonara¹, Pinky J. Brahmbhatt²

¹Student (ME-CSE), Electronics and Communication, L. D. College of Engineering, Ahmedabad, India

²Associate Professor, Electronics and Communication, L. D. College of Engineering, Ahmedabad, India

ABSTRACT: Video surveillance has long been in use to monitor security sensitive areas such as banks, department stores, highways, crowded public places and borders. The advance in computing power, availability of large-capacity storage devices and high speed network infrastructure paved the way for cheaper, multi sensor video surveillance systems. Traditionally, the video outputs are processed online by human operators and are usually saved to tapes for later use only after a forensic event. The increase in the number of cameras in ordinary surveillance systems overloaded both the human operators and the storage devices with high volumes of data and made it infeasible to ensure proper monitoring of sensitive areas for long times. In order to filter out redundant information generated by an array of cameras, and increase the response time to forensic events, assisting the human operators with identification of important events in video by the use of “smart” video surveillance systems has become a critical requirement. The making of video surveillance systems “smart” requires fast, reliable and robust algorithms for moving object detection, classification, tracking and activity analysis.

Keywords: Video-Based Smart Surveillance, Moving Object Detection, Background Subtraction, Object Tracking.

I. Introduction

Video surveillance systems have long been in use to monitor security sensitive areas. The history of video surveillance consists of three generations of systems which are called 1GSS, 2GSS and 3GSS. The first generation surveillance systems (1GSS, 1960-1980) were based on analog sub systems for image acquisition, transmission and processing. They extended human eye in spatial sense by transmitting the outputs of several cameras monitoring a set of sites to the displays in a central control room. They had the major drawbacks like requiring high bandwidth, difficult archiving and retrieval of events due to large number of video tape requirements and difficult online event detection which only depended on human operators with limited attention span. The next generation surveillance systems (2GSS, 1980-2000) were hybrids in the sense that they used both analog and digital sub systems to resolve some drawbacks of its predecessors. They made use of the early advances in digital video processing methods that provide assistance to the human operators by filtering out spurious events. Most of the work during 2GSS is focused on real-time event detection. Third generation surveillance systems (3GSS, 2000-) provide end-to-end digital systems. Image acquisition and processing at the sensor level, communication through mobile and fixed heterogeneous broadband networks and image storage at the central servers benefit from low cost digital infrastructure. Unlike previous generations, in 3GSS some part of the image processing is distributed towards the sensor level by the use of intelligent cameras that are able to digitize and compress acquired analog image signals and perform image analysis algorithms like motion and face detection with the help of their attached digital computing components. The ultimate goal of 3GSS is to allow video data to be used for online alarm generation to assist human operators and for offline inspection effectively. In order to achieve this goal, 3GSS will provide smart systems that are able to generate real-time alarms defined on complex events and handle distributed storage and content-based retrieval of video data. The making of video surveillance systems “smart” requires fast, reliable and robust algorithms for moving object detection, classification, tracking and activity analysis. Starting from the 2GSS, a considerable amount of research has been devoted for the development of these intelligent algorithms. Moving object detection is the basic step for further analysis of video. It handles segmentation of moving objects from stationary background objects. This not only creates a focus of attention for higher level processing but also decreases computation time considerably.

Commonly used techniques for object detection are background subtraction, statistical models, temporal differencing and optical flow. Due to dynamic environmental conditions such as illumination changes, shadows and waving tree branches in the wind object segmentation is a difficult and significant problem that needs to be handled well for a robust visual surveillance system [1].

II. Moving Object Detection

Each application that benefit from smart video processing has different needs, thus requires different treatment. However, they have something in common: moving objects. Thus, detecting regions that correspond to moving objects such as people and vehicles in video is the first basic step of almost every vision system since it provides a focus of attention and simplifies the processing on subsequent analysis steps. Due to dynamic changes in natural scenes such as sudden illumination and weather changes, repetitive motions that cause clutter (tree leaves moving in blowing wind), motion detection is a difficult problem to process reliably. Frequently used techniques for moving object detection are background subtraction, statistical methods, temporal differencing and optical flow whose descriptions are given below [2].

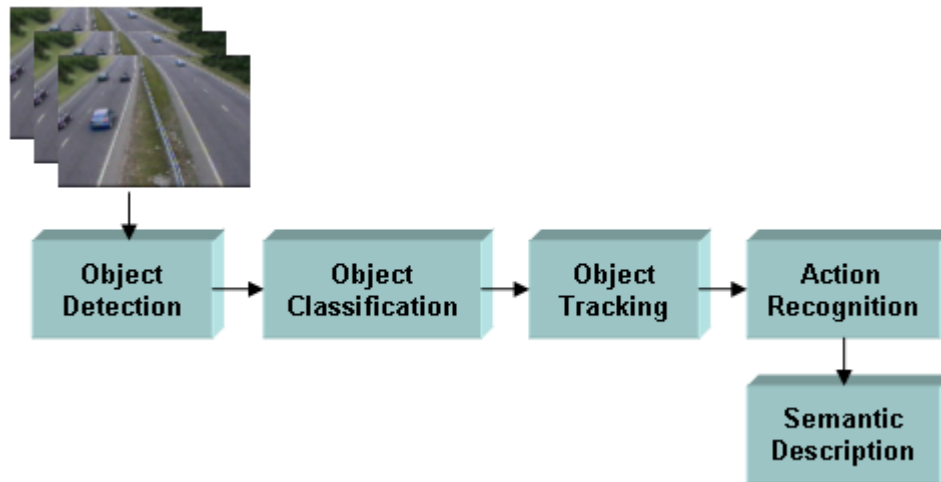


Fig 1: A generic framework for smart video processing algorithms

A. Background Subtraction

Background subtraction is particularly a commonly used technique for motion segmentation in static scenes. It attempts to detect moving regions by subtracting the current image pixel-by-pixel from a reference background image *that is created by averaging images over time in an initialization period. The pixels where the difference is above a threshold are classified as foreground. After creating a foreground pixel map, some morphological post processing operations such as erosion, dilation and closing are performed to reduce the effects of noise and enhance the detected regions. The reference background is updated with new images over time to adapt to dynamic scene changes. There are different approaches to this basic scheme of background subtraction in terms of foreground region detection, background maintenance and post processing. In Heikkila and Silven uses the simple version of this scheme where a pixel at location (x, y) in the current image I_t is marked as foreground if*

$$|I_t(x, y) - B_t(x, y)| > \tau$$

Is satisfied where τ a predefined threshold is. The background image B_t is updated by the use of an Infinite Impulse Response (IIR) filter as follows:

$$B_{t+1} = \alpha I_t + (1 - \alpha) B_t$$

The foreground pixel map creation is followed by morphological closing and the elimination of small-sized regions. Although background subtraction techniques perform well at extracting most of the relevant pixels of moving regions even they stop, they are usually sensitive to dynamic changes when, for instance, stationary objects uncover the background (e.g. a parked car moves out of the parking lot) or sudden illumination changes occur [3].

B. Statistical Methods

More advanced methods that make use of the statistical characteristics of individual pixels have been developed to overcome the shortcomings of basic background subtraction methods. These statistical methods are mainly inspired by the background subtraction methods in terms of keeping and dynamically updating statistics of the pixels that belong to the background image process. Foreground pixels are identified by comparing each pixel's statistics with that of the background model. This approach is becoming more popular due to its reliability in scenes that contain noise, illumination changes and shadow. The W4 system uses a statistical background model where each pixel is represented with its minimum (M) and maximum (N) intensity values and

maximum intensity difference (D) between any consecutive frames observed during initial training period where the scene contains no moving objects. A pixel in the current image I_t is classified as foreground if it satisfies:

$$|M(x, y) - I_t(x, y)| > D(x, y) \text{ or } |N(x, y) - I_t(x, y)| > D(x, y)$$

After thresholding, a single iteration of morphological erosion is applied to the detected foreground pixels to remove one-pixel thick noise. In order to grow the eroded regions to their original sizes, a sequence of erosion and dilation is performed on the foreground pixel map. Also, small-sized regions are eliminated after applying connected component labelling to find the regions. The statistics of the background pixels that belong to the non-moving regions of current image are updated with new image data. As another example of statistical methods, Stauffer and Grimson described an adaptive background mixture model for real-time tracking. In their work, every pixel is separately modeled by a mixture of Gaussians which are updated online by incoming image data. In order to detect whether a pixel belongs to a foreground or background process, the Gaussian distributions of the mixture model for that pixel are evaluated [4].

III. Object Detection and Tracking

The overview of our real time video object detection, classification and tracking system is shown in Figure 3.1. The proposed system is able to distinguish transitory and stopped foreground objects from static background objects in dynamic scenes; detect and distinguish left and removed objects; classify detected objects into different groups such as human, human group and vehicle; track objects and generate trajectory information even in multi-occlusion cases and detect fire in video imagery. In this and following chapters we describe the computational models employed in our approach to reach the goals specified above. Our system is assumed to work real time as a part of a video-based surveillance system. The computational complexity and even the constant factors of the algorithms we use are important for real time performance. Hence, our decisions on selecting the computer vision algorithms for various problems are affected by their computational run time performance as well as quality. Furthermore, our system's use is limited only to stationary cameras and video inputs from Pan/Tilt/Zoom cameras where the view frustum may change arbitrarily are not supported. The system is initialized by feeding video imagery from a static camera monitoring a site. Most of the methods are able to work on both color and monochrome video imagery. The first step of our approach is distinguishing foreground objects from stationary background. To achieve this, we use a combination of adaptive background subtraction and low-level image post-processing methods to create a foreground pixel map at every frame. We then group the connected regions in the foreground map to extract individual object features such as bounding box, area, center of mass and colour histogram [5].

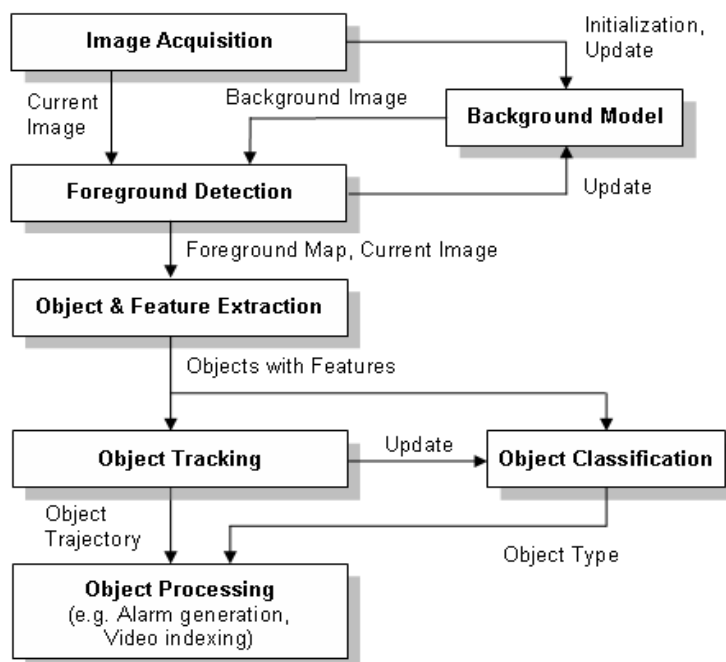


Fig 2: The system block diagram.

Our novel object classification algorithm makes use of the foreground pixel map belonging to each individual connected region to create a silhouette for the object. The silhouette and center of mass of an object are used to generate a distance signal. This signal is scaled, normalized and compared with pre-labeled signals in a template database to decide on the type of the object. The output of the tracking step is used to attain temporal consistency in the classification step. The object tracking algorithm utilizes extracted object features together with a correspondence matching scheme to track objects from frame to frame. The color histogram of an object produced in previous step is used to match the correspondences of objects after an occlusion event. The output of the tracking step is object trajectory information which is used to calculate direction and speed of the objects in the scene. After gathering information on objects' features such as type, trajectory, size and speed various high level processing can be applied on these data. A possible use is real-time alarm generation by pre-defining event predicates such as "A human moving in direction d at speed more than s causes alarm a_1 ." or "A vehicle staying at location l more than t seconds causes alarm a_2 .". Another opportunity we may make use of the produced video object data is to create an index on stored video data for offline smart search. Both alarm generation and video indexing are critical requirements of a visual surveillance system to increase response time to forensic events. The remainder of this chapter presents the computational models and methods we adopted for object detection and tracking [6].

A. Object Detection

Distinguishing foreground objects from the stationary background is both a significant and difficult research problem. Almost the visual surveillance systems' entire first step is detecting foreground objects. This both creates a focus of attention for higher processing levels such as tracking, classification and behaviour understanding and reduces computation time considerably since only pixels belonging to foreground objects need to be dealt with. Short and long term dynamic scene changes such as repetitive motions (e. g. waiving tree leaves), light reflectance, shadows, camera noise and sudden illumination variations make reliable and fast object detection difficult. Hence, it is important to pay necessary attention to object detection step to have reliable, robust and fast visual surveillance system. Our method depends on a six stage process to extract objects

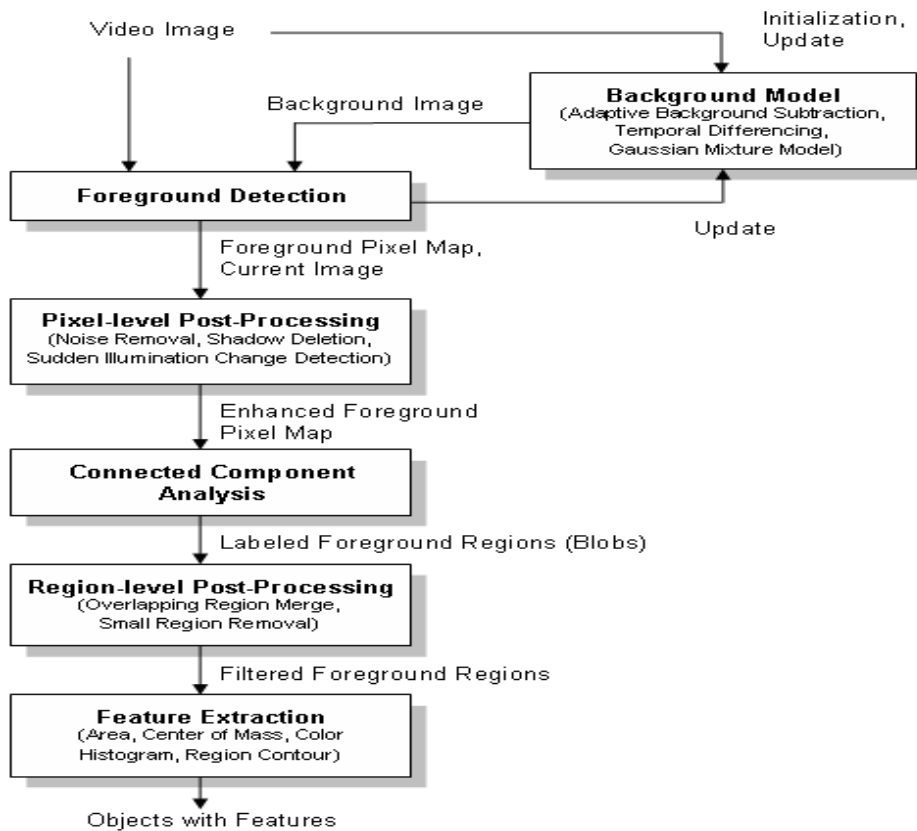


Fig 3: The object detection system diagram.

With these features in video imagery, first step is the background scene initialization. There are various techniques used to model the background scene in the literature. In order to evaluate the quality of different background scene models for object detection and to compare run-time performance, we implemented three of these models which are adaptive background subtraction, temporal frame differencing and adaptive online Gaussian mixture model. The background scene related parts of the system is isolated and its coupling with other modules is kept minimum to let the whole detection system to work flexibly with any one of the background models. Next step in the detection method is detecting the foreground pixels by using the background model and the current image from video. This pixel-level detection process is dependent on the background model in use and it is used to update the background model to adapt to dynamic scene changes. Also, due to camera noise or environmental effects the detected foreground pixel map contains noise. Pixel-level post-processing operations are performed to remove noise in the foreground pixels [7].

B. Foreground Detection

We use a combination of a background model and low-level image post-processing methods to create a foreground pixel map and extract object features at every video frame. Background models generally have two distinct stages in their process: initialization and update. Following sections describe the initialization and update mechanisms together with foreground region detection methods used in the three background models we tested in our system [8].

IV. Results And Analysis

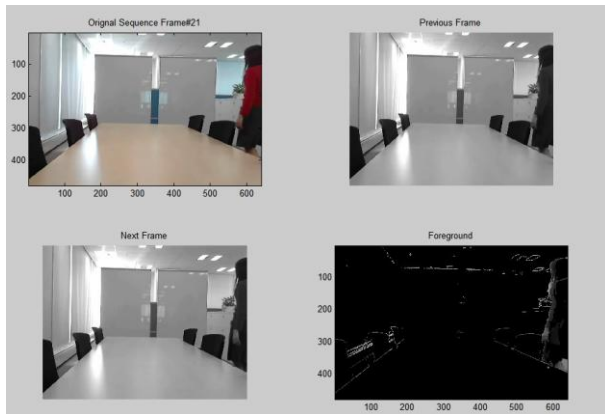


Fig. 4(a)

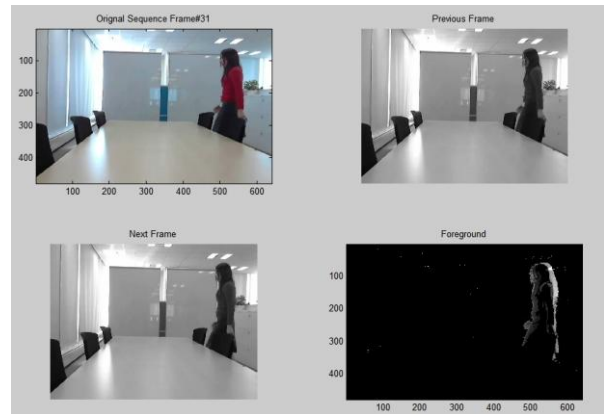


Fig. 4(b)



Fig. 4(c)

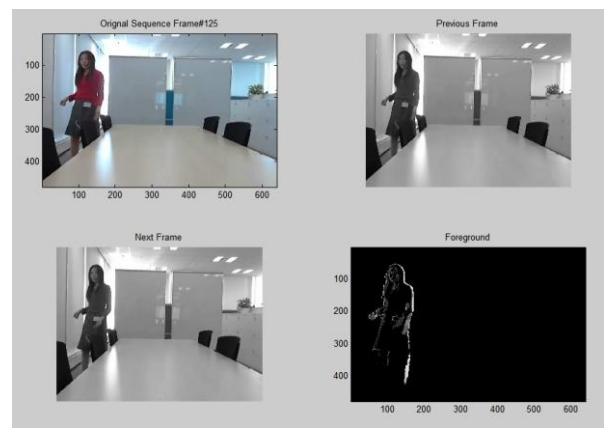


Fig. 4(d)

Fig. 4 Position wise detection of moving object along with their corresponding reference frames

V. Conclusions and Future Work

In this work we have described a unique moving object detection technique based on separation of background and foreground. The approximate position of moving object is captured by comparing the reference frame with consecutive frames.

In this work we have focussed mainly on the detection of a single object from a video sequence. As a part of future work look forward to incorporate methods to enable our algorithm to detect multiple objects present in the video sequence. Also we propose to work on video sequences having complex background.

REFERENCES

- [1] Komagal, E.; Vinodhini, A.; Srinivasan, A.; Ekava, B.” Real time Background Subtraction techniques for detection of moving objects in video surveillancesystem” Computing, Communication and Applications (ICCCA), 2012.
- [2] Soumya. T “A Moving Object Segmentation Method for Low Illumination Night Videos” Proceedings of the World Congress on Engineering and Computer Science 2008.
- [3] A. Amer. Voting-based simultaneous tracking of multiple video objects. In Proc. SPIE Int. Symposium on Electronic Imaging, pages 500–511, Santa Clara, USA, January 2003.
- [4] R. Bodor, B. Jackson, and N. Papanikolopoulos. Vision-based human tracking and activity recognition. In Proc. of the 11th Mediterranean Conf. on Control and Automation, June 2003.
- [5] H.T. Chen, H.H. Lin, and T.L. Liu. Multi-object tracking using dynamical graph matching. In Proc. of IEEE Computer Society Conference on Computer Vision and Pattern Recognition, pages 210–217, 2001
- [6] Lian Xiaofeng; Zhang Tao; Liu Zaiwen “A Novel Method on Moving-Objects Detection Based on Background Subtraction and Three Frames Differencing Measuring Technology and Mechatronics Automation (ICMTMA), 2010 International Conference on, Issue March 2010.
- [7] Jin Wang; Lanfang Dong “Moving objects detection method based on a fast convergence Gaussian mixture model Computer Research and Development (ICCRD), 2011 3rd International Conference on, Issue March 2011.
- [8] C. B. Liu and N. Ahuja. Vision based fire detection. In IEEE International Conference on Pattern Recognition, Cambridge, UK, August 2004.

A production - Inventory model with JIT setup cost incorporating inflation and time value of money in an imperfect production process

R. Chakrabarty¹ T. Roy² and K. S. Chaudhuri³

¹Department of Mathematics, Vidyasagar College for Women, 39, Sankar Ghosh Lane, Kolkata-700006, India

²Department of Mathematics, Vidyasagar College for Women, 39, Sankar Ghosh Lane, Kolkata-700006, India

³Department of Mathematics, Jadavpur University, Kolkata-700032, India

Abstract: A production inventory model with Just-In-Time (JIT) set-up cost has been developed in which inflation and time value of money are considered under an imperfect production process. The demand rate is considered to be a function of advertisement cost and selling price. Unit production cost is considered incorporating several features like energy and labour cost, raw material cost and development cost of the manufacturing system. Development cost is assumed to be a function of reliability parameter.

Considering these phenomena, an analytic expression is obtained for the total profit of the model. The model provides an analytical solution to maximize the total profit function. A numerical example is presented to illustrate the model along with graphical analysis. Sensitivity analysis has been carried out to identify the most sensitive parameters of the model.

I. Introduction

In the manufacturing system, a production process is not completely perfect. Producer may produce defective items from the very beginning or it may happen that at the beginning of the production process, all the produced items are non-defective. Consumers in the super market judge the goods on the basis of both quality depending upon defective or non-defective goods and price. The choice of quality is often an important factor to an industry. A lower quality product results in lower effectiveness with which a manufacturer meets consumers' demands. Productivity of a manufacturer is also a measure of transformation of efficiency and is considered as the inventory turnover ratio. The higher turnover causes much more productivity with which a manufacturer uses its inventory. Considering all the above factors, our attention is to determine the quality factor and maximum stock level so that the integrated total profit is maximized.

Volume flexibility is a major factor of flexible manufacturing systems (FMS) which helps to meet the market-demand at the optimal level. Many researchers have published their article in this direction. Sethi and Sethi (1990) presented five flexibilities at the system level and these are based on producers, routing, product and volume flexibility. Yan and Chang (1998) analyzed a general production inventory model in which there were production rate, deterioration rate and demand rate as a function of time. Skouri and Papachristos (2003) extended the model of Yan and Chang (1998) considering the backlogging rate which is a time dependent function and they introduced an algorithm for the solution of this problem. Rosenblatt and Lee (1986) and Porteus (1986) proposed an EMQ (economic manufacturing quantity) model. In these models, they assumed that the manufacturing process is in control state at the beginning of the production run and it may be shifted to an out-of-control state after a certain time. These defective products are repaired/reworked at a cost. Khouja and Mehrez (1994) extended a classical inventory model to the production model in which the production rate is a variable under managerial control and production cost is a function of production rate. Sana et al. (2007 a,b) discussed the EMQ model in an imperfect production system in which the defective items are sold at a reduced price. In this model, the demand function of defective items is a non-linear function of reduction rate. Some of the works in this direction are due to Khouja (1995), Mondal and Maiti (1997), Bhandari and Sharma (1971) and Bhunia and Maiti (1997). Recently Sana (2010) discussed a production-inventory model in an imperfect production process over a finite time horizon was considered. The production rate varies with time. The unit production cost is a function of production rate and product reliability parameter.

In present competitive market situation, the selling of product and the marketing policies depend on display of stock and advertisement. Advertisement through T.V, Newspaper, Radio, etc., and also through salesman have motivational effect on the customer to buy more. It is seen in the market that lesser selling price causes increase in demand whereas higher selling price decreases the demand. So, we can conclude that the

demand of an item is a function of selling price and advertisement cost. Kolter(1971) analyzed marketing policies into inventory decisions and discussed the relationship between economic order quantity and decision. Other notable papers are due to Ladany and Sternleib (1974), Urban(1992), Goyal and Gunasekaran (1997), Leo(1998), etc., inventory models were discussed incorporating the effects of price variations and advertisement cost in demand.

Most of the articles do not take into account the effect of inflation and time-value of money. In the present economic situation, many countries have worsened due to large scale inflation and consequent sharp decline in the purchasing power of money. Therefore, effects of inflation and time-value of money can no longer be ignored in the present economy. The first article in this direction was presented by Buzacott (1975), taking inflation into account. Misra (1975) also analyzed an article incorporating inflationary effects. Many other researchers extended their ideas to other inventory situations by considering time-value of money, different inflation rates for the internal and external costs, finite replenishment rate, shortage, etc.. Other articles in this direction come from Bierman and Thomas (1977), Datta and Pal(1991), Bose et al.(1995), Ray and Chaudhuri (1997), Roy and Chaudhuri (2006), Roy and Chaudhuri (2007), Sana (2010), Roy and Chaudhuri (2011). Taking the above features into consideration, we develop a production-inventory model with variable set-up cost incorporating inflation and time value of money in an imperfect production process. Demand rate is a linear decreasing function of selling price and the advertisement cost. The unit production cost depends upon labour, raw material charges, advertisement cost and product reliability parameter. In addition, effect of inflation and time-value of money without lead time in finite time horizon are also considered. The total profit function is maximized analytically in this model. The model has been illustrated with a numerical example along with graphical analysis and sensitivity analysis of parameters of the total profit are presented.

II. Notations and Assumptions

This paper is developed with the following *Notations* and *Assumptions*.

Notations :

s : the selling price per unit

A : advertisement cost per unit item

c_h : the holding cost per unit per unit time

c_s : the shortage cost per unit per unit time

c_0 : the set-up cost per production run

c_r : the raw material cost per unit which is fixed

t_1 : the time upto which the production is made and after $t = t_1$ the production is stopped

T : one cycle time

L : fixed cost like energy and labour

D : demand rate

P : production rate which is fixed , $P \geq D$ always.

ψ : product reliability factor

$f(\psi)$: development cost of the production system

$c(\psi)$: unit production cost

ψ_{max} : maximum value of ψ

ψ_{min} : minimum value of ψ

Q : maximum stock level

$q(t)$: stock level at time t

R : disposal or rework cost per unit defective item

a : cost of resource, technology and design complexity for the product when $\psi = \psi_{max}$

b : represents the difficulties in increasing reliability which depends upon the technological design complexity and resource limitation etc

γP : represents die or tool cost which is proportional to the production rate

γ : $r - i$, where r is the interest rate per unit currency and i is the inflation rate per unit currency

g, h : constant values

Assumptions :

- The demand rate D depends on the sum of the advertisement cost and is a decreasing function of the selling price, i.e $D(A, s) = A + g - hs$, where $g > 0$ and $h > 0$

- The unit production cost $c(\psi) = L + c_r + \frac{f(\psi)}{P} + \gamma P$

- During the production period, the defective items are produced. The smaller value of ψ provides better quality product. The development cost of the production system is given by $f(\psi) = ae^{\frac{(\psi_{max}-\psi)}{\psi-\psi_{min}}}$, $\psi \in [\psi_{min}, \psi_{max}]$

- Selling price s is determined by a mark-up over a unit production cost $c(\psi)$ i.e. $s = \mu c(\psi)$, μ is the mark-up.

- JIT setup cost $= \frac{c_0 D}{Q}$ has been considered which depends upon the demand rate.

- Shortages are not allowed.
- Lead time is assumed to be zero.

III. Development of the model

During the interval $[0, t_1]$, the stock-level $q(t)$ gradually increases due to production and demand until the production is stopped and stock-level $q(t)$ is at maximum level Q at $t = t_1$. In the interval $[t_1, T]$ only demand occurs. So stock level $q(t)$ gradually decreases due to demand in the interval $[t_1, T]$ until it is zero at $t = T$. The cycle repeats itself again. The pictorial representation of the model is given in the Fig.1. Insert Fig-1 here The stock level $q(t)$ at any time t can therefore be represented by the following differential equations :

$$\frac{dq(t)}{dt} = P - D, \quad 0 \leq t \leq t_1 \quad (1)$$

and

$$\frac{dq(t)}{dt} = -D, \quad t_1 \leq t \leq T \quad (2)$$

with initial and boundary conditions are $q(t) = 0$, when $t = 0$ and $t = T$ and $q(t) = Q$, when $t = t_1$

The solution of the differential equations (1) and (2) are

$$q(t) = (P - D)t, \quad 0 \leq t \leq t_1 \quad (3)$$

$$= (T - t)D, \quad t_1 \leq t \leq T \quad (4)$$

From (3), we have

$$t_1 = \frac{Q}{P - D}. \quad (5)$$

From (4), we have

$$T = \frac{QP}{D(P - D)}. \quad (6)$$

The present value of total revenue is

$$\begin{aligned} C_{REV} &= \int_0^T s D e^{-\gamma t} dt \\ &= \frac{sD}{\gamma} (1 - e^{-\gamma T}). \end{aligned} \quad (7)$$

The present value of production cost is

$$C_{PRO} = \int_0^T c(\psi) D e^{-\gamma t} dt$$

$$= \frac{c(\psi)D}{\gamma}(1 - e^{-\gamma T}). \quad (8)$$

The present value of holding cost is

$$\begin{aligned} C_{HOL} &= \int_0^T c_h Q e^{-\gamma t} dt \\ &= \frac{c_h Q}{\gamma}(1 - e^{-\gamma T}). \end{aligned} \quad (9)$$

The present value of set up cost is

$$\begin{aligned} C_{SET} &= c_0 \int_0^T \frac{D}{Q} e^{-\gamma t} dt \\ &= \frac{c_0 D}{\gamma Q}(1 - e^{-\gamma T}). \end{aligned} \quad (10)$$

The present value of reworked cost is

$$\begin{aligned} C_{REW} &= \int_0^T R \psi P e^{-\gamma t} dt \\ &= \frac{R \psi P}{\gamma}(1 - e^{-\gamma T}). \end{aligned} \quad (11)$$

The total profit incorporating inflation and time value of money is given by

$$\begin{aligned} \pi(Q, \psi) &= [C_{REV} - C_{PRO} - C_{HOL} - C_{SET} - C_{REW}] \\ &= \frac{1}{\gamma} \{sD - c_h Q - Dc(\psi) - R\psi P - \frac{c_0 D}{Q}\} \times (1 - e^{-\gamma T}). \end{aligned} \quad (12)$$

Now, the problem is to determine the optimal values for Q and ψ such that π in (12) is maximized. However, it is a two dimensional decision-making problem for a retailer.

IV. Optimal solution and theoretical results

The necessary conditions for $\pi(Q, \psi)$ to be maximum are

$$\begin{aligned} \frac{\delta \pi(Q, \psi)}{\delta Q} &= \frac{1}{\gamma} (-c_h + \frac{c_0 D}{Q^2})(1 - e^{-\gamma T}) \\ &+ \frac{1}{\gamma} \{sD - c_h Q - Dc(\psi) - R\psi P - \frac{c_0 D}{Q}\} \gamma e^{-\gamma T} = 0. \end{aligned} \quad (13)$$

and

$$\begin{aligned} \frac{\delta \pi(Q, \psi)}{\delta \psi} &= \frac{1}{\gamma} \{(\mu - 1) \frac{\delta c(\psi)}{\delta \psi}\} D(1 - e^{-\gamma T}) + \frac{1}{\gamma} \{(\mu - 1)c(\psi) \\ &- \frac{c_0}{Q}\} \frac{\delta D}{\delta \psi} (1 - e^{-\gamma T}) + \frac{1}{\gamma} \{(\mu - 1)c(\psi) - \frac{c_0}{Q}\} D \gamma \\ &e^{-\gamma T} \frac{\delta T}{\delta \psi} - (c_h Q + R\psi P) e^{-\gamma T} \frac{\delta T}{\delta \psi} - \frac{RP}{\gamma} (1 - e^{-\gamma T}) = 0. \end{aligned} \quad (14)$$

After rearranging the terms in (13) and (14), we get

$$-\gamma (sD - c_h Q - Dc(\psi) - R\psi P - \frac{c_0 D}{Q}) e^{-\gamma T} \frac{\delta T}{\delta Q} = (\frac{c_0 D}{Q^2} - c_h)(1 - e^{-\gamma T}). \quad (15)$$

and

$$\frac{1}{\gamma} \{(\mu - 1) \frac{\delta c(\psi)}{\delta \psi}\} D(1 - e^{-\gamma T}) + \frac{1}{\gamma} \{(\mu - 1)c(\psi) - \frac{c_0}{Q}\}$$

$$\frac{\delta D}{\delta \psi} (1 - e^{-\gamma T}) + \frac{\gamma e^{-\gamma T}}{1 - e^{-\gamma T}} \frac{\delta \Gamma}{\delta \psi} \pi(Q, \psi) - \frac{RP}{\gamma} (1 - e^{-\gamma T}) = 0. \quad (16)$$

Applying (16), we have $J_1(\psi) = 0$ where

$$J_1(\psi) = (\psi - \psi_{min})^2 \frac{1 - e^{-\gamma T}}{\gamma} \frac{\delta c(\psi)}{\delta \psi} \{(\mu - 1)D - h\mu(\mu - 1)c(\psi) + h\mu \frac{c_0}{Q}\} \\ - (\psi - \psi_{min})^2 RP \frac{1 - e^{-\gamma T}}{\gamma} + (\psi - \psi_{min})^2 \frac{\gamma e^{-\gamma T}}{1 - e^{-\gamma T}} \frac{\delta \Gamma}{\delta \psi} \pi(Q, \psi). \quad (17)$$

Applying (15) and (17), we have the following propositions:

Proposition 1. If $c_h Q^2 - c_0 D > 0$, then $\frac{\delta^2 \pi}{\delta Q^2}$ is negative .

Proof. We first obtain second-order derivative of $\pi(Q, \psi)$ from (13) and using (15), we have

$$\frac{\delta^2 \pi}{\delta Q^2} = -\frac{2c_0 D}{\gamma Q^3} (1 - e^{-\gamma T}) + \frac{1}{\gamma} \left(\frac{c_0 D}{Q^2} - c_h \right) \gamma e^{-\gamma T} \frac{\delta \Gamma}{\delta Q} + \left(\frac{c_0 D}{Q^2} - c_h \right) e^{-\gamma T} \frac{\delta \Gamma}{\delta Q} \\ - \gamma (sD - c_h Q - Dc(\psi) - R\psi P - \frac{c_0 D}{Q}) e^{-\gamma T} \left(\frac{\delta \Gamma}{\delta Q} \right)^2 + (sD - c_h Q \\ - Dc(\psi) - R\psi P - \frac{c_0 D}{Q}) e^{-\gamma T} \frac{\delta^2 \Gamma}{\delta Q^2} \\ = -\frac{2c_0 D}{\gamma Q^3} (1 - e^{-\gamma T}) + 2 \left(\frac{c_0 D}{Q^2} - c_h \right) e^{-\gamma T} \frac{\delta \Gamma}{\delta Q} + \left(\frac{c_0 D}{Q^2} - c_h \right) (1 - e^{-\gamma T}) \frac{\delta \Gamma}{\delta Q} \\ = -\frac{2c_0 D}{\gamma Q^3} (1 - e^{-\gamma T}) - \frac{2}{Q^2} (c_h Q^2 - c_0 D) e^{-\gamma T} \frac{\delta \Gamma}{\delta Q} - \\ \frac{1}{Q^2} (c_h Q^2 - c_0 D) (1 - e^{-\gamma T}) \frac{\delta \Gamma}{\delta Q} < 0$$

Proposition 2. As $\psi \rightarrow \psi_{min}$, $J_1(\psi) \rightarrow \infty$.

Proof. From (17), we have ,

$$J_1(\psi) = \frac{1 - e^{-\gamma T}}{\gamma} \frac{ab}{P} e^{\frac{b(\psi_{max} - \psi)}{\psi - \psi_{min}}} (\psi_{min} - \psi_{max}) \\ \{(\mu - 1)D - h\mu(\mu - 1)c(\psi) + \frac{h\mu c_0}{Q}\} + \frac{\gamma e^{-\gamma T}}{1 - e^{-\gamma T}} \\ \pi(Q, \psi) \frac{QP(P - 2D)}{(PD - D^2)^2} \frac{h\mu ab}{P} e^{\frac{b(\psi_{max} - \psi)}{\psi - \psi_{min}}} (\psi_{min} - \psi_{max}) \\ - (\psi - \psi_{min})^2 \frac{RP}{\gamma} (1 - e^{-\gamma T}) \quad (18)$$

From (18), we have $J_1(\psi) \rightarrow \infty$ as $\psi \rightarrow \psi_{min}$. So we may formulate a lemma as follows.

Lemma. If $J_1(\psi_{max}) < 0$, then $J_1(\psi) = 0$ must have at least one solution in $[\psi_{min}, \psi_{max}]$, otherwise $J_1(\psi) = 0$ may have or may not have a solution in $[\psi_{min}, \psi_{max}]$. Also the solution gives a maximum value of

π , since $\frac{\delta^2 \pi}{\delta \psi^2}$ is negative at that solution.

V. Numerical example

To illustrate the proposed model, we consider the following parameter values of some product in appropriate units: $c_h = \$2$, $c_r = \$15$, $\psi_{max} = 2.2$, $\psi_{min} = .01$, $\gamma = \$.19$, $P = 160$ units, $L = \$2000$, $c_0 = \$50$, $a = \$20$, $b = .25$, $R = \$15$, $A = \$2000$, $g = 55$, $h = .25$, $\mu = 5$. We obtain the optimal solution of the model as $\pi^* = 402585$, $Q^* = 314.639$, $\psi^* = 2.00375$.

Insert Fig-2 here

VI. Sensitivity analysis

Using the Numerical Example, the sensitivity of each of the decision variables Q^* , ψ^* , and the maximum total profit $\pi^*(Q^*, \psi^*)$ to changes in each of the 8 parameters P , a , b , c_0 , γ , g , ψ_{max} , and ψ_{min} is examined in Table 1. The sensitivity analysis is performed by changing each of the parameters by -25%, -10%, +10% and +25%, taking one parameter at a time and keeping the remaining parameters unchanged. From Table 1, we can analyze the following cases.

- When P increases by 10%, then Q^* decreases and the total average profit π decreases by 31.88%. When P decreases by 10% and 25% respectively, then Q^* increases but ψ^* decreases and the total average profit increases by 31.48% and 79.26% respectively. The above discussion illustrates that the production rate parameter is highly sensitive.

- The parameters a , b , c_0 , ψ_{min} are insensitive.

- When γ is decreased by 10% and 25% respectively, then Q^* increases but ψ^* decreases and the total average profit π is increased by 46.45% and 138.95% respectively. So γ is highly sensitive.

- When g increases, then Q^* also increases but ψ^* decreases. The total average profit is increased by 92.52% and 58.14% due to change of g by 25% and 10% respectively. So it is clear that g is highly sensitive.

- When ψ_{max} is increased by 10%, then Q^* increases and the total average profit π increases by 1.74%.

Insert Table 1 here

VII. Conclusions

The following features are observed in the present model.

1. Since demand for the product in an industry is dependent on several features like price, time and advertisement cost, so in this model, demand has been considered as a sum of two functions, advertisement cost and linear decreasing function of selling price.
2. In this model, product quality factor is an important variable which determines the unit production cost and development cost of the production system. Also selling price is dependent on unit production cost.
3. Since effects of inflation and time-value of money can no longer be ignored in the present economy, so we consider here effects of inflation and time value of money.
4. Deterioration of inventory which is a common feature in the inventory of consumer goods, has been considered in this model.

We solve this problem analytically and numerically. The sensitivity of the solution to changes in different parameters has been discussed.

The model can be extended in several ways:

- a. We might extend the proposed profit function stochastically.
- b. We could extend the model by considering the production rate which is either variable or linear increasing function of demand.
- c. The model can also be extended by taking into consideration shortages and lead time.

REFERENCES

- [1] Beirman, H, Thomas, J. Inventory decisions under inflationary condition. *Decision Science* **8**, (1977) 151-155.
- [2] Bhandari, R. M., Sharma, P. K. The economic production lot size model with variable cost function, *Opsearch* **36** (1999) 137-150.
- [3] Bhunia, A. K., Maiti, M. An inventory model for decaying items with selling price, frequency of advertisement and linearly time-dependent demand with shortages, *IAPQR Transactions* **22** (1997) 41-49.
- [4] Bose, S., Goswami, A. and Chaudhuri, K.S. An EOQ model for deteriorating items with linear time-dependent demand rate and shortages under inflation and time discounting, *Journal of the Operations Research Society* **46** (1995) 771-782.
- [5] Buzacott, J. A., Economic order quantities with inflation. *Operations Research Quarterly* **26** (1975) 553-558.
- [6] Datta, T. K., Pal, A. K., Effects of inflation and time-value of money on inventory model with linear time-dependent demand rate and shortages. *European Journal of Operational Research* **52** (1991) 1-8.
- [7] Goyal, S.K., Gunasekaran, A. An integrated production-inventory-marketing model for deteriorating items, *Computers and Industrial Engineering* **28** (1997) 41-49.
- [8] Khouja, M., Mehrez, A., An economic production lot size model with imperfect quality variable production rate. *Journal of the Operational Research Society* **45(12)** (1994) 1405-1417.
- [9] Khouja, M. The economic production lot size model under volume flexibility, *Computer and Operations Research* **22** (1995) 515-525.
- [10] Kotler, P. Marketing Decision Making: A Model Building Approach, Holt Rinehart and Winston, New York, 1971.
- [11] Ladany, S., Sternleib, A. The intersection of economic ordering quantities and marketing policies, *AIIE Transactions* **6**(1974)35-40.
- [12] Leo, W. An integrated inventory system for perishable goods with back ordering, *Computers and Industrial Engineering* **34** (1998) 685-693.
- [13] Mandal, M., Maiti, M. Inventory model for damageable items with stock- dependent demand and shortages, *Opsearch* **34** (1997) 156-166.
- [14] Misra, R. B.. A study of inflationary effects on inventory systems. *Logistic Spectrum* **9** (1975) 260-268.
- [15] Porteus, E. L.. Optimal lot sizing, process quality improvement, and setup cost reduction. *Operations Research* **34** (1986) 137-144.
- [16] Ray, J., Chaudhuri, K.S.. An EOQ model with stock- dependent demand, shortages, inflation and time discounting. *International Journal of Production Economics* **53** (1997) 171-180.
- [17] Rosenblatt, M. J., Lee, H. L.. Economic production cycles imperfect production processes. *IIE Transactions* **17** (1986) 48-54.
- [18] Roy, T. and Chaudhuri, K. S.. Deterministic inventory model for deteriorating items with stock level-dependent demand, shortages, inflation and time-discounting, *Nonlinear Phenomena in Complex System* **9(10)**, ((2006) 43-52.
- [19] Roy, T. and Chaudhuri, K. S.. A finite time-horizon deterministic EOQ model with stock level-dependent demand, effect of inflation and time value of money with shortage in all cycles, *Yugoslav Journal of Operation Research* **17(2)** (2007) 195-207.
- [20] Roy, T. and Chaudhuri, K.S.. A finite time horizon EOQ model with ramp-type demand rate under inflation and time-discounting, *Int.J. Operational Research* **11(1)**, (2011) .
- [21] Sana, S., Goyal, S. K., Chaudhuri, K. S., 2007. An imperfect production process in a volume flexible inventory model. *International Journal of Production Economics* **105** 548-559.
- [22] Sana, S., Goyal, S.K., Chaudhuri, K.S.. On a volume flexible inventory model for items with an imperfect production system. *International Journal of Operational Research* **2(1)** (2007b) 64-80.
- [23] Sana, S. S. A production-inventory model in an imperfect production process, *European Journal of Operational Research* **200** (2010) 451-464.
- [24] Sethi, A. K., Sethi, S. P.. Flexibility in manufacturing: a survey. *International Journal of Flexible Manufacturing Systems* **2** (1990) 289-328.
- [25] Skouri, K., Papachristos, S.. Optimal stopping and restarting production times for an EOQ model with deteriorating items and time-dependent partial backlogging. *International Journal of Production Economics* **81-82** (2003) 525-531.
- [26] Urban, T. L. Deterministic inventory models incorporating marketing decisions, *Computers and Industrial Engineering* **22** (1992) 85-93.
- [27] Yan, Y., Cheng, T.. Optimal production stopping restarting times for an EOQ model with deteriorating items. *Journal of the Operational Research Society* **49** (1998) 1288-1295.

Table 1: Sensitivity analysis

Effects of P , a , b and c_0 on profit (Example 1)

para- meter	% change in the parameter	Q^*	ψ^*	% change in π
	+25	-	-	-
P	+10	218.59	-	-31.88
	-10	404.57	1.8577	31.78
	-25	522.564	1.75612	79.26
	+25	313.743	-	-.332
a	+10	314.28	2.09023	-.134
	-10	314.994	1.91292	.136
	-25	315.551	1.76669	.343
	+25	-	-	-
b	+10	314.671	2.09024	-.0025
	-10	314.606	1.91086	.0042
	-25	314.571	1.75728	.014
	+25	314.667	2.00376	-.0005
c_0	+10	314.65	2.00376	-.0002
	-10	314.627	2.00375	.0002
	-25	314.611	2.00376	.0004

Table 1: Continued

Effects of γ , g , ψ_{max} and ψ_{min} on profit (Example 1)

para- meter	% change in the parameter	Q^*	ψ^*	% change in π
	+25	-	-	-
γ	+10	-	-	-
	-10	446.426	1.77377	46.45
	-25	691.7	1.55078	138.95
	+25	574.883	1.51213	92.52
g	+10	481.597	1.64376	58.14
	-10	-	-	-
	-25	-	-	-
	+25	-	-	-
ψ_{max}	+10	318.832	-	1.74
	-10	314.697	1.88921	.038
	-25	314.758	1.70794	.099
	+25	318.832	-	1.74
ψ_{min}	+10	314.639	2.00423	0
	-10	314.639	2.00327	0
	-25	314.638	2.00253	0

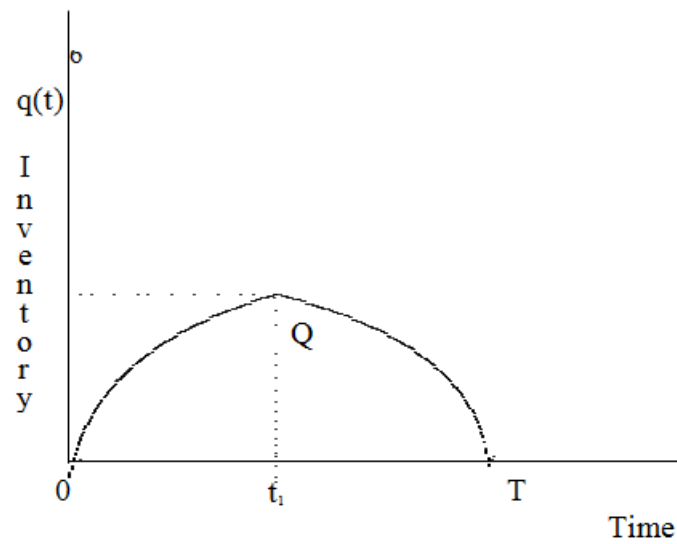


Fig 1: Graphical representation of Model

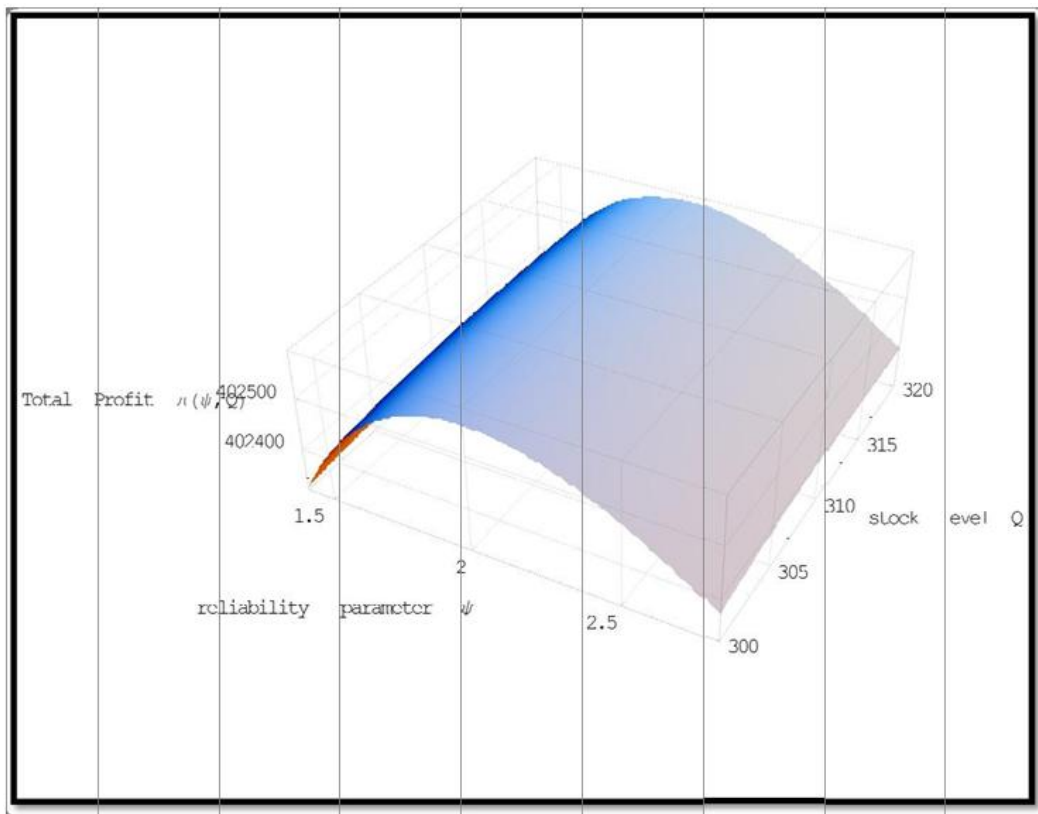


Fig. 2: Maximum total profit $\pi(Q, \psi)$ versus Q and ψ of Example

Wavelet Based Analysis of Online Monitoring of Electrical Power by Mobile Technology

P. Ram Kishore Kumar Reddy

Associate Professor, Department of EEE, MGIT, Hyderabad, India

ABSTRACT: Electrical automation is an important option for obtaining optimal solution while monitoring the electrical power consumption. While using the conventional methods the errors in continuous monitoring of power consumption is more. But the system requires not only the monitoring of the energy but also requires the analysis of the monitored energy. In this paper wavelet analysis is used for the analysis of the monitored energy/power which is monitored by GPRS technology. By using the GPRS mobile technology the energy consumption is monitored continuously and the observed data is interfaced to the computer by RS 232 port. By using MATLAB the monitored data is processed to obtain in depth analysis of the monitored power. The proposed method not only monitors the data but also provides efficient means to analyze the observed data by Wavelet Transform

Keywords: Energy monitoring, GPRS system, Hardware system, Multi Resolution Analysis, Real time monitoring wavelet transforms

I. Introduction

On line Monitoring of the electrical energy in terms of voltage and current is very important for taking appropriate steps basing on the observed data. Online monitoring of energy supports remote monitoring of electrical energy if the system is interfaced with mobile technology such as GSM (Global System for Mobile Communications) or GPRS (General Packet Radio Service) systems. GSM is an interface connects the automated meter to home appliances [1]. Similarly GPRS system interfaces the electrical energy to be monitored to remote units where the monitored energy is observed continuously to take corrective measures if any sort of anomalies are observed. In general voltage profile, current profile, KWH profile is monitored continuously as the load is changing continuously. Basically the monitored electrical variables will be measured by the meter which consists of microcontroller programmed to monitor the variables and the meter consists of a modem which communicates the observed variables to remote units by GPRS technology. At the sight of remote unit, appropriate decision will be taken with the help of monitored data[2]. As an illustration, if the measuring instrument consists of the said characteristics then it is called intelligence meter where logistics can be implemented such as the meter disconnects the supply to home appliances or industrial customers if the consumer consumes more than the intended power. That is the control center can monitor remotely about the level of energy consumption by a particular consumer and can take the appropriate decision.

In order to achieve the online monitoring of electrical power, microcontroller based designs can be preferred due to its versatile features while processing the data corresponding to the parameters. During the past years a number of researches contribute with the help of microprocessors and controllers for continual monitoring of system parameters. During theft of the power there will be corresponding changes in the Power levels and these changes in the magnitude needs to be monitored via online process. While doing so wavelet analysis can be implemented by interfacing the monitored data with PC by using RS 232 port. Wavelet analysis identifies even slight changes in the monitored data and thus facilitates indepth analysis of the monitored power.

Thus Real-time monitoring of electrical power necessitates great abilities of data-handling and data-processing. These requirements limit the possibility of monitoring, in spite of the fact that microprocessor-based monitoring systems have observed vital development in their storage and computational power[3]. Development of compact algorithms will benefit power quality because they will allow monitoring of more points simultaneously for large systems, and, they will help in building powerful embeddable monitoring architectures within small power devices.

II. Online Monitoring System

The introduction of wireless communication has allowed many technical applications around the world to carry out technical activities in a novel way. General Packet Radio Service is a new, high-speed, packet-switching technology, for GSM networks. It makes sending and receiving large volumes of data over a mobile telephone network possible. A simple way to understand packet switching is to relate it to a puzzle.

GPRS offers a continuous connection to the Internet for mobile phone and computer user's. In most of the applications data communication require continuous data transfer especially in the cases of energy monitoring applications. GPRS provides a significant advances to mobile data usage and usefulness..Its main innovations are that it is packet based, that it will increase data transmission speeds, and that it will extend the Internet connection all the way to the mobile PC – the user will no longer need to dial up to a separate ISP.

GTPRS will complement rather than replace the current data services available through today's GSM digital cellular networks, such as Circuit Switched Data and Short Message Service

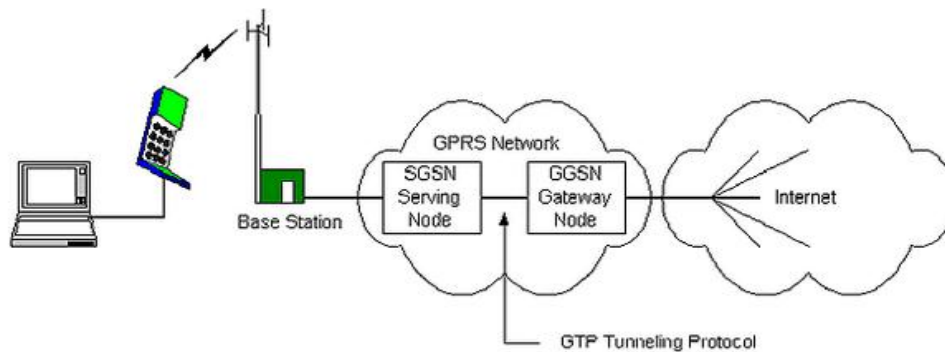


Figure.1 Schematic diagram of GPRS

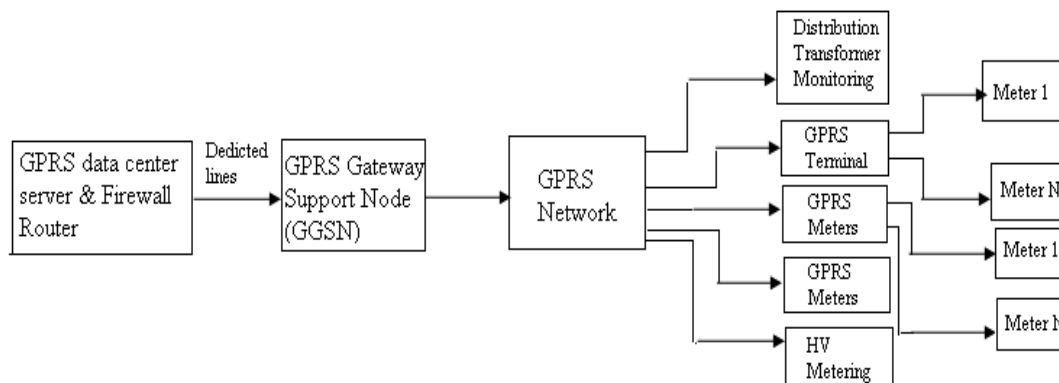


Figure.2 Architecture of GPRS system

To realize the online monitoring of the data, ATmega162 microcontroller which is shown in Figure.3 has been used to process the electrical data. Code is dumped on to the microcontroller (pin diagram shown in fig 3) to control the electrical data to be monitored such as current, voltage and KWh [4]. At the sending end and receiving end GPRS modem is established, and the monitored data is transmitted using GPRS at sending end and the same data is received at remote location by using GPRS at receiving end [5]. The proposed hardware model is shown in fig4. The module shown in fig4 is at sending and receiving end to transmit and receive the monitored data by the microcontroller.

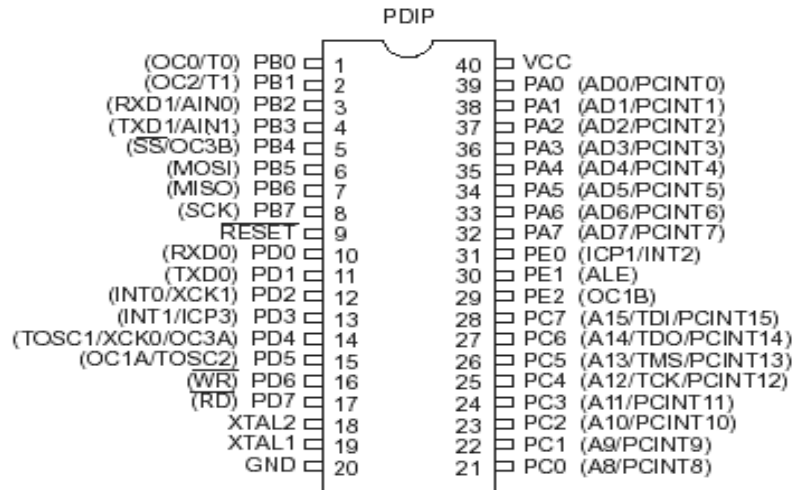


Figure.3 Pin diagram of ATmega162 Microcontroller

In the laboratory the module is tested for variable inductive load such that the corresponding data is received by the modem at receiving end which has been interfaced with PC for further analysis with Wavelet Transform in MATLAB environment.

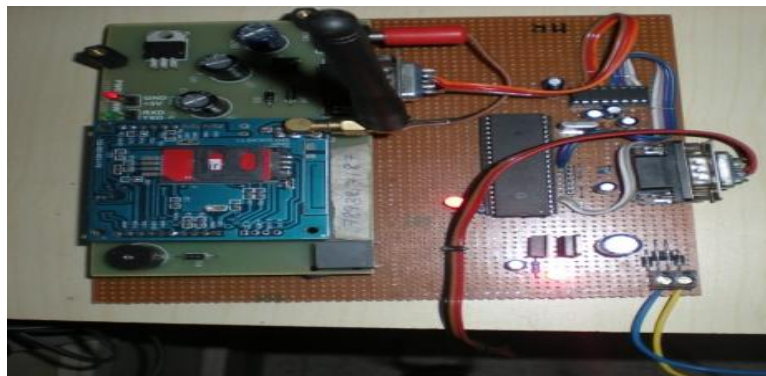


Figure.4 Hardware model for automated monitoring

As an illustration the observed data is given in the following table.
 V=210 volt, Meter can measure up to 12A, KVA=2.0, R-L load

S.No	Voltage	Load current in AMPS
1	209	1
2	209	2
3	209	3
4	209	4
5	209	5
6	209	6
7	208	7
8	208	8
9	208	9

S.No	Time in Minutes	KWh Measured from Energy meter
1	5	0.142
2	10	0.200
3	15	0.424
4	20	0.546
5	25	0.723
6	30	0.788
7	35	0.967
8	40	1.116
9	45	1.266
10	50	1.417
11	55	1.554
12	60	1.698

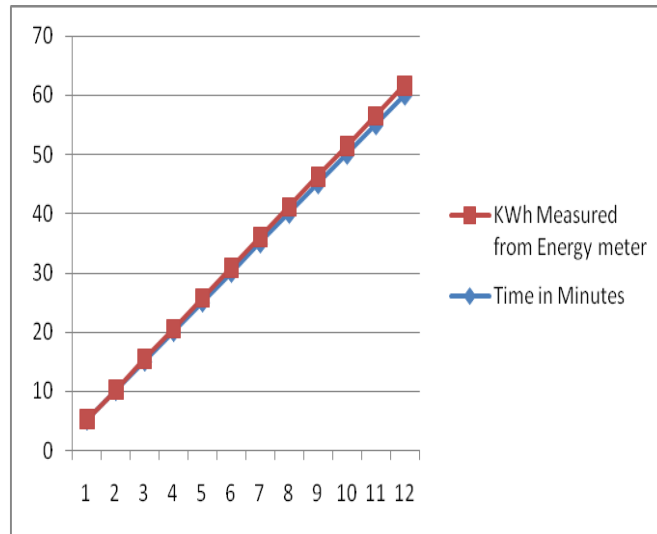


Figure.5 Load variation with corresponding kWh

III. Wavelet Multi Resolution Analysis

The main idea of wavelet multi-resolution analysis is that any function $f(t)$ can be approximated step by step and the approximation of each step is just to smooth $f(t)$ by a lower-pass function $\phi(t)$ which will also expand or contract according to the step. $f(t)$ is approximated in different precision in different steps. Mallet algorithm is adopted to decompose the signal. The signal to be analyzed is to decompose at different dilations and shifted till in-depth resolution of the signal is achieved. Firstly the high-pass filters $h[n]$ and low pass filter $g[n]$ the load signal s can be decomposed into two sub serials $c1[n]$ and $d1[n]$. The transform is an orthogonal decomposition of the signal [6]. The $c1[n]$, named the approximation of signal s contains the low frequency component of the signal s and $d1[n]$ is the detail of the signal is associated with the high frequency component of the signal s . The further step by expanding the scale function $\phi(t)$ the approximation $c1[n]$ is again decomposed into $c2[n]$ and $d2[n]$. By using the Wavelet analysis in the PC, the monitored data is analyzed to observe the discontinuities in the observed data. While applying wavelet transform, detailed and approximate coefficients are obtained and these values provides information regarding any sort of anomalies in the observed data shown in fig 6.

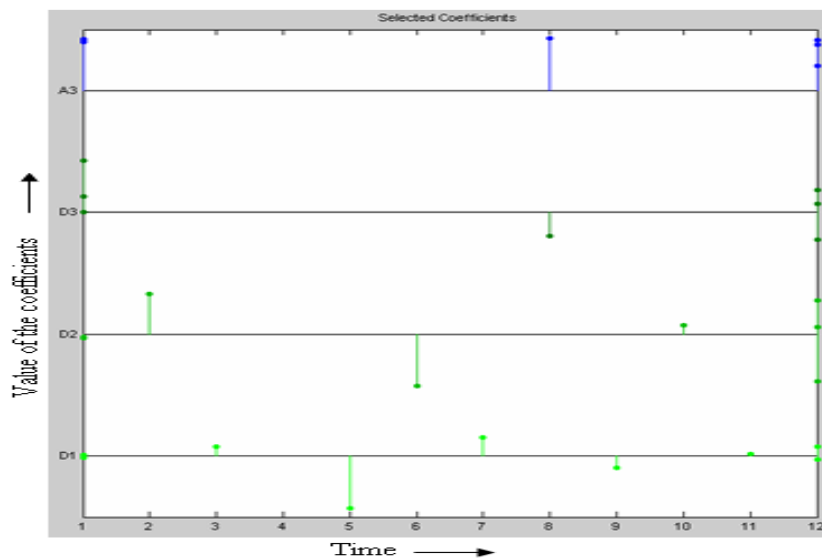


Figure.6 Selected coefficients

This concept can be extended even to monitor the condition monitoring of the power transformer with respect to temperature, voltage, and overload condition.

IV. Conclusion

A real time energy monitoring system for simple load is proposed and developed and its automation closer to real time is realized with microcontroller based GPRS system. The developed approach is low and able to identify anomalies in monitored data with the help of approximate and detailed coefficients as the receiving end GPRS system is interfaced with PC by RS232 port. The developed system is tested in laboratory with variable resistive and inductive load.

REFERENCES

- [1] Fabio Borghese, "Evaluating The Leading-Edge Italian Telegestore Project", ENEL, Business Development Executive, Infrastructure and Networks Division.
- [2] Gerwen, R.J.F., Jaarsma, S. and Koenis, F., Cost Benefit Analysis for Automated Metering, Metering International, issue 4, 2005
- [3] Information on automated metering project on Continuum website: <http://www.continuum.nl>, visited June 8, 2006.
- [4] Information on website Oxxio: <http://www.oxio.nl> visited June 8, 2006 and brochure C 06-05-02.
- [5] Sungmo Jung, Jae-gu Song, Seoksoo Kim, "Design on SCADA Test-bed and Security Device," International Journal of Multimedia and Ubiquitous Engineering, Vol. 3, No. 4, October, 2008
- [6] S. Mallat, "A Theory for Multiresolution Signal Decomposition: The Wavelet Representation", IEEE, Trans. on Pattern Anal. and Mach. Intel., vol. 11, pp. 674-693, 1989